Keywords:
Superconducting cables
Underground transmission cables
Superconductors
Cryogenic cables

EPRI TR-103631
Project 7911-10
Final Report
September 1994

Design Concepts for a Superconducting Cable

Prepared by
UNDERGROUND SYSTEMS, INC., Armonk, NY

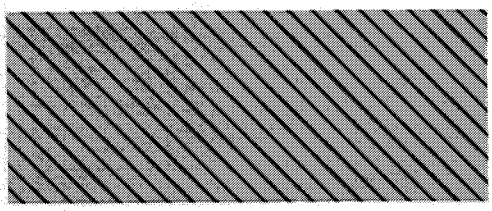

(continued on back cover)

Design Concepts for a Superconducting Cable

Superconducting cables carry higher currents and, depending upon the design, can experience substantially lower transmission losses than conventional cables. This report discusses previous approaches to designing superconducting cables, describes the technical issues that must be considered when designing a high-temperature superconductor (HTS) cable, and presents several design concepts for an HTS cable.

INTEREST CATEGORIES

Underground cables
Advanced delivery system technology

KEYWORDS

Superconducting cables
Underground transmission cables
Superconductors
Cryogenic cables

BACKGROUND Since discovery of the HTS materials in 1987, the industry has discussed the potential of HTS-based power applications, such as transmission cables. A significant amount of work performed in the 1970s focused on designing and building cables using low-temperature superconductors. Most of the studies assessing HTS cables have used the design developed for low-temperature superconductor (LTS) cables, thus minimizing the advantages of the new HTS materials for power applications. This report emphasizes unique HTS design issues.

OBJECTIVES To determine the technical issues associated with designing an HTS cable system; to develop several design concepts for an HTS cable system.

APPROACH The project team's first task was to understand the physics of superconductivity. Using this information and their expertise in conventional transmission cable manufacturing methods, they next assessed the technical challenges associated with designing an HTS cable system. Finally, they developed several HTS cable design concepts.

RESULTS This report describes LTS history, evolution, and applications; the characteristics of various HTS families; and the general theories of conduction and loss in superconductors. Specifically, the report discusses at length several projects undertaken in the 1960s and 1970s to develop superconducting cables using LTS material and to construct cryoresistive cables. These previous efforts revealed several important lessons. First, HTS cables offer a significant advantage over LTS cables, namely, the use of liquid nitrogen as a coolant. This advantage facilitates application of commercial materials and manufacturing techniques, improves the economics of the HTS system, and makes the system more commercially viable. Second, previous efforts to design superconducting cables maintained the electrical insulation at cryogenic temperatures. An alternative approach involves placing thermal insulation (or dielectric) between the conductor and the electrical insulation, allowing the dielectric to operate at ambient temperature. This report identifies the advantages and limitations of both the cryogenic dielectric and the room temperature dielectric design concepts. In addition, the report describes methods for calculating magnetic fields, superconductor losses, cable system losses, and hydraulic flow parameters. Finally, the report addresses thermal models and electrical characteristics.

EPRI PERSPECTIVE Only recently has HTS tape been manufactured in relatively long lengths (hundreds of meters), with critical current density and mechanical characteristics approaching the requirements for a transmission cable. Documented in this report are the requirements for HTS tape, the challenges in manufacturing an HTS cable, and a general description of HTS performance capabilities. The information in this report will serve as the foundation for subsequent prototype and full-scale demonstrations of an HTS cable.

PROJECT
RP7911-10
EPRI Project Manager: Donald W. Von Dollen
Power Delivery Group
Contractor: Underground Systems, Inc.

For further information on EPRI research programs, call
EPRI Technical Information Specialists (415) 855-2411.

Design Concepts for a Superconducting Cable

TR-103631
Research Project 7911-10

Final Report, September 1994

Prepared by
UNDERGROUND SYSTEMS, INC.
84 Business Park Drive, Suite 109
Armonk, New York 10504

Principal Investigator
John Engelhardt

Prepared for
Electric Power Research Institute
3412 Hillview Avenue
Palo Alto, California 94304

EPRI Project Manager
D.W. Von Dollen

Underground Transmission
Power Delivery Group

DISCLAIMER OF WARRANTIES AND LIMITATION OF LIABILITIES

ORGANIZATION(S) THAT PREPARED THIS REPORT:
UNDERGROUND SYSTEMS, INC.

ORDERING INFORMATION

Requests for copies of this report should be directed to the EPRI Distribution Center, 207 Coggins Drive, P.O. Box 23205, Pleasant Hill, CA 94523, (510) 934-4212. There is no charge for reports requested by EPRI member utilities.

ABSTRACT

Superconducting cables carry higher currents and, depending upon the design, can experience substantially lower transmission losses than conventional cables. This report discusses previous approaches to designing superconducting cables, describes the technical issues that must be considered when designing a high-temperature superconductor (HTS) cable, and presents several design concepts for an HTS cable. The report identifies low-temperature superconductor (LTS) history, evolution, and applications; the characteristics of various HTS families; and the general theories of conduction and loss in superconductors. In addition to this historical perspective, the report describes methods for calculating magnetic fields, superconductor losses, cable system losses, and hydraulic flow parameters. Finally, the report addresses thermal models and electrical characteristics.

CONTENTS

LIST OF ILLUSTRATIONS

LIST OF TABLES

1

HIGH TEMPERATURE SUPERCONDUCTOR MATERIALS

Introduction to Superconductors

This section presents a historical review of the scientific and technological landmarks in the field of superconductivity leading to the development of High Temperature Superconductor (HTSC) materials. This is followed by a summary of the complex physical phenomena underlying the fascinating behavior of these materials. The material is presented from the perspective of the cable system design engineer who needs to understand the functional behavior of the new High Temperature Superconductors to properly apply them to the specific application.

Superconductivity is the property of certain materials to conduct a direct electrical current without a voltage drop or power dissipation when their temperature is below a critical temperature (T_c), in contrast to metallic conductors which remain resistive even though cooled to a temperature of absolute zero (Figure 1-1). Above T_c, the behavior of a superconductor is similar to that of ordinary metal. Materials which need to be cooled to extremely low temperatures, below 20 degrees Kelvin, to obtain superconductivity are referred to as Low Temperature SuperConductors or LTSC materials. Materials which display superconductivity at higher temperatures, in the range of 77 degres Kelvin, are called High Temperature SuperConductors or HTSC materials. The LTSC materials require a helium-based cryogenic system while HTSC materials can function in systems that use hydrogen, neon or even nitrogen as the cryogen.

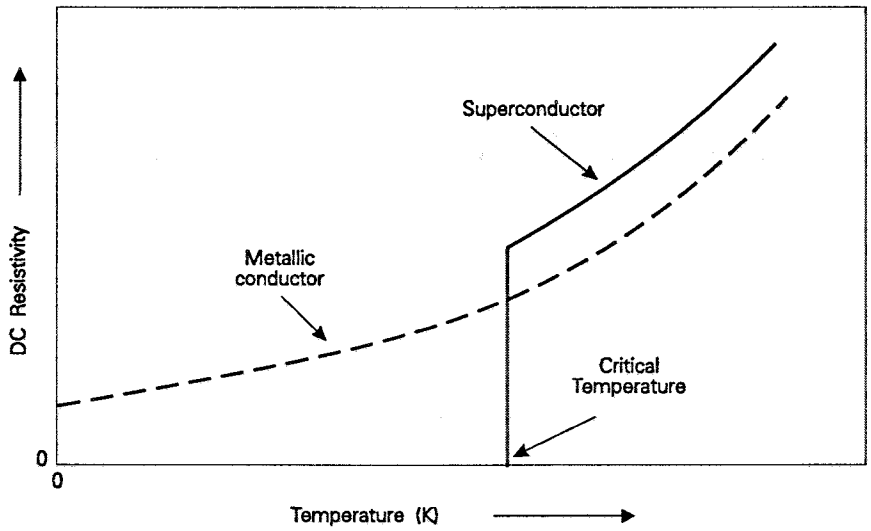

Figure 1-1 The dc resistivity of superconductors drops to zero below T_c in contrast to the resistivity of metals.

The existence and sustenance of the superconducting state is influenced by two parameters in addition to temperature, namely the current density (J) and magnetic field intensity (H) to which the material is subjected. The nature of the relationship among these three parameters is depicted in the three dimensional graph of Figure 1-2. The superconductive state is, in practice, maintained only when T, J and H are below the T-J-H surface shown in the figure.

The classification of superconductors into various types is based on the (H, T, J) characteristics of the material. HTSC and LTSC materials are distinguished by the T_c of the material, as already mentioned. Superconductors are also broadly classified as Type I and Type II. Type I materials are referred to in the older literature as "Pippard" or "soft" materials, whereas Type II materials are referred to as "London" or "hard" materials. Superconductors can also be classified on the basis of their chemical composition, e.g., the Perovskites. The phenomenological differences among the different types of superconductors and the engineering implications from the viewpoint of the cable engineer are discussed in detail in this section.

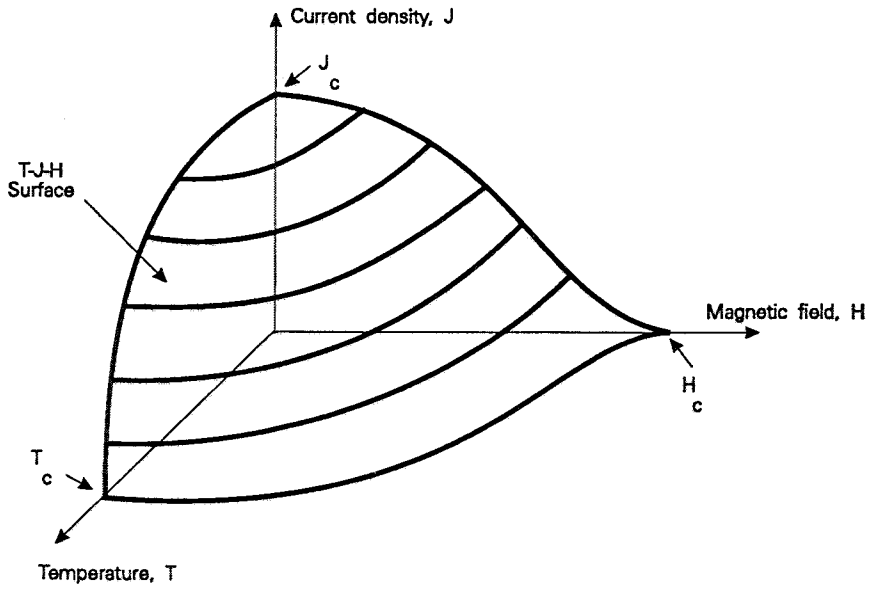

Figure 1-2 The superconducting state is maintained only when the three parameters, T, J and H do not exceed the respective critical values.

The evolution of superconductivity to the present state of the art can be broadly divided into three periods. The first period covered fifty years from 1911 to 1961 during which physicists worked with the elemental Type I materials which had little practical use due to their inherently low magnetic field tolerance. Near the end of this period, the BCS microscopic theory which explains the underlying physics of the phenomenon emerged[1]. The name BCS is generated from the initials of Bardeen, Cooper and Schrieffer who derived this theory in 1957 while at the University of Illinois.

About 1961, the high magnetic field and current capability of Type II materials was confirmed experimentally. The next 25 years represent the second period in the history of superconductors during which the emphasis shifted from the science of the phenomenon to it's application. Type II materials could carry large currents in very high magnetic fields, and their development into engineering materials stimulated many useful applications of superconductivity. Most involved the construction of powerful magnets for a variety of devices. Power transmission cables were one of the earliest

applications proposed, but their development took over two decades. When finally demonstrated, changes in Utility needs and unfavorable economics prevented their commercialization.

In 1986, the third period in this technology began when some Perovskite compounds were found to be superconducting at temperatures higher than known LTSC elements and metallic alloys. In 1987, perovskites were developed that exhibited a superconducting transition temperature above 77 K, the boiling point of liquid Nitrogen. This development promises to have a dramatic impact on the application of superconductivity to a multitude of technologies as a result of the simplification of the cryogenics needed to control the operating temperature these new materials require.

The following historical review is divided into two parts, viz., the LTSC materials and HTSC materials. The accepted theories of superconductivity are briefly described.

Low Temperature Superconductors

History. Throughout the nineteenth century scientists were intrigued by the uncertainty of the behavior of the resistivity of metals at very low temperatures, but they lacked the ability to study materials in that environment. Only in 1898 was James Dewar able to liquify Hydrogen at 20.5 K[2]. Some scientists including Dewar were predicting that resistivity would go to zero as the temperature went to (absolute) zero, but others, such as Lord Kelvin, expected an upturn in the resistivity-temperature characteristic near absolute zero[3].

In 1908, Kamerlingh Onnes, Professor of Experimental Physics at the University of Leiden in the Netherlands, liquified Helium at 4.2 K, and with vacuum was able to reduce its temperature to 1.7 K[4]. Onnes was mostly enthralled with the cryogenic challenge but was also intrigued by the low temperature resistivity mystery, so he began to explore the low temperature resistance characteristics of simple metals. To this end,

he designed a very thorough experimental procedure and assembled an experimental team to perform the electrical measurements while he kept the Helium liquefier in operation. The electrical measurements were done using a four-wire Wheatstone Bridge scheme with a sensitive galvanometer detector. Onnes personally sided with Lord Kelvin and expected resistivity to rise, possibly to infinity, at absolute zero. Their first studies were on platinum and gold which both showed a leveling of resistance at about 4 K. This behavior was attributed to impurities, so Onnes elected to try mercury, because it was easy to purify by repeated distillation.

The first indications that the mercury sample's resistance dropped suddenly to zero near 4 K were naturally interpreted as a problem with the apparatus. However, this behavior, illustrated in Figure 1-3, was observed with every run and finally accepted as a real characteristic of this material.

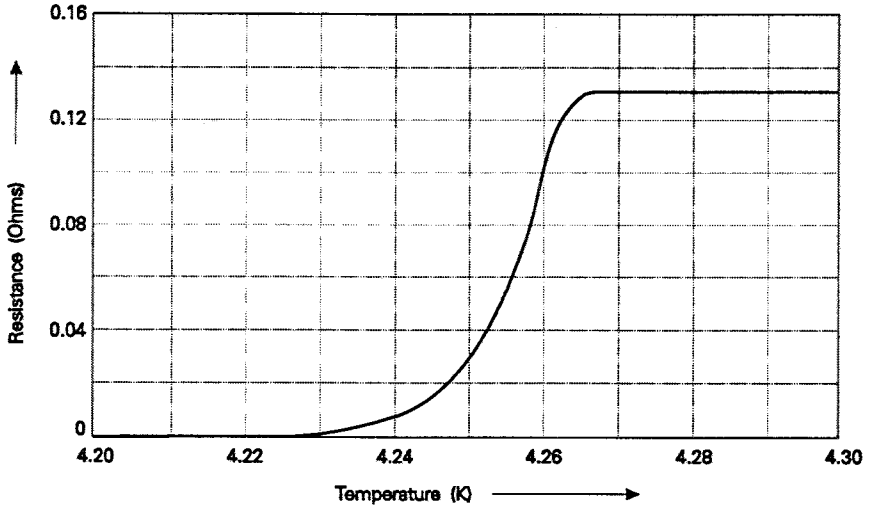

Figure 1-3 Onnes measured a sharp drop in the resistance of mercury at 4.25 K. Source: Reference 2

Onnes labeled the temperature at which the transition occurs the "critical temperature", T_c, and is credited with naming the phenomena "Superconductivity". Onnes first reported his findings to a disinterested audience at the first Solvey Congress in Brussels in October 1911. The "official" publication crediting him with the discovery of

superconductivity was his Communication No. 124c dated November 1911 titled "On the sudden change in the rate at which the resistance of mercury disappears"[5].

Before the disruption of World War I, Onnes managed to measure the onset of superconducting behavior in indium at 3.4 K, tin at 3.7 K, and lead at 7.2 K, but he also observed that the zero resistance state was destroyed by too much current flow or by the application of a relatively small magnetic field. He received the Nobel Prize in physics in 1913 for his work on the properties of matter at low temperatures.

Interestingly, the early projections for the applications of superconductivity were as a means to produce stronger magnetic fields without iron cores, which raised the possibility of lossless machinery. Only one article appeared in which lossless power transmission was mentioned as a potential application for superconductivity.

World War I was not the only impediment to development of the science of superconductors. From 1908 until 1925 Onnes' was the only lab in the world equipped with the ability to liquify Helium. By the end of World War II in 1945 perhaps 5 or 6 labs possessed this capability. However, shortly after World War II, Sam Collins, working at M.I.T., developed a continuous liquefier which soon became commercially available. This development began an era of extensive experimental work in all aspects of low temperature phenomena.

The unique magnetic properties of superconductors were discovered in 1933, when Walter Meissner and Robert Ochsenfeld, working in Berlin, established what came to be known as the "Meissner effect"[6]. When a superconductor is exposed to a magnetic field, currents are induced near the surface of the material which exactly counteract the field and effectively shield the interior of the superconductor from penetration of the magnetic field. If the magnetic field becomes too strong, the superconductor is penetrated and switches to the normal state. However, if the field is lowered below this critical value,

the material instantly returns to the superconducting state. This possible behavior had been suggested by Silsbee[7] of the U.S. National Bureau of Standards as early as 1916. If the superconducting phenomenon was simply that of perfect conduction, the field that had penetrated into the body of the material and caused the transition to the normal state would be trapped by supercurrents near the surface if the material returned to the superconducting state. Meissner and Ochsenfeld observed that the superconductor actually expels the penetrated flux on returning to the superconducting state due to a lowering of the field or a reduction of the sample's temperature, as shown in Figure 1-4. This was the first clear indication that superconductivity is a form of phase transition and that superconductivity is a unique thermodynamic state.

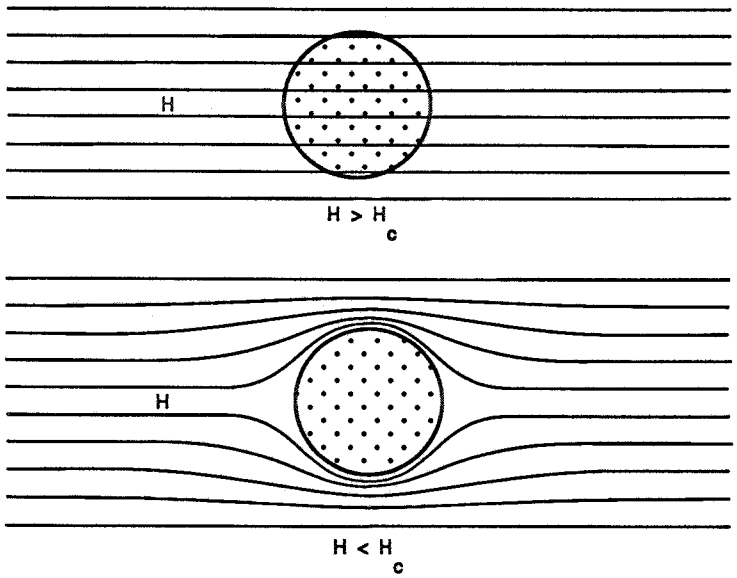

Figure 1-4 The "Meissner Effect" is a fundamental phenomenon exhibited by superconductors wherein the magnetic flux is excluded from the material.

The Meissner effect was the first major breakthrough toward the understanding of superconductivity, as it demonstrated the difference between a superconductor and what might be considered a perfect conductor. Superconducting material is perfectly

diamagnetic (internally **B** must equal zero) in fields that are below a critical level, H_c, except in a thin layer at the surface of the material related to the critical current density. The maximum critical field is achieved at absolute zero (designated by H_0), and the critical field falls roughly parabolically with increasing temperature, reaching zero at T_c. This characteristic established that the superconducting state is a distinct, reversible thermodynamic phase, a conclusion of great significance to the theorist.

In 1934, Gorter and Casimir working at Leiden introduced a phenomenological representation of a superconductor, the "two-fluid model", in which they reasoned that between absolute zero and T_c, the metallic conduction electrons would be in either a normal state or the superconducting state[8]. At absolute zero, all electrons would be superconducting, while at T_c all would be normal as shown in Figure 1-5. The mathematics associated with this model properly predicted the observed parabolic dependence of the critical field on temperature mentioned above, except as the temperature approaches zero where the relation becomes closer to exponential.

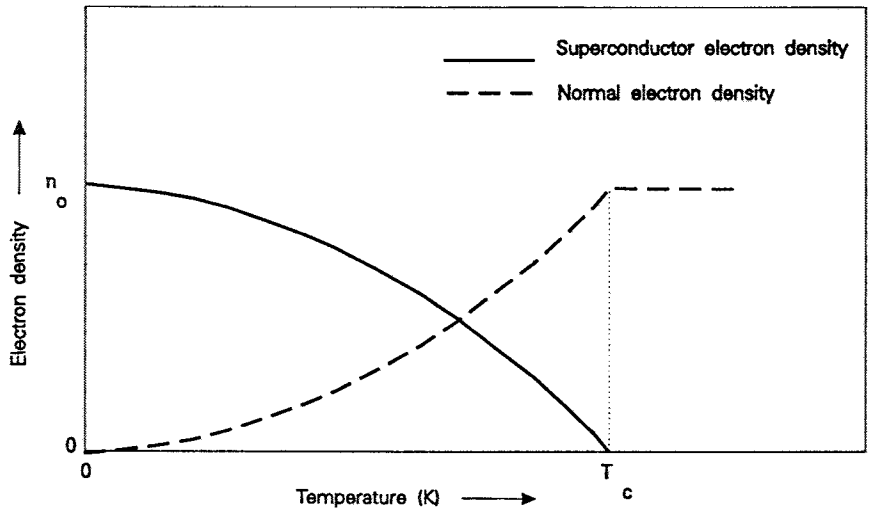

Figure 1-5 At absolute zero, all electrons are superconducting. At T_c, all the electrons are normal.

A major advance in superconductivity came in 1935 with the macroscopic theory of Fritz and Heinz London[9]. The London brothers had followed Kurt Mendelssohn out of Nazi

Germany in 1933 to Oxford University in London where Mendelssohn had set up the first Helium liquefier in England. They derived a phenomenological description of the Meissner effect in the form of modifications to Maxwell's field equations. One outcome of the London equations was that they predicted that the magnetic field falls off exponentially from the surface into the body of the superconductor with a characteristic length parameter λ. The depth of field penetration λ is a function of the material and is in the range of tens of nanometers (several hundred angstroms) for the elemental superconductors known at that time as depicted in Figure 1-6. The "London penetration depth" λ continues to be a fundamental material parameter in the mathematical treatment of superconductivity.

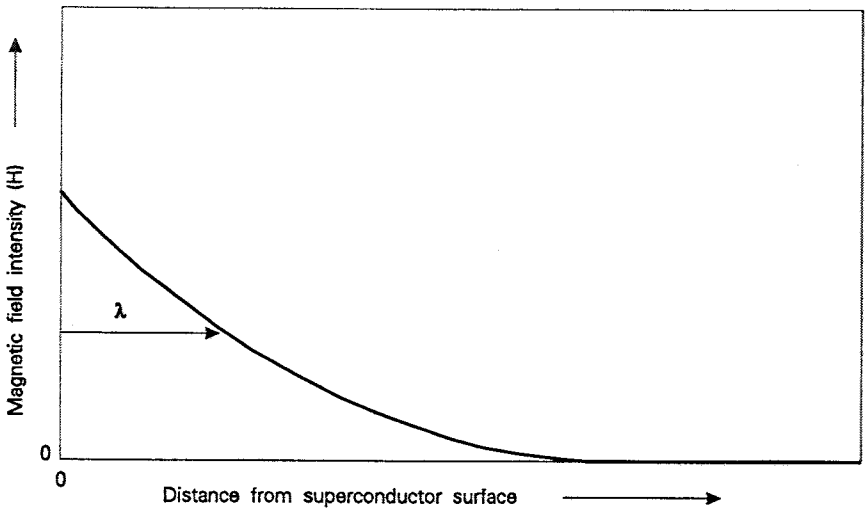

Figure 1-6 The depth of field penetration is a fundamental characteristic of the superconductor material.

The London brothers were pioneers in other aspects of the technology. They were the first to suggest the possibility of an energy gap between the superconducting ground state and the lowest-level excited states in the electron energy spectra, and Fritz London in 1950 casually proposed that flux entering the superconductor would be quantized at a level of hc/e, Planck's constant times the speed of light divided by the charge of an electron[10]. Had he known that the ground state involved electron pairs, he would have

predicted the correct quantum, hc/2e. Heinz London is credited with the discovery of the "anomalous skin effect", a phenomenon that increases conduction loss at very high frequencies where the skin depth becomes comparable to the electron mean free path[11]. The anomalous skin effect applies to normal metals as well as superconductors.

In 1937, the Russian physicist Lev Landau developed a general theory of second order phase transitions[12]. In that time frame, Landau was concerned with the superfluid phase transition of Helium at 2.17 K. A first order phase transition is one with discontinuities in internal energy and density which result in the absorption or evolution of heat, such as the melting of a solid. A second order phase transition involves no change in internal energy and no evolution or absorption of heat; however, discontinuous jumps occur in the heat capacity, coefficient of thermal expansion, and some other physical properties. The transition of a ferromagnetic substance to a paramagnetic substance at the Curie temperature and that of a superconductor from the normal to superconducting state in zero field are examples of second order phase transitions. In the presence of a field below H_c, latent energy associated with the expulsion or entrance of the internal field changes the phase transition to first order.

As World War II approached, the understanding of superconductivity had made significant progress, but scientists were still working with the soft Type I superconductors which had no useful application because of their limited current and field capability. One Russian physicist Shubnikov, working in the Ukraine in 1937, studied superconductivity in alloys and observed the unusually high field capability of what are now known as Type II superconductors[13]. Shubnikov was arrested during Stalin's purges and died in prison.

All of the theoretical descriptions discussed above were phenomenological, in that they described the observed behavior of superconducting materials but did not offer any hypothesis concerning the underlying physical cause of the phenomenon. Progress was

slow, as the theoretical tools required to unravel the mystery were evolving in the same time frame. The field of quantum mechanics and the particle-wave duality era of theoretical physics was introduced in the twenties and was just reaching maturity by 1940. Following the war, physicists began to close in on the microscopic idiosyncrasies of superconductivity, aided by the rapid developments in the solid state physics, and the increasing availability of liquid helium.

In 1944, Vitaly Ginsburg, a young Russian physicist, suggested the possibility of an energy gap between the lowest level ground state of superconducting electrons and the first level of excitation in the normal state[14]. This idea was also suggested by Daunt and Mendelssohn in London in 1946[15].

In 1950, Ginzburg and Landau introduced their psi (Ψ) theory where Ψ is an "effective wavefunction" for electrons in the superconducting state[16]. The Ginzburg-Landau Theory was a phenomenological extension of London theory regarding the number of electrons in the superconducting state and their likely positions. It stipulated that the superconducting electrons condense into a macroscopic quantum state which is described by the Ψ wave function with the same phase throughout the body of the superconductor. This theory accounted for the observed behavior in high fields, especially near the transition to normality and was the first suggestion that electrons in the superconducting state are all in the same quantum state, an idea contrary to the Pauli principle which allows only one free electron to occupy each quantum state in a normal material.

Ginzburg and Landau applied their theory to superconductivity with sufficient insight that they were able to derive many of the fundamental equations which govern superconducting systems. These include the equation which relates the maximum magnetic field which can be tolerated at a temperature T to that tolerated at absolute zero temperature, and equations for the characteristic lengths $\lambda(T)$ and $\xi(T)$, which are

the temperature-dependent magnetic field penetration depth and electron correlation length, respectively. Incidentally, Gor'kov showed in 1959 that the Ginzburg-Landau equations can be derived from BCS theory[17]. What was missing in 1950 was the mechanism by which electrons form Cooper Pairs.

Another clue was put forth in 1950, independently by Maxwell and by Reynolds, et al. They observed that the critical temperature of isotopes of mercury is related to the isotope mass, which implied that superconductivity must involve an interaction between the electrons and the material lattice and more specifically, the phonon spectrum of the lattice[18]. Isotopes are derived from the base element by the addition of one or more neutrons to the atomic nucleus, changing the mass of the nucleus but neither the electrical or chemical nature of the atom. Prior to this discovery, physicists had presumed that the lattice structure was irrelevant to the transition because so many different superconducting structures had been found. This discovery was called the Isotope effect, and subsequent experimentation around the world established this type of relation for most, but not all superconducting elements.

In 1953, Pippard advanced another step with the concept of "nonlocality" of the interaction of the superconducting electrons and internal electromagnetic fields. He introduced a coherence length, ξ, which is a characteristic length for the exponential decay of such field affects on the superconducting electrons[19].

In 1954, the existence of the energy gap was experimentally confirmed by Corak, et al with precise measurements of the electronic specific heat[20]. When compared to the normal specific heat at the transition temperature, the increase in specific heat requires a minimum excitation energy per particle. This energy is made available by the condensation of the electrons into the lowest energy level, known as the ground state.

The microscopic explanation of the phenomenon which generates the superconducting state was finally developed in 1957 by John Bardeen, Professor of Physics at the University of Illinois, Leon Cooper, a post doctoral associate recruited from Princeton by Bardeen, and Robert Schrieffer, a graduate student of Bardeen's. Their theory, which is based on the condensation of electrons into pairs, has became known as the BCS theory. The electron pairs are known as "Cooper Pairs" to acknowledge that the pairing concept had been suggested by Cooper in 1956[21].

According to BCS Theory, superconductivity arises when at low temperatures, electrons form Cooper pairs. There is the usual coulomb repulsion between the electrons of a Cooper pair, but an attraction between the electrons of a pair is introduced by the phonon-electron interaction at sufficiently low temperatures. If the net result between these two forces is attractive, Cooper pairs are formed with energies in the range of $3.53k_BT_c$ (k_B is Boltzmann's constant) symmetrically about the Fermi level. The energy spectrum of a given Cooper pair of electrons is therefore at $\pm\Delta$ situated about the Fermi level E_F leading to the width specified as $\pm 2\Delta$ between the electrons of the Cooper pair

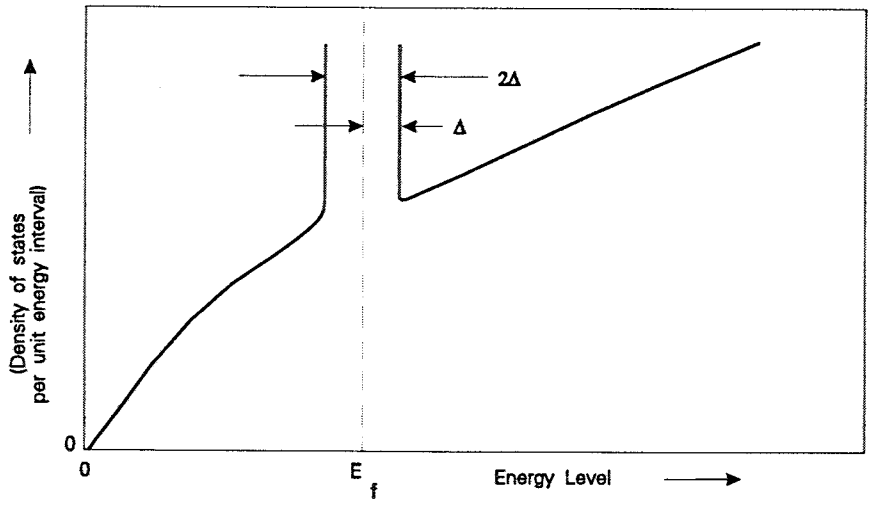

Figure 1-7 The energy spectrum of a Cooper pair of electrons is situated symmetrically about the Fermi level.

as illustrated in Figure 1-7. The electrons which form Cooper Pairs cannot exchange energy with the lattice in a manner which conserves energy, as at superconducting temperatures corresponding quantum energies are not available in the Cooper Pairs and lattice. The net attractive force between the electrons can be reduced by increasing the temperature to T_c which destroys superconductivity. The width of this gap reduces to zero at T_c and is maximum at 0 K as schematically shown in Figure 1-8.

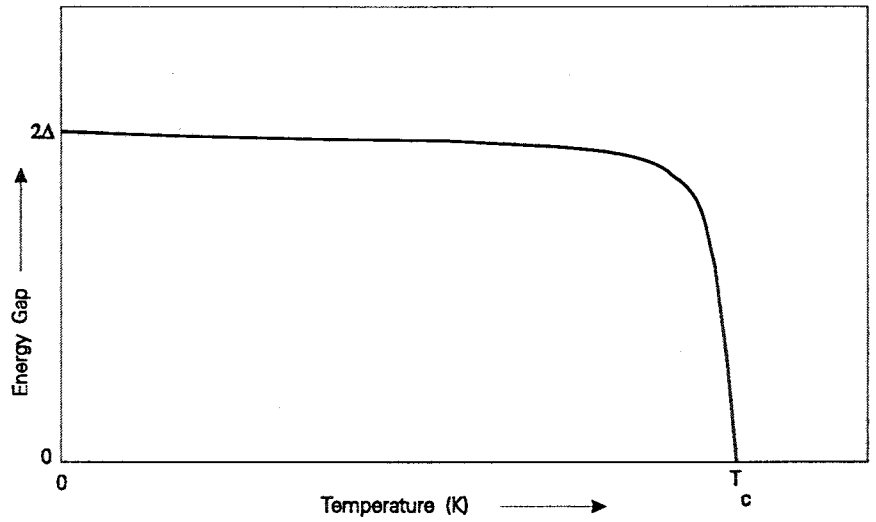

Figure 1-8 The width of the energy bandgap between the Cooper pair of electrons is a maximum at 0 K and reduces to zero at T_c.

Bardeen, Cooper, and Schrieffer described the mechanism by which this occurs, for which they received the Nobel Prize for physics, but not until 1972.

Following the introduction and acceptance of the BCS microscopic theory, most workers in the field believed that the mystery was solved. Efforts turned to the exploration for new superconducting materials and the application of the new theory to improve the properties of known materials. However, in the late fifties, almost five decades after Onnes discovery, most known superconductors were either Type I or rather poor Type II and had almost useless characteristics of current and field tolerance. Essentially all

of the experimental work leading up to the BCS Theory had been carried out on the Type I superconductors because they were well behaved. It should also be noted that most work prior to BCS had dealt with steady fields and dc currents, except for some exploration of surface behavior at very high frequencies.

Two experiments confirmed the quantum nature of the phenomenon as described by the London modifications of Maxwell's equations, the Ginzburg-Landau wave function, and the BCS theory. The first came from Ivar Giaever working at GE in Schenectady, New York in 1959 and 1960. He had been studying the tunneling behavior in semiconductors when he heard of the energy gap in superconductors and the concept that this quantum phenomena occurred on a macro scale because of the relatively large coherence distances, sometimes referred to as "Pippard non-locality". He performed experiments on aluminum at 1.2 K that measured the voltage at which electrons begin to tunnel through a thin insulating barrier and confirmed the existence of the energy gap once the material entered the superconducting state[22]. His technique established a simple procedure for the measurement of the energy gap.

The second confirmation was suggested in 1962 by Brian Josephson, a graduate student at Cambridge University working under Brian Pippard. As he studied the nature of superconductivity and Giaever's paper on tunneling, he wondered why the Cooper pairs hadn't tunneled through the insulator at zero voltage, since the insulator thickness was less then the coherence length. He worked out the solution of the current flow through a thin insulator separating two superconductors, and predicted that current would flow with no voltage across the insulator, and if a small dc voltage was impressed, current would not just flow, it would oscillate at a frequency equal to 2eV/h! Josephson's theoretical work was published[23] "in the hope that someone might try the experiment". The "experiment" was performed by J. Rowell, et al at Bell Labs in 1963, confirming Josephson's remarkable prediction[24].

In retrospect, Giaever had seen the evidence of Josephson tunneling but had discarded the behavior as shorts in the insulating layer he was studying. The irregularity of the effect was due to the extreme sensitivity of the "free" Cooper Pairs to magnetic fields. Even the Earth's field could easily quench the pairs once they left the body of the superconductor if the alignment was appropriate. The "Josephson junction" has become the basis for many electronic devices including the SQUID (Superconducting Quantum Interference Device), which is one of the most sensitive magnetic field sensors available. The typical V-I characteristic of such a device is shown in Figure 1-9.

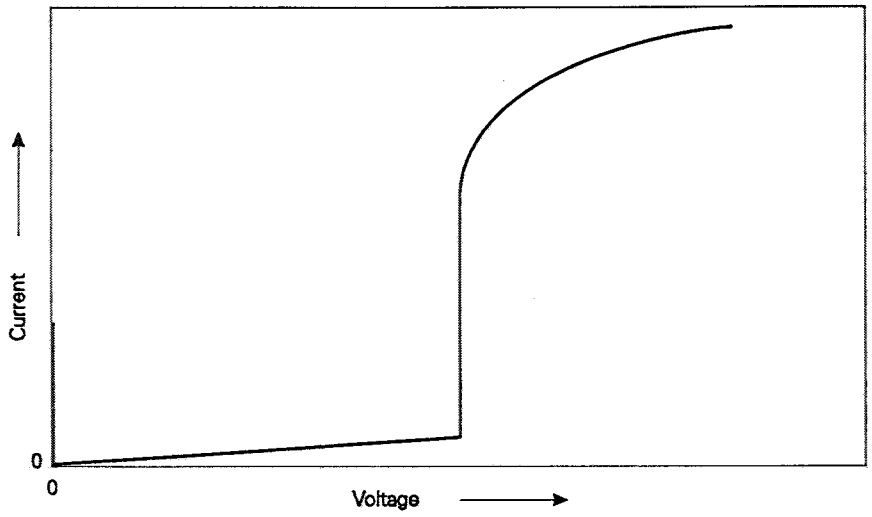

Figure 1-9 The SQUID is one of the most sensitive magnetic field sensors available and is based on the Josephson junction effect.

The Josephson junction has become well-known in the field of the new High Temperature Superconductors. HTSC materials, notably the Yttrium-based family, have a small coherence length which makes any disruption in the structure, such as a grain boundary, behave as a Josephson junction rather than the fully conducting connection that is necessary for a current-carrying application (i.e. a power transmission conductor). When unwanted, Josephson junction behavior is known as "weak link" behavior. Weak links are one of the major materials problems holding back the advancement of 1-2-3 materials in polycrystalline form.

While the BCS theory properly accounts for the microscopic behavior in the superconducting state, it does not relate this electronic activity to the atomic or molecular structure and thus does not help the physicist in his search for better materials by giving him the ability to predict critical temperature and fields from first principles. Neither did it point the way toward Type II behavior and the intermetallic compounds and alloys. The phenomenological theory of Ginzburg and Landau opened that door, via a clever examination of the mathematics of the surface energy.

Evolution of modern LTSC's. Early in the fifties, several significant steps had been taken toward the development of practical materials. George Hardy and John Hulm at the University of Chicago had investigated several intermetallic compounds with a crystal structure known as "A15". Compounds of Niobium generally have this structure. In 1954, B. T. Matthias, et al published critical temperature and field data for many elements, alloys and compounds, including the compound of Niobium and Tin, Nb_3Sn, which showed the highest critical temperature at that time of about 18 K[25]. In general, those working on the classification of materials lacked the ability to create sufficient fields to determine the upper limits of J_c and H_c for these newer materials.

In 1952, a young Russian theoretician Alexei A. Abrikosov predicted the existence of different type of superconductor in which magnetic fields could penetrate the superconductor without causing it to go normal. His prediction, published in 1957, was based on the nature of the surface energy that must exist at the boundary between a normal region and a superconducting region when the material is exposed to a magnetic field, according to the Ginzburg-Landau Theory[26]. This surface energy is required to balance the total energy when the internal energy of the two states differ because of the work done to exclude the field. The surface energy is proportional to a factor which is equal to the coherence length minus the penetration depth. For the pure elemental materials which had been studied up to this point in time, these parameters always

resulted in a positive surface energy since the coherence length is larger then the penetration depth.

Abrikosov asked the question "what if the coherence length were smaller than the penetration depth?". He answered this question with the hypothesis that the surface energy would then be negative, and this would allow some of the material to switch to the normal state without destroying the superconducting state in the remainder of the material. In so doing, the field could penetrate into the superconducting phase, thereby raising the macroscopic field tolerance and current capacity of the material. If this hypothesis were correct, the material would behave as a Type I superconductor up to a small field, H_{c1}, then enter a mixed state in which some of the material would be normal. Because the system energy is reduced by the flux penetration, the flux penetrates in the smallest units as possible, which maximizes the surface area. This results in the penetration of single flux quanta. At a relatively high field, H_{c2}, the material would be fully penetrated by the field, and any increase in field would drive the material completely normal. Recall that behavior of this type had been observed as early as 1937 by Schubnikov. This new type of behavior was initially called "superconductivity of the second kind" to designate that it differed substantially from the first kind. Abrikosov is credited with naming the family of materials that fall into this category "Type II superconductors", and by inference, the elemental materials became known as "Type I".

Figure 1-10 compares the current flow pattern in normal, Type I and Type II cylindrical conductors. Type II materials behave like Type I materials for magnetic fields below a critical level H_{c1}. When the fields are increased above H_{c1}, however, Type II materials allow bulk penetration of magnetic flux. This penetration continues until the magnetic field is increased above the upper critical level H_{c2}. Since the energy of the superconductor is not utilized in expelling flux, the critical current density is generally - much higher in Type II materials than in Type I materials.

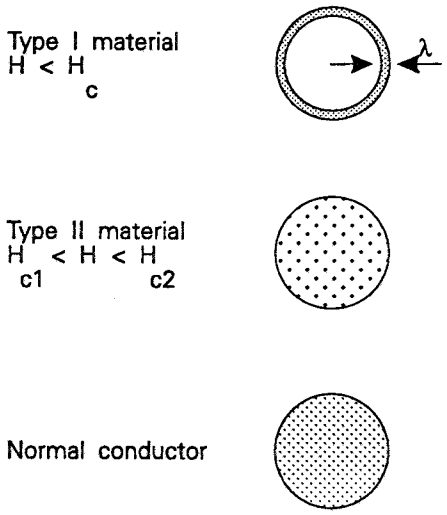

Figure 1-10 The current flow pattern in Type I, Type II and normal materials.

Starting in the late fifties, physicists turned their attention to the improvement of the Type II materials already identified and the search for new materials with higher transition temperatures and/or higher field capabilities. A significant amount of effort was directed toward the study of alloying and compounding in relation to the predictions of the BCS Theory and those of Abrikosov. The two elements, Niobium and Vanadium were known to exhibit Type II characteristics in the pure state, and they served as the starting point for many materials investigations.

The first success came at Bell Labs in 1961 when a group headed by Eugene Kunzler measured an upper critical field of 8.8 Tesla (88 kGauss) with a critical current of 100,000 Amps/cm^2 in a wire made of Nb_3Sn at a temperature of 4.2 K[27]. This achievement is considered the starting point for Type II superconductors of engineering significance. By 1963, Bell Labs had made a "lossless" solenoid which produced a field of 7.0 Tesla using a Nb_3Sn conductor[28]. In quick succession, the intermetallic A15 compounds Vanadium-Gallium (V_3Ga), Vanadium-Silicon (V_3Si), Niobium-Gallium (Nb_3Ga) and Niobium-Aluminum-Germanium (Nb_3Al) were discovered along with the Niobium alloys Niobium-Zirconium (NbZr) and Niobium-Titanium (NbTi). All of these materials

exhibit high field capability and critical temperatures above 10 K. In 1969, the compound Niobium-Germanium (Nb_3Ge) was found to have a critical temperature in the range of 23 K, a level above the liquefaction temperature of Hydrogen (20 K)[29]. This advance represented the first step up in possible cryogens.

No breakthroughs in critical temperature occurred during the seventies and eighties, until the perovskites burst onto the scene in 1986, but the low temperature materials created a mature industry serving the scientific community and the medical industry thanks to the proliferation of Nuclear Magnetic Resonance Imaging (MRI) equipment for medical diagnostics.

Applications. Superconductivity came of age in the 60's due, in part, to the tremendous expansion of cryogenics technology fostered by the space age and other large scale applications such as the transport of liquified natural gas. By 1970 multi-filament Niobium-Titanium conductor in a copper or aluminum matrix could be purchased in a variety of shapes and sizes for magnet construction, and Niobium-tin conductor could be purchased in a thin film configuration on stainless steel tape with copper cladding for stability. Large superconducting magnets were being used for scientific research, and large machines with superconducting dc field coils had been demonstrated. Superconducting Magnetic Energy Storage (SMES) became an attractive application that was under study, and the potential for "lossless" power transmission had been re-established with several development programs underway.

Early applications of low temperature superconductors fall into two categories: electronics and high energy applications. Electronic applications are based on many different uses of Josephson junctions and generally take advantage of the extremely low noise inherent in the devices because of their low operating temperature. Josephson junctions are the basis for SQUIDs (Superconducting Quantum Interference Devices) which are used as magnetometers which can detect very small magnetic fields. SQUID

applications include voltmeters with a sensitivity of 10^{-15} volts, medical, biological and geophysical magnetometers, low power fast digital memory devices and logic gates. Analog applications include mostly radio frequency and higher frequency devices which require low noise, such as mixers for radio telescopes. The precise relationships between the voltage and frequency associated with the Josephson junction have been put to use by the U.S. National Bureau of Standards in a quantum device that has become the legal standard for the Volt. The cryotron switch is a less popular electronic application which uses magnetic quenching of a superconducting pathway as a switch. The cryotron is relatively slow and not interesting as a computer device. It is used occasionally in medium power switching applications, often in conjunction with superconducting energy storage current loops.

High energy uses of superconductors have been almost exclusively related to their use in high field magnets for research purposes and several industrial applications. One of the first wide-spread applications was for windings in particle beam control magnets in accelerators for high energy physics. The development of nuclear magnetic resonance imaging systems (MRI) into a major medical diagnostic industry has created a commercial market for large quantities of medium technology low temperature superconducting wire and medium field superconducting magnets. A few other specialized applications have developed, such as high field magnetic separation; however, the number of systems installed has been very small. Maglev rail transportation using LTSC magnets is in an active development stage in Japan, but Germany has abandoned LTSC in favor of conventional magnets in their Maglev program. Not too much work has been done with LTSC motors.

Many potential applications in the power industry were developed to the demonstration level in the seventies. Included in this category are superconducting generators, SMES, and power transmission cables. However, the major reshaping of the energy industry

in the eighties caused interest in these power applications to fade, as did the hopes for supercomputers using LTSC Josephson junction devices.

High Temperature Superconductors

History. The breakthrough came in January 1986. K. Alex Muller, a professor of Physics at the University of Zurich and a fellow at IBM's Zurich Laboratory, and J. Georg Bednorz, a young physicist at the IBM Lab had been studying the possibilities for higher T_c's in oxides for two and a half years based on work reported in 1973 by D.C. Johnston, et al at the University of California, San Diego, on a lithium-titanium oxide[30], and results published by A. Sleight, et al at DuPont in 1975 on a barium, lead and bismuth oxide which had a T_c of 13 K[31]. In 1985, C. Michel at the University of Caen published a series of papers on metal-like conductivity that they had observed on some perovskite copper oxides[32]. Bednorz and Muller decided to examine the behavior of those oxides at low temperatures for a possible superconducting transition. When they ran the experiment on a lanthanum-barium-copper oxide they found the sought-after transition at 30 K, 7 K higher than the previous high of the niobium-germanium A15 compound! They had both been working in their spare time on this quest for new superconductors, and didn't want to jump the gun by premature publication. They ran several experiments to solidify their results, and submitted an article "Possible high T_c superconductivity in the Ba-La-Cu-O system" to the German periodical Zeitschrift fur Physik in April 1986. The article appeared in the September 1986 issue[33]. Neither Muller nor Bednorz had publicized the discovery in the interim. In fact, they hadn't even disclosed their results to other scientists at IBM.

Paul Chu had been working in the field of superconductivity for over twenty years and had worked his way from the tutorage of Bernd Matthius at UC, San Diego through Bell Labs to an assistant professor position at Cleveland State and, finally, a full professorship at the University of Houston in 1979. Since the mid-seventies Chu had also been searching for higher T_c superconductors in unusual materials and had been especially

interested in the effects of very high pressure on T_c as a key to the role of the atomic structure. He had been in Washington D.C. for the month of October, where he maintained an administrative position with the National Science Foundation. When he returned to his office in early November, he found a copy of the Bednorz-Muller article near the top of the pile on his desk. He immediately sensed that this could be the breakthrough, and that others would be alerted as well. He redirected his whole group to pursue first the confirmation of the 30 K T_c in the Bednorz-Muller La-Ba-Cu-O compound and then to explore the composition for possible higher T_c's. The group quickly confirmed the 30 K transition temperature.

Just before Thanksgiving, Chu and his group saw an indication of superconductivity at 73 K in a variation of the Bednorz-Muller compound with a smaller percentage of copper, but the sample was unstable in the atmosphere overnight and its superconductivity had disappeared the next day. X-ray diffraction analysis of Chu's samples implied that the superconducting phase was the 2-1-4 phase, indicating the approximate ratio of La to Ba to Cu in the oxide formula. Chu next turned to study the effect of pressure on T_c for the La-Ba-Cu-O material. He was able to raise T_c above 40 K by applying ten thousand atmospheres of pressure to the sample. This result suggested substitution of smaller atoms for the large barium atom, and possibly the lanthanum, but Chu's group was too busy with high pressure examinations to try to synthesize new compounds.

Chu attended the Fall meeting of the Materials Research Society in Boston the first week in December, and presented his data confirming the Bednorz-Muller discovery in the La-Ba-Cu-O compound, an important step toward the general acceptance of the IBM results[34]. In a surprising "statement" following Chu's paper, Koichi Kitazawa of the Department of Industrial Chemistry at the University of Tokyo presented a more thorough compilation of data confirming the IBM results. It was then that Chu realized he was in a race. Later during that meeting he contacted his friend and one-time

student Maw-Kuen Wu who was an assistant professor at the Huntsville campus of the University of Alabama, Wu agreed to join in the hunt and help with the synthesis and characterization of some of the variations of the copper-oxide compounds that Chu had in mind. Chu also engaged Art Freeman of Northwestern University, a well-known theoretician and specialist in atomic structure calculations to join his effort.

Wu's first synthesis was a lanthanum-strontium-copper oxide which showed a transition at 39 K without pressure assistance. In that same time frame, before Christmas, Chu's group had raised the pressure to twelve kilo-atmospheres and achieved a T_c above 50 K in the La-Ba-Cu-O system. Chu and his co-workers submitted their initial pressure results on T_c to the weekly Physical Review Letters in mid-December[35]. Their article was published in the January 26, 1987 issue, along with an article from Robert Cava, et al of Bell Labs. Cava's group had measured a T_c of 36 K on the La-Sr-Cu-O compound and submitted their paper two weeks after Chu's submission, yet it made the same issue[36].

During discussions at a New Year's Eve celebration in Houston, Chu, Wu and Jim Ashburn, a member of Wu's Huntsville team decided to try some rare earth substitutes for lanthanum. They agreed to try three; lutecium, ytterbium, and yttrium. On January 29, 1987, the group at Huntsville measured a T_c of 93 K on a sample of yttrium-barium-copper oxide. The following day Wu flew to Houston with the sample where the 93 K value was immediately confirmed in Paul Chu's lab. After a few days of confirmation studies, a paper was submitted to Physical Review Letters which was titled "Superconductivity at 93 K in a new mixed-phase Y-Ba-Cu-O compound system at ambient pressure", co-authored by the key players of both the Huntsville and Houston groups[37]. A second paper titled "High-pressure study of the new Y-Ba-Cu-O superconducting compound system" was also submitted to PRL[38]. Both were published in the March 2nd issue.

Paul Chu first publicized their discoveries with a news conference on February 16 that covered the front page of the Houston Chronicle's afternoon edition. That marked the first publication of the yttrium substitution, inadvertently revealed by the University's Dean. The same information turned up in China in the February 25 issue of the People's Daily as reported from the Beijing Institute of Physics. While the Houston article went unnoticed, the China announcement was picked up by most workers in the field. Within days, the yttrium-barium-copper oxide T_c of 90 Plus K had been confirmed by Bellcore, IBM, Argonne, Bell Labs, Northwestern, as well as several labs in Japan and probably many others around the world.

All that remained to complete the picture was the identification of the particular phase structure that was responsible for the superconducting behavior. To this end Chu enlisted the help of another old friend, Ho-Kwang "Dave" Mao at the Geophysical Laboratory of the Carnegie Institute in Washington. Mao, with help from Robert Hazen and others was able to zero in on the Perovskite structure with the composition $YBa_2Cu_3O_X$ where x is slightly less than seven, now known as the famous "1-2-3". At the Spring meeting of the American Physical Society in New York on March 18, presentations lasted well past one A.M. Speaker after speaker presented confirming results, phase identification, and other helpful bits of information, each with a slightly different focus. This meeting has been heralded as the "Woodstock" of modern physics and enjoyed unprecedented TV and news coverage. High Temperature Superconductors had arrived!

As the end of 1987 approached, Hiroshi Maeda, heading a group at the Tsukuba Laboratories in Japan reported their discovery of the start of a transition at 110 K in a bismuth-strontium-calcium-copper oxide[39]. Their material contained two superconducting phases, one which had a T_c of about 105 K and another with a T_c of 85 K.

In February 1988, Allen Hermann and Zhengzi Sheng of the University of Arkansas displayed a poster at the World Conference on Superconductivity in Houston which reported a T_c of 120 K with a thallium-barium-calcium-copper oxide[40]. This combination of elements had several phases that superconduct, but all seem to have about the same transition temperature.

In this time frame, an endless parade of record breaking discoveries was anticipated as more and more of the possible combinations were synthesized and evaluated. Indeed, many new ceramic superconductors have been discovered, including new families of materials, but none have come close to matching the T_cs' of the three perovskites just mentioned.

As of the end of 1991, the latest and most exciting discovery is that of the carbon compounds nicknamed "Buckyballs". This new class of material is characterized by a unique atomic arrangement of carbon atoms in a molecular structure that mimics a geodesic dome, much like a soccer ball as illustrated in Figure 1-11. This class of carbon compound has been officially named "Fullerenes" after the late R. Buckminster Fuller who is credited with incorporating the geodesic dome into his architectural designs.

Buckyballs were first observed in 1985 but not until 1991 was their potential as superconductors discovered by Robert Haddon, Art Hebard and Don Murphy at Bell Labs. They doped Buckyballs with potassium and found a T_c of 18 K. Another try with potassium and rubidium resulted in a T_c of 28 K. Advantages claimed for these unusual molecules are their ease of synthesis and the resulting superconducting properties appear to be isotropic in sharp contrast with the anisotropy of the copper oxide HTSC materials[41].

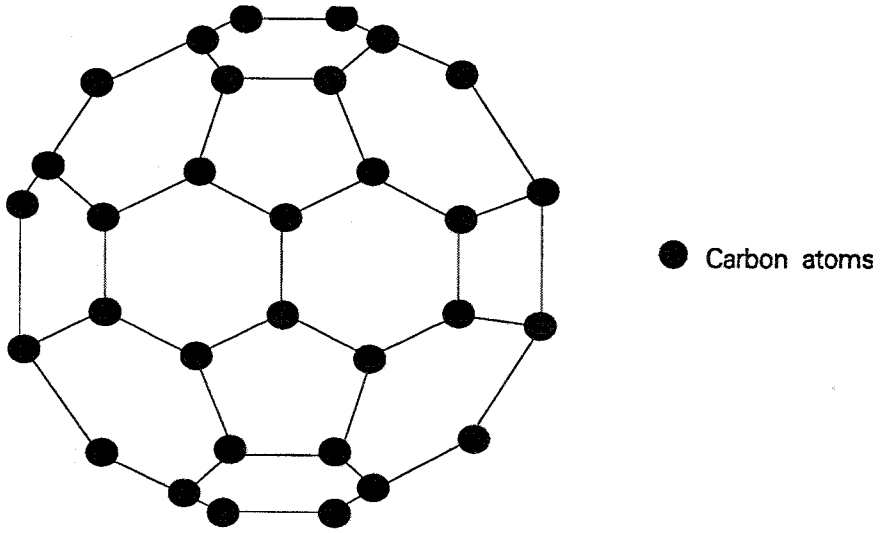

Figure 1-11 The molecular structure of Buckyballs resembles that of a geodesic dome, much like a soccer ball.

Yttrium-Barium-Copper Oxide, (YBCO). YBCO (or 123) was discovered in the U.S. but the compound has been studied extensively throughout the world. The material has a critical temperature of about 93 K, which is above 77 K, the boiling point of liquid nitrogen, but not by very much. YBCO is a multi-phase ceramic. The 1-2-3 phase is actually represented as $Y_1Ba_2Cu_3O_{7-x}$, and its superconducting properties are sensitive to the value of x, being better as x goes to zero. The most common phase is the 2-1-1 phase which does not exhibit any superconducting behavior. 2-1-1 is a greenish translucent substance while 1-2-3 is a dull black opaque material. It has been established that the yttrium is not critical to the superconducting properties of 1-2-3 and any of the rare earths (atomic numbers 57 to 71) can be substituted for yttrium (atomic number 39) with only a small effect on superconducting properties. Thus, this compound is sometimes written as $(RE)Ba_2Cu_3)_7$. Those in the yttrium group (atomic numbers 67-71) yield results similar to yttrium, but Gadolinium (Gd) might have even better properties. Most of the rare earths are not as reactive as yttrium which also might favor their development. However, yttrium continues to be the workhorse of the 1-2-3 compound.

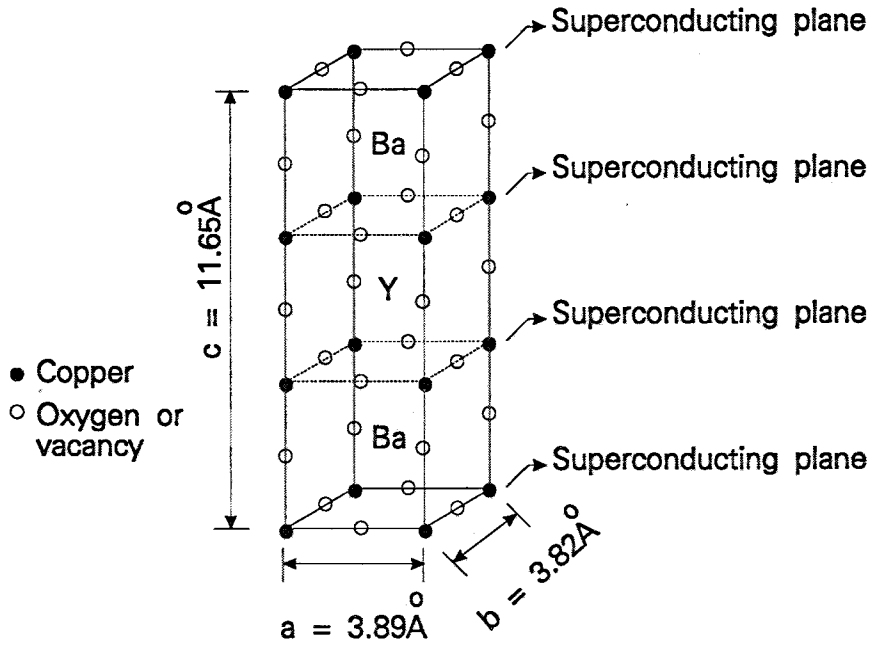

Figure 1-12 The unit cell structure of the orthorhombic 1-2-3 ceramic indicating the superconducting planes.

The 1-2-3 phase has either an orthorhombic or tetragonal crystal structure, depending on oxygen stoichiometry. Figure 1-12 depicts the unit crystal cell structure of this ceramic in the orthorhombic form. If x is larger than 0.6, the structure will be tetragonal and the ceramic will not superconduct. Achieving the optimum oxygen stoichiometry and maintaining it through the full processing procedure has become an art. The superconducting charge flow tends to be in the CuO_2 planes which are parallel to the a-b plane of the crystal (see Figure 1-12). Conduction in the c-axis direction is poor and accounts for the anisotropic behavior of the crystal. Thin films that have the c-axis perpendicular to the plane of the film have the best performance, with J_c's approaching 10^7 amps/cm^2 and H_{c2}'s of several hundred tesla, at 77 K.

Having the correct crystal structure is only part of the problem in the production of bulk, polycrystalline material. Because the coherence length is very small (on the order of the unit cell dimensions), the crystals have to be closely aligned and in the proper orientation to achieve an acceptable connection for current flow. In bulk material, the

tendency of the grain structure is to align at random with small amounts of the other phases separating the grains. Figure 1-13 illustrates a typical bulk ceramic microstructure. Such a microstructure contains several inhomogeneities, structural and chemical, such as grain boundaries, twinning boundaries and various other defects. Unless bulk YBCO is "melt textured" (a type of ceramic fabrication process which is described in later sections), it generally exhibits weak link behavior characterized by a very rapid reduction of critical current with applied magnetic field. Typical bulk samples of such material have critical current densities only in the range of 500 to 1000 A/cm^2 and a sensitivity to magnetic fields such that an external AC magnetic field of 100 Gauss can result in a resistivity greater than the resistivity of Copper at 77 K. However, with melt texturing, weak links can be reduced through improved grain orientation. Increases in the critical current of as much as two orders of magnitude have been achieved with decreases of the sensitivity to magnetic fields to the point that the fields have little effect on J_c over the range of interest for cable technology (300 to 1000 gauss).

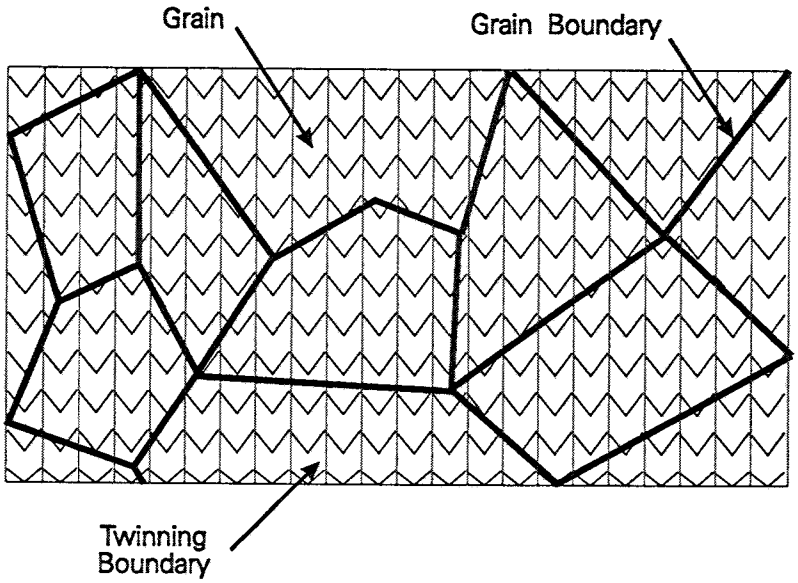

Figure 1-13 Schematic of a typical microstructure illustrating grains, intergranular boundaries and twinning boundaries.

Meter-long melt textured YBCO fibers have achieved critical current densities at 77 K in the range of 20,000 A/cm^2 in self-field, and close to 100,000 A/cm^2 has been claimed in shorter samples in zero field. However, melt texturing of YBCO is so far a very slow process. Treatment rates are measured in mm/hour. Many in the field believe that this shortcoming will be difficult if not impossible to overcome in the scale-up to a commercial production process. It may be noted that while T_c and H_c could generally be considered intrinsic properties of the specific material, J_c is largely a function of the ceramic microstructure and can vary several orders of magnitude depending upon the material processing techniques.

If Type II superconductors are to be practical for large transport current densities, the losses caused by the movement of flux lines must be minimized. Consider the case of a Type II superconductor in the shape of a cylindrical wire carrying DC current. Below H_{c1}, the behavior of the material is identical to a Type I material. In the intermediate region ($H_{c1} < H < H_{c2}$), the Type II material enters the mixed state in which single quanta of flux penetrate the superconductor (see Figure 1-10). The circumferential magnetic self field caused by the surface transport current would cause the penetration of magnetic flux into the material in the form of circumferential flux quanta created at the wire surface. These would tend to minimize their energy configuration by decreasing their radius. In the limiting case, the flux quanta could shrink to the center of the wire and disappear. The dissipation of energy caused by the movement of flux lines must be arrested for Type II materials to be lossless and therefore to be superconducting. Motion of flux quanta can be inhibited through increasing impurities within the superconducting alloy or ceramic microstructure, as such impurities tend to "pin" flux. These are extrinsic material properties which depend on material processing. As the performance of Type II materials depends on such extrinsic properties, the manufacture of Type II superconductors is as much an art as science.

YBCO pins flux very effectively at relatively high temperatures, and this is one of its major advantages. Some believe that the inactive portions of the crystal lattice serve as pinning sites, in addition to interstitials (contaminants within the crystal lattice) and grain boundaries which may house contaminants. There is a clear conflict regarding grain boundaries since good transport requires close clean contact while good flux pinning may require poor dirty contact. However, this conflict is potentially surmountable, as epitaxial thin films have grain boundaries and can also have excellent transport properties which imply excellent flux pinning. However, these properties have not yet been attained in bulk YBCO which, at best, has a critical current density an order of magnitude below that of the best epitaxial thin films.

YBCO materials are highly sensitive to the oxygen content of the lattice, which must be in fairly narrow range for good superconducting properties. Processing of YBCO to obtain the proper phase and oxygen stoichiometry requires treatment at high temperatures, over 600 C for sintering and over 900 C for any type of melt process. If cladding of the material is necessary, silver is the preferred metal because it allows oxygen to pass through the cladding without reaction. Other metals that have melting points above about 1000 C will react with the oxygen needed for proper stoichiometry. At room temperature, HTSC materials are poisoned by Cu which can diffuse into the lattice and are sensitive to moisture, especially in an unclad state.

Melt textured material takes the form of a dense ceramic with reasonable tensile strength but very little strain tolerance or fracture toughness. Bulk polycrystalline YBCO with adequate grain boundary behavior cannot tolerate local bending strains more than about 0.01%. This means that any "flexible" structure will have to be built with very thin filaments or layers which are supported by a normal elastic matrix that provides compressive forces to the YBCO while dominating the mechanical behavior of the composite.

Bismuth-based Copper Oxides, (BSCCO and PbBSCCO). BSCCO (bismuth strontium calcium copper oxide) was discovered in 1988 in Japan and Germany (It's not clear who was first). Most of the early work on these compounds has been Japanese. However beginning in 1989, the U.S. scientific community began to come up to speed with this material, driven by the weak link difficulty with YBCO. The evolution of the properties of BSCCO materials processed in the U.S. is now paralleling the Japanese and German results, but lagging by about a factor of two.

BSCCO is also a multi-phase ceramic which can be structured with several chemical variations. One general formula is $Bi_2Sr_2Ca_nCu_{n+1}O_{2n+2}$ where n is one or two. These two phases are designated 2-2-1-2 which has a T_c of about 85 C, and 2-2-2-3 with a T_c of roughly 105 C. The 2-2-2-3 phase is difficult to separate relative to the dominant 2-2-1-2 phase, and this has slowed progress for those who believe that the higher T_c is necessary. These BSCCO materials form a flaky type of structure similar to mica, which eases the problem of obtaining reasonable intergrain conduction. BSCCO is more ductile than YBCO and does not degrade by exposure to moisture. These advantages together with the higher T_c of the 2-2-2-3 phase make this material a preferred candidate for a LN_2-cooled power transmission cable. The crystal structure is highly anisotropic like YBCO with supercurrent flow concentrated in the CuO_2 planes which are aligned with the a-b plane. The c-axis tends to align itself perpendicular to the surface of the flake structure which simplifies the problem of orienting the c-axis orthogonal to the intended direction of current flow.

The early BSCCO materials have exhibited very good field tolerance at temperatures below about 40 K, where thermally-induced flux creep disappears. BSCCO tapes can provide higher fields than the conventional LTSC materials, NbTi or Nb_3Sn at 4.2 K, and could do so even at 20 K, a growing field for space and military applications which would use liquid hydrogen as the cryogen. For use at 4.2 K or 20 K, the difference between 85 K and 105 K critical temperature has little significance. Unfortunately, at

higher temperatures like 77 K, the weak inherent flux pinning of this material causes losses at high current densities. This characteristic is being overcome by improving both the crystal structure and the microstructure to obtain more pinning sites with higher pinning forces. One improvement has resulted from the addition of lead, either as a dopant or a chemical companion of the bismuth. This family is known as PbBSCCO and exhibits a dramatic improvement in it's superconducting properties at 77 K.

BSCCO and PbBSCCO are made into wires or tapes by forming films on a silver substrate with subsequent folding or rolling, or by powder-in-tube methods where the tube is silver or at least silver-lined. Mechanical reduction is combined with heat treatments and oxygen annealing to arrive at a finished tape or wire, tape being the more common form. A melt-texturing treatment improves the critical current and field tolerance. The field tolerance at 77 K has been improved to the point where PbBSCCO exceeds YBCO in the moderate fields required by transmission cables. The best results have come from Vacuumschmelze in Germany[42] and Sumitomo in Japan[43]. Critical currents on the order of 30,000 Amps/cm^2 in fields of 1000 gauss parallel to the tape surface have been obtained on centimeter lengths of tape. This level of performance might be sufficient to warrant the manufacture of a prototype cable if the AC losses are acceptable over the operating range of temperature and field.

Thallium-based Copper Oxides, (TBCCO). The thallium-based family of superconductors was discovered in the U.S., and the U.S. appears to be leading the world in the performance of these compounds, especially at 77 K. However, for a time the best conductors made of these materials were reported from Japan, with performance comparable to PbBSCCO. Thallium is, of course, a highly toxic element known for its wide-spread use as a rat poison. It has a high vapor pressure and, when combined with moisture will easily pass through human skin, resulting in insidious symptoms that resemble common influenza. As a result, only laboratories equipped to handle toxic materials can work with thallium-based superconductors. In the early days thallium was

considered to be impractical because of its toxicity, but as its performance improved, this aspect of the thallium materials has been overcome. Many of the compounds involved in the fabrication of all of the superconductors are, however, toxic to some degree, and certainly not intended for human consumption. For instance, barium is a heavy metal like thallium, and has also been used for rat poison, yet it is quite common in most ceramics laboratories. In their final copper oxide form, the thallium materials present only a minor hazard, which is reduced even further by the cladding they receive for mechanical and environmental protection. The high vapor pressure of thallium does present a processing problem for these materials because they contaminate the sophisticated vacuum and environmental chambers generally used in the lab for conversion of the raw materials to useable forms. This, of course, will not be a problem in the design of a commercial process.

The general properties and processing of the thallium-based compounds appear to be similar to the BSCCO and PbBSCCO compounds, which is not surprising because they have the same crystal structures and similar chemical formulations except that thallium is substituted for bismuth and barium substituted for strontium. Their general formula is $Tl_mCa_{n-1}Ba_2Cu_nO_{2n+m+2}$, where m is one or two and n is one, two or three. T_c is proportional to the value of n, increasing from 80 K to 105 K to 125 K as n goes from one to three. In this representation, n signifies the number of CuO_2 planes in the crystal structure. The crystal structure of all three compounds is tetragonal (a=b) which means that crystal growth can take place with more than one phase present. This complicates the separation of specific phases. Luckily all phases are superconducting with T_c's above 80 K, but the most desirable phases, 1-2-2-3 and 2-2-2-3 which have the highest T_c are difficult to isolate.

Thallium has been used mostly for the fabrication of thin films. Sumitomo has reported a J_c of 3,200,000 amps/cm^2 in zero field at 77 K[44], and Argonne has extrapolated a level of H_{c2} at zero K of 1000 tesla[45]! Results so far in bulk applications and wire or tape

have been disappointing, with J_c's in the range of 1000 to 10,000 amps/cm^2. However, in December of 1991, GE announced achieving record-breaking performance with a polycrystalline thallium thick film (3.2 micron thickness) which displayed a J_c of over 100,000 amps/cm^2 at 82 K in zero field, falling only to perhaps 50,000 amps/cm^2 at 500 gauss at 77 K[46]. Material with this level of performance will clearly be adequate for power transmission cable applications.

Theories of Superconductivity

BCS Theory and electron pairing. The BCS Theory was a major accomplishment in the field of physics, for it explained how the phenomena of superconductivity works and provided the formulations necessary to calculate with confidence how a Type I superconductor would behave under varying conditions of field, temperature and geometry. This theory enabled physicists to describe, on an atomic scale, the mechanisms which result in the ability of some materials to transport a DC steady current without resistive energy dissipation, or once started, to circulate a persistent current seemingly forever.

Current flow in a normal metal conductor requires a voltage gradient to counteract the resistance of the metal. The atomic structure of metals is such that the outermost electrons easily move out of their atomic orbits and create a "Fermi sea" of electrons which move about in a random pattern, repeatedly colliding with the lattice of metallic atoms. Both the electrons and the lattice are thermally activated and their combined energies constitute the specific heat of the material. Inelastic collisions of electrons with the lattice structure exchange energy by changes in electron momentum, both velocity and direction. In the absence of transport current, inelastic collisions of electrons with the metal lattice structure cause an exchange of energy between electrons and the lattice which assures that they remain in thermal equilibrium. The average distance that electrons can move between collisions is known as their mean free path. Current flow occurs when a voltage is applied. The electric field exerts a force on the electrons that

results in a relatively slow drift in the direction opposite that of the field. Energy is dissipated because the field accelerates the electrons so that more energy is transferred to the atomic structure by each collision. This results in heating of the metal, and is called "Joule Heating", well-known to the electrical engineer.

In a superconductor, electrons conduct current without interacting inelastically with the metal. As a result, no energy is transferred from the electrons to the metal, and no power dissipation occurs in conducting the current. The primary contribution of the BCS theory is its description of the mechanism by which electrons form pairs, known as "Cooper Pairs", below T_c. Pairing of electrons requires an attractive force which overcomes the Coulomb repulsion caused by the electron charge. This attractive force arises from the interaction of the electrons with quantized vibrations of the metal lattice, known as "phonons".

The importance of pairing to superconductivity is derived from some fundamental aspects of quantum mechanics. An electron has a spin of one-half. This results in an asymmetric Schroedinger wave function which requires that when two electrons are interchanged, the wavefunction reverses sign. Thus, while the electrons are not distinguishable, they are also not interchangeable. This establishes the requirement that no two electrons (or any particle with half integral spin) can occupy the same quantum state. A metal has many conduction electrons and therefore a very large number of states which have an essentially continuous energy distribution. The electrons and the metal lattice can exchange energy in any amount down to absolute zero temperature. In other words, the exchange of energy between the lattice and electrons in a normal metal is essentially continuous and not quantized.

If particles have an integral spin they will have even wave numbers and two such particles can be interchanged with no change to the wave function. Then all such identical particles can occupy the same quantum state. Cooper Pairs satisfy this criterion

because they have spin zero, as the two electrons forming the pair have opposite spin. At low temperatures, all the Cooper Pairs can "condense" into this ground quantum state which is separated from the first excited state by a finite energy gap. This has two effects. Electrons cannot transfer energy to the lattice because essentially no electrons are in an excited state from which they can fall into the ground state and give up energy. The lattice cannot transfer energy to the electrons at superconducting temperatures because the energy of lattice excitations (phonons) is too small to bridge the electron gap. Since the electrons can only absorb energy in an amount which elevates the electron from the ground state to an excited state above the energy gap, no interaction is possible. Thus the electron pairs travel through the lattice without interaction, yielding superconductivity as shown simplistically in Figure 1-14.

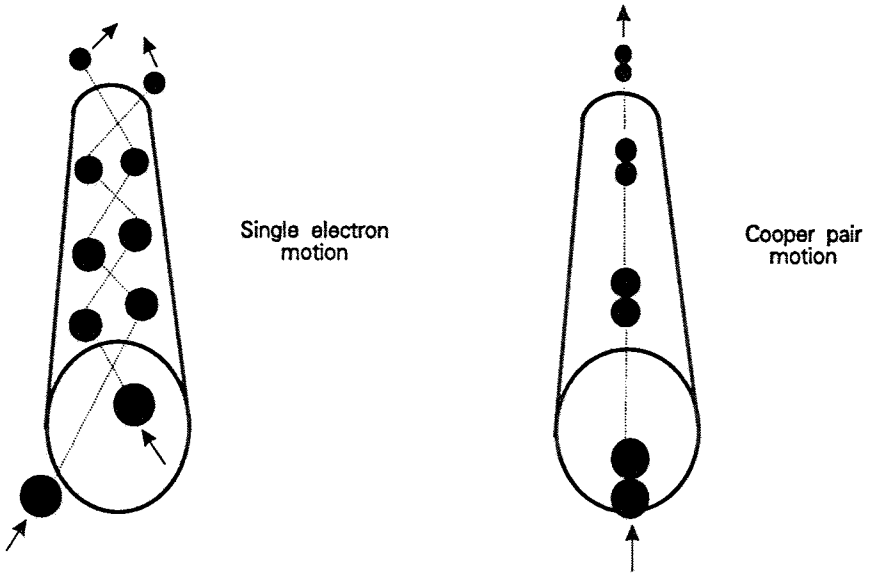

Figure 1-14 Current flow in metals is dissipative due to inelastic electron collisions with the lattice. Cooper pairs lead to lossless current flow.

The above simplified view of the electron pairing mechanism may help the electrical engineer unskilled in quantum mechanics to understand the macroscopic behavior of superconducting materials, and in particular the way they interact with magnetic fields. The interested reader should refer to any good text on the subject or any of the

references cited for a more complete examination of the theory. However, before doing so one should consider a statement by L. Solymar, professor of engineering at Oxford University in a lecture to undergraduate engineering students on the electrical properties of materials, as he entered the topic of superconductivity[47].

> "The microscopic theory is well beyond the scope of an engineering undergraduate course and, indeed, beyond the grasp of practically anyone. It is part of quantum field theory and has something to do with Green's functions and has more than its fair share of various operators. ....."

The BCS theory does not, however, address some aspects of the technology. The theory does not allow a scientist to pre-determine any of the primary superconducting variables of a material i.e. T_c, J_c or H_c from first principles, and it does not, by itself, describe the behavior of Type II materials when operating in a field above H_{c1}, in the mixed state. BCS is the glue that binds the phenomenological "observations" of Meissner, Gorter and Casmir, the London brothers, Ginzburg and Landau, Pippard, Corak, Giaever, Josephson, and many others together in a unifying fundamental theory.

The HTSC copper oxide materials exhibit some "BCS-like" characteristics but do not superconduct by an electron pairing mechanism; rather, they appear to have a pairing of "holes" in the atomic orbits of the lattice. The predominant similarity to BCS is that the mechanism involves the pairing of charge carriers, but that is where the similarity ends. As of the end of 1991, no "new" theory for the superconducting mechanism of the copper oxide family is widely accepted and theorists around the world are engrossed in the quest for "BCS-2".

Intuitive visualization of superconductive behavior. The consequences of the superconducting state follow from fundamental considerations of the interaction of electrons that are free to move without energy dissipation, but in a macroscopically

unified manner, with external stimuli in the form of applied magnetic and/or electric fields. The first unusual aspect of this behavior to be described was the Meissner effect, the expulsion of a magnetic field, and the subsequent establishment of circulating currents near the surface of the material which exactly counteract an external field.

When a material in an external field is brought into the superconducting state, say by lowering its temperature, the motion of the charge pairs is disturbed by the field, but the change in motion results in a change of the magnetic field that is a result of their motion, such that the external field is counteracted. In a normal metal the random orientation of the charge motion and its changes cancel each other and do not affect the macroscopic field. In the body of the superconducting material the charge motion is not random but macroscopically unified. Internal currents are created by the charge motion which exactly counteract the field and move the field toward the surface of the material. However, this counteracting charge motion cannot go past the surface, so a current continues to flow such that the field of the current at the surface exactly counteracts the external field. These surface currents are analogous to eddy currents, except they are the result of a steady field, not a time-varying field as is required for eddy current generation in a normal metal.

The superconductor cannot support an infinitely large current density, so the current that is shielding the external field flows in a surface layer that penetrates into the body of the material. A convenient way of visualizing this behavior is to consider that current flow in a superconductor exists in one of two local states; zero current density, or a current density equal to the critical current density of the material at that field level and temperature. The depth of penetration of the shielding current will then be equal to the required magnetization current divided by the critical current density. When the external field equals H_c, the critical field, the penetration depth equals λ, the London penetration depth. Any increase in field will drive the material back to the normal state by providing that energy needed to put the electrons back into a Fermi state.

The Meissner phenomenon can, however, be dependent on the superconductor geometry relative to the field configuration. Consider the case of a Type I superconductor in the form of a sphere in an ambient field $H < H_c$ as shown in Figure 1-15. The expulsion of flux in this case creates distortions at specific regions on the surface of the material which results in the field in those regions exceeding H_c even though the applied field is less than H_c. This state where macroscopic superconducting and normal regions coexist is called the "intermediate state" and is a characteristic of Type I materials.

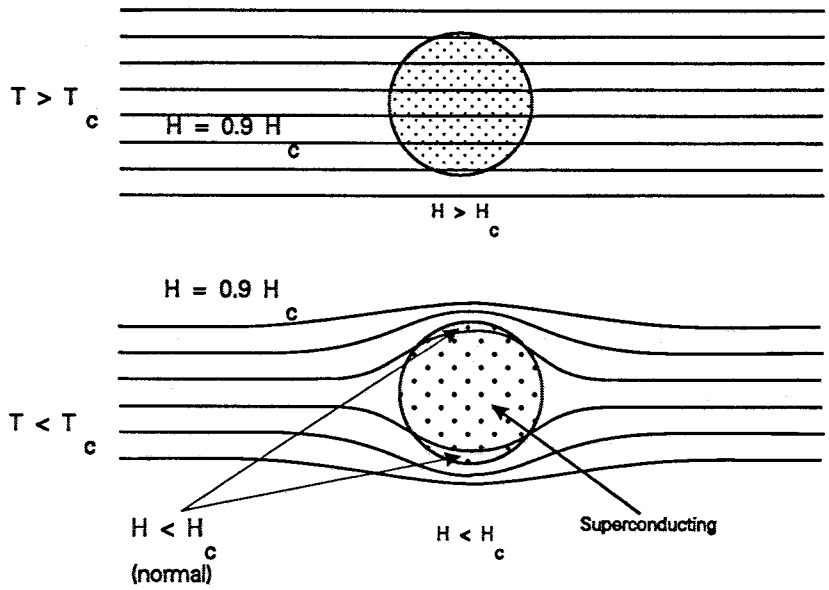

Figure 1-15 The presence of an "intermediate state" wherein the superconducting and normal regions coexist is typical of Type I materials.

When a transport current is imposed on a Type I superconducting body, the same mechanisms apply. Any current tending to flow in the body of the material is forced to the surface by its own magnetic field interactions. The current is forced to flow in the surface layer and is limited by the surface field that it creates, which cannot exceed H_c, and the penetration depth which is limited to λ.

Type I and Type II superconductors. The above discussion has centered on isotropic Type I material in steady field conditions. Type II behavior in the mixed state, behavior in time-varying fields, and anisotropic materials can complicate this picture beyond belief. However, this simple concept that internal currents always flow at a local density of J_c or zero so that external fields at any superconducting-normal boundary are counteracted, can simplify the visualization of the activity internal to the superconducting material because the behavior of the superconductor is always consistent with this concept.

The behavior of Type II materials is truly astounding. Superconductors in the pure elemental form, with the exception of niobium and vanadium, are Type I superconductors, for which penetration of the magnetic field into the superconductor causes it to go normal. Such materials are of limited practical use, because they cannot carry large superconducting currents or superconduct in the presence of a large magnetic field.

Roughly speaking, a magnetic field destroys superconductivity (electron pairing) when the radius of curvature of the electron pairs moving in the magnetic field (the Larmor radius) is less than the distance over which they are correlated. The Larmor radius depends on the magnitude of the magnetic field perpendicular to the direction of electron motion and the velocity of the electrons. By adding impurities to a superconductor the electron mean free path can be decreased and the distance over which electrons are correlated reduced, along with the electron velocity. Since the mean free path can be brought down by orders of magnitude to nearly atomic dimensions, the addition of impurities should effect an enormous increase in the field to which a Type I superconductor can be subjected. The addition of such impurities has little effect on the thermodynamic properties of the metal so long as the impurity concentration is low, but another effect of adding impurities, which is more difficult to explain conceptually, is the conversion of the surface energy at a normal-superconductor interface from a

positive value to a negative value. The consequence of the change in the sign of the surface energy is that the entrance of a flux line into the body of the material, which causes a very small filament to go normal, decreases the internal energy of the system. The breaking up of the superconductor into normal and superconducting regions thus becomes more energetically favorable than going totally normal, as would a Type I superconductor where the surface energy adds to the energy of the system.

When the field rises above H_{c1}, the negative surface energy actually reduces the internal energy if some of the field penetrates into the body of the material. The penetrating field sets up an array of infinitesimally small flux lines or filaments of normal material parallel to the field. Each filament is surrounded by a fluxoid of shielding current which falls off exponentially from the normal-superconducting boundary created by the flux line. As the field rises, more filaments are created until the body of the material is saturated with filaments. At this point, the external field will equal H_{c2}, and the material is said to be at its critical state, unable to absorb another filament. Any increase in field or flux depinning would cause the collapse of the superconducting state and the onset of losses.

Each filament of flux is quantized with the value of hc/2e, which is approximately 2 X 10^{-7} Gauss-cm^2. The filaments are able to pack themselves into the material with a spacing on the order of the penetration depth so that the fluxoids of current don't overlap. When the field is between H_{c1} and H_{c2}, the material is in the "mixed" state.

The ability of Type II materials to tolerate large fields by admitting flux is, by itself, not sufficient to make the material suitable for applications such as transmission lines. A problem arises when the material is asked to transport current. The interaction of transport current with the fluxoids causes a Lorentz force to be exerted on the filament, the magnitude and direction of which is obtained by the vectorial cross product of the current and the field vectors. If this force causes the fluxoid to move, energy will be

dissipated (a force acting through a distance). In order to minimize or eliminate the energy dissipation, the fluxoid must be pinned in place. Pinning in conventional Type II superconductors is accomplished through processing of the alloy to produce pinning sites (impurities) at the grain boundaries. The coherence length of conventional Type II superconductors is such that the grain boundaries do not affect the electron pair transport across the boundary. In high temperature superconductors, however, pinning must be stronger as a result of the larger random thermal fluctuations at the higher operating temperature. Pinning sites can be achieved in epitaxial thin films by simple grain boundaries and in bulk materials by the introduction of impurities, grain boundaries or crystal imperfections.

AC loss mechanisms. In a perfect conductor, the skin depth would be zero, and no losses would occur during conduction of an AC current. A Type I superconductor or Type II superconductor operating below H_{c1} (the field at which flux begins to penetrate) essentially meets this criterion, and the theoretical loss is zero. In reality, some loss still occurs as a result of surface imperfections in the superconducting layer. For HTSC superconductors, H_{c1} is in the range of 100 Gauss, which is just too low to facilitate design of a cable with a practical conductor diameter and operating current which does not produce a magnetic field greater than H_{c1} at the conductor surface.

In Type II superconductors, flux moves in and out of the superconductor with each AC cycle. This causes power dissipation. The equation for loss in a cylindrical conductor can be derived from Maxwell's equations and the assumption that all changes in current occur from the outside surface. Thus, if the AC current in a cylindrical superconductor is raised, a surface current will flow on the surface until the field at the surface reaches H_{c1}. At this point, flux and current will start to penetrate into the superconductor. As the current is increased, it penetrates further into the superconductor, always flowing at the critical current density. Penetration could continue until the surface field reaches H_{c2}, which defines the critical current for the geometry. Once the peak current is

reached and the current starts to reduce, a completely counter-intuitive phenomenon occurs. The current on the surface starts to flow in the opposite direction, while the remaining current in the bulk continues to flow as it was at the time of the peak current. As the current continues to drop, the reverse current penetrates from the outside, so that when the net current reaches zero, equal currents at the critical current density are flowing in opposite directions within the superconductor with a boundary separating the currents at some radius R_i. As the current continues to the reverse peak, the boundary radius R_i moves inward until at the opposite peak, all the current is flowing in the reverse direction, and R_i has reached its minimum value, the current penetration depth.

The combination of this type of current flow and Maxwell's equations lead to an AC loss. A hollow cylindrical superconductor with radial thickness much less than the outer radius, R_o, will experience a loss expressed, to first order, as:

$$Q = \frac{2f}{3\pi R_o} x \left(\frac{I^3}{J_c}\right) x\ 10^{-7}\ \ \frac{W}{m} \qquad (1\text{-}1)$$

where I is the conductor current, J_c the critical current density, and f is the frequency of the AC current.

This loss mechanism is best described as a hysteretic loss mechanism. This mechanism was first studied by C. P. Bean in 1962 who published an analysis that has become known as the "Bean Critical State Model"[48]. Appendix I contains a summary of the application of the Bean model to the transmission line problem that was done by E. W. Collings of Battelle for the STI program.

The hysteretic loss should be the predominant loss for an AC transmission line. However, other losses must also be evaluated. Eddy current loss will occur in any normal material that is exposed to the AC magnetic field caused by the transport current. Careful design of the normal metallic components is required to minimize the

magnitude of eddy current loss, but most of the superconducting tapes or wires being developed, especially those produced by some form of the powder-in-tube method, will have a metal sheath located in the field of the transport current. The mathematical calculation of eddy current loss for all aspects of the various cable designs is presented in Section 3.

A minor contribution of loss in AC cables will come from the flow of normal electrons in the superconductor under the influence of the reactive axial voltage gradient developed by the flow of the superconducting electrons. In theory, all of the conduction electrons will condense into the superconducting state only at absolute zero temperature. For any temperature above zero but below T_c only a fraction will go superconducting. This fraction was given by the Gorter-Casmir two-fluid model as:

$$n(T) = n_0 (1-t^4) \quad where \quad t = \frac{T}{T_c} \tag{1-2}$$

In this relation, n(T) is the superconducting electron density at temperature T, and n_0 is the electron density at zero temperature. The normal fraction is just {1 - n(T)}. Since HTSC materials in LN_2 transmission lines will be operating in the upper end of the temperature range, this loss can be appreciable. It will depend on the normal conductivity of the material at the operating temperature, which can be derived from the resistivity-temperature characteristic determined experimentally for the material, corrected for the contribution of any normal metal that may enter into the normal path. This calculation is also presented in Section 3.

Properties of HTSC Superconductors

Critical Parameters, Tc, Jc, and Hc

The critical temperature T_c at which a material becomes superconducting, the maximum critical current J_c which it can carry in the superconducting state, and the maximum magnetic field H_c (or H_{c2}) to which it can be exposed while remaining in the superconducting state are interrelated. For the purpose of rough estimation,

$$H_c(T) = H_c(0)\ x \left(1-(\frac{T}{T_c})^2 \right) \quad Amps/m \tag{1-3}$$

That is, the maximum magnetic field at any operating temperature, T, is related to the maximum magnetic field at (absolute) zero temperature by a factor which depends on the square of the ratio of the operating temperature to the critical temperature (for zero field and zero current). Since a current cannot flow through a superconductor without generating a magnetic field, this equation also relates the maximum current which can be carried for a given geometry as a function of temperature, $J_c(T)$. The superconducting region of current, temperature, and magnetic field are often conceptualized as in Figure 1-2. However, such a plot is only qualitative unless a specific geometry is defined.

Differences Between HTSC and LTSC Materials

The primary differences in the superconducting properties of HTSC and LTSC materials result from the differences in the material properties and in the distance over which electrons are correlated in the two materials. A much smaller correlation length is what gives HTSC materials their outstanding magnetic properties (exceedingly high H_{c2}). In a Type II superconductor, H_{c1} (the magnetic field above which flux starts to penetrate) is generally quite low, of order 100 G. Thus for almost any practical application, the superconductor must operate in the mixed state in which quantized vortices of magnetic flux have penetrated the material. When a current flows through such a material, a force acts on the vortices. If the vortices move, a force is acting through a distance, which results in power dissipation. Thus the vortices must be "pinned" by a force sufficiently great to resist the combination of the magnetic force which results from the interaction with a current flowing through the material and the random thermally induced forces which become significant at temperatures around boiling point of Nitrogen. Thus the "real world" electrical properties of most superconductors depend on extrinsic material properties, such as the strength of pinning centers in the material. In LTSC materials, the same impurities which are added to convert the Type I superconductor into a Type

II superconductor also aid in pinning. Pinning can be improved by altering the metal crystal structure with treatments such as cold working. The manner in which such treatment is undertaken is part of the "art" in making modern LTSC conductors. In LTSC materials, imperfections at intergrain boundaries within the metal do not degrade the superconducting properties, as the distance over which electrons are correlated is great compared to the width of the grain boundary.

HTSC materials have several problems related to the above considerations. Most important, the distance over which electrons are correlated is very small compared to LTSC materials. This results in a deleterious effect of most mismatches at grain boundaries. Further, some of the HTSC materials, notably YBCO, have very complex phase diagrams with non-superconducting liquid phases which can easily form during processing and flow between grains. These give rise to intergrain Josephson junctions and weak linked behavior (rapid drop in the critical current with applied magnetic field). Improved understanding of the phase diagram of YBCO, along with melt texturing, has largely overcome this problem, so that the effect of misalignment at intergrain boundaries is the primary problem remaining.

Both bismuth and thallium-based materials appear to have much less of a weak link problem caused by non-superconducting phases formed during processing, and both have structures which allow for alignment by mechanical processing and improved electromechanical properties of the completed conductor. However, the problem of short electron coherence length and the effect of mismatch at grain boundaries remains. The magnitude of the problem can be illustrated by comparing results on epitaxial films with those for the bulk material. An epitaxial film is grown on a substrate which nearly matches the crystal structure of the film to be grown. This allows the film to grow with a minimum of major defects (e.g., high angle grain boundaries). At 77 K, HTSC materials have achieved current densities in the range of 10^7 A/cm^2 in epitaxial films. Melt-textured bulk materials have achieved in the range of 100,000 A/cm^2 in small

samples, short lengths of wire have achieved about 50,000 A/cm^2, and about 20,000 A/cm^2 has been achieved in the best significant lengths of wire. Thus the current density achieved in significant lengths of wire is almost three orders of magnitude below the intrinsic critical current of the material, and this difference is largely the result of the effect of the short coherence length interacting with crystal mismatches at grain boundaries. However, very steady progress is being made in properties of HTSC wires. A 50,000 A/cm^2 wire should be adequate for the manufacture of a practical HTSC power cable.

The above comparisons could be viewed as slightly misleading, as the materials for which performance has been quoted differ. The wires are primarily bismuth-based material, while the epitaxial films and bulk materials are YBCO. Achieving a strong pinning force appears to be more difficult for bismuth-based materials than for YBCO, and melting of the flux lattice is one of the limitations of 77 K superconductivity for bismuth-based materials. However, the addition of lead to the material appears to overcome the problem, at least for the current densities presently achieved in bismuth-based wires. In both YBCO and bismuth-based materials, critical current densities have sometimes been improved through defect creation with bombardment by energetic neutrons, heavy ions, or electrons.

In summary, the primary differences in the electrical properties of LTSC and HTSC superconductors result from the much shorter electron pair coherence length in the HTSC materials. While this short coherence length undoubtedly gives HTSC materials some of their good superconducting properties (very high H_{c2}), it also results in problems related to the deleterious effect of misaligned grain boundaries in bulk material.

Technologies for material fabrication

All HTSC materials known to date are highly complex chemically and exist in a

metastable state at room temperature. The metastable nature of the material at room temperature and operating temperature results in distortion of adjacent layers of the material. All the materials have complex phase diagrams, and the phases of interest can exist over a very limited set of equilibrium conditions. As well, the chemical formulae do not always accurately reflect the chemical composition. These considerations combine to increase the expected difficulty of manufacturing high temperature superconductors in a continuous process.

Bulk YBCO can be manufactured reproducibly, but high angle grain boundaries and/or the ingress of non-superconducting liquid phases between the grains degrade the material. These problems with bulk YBCO can be overcome to a large degree by using extreme care in the process, and by melt texturing, which is discussed below. Even with melt texturing, the critical current achieved for bulk YBCO is still an order of magnitude below that achieved for epitaxial thin films.

Bismuth materials are chemically more complex than YBCO, especially after addition of lead to improve flux pinning and facilitate synthesis of the 110 K phase of the compound. The bismuth family of materials exists in several HTSC phases, but the 2-2-2-3 phase has the highest T_c, 110 K. The next highest T_c phase, 2-2-1-2, has a T_c of only 80 K, which makes this phase undesirable for a LN_2-cooled transmission line.

The thallium-based compounds include a phase with a T_c of 125 K, the highest yet known, and the other phases that tend to form have T_c's above 100 K. The highest T_c phase does not appear to form under conditions of equilibrium but only as an intermediary compound in a chain of kinetic reactions. It thus will decompose under the same conditions at which it forms.

The available data suggest a correlation between thermodynamic instability and increased transition temperature, although no theoretical basis for such a correlation has

emerged. If this proves to be the case, the manufacture of high transition temperature superconductors may require techniques capable of fabricating a nonequilibrium structure 'in situ', such as molecular beam epitaxy. In any case, successful material fabrication will clearly require a highly skilled approach and sophisticated equipment, all of which can be expected to impact the cost of development and early trials. The situation is similar to the development of the LTSC materials, and product costs should drop as market for the materials develops, along with at least some degree of competition in the field.

Bulk Formation Techniques

Shake & Bake. This is the simplest method for making YBCO. Appropriate chemicals are mixed together through grinding. They are then sintered at appropriate temperature (in the range of 1000 °C). Often this is followed by repeated grinding and sintering to assure excellent mixture of the components. If a bulk shape is desired rather than a powder, it is achieved by sintering or partially melting in a mold, possibly under mechanical pressure. Finally, a treatment in a controlled oxygen atmosphere is used to attain the desired oxygen concentration in the lattice. The quality of the initial compounds is crucial. As well, YBCO has a very complex high temperature phase diagram, and avoiding liquid nonconducting phases during processing is difficult. Once formed, such phases tend to flow between the superconducting grains to produce weak links, essentially Josephson junctions between the grains, which make the critical current density very sensitive to magnetic fields.

Powder-in-Tube. A silver tube is filled with superconducting compound in powder form or precursors (compounds which can be transformed into a superconductor through further processing). Through combinations of mechanical and thermal processing, the material is converted into a thin filament (wire) or tape with good superconducting properties. This method has been successfully pursued for bismuth- and thallium-based compounds which are processed into a silver-clad tape with very

uniform J_c in the range of 10,000 to 20,000 A/cm^2 over meters of length. Silver is used because it is permeable to oxygen, and an oxygen treatment is normally required to achieve the desired oxygen concentration in the superconductor. Also, the silver does not diffuse into the superconductor material as do most other metals.

Deposition on a Surface

Draw from melt. If the superconducting compound or a precursor can be formed as a melted glass, then either a superconducting fiber can be pulled from the melt, or a surface can be pulled through the melt to acquire a superconducting coating (or the precursor thereof) on its surface.

Laser ablation. One or more targets of the relevant compounds are irradiated with a high energy laser beam which evaporates the material from the targets. The resulting vapor coats the surrounding surfaces, which include the heated deposition substrate. Methods such as laser ablation can result in very high quality thin films on substrates which match fairly closely the crystal lattice parameters of the superconductor (such films are known as epitaxial). However, the properties are degraded toward those of the bulk superconductor when the coating is deposited on any other type of surface.

Sputtering. Sputtering is a process by which atoms are evaporated from a target held at negative potential by bombardment with a gas plasma. The liberated atoms are directed toward a heated substrate where they attach themselves. A wide range of variations is possible, including sputtering from several targets onto the (heated) substrate, off axis sputtering from a single target, etc.

Metal-organic chemical vapor deposition (MOCVD). Organic compounds which contain the required metallic elements are evaporated into an inert gas mixed with oxygen, which caries the vapor into a reaction vessel with a heated substrate onto which the metal atoms are deposited.

Plasma deposition. The chemical components are injected into a stream of gas which is passed through a region in which it is thermally ionized with an electric arc or flame. This ionized gas stream is then "blown" onto a surface. The ionized solids tend to stick to the surface. The process variables (carrier gas, ambient gas, temperature, etc.) allow for a wide range of operation conditions and results.

Paints. Various chemical solvent approaches have been taken to deposit the superconducting precursors, typically formed through the "shake & bake" process, on a substrate. These include doctor blade, spray painting, etc. For YBCO, these methods generally result in mediocre superconductors unless a very slow melt texturing is employed after deposition.

Post-Forming Treatments

Sintering. Many forms of HTSC fabrication work with chemical precursors which are converted to a superconductor by sintering after the material has been worked into the desired physical form. This is necessary because the HTSC materials are non-ductile ceramics. Even where the starting materials are superconductors, diffusion of oxygen into the materials is often required after heat processing. The permeability of silver to oxygen and minimal reaction of silver with the superconductor makes it the most popular cladding and precludes the use of non-noble metals for this task.

Melt texturing. The quality of YBCO elements can be increased greatly through the use of "melt texturing". This is a process of bringing the sample to the point that recrystallization can take place under conditions of a controlled temperature gradient which results in the preferential growth of superconducting crystals in the desired direction (of current conduction). Unfortunately this process is extremely slow. Processing speeds are usually measured in mm/hour.

Practical HTSC Conductor Application

Cryostability

Cryostability, i.e., the stable superconducting operation of a system in spite of small thermal perturbations of the system, is of much less concern for HTSC systems than LTSC systems. The heat capacity of all materials goes to zero as the temperature goes to absolute zero. Thus at the very low temperatures at which LTSC systems operate, both the cryogen (liquid or supercritical He) and the superconductor have very low heat capacity. Thus any perturbation of the system which generates heat, such as a "flux jump" (rearrangement of flux within the system) or physical motion of the conductor, can cause a significant increase in the temperature of the superconductor. If the increase is sufficient to cause the superconductor to go normal in a small region, a large increase in the power dissipation in the superconductor will result. In the absence of adequate stabilizing factors, such a normal region will cascade down the conductor causing a total "quench" of the system. Stabilizing factors include adequate quantities of normal metal of low thermal resistivity, adequate thermal transfer from the superconductor to the cryogen, a large heat capacity in the cryogen, and operation at the lowest practical temperature, that is, as far below T_c as possible.

At 77 K, the heat capacity of materials and the cryogen is much greater than in the region of 5 K. Thus, cryostability is much less of a concern. However, HTSC materials are ceramics which have much lower thermal conductivity than the LTSC metallic alloys. Thus, cryostability must be addressed in the design of a conductor. However, the heat capacities of all the involved materials are so much greater at 77 K that a cable can easily be designed to be cryo-stable. In one design calculation, a 10 cycle, 50 KA fault would heat the superconductor, a 3-mm thick Cu stabilizer (the wall of the cryogen channel) on which superconductor is installed, and the LN_2 within the cryogen channel by less than 3 K. Certainly the HTSC material will instantly go normal during the fault because of the increase in magnetic field; however, since the superconductor only increases its temperature by 3 K it will remain well below T_c, and return to the superconducting state

as soon as the current and field are reduced, as they would be when the circuit clears. The cable and its cooling system can be designed so that it will return to its full superconducting capability and be available for operation within seconds of fault clearing.

An analysis of the cryostability in a DC power transmission line was done by E. W. Collings for the STI program. His report (in two parts) is included as Appendix II. This analysis presents the methodology for making the calculations necessary to determine that a given structure will be stable in operation.

Heat Transfer Requirements

Power will be dissipated by an AC superconductor cable as a result of AC losses, dielectric losses (if the dielectric operates at cryogenic temperature[49]), and heat leak through the cryostat along the entire cable length. Additional heat in-leak will occur at the terminals, at the splices in the cable and/or splices in the cryostat. These mechanisms should account for the majority of the thermal load on the refrigeration system. The LN_2 cryogen will be refrigerated to some temperature T_1, enter the cable, and increase in temperature more or less linearly with distance until it emerges at T_2 at the far end of the cable or at an intermediate refrigeration point in a very long cable. The values of T_1 and T_2 will be fixed by the properties of the cryogen (minimum temperature T_1), HTSC material (maximum temperature T_2), and economics. T_1 can be below 77 K, but must be greater than 65 K, the freezing point of N_2. For present HTSC materials, T_2 will probably be in the range of 77 K and not greater than 80 K. This provides an operating temperature range of as much as 15 K. If 5 K of this is left for heating during faults and degradation of the thermal characteristics with time, a 10 K practical operating range is defined.

The cryogen flow rate must be adequate to remove the heat load without excessive warming of the cryogen as it passes down the cable. The flow rate for a given cryogen

duct diameter is easily calculated based on the heat capacity of the cryogen and the values of T_1 and T_2. The combination of the flow rate, duct diameter, and the empirical duct "friction factor" determine the pressure drop from one end of the cable or cooling section to the other. This pressure drop must remain within reason, say in the range of 1 MPa or 150 psi. The pressure drop for constant temperature rise and heat load depends on the inverse 5^{th} power of the cryogen duct diameter, so small changes in duct diameter have a large effect on the pressure drop.

The refrigeration system which cools the LN_2 from T_2 to T_1 will probably use helium as its working fluid. The use of nitrogen as the refrigerator's working fluid below 77 K poses problems associated with subatmospheric pressure. Helium is the most suitable working fluid, primarily because it is the most common refrigerent for cryogenic applications operating below about 80 K. Hydrogen could be used, but it is rather dangerous. Thermodynamic data and extensive experience in use as a refrigeration working fluid are lacking for the other gas candidates neon and argon. Helium is presently used in most low temperature refrigeration systems, including those designed to work at 77 K.

The refrigeration system must be failsafe. It must provide cooling in spite of inevitable component failures and required maintenance. This can be achieved through system or component level redundancy and with storage reservoirs of cold LN_2. Large commercial refrigeration systems such as those used to make LN_2 are highly reliable and fail most often from interruptions of the electrical supply. However, they are shut down periodically for maintenance, and are not required to be uninterruptable.

Rate of Progress and Summary

1987 was a year of orientation by many research groups that had to come up to speed in the technology of the new yttrium 1-2-3 material. Reminiscent of Onnes' experience, once the hoop-la settled down, the 1-2-3 material was found to have disappointing

practical capabilities. Its ability to carry current in bulk form was found to be poor and easily quenched by relatively small magnetic fields. Results quickly began to improve, however, especially in thin films that likely benefitted from crystal alignment which minimizes the impact of their anisotropy.

The materials opened a new world to theorists, who quickly established that BCS theory did not apply in many respects to these materials. The charge transfer was found to imply a pairing of charges, but the material exhibits p-type behavior. The implication is that "hole-pairs", not Cooper's electron pairs, provide the lossless charge transfer. The materials are clearly Type II, and thin films showed possible levels of H_{c2}, the upper critical field, in liquid helium that were in the range of hundreds of Tesla, much higher then the A15 LTSC compounds. T_c was the most publicized parameter by which progress was judged. Initial levels for bulk samples at 77 K were in the range of 10 to 100 Amps/cm^2 in zero field and thin films weren't much better, but by the end of 1987 single crystal bulk material had achieved almost 10,000 Amps/cm^2 in zero field, and thin films were over a million Amps/cm^2.

1988 was similar to 1987, with the exception that the bismuth and thallium structures were added to the list. Work on the bismuth material was concentrated in Japan, perhaps because it was discovered there, and several Japanese Companies established strong patent positions. The U.S.-discovered thallium material was also slow to get started, most likely because its toxicity restricted experimentation to those labs that were equipped with elaborate toxic materials handling capability. Progress dropped off in 1988, and the problem of grain boundary limitations in polycrystalline samples of the 1-2-3 material became the focus of much work. J_c's were held to under 1000 Amps/cm^2 for wire and tape forms of polycrystalline bulk material. For comparison, copper in conventional transmission cable applications operates at about 100 Amps/cm^2.

In 1989, things seemed to get worse, prompted by very poor flux creep resistance and continued weak link problems. 1989 was the year that some proclaimed "the party's over" for HTSC material. Fortunately the scientific community kept working to improve the HTSC capabilities, and more labs started to explore bismuth and thallium compounds, which both seemed to have better inter-grain transport characteristics. Moderate progress was made by the end of 1989.

In the fall of 1989 E. W. Collings traveled twice to Japan funded, in part, by the STI Program. Appendix III presents his report derived from those trips in which he summarizes the state-of-the-art in Japan at that time. It also includes an appendix on Solidification Processing prepared by A. J. Markworth of Battelle.

1990 was a year of steady progress which indicated that these materials would eventually achieve the properties necessary for many, if not all, targeted applications. Fortunately the field and current transport capabilities required for transmission cable applications are on the low end of the scale for conventional power-related equipment. Work with the bismuth materials accelerated, but still lagged behind the Japanese. The limitation of the 1-2-3 material was firmly established to be the "weak link" problem of current transport between grains, while the bismuth compounds suffered more from weak flux pinning and subsequent loss of transport capability at liquid nitrogen temperatures. Melt texturing of 1-2-3 significantly improved the J_c and crystallization, but weak links between crystals still dominate performance.

During 1991, performance levels were achieved in some labs that are sufficient for a power transmission cable application. As the end of 1991 approached, the concern for the STI program was the inability of the manufacturing sector to produce superconducting wire or tape in the continuous lengths suitable for cable trials. The processing equipment needed to transform a laboratory scale production of short trial lengths to a commercial scale capable of producing continuous lengths on the order of

500 to 1000 meters exists with only a few producers, not necessarily those that have achieved acceptable results. Commercial positioning for proprietary advantage among the potential suppliers of wire or tape also became evident, slowing the evaluation process.

In 1992, the development of HTSC conductors is progressing rapidly. Short lengths of flexible conductor elements have reached 40,000 A/cm^2, which, if the AC losses conform to theory, is almost sufficient for a practical HTSC cable. Given the rate of progress over the past year, 1991, achieving this level of performance in long lengths of conductor is just a matter of time.

In summary, HTSC power cable has the potential to be a practical and cost effective technology. In short lengths, conductor materials (tapes or wires) appear to have achieved the electrical and mechanical properties necessary for manufacturing a power cable. With time, these properties should be routinely achieved over very long lengths to enable the manufacture of practical conductors for power transmission cables.

References

1. J. Bardeen, L.N. Cooper and J.R. Schreiffer, *Physics Review*, vol. 108, December 1 1957, p. 1175.

2. James D. Doss, Engineer's Guide to High-Temperature Superconductivity, New York, John Wiley & Sons, 1989.

3. R. de Bruyn Outober, *IEEE Transactions on Magnetics*, vol. MAG-23, March 1987, p. 355.

4. P.F. Dahl, *Kammerlingh Onnes and the discovery of superconductivity: The Leyden years, 1911-1914*, Historical Studies in Physical Sciences, vol. 15, Part 1, p. 1.

5. H.K. Onnes, *Leiden Communications.*, 124c, 1911.

6. W. Meissner and R. Ochsenfeld, *Naturwissenshaften*, vol. 21, 1933, p. 787.

7. F.B. Silsbee, *Note on electrical conduction in metals at low temperatures*, vol. 14, Scientific Papers, U.S. Bureau of Standards, p. 301.

8. C.J. Gorter and H.B. Casimir, *Z. Techn. Phys.*, vol. 15, 1934, p. 539.

9. F. London and H. London, *Proceedings of the Royal Society (London)*, vol. A149, 1935, p. 71.

10. F. London, *Superfluids, vol. I*, Wiley, New York, 1950, p. 152.

11. F. London, *Une Conception nouvelle de la supraconductibilite*, Hermann & Cie., Paris, 1937.

12. L.D. Landau, *Phys. Z. Sowjet.*, vol. 11, 1937, p. 129.

13. L.W. Shubnikov, W.I. Kotkevich, J.D. Shepelev and N.J. Riabinin, *J.E.T.P. USSR*, vol. 40, p. 221.

14. V.L. Ginzburg, *J.E.T.P. USSR*, vol. 14, 1944, p. 134.

15. J.G. Daunt and K. Mendelssohn, *Proceedings of the Royal Society (London)*, vol. A185, 1946, p. 225.

16. V.L. Ginzburg and L.D. Landau, *Zh. Eksperim. i. Teor. Fiz.*, vol. 20, 1950, p. 1064.

17. L.P. Gor'kov, *Zh. Eksperim. i. Teor. Fiz.*, vol. 36, 1959, p. 1918.

18. E. Maxwell, C.A. Reynolds, B. Serin, W.H. Wright and L.B. Nesbitt, *Physics Review*, vol. 78, 1950, p. 487.

19. A.B. Pippard, *Proceedings of the Royal Society (London)* ,vol. A216, 1953, p. 547.

20. W.S. Corak, B.B. Goodman, C.B. Satterthwaite and A. Wexler, *Physics Review*, vol. 102, May 1 1956, p. 656.

21. L.N. Cooper, *Physics Review*, vol. 104, 1956, p. 1189.

22. I. Giaver, *Physics Review Letters*, vol. 5, August 15 1960, p. 147.

23. B.D. Josephson, *Physics Letters*, vol. 1, July 1 1962, p. 251.

24. J.M. Rowell, P.W. Anderson and D.E. Thomas, *Physics Review Letters*, vol. 10, p. 334.

25. B.T. Matthias, T.H. Geballe, S. Geller and E. Corenzwit, *Physics Review*, vol. 95, September 15 1954, p. 1435.

26. A.A. Abrikosov and L.P. Gor'kov, *J.E.T.P. USSR*, vol. 32, 1957, p. 1781.

27. J.E. Kunzler, *IEEE Transactions on Magnetics*, vol. MAG-23, March 1987, p. 396.

28. C. Laverick, *Superconducting Magnet Technology*, Advanced Electrical and Electron Physics, L. Marton, ed., New York, Academic Press, 1967.

29. T.H. Geballe and J.K. Hulm, *Science*, vol. 239, January 22 1988, p. 367.

30. D.C. Johnston, H. Prakash, W.H. Zachariasen and R. Viswanathan, *Material Research Bulletin*, vol. 8, 1973, p. 777.

31. A.W. Sleight, J.L. Gillson and P.E. Bierstedt, *Solid State Communications*, vol. 117, 1975, p. 27.

32. R.M. Hazen, *Scientific American*, vol. 258, June 1988, p. 74.

33. J.G. Bednorz and K.A. Muller, Z. *Phys.*, vol. B64, 1986, p. 189.

34. R.M. Hazen, *The Breakthrough-The Race for the Superconductor*, Summit Books, New York, 1988.

35. C.W. Chu, P.H. Hor, R.L. Meng, L. Gao, Z.J. Huang and Y.Q. Wang, *Physics Review Letters*, vol. 58, January 26 1987, p. 405.

36. R.J. Cava, R.B. van Dover, B. Batlogg and E.A. Rietman, *Physics Review Letters*, vol. 58, January 26 1987, p. 408.

37. M.K. Wu, J.R. Ashburn, C.J. Torng, P.H. Hor, R.L. Meng, L. Gao, Z.J. Huang, Y.Q. Wang and C.W. Chu, *Physics Review Letters*, vol. 58, 1987, p. 908.

38. P.H. Hor, L. Gao, R.L. Meng, Z.J. Huang, Y.Q. Wang, K. Forster, J. Vassilious, C.W. Chu, M.K. Wu, J.R. Ashburn and C.J. Torng, *Physics Review Letters*, vol. 58, 1987, p. 911.

39. H. Maeda, Y. Tanaka, M. Fukutomi and T. Asano, *Japanese Journal of Applied Physics*, vol. 27, February 1988, p. L209.

40. Z.Z. Sheng, W. Kiehl, J. Bennett, A. El Ali, D. Marsh, G.D. Mooney, F. Arammash, J. Smith, D. Viar and A.M. Hermann, *Applied Physics Letters*, vol. 52, May 16 1988, p. 1738.

41. M.W. Browne, "Chemists' New Toy Emerges as Superconductor," *The New York Times*, September 3 1991, p. C1.

42. K. Krauth, paper presented at the *NATO Advanced Study Institute on Physics and Material Science of High-T_c Superconductors*, Bad Windshein, FRG, August 13-26 1989.

43. K. Sato et al. paper presented at the *Proceedings of Second International Symposium on Superconductivity (ISS)*, Tsukuba Science City, Japan, November 14-17 1989.

44. T. Doi et al., *Physica C*, vol. 183, November 10 1991, p. 67.

45. J.H. Kang et al., *Applied Physics Letters*, vol. 53, 1988, p. 2560.

46. J.E. Tkaczak, Paper presented at the *Material Research Society* Meeting, Boston, MA, December 5 1991.

47. L. Solymar and D. Walsh, *Lectures on the Electrical Properties of Materials*, Oxford, Clarendon Press, 1970, p. 311.

48. C.P. Bean, "Magnetization of Hard Superconductors", *Physics Review Letters*, vol. 8, March 15 1962, p. 250.

49. *Development of Cross-Linked Polyehtylene Insulated Cable for Cryogenic Operation*, Final Report EL-3907, EPRI Project RP 7892-1, EPRI, Palo Alto, CA, February 1985.

2

HTSC CABLE CONCEPTS

Summary of Historical Concepts

Introduction

A detailed review of the history of the development of superconducting cable technology was undertaken to illustrate the evolution of concepts put forth in the past and the way in which they were coupled to the ever-changing needs of the utility industry. It will be seen that there was a large spread in the ideas that were initially publicized, but these concepts narrowed considerably as the realities of practical cable systems entered the analysis. Rapid and continued growth of the use of electricity in the mid-sixties initiated a major thrust of R&D for very high capacity underground transmission systems. Superconducting cables were seen as the ultimate solution with no apparent limit to the amount of power they could transport. Had that future materialized it is likely that superconducting cable systems would be commonplace today. However, the energy crisis of the early 70's reversed the trend toward energy parks and hugh transmission corridors and slowly shifted R&D goals away from very high capacity toward engineering improvements and lower costs with existing technologies. Along the way many good ideas emerged and much of the detailed engineering necessary to design, test and build complete superconducting transmission systems was performed and published.

There are two differences between LTSC's and HTSC's that are thermodynamically fundamental and cause HTSC's to have a much higher probability of commercial application for power transmission cables in today's utility environment than LTSC-based cable designs. The first is that for an ideal Carnot cycle, the amount of work theoretically required to transfer a Watt of heat from a body at low absolute temperature T_l to a heat sink at a high absolute temperature T_h, varies as $(T_h/T_l-1)^1$. The Carnot cycle defines the best possible transfer using an ideal reversible process. The ratio of the ideal heat required to remove a watt of heat at 77 K to that at 4 K relative to a heat sink at 300 K is 25.6. However, the real world must use an irreversible process whose actual efficiency gets worse as the low temperature gets lower. As a result, the best numbers are about 500 Watts/Watt for transfer between 4 K and 300 K and 10 Watts/Watt for transfer between 77 K and 300 K. Thus the energy "cost" of a Watt of loss when operating in liquid helium in the range of 4 K is about 50 times greater than operation at 77 K, the temperature of liquid nitrogen. Notice that the efficiency can be about doubled by working at 8 K rather then 4 K.

The second major difference between these classes of superconducting materials is their inherent thermal stability. The heat capacity of all materials decreases as their temperature decreases, and goes to zero at absolute zero. Thus at temperatures near absolute zero the heat capacity of materials is very small. In a LTSC transmission cable a small "dose" of heat at some localized point can cause that region to heat up above it's critical temperature and/or field for the current being carried and switch to the normal state, which results in a sudden jump in local heat creation. This effect will propagate away from the local area along the conductor causing a "quench". This phenomena is fully described in Appendix B of Section 1. Heat can be generated by mechanical motion of the conductors as a result of magnetic forces, by "flux jumping" (a sudden change in the configuration of the vortices within the sample), and several other phenomena. These problems require very careful attention to the stabilization of the superconductor with a normal metal such as copper or aluminum, and this aspect of LTSC application

was a primary factor in the design of practical LTSC conductor assemblies, not only for fault current capability, but also for stable operation at normal current loadings. High temperature superconductors have much greater heat capacity because they operate in the range of liquid nitrogen temperature, as do the metals which might be used for mechanical support of the superconductor. Also, liquid nitrogen at 77 K has a much higher heat capacity than liquid helium at 4 K or supercritical helium at 8 K. Thus the overall thermal environment for the HTSC system has much more thermal mass than it's LTSC counterpart. Studies to determine the amount of normal metal required for fault current stabilization have established that thermal stability is achieved with almost no metal backing, due largely to the high heat capacity of the liquid nitrogen cryogen.

These factors result in the possibility of substantial differences in cable designs using the two classes of superconductor. The review of LTSC design concepts should not, therefore, suggest that these concepts are appropriate or optimum for HTSC cables. Nevertheless, one finds that almost every conceivable approach has been discussed in the more than 30 years of literature concerning LTSC cables.

The following discussions look at prior work in some detail and attempt to relate that work to the present analysis and to future potential cable system applications as HTSC materials evolve into useable and economically viable conductor alternatives.

Overview of Historical Activity - the sixties

While Omnes discovered the phenomena of superconductivity in 1911 and its potential application for the "lossless" transmission of electric power was suggested in 1913[2], the idea of a superconducting transmission line lay dormant until 1961 when it again surfaced in a pair of articles by McFee[3,4] who suggested superconducting cables using Pb or Nb_3Sn superconductors for power transmission. McFee was a Professor of Electrical Engineering at Syracuse University with experience in cryogenics. He proposed an "interleaved coaxial" cable design comprised of lead foil layers separated

by 100 mils of paper operating at 30 kV between layers. Each lead layer was to carry a maximum surface current density of 300 amps/centimeter (below the H_c of lead) so that 20 layers could carry 90,000 amperes (RMS). The actual arrangement of dielectric and conductor layers is not clear; presumably alternate layers of lead foil were grounded, or perhaps connected to different phases. Also, the means to enforce the current distribution were left to the reader's imagination. The Power transmission capacity of this cable was stated as 2700 MVA resulting from 90,000 amps at 30 kV, implying that McFee was considering a single phase application. The cable would be cooled by liquid helium held at 4.2 K and use a heat shield provided by liquid nitrogen at 77 K. McFee suggested vacuum as the thermal insulating medium and implied that vacuum might be used for the dielectric insulation as well to eliminate dielectric loss. His published cable concept is illustrated in Figure 2-1.

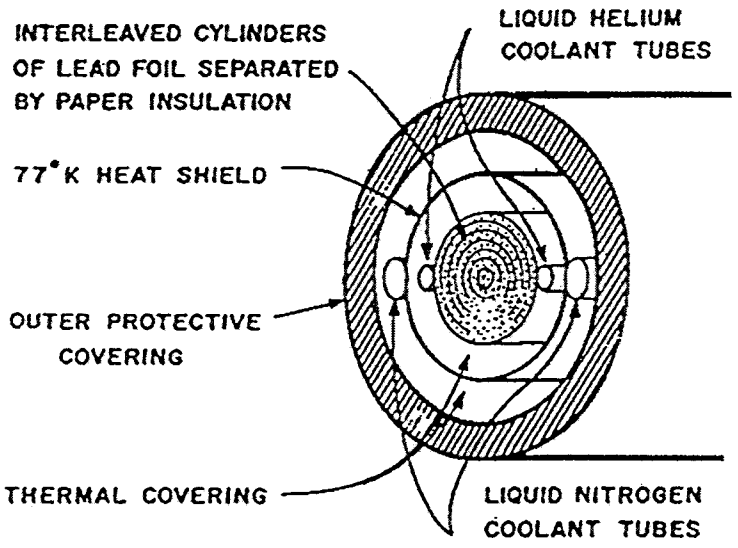

Figure 2-1 First transmission cable concept suggested by McFee[3].

McFee recognized some of the problems facing the designer of such a transmission system. Foremost was the question of reliability of the many refrigeration systems needed to provide the cooling for a line of significant length using a guide of one

cooling station every few miles. Also mentioned is the problem of heat in-leak due to mechanical supports, and the current leads into and out of the ends of the line, a subject with which McFee had some prior experience[5]. He pointed out that such a line could carry the output of a generator directly without the need for transformation to higher voltage.

In 1962 Kafka of Siemens in Germany filed a US patent application covering a three-phase superconducting system in which each phase was a coaxial cable carrying phase current on its inner conductor and equal return current on its superconducting outer conductor[6]. Kafka's Patent included the desirability of designing the cable to minimize it's characteristic impedance and maximize power transfer capability. Multiple cables per phase could be employed to provide any desired power level. Also claimed in this patent is the concept of multi-layer vacuum thermal insulation and multiple levels of heat shielding provided by fluid gases of successively higher boiling points, e.g. nitrogen at 77 K, methane at 111 K, ethylene at 170 K, CO_2 at 220 K, etc.. Cable cross-section drawings included in this patent are shown in Figure 2-2.

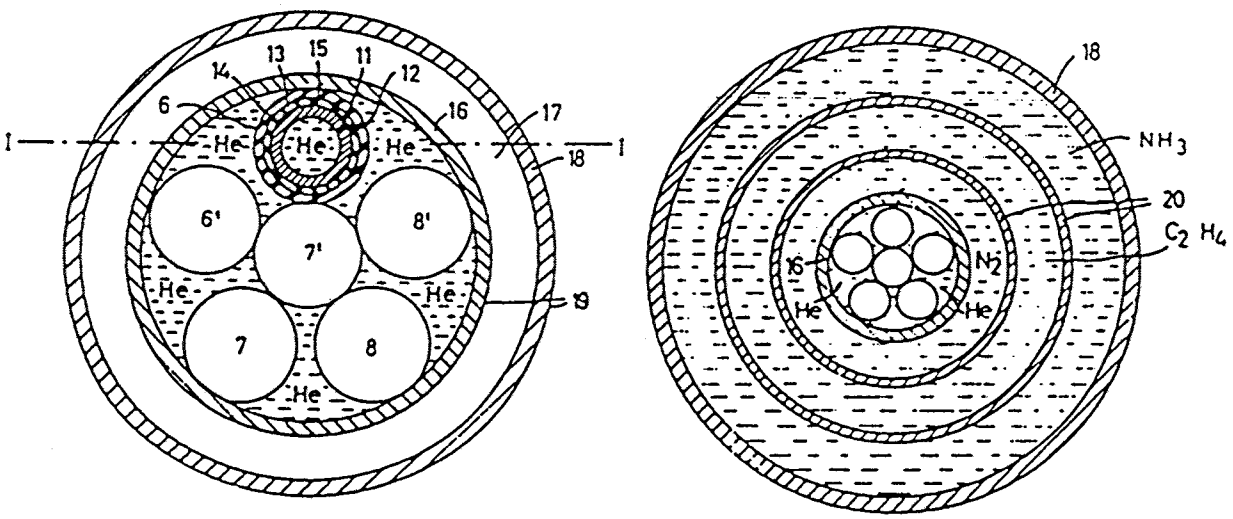

Figure 2-2 Kafka's cable drawings in U.S. Patent 3,292,016[6].

Professor P.A. Klaudy of the Technical University of Graz, Austria mentioned some possible superconducting transmission cable concepts at the 1965 Cryogenic Engineering Conference in Houston, Texas[7]. His presentation was included in the session titled "Superconductivity and Magnets" in a conference generally concerned with space applications of cryogenics. After a brief introduction on the use of cryo-resistive or superconducting materials in transformers, he switched to the possibilities of low temperature materials for use in power transmission cables, specifically superconductors cooled by liquid helium. Klaudy observed that a solid superconducting wire of radius R carrying a uniform current density J has a surface field equal to RJ/2, and this field is lowered by making R small. He therefore suggested that cables should be made of a multiplicity of small conductor sets carrying opposite currents arranged either coaxially or in pairs for the DC case, and triaxially or as triplets for the three-phase AC case, recognizing that a lower limit of radius is defined by the dielectric strength of the insulation and the voltage between conductors (line-to-line). The relatively small pairs or triplets were not shielded from each other so Klaudy introduced a correction factor to be used to adjust the calculated surface magnetic field. He also suggested the use of Type II superconductors to improve the field tolerance and noted that the close spacing of current bundles that each add vectorially to zero greatly reduces the surface magnetic fields acting on the enclosure and subsequent eddy current loss. A 150 MVA 10 kV cable design based on a corrugated cryostat assembly was presented which is shown in Figure 2-3.

This system contained 860 mini-three-phase triplets each carrying 10 amps three phase for a total current of 8600 amperes. Again the concepts of power transmission at generator voltage and a liquid nitrogen heat shield mentioned by McFee were carried forward. Professor Klaudy went on to build one of the two successful full-scale prototype superconducting cable systems in the world. That project is described in detail later in this Section.

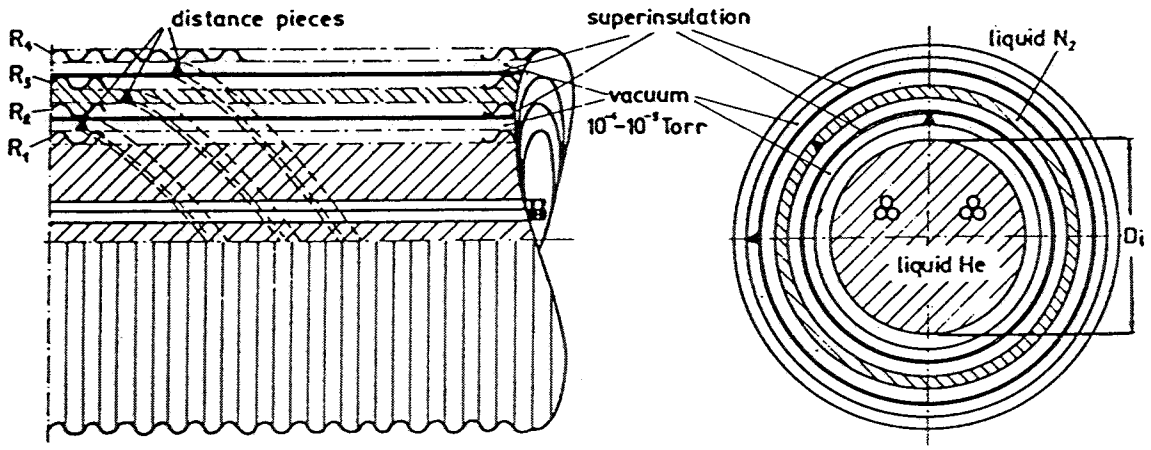

Figure 2-3 Professor Klaudy's First Superconducting Cable Concept[7].

In 1966, M. Aupoix and F. Moisson-Franckhauser of General Electric in France filed for patent rights on some unusual arrangements of sheet conductors, either cryo-resistive or superconducting, for poly phase AC power transmission[8]. Their intent is to provide a large conductor surface area for a given cable volume which will improve the utilization of the conducting material. These designs are shown in Figure 2-4.

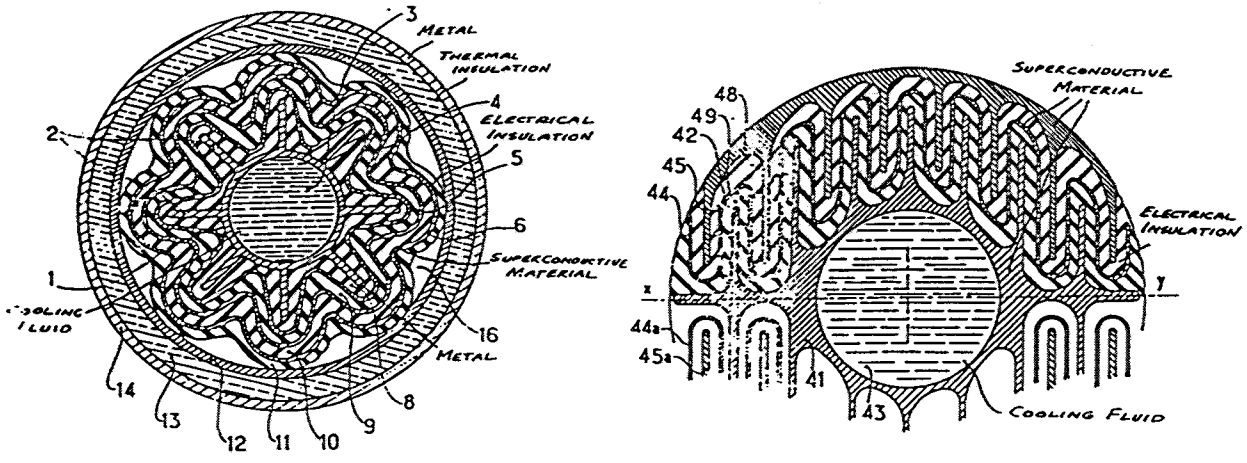

Figure 2-4 Cable designs of patent 3,502,783[8] (GE - France)

Aupoix and Moisson-Franckhauser received two more U.S. patents in the field. Patent 3,600,498, filed in 1969, presented the arrangement shown in Figure 2-5[9]. Patent 3,730,966, filed in 1972, shows a more complete flexible coaxial cable construction[10]. Its drawing is reproduced in Figure 2-6.

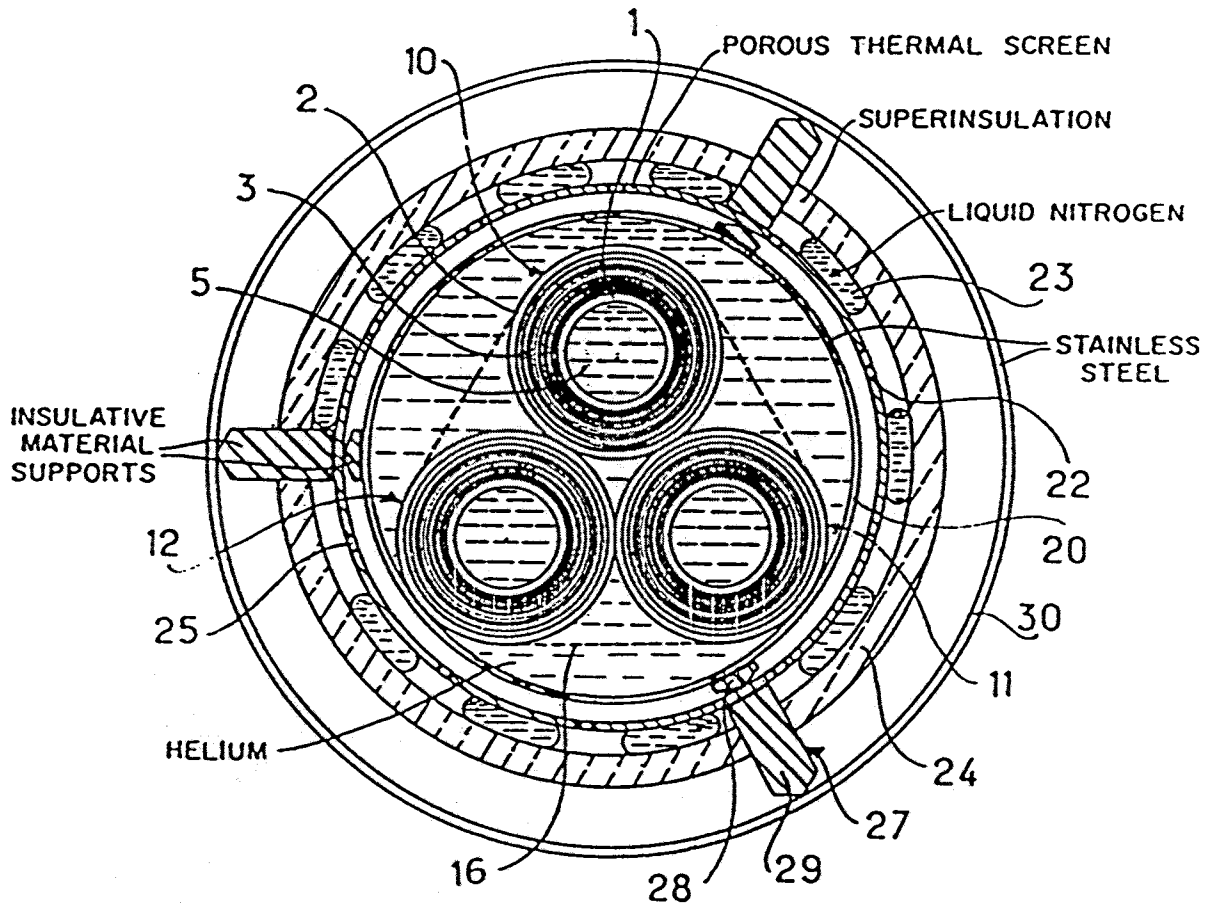

Figure 2-5 Cable system design of patent 3,600,498 (GE - France)

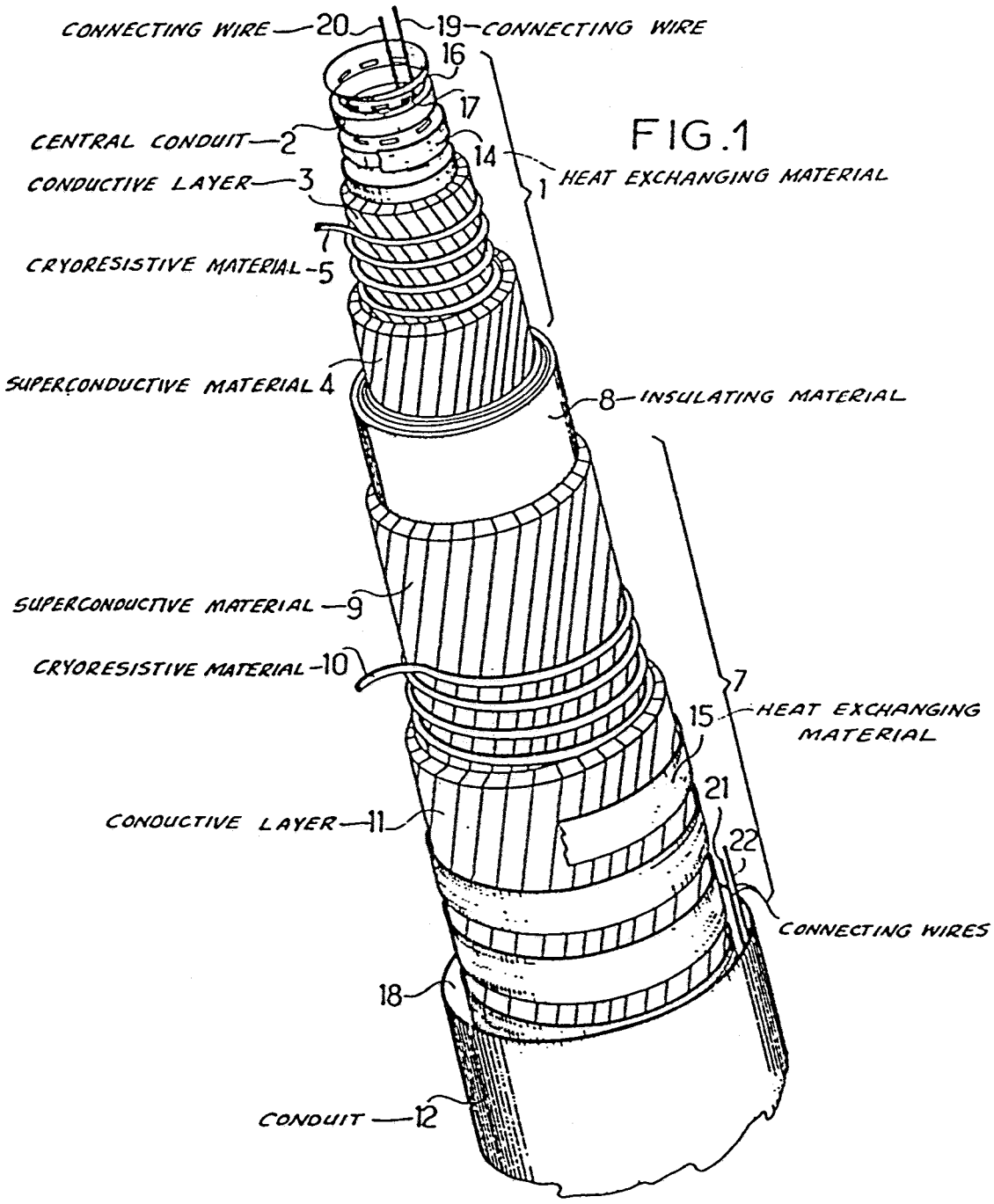

FIG.1

Figure 2-6 Cable design of patent 3,730,966 (GE - France)

In 1967 Garwin and Matisoo of IBM authored an IEEE Proceedings Paper[11] that presented an interesting analysis of an ambitious transmission scheme that would solve the long distance-high capacity-high cost riddle that was blocking the development of truly efficient generation parks in remote areas, and interconnections of bulk power systems separated by large distances. They reasoned that long distance transmission of electrical energy could be more cost effective than transportation of coal to local generation plants, and there could be economies of pooling between large systems whose peak loads are offset from each other. They analyzed a DC bi-pole arrangement that would transmit 100 GW 1000 km at +/- 100 kV. Nb_3Sn was selected as the superconductor because of its high field capability (10 Tesla at J=200,000 amp/cm^2 at 4 K). The current in this line would be 500,000 amps, but would require only 5 cm^2 of superconductor cross-section operating at one half of its critical J_c. While truly a "blue-sky" proposal, there were several subtle points regarding superconducting cable design that warrant mention. The hysteretic losses due to load variation and start-up are analyzed on the basis of the Bean model for hysteretic loss. They found that small load variations would be acceptable but up to five days might be required to bring the current to its steady value. The possibility of "anelastic" loss in AC superconducting cables due to magnetic forces was suggested, and the steady mechanical force acting on each conductor was calculated and shown to be tolerable. Their design used frequent liquid/gas separators to bleed gas from the liquid line into the gas return line and frequent small booster pumps to keep the axial pressure drop small. They noted the high energy stored in the magnetic field (the cable's inductance) and provided resistive shunts with a ten ton mass at each cooling station to absorb this energy safely in the event of the loss of load. Finally, they acknowledged the reliability issue by providing a back-up conventional transmission line paralleling the superconducting line. The backup could be switched in sections thereby allowing a section of the superconducting line to be serviced. Many of these concepts are claimed in a patent issued to Garwin in September 1967 which had been filed in 1963[12]. Their cable system concept is illustrated in Figure 2-7.

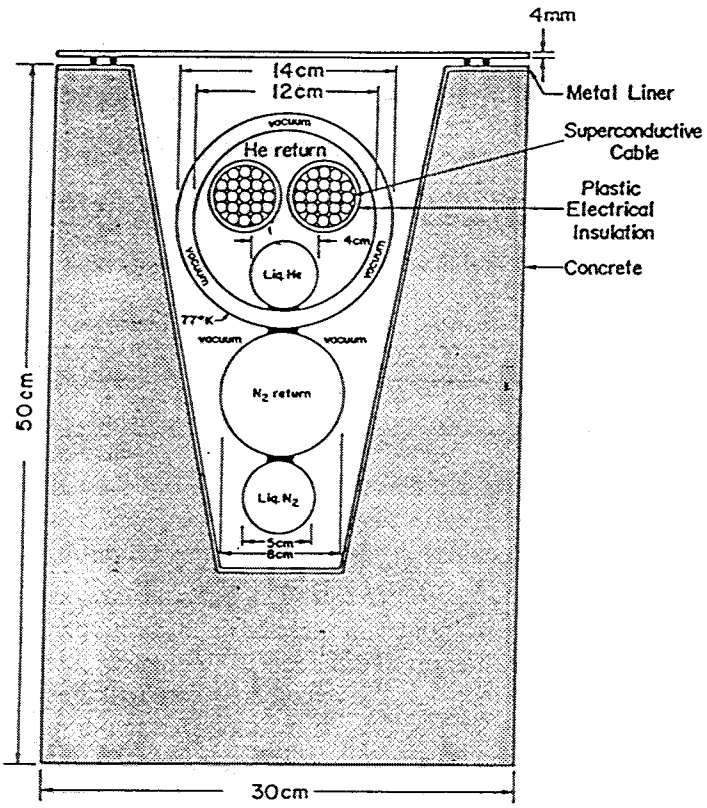

Figure 2-7 The Long Distance DC System proposed by Garwin and Matisoo.

The paper of Garwin and Matisoo was a precursor of more thoughtful studies that would begin to emerge in 1968. However, a 1967 survey of over one hundred utilities, consultants and manufacturers by Electric Light and Power Magazine on the future trends in underground transmission[13] produced only one mention of the possibility of cryogenic cables. Two papers (1963 and 1966) by Dr. Wilkinson in the British IEE Proceedings[14,15] considered the economic practicality of cryogenic options (cryo-resistive and superconducting) for transformers and cables and concluded that this technology would not be competitive. Meanwhile, the extension of conventional technologies was gathering momentum. 1967 was the year that Westinghouse and the newly-formed Electric Research Council agreed to build the Waltz Mill Test Facility to test and demonstrate 500 kV cable systems, new types of cables for 138 kV, and ultimately be able to test cable systems to UHV levels.

Fortunately, other work on cryogenic transmission systems was going on in 1967 that was more positive. In the UK, BICC was involved in a study for the CERL on superconducting cable options. In his discussion of Wilkinson's second paper, published in the 1967 IEE proceedings[16], D. Edwards presented three designs which are shown in Figure 2-8.

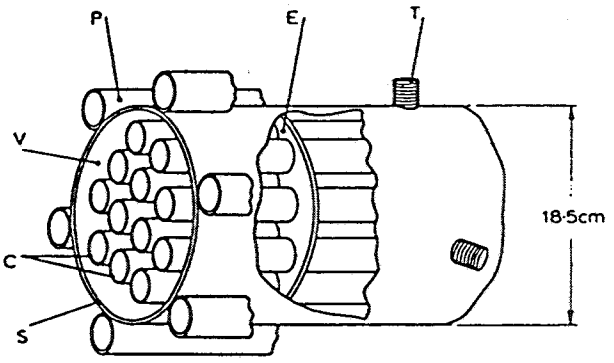

Fig. D

Multitube conductor system

33kV a.c., 750MVA; vacuum insulated

C Composite conductor with niobium outside
V Vacuum electrical insulation
S Composite screen with niobium inside
P Aluminium pipes for liquid helium, screen cooling
E Electrically insulating spacers
T Thermally insulating spacers

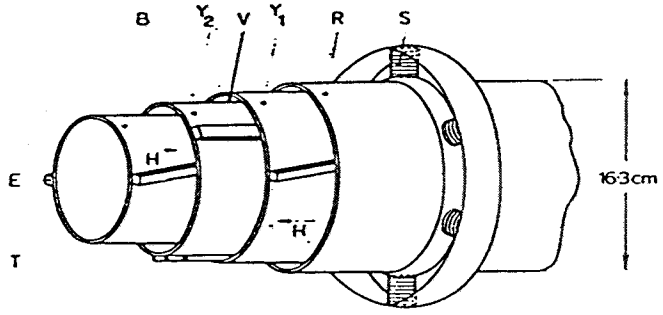

Fig. E

All-coaxial conductor system

33kV a.c., 750MVA; liquid-helium insulated

R Red-phase conductor (niobium inside)
Y_1 Split yellow-phase conductor (niobium outside)
Y_2 Split yellow-phase conductor (niobium inside)
B Blue-phase conductor (niobium outside)
V Vacuum thermal insulation between go and return flow paths
T Thermally insulating spacers
E Electrically insulating spacers
S Electrically and thermally insulating spacers

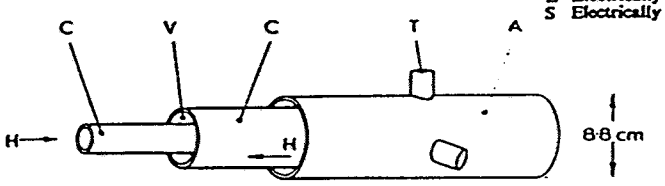

Fig. F

Coaxial-conductor system

33kV d.c., 750MVA; vacuum insulated

C Conductors; inner with niobium outside and outer with niobium inside
V Vacuum electrical insulation
T Thermally insulating spacers
A Aluminium outer tube

Figure 2-8 Early concepts by BICC for the CERL in the UK.

A group at Simplex headed by P. Graneau was testing a vacuum insulated cryo-resistive prototype which will be discussed later in this section. Studies were also underway in France, West Germany, Austria and the USSR, but results had not yet reached the literature. Experimental cable models or prototypes had been built and were producing data in the US, UK and France, and would come on line soon in Germany. The 12th International Conference on Cryogenic Techniques held in Madrid in October 1967 was the first to have a special session on the use of superconducting materials for the generation and transmission of electric power.

In 1968 cryogenic transmission came down from the sky. The ERC issued contracts to General Electric to develop a cryo-resistive cable system, and to Union Carbide, Linde Division to study the use of Niobium in a superconducting cable design. These programs will be discussed in detail later in this section. An article in Business Week[17] identified five U.S. Companies with significant interest in power applications of cryogenics in addition to Union Carbide and GE. Mentioned were North American Rockwell, Westinghouse, Norton, Avco and Dynatech. In 1970 an article in the USSR[18] stated that over 400 US companies were involved in the technology of superconductivity.

In 1969, Japan showed its first interest in cryogenic transmission systems with an economic study by S. Ihara and T. Horigome of the Electrotechnical Laboratory, Ministry of International Trade and Industry[19]. They found that superconducting cables were the most attractive for high power DC applications.

An international Conference was held in London in March, 1969 organized by the British Cryogenics Council covering "Cryogenics in Fuel and Power Technology". This Conference was divided into two sessions; one on cryogenic transfer of Liquified Natural Gas (LNG) and the other on the potential of cryogenics in electrical power applications. The LNG session drew slightly more participants. Several papers on DC and AC transmission were given, including a presentation by GE on the preliminary results of

their study[20]. Pastuhov and Ruccia of Arthur D. Little suggested utilization of a cryogenic environment for the combined transfer of LNG and electric power[21]. Designs for a hydrogen-cooled cryo-resistive system and a helium cooled superconducting system are shown in Figure 2-9.

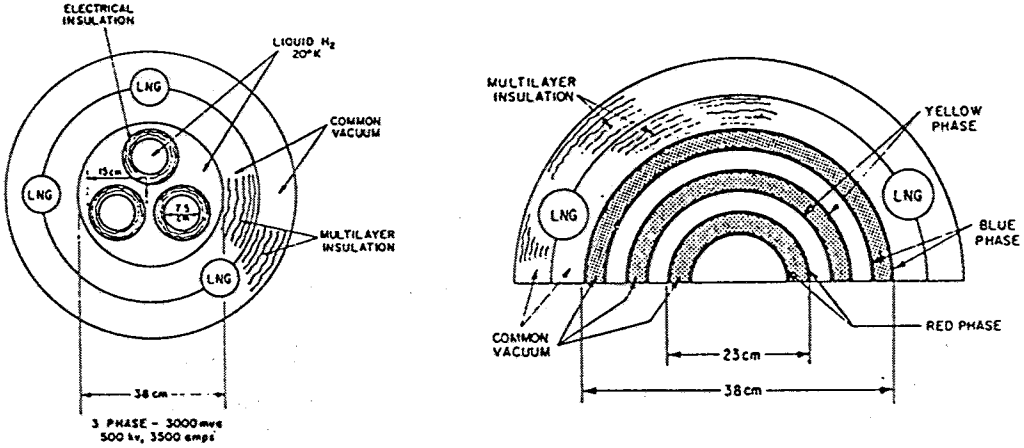

Cryo-resistive Concept Superconducting Concept

Figure 2-9 Possible designs for a pipe-line carrying LNG and electric power.

In the session on DC cables, Voigt of AEG-Telefunken in West Germany compared a conventional DC paper-oil cable to a liquid hydrogen cooled cryo-resistive cable and a helium cooled superconducting cable, the latter two being arranged with dielectrics at room temperature such that the over-all diameter of the three cables was the same[22]. These designs are shown in Figure 2-10.

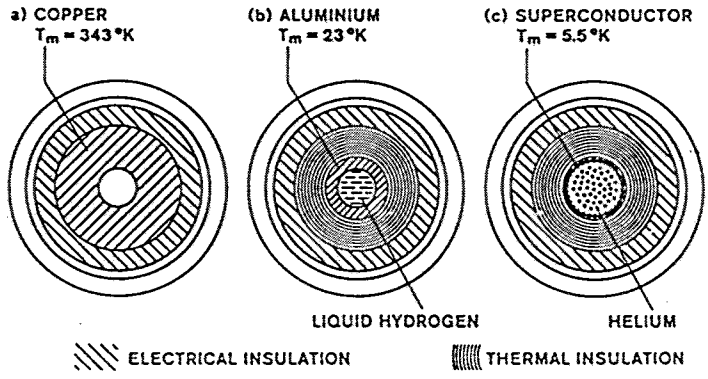

Figure 2-10 Room temperature dielectric DC cables compared by AEG-Telefunken.

Aupoix et al of GE - France presented data and a photographic summary of a 20 meter long test setup that had demonstrated a capacity of 80 MW (4,000 amps at 20 kV) which could be scaled to 2,000 MW at +/- 125 kV[23]. Rogers et al of BICC/CERL in the U.K. summarized test results on a 2.7 meter long coaxial superconducting AC cable model that included novel superconducting current transformers at each end to obtain up to 5,000 amps AC in the shorted test cable with a greatly reduced heat in-leak for the leads of the current source[24]. Rogers also presented an economic study which found that superconducting cables are more economical than conventional 275 kV oil-filled cable in the power range of 1000 to 4000 MVA[25]. Cryo-resistive cables were found to be more costly than 275 kV oil-filled cables.

In summary, at the end of the sixties the trend for superconducting cables was to use niobium operating between 4 and 5 K with the magnetic field kept below its critical field H_{c1}, thought to be about 1200 amps/cm. In this mode the current would be limited to a surface current and hysteretic loss would be avoided. Cryo-resistive conductor designs favored high purity aluminum operating at about 20 K where its resistance ratio (room temperature resistivity divided by low temperature resistivity) is several hundred to one, rather then at 77 K where both copper and aluminum have a resistance ratio of about 8:1. Many cable system concepts had been proposed and some had been built and successfully tested on a laboratory scale. The stage was set for more detailed studies and experimental installations that occupied many organizations throughout most of the seventies, some even extending into the eighties.

LTSC Cable Projects

There were four projects on superconducting cables in the late sixties and seventies that warrant specific analysis because of their involvement with the problems of the application of superconducting cables and the extent of their programs. In addition, there were several projects in Europe and the U.S.S.R. that warrant mention because of novel ideas and contributions to the state of the art. These are discussed below:

Union Carbide Rigid System. The Research group of the Linde Division of Union Carbide began privately studying superconductors in 1963 because of their commercial interest in general cryogenic technology and the possibility that superconducting transmission systems could significantly increase the activity in that market place. Their early work concentrated on the AC losses of small wires of Niobium. In 1968 they obtained funding from EEI as part of the new Electric Research Council's underground transmission research and development program to study the AC losses of Niobium tubes, and perform an initial economic study of the viability of the rigid tubular system using liquid helium as both the coolant and the dielectric, with spacer supports. The results of this effort are presented in a comprehensive Final Report[26].

The experimental portion of this first program studied 20 foot-long tubular conductors installed as a shorted coaxial pair in a 24 foot long, 40 cm I.D. cryostat coupled to a 10,000 ampere AC current supply, as shown in Figure 2-11.

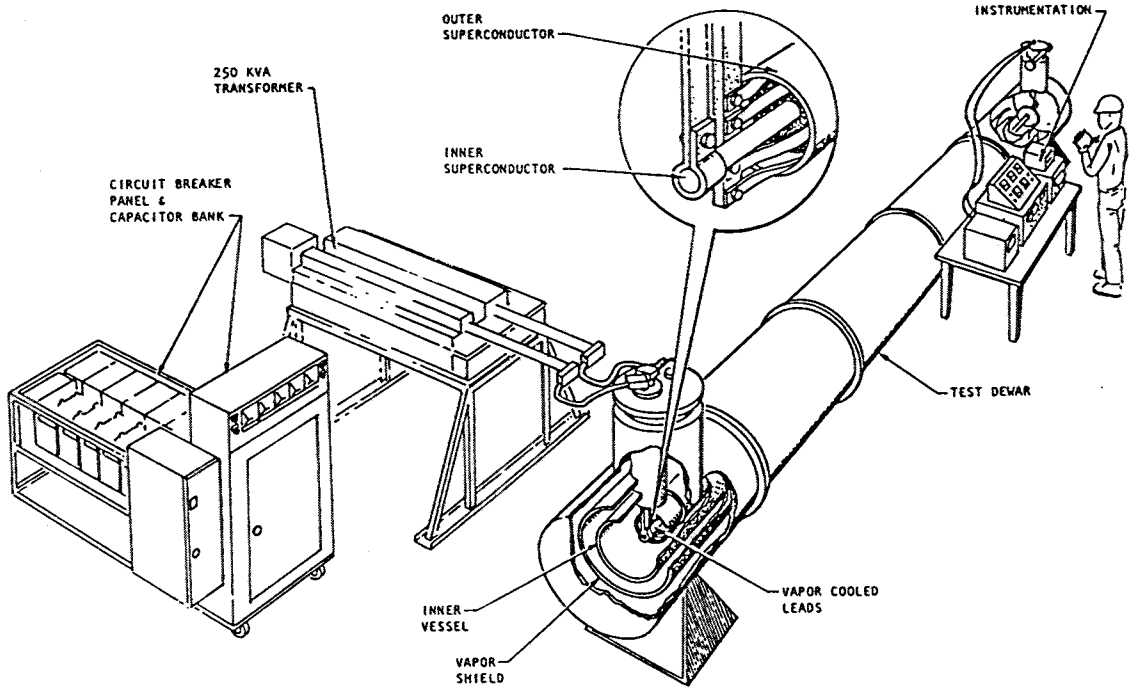

Figure 2-11 Experimental set-up for AC loss measurements on niobium tubes[26].

Niobium tubes 1 and 3 cm in diameter were tested as well as a 1 cm composite tube made by electroplating a copper tube with niobium. The outer return conductor was a 9 cm niobium tube for the 1 cm samples and 27 cm diameter niobium pipe for the 3 cm tube sample. The final report[26] contains an excellent summary of the problem of AC loss measurements in tubular conductors and the equipment needed to provide test currents up to 10,000 amperes, as well as interesting data on loss magnitudes as a function of magnetic field, material properties, temperature and non-uniform field conditions, all of which were found to be predictable from a knowledge of basic material properties. AC Loss for the 3 cm diameter tube was found to be only 15 mW/m carrying 5000 amperes RMS where the peak surface field is 750 amp/cm.

In conjunction with the experimental set-up vapor-cooled current leads were developed to reduce the heat leak at the feed end of the test bed. While not as efficient as planned, this approach worked well up to about 7000 amperes.

The system study portion of this program looked at cost estimates for a three phase coaxial system contained in a single cryostat, as depicted in Figure 2-12.

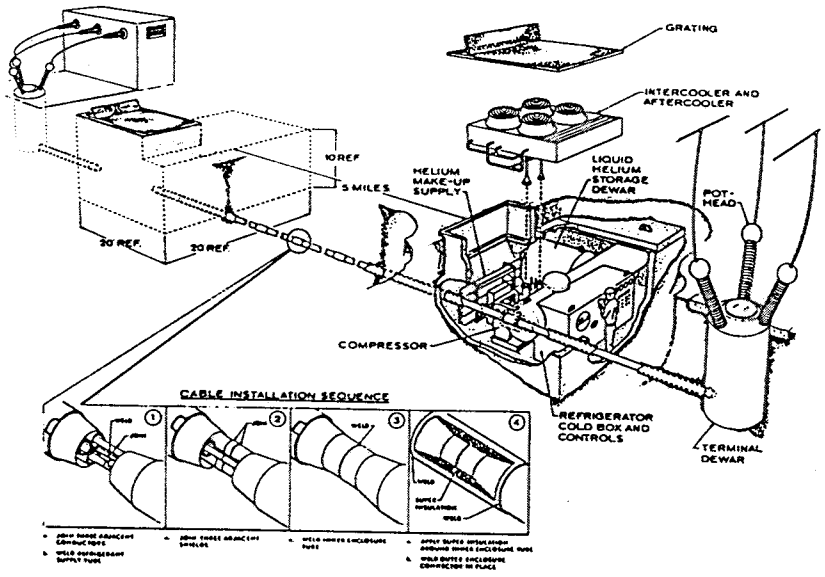

Figure 2-12 Union Carbide's rigid AC cable system[26].

Three possible arrangements of the three conductors in a single cryostat were defined, as shown in Figure 2-13, which also details the current flow on the inner and outer surfaces of the middle conductor in the concentric triaxial configuration.

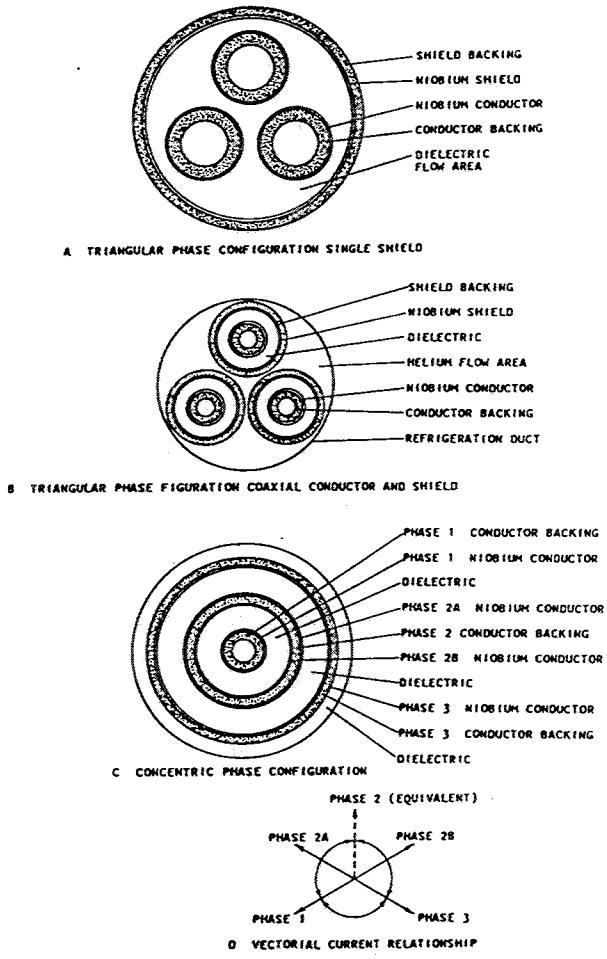

Figure 2-13 Union Carbide's superconducting AC power cable configurations[26].

Only the coaxial designs (b and c of Figure 2-13) were analyzed, with emphasis on the triangular arrangement. Designs for a 1000 MVA 138 kV, 4200 amp system were developed around a surface field of 564 amps/cm. The triangular coaxial arrangement had an outside diameter of about 36 cm compared to about 32 cm for the concentric triaxial case. Included in the design study was a preliminary solution for terminations.

An analysis of the improvement needed in cryogenic enclosure performance suggested the possible elimination of a liquid nitrogen shield by the use of "multishields" cooled by helium vapor bled from the main flow stream. Refrigeration system design was discussed in detail and a compact manhole installation was shown to be feasible for stations along the route.

The stabilization of the superconductor to overloads and fault currents was analyzed. This led to a three layer system that used a niobium alloy such as niobium-titanium between the niobium layer and the base metal (copper). This approach, also suggested by Taylor of BICC at the 1969 London Conference[27], would take advantage of the high field capability of the alloy but not suffer from it's higher AC loss.

If there was a weakness in this first study it was the lack of a good data base on the dielectric properties of liquid helium, and the combination of liquid helium and solid supports. The choice of a working stress has a major effect on the system dimensions and cost. Linde chose a design working stress of 20 kV/mm at BIL but may have misapplied this parameter in their design equations. The resulting 138 kV triangular coaxial configuration had a maximum stress of 40 kV/mm peak impulse (at 600 kV BIL) and a working stress of 5.35 kV/mm RMS at 80 kV phase to neutral. Linde used the average stress in their determination of the system dimensions. In subsequent design studies, Linde reduced the maximum design stress to 15 kV/mm impulse and 2 kV/mm RMS[28], more reasonable parameters but still optimistic for large gaps with the large surface area of a long cable system.

The results of this study were summarized in a paper presented at the winter power meeting in New York in 1970[28] and several other papers in that time frame. The success of the first stage led to a proposal to EEI in mid-1969 for a 12-year program estimated to cost about $8,000,000. A 3.5 year second stage program was jointly funded by EEI and the U.S. Department of Interior in late 1971 but was quickly taken over by the newly

formed EPRI and the U.S. Energy Research and Development Agency (ERDA). This phase two program was designated EPRI Project RP7807-1 and ERDA Contract No. E(49-18)1420.

The second stage of this program expanded the experimental work to include model and full-scale voltage testing and a full-scale high-current, high voltage test bed in a 14 meter long, 40 cm I.D. prototype cryostat equipped with two high current, high voltage terminations developed and supplied by Westinghouse under a sub-contract. Their termination design was essentially a vapor-cooled current lead in a vacuum-insulated cryostat that served as the high voltage conductor with its outer diameter at room temperature. The voltage isolation was a conventional epoxy-molded stress control device in an SF_6-filled fiberglass or porcelain bushing.

The conductor design was changed to a composite of niobium, copper and invar, with the low expansion invar dominating the mechanical behavior of the assembly. This change was accompanied by the design of an explosively welded joint that could be mechanically anchored to the enclosure. This eliminated the need for bellows-type expansion joints in the conductor and shield tubes. Losses were measured on a 6 meter 1 cm diameter composite conductor and a 12 meter 8 cm diameter composite with acceptable results. The invar composites were developed and supplied under a subcontract with the International Nickel Company (INCO).

High voltage tests of liquid helium and prototype spacers between spherical electrodes and in a vertical coaxial model cell supported the design stress levels mentioned above. However, when full-scale tests were made in a horizontal dewar 6 meters long with a bushing at each end holding two separate coaxial test cells, the results were disappointing. Breakdown levels as much as 3.5 times less than those expected were experienced when spacers were included between the electrodes. While conditioning

was found to improve the breakdown level, the actual cause of the poor performance was not determined though particle contamination was suspected.

The multishield type of cryostat selected in the first phase was designed and a 13 meter 34 cm I.D. test bed constructed which contained a joint at its center. The cryostat sections were factory sealed and evacuated. The joint was contained in a 4 meter long sleeve also vacuum-insulated and sealed at the factory so that no vacuum-tight field welds had to be made. The performance of this assembly was good with the exception of the heat-leak of the joint which prompted additional experimental and design work. The projected overall average heat leak, assuming the joint problems could be resolved, was 0.375 watts/meter.

The difficulties of full-scale testing came to light when high current loss measurements were attempted on an insulated single phase assembly. Unfortunately, the presence of the high voltage precluded the use of a coaxial conductor arrangement so the return current was carried by an external lead between the two terminations. Insulating spacers were used to prevent circulating currents from flowing in the cryostat members, but the impact of eddy current losses in the steel outer pipe of the cryostat had not been anticipated. As a result, the test bed that had been built with a current capability of 10,000 amperes was able to obtain meaningful data only up to 2,000 amps.

System designs were developed for the five voltage classes from 69 kV to 500 kV which covered capacities from 1,100 to 34,700 MVA. A revised cost analysis was performed under a subcontract to Gibbs and Hill for a 3400 MVA, 138 kV (14,140 ampere) system 40 km long.

In 1975 a study was performed with the Commonwealth Edison Company which identified three scenarios in the transmission system of the 1990's that might utilize Linde's rigid superconducting system[29]. Normal and contingency load flow studies

were performed for a 30 mile single circuit rated 3400 MVA at 138 kV, four 345 kV circuits ranging from 24 to 51 miles in length, and a single 37 mile 230 kV circuit, the latter two cases being associated with the (planned) 765 kV network and therefore required transformers at each end of each line. No load flow problems were detected indicating that in all cases the superconducting cables were technically viable. Future studies were to investigate stability and transient phenomena, and the economics of these options, but these studies were not done, presumably because of the project termination. The conclusion of this initial study was that these cables have too much capacity. To be used effectively it is necessary to select the power level required first, then determine which voltage best matches the superconducting system.

About half way through this 42 month program a proposal was prepared and submitted to EPRI/ERDA for the next phase which was to build a full size prototype three phase system 40 feet long with one trifurcating termination[30]. This two-year program would be followed by an eight-year program which would install a 250 to 1000 foot-long system in a long-term test facility (presumably Waltz Mill), test it for four years, and summarize the results which would finalize commercial design parameters. At that time Linde was confident that the goals of the present program would be met. However, in view of the difficulties that arose during the second half of the phase two effort (which included a four month extension designated RP7807-2), EPRI and ERDA decided to terminate the program rather than fund phase three, the next two-year prototype stage proposed. As a result Linde issued a final report in two parts covering the completion of phase two. The first part was an abbreviated summary of the work done in phase two[31]. The second part provided a detailed description of the cryogenic envelope development work and the refrigeration system details developed in phase two, plus sub-contractor reports by Gibbs and Hill, INCO and Westinghouse[32]. The bulk of the work in the first half of phase two was reported in draft form as a two-part appendix to the technical proposal[30]. These appendices contain the most thorough summary of the engineering calculations and test data produced by this program.

The final activity of this program was participation in the Philadelphia Electric Company's comparative study of various underground transmission alternatives to feed power from a 10,000 MW energy park 66 miles to their load center in Philadelphia, funded by the Department of Energy[33]. The data that was generated in this study has some interesting implications on the economic viability of this particular superconducting system. Of the 15 underground options studied, this system ranked second highest in total cost, exceeded only slightly by the GE cryoresistive cable option (to be discussed later). The lowest cost option was the Brookhaven (BNL) flexible superconducting cable system, also to be discussed later. The Linde 230 kV system, which used three 36 inch diameter pipes, was twice the cost of the Westinghouse three-phase SF_6 Gas Insulated Transmission Line (GITL) system which used five 40 inch pipes, both with comparable trench dimensions. The energy costs of the Linde system were 65% higher than the GITL system and 51% higher than the BNL system. The Linde system had a surge impedance 5.6 times that of the BNL system due to its large dimensions, which, in conjunction with its high current, made it the only system to require series capacitor compensation which accounted for 20% of its total cost. If the termination cost that would have been required to space the compensation out over the length of the line had been included in the analysis, the total system cost would have gone up considerably. These factors, in particular the high costs resulting from this study may have influenced EPRI and ERDA in their decision to terminate this program.

There are two factors that should be mentioned. The first is the choice of niobium as the superconductor which requires a narrow operating temperature range of 4.6 to 5.1 K in contrast with the BNL design which used the A15 compound Nb_3Sn with a design range of 6.7 to 8.5 K. The two systems had about the same loss, but the energy cost of the Linde system was almost twice that of the BNL system. Part of this difference was due to the lower operating temperature and part due to the higher energy cost of re-liquefaction of the helium bleed to room temperature required by the multishield system. The BNL cryostat did not use a multishield or nitrogen shield system and claimed a

lower heat in-leak (460 W/km against 571 W/km). The use of Nb_3Sn instead of niobium and a higher operating temperature may have resulted in a significant reduction in overall costs. The second factor was the use of helium as the primary dielectric. While this was the only option short of a solid material, the very low stress coupled with the lower design field necessitated by using niobium rather then Nb_3Sn results in large system dimensions which heavily impact all costs, including the high surge impedance and compensation penalty suffered by this system. The rigid tubular system is an attractive option for its ease of conductor fabrication and general simplicity. Perhaps some innovation in the dielectric area that would raise the operating stress and reduce system dimensions together with simplified splicing techniques could result in a more economically attractive system based on the rigid concept.

One section of Linde's 1974 proposal to EPRI and ERDA was funded by EPRI. This was a one year design study to layout a helium refrigeration system suitable for a general multi-bay long term test facility. The report of this work[34] presents a helium-based system with controlled output streams at several temperatures from 4.5 K to 80 K that could simultaneously supply primary temperature control and shielding temperature control for several LTSC systems under test (cables and Generators).

Professor Klaudy and the Cable Project at the Arnstein Power Station, Austria. Professor Klaudy of the Anstalt fuer Tieftemperaturforschung, ATF (the Institute for Cryogenics) in Graz, Austria began promoting superconducting cables in 1965 with lectures and publications in Europe and the United States. In the late sixties he lectured extensively on such cables and performed experimental work to measure the AC losses of LTSC materials using a specially designed AC resistance bridge built for samples with a high inductance to resistance ratio[35]. Also in this time-frame a graduate student, J. Gerhold, was obtaining dielectric data on cryo-vacuum, liquid and gaseous helium, and various solids immersed in low temperature helium.

In the late sixties, Klaudy built two cable models working in conjunction with AEG in Austria, Kabelmetal of Hannover, Germany, and Linde in Munnich. The first was 14 meters long and contained several triplets of small niobium wires with low voltage insulation suitable for three-phase current and loss measurements. The second model was 50 meters long and used 4 mm diameter copper wires coated with lead (the superconductor) and insulated with paper to a design voltage of 20 kV. These constructions were similar to those shown in Figure 2-3. The 50 meter model was used for cryogenic studies as well as electrical studies. The concept of a constant temperature system which utilized continuous Joule-Thompson expansion of the helium stream to counteract the heat absorption required by heat in-leak and losses was demonstrated on this model[36]. In the fall of 1970 this model stimulated enough interest from Steweag, the Austrian utility, to initiate a full scale trial of a superconducting cable in the high voltage grid, the beginning of Klaudy's Arnstein Power Station demonstration project[37].

The Arnstein Project consisted of a 50 meter full-size single phase cable installed so that it could be switched into one phase of an overhead 60 kV transmission line exiting the Arnstein hydro-electric generating facility. The cable was fabricated by Kabelmetal and consisted of seven concentric corrugated tubes. The outside diameter over the polyethylene jacket was 21.6 cm[38]. The superconductor was formed by a 70 micron layer of niobium that was deposited on the outer and inner surfaces of the first two copper tubes to form the phase conductor and its shield conductor. The deposition process required significant development which accounted for much of the program time between its inception in 1970 and cable installation in 1977. The process finally adopted successfully was a brushing operation that deposited a thin layer of copper onto a niobium strip by cold-welding. The copper layer was then built up to the required thickness by electroplating.

The Arnstein cable was insulated with about 500 mils of paper to be suitable for operation at 110 kV even though it was connected into a 60 kV line. The paper was

impregnated with static helium held at 10 atmospheres pressure. Temperature was controlled at about 6.5 K by parallel helium flow inside the inner corrugated copper/niobium conductor and outside the corrugated stainless steel pipe which tightly covered the outer corrugated copper/niobium conductor. This stainless steel pipe over the outer conductor pipe was necessary to contain the high pressure helium gas used to impregnate the paper insulation. Isolation bushings at each end provided helium access to the conductor core. Helium was returned to the refrigerator from the far end in an external vacuum-insulated return pipe. This cable is illustrated in Figure 2-14.

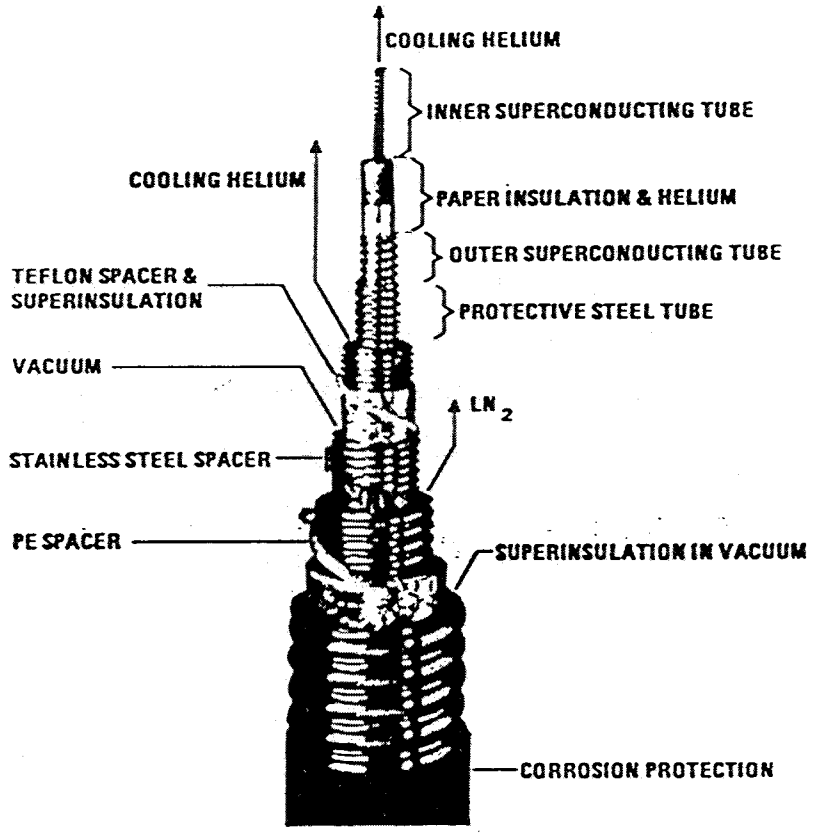

Figure 2-14 Cable tested at the Arnstein Power Station by Professor Klaudy[38].

Though the cable was installed in 1977, it was not cooled and energized until the fall of 1979. It operated for five test periods during the remainder of 1979 and throughout 1980

for a total time of 190 hours at operating voltage (nominally 38 kV phase to ground), making it the first, and only, superconducting cable to carry commercial power in a real utility system. While it carried (one phase of) the full output of the power station on occasion, this was less then 1000 amperes. Following the in-service experience, the cable system was subjected to a high voltage AC test which resulted in a terminal failure at 135 kV. A final current test was made with the end shorted to confirm the cable's ability to carry 1000 amperes.

Following the Arnstein test, Klaudy and Gerhold suggested the simplified design shown in Figure 2-15.

1 - Cooling helium
2 - Niobium-plated copper
3 - CB paper shield
4 - Paper insulation
5 - Metalized CB shield
6 - Cooling helium
7 - Niobium-plated copper
8 - SS Inner tube of cryostat
9 - Improved Superinsulation
10 - SS Outer tube of cryostat
11 - PVC Jacket

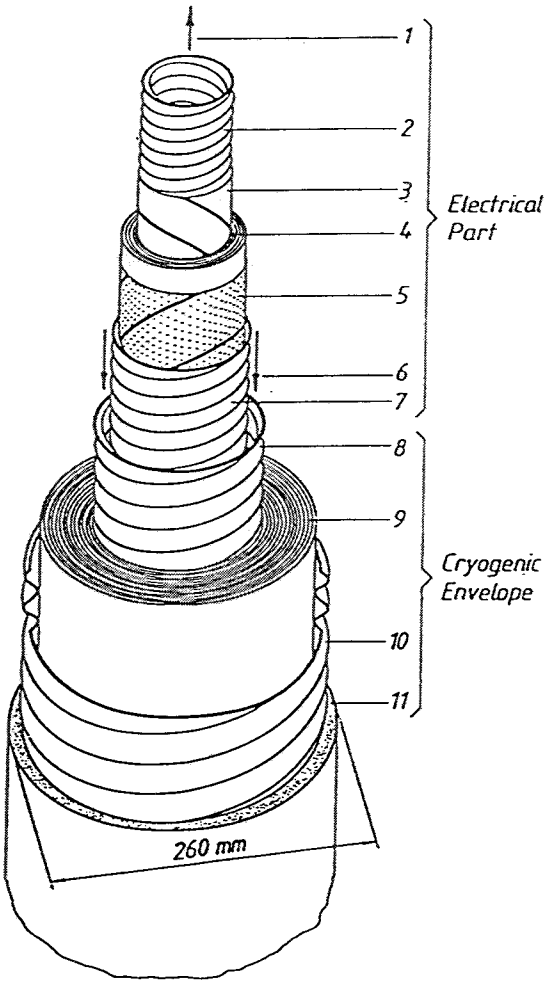

Figure 2-15 Klaudy's improved cable with high performance superinsulation[39].

This concept which does not use the liquid nitrogen intermediate shield is made possible by an improved superinsulation construction which uses a crossed weave of polymer rods to separate layers of reflecting foil. They also point out that the large cryostat (O.D. of 26 cm) can be installed in short lengths of about 250 meters using only mechanical/thermal joints. The smaller cable core can be manufactured in longer lengths, up to 1 km and easily pulled into the installed cryostat. The number of superconducting joints with electrical insulation is thus reduced by a factor of four[39].

Brookhaven AC Cable Program. The largest US program for development of HTSC AC power cable was undertaken by Brookhaven National Laboratory (BNL) during the 1970's and 1980's, resulting in a cable which was operated during extended test periods at rated current and voltage. This cable was insulated with plastic tape impregnated with supercritical helium gas. The two coaxial conductors each consisted of two layers of counter-spiraled superconducting tapes installed so as to minimize the axial magnetic field. The project involved the development of several new materials and technologies, including the Nb_3Sn superconducting tape, an oriented plastic tape suitable for high voltage cable applications and the actual manufacture of a plastic tape-insulated cable, a termination design based on an epoxy-impregnated paper stress control build-up, an impressive refrigeration plant to control system temperatures in the range of 8 K, and an elaborate computer instrumentation and dynamic control system.

Interest in superconductor applications at BNL was an extension of development work on superconducting pulsed magnets that could be used in a very high energy synchrotron. During 1969 and 1970 an "ad hoc" committee of scientists and engineers from the Accelerator Department and the Department of Applied Science held informal discussions on possible commercial applications of superconductivity such as large machines and transmission lines. During 1970, casual AC loss measurements were made on half-inch wide Nb_3Sn ribbons commercially available from RCA. Encouraging results prompted a proposal to the National Science Foundation (NSF). In March 1971 this

group received funding from the NSF (Grant AG-251) to perform a study on the possible application of superconductivity to the transmission system of the 1990's. The result of this study was a report published first in December 1971[40] and in final form in March 1972[41].

The 1971 study report presents a brief but concise summary of the thinking in the utility industry at that time on the future needs of the industry supporting the quest for high capacity transmission systems, and a good summary of the work under way around the world on the various high capacity alternatives under study. The conclusions of this work set the stage for the major program to follow. Nb_3Sn was selected over niobium because of its higher operating temperature and greater field capability in spite of a higher AC loss characteristic. BNL reasoned that the high field capability would tolerate a fault ten times the normal current without going normal, and were the first to recognize that the three degree increase in the refrigerator output temperature would allow system design based on supercritical helium rather than liquid helium or a two phase system. Supercritical helium has a higher thermodynamic efficiency that would almost halve it's energy cost for the same heat load, thereby easily justifying the higher operating loss. This unique material also has a positive Joule-Thompson coefficient in the temperature range of interest which simplifies axial temperature control. The high AC loss under fault conditions would be of short duration and cause only a minor system disturbance.

Two cable concepts were suggested: The first was designated the "ribbon" concept which used flat ribbons with two or four layers of Nb_3Sn on a substrate of niobium or Hastelloy. Ribbons are interleaved with return ribbons in the single phase case or other phase ribbons in the three phase case. Such a construction is shown in the simplified diagram of Figure 2-16.

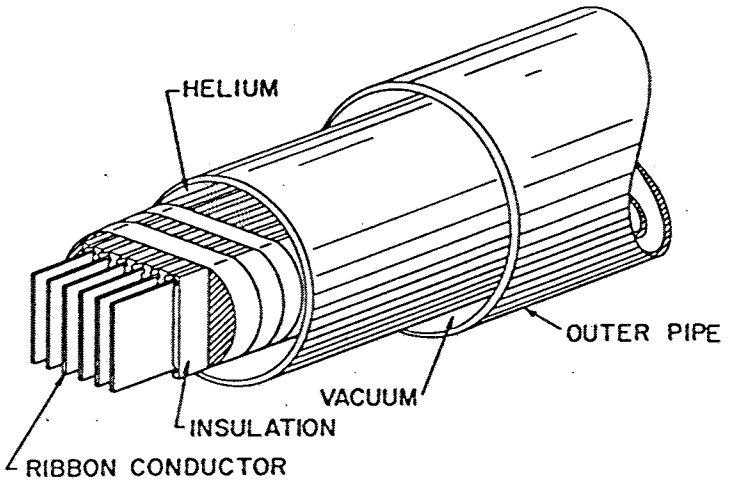

Figure 2-16 BNL's Ribbon Cable concept[41].

Multiple assemblies are paralleled to achieve any desired current level. The operating voltage is applied between ribbons which are insulated by tape wrappings. This construction has a very low inductance and relatively high capacitance, yielding a low characteristic impedance which is amenable to high current and low voltage operation. A single phase model is easily built by coiling two ribbons which are connected together at one end. AC loss measurements were made on two commercially available ribbons supplied by RCA and GE. Their characteristics were found to be acceptable starting points based on typical design calculations.

The second concept suggested by BNL was a flexible coaxial cable. This construction favored the dielectric because of the elimination of the ribbon edges which enhance the stress and was therefore applicable to higher voltage, lower current designs. The superconductor would be deposited on the appropriate surface of the individual conductor segments of both the inner and outer conductors.

Coaxial cables could be made to the optimum dimensions for magnetic field and electric stress, and used in multiples of three in a common cryostat to achieve any desired capacity. The possibility of eliminating the outer return superconductor to halve the AC

loss at the expense of eddy current losses in the cryostat was mentioned, noting that with multiple cables per phase the eddy loss is reduced, possibly to tolerable levels.

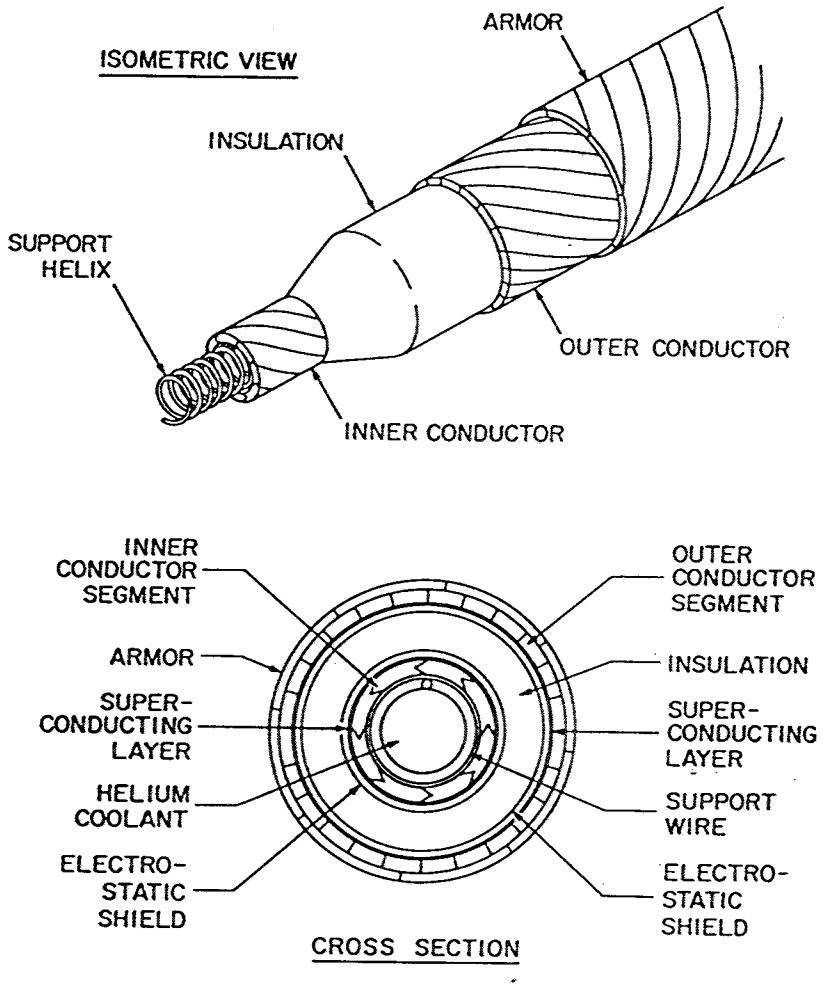

Figure 2-17 BNL's first flexible coaxial cable concept[41].

This preliminary study was very thorough. It included sections on cooling system calculations and configuration, system implications, fault consequences, and mention of material costs and availability, particularly helium and niobium. A section also considered DC transmission but concluded that AC would be the more appropriate target for development because AC designs are easily be converted to DC, but the reverse is not true. DC cables were shown to be desirable for very long distances and

very high power ratings which might be of interest to the utility industry for some scenarios. The study's conclusions identified five advantages of superconducting cables which are quoted[41] below:

1. The critical length may be as long as several hundred miles.

2. The cable may be designed to achieve surge impedance loading.

3. Heavy fault currents may be carried without tripping and the line will carry rated current immediately after the fault.

4. Extended overload currents may be carried for many hours. Following a suitable recovery period at rated current the overload cycle may be repeated indefinitely without degradation of the insulation.

5. Cable rating is not dependent on soil conditions.

In December 1971 BNL submitted a proposal to the National Science Foundation to develop a flexible AC superconducting cable system, concentrating first on fundamental experimental work to establish and improve material capabilities of both the superconductor and potential plastic tape dielectrics, followed with the construction of a half mile coaxial cable to be operated in series with the 69 kV high voltage supply to the BNL complex. A time-period of ten years to produce a cable system for utility evaluation was suggested. The first year of this program was funded under NSF Grant AG-381 which commenced in May 1972. The principle investigators were designated to be E.B. Forsyth, an Electrical Engineer of the Accelerator Department and J.M. Hendrie, Senior Physicist of the Department of Applied Science. However, J.M. Hendrie left BNL to accept a two year position with the Atomic Energy Commission, leaving E.B. Forsyth as the sole principle investigator, the position he held for the duration of the project. A second supplemental proposal was submitted in August 1972 which requested increased funds for an accelerated program, illustrating the sense of urgency that existed in the utility R&D community in that time frame.

In 1975 the project funding was moved to ERDA and the scope of work was integrated into a national program for power transmission. This move was accompanied by a reduction in the budget and overall scope of work. The intended half-mile demonstration cable to be inserted in the 69 kV feed to the BNL complex was changed to a 100 meter test bay, but upgraded to the 138 kV class. The two test cables, which were manufactured by BNL, were installed in the cryostat in November 1981. Full-scale testing began in October 1982. Tests were done for relatively short time periods over the next four years, the longest period of continuous operation being about four weeks. Testing confirmed the cable system's ability to carry a normal current of 4100 amperes and an emergency current of 6000 amperes at the 138 kV operating voltage, 80 kV phase-to-ground[42]. Impulse tests on the system at the completion of the operating tests resulted in a terminal failure in a stress cone at 488 kV. The program for superconducting cable development was terminated in mid-1987 and the foster program for the development of plastic tape dielectrics for room temperature cables was terminated in mid-1989.

Documentation of all aspects of the program can be found in a series of 164 Technical Notes which include quarterly reports through 1975, and semi-annual reports thereafter. This project was also the most prolific of any. Papers were published at the rate of ten to twenty per year and total several hundred. These works appeared in the journals of a variety of technologies.

The project proceeded along four parallel paths defined in the initial proposal.

1. Materials development on both superconductor and dielectric materials.

2. Laboratory Measurements of fundamental materials properties.

3. Cable system engineering, including functional requirements and cable design, cryogenics technology, and test facility requirements.

4. Prototype cable tests to evaluate materials and design in cable models and full-scale prototype assemblies.

The first challenge was the development of Nb_3Sn in tape form. This material is a brittle, weak metallic compound formed by the high temperature reaction of niobium and tin. To be useful it requires a metallic substrate to provide mechanical strength. The evolution of this compound into the "commercial" tape used for the cable demonstration required several years of intensive work by BNL scientists and several tape suppliers. Not only the metallurgical formation but also the combination of metallic partners to provide current stabilization and mechanical strength had to be optimized, a process that required extensive metallurgical facilities and physical and electrical test equipment capable of both room temperature and cryogenic temperature studies.

During this development process the functional requirements were also evolving. The initial cable design was based on single layers of tape for the inner and outer conductor, as shown in Figure 2-17. However, analysis for the ideal lay of each layer yields three independent criteria that cannot be simultaneously accommodated[43]. This gives rise to axial fields either inside the inner or outside the outer superconducting layers, in addition to the circumferential field in the dielectric space. These fields result in eddy current losses in the normal metal layers on both sides of the superconducting tapes, or circumferential currents in any metal path surrounding one phase. By the end of 1975 it had become clear that at least two layers in opposite directions were beneficial for each conductor in the coaxial configuration to eliminate axial fields external to the dielectric annulus and subsequent core and armor losses due to eddy currents. In conjunction with this problem, BNL studied a three layer concept (one layer for the inner conductor) that would reduce costs while still yielding very low axial fields. The four layer design was adopted, however, even though the three layer concept showed some promise.

The analysis of losses also considered the actual current paths in the superconducting surfaces and whether currents flowed on or around the tape edges. Some production techniques produced tapes with superconducting material on the edge and others did not. The tapes used for the test cables were slit from a wide sheet after heat treatment. Its edges were not superconducting. Though several papers were written on this subject, some believe that this situation has not yet been fully explained[44,45,46]. The final test cable had inner conductor losses that were about four times greater than expected and losses in the outer return conductor that were about seven times those expected.

The tape construction selected for the demonstration cable was manufactured by IGC and is illustrated in Figure 2-18.

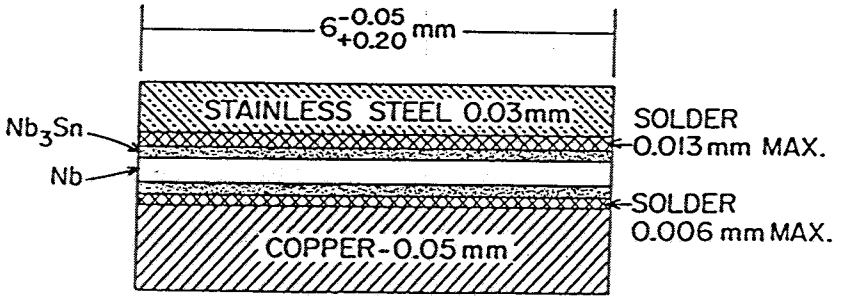

Figure 2-18 Cross-section of Nb_3Sn tape used in BNL cable[47].

The second challenge was the development of a suitable plastic tape to be used for the cable dielectric. Two uncertainties faced the designer: The first was the use of supercritical helium as the impregnant. Electrical data on supercritical helium in the temperature range of 7 to 9 K with pressures up to 10 atmospheres was non-existent. The second was the selection of the optimum material for the plastic tape. Requirements included extremely low dissipation factor (tan δ), high dielectric strength, mechanical properties close to paper (high tensile and compressive modulii, moderate surface friction, etc..), and cryogenic compatibility. Screening tests required the construction of several new test facilities, most with a cryogenic environment. Dielectric studies began with sheets but soon graduated to cylindrical cable models. The National Bureau of

Standards at Gaithersberg, Md. assisted with the design of test cells and the measurement of tan δ in liquid helium. The Battelle Memorial Institute was enlisted to assist with mechanical and thermal screening of material candidates.

A trial cable (without superconductors) was manufactured by Anaconda in 1975. This cable used three different materials, each in a 500 foot section, taped on a 1500 foot length of 542 kcmil six-segment self-supporting conventional hollow core LPFF copper conductor (O.D.=.906") provided by Pirelli Canada. The plastic tapes used were 25-.004" polyethylene, 33-.003" polycarbonate, or 25-.004" polysulfone. Half of the polysulfone and all of the polyethylene lengths were taped over a 25 mil porous teflon bedding. Soon after the production of this cable Anaconda closed its Hastings-on-Hudson, N.Y. plant. BNL took this opportunity to purchase an old low voltage taping line so that they could manufacture test cables in-house.

The Anaconda cables performed moderately well but suffered from problems with the unusual mechanical characteristic of the polymer tapes, as expected. As a result, a more involved material development program was initiated to "engineer" a plastic tape that would satisfy the stringent demands of this very low loss cryogenic application. An EPRI-sponsored study of taping theory was performed jointly by Phelps Dodge and BNL. This study quantified target levels of the combination of mechanical properties needed to enable the manufacture of a mechanically stable structure[48].

General Cable developed a two layer self-supporting conductor made of 1 mm thick bronze tapes supported by an aluminum tube which is subsequently dissolved away by hydrochloric acid. They produced 2000 feet with an O.D. of 2.37 cm in 1976 for superconductor and dielectric taping trials. 1000 feet of a slightly larger core (O.D. of 2.79 cm) was supplied in 1979 and used for the actual test cable.

In 1977 General Cable produced a prototype cable similar to the Anaconda cable. It was made on the two layer core previously produced and included three different materials, 350 feet of each. The first material was a 2.4 mil polycarbonate, the second was a 4 mil polyethylene, and the third was an embossed version of the 2.4 mil polycarbonate with an effective thickness of 3.4 mils. The insulation thickness for all sections was 300 mils total. This cable produced some interesting data, especially at room temperature when pressurized with SF_6.

In response to the material characteristics identified by the Phelps Dodge study, Battelle developed an very high modulus (VHM) polyethylene tape that also showed considerable anisotropy between its tensile and compressive modulii, a desirable trait of paper. Other steps to higher modulii include the lamination of thin tapes. This was tried with polypropylene which produced tapes with the best combination of properties yet. The test cables were made using 2-ply 4 mil thick and 3-ply 5 mil thick polypropylene tapes that had been surface treated with a teflon spray to improve their static coefficient of friction. The test cable had a wall thickness of 400 mils and exhibited excellent mechanical (bending) properties, a remarkable achievement. Figure 2-19 illustrates the test cable construction that was manufactured on the BNL taping line and installed in the 100 meter two-cable cryostat for full-scale voltage and current tests.

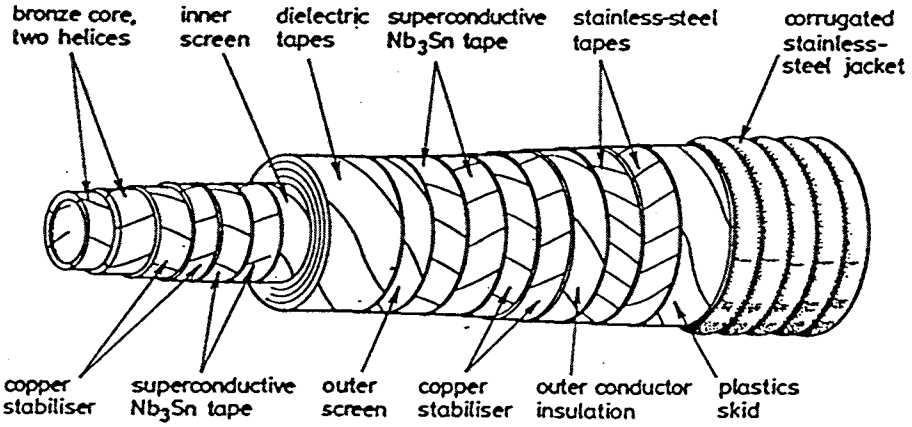

Figure 2-19 Cable construction of BNL full-scale test cables.

In the course of the dielectric development it became apparent that much of the improvements would be applicable to room temperature cables, but operating conditions would most likely include impregnation with a dielectric fluid. A parallel effort to develop a polymeric tape for ambient temperature HPOF pipe-type cables was initiated in 1976 and carried for the duration of the program. The primary difference was the fluid impregnation. Embossing of the tape to stabilize the coefficient of friction and provide pathways for the flow of helium had been tried, but found to be counter-productive. However, embossing was thought to be mandatory for fluid-impregnated room temperature cables to allow fluid to flow within the tape structure. The other problem associated with fluid impregnation was swelling. Highly oriented material was found to be the most resistant to swelling in standard hydrocarbon dielectric fluids, which was consistent with the very high modulii being sought for tape-ability. A separate test bay was built to allow testing of ambient temperature cables made on conventional metal conductors.

During the development of taping practice and evaluation, BNL utilized a soft X-Ray technique to examine the taping patterns in finished cables. The process was made available to the cable industry and used to examine 500 kV HPOF test cables at the EPRI Waltz Mill Test Facility and in laboratories doing post-mortem analysis of these test cables. The process was used in the field by Con Edison during their 345 kV TMB repair program and by LILCO to QC molded splices on 69 kV extruded cable. Fault damage assessment and soft spot analysis was done on 345 kV TMB faults experienced by Northeast Utilities, PSE&G and LILCO. This technique was also applied to non-lapped cables, to check extrusion symmetry for 138 kV XLP cables, molded joints in a six-mile submarine cable, and joints in an experimental glass-insulated cable assembly[49].

Several realistic power system application studies were performed throughout this program to focus design goals and evaluate the viability of the flexible superconducting cable system. The first, done in 1973, was a rough look at the hudson valley 345 kV

corridor which feeds power into the heart of the Con Edison System[50]. A combination of six overhead lines from Millwood to Sprain Brook (32.2 km) and eight pipe cables from Sprain Brook to Farragut (32.2 KM) with a rated capacity of 8000 MVA was projected for 1980. Beyond 1980 it was likely that this capability should be doubled. The installation of one 8000 MVA or two 4000 MVA superconducting cables directly between Millwood and Farragut (64.4 km) was analyzed for system implications. Flexibility in the cable design to match impedance requirements was exploited to produce cables that integrated well into the system without additional power flow controls or compensation. Faults and overloads were studied in some detail as to the capability of these first cable designs. The use of Nb_3Sn provided more than enough field capacity to handle a 4-cycle fault with a peak current twenty times rated current without going normal. Overload capacity at 20% above rated load was estimated to be several hours, corresponding to an LTE situation. Much higher loads could easily be tolerated for several minutes to satisfy STE requirements. A superconducting DC cable system alternative was briefly studied, but the conversion cost alone was estimated to be greater than the cost of a conventional underground AC cable installation.

The first major case study with a utility partner was initiated in 1973 with LILCO in parallel with the transmission planning for the 4800 MW nuclear plant to be built at Shoreham[51]. One plan required two parallel 42.5 mile 345 kV superconducting cables, each with a 4800 MVA continuous rating, or three parallel 42.5 mile 230 kV superconducting cables, each with a continuous rating of 2400 MVA, to carry the full output of the shoreham complex[52]. Two other plans involved lower ratings and combinations of superconducting cables roughly 22 miles long with overhead lines. BNL developed technical designs for these cable options and issued sub-contracts to PTI and the Cryenco Division of Cryogenic Technology, Inc. (CTI) to develop installation and cryogenic envelope costs, respectively[53]. The double circuit 345 kV plan was studied in more detail following preliminary considerations. PTI performed a study of switching surge overvoltages, fault current magnitudes, and arrester and breaker duty for such an

installation. The conclusions of this study caution that switching surge waveforms give rise to larger than normal high frequency contents, and transients due to system faults take longer to decay, both a consequence of the low loss conductor characteristic.

Results of the detailed cost analysis yielded a superconducting system cost for the most interesting case only twice that of the base 345 kV overhead scheme which included a full length double circuit and a single circuit to an intermediate substation. The conventional underground alternative, nine 345 kV HPFF circuits, was twice the superconducting system cost.

The cable design for all cases was similar to that shown in Figure 2-17. A single layer superconductor helix was assumed for both the inner and outer conductors. The maximum operating stress in the cable was 10 kV/mm and the current density was 420 amperes/cm at 4800 MVA. The cryostat features thermal shields formed by the return flow of the helium stream; internal helium flow is unidirectional. A separate helium return pipe is not required. The overall system appears in Figure 2-20.

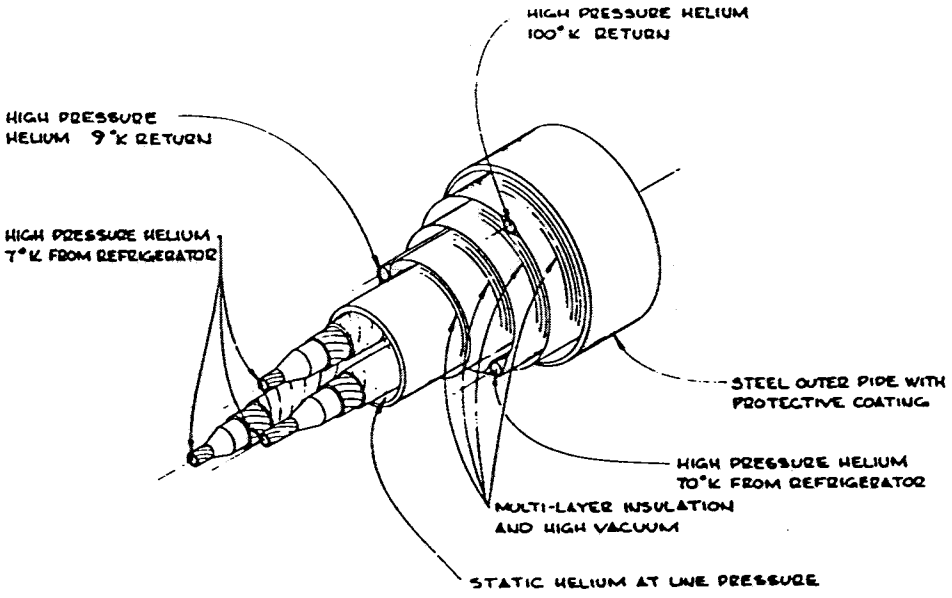

Figure 2-20 Superconducting system used in BNL-LILCO Study[51].

The cryostat was found to be the major cost item (57% of the material cost) prompting a considerable effort to improve this part of the system. This effort led to the far-end expansion temperature control scheme and a cryostat with no intermediate shield, a revolutionary concept in 1974. However, because of a large pressure difference between the conductor core and the return channel in the cryostat space surrounding the cables created by the counter flow scheme, each cable requires a hermetic seal to keep helium from flowing radially outward through the dielectric. Another design change destined to have a large impact on cable cost was the use of two opposite lay helices for the inner and outer conductors, essentially doubling the amount of superconducting material in the cable construction. In 1976, following another study which also highlighted the high cost of the original shielded cryostat, the LILCO study was repeated using the new cryostat design but also a revised cable construction based on the double layer superconductors and a reinforced lead sheath over each cable. The net result was an increase of 33% in the superconducting cable system cost, even after adjusting the early study to 1976 dollars. A variation which increased the operating stress to 15 kV/mm reduced the cost to about the level of the 1973 study, highlighting the sensitivity of EHV cables to dielectric performance.

The second case study, alluded to above, was for a long distance (350 miles) application connecting coal mine-mouth generation parks (10,000 MVA) in Ohio and western Pennsylvania to the PJM power pool[54]. This study by BNL and PTI was done in 1975 and followed an earlier study by a consortium of Pennsylvania utilities including General Public Utilities (GPU) Service Corporation, Pennsylvania Power & Light and the Philadelphia Electric Company which had evaluated a three circuit 1300 kV overhead system.

This study looked at three schemes to deliver 10,000 MVA to two substations in the PJM pool. The least expensive had two circuits 310 miles long and one circuit 350 miles long, each circuit rated at 4260 MVA normal with a contingency of 5200 MVA at 500 kV, the

PJM system voltage. The superconducting system was arranged with an average distance between refrigeration stations of 38 miles. The cables were designed with an operating stress of 10 kV/mm and two levels of current density, the lower density yielding a lower surge impedance. The hermetic seal over each cable was provided by a stainless steel corrugated tube, the same concept used for the BNL test set-up as shown in Figure 2-19. The three stainless steel tubes were to be supplied in the longest lengths shippable and pulled into the enclosure during the enclosure installation, with one welded joint between cable splice points. The cables were then pulled into the three tubes as in a conventional pipe-type cable installation.

The superconducting cables were found to behave in a manner similar to the 1300 kV overhead system regarding system stability, power flow, compensation requirements and fault duty. Switching a circuit on resulted in tolerable surge voltages with series resistor damping. Though breaker arrester duty was severe, the same problems were identified with the overhead system.

The cost comparisons of this study were in line with the LILCO study. The capital cost of the superconducting system was 2.8 times that of the 1300 kV overhead system. When the capitalized cost of losses were included this ratio increased to 3.6. The superconducting system cost of losses were twelve times that of the overhead system and increased the capital cost of the superconducting system by 39% compared to a 9.2% increase for the overhead option[55]. An interesting aspect of the high cost of losses: the superconducting system consumes its energy from the distribution system, not the transmission system, and therefore must include the overhead associated with substation and distribution costs. No mention was made that the obvious system for this application was a DC system.

The third system study was done as a part of the DOE-funded study by the Philadelphia Electric Company mentioned earlier[33]. This study is considered to be the most

comprehensive evaluation of all the high capacity systems being promoted in this time frame (the 70's). This hypothetical project considered all feasible concepts (a total of 16) for the transmission of 10,000 MVA from an energy park in mid-Pennsylvania 66 miles to a substation in Philadelphia, considering all aspects of such a project as realistically as possible. The 230 kV three-circuit BNL-designed system was the lowest cost all underground alternative, beating a 500 kV 3-phase GITL rigid system by 3.4% and 500 kV SCFF cables by 5.4%. The lowest cost pipe-type cable system, the 500 kV PPP option, was 20.7% higher in cost. That option required 16 pipe cable circuits as opposed to the three circuits required by the BNL system.

The cable design used in this study was based on an operating stress of 10 kV/mm and a current density of 425 amp/cm based on a circuit rating of 5100 MVA continuous. The cable used a reinforced lead sheath as the hermetic seal. The outside diameter of the cryostat was 20 inches. Only two refrigeration systems and one expander were required (per circuit) along the route. Expanders were also needed at each end of each circuit. A small amount of series capacitive compensation was required in comparison to the Linde rigid superconducting system and the 500 kV overhead/underground base case. These three systems were the only ones which operated above their surge impedance loading (SIL). No shunt reactors were required, as they were for the AC fluid filled systems, both HPFF and SCFF. Even though the parameters of this application were particularly favorable to the BNL system, the cost triumph marked a significant achievement for the BNL program.

During the project, work on the cryostat design was extensive, not only for the system design but also for the numerous test beds that were built and used to test progressively larger conductor assemblies, dielectric materials, and prototype cables. Coaxial conductor assemblies were tested in one meter and twelve meter cryostats. Fully taped cable samples were tested in a one meter dewer and two twenty meter cryostats, one of which was a flexible three inch I.D. four-tube corrugated assembly provided by

Kabelmetal, similar to that used for Klaudy's Arnstein cable described earlier, which used a liquid nitrogen-cooled shield. Heat leak tests into the nitrogen, as is appropriate for a HTSC cable system, were relatively high at 3.7 watts/meter, about twice the design value. However, the assembly was in a bent configuration (90 degrees) which may have affected the results. The twelve meter rigid cryostat had a heat leak to the liquid nitrogen shield of less then 0.5 watts/meter, as did the twenty meter rigid cryostat built by BNL. The twenty meter cryostat built by BNL was the basis for the design specification for the 100-meter five-section cryostat for the demonstration cables, which was purchased from the low bidder, the Minnesota Valley Engineering Company (MVE). The test cryostat consisted of an 8 5/8" by 0.109" wall 304 stainless steel inner pipe (IPS Schedule 5S) and a 16 " O.D. by 0.25" wall schedule 20 carbon steel outer pipe. The support scheme was a bicycle-wheel type wire cage assembly. Each 60 foot factory section was evacuated and permanently sealed at the factory. A spare section was purchased for backup, and a dimensionally compatible stainless steel corrugated section (8" I.D. x 15.35" O.D. x 18.9 meters long) was purchased from Kabelmetal.

The MVE sections were delivered to BNL in the fall of 1977 and the Kabelmetal flexible section was received in August 1979. All enclosures had design levels of heat leak of about 0.5 watts/meter to supercritical helium at 6 K. The five MVE sections installed in the test line were tested for heat leak in 1984 and found to be acceptable. The Kabelmetal section was not measured. One aspect of concern to cable engineers is the durability of the vacuum in factory-evacuated hermetically sealed cryostats. To this end BNL recorded the vacuum levels (at ambient temperature) in the six MVE sections and the Kabelmetal section through the end of the project. This data together with an additional measurement taken in September 1992 are shown in Figure 2-21. The Kabelmetal section lost vacuum sometime between 1986 and 1992. It is likely that an "O-ring" seal on one of the pump-out ports failed. Kabelmetal did not have the capability to provide cold-welded pinch ports used by MVE when this section was manufactured.

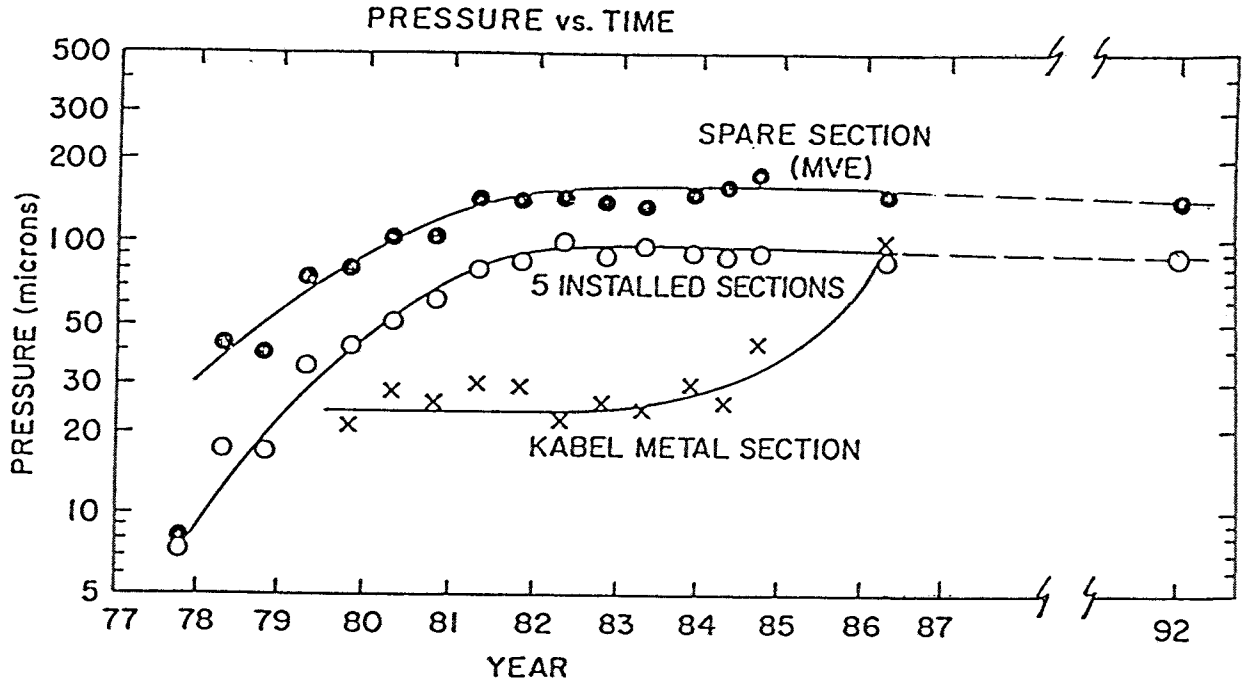

Figure 2-21 Ambient temperature vacuum level for BNL's factory sealed cryostats.

This brief review has barely scratched the surface of the amount of engineering and experimental information that was developed and accumulated over the course of this program, and which is available in the literature and in the series of progress reports. In particular, there is valuable information on the problem of cryogenic splices and terminations, test facility design and construction, refrigeration system design, construction and performance, the taping of thick walls with plastic tapes, the metallurgy of LTSC materials and the evaluation of their electrical and physical properties, and so on. Extensive review of this information base should be a pre-requisite for anyone contemplating serious involvement in the technology of superconducting cable systems, either LTSC or HTSC.

Los Alamos DC Cable Program. Los Alamos National Laboratory (LANL) carried out a project for the development of a DC superconducting power transmission line (SPTL) which began in the fall of 1972 with funding from the Division of Applied Technology of the Atomic Energy Commission[56]. In 1975, ERDA assumed financial responsibility for the LANL program and the BNL program. The program funding was cut back by DOE in 1978 so that the scope had to be reduced, eliminating the planned 300 meter test section designed to demonstrate a 25 kAmp capability at 100 kV (2500 MW/cable). Further reductions in DOE's budget resulted in the termination of the program at the end of fiscal 1979 (mid-1979), before a full-scale cable could be built and tested[57].

The program began with the creation of task groups to perform the following four functions:

1. Superconductor materials: purchase and fabricate samples of superconducting material, characterize them, and develop geometries for conductor experiments.

2. Critical Current Measurements: Design, build and operate the apparatus to obtain critical current data on material samples provided by Task Group 1.

3. Test Bed: Design, build and operate the cable test beds.

4. Power Engineering: Perform calculations and system studies to insure that the cable design parameters remain realistic as progress is made.

The first two years of this program concentrated on the study of superconducting materials with the highest possible operating temperatures, notably Nb_3Sn and $Nb_3(Ge,Al)$, targeting an operating temperature in the range above 13 K. One cooling technique thought possible was the use of slush hydrogen rather than supercritical helium as the triple point of hydrogen is 13.9 K. In 1975 EPRI joined the effort by funding a one-year program specifically to develop Nb_3Ge[58]. This EPRI program was continued to a successful conclusion, achieving critical currents over 4,000,000 amps/cm^2 with this material which has a T_c of 32.2 K[59].

An interesting DC transformer technique was developed to measure the critical current of relatively large tubular samples. One sample made by soldering four 1/2 inch wide tapes longitudinally to the surface of a 3/4 inch copper tube carried 29,500 amperes in response to the DC field set up by a toroidal iron core with a generous superconducting tape primary winding. The sample was arranged in the center of the toroid with a coaxial return made of superconducting tapes that passed over the toroid to form the secondary loop. This technique takes advantage of the unique flux exclusion property of superconducting material which causes shielding current to flow to counteract the presence of a field, even a DC field! A second trial was made with four new tapes soldered on top of the original four. It was expected that this assembly would have a critical current well over 50,000 amperes, but when tested I_c was only 39,000 amps. Field affects and unequal current sharing were probably responsible for these "poor" results. Tubular structures wherein the superconducting material is placed on the outer surface of a metal tube by plasma-arc spraying, sputtering, or a CVD process were pursued in addition to the soldered tape method just mentioned.

A test bed that could measure short tape or wire samples on the order of a foot long was built, and a twenty meter test bed was also constructed in a hairpin configuration suitable for testing long samples of tapes or wires. A 50,000 ampere, 2 volt current source was built using a bank of submarine batteries. A modular transistor controller was also designed and built to enable controlled high current testing. Later in the program a 3.25 MW power supply with a DC capability of 35,000 amperes was installed.

Several methods to produce multifilimentary (mf) wires were developed and evaluated. The final selection for the test cable was a multifiliment Nb_3Sn structure in a copper matrix forming a wire that could be stranded into multi-strand cables and formed into a helical structure over a simple former. Several assembly options using mf wires were identified as shown in Figure 2-22.

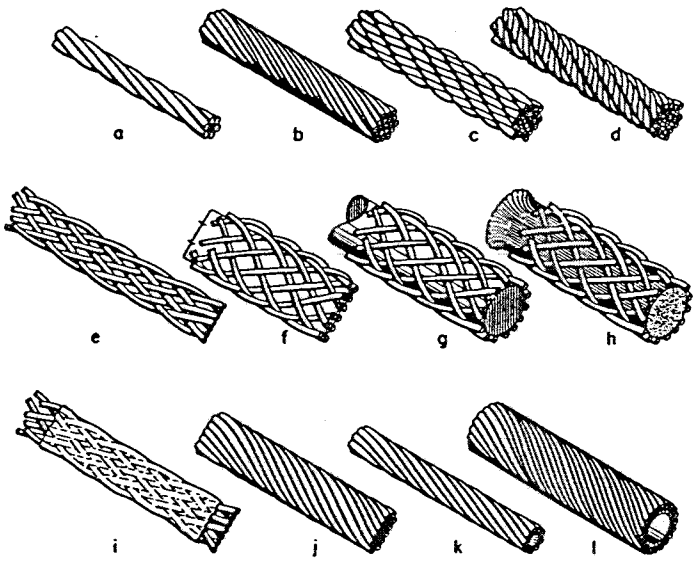

a,b - Concentric lay, hexagonally packed.

c,d - Rope lay options.

e - Flat braid.

f - Flattened circular braid.

g,h - Circular braid over cores.

i - Solder-covered flat braid.

j - Roebal transposition.

k,l - Spiral wraps on solid wire and hollow tube.

Figure 2-22 Various assembly options for multifilimentary LTSC wire[60].

Early in the program two cable designs were identified. The first was a flexible coaxial cryogenic monopole design similar to the BNL flexible cable. This cable has a superconducting conductor and outer return conductor in a corrugated sheath to separate the go and return helium streams. It is pulled into a rigid cryostat. The cryogen enters the conductor and returns in the space between the cable and the inner wall of the cryostat, making this system a self-contained (monopole) system. As in the BNL design, the counterflow acts as the final heat exchanger leading to the far-end expander in the refrigeration scheme. This concept is illustrated in Figure 2-23. Figure 2-24 provides dimensions for a system rated at 5 GVA at 100 kV. The conductor and return current is 50 kAmperes.

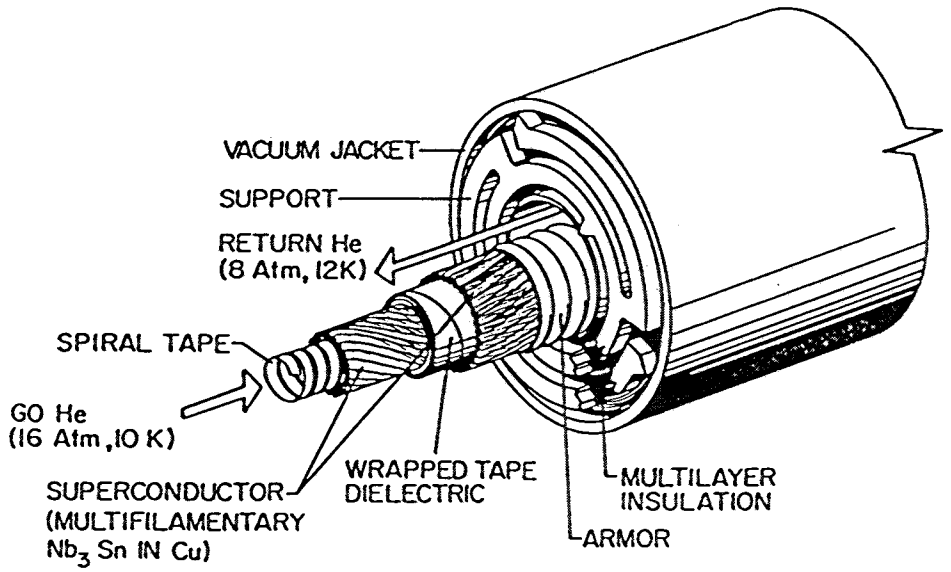

Figure 2-23 LANL's cryogenic dielectric coaxial monopole DC LTSC concept[57].

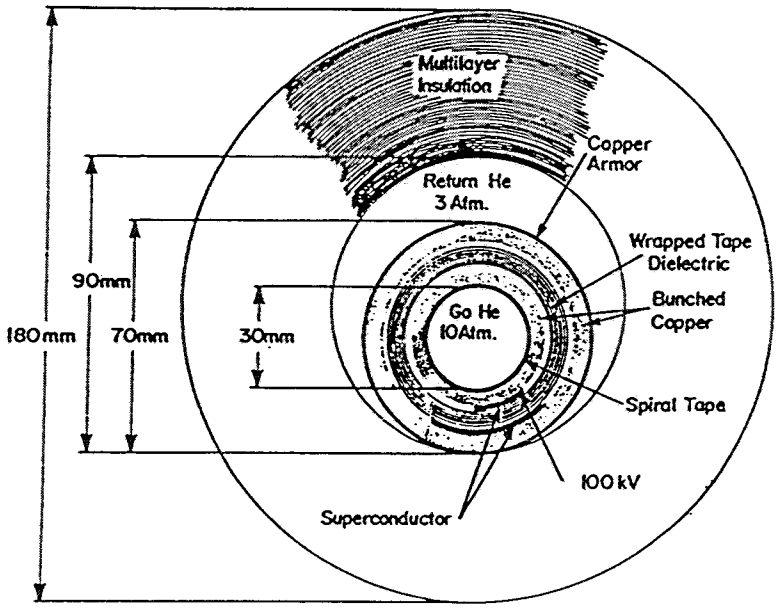

Figure 2-24 LANL's cryogenic DC system for 5 GVA at 100 kV[61].

LANL's second design used a superconducting conductor inside a flexible cryostat made of corrugated tubes. The outer wall of the cryostat is at the same voltage as the conductor, but at room temperature. The dielectric is placed over the cryostat and can be any conventional material because it operates at room temperature. LANL called this design the "Small Line Design" because it does not provide a superconducting return. It is more suitable for bipole operation where the voltage is high and the current is low. Two cables are used, one for each pole, which also provides the second hydraulic path needed for the cryogen. Otherwise, a thermally insulated return line would be necessary. This design is shown in Figure 2-25.

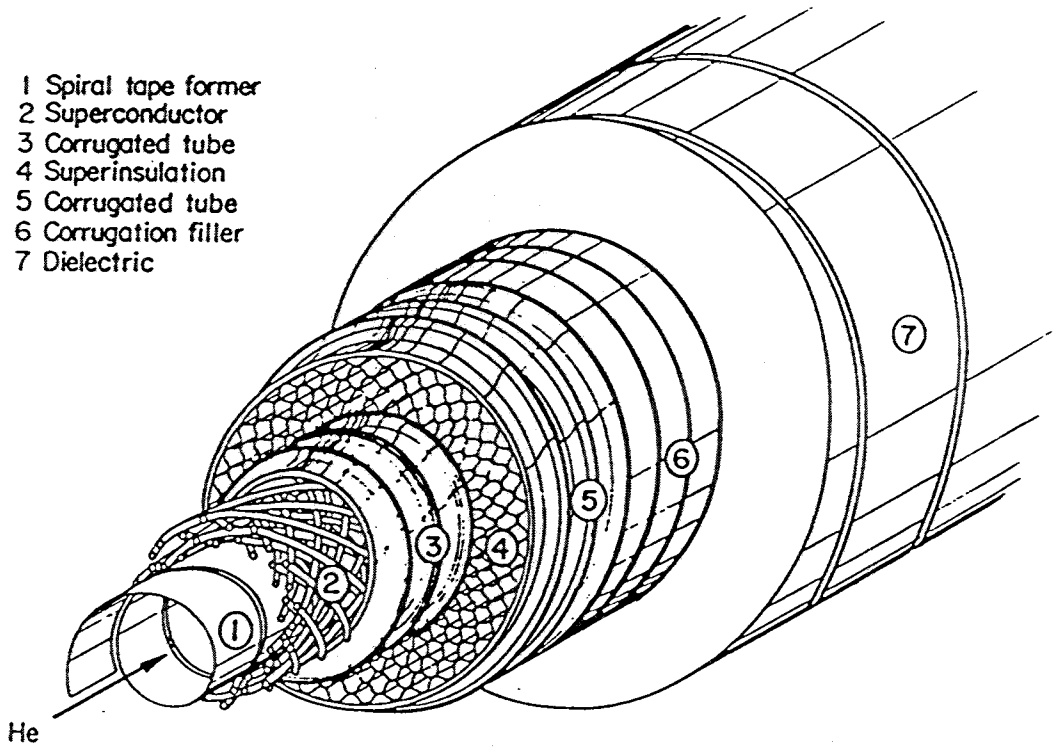

Figure 2-25 LANL's "Small Line Design" room temperature dielectric cable concept[57].

A program to study dielectrics was initiated in 1975, with Oak Ridge National Laboratory scheduled to do the experimental work as part of an ERDA program supporting cryogenic studies. This program was terminated in mid-1976[62]. As a result, LANL decided to build their own dielectrics laboratory. Some of the dielectric test equipment at Oak Ridge was transferred to LANL, notably an eight position sphere-to-plane test cell which was modified to a six position shaped electrode configuration. LANL purchased a +/-300 kV, 10 ma corona-free test set, and a 600 kV, 60 kJ impulse generator. They set up a 17 meter horizontal cryostat with a 10 cm bore to be used for high voltage tests on full scale cable models and a 2 meter cryostat that could accommodate a mandrel with an active coaxial length of about 27 cm between stress cones.

Much effort was devoted to the design and manufacture of bushings for the high voltage test cryostats. The apparatus for vacuum casting epoxy and epoxy-film combinations was developed and used to produce 50 kV and 100 kV bushings for the multi-cell cryostat and short cryostat respectively. A 300 kV bushing was purchased from Lapp to be used on the 17 meter cryostat.

Material candidates for a lapped cable dielectric were screened on the basis of DC breakdown tests in the multi-cell cryostat. Two papers and PPP were selected for coaxial model tests for DC and impulse strength, as well as two runs that tested combinations of polyethylene and paper. However, the dielectrics program suffered from the rush created by the early cancellation of the program. In spite of a careful approach and close attention to detail in the handling of samples, the breakdown data had wide dispersion. There wasn't enough time to fine-tune technique and do the replications demanded by very high stress cell testing.

The 17 meter cryostat was never used for high voltage testing. It was used to confirm the hydro-dynamics of counter-flow cooling using a piece of 300 kV fluid filled paper

cable made by Phelps Dodge. This cable was unusual in that it used a .75" O.D. x .065" wall copper tube as it's conductor, demonstrating the viability of building a taped cable over a solid tube. The cable had a fluted lead sheath to supply fluid to the dielectric since the conductor was hermetically isolated from the dielectric. The cross-section of this cable is shown in Figure 2-26.

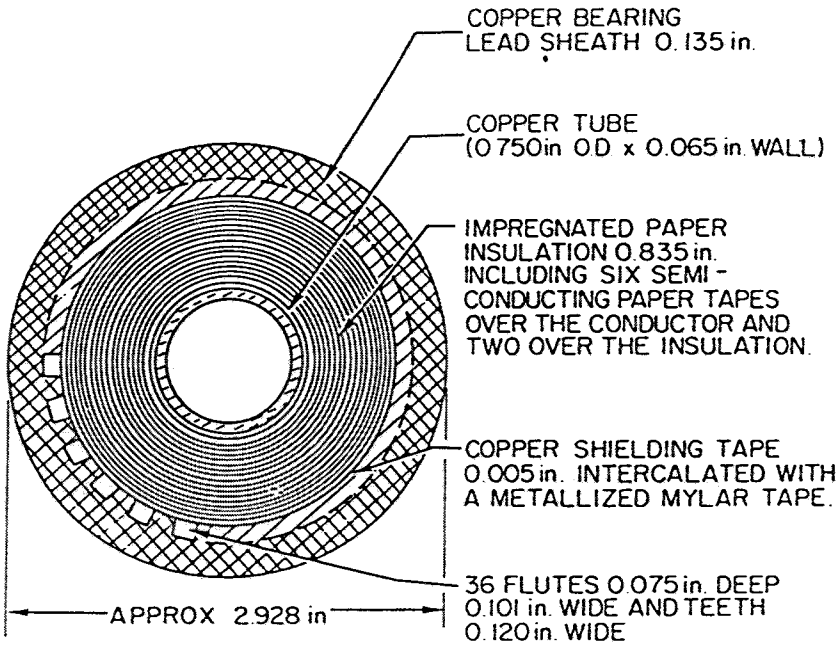

Figure 2-26 Tubular conductor fluid-filled 300 kV DC cable used for flow tests[57].

The power engineering studies concentrated on establishing the functional requirements of the cable system for long distance DC transmission in a large AC electrical system, or between large systems. A subcontract was given to New Mexico State University to perform load flow and system studies with various DC transmission lines integrated into an AC system. Engineering studies throughout the project concentrated on the nature of the abnormal voltage and current that a cable could be exposed to in service. These include harmonics introduced by the load, ripple currents created by the inverter, fault

currents and voltages, and transient overvoltages caused by system disturbances. Conclusions of this work were that no major problems existed for a well-designed cable. AC losses due to harmonics and ripple currents could be kept at a tolerable level, as well as fault currents which are basically limited to the capacitive discharge current of the cable. The main source of overvoltages are wave reflections which will result in significant transient voltages. However, the normal relation between operating stress and BIL will provide sufficient margin to tolerate these voltages without damage.

An early target for a demonstration cable was the EPRI/Con Edison 100 MVA DC Test Link project at the Astoria Generation plant in Queens, New York for which LANL would supply a 600 meter room temperature dielectric system. The more general target was for a 10 GVA system using either of the two concepts. The room temperature dielectric design would provide this capacity with a current of 12,500 amperes in two cables at +/- 400 kV while the cryogenic dielectric would do this job with 100,000 amperes at 100 kV in a monopole configuration.

The DOE/Philadelphia study[33] provided the only comparative analysis opportunity for the LANL design team. The system design submitted was for three independent coaxial monopoles each rated at 7.5 GVA (25 kAmp at 300 kV). This rating was a continuous rating even though it represented the second contingency for the overall system. Because of the short length of this study, 66 miles, the DC systems were not expected to be the lowest cost. Of interest is the comparison between the LANL superconducting system and the "conventional" DC design which was a +/- 600 kV, 4000 kcmil copper conductor SCFF system that used eight cables arranged as four bipoles with each bipole having a 4000 kcmil copper ground conductor insulated for 15 kV. The LANL system was almost 20 % higher in total cost. The three superconducting cables cost 26 % more than the eight 4000 kcmil 600 kV SCFF cables plus the four 4000 kcmil 15 kV ground cables. Together with the refrigeration packages, the LANL cable system was 70 % higher in cost than the SCFF system. The substation cost was also higher for the

superconducting system, by 10 %. On the plus side, the capitalized cost of losses for the LANL system was only 80 % of that of the SCFF system, but the cost of losses was only 20 % of the total cost, hardly compensating for the higher cable system cost.

After reviewing the results of the comparisons in the DOE/PECo study, LANL made a quick estimate of the cost impact of using three bipoles at +/- 300 kV, each consisting of two room temperature dielectric "small line" cables with a contingency rating of 6,667 amperes, plus a seventh superconducting conductor insulated for 20 kV to serve as the independent ground. This in essence replaced three large rigid cryostats with seven small flexible cryostats. Some cost savings were also anticipated for superconducting material and the refrigeration equipment. However, a rough estimate suggested the total cost could be reduced by only about 10 %. More detailed calculations were not done.

Superconducting Programs in Europe. The Research Laboratories of the CEGB in Great Britain carried on a program that began in 1967 and lasted ten years. Studies by the CEGB had established that higher voltage, lower current superconducting system was desirable for the transmission system of the British Isles[63]. 4,000 MVA at 275 kV (8400 amperes) and 5000 MVA at 400 kV (7200 amperes) were identified as reasonable targets. Lower voltage higher current options were not considered because of the severe breaker requirements. Also, the above capacities are in the range of the surge impedance load of coaxial superconducting cables with taped dielectrics, leading to the elimination of series or shunt compensation.

CERL constructed an eight meter cryostat with a 30 cm bore utilizing a 150 watt helium refrigerator that had been used for a magnetohydrodynamic generation research program in the sixties[64]. Work in this test bed began with niobium coated copper tubes in a coaxial arrangement (far end shorted) similar to the Linde studies. Later work studied flexible taped conductors using first a single layer for the inner and outer conductors and finally a double layer with opposite lay for each. Their choice of

superconductor tape was niobium on either an aluminum or copper substrate, the latter finally winning out because the heat capacity of copper is about twice that of aluminum at 5 K. The test bed did not use the superconducting transformer that BICC had developed. A brute force current supply was used which had a 10,000 ampere steady capability and shorter time capability up to 70,000 amperes for one second. The test bed is illustrated in Figure 2-27. Compare this arrangement to that used by Linde, shown in Figure 2-11.

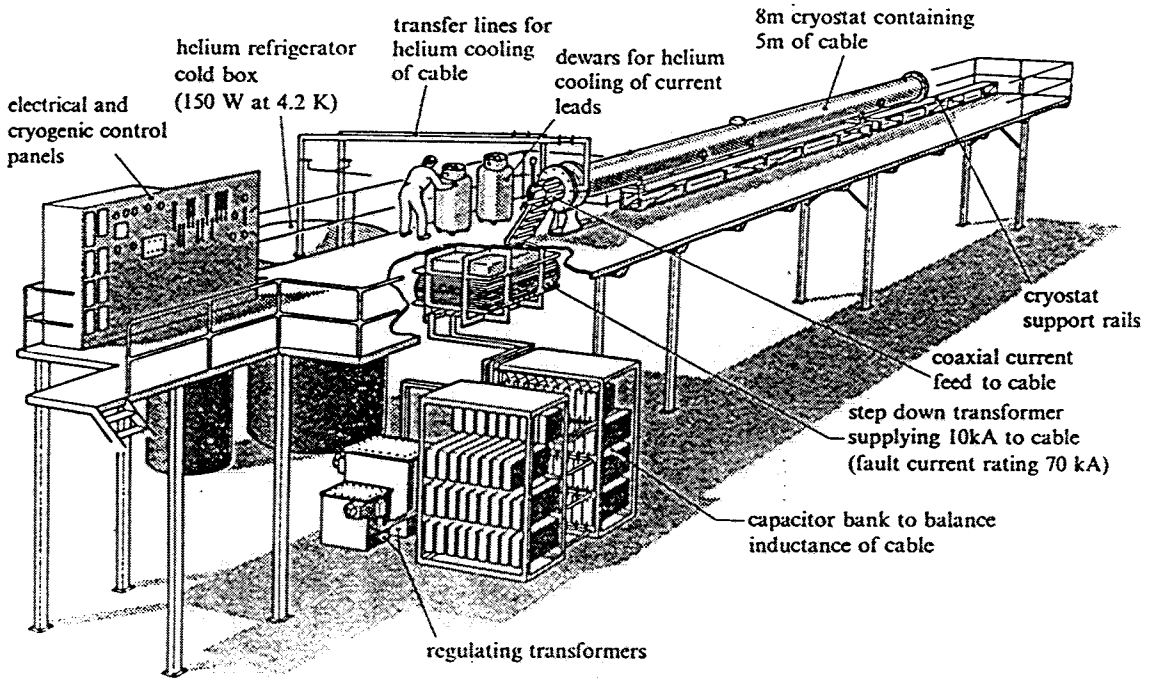

Figure 2-27 CERL's superconducting coaxial cable test bed[65].

The use of polyethylene tapes impregnated with supercritical helium was selected early in the program and assumed to be viable based on supporting work by BICC on gas-impregnated polyethylene taped cables for room temperature EHV applications. Early designs at 275 kV used a maximum stress of 8 kV/mm at operating voltage[64]. Later studies suggested that 10 kV/mm would be required to make the system cost-effective at 400 kV[66].

The overall system arrangement was similar to the BNL design. An early version is shown in Figure 2-28 below. Supercritical helium in the 4 to 5 K range flows in the core and space outside the neutral conductor inside the helium return tube, going in the two smaller tubes and returning in the larger tube. The tubes are thermally isolated by vacuum in the interstice between tubes. A liquid nitrogen inner shield is used, covered with superinsulation. The rigid helium return tubes are made of a low-contraction alloy with periodic bellows to reduce stress at low temperature. The outer casing is steel with an O.D. of 46.5 cm.

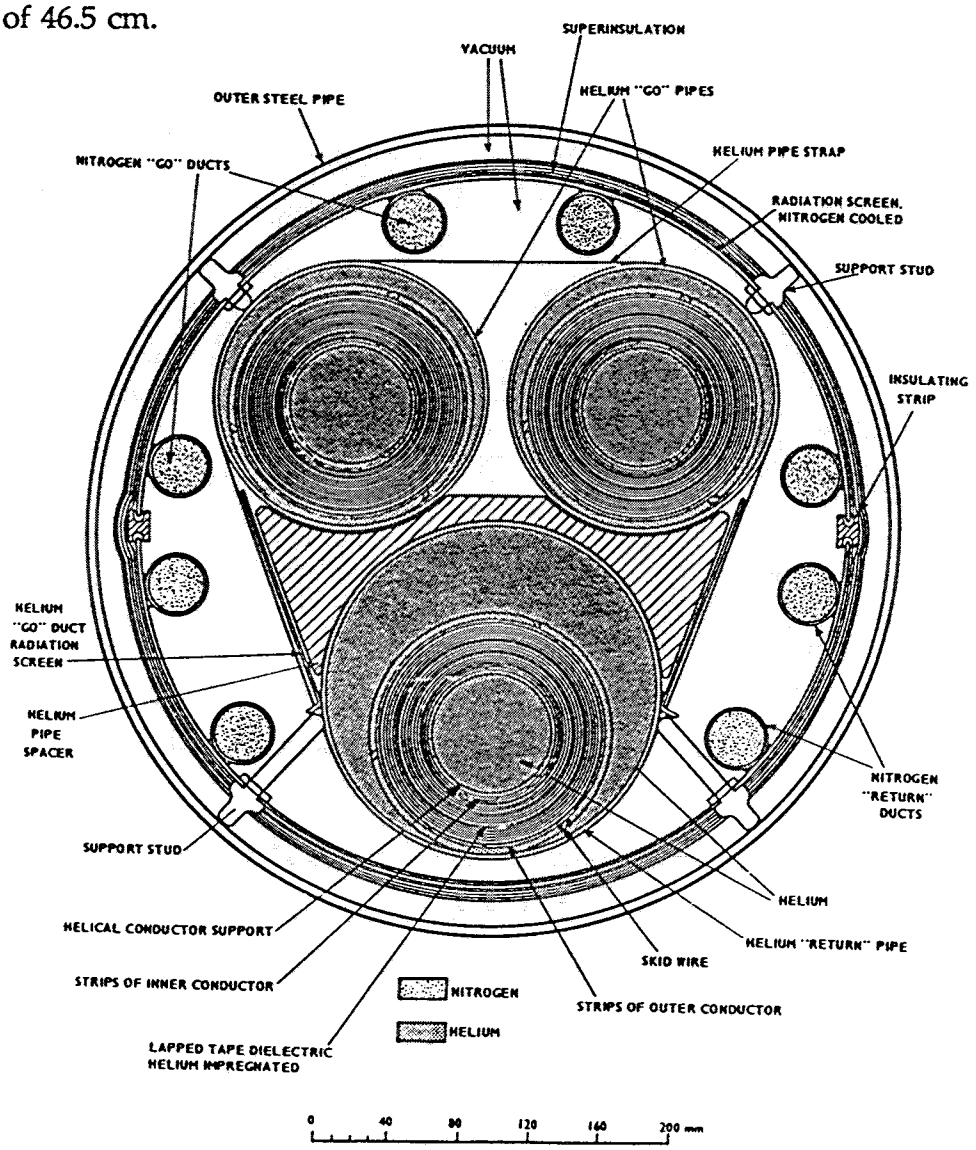

Figure 2-28 General arrangement of early CERL design[63].

A later version of this assembly is shown in Figure 2-29. While fundamentally the same, some refinements are evident. A carriage has been added to allow continuous installation of the helium return tubes, which are now corrugated stainless steel. The number of nitrogen feed tubes has been reduced to two. A full-size model of this assembly was built, detailing the intricate carriage design. Figure 2-30 shows the installation plan that takes advantage of this design.

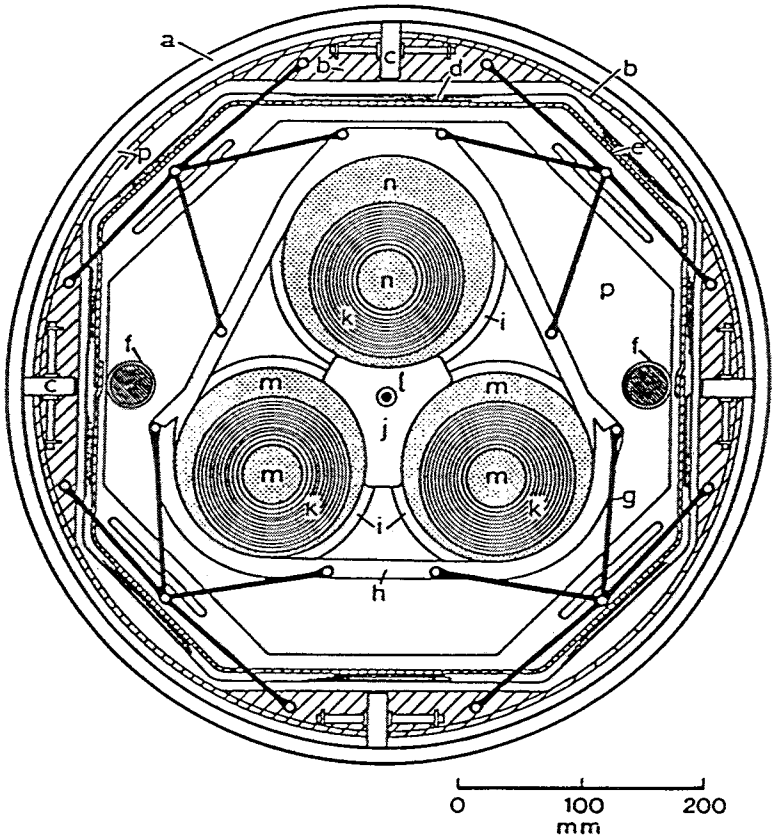

FIG.1 CROSS SECTION OF A THREE PHASE 5 GVA 400kV SUPERCONDUCTING CABLE

a OUTER STEEL PIPE
b CARRIAGE
c CARRIAGE WHEELS
d SUPERINSULATION
e HEAT SHIELD
f NITROGEN PIPES
g SUPPORT STRUTS
h CORE BINDING FRAME
i CORRUGATED STEEL HELIUM PIPES
j HELIUM PIPE SPACER
k CABLE CORES
l PULLING WIRE
m & n HELIUM GO AND RETURN FLOWS
p VACUUM

Figure 2-29 General arrangement of the final assembly design[67].

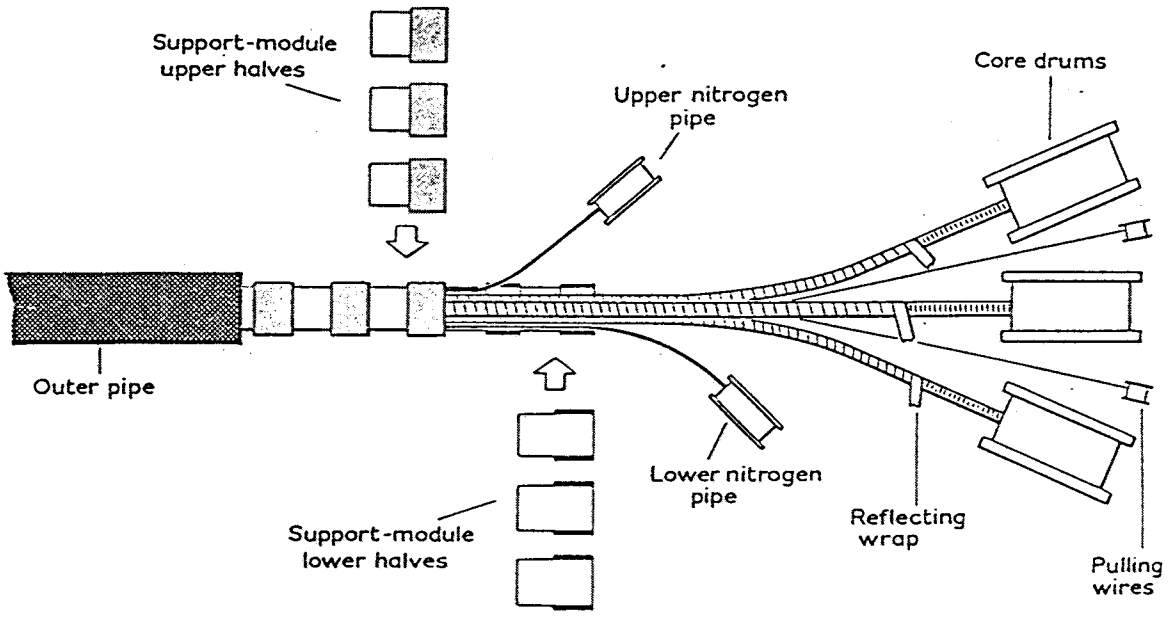

Figure 2-30 On-site installation plan for superconducting cable system[68].

The CERL cable design followed the BNL evolution. It began as a very simple coaxial cable with a single layer of superconducting tapes for the inner and outer conductors with polyethylene tape as the dielectric. A skid wire held the outer conductor intact and allowed long cable lengths to be installed in the rigid helium return pipes. This concept is shown in Figure 2-31.

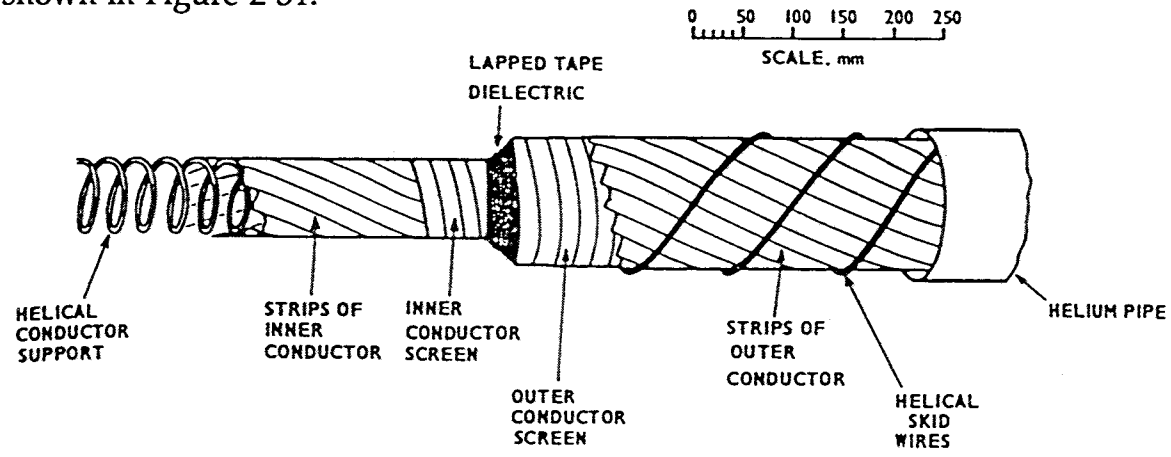

Figure 2-31 Early CERL flexible cable design[63].

By the end of the program a double layer of superconducting tapes, opposite lay, had been adopted. By this time work on the dielectrics established the necessity of very careful screen design and had produced a combination of screens and bedding tapes to be used on both sides of the dielectric. A new ribbed plastic support was designed to replace the usual steel spring. The superconducting tape is a copper tape with a thin (25 m) coating of niobium all around. The tape measures 10 mm wide by 1 mm thick and uses copper with a low temperature resistance ratio of 200. This amount of copper provides sufficient stabilization so that additional metal tapes are not required. This final cable concept is shown in Figure 2-32.

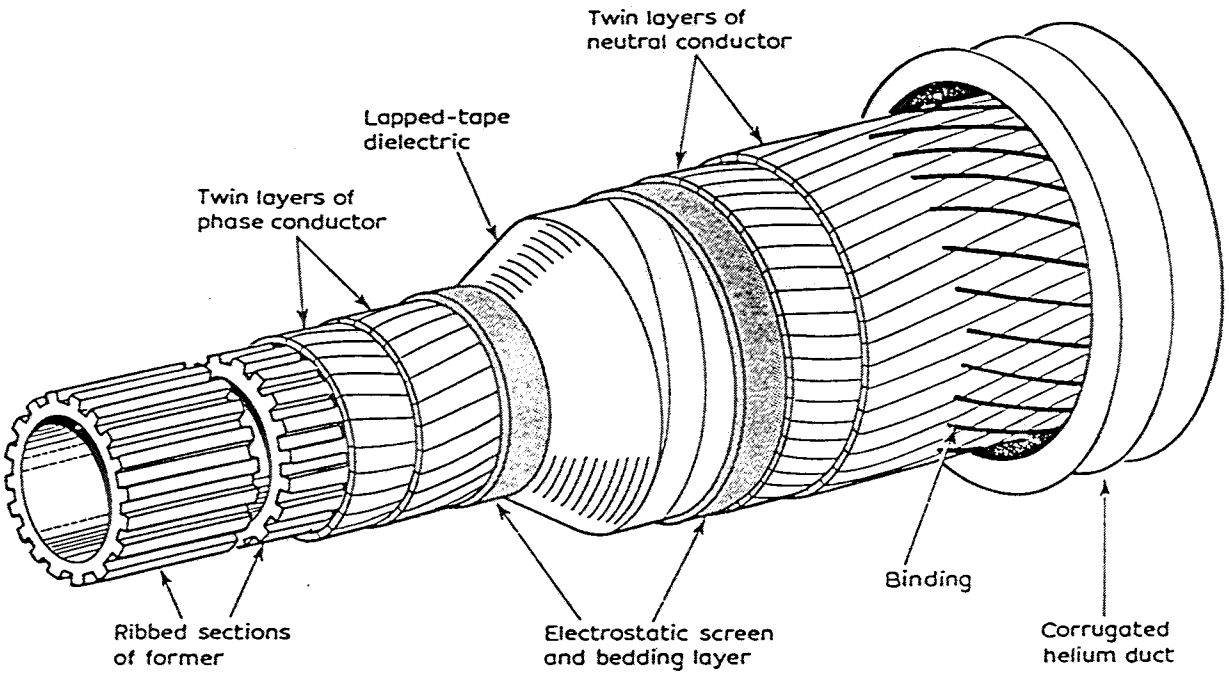

Figure 2-32 Final flexible cable concept of CERL program[68].

In Germany, Siemens AG built and tested a 35 meter single phase cable culminating an eleven year program that began in 1968[69]. The early design was a rigid tubular design similar to the Linde design, except a fourth inner duct with thermal insulation was

included in the cryostat to isolate the go and return flows. The final concept was a flexible coaxial cable which used niobium-plated aluminum wires rather than tapes. Their three phase assembly is illustrated in Figure 2-33.

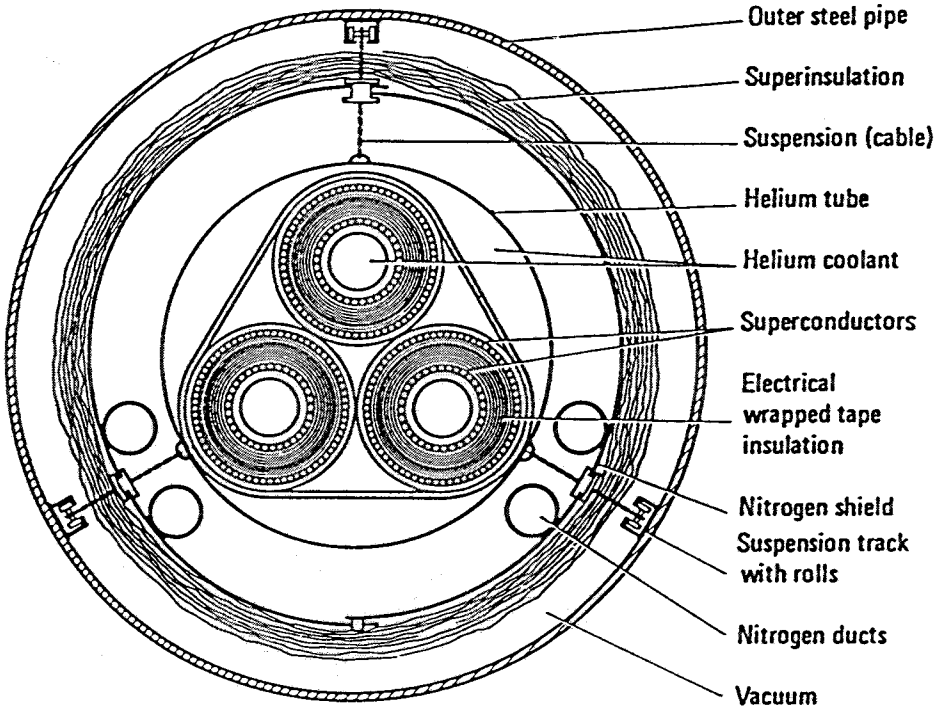

Figure 2-33 Siemens concept for a 110 kV, 10 kA AC cable system[69].

The cryostat has some interesting innovations. The outer steel pipe enclosure is equipped with three small tracks that allow the inner parts of the cryostat to be "rolled" into the outer pipe. The liquid nitrogen shield is made of four sections of copper, each with its own nitrogen duct soldered in place. The helium tube is rigid with corrugated sections periodically to account for contraction. This design is similar to the CERL design shown in Figure 2-29, but appears to be much simpler. A five-meter section was carefully characterized for thermal performance. The heat leak from ambient to the liquid nitrogen shield was 2 watts/meter and the leak into the helium duct was 0.1 watts/meter. This data is consistent with most constructions of this style.

liquid nitrogen shield was 2 watts/meter and the leak into the helium duct was 0.1 watts/meter. This data is consistent with most constructions of this style.

The cable is notable for its use of single layer conductors made of 3 mm diameter wires. Two wire structures were developed, the first being a co-extrusion of niobium over an aluminum core and the second being a Nb_3Sn made on a copper core by the solid state diffusion process. The latter was the preferred choice because of its higher operating temperature, other parameters being about equal. The test cable was made with the niobium-aluminum wire because of time restrictions on the wire production.

The dielectric was an alternating mixture of a 4 mil high density polyethylene film tapes and fibrous tapes, the latter known as Tyvek. Again, time restraints on the test cable production prevented the use of laminated or cross-linked HDPE tapes which were preferred because of better mechanical properties. The operating stress was 5 kV/mm. Partial discharge inception was found to be 10.4 kV/mm and an AC breakdown stress was 13 kV/mm. It was thought that the axial field in the stress cones was responsible for the relatively poor performance of this dielectric design.

The use of a single layer conductor assembly causes an axial field in the core and outside of the outer conductor. This does not cause additional loss because there are no metal components in these areas, the core support and the skid wires being plastic. Also, the stabilizing metal is the aluminum core of each wire and is totally surrounded by superconductor, therefore shielded from all fields. However, in the single phase configuration, the helium pipe experiences this field and would suffer eddy current loss. The three phase arrangement would experience a reduced loss due to the three phase field cancellation, but local eddy currents would still exist as in conventional pipe-type cables. The helium pipe in the 35 meter test bed was made of invar and internally coated with niobium to eliminate the eddy current loss. The total current losses measured in the test bed were less than one watt at 10,000 amperes (about 0.03

watts/meter). Siemens recognized the problem of the single layer conductor and suggested that "real" cables would probably use a double layer. A photograph of the test cable is shown in Figure 2-34.

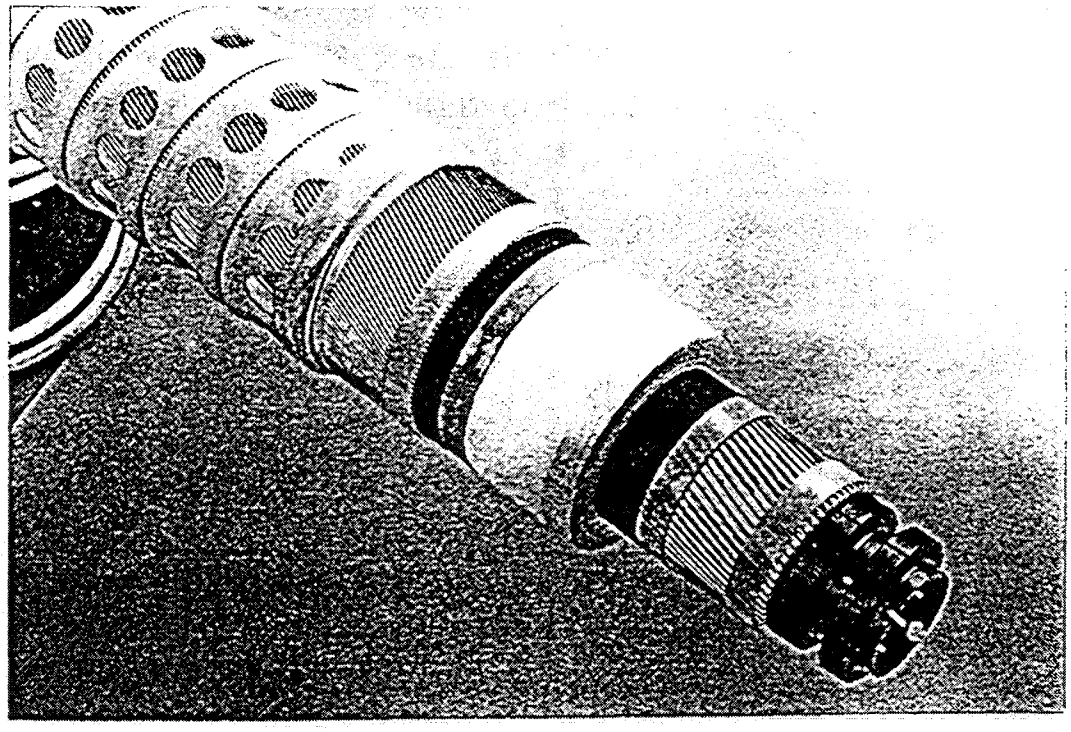

Figure 2-34 Photograph of Siemens 110 kV, 10 kA test cable[69].

It should be noted that in 1974 G. Bogner of the Research Laboratories of Siemens AG, Erlangen, Germany authored an extensive and complete treatise on the science and engineering of superconducting cables[70]. This 147 page chapter is still the most thorough work on this subject one can find in the literature.

The other program in Germany was that of AEG-Telefunken. Their work started in the late sixties with the manufacture of DC test samples up to fifty meters in length in conjunction with Kabelmetal AG and Linde AG. This program continued through the seventies also with funding assistance from the federal government. The DC cable that evolved consisted of a single layer of Nb_3Sn tapes stabilized with copper on both sides

assembled over a Teflon former, insulated with cable paper with carbon black paper screens and a metalized paper outer shield. This single conductor cable is placed inside a four-tube corrugated cryostat with a liquid nitrogen shield manufactured by Kabelmetal, identical to that used by Professor Klaudy at Arnstein. A photograph of the cable tested appears in Figure 2-35.

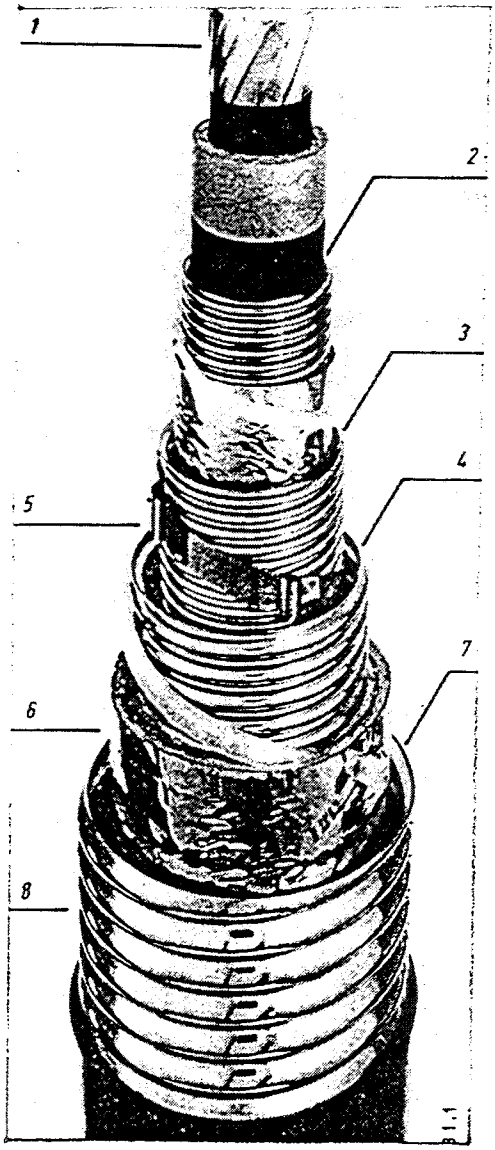

1 - Nb_3Sn Tapes, single layer and helium in core.

2 - Paper dielectric system and helium channel.

3 - Vacuum and superinsulation.

4 - Flowing liquid nitrogen.

5 - Metal separator.

6 - superinsulation.

7 - Vacuum.

8 - Outer tube of cryostat, with PE jacket.

Figure 2-35 Photograph of AEG 200 kV, 10 kA DC test cable[71].

This cable was tested in two different test beds. The test for current also demonstrated that the cable will function in the bent state. A circular ring was set up with four iron core current transformers spaced at ninety degrees. The cable was joined to itself to form a superconducting one turn secondary. The DC critical current of the cable was found to be 25 kA in this unique test bed. The second test was more conventional. The cable was arranged with a terminal at each end. A test program equivalent to the qualification program recommended by CIGRE in conformance with IEC specifications was performed, but the cable system failed at 240 kV DC (18 kV/mm maximum stress) in a terminal[72]. Because of the terminal failure, surge tests were not performed.

Several programs were carried out in the U.S.S.R. For the years 1973 through 1980 there was a formal technical exchange program between the U.S. and the U.S.S.R. on the topic of superconducting transmission[72]. BNL was the principle party from the U.S. and the Kryzhanovsky Power Engineering Institute in Moscow was the seat of the Soviet side of this exchange. The agreement was cancelled in 1980 as a reaction to the Afghanistan invasion. Much effort was focused on cryoresistive cables but two types of superconducting cable were built and tested. As in other countries a rigid tubular construction was the first concept put forth. An eight meter test cable was built using Nb_3Sn tapes soldered to a copper tube with Mylar taped insulation. This cable demonstrated a 21 kA capability. In the early eighties a 100 meter trial cable was installed at the Mosenergo Substation. There are no further details of that installation, and no high voltage testing was done on this construction. A fifty meter flexible cable using Nb_3Sn tapes over a single layer copper core was built at the Moskabel plant for a program at the All Union Scientific Research Institute of the Cable Industry in Podolsk. This coaxial cable used conventional paper for its dielectric and was installed in the popular Kabelmetal four-tube corrugated cryostat. The cable had a design rating of 2400 MVA at 110 kV (12.5 kA). A conventional U-shaped layout with two terminations was used for the test set-up. As of 1982 the cable had undergone cryogenic and current tests, but no high voltage tests[73].

Programs began in France in the mid sixties. The principle organizations involved were the engineering and laboratories of Electricite de France (EDF), Compagnie General d'Electricite (GE), Cables de Lyon and Air Liquide. Cryoresistive cables sized for 1000 MVA and both AC and DC superconducting cables sized for 3000 to 5000 MVA were studied analytically and experimentally. The superconducting system designs are illustrated in Figure 2-36 below.

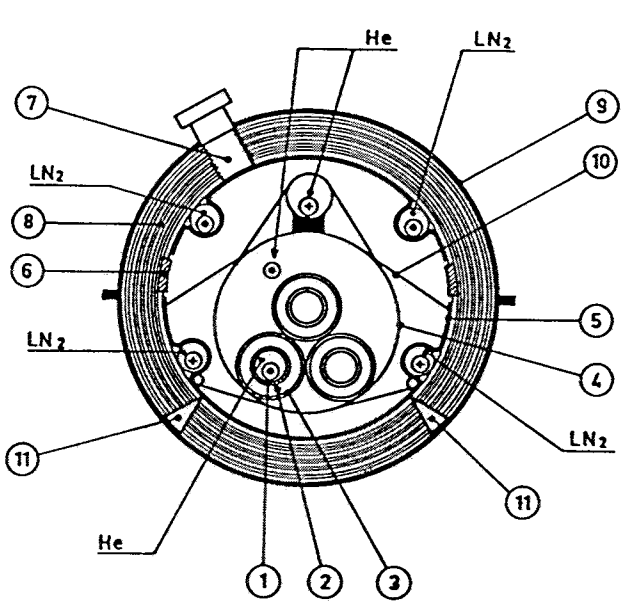

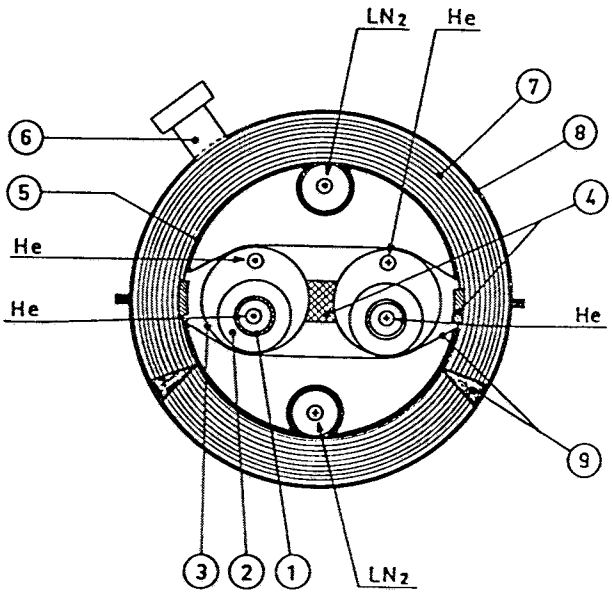

Three-phase 5 000 MVA superconducting A.C. cable.

1 - *Phase conductor (copper shunted niobium).*
2 - *Polyethylene film ribbon.*
3 - *Electromagnetic shield (copper shunted niobium).*
4 - *Invar 4 K vessel.*
5 - *77 K (invar and aluminium isotherms) thermal shield.*
6 - *Thermally insulating spacers.*
7 - *Pumping funnel.*
8 - *Superinsulation.*
9 - *700 mm outer diameter 300 K steel vessel.*
10 - *Hanger device system.*
11 - *Thermally insulating support carrier.*

5 000 MVA superconducting D.C. cable.

1 - *Copper stabilized Nb_3Sn pole conductor.*
2 - *Mylar film ribbon.*
3 - *4 K vessel.*
4 - *Thermally insulating spacers.*
5 - *77 K thermal shield (invar + aluminium isotherms).*
6 - *Pumping funnel.*
7 - *Thermal insulation (vacuum superinsulation).*
8 - *300 mm outer diameter steel 300 K vessel.*
9 - *Hanger device systems.*

Figure 2-36 AC and DC superconducting system concepts of EDF[75].

The AC cables were based on niobium coated copper tapes and the dielectric was liquid helium-impregnated polyethylene film. The DC designs used Nb_3Sn tapes with a Mylar tape dielectric impregnated with supercritical helium, taking advantage of the higher operating temperature of the Nb_3Sn material. Dielectric studies were also performed on

Mylar tape cable models operating in vacuum so that the dielectric could be made a part of the thermal insulation system. This concept was not pursued to the prototype stage.

The best reflection of R&D work in the European Community is via the CIGRE Working Group 21, which can also include members from all other parts of the world when there is interest. By 1982 the work on superconducting transmission had all but stopped. The situation is summarized by the following comment of C. Jacobsen, the WG-21 Special Reporter for the 1982 CIGRE General Meeting in Paris, taken from his Special Report from Group 21[75].

> "....
>
> Techniques are available today, or in the final stages of development, which permit the transmission of up to 10 GVA (21-04). Paper-insulated OF-cables (low or high pressure OF) rated up to 525 kV AC and conductor cross-section to approximately 2500 mm^2 copper (21-06) are available. XLPE and PE cables approximately 275 kV AC at approximately 1000 mm^2 copper (21-09) and EPR insulated cables to approximately 132 kV AC. In the naturally-cooled mode, technical solutions are available, permitting transmission capabilities of approximately 1500 MVA in OF cables. Through externally forced cooling it is possible to increase the capacity to approximately 2000 MVA (21-03). When internal conductor cooling is used, higher ratings may be achieved (21-01). For still higher ratings, compressed gas insulated cables (CGIT) are available (21-04).
>
> This situation has virtually eliminated interest in cryo-cables and superconducting cables.
>
> ....."

Cryoresistive Cable Projects

The evolution of the cryogenics industry brought on by the development of the Collins cryo-generator in the late fifties, and fed by the "race to space" during the sixties also spawned interest in high capacity cables that used copper or aluminum conductors cooled to very low temperatures, in parallel with the interest in viable superconductor systems discussed above. In this time frame the unusual behavior of the resistivity of

metals at very low temperatures occupied many research laboratories. Linear extrapolation of the resistivity verse temperature characteristic from the normal temperature range to the point of zero resistivity intercepts the temperature axis in the range of 30 to 60 K, specifically for 100 % IACS conductivity copper the zero intercept is at 38.65 K and for 64 % IACS conductivity aluminum this value is 56.65 K. The question of what happens to the resistivity at temperatures below this intercept intrigued many, including Omnes as mentioned in Section 1. For metals that are not superconductors, their resistivity approaches zero and levels off as the temperature is lowered. The ratio of the resistivity at 273 K to that at 4 K has been labeled R or sometimes RRR, either standing for the Relative Resistivity Ratio so defined. The purity of the metal determines how large its R value will be. The graph in Figure 2-37 illustrates this behavior for high purity copper and aluminum, each with an R of 1000, and typical copper with an R of 100.

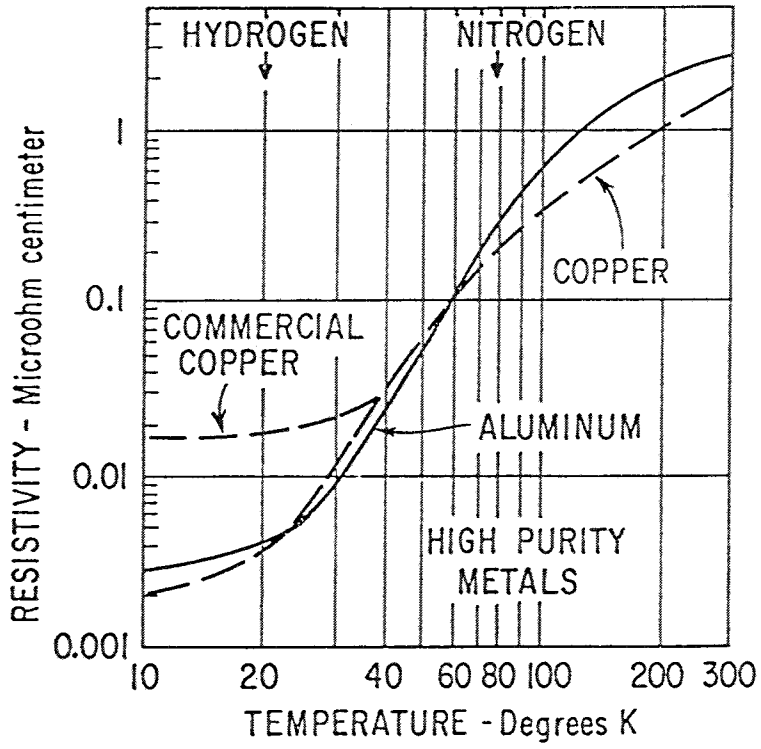

Figure 2-37 Resistivity verse temperature, copper and aluminum[76].

It can be seen that at 20 K the resistivity is roughly three orders of magnitude lower than at 300 K, and aluminum is actually lower than copper in the 25 to 55 K range. In contrast, the resistivity at 77 K, liquid nitrogen's temperature, is reduced by less than an order of magnitude. The energy cost of refrigeration is about 100 watts/watt at 25 K verse 10 watts/watt at 77 K. Thus, the 25 K range has the potential for an order of magnitude reduction in the final cost of ohmic losses, other things being equal. For this reason, the first studies of cryoresistive cables focused on the use of hydrogen as the cryogen so that operating temperatures around 25 K could be used. The only problem associated with the use of hydrogen was the safety question, but safety was claimed to be no different than a natural gas pipeline, of which there were thousands of miles installed in all kinds of conditions.

Many factors combined to shift the focus to the liquid nitrogen level in spite of the efficiency advantage of the hydrogen system. Perhaps the most convincing turned out to be the high cost of the extra-high purity metals needed to take advantage of the lower temperature, when compared to conventional copper or aluminum that would be used at 77 K. Other factors included: higher heat leak at 20 K because of the larger temperature difference, smaller skin depth at 20 K (about 15 mils in 1000 RRR copper) which complicates the design and manufacture of the very large conductors being considered, shorter development time for a nitrogen-impregnated dielectric, more realistic (smaller) power ratings, and, finally, a less complex refrigeration system for the nitrogen system. By 1970 most researchers had dropped the quest for a hydrogen system and concentrated on liquid nitrogen.

Cryoresistive systems do not require exotic cable concepts; they essentially depend on brute force. The most challenging aspect of this cable was the dielectric question. Since currents could only be increased by a factor of about three, these systems tended toward EHV voltage levels. To show an advantage in MVA capability it was necessary to use the largest conductors available so that the capacity of an EHV overhead line with

bundled conductors could be matched. This philosophy tended to dictate the design targets for system developers.

The most relevant aspects of the cryoresistive system to potential HTSC systems are the engineering of the liquid nitrogen cooling system and the performance of dielectric materials impregnated with liquid nitrogen. Both of these topics are covered elsewhere in this Document. Therefore, only an overview of the two US projects will be given.

General Electric Taped Cable Program. GE's Research Lab was one of the first to explore the dielectric properties of materials at cryogenic temperatures[76]. This interest together with their position in the electrical utility industry led to a proposal to develop a cryo-resistive cable for high power capacity. A three-part program was funded by the Edison Electric Institute and the Tennessee Valley Authority and began on February 1, 1968. Each part lasted about one year and was fully documented with an interim report[77,78,79].

In the first year dielectric properties in liquid nitrogen, hydrogen and helium were gathered, cable concepts developed (the main question was rigid or flexible?), conductor and shielding designs were postulated, and preliminary cost estimates made to evaluate each of the concepts[77]. By the end of Part A, a flexible system using aluminum conductor insulated with polyethylene paper (Tyvek) impregnated with liquid nitrogen was selected as the most appropriate solution for further development. The design capacity was set at 3500 MVA at a system voltage of 500 kV, requiring a phase current of 4000 amperes. Dielectric studies with cylindrical cable models determined the AC breakdown stress to be between 900 and 950 volts/mil (35.4 to 37.4 kV/mm) and the impulse strength to be 2300 vpm (90.5 kV/mm) at 80 psig. An optimistic design stress of 400 vpm (15.7 kV/mm) was selected. With this design stress, impulse breakdown would occur at 1656 kV, limiting this design to a BIL of 1550 kV. At this point it should have been recognized that these dielectric strengths were only 70 to 80 % of good

cable papers impregnated with dielectric fluid. On the other hand, the power factor (tan δ) of the Tyvek/nitrogen material was on the order of 0.01 %, three times lower than the requirement established by system studies.

The second year was spent doing detailed design studies for the 3500 MVA flexible system[78]. These included designs for terminals and splices (both normal and nitrogen feed-type) and extensive work evaluating refrigeration options. The cross-section of the proposed 3500 MVA 500 kV cable is shown in Figure 2-38.

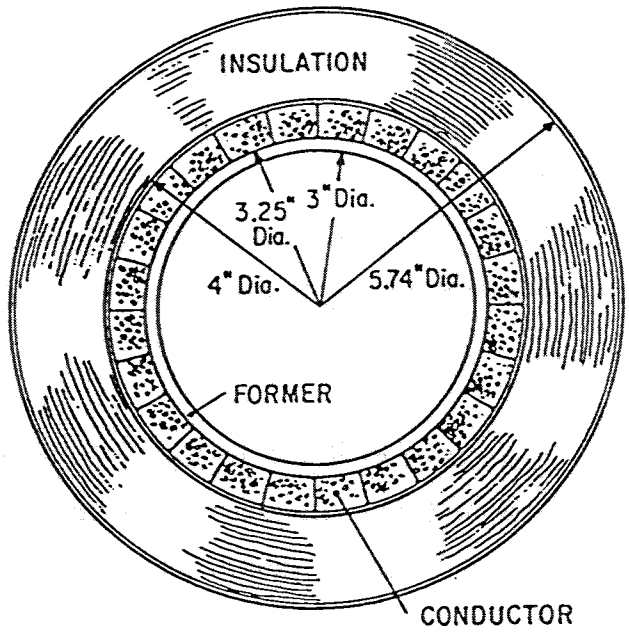

Figure 2-38 GE's 3500 MVA 500 kV cryoresistive cable concept[78].

A two-stage neon refrigerator with a capacity of 1 megawatt at 65 K was selected as the base unit that could handle five miles of cable at its rated load. A thermally insulated return pipe was required by this design as shown in Figure 2-39 to avoid counterflow heat exchange across the cable dielectric. The questions of reliability, redundancy and availability were addressed. Finally, a single-ended test setup was designed to allow high voltage testing to be done on a forty-foot trial cable. This would be the basis for the third year's program.

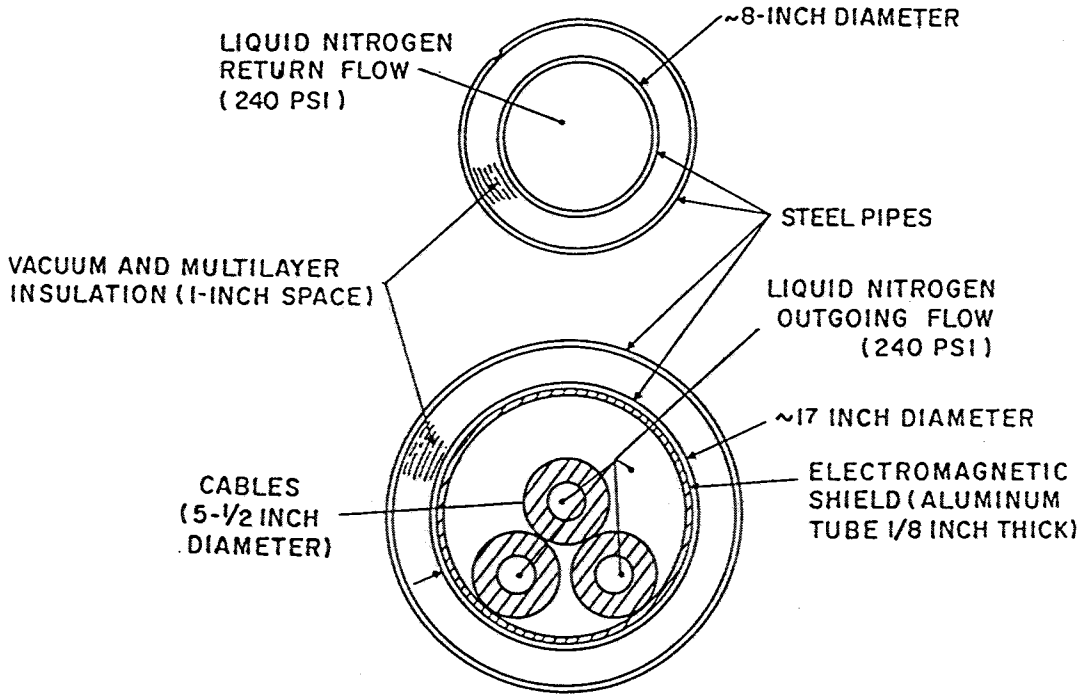

Figure 2-39 Assembly of 3500 MVA 500 kV GE cryoresistive system[78].

In the third year, a prototype cable was manufactured by Phelps Dodge and tested in the Phelps Dodge EHV laboratory. This cable was insulated with 850 mils (21.6 mm) of Tyvek using 5 mil and 8 mil tape thicknesses, and hand-carried to the test lab without bending. Two AC breakdown tests were made with disappointing results. This test cable was designed for a maximum operating stress of 425 vpm (16.7 kV/mm) at 290 kV conductor to shield. The first setup operated at 290 kV for four days, but when the voltage was raised to 350 kV very high discharges occurred which caused the test to be aborted. The problem was found to be particles on the surface of the stress cones. A second length of cable was installed with improved hardware. This cable failed at 435 kV (640 vpm or 25.2 kV/mm) after forty hours at rated voltage and fifteen hours at 1.3 times rated voltage (375 kV). The maximum stress at breakdown was only 640 vpm (25.2 kV/mm). The cross-section of this prototype cable is shown in Figure 2-40.

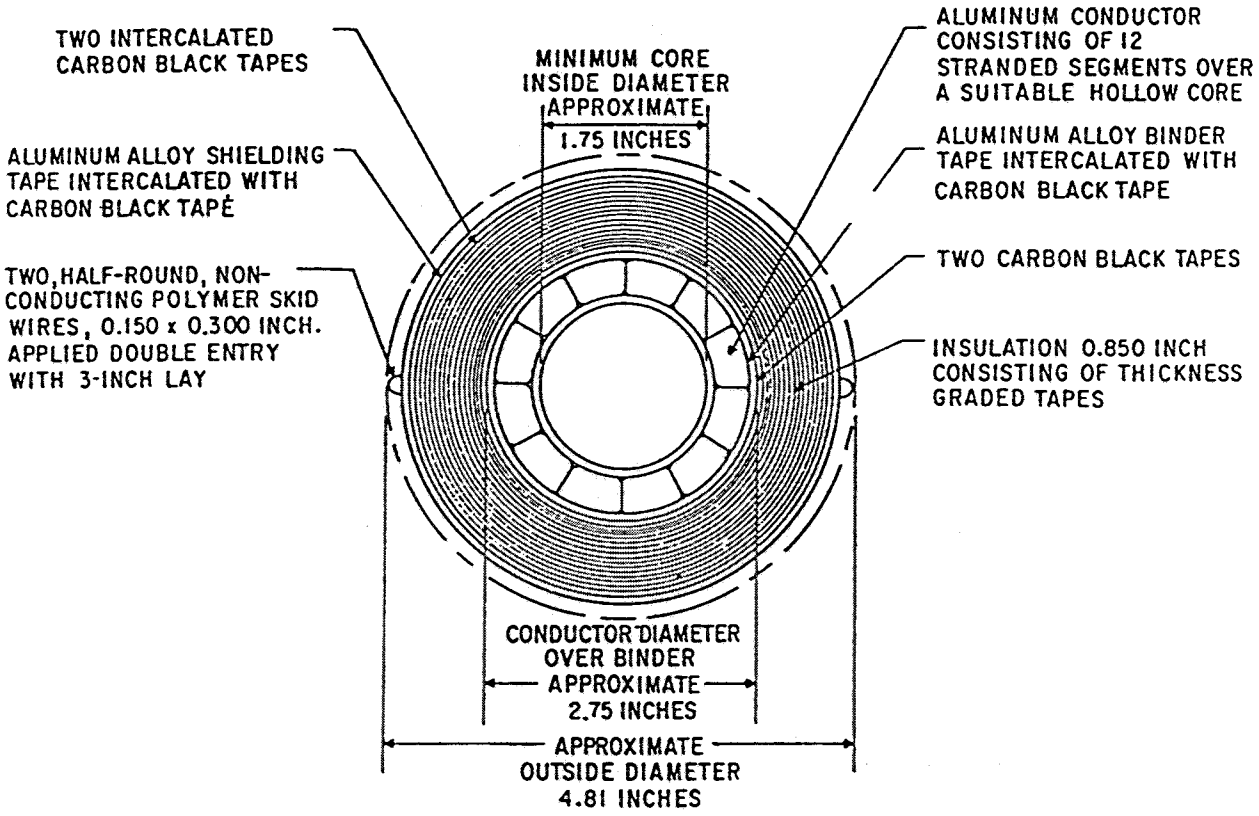

Figure 2-40 Prototype cryoresistive cable made by Phelps Dodge for GE[78].

Following this initial program, GE proposed a ten-year long-term program to complete the development of commercial cryoresistive cable systems. The first five years would refine the dielectric system and design and build a 1000 foot three-phase current-loaded test cable demonstration facility. EEI, DOI (ERDA) and TVA funded a two-year program (Phase II) from April 1972 to April 1974 which addressed the dielectric situation, assessed fiber-reinforced epoxy pipes with foam insulation, designed cable accessories, and prepared a specification for the proposed test facility[80].

Three dielectric materials were studied experimentally in a 50 kV multi-sample cryostat and three 200 kV cylindrical cryostats. The materials were an improved calendared and higher density polyethylene spun-bonded paper, conventional cable paper, and PPP.

Paper had the highest AC strength but a high dissipation factor. The calendared polyethylene paper had a much higher strength than the early Tyvek and very low dissipation factor. The PPP materials were in between in both parameters.

Phase III followed, supported now by EPRI and ERDA, for the period April 1974 through March 1977. Paper was selected as the dielectric for another full-sized cable trial because it had demonstrated the highest dielectric strength. Analysis of the high loss aspect of paper showed that total system losses would increase by about ten percent. The emphasis was also shifted to a foam-insulated enclosure, based on the findings in Phase II[80]. The electromagnetic shield was placed outside of the foam thermal insulation. A FRP pipe contained the liquid nitrogen at high pressure and was the inner member of the thermal insulation system, as shown in Figure 2-41.

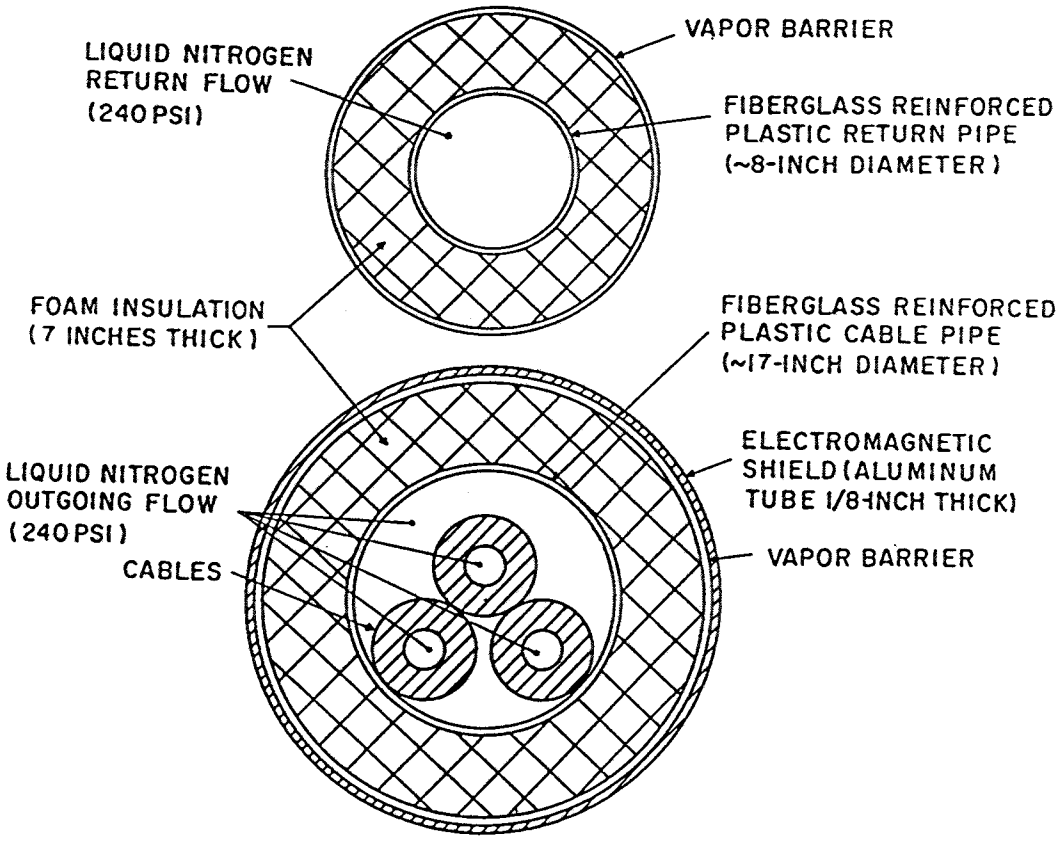

Figure 2-41 Foam-insulated cryo-resistive system proposed by GE[80].

The second trial cable was built and tested by Anaconda. 1000 feet of a large (4632 kcmil, O.D. of 3.03") eight segment hollow core aluminum conductor was fabricated. Two sections, each about 350 feet were insulated with conventional EHV cable papers. The first had a 0.860" wall and the second had a 0.550" wall, made by omitting the final 310 mils of tapes in the taping operation. The reduced wall was made to insure that an AC breakdown could be obtained within the 500 kV test limit of the Anaconda High Voltage laboratory. A foam-insulated FRP double ended test setup was supplied by GE which included foam insulated FRP tubular terminations. Four pieces of the 550 mil wall cable and one piece of the 860 mil wall were tested to breakdown with an AC step schedule. All of the failures were associated with the terminations (one involved the power factor gap at the base of the termination). The highest cable stress demonstrated was 860 vpm (33.9 kV/mm), more than twice the rated stress.

The final report of the work done in this three year period[81] contains a wealth of information and engineering analysis on foam-insulated FRP pipes, cable splice and termination design, test station design, liquid nitrogen refrigeration systems and total system analysis.

The GE system was one of the candidates in the Philadelphia study[33]. Four 3750 MVA, 500 kV (4330 amperes) circuits were required, each with a non-hollow 5000 mm^2 (9700 kcmil) aluminum conductor insulated with 2.34 cm (920 mils) of paper. An optimistic refrigerator efficiency of 7.8 watts/watt was claimed. Unfortunately for this technology, this system was the highest cost alternative in this study. The refrigeration plant capital cost plus the capitalized cost of losses was 52% of the total cost of this system. EPRI and ERDA elected not to continue with Phase IV of this program.

In 1977 another system study was funded by DOE (Contract EC-77-C-01-5087) which was performed by the Public Service Electric & Gas Company and GE[82]. This study compared the GE cryoresistive cable system to a conventional heavily forced cooled

HPFF alternative for a 3000 MVA 500 kV 34 mile underground system to be inserted in the PSE&G 500 kV overhead network. This study gave GE a chance to develop algorithms that could be used to identify those aspects of their design that were the most sensitive to cost reduction. Modifications of design parameters resulted in cost reductions of 10 to 40% relative to the Philadelphia study[33]. The study compared two versions of a single circuit cryoresistive cable against a three-circuit HPFF cable installed sequentially over fifteen years. The two cryoresistive options were a multi-layer vacuum-insulated pipe and a foam-insulated FRP pipe. The multi-layer vacuum-insulated pipe was less costly than the foam/FRP system and about equaled the cost of the HPFF system.

Graneau's vacuum-insulated cryoresistive cable. Graneau's concept was based on the use of vacuum as a combined dielectric and thermal insulation in a surprisingly simple configuration that consisted of three conductor "pipes" supported by occasional spacers in an evacuated outer pipe. Work began in 1967 while Graneau was in the R&D laboratory of the Simplex Wire and Cable Company with the initiation of an internally funded program[83]. The initial concept consisted of three aluminum tubes in an aluminum shield covered with multi-layer superinsulation. Only the conductor tubes contain liquid nitrogen at high pressure. The rest of the system is evacuated. This concept is shown in Figure 2-42.

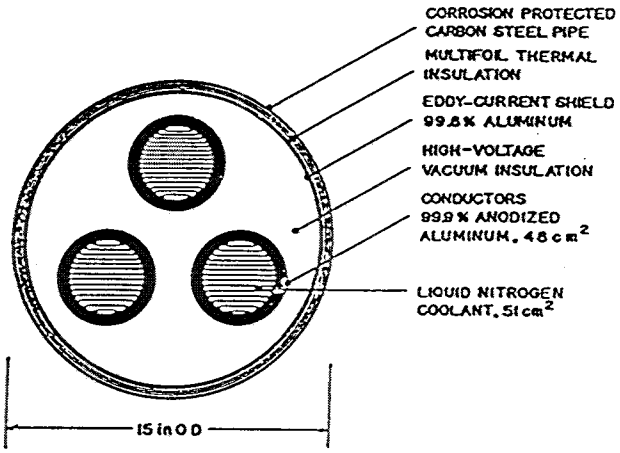

Figure 2-42 Graneau's initial vacuum-insulated system concept[84], sized for 345 kV.

A test stand was built for the dielectric testing of 10-foot coaxial cable models which achieved maximum test levels of 150 kV AC and 770 kV impulse which correspond to a maximum stress on the surface of the conductor of 142 vpm AC and 730 vpm impulse. The conductor dimensions were 2" OD for the inner conductor and 5.75" OD for the outer conductor.

Dielectric studies found that initial conditioning of the electrode surfaces was required, and would entail a substantial effort, possibly with a high temperature outgassing phase in addition to energization with a high voltage source capable of repeated sparking. This conditioning must be done after the final evacuation due to the surface absorption of any gas present in the vacuum space. Studies on the destructive risk of such voltage conditioning with a low impedance source were perhaps unconvincing. Implications were that occasional sparkovers would occur based on the statistical nature of the breakdown of vacuum gaps associated with very large surface areas, but these would be cleared without damage to the affected areas, just as in overhead lines.

In 1969 a test terminal using a clear Pyrex glass bushing was installed at the ERC/Westinghouse Waltz Mill test facility. The results of this trial were not published implying that this experience was unsuccessful[85]. A U.S. Patent, 3,522,360, issued July 28, 1970, was obtained which covers an ion-shield concept for vacuum-insulated systems. The same concepts are used in the spacers developed at Simplex.

In the early seventies Graneau left Simplex and formed his own company, the Underground Power Corporation. A grant from the National Science Foundation allowed his work to continue at M.I.T. Part of the academic work done for this concept involved the affect of the magnetic field caused by current flow on charged particles in the vacuum space. A double ended test loop test loop capable of high voltage testing with up to 3000 amperes of circulating current was built at M.I.T. While designed for

a 138 kV voltage level, tests were conducted to 133 kV, the phase to ground voltage for a 230 kV system, and held for 50 hours while transporting 3 kAmps[86].

A parallel program to continue the development and demonstration of a termination for the vacuum insulated transmission line was funded in 1972 by DOI and EEI. This program was later taken over by EPRI and ERDA. Underground Power Corp. had the assistance of Vacuum Barrier Corporation, the Lapp Insulator Division of the Interpace Corporation and M.I.T. for this project[87]. A second 138 kV termination was installed at Waltz Mill in the mid-seventies. While AC behavior was tolerable, withstanding up to 170 kV AC, impulse testing was not. Impulse tests were performed using a discharge circuit superimposed on the AC voltage wave, presumably at rated AC voltage (80 kV). A minimum breakdown level of 200 kv negative polarity was experienced, and a total of nine breakdowns occurred between 200 and a high of 272 kV. The highest impulse withstood was about 265 kV. The conclusion of this test series was that this terminal had a BIL of 200 kV. Most conventional 138 kV transmission systems are tested to insure a BIL of at least 650 kV.

Graneau proposed a vacuum insulated system for the Philadelphia Electric study, but it was not included in the system analysis or the cost comparisons because of incomplete data and serious questions about the general viability of this concept. The concept put forth used 27,000 kcmil hollow extruded aluminum sector-shaped conductors, each with a four inch bore carrying liquid nitrogen in the pressure range of 515 to 880 psi. That's 61 atmospheres! The temperature range was 65 to 130 K. The design also featured, for the first time in Graneau's publications, a complete triangular ground shield isolating the three phases electrostatically. The system relied completely on vacuum for thermal insulation. There was no radiation shielding or supplemental external insulation. The study does not mention the number of circuits required at 345 kV or the current rating for this proposal. This final system concept is illustrated in Figure 2-43.

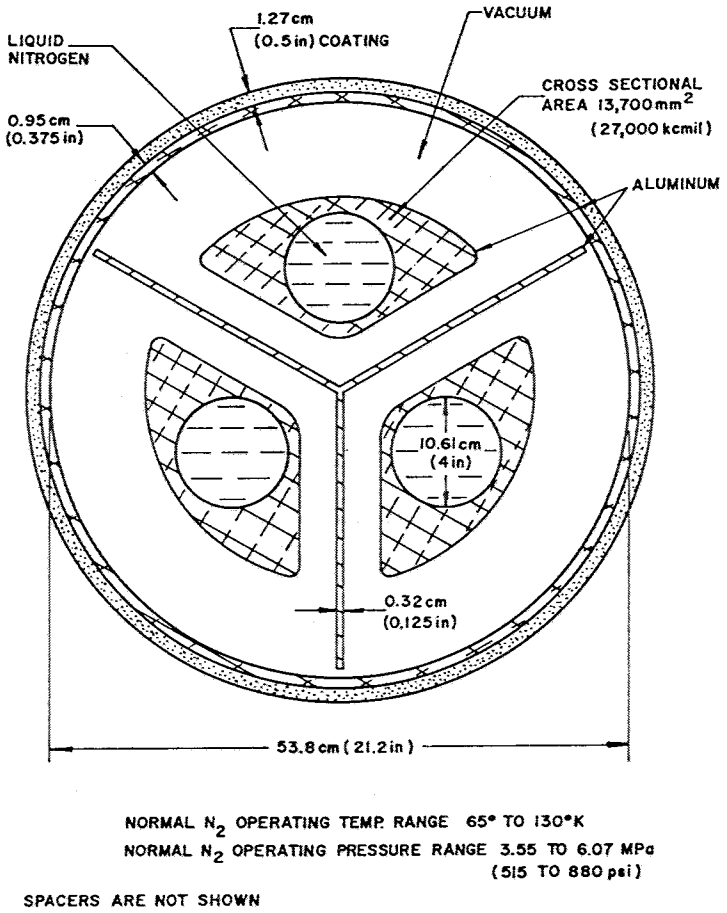

Figure 2-43 Graneau's vacuum-insulated cryoresistive cable for the PECo study[33].

Summary: Offshore cryoresistive projects. In the seventies many countries had active cryoresistive cable projects but Japan was by far the most active, due to the interest of the Japanese utilities and their research laboratories, which thereby involved all of the active high voltage cable manufacturers. The companies that built and tested trial cables, most for the 154 kV class, included Fujikura, Furukawa, Showa, Hitachi and Toshiba[88]. Test bed lengths were in the range of 10 to 25 meters. Cryoresistive cables were viewed as an intermediate step toward superconducting cables. The R&D emphasis was on dielectric materials, with Tyvek ranking high. Test cables were built using paper and Tyvek, but PPP in various forms was recognized as the most likely to succeed.

In the late seventies, as interest in high capacity systems was fading, Furukawa proposed a novel compromise[89], the use of a LPFF paper dielectric placed between thermal insulation layers such that the dielectric would operate in the range of -40 to -80 C. At this temperature low viscosity fluids such as DDB remain fluid and can be pressurized in the normal fashion, except that thermal duty on the pressurization system is greatly reduced because the dielectric operates at essentially constant temperature. This concept, in a single conductor form, is shown in Figure 2-44.

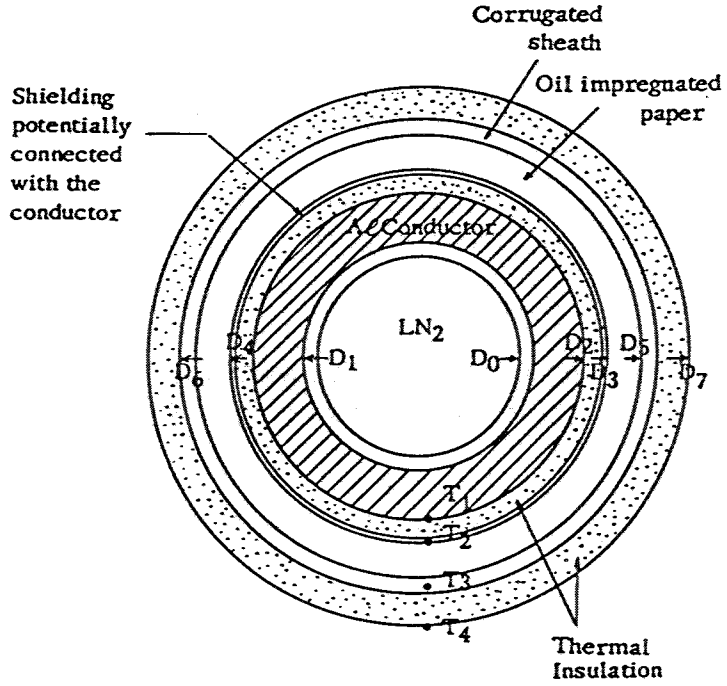

Figure 2-44 Furukawa's intermediate temperature LPFF cryoresistive cable concept[89].

In France, the EDF considered cryoresistive cables to be straight-forward in design and construction. However, the high losses made this technology non-competitive with conventional alternatives or superconducting cables. A design that was analyzed in some detail used Tyvek as the dielectric, and aluminum conductor and superinsulation. This is shown in Figure 2-45. The thermal enclosure is slightly different from those proposed for superconducting cables in Figure 2-36.

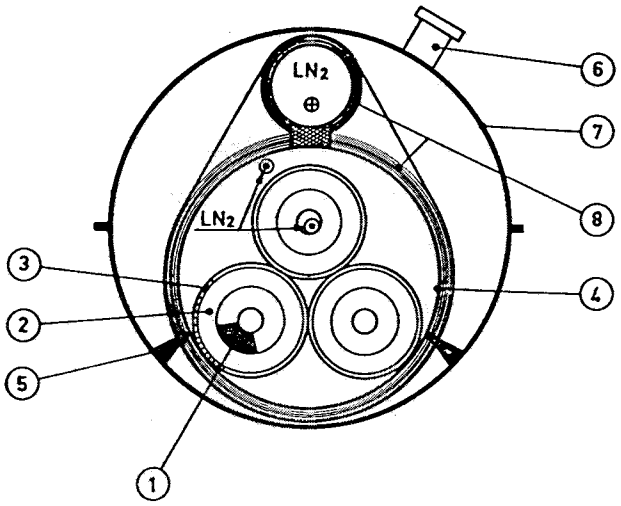

Three-phase cryoresistive A.C. cable (1 000 MVA).

1 - Aluminium conductor.
2 - Fibrous polyethylene sheet ribbon (Tyvek).
3 - Aluminium electromagnetic shield.
4 - Invar 77 K vessel.
5 - Hanger system.
6 - Pumping port hole.
7 - Steel 300 K (500 to 600 mm) vessel.
8 - Thermal insulation (vacuum superinsulation).

Figure 2-45 French concept of cryoresistive system[75].

Cryoresistive studies in the U.S.S.R. continued into the eighties. In 1983, four experimental cable systems were reported under test, each made in a different manufacturing facility[73]. Paper dielectrics were used in all cases, the differences between constructions being in the conductor design and material, aluminum being the preferred choice for economical reasons. By contrast, work on cryoresistive concepts in Germany was terminated by 1975 because of the poor economics found for this type of system.

As of 1992 we know of only one active project on cryoresistive cable systems which is taking place at KERI, the Korea Electrotechnology Research Institute.

Liquid-Nitrogen Cooled HTSC Cable Concepts

Impact of HTSC Materials on Power Transmission Cables

The discovery of HTSC materials which hold the promise of operation in the 77 K temperature range has stimulated a re-evaluation of superconducting power transmission systems which can be based on liquid nitrogen cryogenics rather then the helium-based systems required for LTSC cables. The full impact of the new HTSC materials won't be known until they reach practical performance levels, but the shift to the higher temperature range has a significant impact on other aspects of a superconducting cable system, most notably on the refrigeration system, its energy consumption, and the losses that can be economically tolerated.

All AC LTSC designs were driven by two factors that may not apply to HTSC-based cable systems. First, the refrigeration energy cost for cooling cables to temperatures below 10 K is 300 watts/watt or higher. This placed the utmost demands on the minimization of losses. Secondly, system capacity targets were set at very high levels in anticipation of continued growth and economies of scale. Cable designs were required that could not use conventional cable concepts and materials because of the necessity to reduce ohmic and dielectric losses to the absolute minimum possible. HTSC cable systems operating in the 65 to 80 K range will require only about 10 watts of power to extract one watt of cable loss and heat inleak. This dramatic reduction in energy consumption will have a major impact on the potential of HTSC cable systems. They will be economically competitive over a broader range of applications including the lower power circuits now being installed by utilities. The capitalized cost of energy over the life of the system can be from 30 to 60 percent of the total system cost for modern HPFF cable systems installed for bulk power transfer of 500 to 1000 MVA. If the HTSC alternative can halve the energy consumption, it can tolerate material and installation costs that are fifty percent higher than pipe cable systems. With some luck in the control of AC conductor loss with the new materials, energy reductions of three to four times might be obtainable. The fact that higher losses can be tolerated, within

reason, will give the cable designer flexibility in his design options. In the discussions that follow, this aspect of superconducting cable design will be developed.

The comparison between LTSC systems and possible HTSC systems identify some subtle differences that might lower the cost of the HTSC cable. The conductor configuration can be simplified, depending on the forms that evolve for the HTSC material, to minimize the component and fabrication expense. The dielectric can be LN_2-impregnated PPP or even paper, both of which can be applied with existing commercial equipment and minimal demonstration. Finally, the cables may not require a superconducting outer conductor to minimize losses. This could reduce the amount of superconducting material by more than half relative to the fully coaxial design of the LTSC system, and simplify cable assembly and handling as well.

The requirements for thermal insulation differ little for the two cases. Radiative heat transfer varies as $T_H^4 - T_L^4$, where T_H is the high temperature surface and T_L is the low temperature surface. Since the difference between ($300^4 - 5^4$) and ($300^4 - 77^4$) is negligible (about 0.5%), radiative heat in-leak is essentially the same whether the low temperature is 5 K or 77 K. The quality of the thermal insulation may be slightly more difficult to achieve at 77 K than at 5 K because of reduced self- or cryo-pumping. At 5 K all gases except helium are solids with low vapor pressures. The vapor pressure of hydrogen at 5 K could be a problem, but hydrogen is easily removed with "getters", compounds that absorb gases when cooled. Thus, such a system is essentially self-pumping because it condenses out all gas except helium and creates an ultra-high vacuum. 77 K is the boiling point of N_2 and only slightly below the boiling point of O_2. These most abundant gases in the atmosphere have high vapor pressures at 77 K, and relatively little cryo-pumping will take place. This situation requires aggressive use of "getters", pre-flushing with a high boiling point gas like CO_2, and maintenance of high vacuum within the cryostat. The conductive heat in-leak will be reduced by about 25% because this heat leak depends linearly on the temperature difference. Since the

conductive heat leak is roughly equal to that of the evacuated superinsulation, the actual heat in-leak is likely to be about 10% lower for the system that operates at 77 K.

Conventional power transmission cables are comprised of a conductor assembly surrounded by a dielectric system which in turn is enclosed in a grounded metallic member that serves as the dielectric shield, and a system enclosure which contains the operating pressure necessary for proper dielectric function and protects the cable from the earth environment. The pressure medium is a dielectric fluid or Nitrogen gas. The conductor material is stranded copper or aluminum, depending on the economic trade-offs at the time of manufacture. The dielectric is vacuum-dried fluid-impregnated paper or PPP. The enclosure may be a steel pipe holding all three phases (HPFF), or lead or aluminum sheaths over each phase (SCFF).

Ohmic losses occur in the conductor when the cable carries current. Ohmic losses also occur in the dielectric shields and enclosure due to induced circulating currents, eddy currents and hysteresis caused by the AC magnetic fields created by the currents in the three conductors. Dielectric losses occur in the dielectric due to the applied voltage. These losses appear as heat and cause the cable temperature to rise until the heat dissipation to the surroundings balances the heat generated by the losses. Thermal degradation of the cellulose in the dielectric limits the temperature at which the system can operate and there-by establishes and limits the power transfer capability of the system.

The concept of a superconducting cable is to replace the metallic conductor with a superconductor that can carry a larger current with lower ohmic loss. The complication is the necessity to maintain the temperature of the superconductor at a cryogenic level. This requires a channel for the flow of the cryogen and a cryostat to thermally insulate the superconductor and cryogen from the surroundings. Fortunately the superconductor can support a very large current density so little material is needed for the conductor

function. This leaves space for the cryogen channel and cryostat and allows a superconducting cable to be comparable in size to, or smaller than a conventional cable, an important consideration since more than half the cost of conventional underground installations is the digging of the trench to house the system.

LTSC designers quickly found that the AC magnetic fields acting on normal metal components created unacceptable losses in the cable shields and enclosures due to eddy currents and circulating currents. Their only option was to make the outer shielding of the cable also superconducting. In this coaxial form the outer superconductor will experience an induced current equal and opposite to the current in the inner conductor which confines the magnetic fields to the space between the two and eliminates the driving force for eddy currents and circulating currents in the outer metallic components. The truly coaxial cable has the lowest inductance possible for a given dielectric spacing, which results in the lowest surge impedance obtainable. However, the cryogenic aspects of the cable are more complex because the entire cable must be maintained at the cryogenic level. The dielectric must therefore be able to function immersed in the cryogen at low temperature and dielectric losses must be removed by the cooling system. Thus, all AC LTSC cable designs have required cryogenic dielectrics and two coaxial superconductors for each phase. Cost and space considerations favored the placement of the three phases in one large cryostat. The rigid design developed at Union Carbide and the flexible design demonstrated at Brookhaven shared this overall arrangement, as did most cable concepts put forth around the world. While the coaxial, fully cryogenic cable may be necessary for very high current applications of the future, the lower power levels in use today and for the near future open the door to simplification and subsequent cost reductions that take advantage of the reduced refrigeration penalty afforded by a liquid nitrogen cryogen.

As the first consequence of a smaller current carrying requirement, one asks if the superconducting outer shield is still mandatory or would it be possible to revert to

conventional shield structures and tolerate the additional losses? The answer is yes! With careful shield optimization the shield loss can be reduced to an acceptable level. The next question is what about magnetic field interactions? The effect of normal fields on the surface of a superconductor may be severe, but at lower currents and fields, it too may be tolerable. The lack of phase-to-phase magnetic isolation raises the inductance and surge impedance and reduces the surge impedance load, but at lower power levels a lower SIL is desirable. The most significant consequence affects the dielectric. If the outer shield is not superconducting, there is no reason for the dielectric to operate at cryogenic temperature. This means that a very simple design put forth for LTSC DC cables in the early seventies could be applied to HTSC AC cables. This concept placed the conductor inside a small flexible cryostat which was covered with a dielectric that operates at room temperature.

One lesson learned during the development of LTSC cable systems was that a new dielectric design for a high voltage cable system and its subsequent qualification is not a trivial task. Many researchers found that the introduction of a new dielectric system was far more difficult than qualifying a radically new superconducting conductor assembly. Dielectric concerns contributed to the lack of acceptance of LTSC concepts. The Kabelmetal system which used conventional paper impregnated with supercritical helium was the only system to be demonstrated by connection into a Utility's operating transmission line. The use of a well-developed dielectric system operating at room temperature will eliminate this formidable hurdle and increase the probability of an early successful system demonstration. We have therefore focused on the room temperature dielectric cable concept as our first choice for immediate development, recognizing, of course, that fully coaxial, cryogenic dielectric systems may also be of interest for future higher power levels.

Room Temperature Dielectric Designs

AC Cable Systems. Figure 2-46 illustrates a room temperature dielectric pipe-type cable system built around an HTSC superconducting conductor assembly which provides, in one structure, the cryogen channel, the superconductor, and the cryostat. The conductor assembly in its simplest form is comprised of a corrugated tube coated with a superconducting layer that carries the current, enclosed in a corrugated vacuum-insulated cryostat that provides the thermal isolation. Pressurized liquid nitrogen flows in the hollow core to control the temperature of the superconducting layer. The entire cryostat is at line potential inside the dielectric. In a single pipe type arrangement, the cryogen flows out one phase and back in the other two. With two pipes, flow can be in the same direction in each conductor in a pipe, out in one pipe and back in the other. The cable's dielectric is applied over the cryostat so that it operates at ambient temperature. This allows proven conventional materials to be used for the dielectric, such as fluid-impregnated PPP.

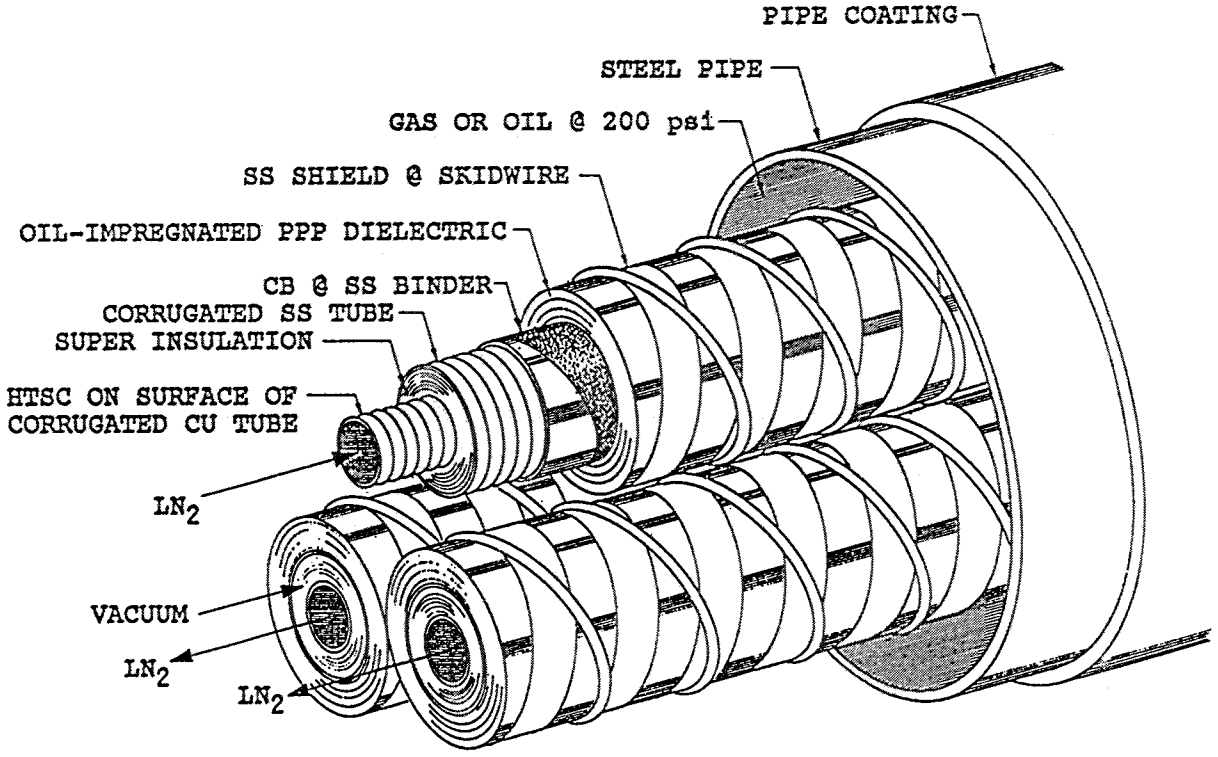

Figure 2-46 Room Temperature Dielectric HTSC HPFF cable system.

The cable dielectric, its shielding and the steel pipe enclosure are conventional in every respect. Comparison of this assembly with a standard pipe-type cable reveals that only the conductor has been changed. If the cryostat assembly can be made in the diameter range of normal copper or aluminum conductors, which is three to six centimeters, the physical size and appearance of the cables will be identical to conventional practice and they will be easily assimilated by the cable industry/utility infrastructure. Being similar to conventional pipe cable, this design could be retro-fitted into existing pipes, affording a significant increase in capacity between two stations without the civil construction required by the installation of new pipes. The savings in civil costs are expected to exceed the somewhat higher cost of the conductor assembly, yet to be clearly defined.

Other forms of HTSC are easily accommodated. Figure 2-47 illustrates a similar design which uses two opposite-lay layers of HTSC tapes over a stainless steel former inside the inner corrugated tube.

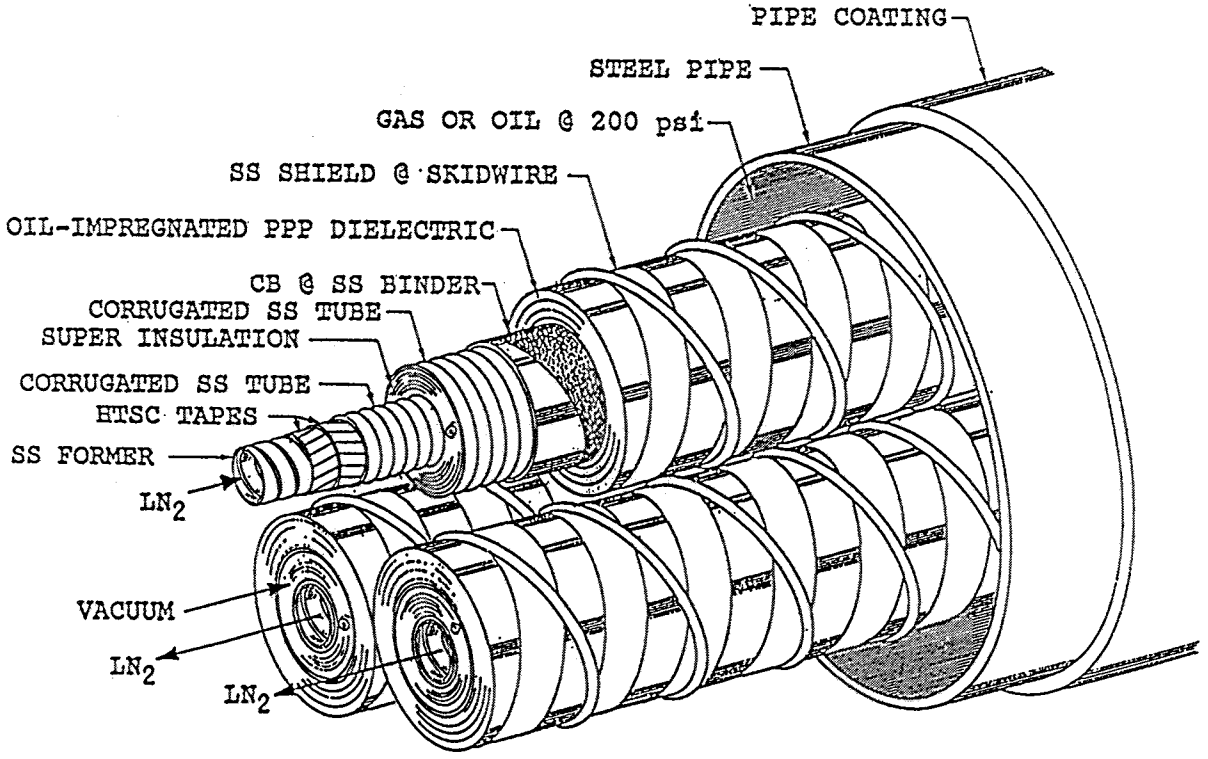

Figure 2-47 Room Temperature Dielectric taped conductor HTSC HPFF cable system.

The room temperature dielectric cable concept has many advantages in comparison to the cryogenic dielectric cable beyond the use of an established dielectric system. Only the heat in-leak and the AC and eddy current losses in the superconductor assembly load the refrigerator. Dielectric losses and ohmic losses in the cable shields and enclosure are conducted to the earth; they do not have to be removed by the refrigeration system. This reduces the overall system energy requirements, reduces the size of refrigeration packages and lowers the flow requirements which extends the distance between cooling plants for a given channel diameter. Thermal contraction phenomena are limited to the former, the HTSC tapes, wires, or coating, and the corrugated inner wall of the cryostat. The remainder of the cable components operate at a temperature slightly above the earth ambient. The mass of material that must be cooled is greatly reduced, which simplifies service procedures and reduces down time, an important consideration for large transmission systems. Installation does not entail any special operations except for the splicing of the conductor assembly. Cables will be lighter than conventional cables which could result in longer pulling lengths. The terminations will also be essentially conventional since the thermal insulation is not exposed to the voltage gradient. The use of conventional dielectric materials operating in their normal temperature range makes this system applicable to any voltage level, even EHV levels up to 765 kV.

Perhaps the most important aspect of this design concept is it's ability to be retro-fitted into existing pipes. This capability presents utility planners with a totally new option for upgrading existing urban facilities and a low cost alternative for bulk transfer through heavily built-up urban areas. The concept is adaptable to SCFF cable designs that can be installed in ducts or directly buried. A SCFF design is shown in Figure 2-48 which uses a fluted lead sheath to provide dielectric fluid channels to the insulation. This type of HTSC cable can also be retro-fitted into existing duct systems.

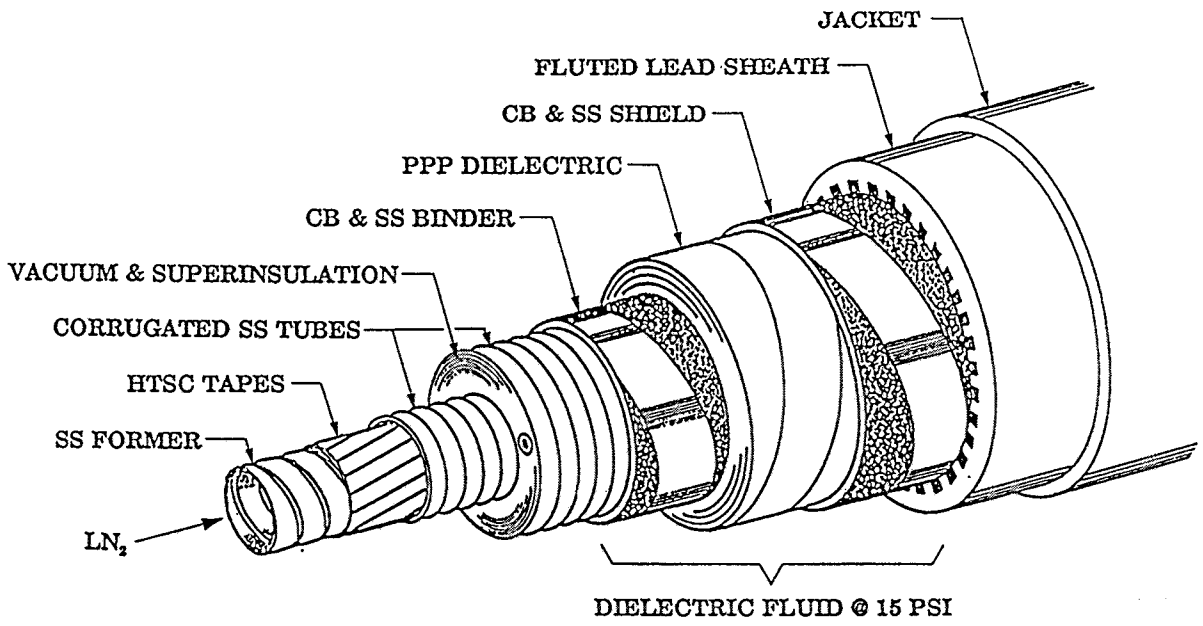

Figure 2-48 Room Temperature Dielectric taped conductor HTSC SCFF cable system.

The limitation of the room temperature dielectric HTSC cable installed in a conventional steel pipe will be its current carrying capability. Eddy current and hysteretic losses in the steel will limit the current that each conductor can carry to the 2000 to 2500 ampere range, decreasing with increasing pipe size. Figure 2-49 graphs the MVA capability of a circuit against its phase current for the common transmission voltages in the US. Shown on this graph are the limits of conventional HPFF pipe cables and the typical ratings of overhead lines. It can be seen that extending the range of the HPFF system up to 2500 amperes more than doubles the capability of conventional underground circuits, and extends the thermal capability beyond that of single circuit overhead lines except at the highest voltage levels. New installations can benefit by the use of a non-magnetic stainless steel pipe to achieve current ratings in the 3500 ampere range which would be close to the SIL for 138 and 230 KV HTSC systems[90]. Thus, this concept can provide the ability to build very long underground circuits that operate at or near surge impedance loading with power transfer capabilities in the 1000 to 1500 MVA range.

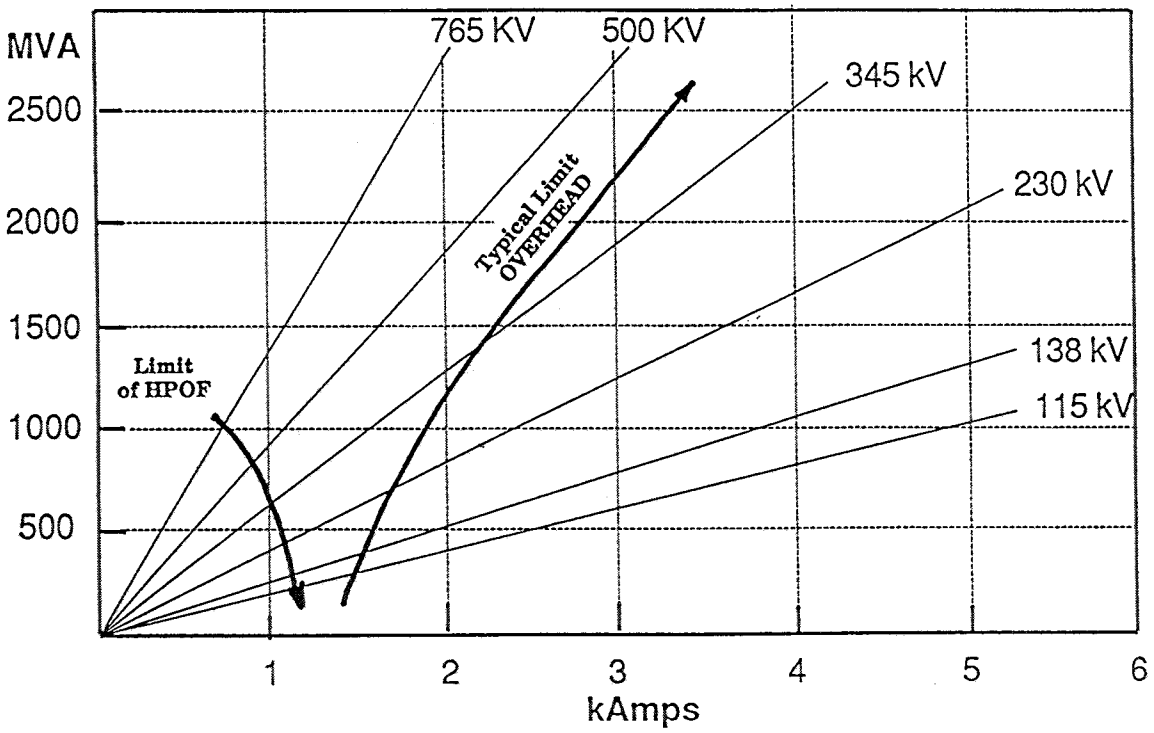

Figure 2-49 Power level for transmission circuits in the US.

The key and only new component of the room temperature dielectric system is the conductor assembly which forms the entire conductor system. Once manufactured, this system can be fully characterized and tested for compliance with its intended service. When its performance has been confirmed, it enters the conventional cable manufacturing process to be insulated, factory tested for dielectric integrity (at room temperature), shipped and installed. At all stages in the life of this system, the conductor function and the dielectric function are separated. Voltage testing can be done without cooling the system, and current testing can be done any time, even before installation in the pipe. With this concept, the challenge facing HTSC proponents is to develop only the conductor assembly and cryostat. A "new" dielectric system is <u>not</u> required.

Figure 2-50 illustrates two approaches to the conductor assembly using wires or tapes. The upper assembly shows a corrugated stainless steel tube as the inner wall of the cryostat, manufactured over a taped conductor. The lower assembly shows how an extruded tube reinforced with a high strength polymer braid might be used to provide a non-conducting high-pressure/vacuum separator. In this case a wire assembly is illustrated. Eddy current losses in the corrugated tube would be eliminated with this construction.

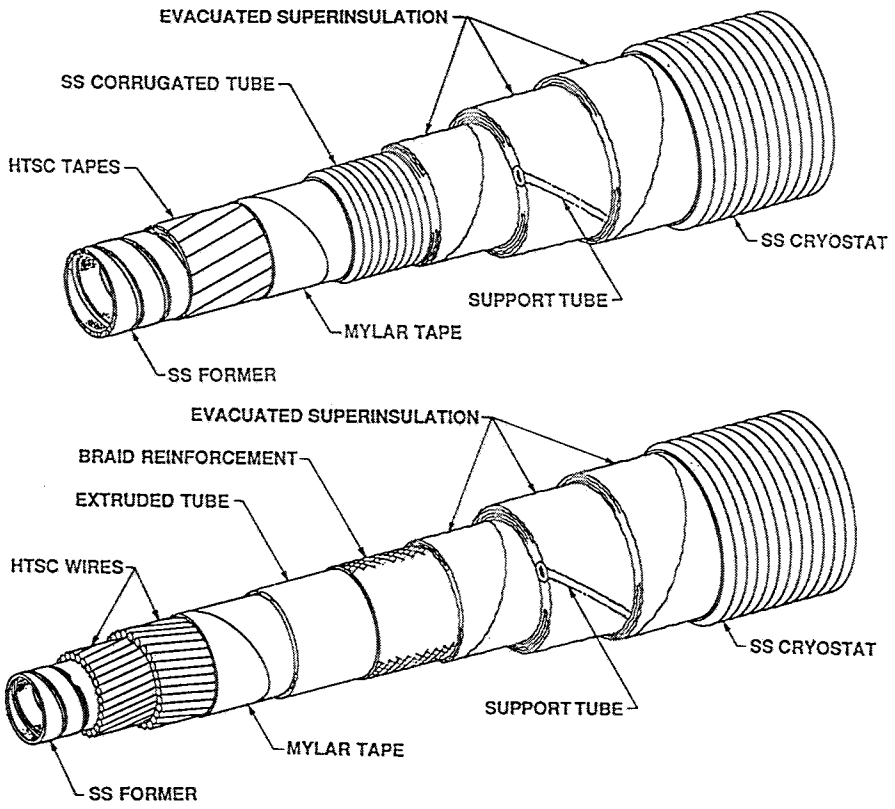

Figure 2-50 Two concepts for the conductor/cryostat assembly.

Another approach uses corrugated wires or tapes of High TC superconducting material applied on the outside of the corrugated cryogen flow tube. The corrugated wire or tape would have the same corrugation parameters as the tube. This assembly has two main advantages. First, it is a means of providing flexibility with reduced stress and strain on the individual wire or tape. Second, it allows for a parallel assembly of the

superconducting elements over the tube, rather than a helical assembly of straight wires or tapes. This advantage would simplify the assembly process because a stranding or cabling machine would not be required. As a result, the individual elements could be supplied on very large reels to minimize their need to bend during the assembly process. These reels could easily be made so large as to match or exceed the final bending radius requirement of the finished cable.

Three such concepts are shown in Figure 2-51, each with a different means to maintain good thermal contact with the corrugated tube holding the flowing liquid Nitrogen. Though tapes are used in this Figure, wires could be applied in the same way.

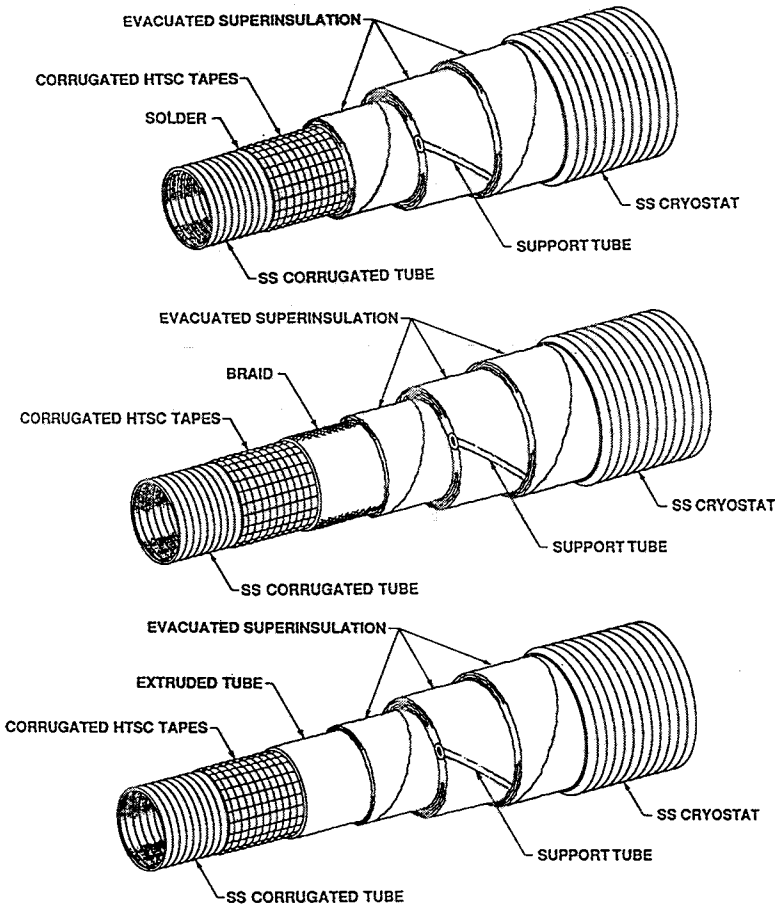

Figure 2-51 Conductor assembly using corrugated tapes.

The corrugations would be imposed on the wire or tape while it is still in the malleable state, prior to any final treatment that is required to convert the material to its superconducting structure. For handling, 3000 feet of corrugated tape one quarter inch wide could be placed on a seven foot diameter drum 36 inches wide in a single layer. The drum could be manufactured with the final corrugation shape to provide robust support for the tape. Such a drum could be easily shipped and handled on a factory floor. By going to multiple layers, such a drum could hold several tapes in parallel, so that only a few such drums need to be set up for payoff in the final assembly operation. The lower tapes would come off the bottom of their shipping drum and the upper tapes would come off the top of their drum. For an assembly of many tapes, the side tapes might come off drums that are laid over on a rotating table.

DC Cable Systems. DC systems can be operated as bipoles or monopoles. Land-based systems are usually configured as bipoles, so that a failure takes out only half of the system capacity. When operating as a monopole the system must have a ground return to complete the circuit. This can be an "earth" return, or it can be a conducting cable return. One advantage of a cable design with a cryogenic dielectric and a superconducting shield for DC applications is that the shield can be used as a lossless return for monopole operation. However, in bipole operation the shield is performing no useful function other than to provide an electrostatic ground for the cable. In bipole operation, therefore, one might just as well use a much simpler room temperature dielectric design which has the advantages of a well-proven dielectric and conventional manufacturing technology. If a component failure puts half the system (for example, one cable) out of service, either a ground return will be necessary, or the normal cable shield will have to be designed with enough cross section to carry the return current. This would also imply a thermal design of the cable system for such operation. An HTSC bipolar DC cable system is illustrated in Figure 2-52. These cables are solid-type paper-lead, the conventional choice for operating voltages up to 300 kV. Higher voltages could be accommodated using a SCFF construction similar to that shown in Figure 2-48.

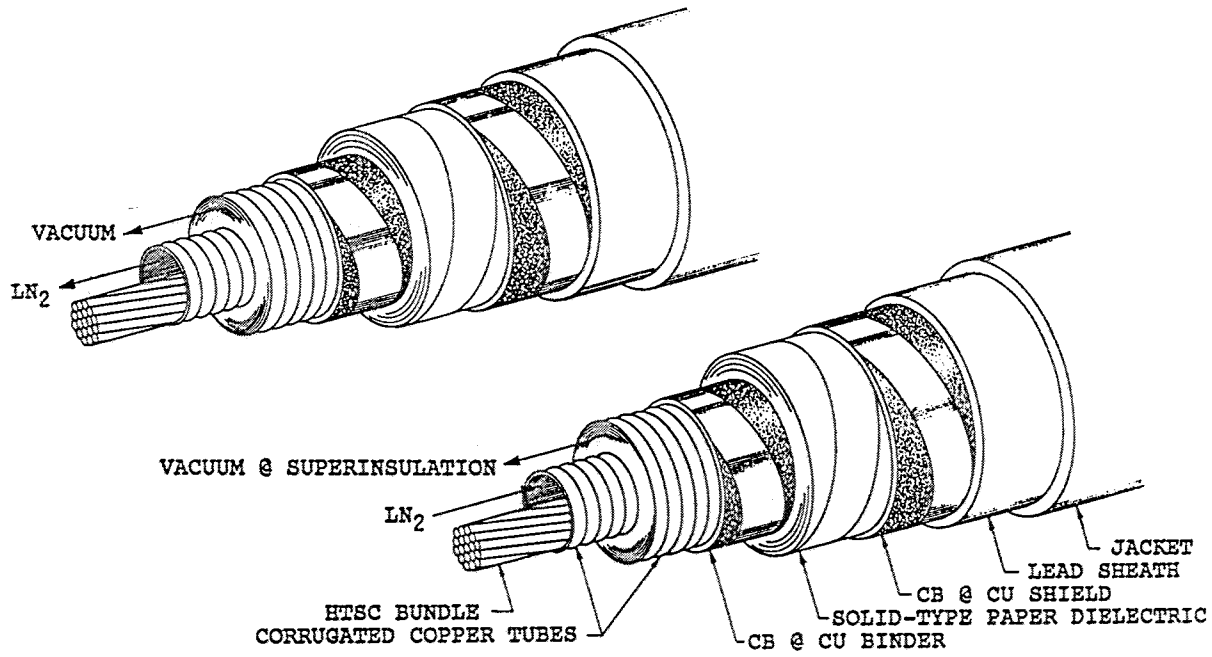

Figure 2-52 Room Temperature Dielectric solid-type bipolar DC HTSC cable system

As seen in Figure 2-52, the conductor for an HTSC cable can have a very simple construction. That shown is based on the availability of HTSC wire robust enough to withstand a stranding operation. Multi-filament wires developed for magnet applications may prove to be a good choice. Of course, the hollow core configurations discussed above for AC use could also be used for DC service.

Much of the complexity in the design and qualification of a conventional DC cable is related to the effect of conductor dissipation-induced temperature gradients within the dielectric on the stress distribution therein. The complexity arises because the DC potential is distributed across the insulation resistively while surges divide capacitively. The dielectric constant has a very small temperature coefficient, but the dielectric resistivity of impregnated laminar materials has a large negative temperature coefficient. At maximum conductor dissipation, this results in a shift of the highest electric field

from the inner portion of the dielectric to the outer portion of the dielectric. However, the surge-induced stress is still maximum at the conductor surface. Thus when a capacitively distributed reverse polarity surge is superimposed on the resistively graded DC stress at maximum conductor dissipation, the difference in the two field distributions increases the stress imposed on the dielectric. This is the worst case condition for conventional DC cable and the one which governs the cable design.

Conductor dissipation related problems are irrelevant to an HTSC DC cable because the dielectric operates at a uniform ambient temperature. The thermal conductivity of the dielectric is vastly greater than that of the thermal superinsulation, so that the temperature gradient across the dielectric caused by the heat in-leak to the cryogenic core should be only a fraction of a degree. At uniform temperature, the potential distribution across the dielectric for DC and AC stresses differs only as a result of the small positive voltage coefficient of conventional DC dielectrics. The distortion caused by this effect is relatively small and results in little increase in stress for a reverse polarity surge. Thus the dielectric design of HTSC DC cable is very much simpler than for conventional DC cable. In the case of a room temperature dielectric HTSC DC cable, insulation technology based on pipe-type, self-contained, or mass-impregnated dielectrics is at hand and well proved.

The use of HTSC DC cable may lead to savings in the converter stations by facilitating a combination of transmission current and voltage which makes efficient use of the thyristor rating. At present, the economic optimum for transmission is normally a higher voltage and lower current than the economic optimum for the converters. For example, the converter stations for a 500 MW monopole at a voltage of about 150 kV and current of 3500 A would cost 10% to 20% less than the same power level transmitted at 400 kV. The estimated price of the terminal equipment for a 1000 MW bipole is $200 to $210 million, including AC and DC filters which typically constitute in the range of 10% of the total price. For transmission using an HTSC power cable, the above prices might

be reduced by 10% to 20% through the use of the optimum combination of voltage and current, as discussed above, and by another 5% if the DC filters are not required for a cable application. This could result in an overall saving on the converter stations in the range of $30 to $50 million relative to stations designed for conventional overhead dc transmission.

Cryogenic Dielectric Designs

AC Cable Systems. The high loss inherent in the room temperature dielectric cable system can be avoided by making the cable truly coaxial. This requires that both the conductor and the cable shield be superconducting. In this case, the shield carries a return current exactly equal to the conductor current and there is no magnetic field external to the outer conductor to cause losses in additional metal components of the assembly, such as the pipe. A typical arrangement using a PPP laminate dielectric is shown in Figure 2-53.

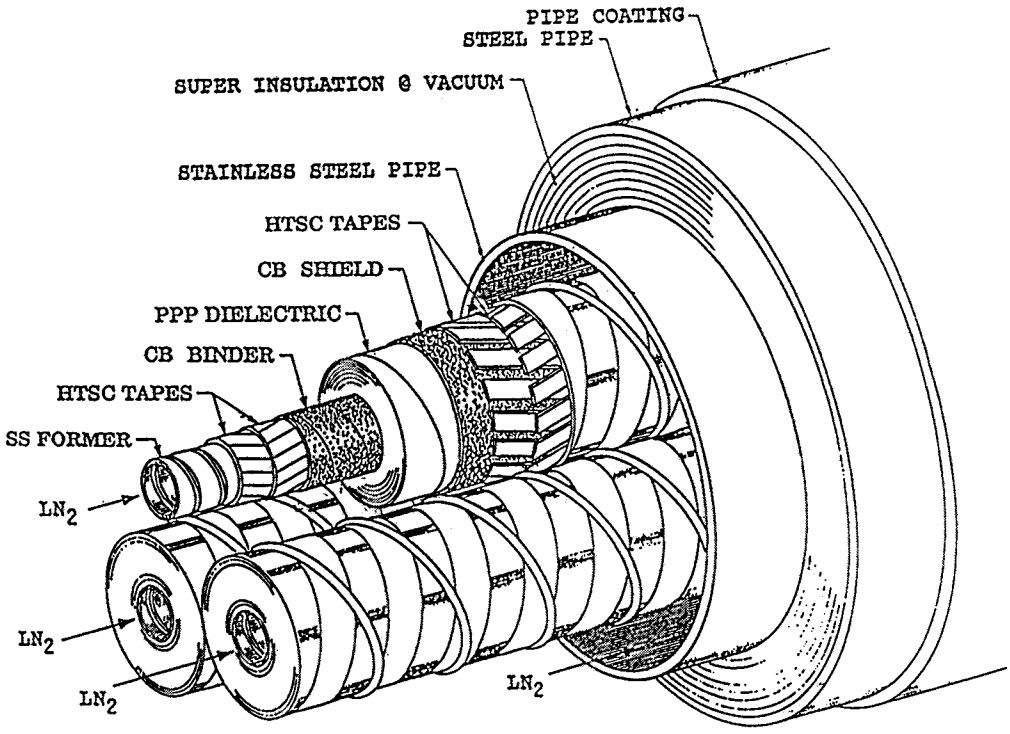

Figure 2-53 Cryogenic Dielectric Coaxial HTSC cable system.

The current carrying capacity of this design is limited only by the capability of the superconducting material. The Brookhaven helium cooled LTSC cables of this design successfully carried up to 6000 amperes on a continuous basis.

The need to maintain the outer shield conductor of the cable at cryogenic temperature requires the cable's dielectric to also operate at this temperature. This changes the logical arrangement of components. For a pipe-type installation, the three cables are placed inside a common cryostat. The hollow core conductor assembly will be similar to the room temperature design. The dielectric can be either a taped structure or an extruded structure but it must be capable of withstanding the low temperature and cycling between room temperature and cryogenic temperature without damage or cracking.

The cryogenic dielectric cable system is well suited to new construction because the relatively large cryostat can be manufactured as a rigid assembly and installed in short sections in the same manner as pipe. Retro-fitting existing pipe is more difficult because it requires a flexible cryostat assembly. It is desirable to make the outer diameter of the cryostat as large as the pipe can accommodate, which results in such a large assembly that shipping lengths are severely limited. A compromise solution that takes advantage of the vacuum capability of the existing pipe is shown in Figure 2-54. This design factory assembles the three superconducting cables into the inner corrugated tube of the cryostat. This tube can be factory tested to insure that it is pinhole free; any defects can be located and repaired. The final assembly of the cryostat takes place in the field using portable equipment to apply the multi-layer insulation and spiral support member. This concept maximizes the space available for the thermal insulation. The smaller diameter of the factory assembly allows shipping lengths that are far more reasonable. The cables in Figure 2-54 are insulated with an extruded polyethylene, and show only a single layer for the inner and outer taped superconductors. This design leads to losses that could be reduced with multiple layers of tape, as shown in Figure 2-53.

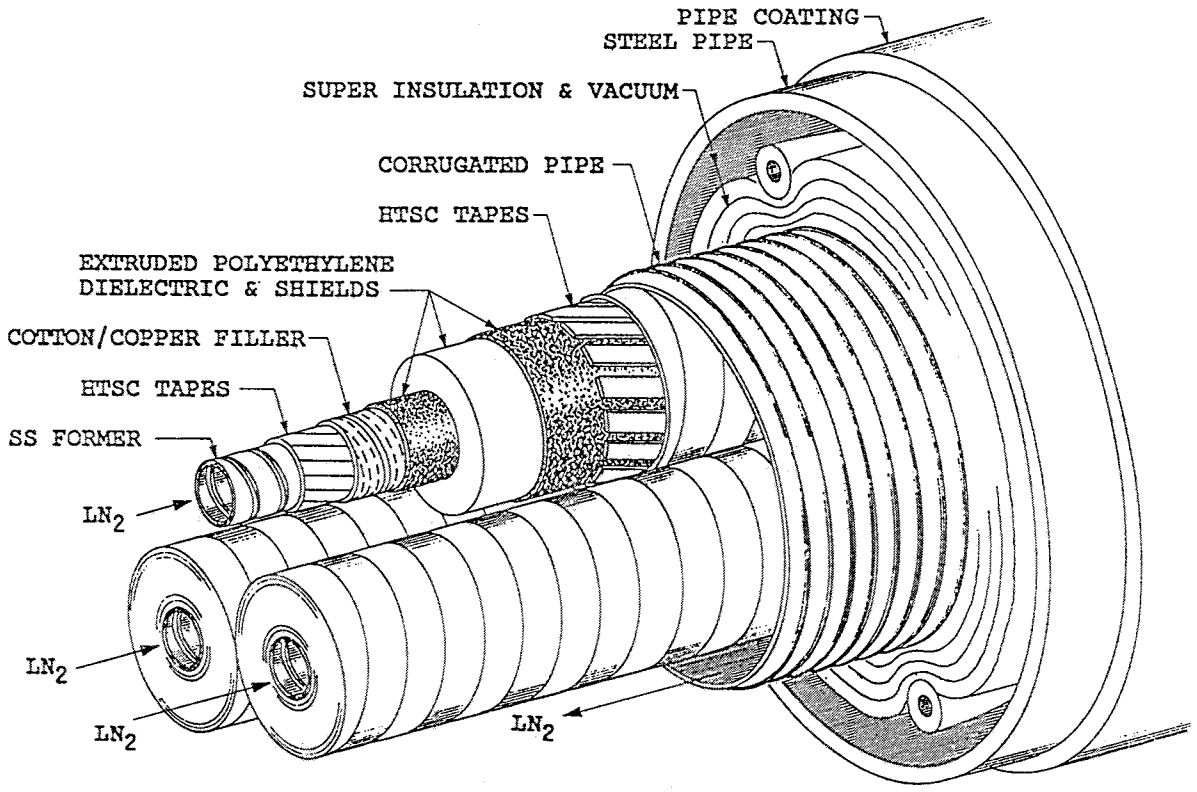

Figure 2-54 Cryogenic Dielectric Coaxial HTSC cable system suitable for retrofit.

For cable systems that must carry only slightly more current than the room temperature dielectric system can accommodate, a non-coaxial cryogenic cable configuration might be a cost-effective solution. Figure 2-55 illustrates an assembly for such a system, derived by combining the earlier LTSC designs with conventional cable technology. This particular design employs a PPP dielectric and a high resistance shield. The current capability of this structure is limited by the magnetic field interaction between conductors and eddy current losses in the shields and enclosure, because the magnetic fields are not shielded. The choice of material for the inner wall of the cryostat could range from copper to provide an eddy current magnetic shield, to FRP pipe to eliminate eddy current loss at low temperature. With this concept, the conductor diameter can be larger than in a room temperature dielectric design, and at modest currents the extra losses may be offset by a lower cable cost.

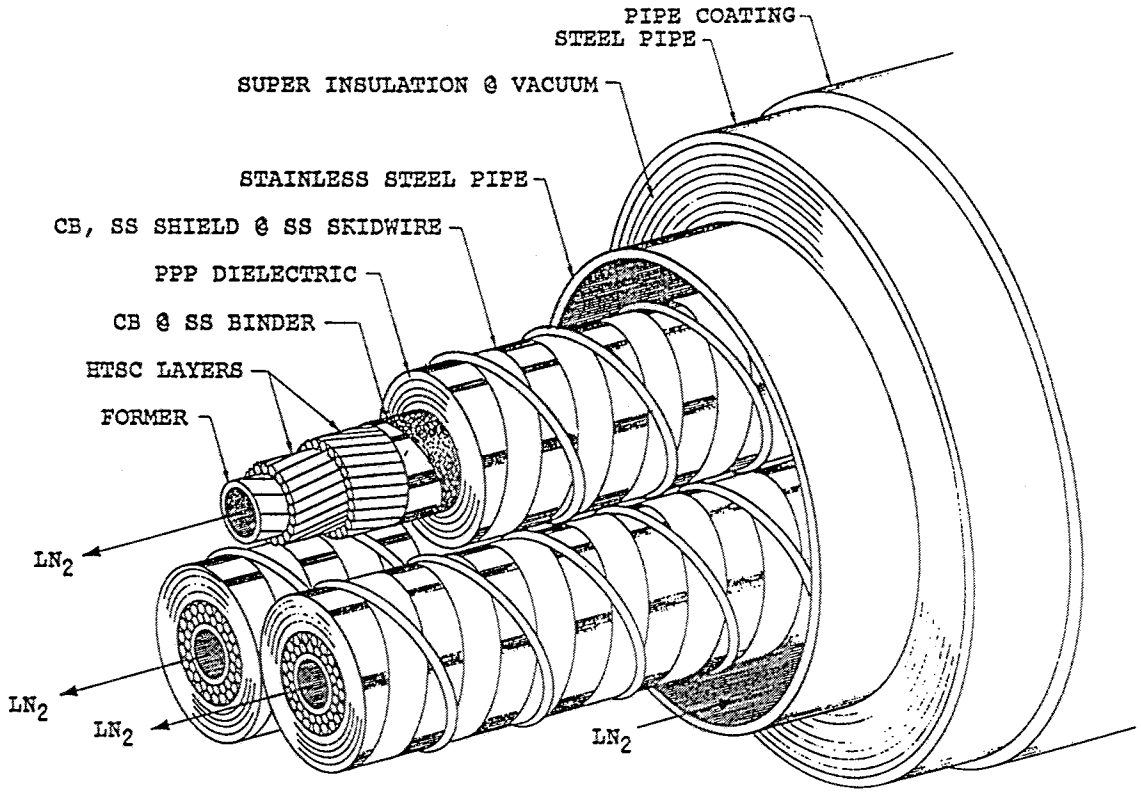

Figure 2-55 Cryogenic Dielectric non-coaxial HTSC cable system.

Because the dielectric operates in the cryogen, dielectric losses must be removed by the refrigerator, which imposes the energy penalty on this loss. Conventional cable paper work well in liquid nitrogen, but its high loss limits its use to 138 kV. PPP has lower loss but will only be attractive up to the 230 kV level. Higher voltages will require a low loss material like the plastic tapes developed at Brookhaven, or an extruded polymer such as polyethylene.

The cryogenic dielectric of choice at this point in time is an extruded polyethylene rather than cryogen-impregnated plastic tapes. Extruded dielectrics for transmission cables have evolved into a mature technology over the last twenty years, while plastic tapes have yet to be successfully demonstrated and adopted by the cable industry. EPRI funded a study of the use of extruded polyethylene at cryogenic temperatures in the

early eighties which demonstrated their viability for operation in liquid nitrogen[91]. More recent work in Japan has confirmed the excellent properties of this material at liquid nitrogen temperatures and similar HTSC cable designs are being developed[92].

The cooling of extruded polyethylene to 77 K actually improves its dielectric behavior relative to temperature-limited operation in conventional cable applications. This extends the voltage levels that are possible for HTSC systems to the EHV range and promises to provide an underground alternative transmission system with the highest power delivery capability that can be imagined in the present scope of utility applications.

The cryogenic dielectric concept is readily applied to the self-contained cable type by the use of flexible individual cryostats for each phase. Liquid nitrogen will flow down the conductor and return in the radial space provided between the outer superconducting layers and the inner wall of the cryostat. Such a design is shown in Figure 2-56.

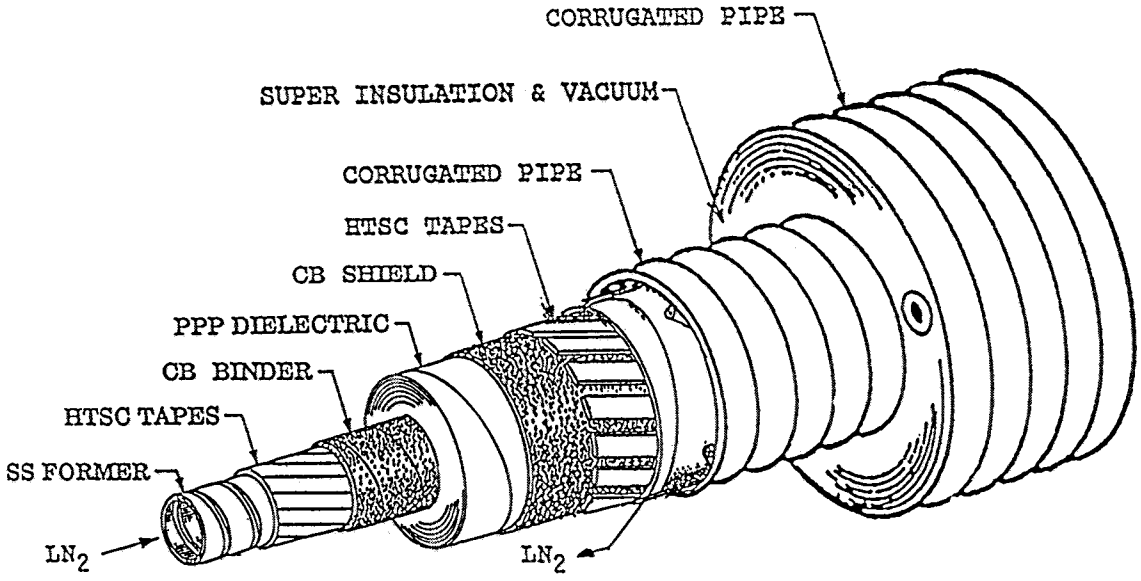

Figure 2-56 Cryogenic Dielectric coaxial HTSC self-contained cable concept.

DC Cable Systems. The general application of HTSC technology to a DC cable system is discussed above in the room temperature dielectric section. The question of dielectric performance with a temperature gradient across the dielectric should be considered if the dielectric provides the primary thermal insulation between the go and return cryogen streams. If the resistivity/temperature characteristic is not flat over the operating temperature range, there may be a redistribution of stress that could lead to increased stress under some conditions of surge or sudden polarity reversal. If so, a reduced design stress may be warranted. Conventional high density cable paper will likely be the best choice for a dielectric material for all voltage levels.

With the cryogenic dielectric system, the designer can select either a coaxial or non-coaxial cable construction. Any of the constructions discussed above are candidates. A simple non-coaxial two cable bipole system in a common cryostat is shown in Figure 2-57. This construction might include a third low-voltage conductor to serve as a ground return.

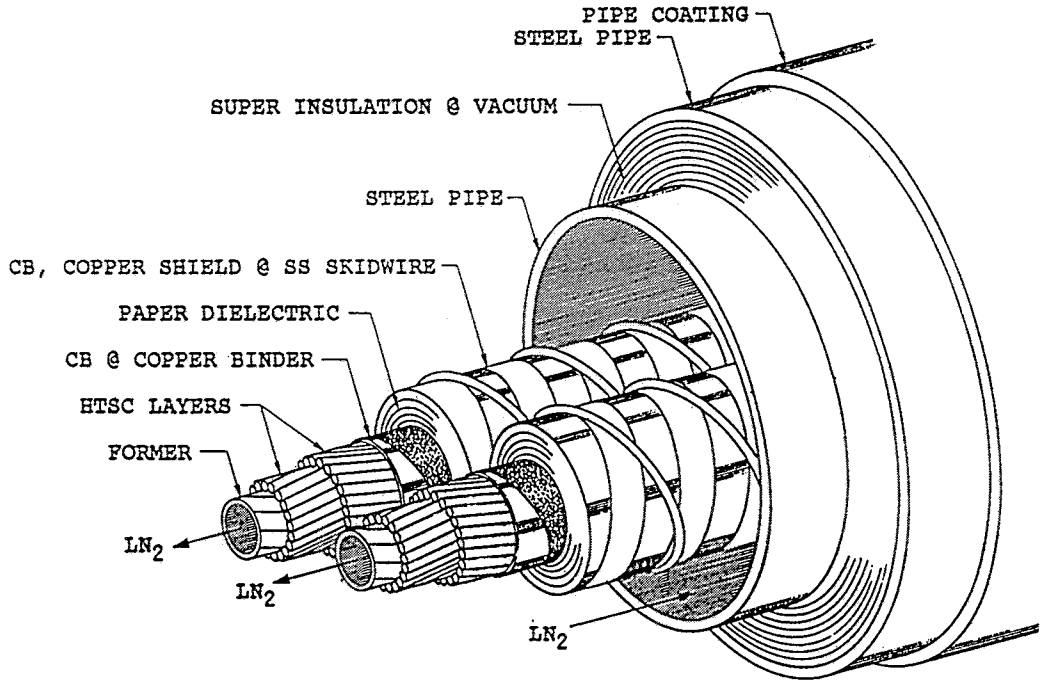

Figure 2-57 Cryogenic Dielectric bipolar DC HTSC cable system.

Summary and Recommendations

The primary advantages of an HTSC cable over conventional cables is the ability to carry more power per circuit with a lower energy cost per megawatt delivered. The former can lead to an economic advantage where space is at a premium or more than one conventional underground circuit is required to satisfy the capacity requirement and a single superconducting circuit does not violate reliability criteria. Two scenarios seem to fall into this category. The first would take advantage of the room temperature dielectric concept to retrofit HTSC cables into existing HPFF pipes. This would be beneficial in urban areas where, because of crowded streets and congested underground corridors, it is difficult and expensive to install new pipes. There are hundreds of miles of cables that have been installed in pipes over the past 40 years in all of the nation's larger cities. As urban load densities shift over time, some of these cable systems have reached their load limits, and many are approaching the end of their expected 40 year life. EPRI's development of PPP which reduces the insulation thickness has enabled Utilities to pull out old paper insulated cables and replace them with higher voltage PPP insulated cables that double the power capacity of the existing pipe. This results in substantial savings in construction costs as well as operation and maintenance savings. In 1989 Con Edison upgraded an old 69 KV paper cable system in lower Manhattan with a 138 KV PPP cable system and doubled the pipe's capacity. By combining the advantage of PPP insulation with an HTSC conductor assembly, an existing pipe's capacity might be increased three to six times. Such a large increase in capacity may not be required in all urban areas due to load growth alone because the power density in many crowded areas is already high. However, significant urban renewal projects that replace low rise slums with high rise, state-of-the-art population centers pose this type of problem to the host Utility. The World Trade Center in New York City is one example of this type of growth. There are now five 138 KV pipe cables feeding that neighborhood substation.

Another opportunity for HTSC cables retrofitted into existing pipes is in the area of inter- and intra-regional bulk transfers motivated by shifting economical generation locations as new units come on line and old, uneconomical units are retired. The major interconnections are EHV overhead networks that necessarily skirt urban areas. Some Utilities like Boston Edison have had to install phase angle regulators to prevent bulk load transfers from taking the low impedance direct underground route through the urban center, which overloaded the pipe cables feeding power into the city, and force the bulk power to go around the area on the overhead system. As the economic motivation for bulk power movement increases, as it is, the overhead routes are going to saturate. By replacing one or more underground cables with HTSC cables, the utility could increase their pass-through capability and their local power density without jeopardizing service to the urban area or building new overhead facilities around the area in sensitive, now suburban environments.

The second scenario will be the undergrounding of sections of overhead lines, either as they approach populated load centers or in remote sections that are forced out of the sky for non-technical reasons. This application will favor EHV circuits where conventional cables don't come close to matching the thermal capacity of the overhead line and the circuit length is not great enough to limit the overhead line loading to levels that could be handled by one conventional circuit. The drawback to the possible application of fully coaxial cryogenic dielectric cable designs for this application is the EHV voltage level. The development and qualification of a cryogenic dielectric capable of EHV levels is many years away. However, as mentioned above, the room temperature dielectric capability is available and qualified now, all the way to 765 KV using PPP. Again, the only missing component is the conductor assembly. Therefore, once a conductor assembly is developed, this scenario could be satisfied by a potentially competitive single circuit HTSC room temperature dielectric cable system.

The reduction in energy used (lost) by an HTSC cable is another potential advantage. Unfortunately, this characteristic is not the panacea that has often been claimed. It does, however, have some merit for circuits that are to be operated at very high load factors, that is, loaded all the time. Our studies show that an AC HTSC cable can achieve a per unit energy savings of about 50% when loading conditions are most favorable. A cryogenic cable system requires a baseline amount of energy to be functional, even before it starts to deliver useable power. While the losses in the transmission circuit are dramatically reduced, the energy consumed by the refrigeration plant to maintain the cryogenic temperature negate much of the savings. Even "lossless" DC HTSC cables will consume considerable energy to balance the heat in-leak. For practical designs of HTSC DC cables, their energy consumption will about equal a conventional cable alternative which is loaded near its thermal limit, making HTSC dc cables attractive only for loads that are higher than the capability of conventional designs which is about 2000 amperes.

For base-loaded systems of medium length, say 10 to 50 miles in areas hostile to overhead construction, the HTSC cable can enjoy a considerable advantage due to it's lower energy costs. The cost of losses for conventional cables when capitalized over the life of the system can approach 25% of the installed cost. In this context even the 50% reduction in energy consumption per megawatt delivered adds to a sizeable cost advantage for the HTSC cable.

References

1. R. Resnick, D. Halliday, Physics, Part 1, John Wiley & Sons, New York, 1977.

2. B.J. Muddock, J.C. Male, "Superconducting cables for AC power transmission", *CEGB Research*, Number 4, September 1976.

3. R. McFee, "Superconductivity - Cryogenic key to low-loss T&D?", *Power Engineering*, Vol 65, page 80, October 1961.

4. R. McFee, "Applications of superconductivity to the generation and distribution of electric power", *Electrical Engineering*, Vol 81, page 122, 1962.

5. R. McFee, "Optimum input leads for cryogenic apparatus", *The Review of scientific Instruments*, Vol 30, No. 2, February 1959.

6. W. Kafka, "Superconducting three-phase current cable", U.S. Patent 3,292,016 filed September 23, 1963, issued December 13, 1966.

7. P.A. Klaudy, "Some remarks on cryogenic cables", *Advances in Cryogenic Engineering*, Vol 11, Plenum Press, 1966.

8. R.L. Garwin, J. Matisoo, "Superconducting lines for the transmission of large amounts of electrical power over great distances", *Proceedings of the IEEE*, Vol 55, April 1967.

9. R.L. Garwin, "Superconducting electrical power transmission systems", U.S. Patent 3,343,035 filed March 8, 1963, issued September 19, 1967.

10. M. Aupoix, F. Moisson-Franckhauser, "Electric cable for polyphase current", U.S. Patent 3,502,783 filed November 30, 1967, issued March 24, 1970.

11. M. Aupoix, F. Moisson-Franckhauser, "Superconductive cable for carrying either alternating or direct current", U.S. Patent 3,600,498 filed December 24, 1969, issued August 17, 1971.

12. M. Aupoix, F. Moisson-Franckhauser, "Cryogenic cable", U.S. Patent 3,730,966 filed January 20, 1972, issued May 1, 1973.

13. K.S. Jacobs, Editor, "What's ahead in underground transmission (UT)? A Special Report", *Electric Light & Power*, August 1967.

14. K.J.R. Wilkinson, "Superconducting windings in power transformers", *Proceedings of the IEE*, Vol 110, December 1963.

15. K.J.R. Wilkinson, "Prospects of employing conductors at low temperature in power cables and in power transformers", *Proceedings of the IEE*, Vol 113, September 1966.

16. D.R. Edwards, Discussion of Reference 14, *Proceedings of the IEE*, Vol 114, pages 1894-1895, December 1967.

17. "Tapping a cool ideal for power", *Business Week*, September 7, 1968.

18. Y.N. Astakhov, V.A. Venikov, E.I. Zuev, V.S. Okolotin, "On non-traditional means of power transmission by low-cooling", *Electric Technology*, (USSR), Vol 2, 1971.

19. S. Ihara, T. Horigome, "Economy of superconducting DC cables", *Electrical Engineering in Japan*, Vol 91, No. 3, 1971.

20. S.H. Minnich, G.R. Fox, "Cryogenic power transmission", *Proceedings: Low temperatures and electric power*, Conference on Cryogenics in Fuel and Power Technology, London, U.K., March 1969.

21. A.V. Pastuhov, F.E. Ruccia, "A total energy transfer system for LNG and electric power", *Proceedings: Low temperatures and electric power*, Conference on Cryogenics in Fuel and Power Technology, London, U.K., March 1969.

22. H. Voigt, "Basic problems of d.c. power transmission by cryogenic cables", *Proceedings: Low temperatures and electric power*, Conference on Cryogenics in Fuel and Power Technology, London, U.K., March 1969.

23. M. Aupoix, F. Moisson, E. Carbonell, "Maquette de cryo-liaison hyperconductrice en courant conyinu", *Proceedings: Low temperatures and electric power*, Conference on Cryogenics in Fuel and Power Technology, London, U.K., March 1969.

24. E.C. Rogers, E.C Cave, R. Grigsby, "A 'superconducting link' for laboratory tests on conductors for superconducting cables", *Proceedings: Low temperatures and electric power*, Conference on Cryogenics in Fuel and Power Technology, London, U.K., March 1969.

25. E.C. Rogers, "A comparison of superconducting and cryo-resistive power cables", *Proceedings: Low temperatures and electric power*, Conference on Cryogenics in Fuel and Power Technology, London, U.K., March 1969.

26. *Superconducting cable system*, Final Report, EEI Project RP 78-7,October 31, 1969.

27. M.T. Taylor, "Composite conductors for a superconducting a.c. power transmission cable", *Proceedings: Low temperatures and electric power,* Conference on Cryogenics in Fuel and Power Technology, London, U.K., March 1969.

28. L.K. Eigenbrod, H.M. Long, J. Notaro, "Conceptual design and economic analysis of a superconducting AC power cable system", *IEEE Transactions on Power Apparatus and Systems,* Vol PAS-89, No. 8, November/December 1970.

29. R.W. Meyerhoff, K. Nurmepuu, R.A. Naatz, K.J. Rooney, "Feasibility of incorporating underground AC superconducting transmission in the Commonwealth Edison system in the 1990's", IEEE Conference Record 76 CH1119-7-PWR, 1976 Underground Transmission and Distribution Conference, Atlantic City, New Jersey, September 27-October 1, 1976.

30. Proposal by Linde Division, Union Carbide, submitted to EPRI and the U.S. Department of Interior in 1974 (the proposal is not dated). The proposal was issued in two parts, a cost proposal and a technical proposal. The technical proposal referenced a two volume appendix which was the draft of an interim technical report on RP7807-1.

31. R. Meyerhoff, H. Morihara, *Superconducting Cable System,* Summary report for the period November 1971 - August 1975, ERDA Contract No. E(49-18)1420 and EPRI Contract EL-402-SY, NTIS CONS/1420-1, May 1977.

32. R. Meyerhoff, H. Morihara, *Superconducting Cable System,* Final Report EPRI EL-402, Project RP7807-2, Vol II, May 1977.

33. Philadelphia Electric Company, *Evaluation of the economical and technological viability of various underground transmission systems for long feeds to urban load areas,* Final Report to DOE under contract No. EX-77-C-01-2055, NTIS HCP/T-2055/1, December 1977.

34. H. Morihara, J.W. Terbot, *Liquid helium refrigerator for testing superconducting system,* EPRI 7839, Final Report, August 1975.

35. P. Klaudy, "Superconducting cables", *Elektronische Zeitschrift,* issue A, Vol 89, No. 14, 1968.

36. P. Klaudy, "Uber tiefstgekuhlte, besonders supraleitende Kabel", *Elektrotechnik und Maschinenbau,* Vol 3, 1972.

37. P. Klaudy, *Arbeiten zur Entwicklung und Erprobung supraleitender Energieubertragungskabel,* Springer-Verlag, Wien, 1978.

38. P. Klaudy, J. Gerhold, A. Beck, P.Rohner, E.Scheffler, G. Ziemek, "First field trials of a superconducting power cable within the power grid of a public utility", *IEEE Transactions on Magnetics*, Vol MAG-17, No. 1, January 1981.

39. P. Klaudy, J. Gerhold, "Practical conclusions from field trials of a superconducting cable", 1982 Applied Superconductivity Conference, November 30-December 3, 1982.

40. E.B. Forsyth, Editor, *Report on Superconducting electrical power transmission studies*, BNL 16339, December 1971.

41. E.B. Forsyth, Editor, *Underground power transmission by superconducting cable*, BNL 50325, March 1972.

42. E.B. Forsyth, R.A. Thomas, "Operational test results of a prototype superconducting power transmission system and their extrapolation to the performance of a large system", IEEE PES Summer Meeting, Vancouver, B.C., July 14-19, 1985.

43. C. Morgan, *Magnetically induced losses in the normal metal parts of a superconducting power transmission line*, Power Transmission Project Technical Note No. 35, Brookhaven National Laboratory, Upton, New York, January 7, 1975.

44. M. Garber, "A 10 m Nb_3Sn Cable for 60 Hz power transmission", *IEEE Transactions on Magnetics*, Vol MAG-15, No. 1, January 1979.

45. G.H. Morgan, F. Schauer, R.A. Thomas, "An improved 60 Hz superconducting power cable", *IEEE Transactions on Magnetics*, Vol MAG-17, No. 1, January 1981.

46. E.B Forsyth, "Energy loss mechanisms of superconductors used in alternating-current power transmission systems", *Science Magazine*, Vol 282, 1988.

47. *Semiannual Report for the period October 1, 1981 to March 31, 1982*, Power Transmission Project Technical Note No. 132, BNL 51569, Brookhaven National Laboratory, Upton, New York.

48. E.B. Forsyth, et al, *Some theoretical considerations affecting the design of lapped plastic insulation for superconducting power transmission cables*, Final Report, Project 7844-1, EPRI EL-269, December 1976.

49. *Semiannual Report for the period April 1, to September 31, 1978*, Power Transmission Project Technical Note No. 83, BNL 50930, Brookhaven National Laboratory, Upton, New York, November 7, 1978.

50. E.B. Forsyth, "Predicted characteristics of superconducting transmission cables", BNL 17894, IEE Conference Publication #107, International Conference on High Voltage DC and/or AC power Transmission, London, U.K., November 19-22, 1973.

51. E.B. Forsyth, G.A. Mulligan, J.W. Beck, J.A. Williams, "The technical and economic feasibility of superconducting power transmission: a case study", *IEEE Transactions on Power Apparatus and Systems*, Vol PAS-94, No. 1, January/February 1975.

52. E.B. Forsyth, *Superconducting cable design for LILCO study*, Power Transmission Project Technical Note No. 20, Brookhaven National Laboratory, Upton, New York, October 3, 1973.

53. E.B. Forsyth, *Superconducting cable design for LILCO study - Revision B*, Amendment to Power Transmission Project Technical Note No. 22, Brookhaven National Laboratory, Upton, New York, December 6, 1973.

54. E.B. Forsyth, J.R. Stewart, "Long distance bulk power transmission using helium-cooled cables", IEEE Conference Record 76 CH1119-7-PWR, 1976 Underground Transmission and Distribution Conference, Atlantic City, New Jersey, September 27-October 1, 1976.

55. *Quarterly report for the period 1 October to 31 December, 1975*, Power Transmission Project Technical Note No. 50, Brookhaven National Laboratory, Upton, New York, January 28, 1976.

56. R.J. Bartlett, et al, *USAEC-DAT DC Superconducting power transmission line project at LASL*, Progress Report #1 for the period November 1, 1972 to March 31,1973, Los Alamos Scientific Laboratory, LA-5271-PR, May 1973.

57. F.J. Edeskuty, *DC Superconducting power transmission line project at LASL*, Progress report #24, Final Report for the period November 1, 1972 to September 30, 1979, US DOE Division of Electric Energy Systems, Los Alamos Scientific Laboratory, LA-8323-PR, April 1980.

58. W.E. Keller, R.D. Taylor, M.P. Maley, L.R. Newkirk, *Development of Nb_3Ge conductors for power transmission applications*, Final Report EPRI TD-200, Project 7838, July 1976.

59. M.P. Maley, L.R. Newkirk, J.D. Thompson, F.A. Valencia, *Development of Nb_3Ge for power transmission applications*, Final Report EPRI EL-965, Project 7855-1, January 1979.

60. W.E. Keller, R.D. Taylor, *DC Superconducting power transmission line project at LASL*, Progress report #9 for the period January 1 to March 31, 1975, US DOE Division of Electric Energy Systems, Los Alamos Scientific Laboratory, LA-6053-PR, September 1975.

61. F.J. Edeskuty, P. Chowdhuri, *DC Superconducting power transmission line project at LASL*, Progress report #15 for the period October 1, 1975 to September 30, 1976, US DOE Division of Electric Energy Systems, Los Alamos Scientific Laboratory, LA-6699-PR, February 1977.

62. H.M. Long, et al, *Cryogenic power transmission technology - Cryogenic dielectrics*, Final Report for the period November 1, 1972 to September 30, 1976, Oak Ridge National Laboratory Contract W7405-ENG-26, July 1977.

63. J.A. Baylis, *Prospects for power transmission by superconducting A.C. cables*, Laboratory Note RD/L/N 79/72, Central Electricity Research Laboratories, Leatherhead, Surrey, U.K., April 1972.

64. J.A. Baylis, "CERL develops superconducting cables", *Electrical Times*, IPC Business Press Ltd, May 24, 1973.

65. J.A. Baylis, "Superconducting cables for a.c. and d.c. power transmission", Philosophical Transactions Royal Society, London, A275, 1973,

66. D.N.H. Cairns, *The operation and economics of superconducting cables in the U.K. transmission system*, Laboratory Note RD/L/N 113/77, Central Electricity Research Laboratories, Leatherhead, Surrey, U.K., September 1977.

67. B.J. Maddock, D.N.H. Cairns, J. Sutton, D.A. Swift, J.E.J. Cottrill, M.B. Humphries, D.E. Williams, "Superconducting A.C. power cables and their application", paper submitted to CIGRE for publication in 1976.

68. B.J. Maddock, J.C. Male, "Superconducting cables for AC power transmission", *CEGB Research*, Number 4, September 1976.

69. G. Bogner, P. Penczynski, F. Schmidt, *Development of a superconducting high power AC cable*, Siemens Research and Development Report, Volume 8, No. 1, 1979.

70. G. Bogner, "Transmission of electric power by superconducting cables", Chapter 7, *Superconducting Machines and Devices - Large Scale Applications*, Edited by S. Foner and B.B. Schwartz, Volume 1 of Series B:Physics, NATO Advanced Studies Institute Series, Plenum Press, New York, 1974.

71. E. Bochenek, H. Voigt, U. Hildebrandt, H. Kuhmann, E. Scheffler, "Supraleitendes flexibles Hochleistungs-Gleichstromkabel", *Elektrotechnische Zeitschrift*, (B), Jg.26, 8/9, 1974.

72. E.B. Forsyth, "The high voltage design of superconducting power transmission systems", *IEEE Electrical Insulation Magazine*, Volume 6, No. 4, July/August 1990.

73. G.I. Meshchanov, I.B> Peshkov, G.G. Svalov, "The results of work carried out in the USSR on creation of superconducting and cryoresistive cables for electric power lines", *IEEE Transactions on Magnetics*, Volume MAG-19, No. 3, May 1983.

74. Z. Croitoru, A. Lacoste, L. Deschamps, "New techniques for power transmission by underground cables. Medium and long terms", *Revue Generale de l'Electricite*, No. "special", June 1974.

75. C. Jacobsen, "Special report for Group 21 (High Voltage Cables)", CIGRE 21-00, Paris, France, September 1-9, 1982.

76. K.N. Mathes, "Electrical insulation at cryogenic temperatures", Electro-Tech., Volume 22, September 1963.

77. G.R. Fox, et al, *Resistive Cryogenic Cable, Phase A Report*, EEI Project RP 78-6, March 1969.

78. G.R. Fox, et al, *Resistive Cryogenic Cable, Phase B Report*, EEI Project RP 78-6, May 1970.

79. G.R. Fox, et al, *Resistive Cryogenic Cable, Phase C Report*, EEI Project RP 78-6, June 1971.

80. G.R. Fox, et al, *Resistive Cryogenic Cable*, Phase II Final Report, EEI Contract 14-01-0001-1483, May 1974.

81. M.J. Jefferies, et al, *Resistive Cryogenic Cable, Phase III*, Final Report EPRI EL-503, Project 7806, October 1977.

82. S.J. Fallick, S.S. Kalsi, K.F. Schoch, J.S. Hickev, F.G. Hajar, "Resistive cryogenic cable systems for underground transmission of electrical energy", *Workshop proceedings: Public Policy Aspects of High-Capacity Electric Power Transmission*, EPRI WS-79-164, Project WS-97-164, September 1979.

83. P. Graneau, "Economics of underground transmission with cryogenic cables", *IEEE Transactions on Power Apparatus and Systems*, Volume PAS-89, No. 1, January 1970.

84. S.B. Afshartous, P. Graneau, J. Jeanmonod, "Economic assessment of a liquid-nitrogen-cooled cable", *IEEE Transactions on Power Apparatus and Systems*, Volume PAS-89, No. 1, January 1970.

85. "Cryogenic Terminal tested at Waltz Mill", *Electrical world*, December 22, 1969.

86. P. Graneau, L.B. Thompson, Jr.,M.O. Hoenig, "High power transmission tests of short VI-LN2 cryocable loop", *IEEE Conference Record, 1976 Underground Transmission and Distribution Conference*, Atlantic City, New Jersey, September 27-October 1, 1976, IEEE pub. No. 76 CH1119-7-PWR, 1976.

87. P. Graneau, L.B. Thompson, "Design and testing of a 138 kV prototype termination for a vacuum-insulated LN2 cryocable", *IEEE Conference Record, 1976 Underground Transmission and Distribution Conference*, Atlantic City, New Jersey, September 27-October 1, 1976, IEEE pub. No. 76 CH1119-7-PWR, 1976.

88. M. Rabinowitz, "Advanced transmission line technologies", *Workshop proceedings: Public Policy Aspects of High-Capacity Electric Power Transmission*, EPRI WS-79-164, Project WS-97-164, September 1979.

89. Z. Iwata, N. Ichiyanagi, E. Kawai, "Cryogenic cable insulated with oil impregnated paper", *IEEE Transactions on Power Apparatus and Systems*, Volume PAS-96, No. 4, July/August 1977.

90. J. Engelhardt, D. Von Dollen, R. Samm, "Application considerations for HTSC power transmission cables", NYSIS Fifth Annual Conference on Superconductivity and Applications, Buffalo, New York, September 24-26, 1991.

91. M. Sosnowski, G. Bahder, G.S. Eager, Jr., *Development of Cross-linked Polyethylene Insulated Cable for Cryogenic Operation*, Final Report EPRI EL-3907, Project 7892-1, February 1985.

92. M. Kosaki, M. Nagao, Y. Mizuno, N. Shimizui, K. Horii, "Development of Extruded Polyethylene-Insulated Superconducting Cable", *Electrical Engineering in Japan*, Volume 109, No. 1, 1989.

3

CABLE DESIGN

Design Development Process

Introduction

This section reviews the design process of an HTSC cable system, presents detailed methods of calculation, and tabulates the available data required to perform in-depth design studies.

Controlling Parameters

The primary controlling parameters for cable design fall into three categories; capacity requirements, system voltage, and circuit length and topology. These three aspects are closely interrelated and are usually beyond the control of the cable designer. The normal utility application requires a specified capacity between two geographical locations, most likely at an existing system voltage. Abnormal situations such as extra high power levels or long distances may offer the cable engineer more flexibility in choosing system parameters such as the optimum voltage and the possibility of DC conversion.

Capacity requirements influence conductor design and voltage selection. The maximum practical current levels may impose lower limits on the voltage option. System voltage primarily impacts the dielectric design and subsequent cable diameters. The wall thickness of the cable dielectric and the cryogen duct diameter are the two predominant dimensional parameters because the cryostat dimensions are essentially independent of

voltage or current requirements, and the superconductor should require negligible cross-section.

In general, the length and location of the circuit establishes the practical distance(s) between cooling stations and may impose restrictions on the minimum cryogen duct dimensions. The total heat load on the cryogen system tends to be constant and will be in the range of one to two Watts per phase-meter. The primary choice for the designer is thus between the use of a dielectric that operates at room temperature or one that operates at low temperatures.

The design parameters of an AC cable are more complex than those for a DC cable as considerations such as AC losses, surge impedance, and reactive (charging) current are important for an AC cable but less applicable to a DC cable. Long AC circuits are sensitive to charging currents which tend to increase with voltage.

The design goal, in general, is to minimize cable diameters simply because this would minimize the amount of material required to build the system and therefore should minimize the system cost. There are, however, some scenarios where this logic may not be appropriate. Retrofitting an existing pipe or duct system is one such application. In this case, the goal may be to maximize capacity, given the restriction of the pipe or duct diameter. This would be done by optimizing the cryogen duct and conductor diameter against the pipe loss which increases with cable size and may limit capacity. In another scenario, specific to long systems, it may be desirable to increase the dielectric wall thickness to increase the surge impedance of the cable and/or decrease the charging requirements.

Configuration Options

AC vs. DC. The first choice in a design "decision tree" is whether the system will be AC or DC. The option may arise when a very long circuit is required, and one design

step may be to evaluate the installation for both options to establish the more economic system. The more general case will pre-determine whether the circuit will be AC or DC. AC is the popular choice for transmission lines, but DC may have some interesting new application opportunities for very long lines (hundreds of miles) of very large capacity.

DC systems can be operated as bipoles or monopoles. Land-based systems are usually configured as bipoles so that a cable failure disables only half of the system capacity. The requirement of a DC cable to carry some or all of the return current on its outer conductor has a significant impact on the choice of cable configurations.

When operating as a monopole, the system must have a ground return to complete the circuit. The ground return can be provided by means of an "earth" return, a low voltage separate normal cable, or by the cable shield itself. If the cable shield is utilized as the ground return, the shield structure must have the capacity to carry the full load current. One advantage of a cryogenic dielectric cable with a superconducting shield is that the shield will act as a lossless return.

In bipole operation, the shield performs no useful function other than to provide an electrostatic ground for the cable. In bipole operation, therefore, one might just as well use a simpler room temperature dielectric design which has the advantages of a well proved dielectric and standard manufacturing technology. If for some reason one half of the system (for example, one cable) is out of service, a ground return will be necessary for the other half, and the capacity of the ground return may dictate the power transfer capacity while in the monopole mode. If this situation must be included in the design, it may be cost effective to employ a superconducting cable with a room temperature dielectric and a normal heavy copper return structure, where the return will carry the full current without overheating (but having a substantial loss). If this condition is expected to be infrequent, the cost of the extra loss during the outage will

be insignificant compared to the cost of providing a fully cryogenic system with twice the amount of superconductor required.

Thermal gradient related problems in the dielectric are not relevant to an HTSC DC cable where the dielectric operates at either a uniform cryogenic temperature or at uniform ambient temperature. In the latter case, the thermal conductivity of the dielectric is vastly greater than that of the thermal superinsulation so that the temperature gradient across the dielectric caused by the heat in-leak to the cryogenic core will be only a fraction of a degree. DC insulation technology based on pipe-type, self-contained, or solid-type mass-impregnated paper dielectrics is at hand and well proved.

DC cables must tolerate small components of AC current inherent in the inverter/converter operation. The magnitudes of these currents are generally below about 1% of the rated DC current, but they occur at fairly high harmonics which result in significant eddy current and hysteretic losses in the superconductors and normal metal components. Eddy current losses increase as the square of the frequency and are proportional to the square of the magnitude of the AC field. If the combined DC and peak AC field exceeds the H_{c1} level in the superconductor, as it most likely will, hysteretic losses will occur which are directly proportional to the frequency but will increase as some power of the AC field magnitude. This power will be in the range of 1 to 4 and will depend on the hysteresis characteristic of the superconductor in its mixed state. The DC current will bias the hysteresis loop, probably in the direction that will increase the loss. If the harmonic current content can be established, a loss calculation should be made to assess the impact on the cryogenic design. This calculation requires the knowledge of the hysteresis loop of the superconductor in the proposed cable configuration.

Rigid vs. Flexible. The next decision facing the designer is the choice between a flexible cable system and a rigid type of system. The most common choice will be the flexible system using well-developed lapped or extruded dielectric materials. However, when high capacities are required, the rigid system may offer the best utilization of superconductor properties, and may thus be the most economic configuration. Such a system would be dimensionally large owing to the low operating voltage stress required with gaseous or vacuum dielectrics. The large dimensions, however, would favor the superconductor performance as this system would result in the lowest magnetic field per unit of current. The application of the superconductor to tubular members should be economically attractive provided suitable manufacturing processes are developed. In such a design, bending stresses are eliminated, and the design focus is on the relative contraction of the superconductor and its substrate(s).

There has been a resistance to the use of rigid Gas-Insulated Transmission Lines (GITL) systems in the U.S. which has limited their applications to relatively short lines and intra-station bus ties. The need for extreme cleanliness during installation and the large number of field joints are problem areas often cited by opponents. Early systems had many service troubles, a situation to be avoided when introducing a new technology. In recent years SF_6 systems have become commonplace in compact substation applications. This wide-spread use has overcome most of the perceived problems with this type of transmission line which is now considered a mature technology. For this reason, rigid configurations for HTSC systems should not be ruled out without evaluation.

The evolution of the HTSC materials may have a negative impact on the possible choice of the rigid system even though it should be the easiest way to accommodate these new materials. The present efforts by those addressing transmission lines as possible markets for HTSC materials have targeted tapes as the preferred format for the material. This

direction has been chosen because tapes can be used for most of the bulk applications so far identified, such as coils for magnets, motors, transformers, and the like.

SF_6 GITL systems are often chosen for very high capacity short bus ties. They have as much inherent capacity as can be envisioned for most likely applications in the near term. In this sense, these systems are more of a competitor than an ally for a short superconducting system.

Cryogenic vs. Room Temperature Dielectric. The major decision at the design stage is the choice between a cryogenic dielectric and a room temperature dielectric cable system. Most past superconducting cable designs have utilized a cryogenic dielectric in which each phase (AC) or pole (DC) is a coaxial cable with a superconducting conductor and a superconducting shield or return. In such a design, equal and opposite currents flow in the superconducting conductor and superconducting ground shield return, assuming that end connections allow such currents to flow. This configuration eliminates magnetic fields outside of the cable shield and thereby eliminates eddy current or magnetic losses in the cryostat or other metallic components that might cover the cables such as skid wires. For a Helium cooled LTSC system, all cryogenic losses must be kept at an absolute minimum; eddy current losses in the cryogenic enclosure would not be acceptable. HTSC cables have the potential to operate with a liquid nitrogen cryogen in the temperature range of 65 to 80 K. The refrigeration costs in this temperature range will be in only 10 to 15 Watts per Watt, which is 25 to 50 times lower than LTSC cables operating below 10 K. This change in operating costs reduces the emphasis on very low losses and opens the door to many attractive design and configuration options including the room temperature dielectric option.

The room temperature dielectric cable system is preferred for its simplicity and low cost. However, it has a limited current carrying capacity due to higher losses in the superconductor, and high pipe or sheath losses outside of the cryogenic system. The

latter will cause the pipe or sheath temperature (and dielectric temperature) to rise over ambient, leading to possible soil instability. Table 3-1 presents results of a calculation of the current that would cause a 30 C rise of the pipe over ambient for a room temperature dielectric pipe cable configuration as a function of pipe size and material using a pipe to cable diameter ratio of 2.4. These calculations, described later, consider only pipe loss and assume a 107 cm (42 inch) burial to the pipe's centerline and an earth thermal resistivity of 60 C-cm/watt. If higher currents are required, a cryogenic dielectric system should be considered. The final choice will depend on the specifics of each option and the superconductor performance in respect to the AC loss parameters.

Table 3-1

Breakpoints for the Room Temperature Dielectric HPFF Cable System

Pipe size, O.D.	Steel Pipe	SS Pipe
5-9/16"	2760 amps	4200 amps
6-5/8"	2700 amps	3915 amps
8-5/8"	2443 amps	3540 amps
10 3/4"	2260 amps	3280 amps
12-3/4"	2133 amps	3100 amps

A balanced design. In an optimum system, the heat load from conductor losses, dielectric losses and heat in-leak through the cryostat should be roughly balanced. Expending substantial sums to reduce the loss of one component far below that of the other components obviously makes no sense. This balancing requires trading off the current-induced ohmic and superconductor losses with the voltage-induced dielectric loss given the available conductor, dielectric materials and configuration. And neither should be made much lower than the heat in-leak unless the cost of so doing is small, or driven by other considerations.

Technical risk. Technical risk must also be factored into the design philosophy, especially as it impacts the use of materials with little or no manufacturing and service experience. Clearly, the lowest technical risk option is offered by the maximum utilization of existing technology. In the case of a superconducting power cable, this concept impacts the choice of the dielectric material more than any other component. The implication is that the use of standard materials such as paper, PPP, or extruded dielectrics, and the room temperature dielectric system in either pipe-type or self-contained configurations should receive first considerations.

A clear advantage of the room temperature dielectric concepts is the ability to retrofit an existing pipe with HTSC cables for the purpose of uprating an old circuit, or the potential to retrofit existing ducts housing very old LPFF cables with HTSC options. Since the cost of new pipe or duct installations can represent more than half of a total cable system cost, retrofitting with a higher capacity HTSC cable provides a major economic incentive for the room temperature configuration, even if the superconducting conductor costs substantially more than a conventional copper conductor.

Room Temperature Dielectric Considerations

AC cables. In general, the use of the room temperature dielectric will be limited by the magnitude of the losses that occur at room temperature. These losses, which include dielectric loss, will be isolated from the cryogen cooling system by the cryostat and incur no cooling penalty, but they will have to be removed by conduction to the surrounding earth, as in a normal cable system. The temperature rise of the dielectric and/or the stability of the earth at elevated temperature will dictate the maximum loading on this type of system.

For systems that have moderate current levels, the room temperature dielectric offers considerable advantages over its cryogenic counterpart. These have been discussed in detail in Section 2 and need not be repeated here. The essence of the argument for this

configuration is the use of conventional materials without the need for an extensive development and qualification program, a much smaller cryogenic mass, and more flexibility in the type and overall size of the cable system.

There are three types of dielectric systems that are well-established for application to the room temperature dielectric concept. Rigid systems use pressurized SF_6 and filled epoxy spacers. Flexible systems use either laminar or extruded dielectrics.

Laminar materials are fluid-impregnated and include paper tapes or PPP tapes (a newly developed laminate of paper and polypropylene) which operate in a pressurized environment. The pressure medium is either a dielectric fluid or, for voltages up to 138 kV, nitrogen gas. Pressurized fluid-filled systems can be configured as Pipe-Type (HPFF or HPGF) or self-contained systems (SCFF), the former being the prevailing choice in the U.S. The operating pressure for pipe-type systems, both fluid and gas, is in the range of 1.5 MPa (200 psig). Self-contained Fluid-Filled (SCFF) laminar cables can operate at low pressure (LPFF) or medium pressure (MPFF). At the present time (1992) room temperature dielectric options for EHV applications in the U.S. (230 kV and above) include only fluid-impregnated paper or PPP laminate, or SF_6 gaseous insulation. In the evolution of these systems, long term qualification test programs have been successfully completed, and have demonstrated adequate performance even for UHV applications up to 765 kV in the U.S., 1100 kV world-wide. High Pressure Gas-Filled (HPGF) PPP cables for 230 kV are currently under development in an EPRI-sponsored program.

Extruded dielectrics are either cross-linked polyethylene or various blends of synthetic rubbers. Extruded systems operate without pressure assistance at voltages up to 138 kV. Extruded cables using XLP are available from foreign manufacturers at voltages up to 230 kV and some utilities have trial installations underway or planned at this voltage.

The independent variable in the dielectric design problem is the thickness of the dielectric required to provide the necessary dielectric strength that will insure reliable operation for the life of the cable. Most dielectrics have a range of operating stress that has been established by an evolutionary process over many years. This stress can be based on the operating voltage or the Basic Impulse Level (BIL) of the system. The AC or impulse stress at radius R is uniquely defined by the following relation between the applied voltage, either operating or surge voltage, and the inner and outer diameters that define the wall thickness, assuming a dielectric of uniform dielectric constant.

$$\sigma = \frac{V}{R \ \ln\left(\frac{D_o}{D_i}\right)} \quad \frac{Volts}{unit\ radius} \tag{3-1}$$

In Equation 3-1, D_o is the outside diameter of the dielectric and D_i is the inside diameter of the dielectric. Two stress values of interest are those occurring at the inner and outer radii, σ_{max} at $R = D_i/2$ and σ_{min} at $R = D_o/2$. The maximum stress is the controlling parameter in most cases. However, laminar cables with large diameter conductors may be limited by the minimum stress because of weaknesses inherent in cable accessories.

GITL systems use SF_6 pressurized in the range of three to five atmospheres. The overall dimensions of GITL systems are proportional to their required ampacity. The relationship between the inside and outside diameters is established by stress considerations. A diameter ratio equal to e (2.72) sets the minimum stress for a given outer diameter and voltage level; diameter ratios larger then e don't make sense because an increase in the inner diameter allows a smaller outer diameter to be used. If a larger conductor is required to carry the current, a diameter ratio smaller then e can be used as dictated by the operating stress guidelines. Systems below 550 kV tend to be controlled by the BIL of the system rather then the AC operating level (System Voltage). At 550 kV and above, the AC operating stress controls the system dimensions.

GITL systems are quite large to accommodate the high currents which make them economically interesting. Room temperature dielectric HTSC applications would take advantage of this size capability to utilize cryostat dimensions comparable to conventional GITL conductors. Based on an impulse design stress of 17.7 kV/mm (450 vpm) or an AC_{rms} stress of 3.15 kV/mm (80 vpm), whichever is limiting, the cryostat outside diameters and the enclosure inside diameters shown in Table 3-2 result from the use of Equation 3-1 and a diameter ratio of 2.72.

Table 3-2

Cryostat and Enclosure Dimensions for RT GITL/HTSC System

System Voltage kV	BIL kV	Cryostat O.D. cm	(in)	Enclosure I.D. cm	(in)
138	650	7.4	(2.9)	20.1	(7.9)
230	1050	11.9	(4.7)	32.3	(12.7)
345	1300	14.7	(5.8)	39.9	(15.7)
550	1550	20.1	(7.9)	54.9	(21.6)

These dimensions illustrate the typical size range for the use of SF_6 as the room temperature dielectric in a rigid isolated phase configuration. Variations in the design stress, the use of a reduced BIL, or the three-in-one configuration are options that may be indicated by a detailed analysis of this choice of dielectric. It is interesting to note that the conductor/cryostat dimensions naturally increase with voltage level. Since the current capability of an HTSC conductor also increases with diameter due to the reduced surface field, the voltage/current characteristics of the GITL/HTSC system will be similar to those of overhead lines, that is, increasing current capability with higher voltage.

From an engineering viewpoint, the wall thickness would seem to be a variable that is determined by the conductor diameter, the voltage withstand requirement, and the

established dielectric strength of the material. Indeed, these stresses are seen to be functions of the inner and outer diameters of the cable which implies that, if the strength is a constant of the material, the wall thickness can vary with the conductor diameter. Industry practice, however, has not adopted this approach for either laminar or extruded cables. Instead, wall thicknesses have been standardized in specifications issued by the Association of Edison Illuminating Companies (AEIC)[1,2,3,4].

Laminar cable systems are defined in detail in AEIC Specifications for HPFF[1] and SCFF[2] cable types. The standard wall thicknesses are shown in Table 3-3 for the most popular system voltages. The BIL for each level is also shown.

Table 3-3

AEIC Wall Thickness for Paper and PPP HPFF Cables

System Voltage kV	BIL kV	Range of Conductor Size mm^2 (kcmil)	Insulation Thickness - mm (mils)	
			Paper	PPP
69	350	85-2027 (3/0-4000)	6.86 (270)	-
115	550	177-380 (350-750) 405-2027 (800-4000)	10.67 (420) 9.53 (375)	6.35 (250)
138	650	253-456 (500-900) 507-2027 (1000-4000)	12.45 (490) 11.18 (440)	7.62 (300) 6.86 (270)
230	1050	507-1013 (1000-2000) 1140-2027 (2250-4000)	18.92 (745) 15.37 (605)	11.43 (450)
345	1300	507-633 (1000-1250) 760-2027 (1500-4000)	25.91 (1020) 22.99 (920)	15.24 (600)
500	1550	1013-2027 (2000-4000)	27.94 (1100)	18.92 (745)
765	2050	1013-2027 (2000-4000)	-	30.48 (1200)

For voltages above 69 kV two wall thicknesses are specified for each voltage level. The two groups are differentiated on the basis of a range of conductor diameters. The

maximum stress at the BIL of the system is used to define the wall thickness for the minimum conductor size of each group in the HPFF spec. For system voltages less then 230 kV an impulse stress level of 78.74 kV/mm (2000 vpm) is used. The higher EHV levels are based on a stress at BIL of 88.59 kV/mm (2250 vpm).

The SCFF specification uses the same wall thickness as developed for paper-insulated HPFF systems, even though SCFF cables use hollow core conductors that have a larger diameter then a pipe-type conductor of the same metal cross-section (size). As a result, SCFF cables operate at slightly lower maximum stresses then their HPFF counterparts, but minimum stresses are higher. PPP has not yet been used in a SCFF cable installation in the US because so few systems of this type are being installed. It has been used in Japan and will most likely be the dielectric of choice if an opportunity for an EHV SCFF system presents itself in the US. An abbreviated qualification program will be required, but this will not be a problem. HTSC EHV applications in the self-contained configuration should select PPP as the dielectric using the same wall thicknesses as those specified for PPP HPFF cables.

The minimum stress can sometimes control wall thickness for cables with a large conductor diameter. The maximum AC stress occurs at the inner diameter of the dielectric. However, as the insulation thickness becomes smaller in relation to the cable diameters, the minimum stress at the outside of the cable increases toward the level of the maximum stress. This trend raises two concerns: The first applies to the performance of splices and terminals. These accessories require a stress cone of some type to begin the transition from uniform cylindrical cable geometry to that of the accessory. The minimum stress is active at the tip of any stress cone and it is very difficult to apply the stress cone material such that its dielectric strength is as high as is achieved in the cable material. The second concern is that the local strength of the cable dielectric is inherently lower in the outer portion of the dielectric than in the inner portion. This is caused by the use of thicker tapes in the outer portion, and the

reduction in interlayer pressure that occurs as the diameter approaches the outside of the wall. Both of these factors result in lower dielectric strength. The AEIC recognizes this problem for PPP laminate dielectrics and recommends that the wall thickness be increased if necessary to limit the minimum stress under impulse to 68.9 kV/mm (1750 vpm).

Efforts to replace paper tapes (or laminates) with totally synthetic material for laminated EHV cables began in the fifties and continue today without a major breakthrough. This area of research has been, perhaps, the most disappointing of all to those in the cable industry, especially those who were convinced that such an archaic material as paper could surely be replaced by an improved synthetic product of modern material science. The work done by the Brookhaven team on polymer films, initiated in conjunction with their LTSC cryogenic cable program and continued in the eighties as an independent room temperature dielectric development program has come the closest to achieving the required combination of properties with biaxially oriented embossed films of polyethylene or polypropylene[5]. Unfortunately, the trend away from UHV cable applications and the very high cost of a full scale demonstration program have resulted in the termination of this program short of the projected goal. For conventional cable applications in the U.S. up to 345 kV, the benefits of the fully synthetic lapped dielectric, lower loss and reduced wall thickness, simply do not justify the time and expense of a full-scale demonstration program, and the higher cost of the material make it non-competitive in today's limited market.

Extruded dielectrics for distribution cables came of age in the fifties and early sixties and began to find application for transmission cables later in the sixties. Cross-linked polyethylene (XLP) and Ethylene-Propylene Rubber (EPR) are the two polymer systems that have received the most attention. These materials are both thermosetting, making them eligible for operation at temperatures in the 130 C range, a criterion that was

intended to provide an economical advantage over paper insulated cables whose emergency temperatures are limited to 105 C.

Extruded transmission cables made in the U.S. were given an extensive qualification program at the 138 kV level in the late sixties and early seventies[6]. However, problems that emerged during this program coupled with sky-rocketing failure rates of polyethylene distribution cables that began in the mid seventies dampened utility enthusiasm for this type of dielectric with the result that most of the U.S. manufacturers abandoned efforts at the 138 kV level and redirected their assets to the distribution cable market. Since the early eighties, only two U.S. manufacturers are willing to supply 138 kV extruded dielectric cable.

The world-wide picture for extruded dielectric transmission cable is essentially the opposite of the U.S. picture. Manufacturers everywhere have invested heavily to develop and optimize the production of heavy walls of XLP, and EPR to a lesser extent. France has almost two decades of successful experience on their extensive 220 kV network. Japan has commercialized 275 kV XLP cables and successfully manufactured cable for a 500 kV demonstration project. Extruded transmission cable applications are growing rapidly while paper insulated cables are losing their market share. Currently some U.S. utilities import XLP cable systems at 138 kV and a few are considering importing 230 kV cable systems.

Contrary to popular U.S. opinion, we believe that either XLP or EPR extruded dielectrics are viable options for self-contained HTSC cable constructions. Their primary advantage is the elimination of the pressurization system. Improved dielectric performance can be expected because the service conditions do not include significant temperature exposure. In fact, thermoplastic polyethylene, which is much easier to extrude because it requires no high temperature cure, would satisfy all dielectric requirements in an HTSC room temperature dielectric application. The thermoplastic polyethylene option could be

quickly developed within the existing U.S. infrastructure and should prove to be an attractive choice in many scenarios.

The AEIC maintains specifications for XLP cables rated 46 through 138 kV[3] and EPR cables rated 5 through 69 kV[4]. Following standard U.S. practice, the AEIC recommends a single wall thickness for each voltage class which covers the conductor size range for each specification. These wall thicknesses are summarized in Table 3-4 for voltages relevant to potential HTSC cable systems. The impulse withstand voltage that must be obtained during qualification testing is shown in Table 3-4 as the BIL. This level is actually about 25% above the system BIL for each voltage class.

Table 3-4

AEIC specifications for XLP and EPR Extruded cables

System voltage kV	BIL kV	Conductor size range mm^2 (kcmil)	XLP Wall Thickness mm (mils)	EPR Wall Thickness mm (mils)
46	310	107-1013 (4/0-2000)	11.3 (445)	11.3 (445)
69	440	253-1013 (500-2000)	16.5 (650)	16.5 (650)
115	690	380-1520 (750-3000)	20.32 (800)	NA
138	815	380-1520 (750-3000)	21.59 (850)	NA

The wall thicknesses shown in Tables 3-3 and 3-4 are recommended as the minimum values to be used for the design of HTSC room temperature dielectric cables, without exception.

DC cables. The dielectric design for a DC cable system has a totally different focus than for AC systems. The difference is due to the mechanisms that control the operating stress. In an AC cable, the capacitive properties of the dielectric are more relevant than the resistive properties because the electric stress distribution is dictated by the dielectric

permittivity of the material. In a DC cable, the resistive properties of the dielectric material establish the electric stress distribution for the steady component of the applied voltage; the capacitance controls the stress due only to AC harmonics, surges, and impulses.

A near-zero conduction characteristic is mandatory for an AC cable to have an acceptable dielectric loss. An ideal zero-conduction characteristic, however, can be fatal to the operation of a DC cable, since in the absence of conductive stress control, space charges accumulate near the extremes of the dielectric. This phenomena results in very high stresses in the inner and outer regions of the dielectric wall, and very low stress in the bulk of the dielectric. Fortunately, the most commonly employed dielectric material, fluid-impregnated paper, has exactly the right properties for DC applications.

The dominant type of DC cable has used fluid-impregnated paper in a solid-type construction referred to as paper-lead or solid-type cable. This unpressurized dielectric system has been used for voltages up to 300 kV and is the only option for very long submarine cables for voltages above 100 kV. Ongoing developmental efforts promise higher limits for this dielectric. Paper can be used at higher voltages if pressurized, easily accommodating system voltages as high as 750 kV.

The operational limitation for paper is it's temperature sensitive conductivity which causes undesirable stress redistribution when a large temperature gradient is imposed on the dielectric by heavy loading. The potential distribution within the dielectric of an HTSC DC cable will not be subjected to this "stress inversion" because the dielectric will operate at nearly a uniform temperature and have a nearly uniform electrical conductivity. There may be a slight departure from an ideal logarithmic stress distribution due to the small positive voltage coefficient of conductivity for conventional fluid-impregnated DC dielectrics. The distortion caused by this effect reduces the maximum stress under steady conditions and results in only a small increase in stress

during a reverse polarity surge, the most severe design condition in normal temperature DC cables[7]. However, since the stress inversion caused by a large temperature gradient which limits the design stress at operating voltage will not apply to the HTSC DC Cable, the room temperature dielectric HTSC DC cable will be able to operate at higher stresses than those used in conventional DC cables. With some developmental effort, a paper insulated solid-type system that takes advantage of the uniform temperature distribution seems feasible for operation up to 500 kV. In any case, the application of standard design criteria will result in a conservative system suitable for immediate construction with no more than the standard qualification requirements. Table 3-5 presents a suggested range of operating maximum stress at the conductor surface for the design of paper insulated solid-type and pressurized cable constructions, based on existing world-wide practice and recent EPRI Studies exploring the upper limits for DC systems[8].

Table 3-5

Room temperature Dielectric - DC design stress

Cable Type	Design Stress - kV/mm
Solid-type	25 - 35
Pressurized	40 - 50

Fluid-impregnated PPP materials might be excellent candidates for DC cable applications. This dielectric should have substantially improved capability over paper, especially when pressurized. However, long-term studies are suggested to substantiate PPP's very high dielectric strength demonstrated to date, and to confirm the capability of PPP to tolerate space-charge effects within the polypropylene film in general, and partial discharges that may occur in an un-pressurized solid-type construction using PPP.

Cryogenic dielectric Considerations

AC cables. The literature contains a substantial amount of data on bulk gas, liquid,

vacuum, laminar and extruded dielectrics operating at cryogenic temperatures[9]. Much of the available data was obtained during the flourishing activity of the seventies. Recent information has begun to appear in conjunction with world-wide interest in the possibilities for HTSC cables. In the seventies, work at liquid nitrogen temperature was performed by those interested in high capacity cryo-resistive cables and those involved in academic studies of fundamental dielectric mechanisms at cryogenic temperatures. Some reported experimental work at liquid nitrogen temperature as a stepping stone toward liquid helium temperature. Most investigators, however, believed that LTSC superconducting cables would prove to be more competitive then cryo-resistive systems and this caused most of the work on cryogenic dielectrics to focus on bulk liquid or supercritical helium, or laminar materials immersed in the helium cryogen.

Since helium-cooled systems pay a large refrigeration penalty for heat removal there was a well-defined need to find suitable materials with exceptionally low dielectric loss characteristics. This led to a search for low loss laminar materials which could be applied with the same equipment used to manufacture paper insulated cables. Most candidates were new polymeric materials that were emerging from the rapidly developing plastics industry. They were available in a fibrous structure (synthetic paper) or as films.

Initial measurements made in dielectrics laboratories tended to study these materials immersed in boiling liquid nitrogen at atmospheric pressure. Such measurements were simple because all one had to do was immerse the sample cell into an open dewar to obtain a temperature close to 77 K. Some labs used closed systems where the liquid nitrogen could be pressurized, but pressure ranges were low. The group at NRC in Canada published perhaps the most thorough study of materials in liquid nitrogen as a function of pressure, but their pressure range was limited to 0.117 MPa (17 psi)[10]. In boiling nitrogen or liquid nitrogen at low pressures the polymeric materials which have desirable low loss characteristics are susceptible to partial discharges that occur in gas

bubbles and it was common to find that AC breakdown stress was just above the partial discharge inception level.

HTSC cable systems will use liquid nitrogen as the circulating cryogen to control the temperature of the superconductor and remove heat. Liquid nitrogen has excellent dielectric properties, comparable to dielectric fluids. The liquid nitrogen will operate at pressures high enough to insure that the liquid remains bubble free, just as is done with conventional SCFF and HPFF paper or PPP systems. The recommended minimum system pressure will be 0.75 MPa (100 psi). Maximum pressures will be as high as 3.0 MPa (400 psi) and will be dictated by the pumping requirements of the system and elevation considerations.

The cryogenic dielectric HTSC system can consider the same three types of system discussed above for the room temperature dielectric option; a rigid tubular system using liquid, gas or vacuum and spacers (as in an SF_6 GITL), a flexible cable insulated with a laminar material, or a flexible cable insulated with an extruded material. The latter two concepts would most likely immerse the dielectric in the liquid nitrogen cryogen and take advantage of the improved breakdown strength afforded by its high pressure.

A rigid tubular superconductor system, if developed, might be an attractive option for a high capacity HTSC system. Some of the earliest cryogenic dielectric concepts were based on rigid tubular members with supercritical helium (Union Carbide) or vacuum (Underground Power Corp.) serving as the bulk dielectric. Such systems were geometrically similar to modern SF_6 GITL systems with the addition of an external cryostat. Candidates for a bulk dielectric material in a rigid HTSC system are the liquid nitrogen cryogen, helium or neon gas, or vacuum. Each would have to interact with supporting materials which could be continuous members such as plastic tubes or I-beams wrapped helically around the inner conductor, or solid spacers as used in GITL systems.

The design problem for these bulk dielectric approaches is the selection of suitable operating stresses and definition of the operating pressure and safe limits for each possibility. Table 3-6 presents estimates of reasonable values that can be used for preliminary studies, and a comparison to stresses used in modern GITL systems.

Table 3-6

Design Stresses for Cryogenic Dielectric Rigid Cables
Temperature Range = 65 - 80 K

Bulk Medium	Operating Stress kV/mm	vpm	Stress at BIL kV/mm	vpm
LN_2 @ 10 atm.	4.0	100	30	762
Helium @ 10 atm.	2.0	50	15	381
Neon @ 10 atm.*	2.0	50	15	381
Vacuum - $<10^{-5}$ torr	1.0	25	6.0	150
SF_6 @ 3 atm., 300 K	3.15	80	17.7	450

Note: stress shown is maximum stress at inner conductor surface
* - Insufficient data, parameters assumed similar to helium

When both the inner and outer portions of each cable must be cold it is desirable to have both the go and the return channels within the same cryostat. When this is done, some degree of thermal isolation between the two channels is required to allow the temperature profile to be controlled from the ends of the cooling loop. Vacuum has a significant advantage in that it can provide substantial thermal insulation as well as the dielectric function. If liquid nitrogen were used as the dielectric there would have to be an additional thermal barrier to thermally separate the streams. Helium or neon might have sufficient radial thermal impedance to provide the bulk of this function but additional layers of thermal insulation might be needed to allow the streams to coexist.

Flexible cables could also benefit by the use of a gaseous dielectric if a suitable flexible support system could be developed along the lines of the Spir-o-line polyethylene tube support structure used for years in high-power, low-loss RF antenna systems[11]. The more likely choices for a flexible cable would be a laminar structure or an extruded polyethylene dielectric.

Laminar fibrous materials such as Tyvek, and polymeric films have extremely low dissipation factors at 77 K but questionable dielectric strength, likely due to poor resistance to partial discharge. Materials such as conventional cable papers show dielectric strengths equal or higher than that at room and elevated temperature but their dielectric loss is an order of magnitude greater than the polymer materials.

Some experience has been gained with fibrous laminar dielectrics in the early cryogenic cable applications described in Section 2. The first cryo-resistive cable manufactured in the GE program employed Tyvek and exhibited disappointing dielectric performance. The second cable, made with conventional cable paper, performed in accordance with its design. Professor Klaudy's LTSC 66 kV cable system also used conventional paper impregnated with supercritical helium. A cryo-resistive cable insulated with paper was made in the USSR and achieved a respectable AC breakdown level of 32.2 kV/mm (818 vpm). Recent work in Japan has established exceptional performance with the new PPP laminates in liquid nitrogen. Several cryo-resistive cables insulated with Tyvek were tested in Japan in the seventies. Those results, while considered satisfactory, also exhibited lower dielectric strength then expected. Reading between the lines in the literature one detects the fact that most of these cables suffered from mechanical deficiencies in the taping structure. This explains why performance extrapolated from cell studies and model cable test data were not achieved in the full scale tests.

The problem with the cellulose-based materials (paper and PPP) that have been successful in cryogenic demonstrations is their high dielectric loss characteristic. This

limits the maximum practical operating voltage at which they can be used. EHV voltages (230 kV and higher) will require a dielectric with lower losses, such as synthetic fibrous or film tapes, or extruded polyethylene. The Brookhaven Project expended a significant effort in developing a polymer film tape with the desirable characteristics of low loss, good mechanical properties and sufficient dielectric strength when impregnated with gaseous helium. These materials seem to be the logical starting point for the development of a low-loss laminar system operating in liquid nitrogen at high pressure for EHV applications.

Another difficulty found in past experience is that the cryo-resistive cables that were tested were quite large because they needed a large cryogen channel and conductor cross-section. As noted earlier, thin dielectric walls on large core diameters result in high minimum stress on the outside of the dielectric. This makes termination of the cable very difficult as evidenced by the fact that most of the cable tests resulted in termination failures. Those tests that achieved breakdown in the cable were at lower levels then anticipated and appear to be correlated with taping defects. The BNL film cables were made on a relatively small core, more in line with conventional practice. Even so, termination of those cables was troublesome, probably because of the very high design stresses attempted. In terms of diameter ratios, HTSC cables will lie between these extremes. Lower stresses are recommended simply because there is no need to push the limits of dielectric technology, at least in the early stages of the development of HTSC cables.

The aging of a dielectric assembly is an important consideration in the development of design parameters for any new dielectric system. Fortunately, cryogenic temperatures have a pronounced beneficial effect on aging mechanisms with the exception of deterioration of polymer materials caused by partial discharge. Aging studies on pressurized samples of paper, PPP and Tyvek in the GE program established that

thermal and stress-induced mechanisms cause insignificant changes in the loss and breakdown characteristics of these materials[12].

After consideration of the history of cryogenic dielectrics and the data in the literature coupled with our own experience, we offer the following recommendations for the preliminary design of HTSC cable systems of this type. Paper and PPP cables can use the same wall thickness philosophy as room temperature paper and PPP cables, with care not to exceed 69 kV/mm (1750 vpm) minimum stress on the outside of the cable at BIL. Cables made with these materials will not require an insulation development program, only the normal qualification program as outlined in the AEIC Specifications. Of course, the manufacturer of an HTSC cable may want to perform his own in-house exploratory program to determine material and manufacturing criteria prior to full-scale cable production. Unfortunately these materials will not be suitable for EHV systems because of their high loss, unless the intended application can tolerate this burden.

The choice of a laminar polymeric material for EHV use is between a synthetic paper and polymer film. Either choice will require additional material studies and possible full-scale trial cables to establish performance limitations. Synthetic papers like Tyvek will perform well if design stress is kept low and satisfactory taping criteria can be established. We recommend the use of the conventional AEIC low stress paper wall thicknesses for synthetic paper systems until long-term full-scale tests determine whether higher operating stress can be achieved. The bi-axially oriented polyethylene or polypropylene films developed at Brookhaven should achieve better performance in full-scale cables once taping parameters in a commercial taping line can be determined. We expect that AEIC PPP wall thicknesses will give satisfactory and consistent performance with a comfortable margin in the liquid nitrogen environment.

An attractive option for a low loss dielectric is extruded polyethylene. The caveat for extruded polyethylene is the accommodation of its large thermal contraction (roughly

3%) on cool-down. There is less experimental data on extruded polyethylene dielectrics, but these materials appear to perform exceptionally well in liquid nitrogen, provided the thermal contraction of the dielectric is allowed to occur without creating excessive mechanical stress. Qualification of an extruded dielectric cable should be relatively simple, since new manufacturing techniques are not involved. Data from the EPRI-sponsored work by CTL[13] and work in Japan[14] show clearly that dielectric performance of extruded polyethylene is significantly improved in liquid nitrogen relative to room temperature performance, and improved even more if the liquid nitrogen is at high pressure. CTL suggested appropriate wall thicknesses for cryogenic XLP dielectrics at 69, 138 and 230 kV of 240, 500 and 750 mils respectively, which seem reasonable in view of the improvement in breakdown strength they observed, without undue attention to the quality of the extrusions which were tested.

Table 3-7 summarizes our recommendations for the wall thickness and choice of material to be used for the preliminary design of cryogenic dielectric HTSC cables, as a function of system voltage.

The fact that an extruded dielectric over a hollow core creates a pressure-tight structure can be used to advantage in the cryogenic system. This eliminates the need for additional components to control or prevent the cross-over of liquid nitrogen from the core to the return channel outside of the cable's shield conductor.

DC cables. The dielectric properties of laminar cable materials tend to improve at low temperatures, and this applies to the resistivity and aging at high stress of paper and PPP tapes when impregnated with liquid nitrogen. The resistivity can increase several orders of magnitude when impregnated with liquid nitrogen. Thermal aging mechanisms are essentially eliminated leaving only stress-dependent aging to be considered. A material's resistance to partial discharge at operating stress coupled with it's ability to pass liquid nitrogen so that the operating pressure is maintained

throughout the dielectric during normal and abnormal operation are important characteristics for the selection of dielectric candidates.

Table 3-7

Wall Thickness of Various Insulations for Cryogenic Dielectric HTSC Cable

System Voltage kV	BIL kV	Wall Thickness - mm (mils)				
		Paper	PPP	Synthetic Paper	Polymer Film	Extruded PE/XLP
69	350	6.86 (270)	5.08 (200)	-	-	6.096 (240)
115	550	10.67 (420)*	6.35 (250)	-	-	10.67 (420)**
138	650	12.45 (490)*	7.62 (300)	12.45 (490)	7.62 (300)	12.7 (500)
230	1050	-	11.43 (450)*	18.92 (745)	11.43 (450)	19.05 (750)
345	1300	-	15.24 (600)*	25.91 (1020)	15.24 (600)	22.86 (900)**
500	1550	-	-	27.94 (1100)	18.92 (745)	25.4 (1000)**

* - may have excessive dielectric loss
** - wall thickness extrapolated from CTL work

There appears to be no experimental data on the DC dielectric properties of laminar materials impregnated with liquid nitrogen at high pressure where discharges do not govern the breakdown strength and life of the material. However, data on AC and impulse strength in liquid nitrogen show clearly that cable paper performance will be similar to or better then fluid-impregnated paper at room temperature. It is not clear whether PPP will offer higher breakdown strength and the possibility of higher operating stress and thinner walls. Pending further research, USI recommends the use

of conventional cable papers selected to suit the application by the cable manufacturer since the mechanical behavior of the paper will play an important role in the success of the cable design. A maximum design stress at the surface of the conductor of 40 to 50 kV/mm (1017 to 1270 vpm), increasing with voltage, with a minimum liquid nitrogen pressure of 0.52 MPa (75 psi) is suggested for preliminary studies. This stress suggests wall thicknesses as shown in Table 3-8 calculated for a conductor assembly diameter of 5.08 cm (2 inches).

Table 3-8

Paper Wall Thickness for Cryogenic Dielectric DC HTSC cables

System Voltage kV	Max. Operating Stress kV/mm (vpm)	Wall Thickness mm (mils)
+/- 100	40 (1016)	2.8 (110)
+/- 250	44 (1118)	6.35 (250)
+/- 400	47 (1194)	10.1 (400)
+/- 600	50 (1270)	15.3 (600)

Many polymeric materials have been suggested for cable insulations at cryogenic temperatures and many have been studied in detail in conjunction with earlier programs. In general these investigations were seeking dramatically reduced AC losses. One polymeric laminar material, Nomex, might prove to be a good DC insulating material in pressurized liquid nitrogen. This paper made of fibrous nylon has properties comparable to cellulose. Its successful use in liquid nitrogen may depend only on the ability to manufacture and cool down a cable assembly taped with Nomex.

Another viable candidate that warrants further investigation is extruded EPR. This material is a good choice for moderate DC voltage applications of conventional cable but has received little attention in cryogenic studies. Rubber materials have long been

known to become very brittle at low temperatures. The development of the synthetic rubbers was partly driven by the desire to create a material with rubber-like properties that was more tolerant of low temperatures. One mechanical property of EPR, its low coefficient of expansion, makes its contraction much less then that of polyethylene when cooled to liquid nitrogen temperature. The dielectric characteristics of the EPR compounds are heavily influenced by their polar molecular structure. This implies that AC loss and, possibly, breakdown strength may improve in liquid nitrogen while its conductivity caused by ionic fillers will be preserved. We believe this behavior makes extruded EPR an interesting possibility for the dielectric of an HTSC DC cable.

Cable Dimensions

Flexible cables for high voltage underground transmission represent a mature niche industry in the U.S. HTSC cables that enter this niche will be manufactured and installed within the framework of the existing infrastructure simply because the present market trends for underground transmission do not suggest investment in new plants or equipment. This existing infrastructure has two types of dimensional constraints that limit the size of cables considered; production equipment diameter limitations, and shipping reel sizes which impact the cable diameter and shipping length.

The dimensional constraints on rigid constructions affect section length rather than system diameters. Lengths are limited to what can be shipped. The standard truck length for pipe is about 14 meters. Longer lengths are possible, up to perhaps 25 meters with special attention to routing. Rail shipment has a limit of about 28 meters on a single standard flat car.

Cable diameters. The dominant production constraint for a flexible cable is the maximum insulation diameter that will fit through the dielectric application equipment. For laminar cables made in the U.S. on existing equipment, this will be slightly less than 13 cm (5.12 inch). The largest laminar cables that have been produced in the U.S. are

the 765 kV PPP HPFF cable made for EPRI by Phelps Dodge (now Cablec)[15], the first Tyvek-insulated cryo-resistive cable made by Phelps Dodge for GE/EPRI[16], and the paper insulated cryo-resistive cable made for GE/EPRI by Anaconda[17]. The insulation diameters of these cables were 11.3 cm (4.33 inch), 11.46 cm (4.51 inch), and 12.07 cm (4.75 inch), respectively. World-wide, larger cables have been manufactured. The largest cable manufactured to date is the 1100 kV SCFF cable made by Pirelli in Italy for a long-term qualification test[18]. This cable has a diameter over the paper dielectric of 12.6 cm (4.96 inch). The hollow core of that conductor has an O.D. of 56 mm (2.2 inch) and a core diameter of 24 mm (0.945 inch).

Extruded thermoplastic polyethylene can be applied in many types of extrusion equipment because cooling can be initiated as soon as the material leaves the extruder die or even within the die for larger wall thicknesses. The polyethylene will solidify in a length short enough that the cable will not sag between the die entry and the first point of supporting contact after solidification. Cross-linked polyethylene must be processed in a more complex process that uses either a vertical extrusion line or a catenary vulcanization line (CV). These larger machines are required so that the cable can hang free while the temperature is raised to initiate the cross-linking process and then lowered until solidification occurs. Weight is the predominant parameter limiting cable size, rather than diameter restrictions that impact the extrusion die design. The weight of an HTSC cable with a hollow core and light superconductor assembly, with or without an internal cryostat, will be only slightly more than the weight of the polyethylene. Therefore, it is difficult to state precisely what the diameter limitation may be. It will undoubtedly depend on the specific extrusion line and possibly be governed by ancillary equipment such as take-up reel size limitations. Considerations of very large extruded cable designs will more likely be limited by shipping and installation constraints.

The length of cable that can be wound on a shipping reel is a function of three reel parameters. The first two are the external dimensions of the reel; its width and its overall diameter. Shipping reel dimensions are limited by the practical and legal criteria of the method of shipment. The largest shipping reels commonly used for truck transportation without special permits are 2.44 m (8 feet) wide and about 3.6 m (142 inches) in overall diameter, exclusive of protective lagging. Larger reels exist and have been used on occasion. Diameters of 3.94 m (155 inches) can be used with the 2.44 m width on the interstate highway system, and wider 3.6 m diameter reels have been shipped by rail. Slightly larger dimensions can be used with the extra bother of special permits and careful routing, often requiring off-hour travel only.

Rail limitations depend on the orientation of the reel. The standard car width is 3.05 m (10′) and the standard height is 5.03 m (16′ 6"). A low bed flat car has a surface 0.61 m (2 feet) above the rail leaving 4.42 m (14′ 6") available for the outside reel height. If the reel axis is across the flat car it is limited in overall width to 3.05 m and a diameter of 4.42 m. If the axis is parallel to the rail the diameter is limited to 3.1 m , but the width can be extended to perhaps 9.1 m (30′). There are many routes that allow load height to reach 5.715 m (18′ 9"). Also, a special low bed car that places the load only 22.86 cm (9") above the rail will extend the useable height for some cases to almost 5.49 m (18′).

The drum diameter of a shipping reel is the third parameter that defines the length of cable of a particular diameter that a reel can hold. The rule of thumb used to estimate the minimum drum diameter for a given laminar cable size is to use a multiple of the cable's outside diameter. The AEIC Specification defines this multiple as a function of the insulation thickness. Specific values of this multiple are 14 for insulation thickness less than 8.89 mm (350 mils), 18 up to thicknesses 20.32 mm (800 mils), and 22 for thicknesses over 20.32 mm (800 mils). An additional constraint to be satisfied is that the drum diameter cannot be less than 22 times the conductor assembly diameter. As the cable diameter increases, so does its minimum drum diameter, causing the maximum

length that will fit on a reel of fixed flange diameter to decrease disproportionately. Typical maximum shipping lengths of the old style 345 kV paper-insulated HPFF cable, which had an outside diameter of about 10.2 cm (4.12 inch) were on the order of one kilometer (3280 feet). The longest lengths of this size cable shipped over the road were for a Long Island Sound Crossing in 1978 and measured just over 2.13 km (7000 feet). Each reel weighed about 45,360 kilograms (100,000 pounds) and measured 3.99 meters (13 ft, 1") wide by 4.7 meters (15 ft, 5") in diameter.

Hydraulic Requirements. The cable system dimensions (basically diameters) are affected by each of the radial components which make up the cable. Essentially all cable designs evolve from a hollow core cryogen channel concept. This core must be sufficiently large to accommodate the cryogen flow necessary for acceptable temperature rise and pressure drop in the cooling loop. Rigid systems tend to have large dimensions for other reasons, so the cryogen channel seldom dictates the system diameters. Flexible cables are limited to a diameter less than 13 cm, which leaves less room for the cryogen channel. Room temperature dielectric cables need to contain the cryostat and the dielectric within the diameter limitation leaving the least space for cryogen flow.

Cryogenic dielectric cables do not require a hermetically sealed cryogen channel. The conductor assembly can be as simple as a spiral former covered with one or more layers of superconducting tapes or wires, provided the dielectric assembly provides sufficient flow impedance to limit the radial flow of the cryogen to a value acceptable to the overall flow scheme. Room temperature dielectric cables, however, need absolutely gas tight containers for the cryostat which must operate at high vacuum levels and yet be flexible to allow reeling, installation, and final positioning. This can be accommodated by a slight degree of corrugation of the cryogen tubes. The added radial space taken by the corrugation and the impact of the corrugation on the fluid flow friction factor can be minimized by making the corrugation pitch short and its amplitude small. A spatially optimum design might be achieved by using a soft metal tubing with

appropriate mechanical support. For AC cable, the superconductor could be either inside the cryogen tube or on the outside surface of the tube in the vacuum space as described in Section 2.

The procedures for calculation of temperature rise and pressure drop are presented later. General guidelines regarding the feasible magnitudes can be inferred from the experience with pipe-type systems. Typical operating pressures are in the range of 1.4 MPa (200 psi) and test pressures are at least 3.4 MPa (500 psi). The pressure capability of thin wall tubes of small diameter (a few cm) easily exceeds nominal pressures in this range. In terms of standard construction practice, the upper limit for pumping pressure will be set by cryogenic pump and pressure control capabilities. A reasonable target is about 2.8 MPa (400 psi).

The lowest pressure in the system, at the circulating pump inlet, must be well above the vapor pressure at the fluid temperature to prevent gas evolution and pump cavitation. In no case should the inlet pump pressure be allowed to operate below 0.35 MPa (50 psi). If a nitrogen-immersed cryogenic dielectric is employed, the lower pressure limit should be raised to the order of 0.7 MPa (100 psi). The dynamics of the pressure behavior of the system under abnormal conditions will most likely influence the selection of the minimum design pressure.

The operating temperature range affects the superconductor behavior, particularly the losses, and the selection of the cryogenic equipment. The superconductor performance is optimum at the lowest practical operating temperature, while the cryogenic performance is optimized at higher temperatures. The feasible range is dictated by the choice of liquid nitrogen as the cryogen. The lowest temperature that can be considered is about 65 K which is just above the triple (freezing) point of nitrogen, 63.149 K. A practical temperature rise will be on the order of 10 K. A small margin should be allowed to avoid freezing in the loop due to minor expansion effects that might occur

in pipe fittings and bends, yielding practical design targets of a cooling plant output temperature of 67 K and a maximum hot-end output from the loop of 77 K. The hot end temperature should be minimized consistent with length and pressure drop restrictions. Designing for a higher superconductor temperature is not recommended because of the falloff of performance as the superconductor temperature approaches its T_c.

Conductor Cross-Section. The superconductor cross section depends on the critical current density of the superconducting elements over the design range of operating temperature. If the useable current density is greater than, say, 20,000 A_{rms}/cm^2, the radial dimension of the superconductor becomes negligible for a reasonable cryogen channel radius. For example, if the superconductor were placed at a mean radius of 1.5 cm, the cable design current was 1500 A_{rms} and the cable conductor operated at 5000 A_{rms}/cm^2, the required superconductor thickness would be only 0.32 mm (13 mils), allowing a 4:1 margin between the maximum operating current and the critical current of the superconductor. For some conductor tape configurations, such as the typical powder-in-tube tapes, the superconductor may occupy as little as 25% of the cross section of the tape; the thickness of the tape would then be 1.28 mm (50 mils). Such tapes have already demonstrated short sample critical current densities in the range of 20,000 to 40,000 A_{peak}/cm^2 at 77 K and performance levels continue to improve. From a practical viewpoint, the required radial dimensions consumed by the superconducting material should be insignificant.

It is unrealistic to suggest a minimum required current density or loss characteristic for the HTSC materials at this time (mid-1992). Performance levels are improving continuously, and the point has been reached where the dimensions of the superconductor have very little impact on the overall cable dimensions. Much will depend on the nature of the material assembly, the amount of normal metal associated with the structure, and manufacturing ramifications. The choice of the actual cross-section of material to be used should await a more detailed knowledge of the candidate

material and the application, in particular the overload and fault current requirements of the cable.

Cryostat Thickness. Thermal insulation considerations are presented in depth in Section 4. A brief summary discussion follows only as it impacts the relationship of the cryostat to other cable dimensions. The thickness of the cryostat depends on a number of factors. The heat in-leak of evacuated super insulation, which is comprised of multiple layers of metallized mylar, is caused by radiation and the thermal conductivity of the mechanical support/separation scheme. The radiation heat transfer decreases as the number of reflective layers increases until thermal conductivity between layers begins to counteract the benefit of additional layers. The two walls of the cryostat have to be separated to accommodate the forces imposed during handling and service in addition to maintaining the inner wall roughly concentric to the outer wall. This requires a fairly robust separator support structure, and the heat leak through this structure will be significant.

Vacuum Barrier, Inc. has for several decades been manufacturing flexible vacuum insulated, corrugated coaxial copper or stainless steel LN_2 tubing in a size range similar to that contemplated for room temperature dielectric cables. With no superinsulation, Vacuum Barrier achieves a heat in-leak of about 2 W/m for a 5 cm ID copper tubing. This can be reduced with several layers of superinsulation to the practical range of 0.5 W/m. This target value has been selected for preliminary design evaluations. An experimental program is required to optimize the design and construction of long lengths of cryostat with attention to the problems of evacuation, outgassing, and suitable performance of the support structure against cost.

Based on a target heat in-leak value of 0.5 W/m, and the data presented in Section 4, a rough estimate of the minimum cryostat dimensions can be made using either the inner or outer diameter, whichever is controlling, and making the ratio of the outer diameter

to the inner diameter equal to 1.4. The diameters to be used for this calculation represent the clearance in the annular space of the cryostat, that is, the maximum outer diameter of the inner tube or the minimum inner diameter of the outer tube. If larger diameter ratios can be accommodated they should be used, up to a ratio on the order of two. Beyond this level, there is minimal gain in performance. These practical guidelines apply equally to small corrugated cryostats and large smooth-walled rigid types of cryostat that would be used for cryogenic dielectric systems.

Cable Shield and skid wires. High voltage cables of all types require a conducting electrostatic shield and grounding structure for the control of dielectric stress, the transport of the dielectric charging or leakage current, and the ability to carry fault currents without damage to the shield components. AC cables experience losses in their shield material due to eddy currents, circulating current and charging current. DC cable design is, on the contrary, influenced by the conduction of the leakage current and relatively small fault current capabilities.

Flexible cables of conventional pipe-type design use a cable shield consisting of one or more metal tapes paralleled by one or two metal skid wires. The eddy current and circulating current losses are proportional to the square of the phase current, and can approach a few Watts per meter. Superconducting cables designed to carry higher currents aggravate the shield loss accordingly. If the cable dielectric is to be cryogenic, the shield losses will have to be removed by the cooling system, thereby incurring the corresponding energy penalty.

The mathematics of shield loss behavior (described in detail below) depend on the axial resistance of the shield such that there will be a particular resistance which gives a maximum loss. The loss falls off to zero as the shield resistance approaches either zero or infinity. This behavior is the primary reason that all AC LTSC cable designs utilized a superconducting shield, the zero resistance option. Of course, a superconducting

shield requires a cryogenic dielectric. A room temperature dielectric cable must have a conventional type of shield structure for which the design calculations suggest the use of a nonmagnetic, high resistivity material such as stainless steel for the metal shield tape and skid wires, opting to increase the shield resistance to achieve tolerable losses. Losses can be further reduced by using hollow skid wires to reduce their conductance, or a low resistivity tough polymer.

Shield tapes are typically 0.076 to 0.127 mm (3 to 5 mils) thick and are applied intercalated with a 25 micron (1 mil) metalized polyester tape which acts as a moisture seal. One metal tape is adequate for normal service and is the standard choice for conventional pipe cable systems. Skid wires are used to facilitate pulling of the three cables into a pipe. They are "D" shaped and are described by their height and width. Two sizes are used, 2.5 x 5 mm (0.100" x 0.200") or a "low profile" 1.2 x 4.7 mm (0.063" x 0.187"). They are applied helically with a 7.62 cm (3 inch) lay in the direction opposite that of the shield tape, in pairs (double entry) evenly spaced except for small cables, where one suffices. This typical shield and skid wire assembly is standard in the industry; only the particular metals vary depending on individual utility preference. Choices include stainless steel, brass, bronze, copper and zinc. The assembly adds about 3.6 mm (140 mils) to the cable diameter for the small skid wires, 5.5 mm (215 mils) for the larger size.

Test cables installed at the EPRI Waltz Mill Long Term Testing Facility have used over-sized 3.8 x 7.6 mm (0.150" x 0.300") high density polyethylene skid wires to provide electrical isolation between adjacent cables and the pipe[19]. This facilitates the measurement of the dielectric condition of the cable throughout a test program. Plastic skid wires of this type could be considered for a typical commercial HTSC cable installation because of the reduced cable weight, but at the expense of a 7.6 mm (0.3") increase in cable diameter unless a smaller size could be established as having adequate wear properties. Also, the polymer has to be semi-conducting (carbon loaded) to

provide electrical contact between cable shields. This contact is required to minimize the axial flow of charging currents. The three phase charging currents add to zero if the three cable shields are connected.

Shield and skid wire designs for cryogenic dielectric cables that are to be installed in a smooth pipe which is the inner tube of the system cryostat can be similar to the conventional assembly described above and will have a similar dimensional impact on the cable and pipe dimensions. The higher loading associated with the choice of a cryogenic dielectric would cause relatively high shield loss which is why these cables will probably require the superconducting shield system. Standard skid wires would still be needed for installation, but since they are outside of any magnetic field, they have no impact on system losses. DC cables installed in pipes would likewise use this construction. Other cable configurations such as self-contained or rigid types would use a shield system specific to the design.

Pipe or enclosure. Dimensional considerations of the pipe or enclosure apply to pipe-type assemblies using the room temperature dielectric concept and to cryogenic dielectric concepts which have a large common cryostat.

Industry practice for pipe-type systems utilize standard pipe sizes of 14.1 cm (5-9/16"), 16.8 cm (6-5/8"), 21.9 cm (8-5/8") and 27.3 cm (10-3/4") O.D. Wall thickness is 6.4 mm (1/4") for normal conditions but may be increased to 9.5 mm (3/8") or 12.7 mm (1/2") for abnormal strength or corrosion conditions and for submarine portions of a circuit.

The maximum diameter limitation for each cable is established by a minimum allowable clearance between the cables and the inside of the pipe. For three cables the clearance is defined as the inside diameter of the pipe minus the diameter of a circle enclosing the three cables in a tight triangular arrangement. This diameter is approximately 2.15 times the individual cable diameter over the skid wires but is sometimes reduced by

acknowledging that the skid wires may "nest". The allowable clearance ranges from 12.7 mm to 25.4 mm (1/2" to 1"), increasing with pipe diameter. Clearance is required to insure that the cables can be pulled into the pipe smoothly and to allow the cables freedom to move about as they expand and contract due to temperature variations caused by their loading. Thermal movement occurs daily and seasonally.

There are two reasons why room temperature dielectric HTSC cables might be designed with a smaller clearance. First, HTSC cables that could be installed or retrofitted in steel pipes would be much lighter than cables of comparable dimensions with a massive copper conductor and would also have less stiffness. As a result, the pulling tensions would be significantly reduced and the pulling operation greatly simplified. The second reason is that thermal motion of the HTSC cable would be essentially eliminated. The thermal contraction of the inner portion of the cryostat and the superconductor assembly will be accommodated within the cryostat. The room temperature components will experience daily variations in temperature due to the shield and pipe losses which will cause a temperature rise above the ambient ground. There will, however, be no stiffness in the assembly that would force a change in length as does a conventional copper or aluminum conductor. It is therefore recommended that the minimum clearance used to establish the maximum cable diameter over the skid wire assembly be reduced to the range of 9.5 to 19 mm (3/8" to 3/4"), varying in 3.2 mm (1/8") increments for the above four pipe sizes.

While there is no hard limit to the minimum cable diameter that can be installed in a given size pipe, there is a dangerous condition that should be avoided. This condition arises when the ratio of the inside pipe diameter to the cable diameter is close to three, particularly below three. If the cables are smaller than one third of the pipe diameter, one cable could theoretically pass freely between the other two. If the ratio is slightly less than three, that cable could get stuck between the other two if the cable tried to cross between them. Very large deformation forces can be generated by the wedging

action under these conditions. It is therefore prudent to avoid pipe to cable diameter ratios in the range of 2.9 to 3.1. It is unlikely that the diameters of realistic HTSC cables will get near this range because the superconductor and cryostat diameters will generally be maximized against the minimum clearance restraint. Table 3-9 lists the suggested cable diameter range for the four standard pipe sizes likely to be encountered in a retrofit scenario.

Table 3-9

Maximum cable diameters for standard pipe diameters

Pipe Size inches	Pipe O.D. x wall thickness cm (in)	Clearance cm (in)	Maximum Cable diameter* cm (in)
5	14.1 x 0.635 (5-9/16 x.25)	1.3 (1/2)	5.39 (2.12)
6	16.8 x 0.655 (6-5/8 x .258)	1.6 (5/8)	6.50 (2.56)
8	21.9 x 0.635 (8-5/8 x .25)	1.9 (3/4)	8.71 (3.43)
10	27.3 x 0.635 (10-3/4 x .25)	2.2 (7/8)	11.1 (4.36)

* Maximum cable diameter is over skid wires

New installations employing room temperature dielectric cable should be designed using stainless steel pipe to reduce the pipe loss thereby allowing a 30 percent increase in current loading as compared to a steel pipe of the same dimensions. Stated differently, the stainless steel pipes exhibit less than two thirds the loss of a steel pipe for the same current. The savings from the loss reduction may be sufficient to justify the higher cost of the pipe, even without considering the increase in capacity. Stainless steel pipes can be used with a wall thickness as small as 3.2 mm (1/8") owing to their higher strength and immunity from most types of underground corrosion. They can also be ordered in non-standard sizes without a cost penalty. There have been trial installations of stainless steel pipe that have demonstrated that installation costs can be reduced as well, with the exception that field bending is more difficult[20]. Stainless steel pipe would be used with

no internal coating but a conventional external coating to provide a dielectric separation that allows a cathodic protection system to be installed.

Since flexible cables of any type are limited in diameter to about 12.7 cm (5"), the largest pipe size required would be about 30.5 cm (12"). This applies to the inner pipe of a rigid cryostat as well as a room temperature dielectric cable pipe, for both, steel or stainless steel. The outside diameter of a cryostat can be estimated by applying a reasonable diameter ratio of 1.4 as discussed above to a 30.5 cm (12") diameter inner pipe with a 3.2 mm (1/8") wall. This yields an inner diameter for the outside pipe in the range of 43.2 cm (17").

Rigid systems that use a gaseous dielectric can require much larger diameters than the flexible designs discussed above. It is difficult to consider practical limitations without an experience base for such systems. Large pipe installations are more common for long-range gas and oil transmission pipes, and for water and sewer applications. Designers that consider this option would do well to acquire help from those experienced in the large pipe field. Some utilities may be reluctant to venture into this new ground unless the economics overwhelmingly favor those concepts.

A final dimensional consideration for the design of a new installation will be the minimum installed bending radius that the pipe and cables can tolerate. Conventional practice limits the bending radius to about 50 times the outside diameter of the pipe when the pipe is bent in the field. The cable should not be bent to a radius tighter than about 25 times its diameter. The cable limit comes into play for factory made bends in the pipe, or in riser pipes that carry individual cables to their respective terminations. Standard practice limits the radius of factory bends to a minimum of 1.83 m (6 ft). One consideration in the selection and evaluation of bends is the effect on pulling tension and on the sidewall bearing pressure of the cables against the pipe during the pulling

operation. It is common and prudent to arrange the pulling direction such that sharp bends are at the beginning of the pull where the pulling tension is at its lowest level.

Methods of Calculation

The development of a detailed cable system design requires calculations of several types. The general goal of the designer is to minimize the total cost of the system over the total life, while still meeting all of the functional requirements. The design process can take many paths; usually there will be constraints that dictate the order in which calculations are made. The first step in the process will determine the dimensions of the system. The second will establish the losses that need to be removed. The third will interrelate the hydraulic parameters, cryogen flow rate, pressure drop and temperature rise with cooling section lengths. The fourth group will explore the mechanical behavior of the system components with respect to manufacturability, handling, installation, and temperature cycling. Finally, it will be necessary to calculate the electrical parameters of the cable systems as required by the utility for integration into their system operation and to predict the response of the system to fault currents and other abnormal conditions of current and/or voltage.

The dimensional parameters are strongly correlated. For example, the cryogen duct diameter impacts the flow resistance, magnetic field at the surface of the superconductor, the AC loss in the conductor, and the application of the superconductor material. These properties are all favored as the duct diameter increases, but at the expense of larger cryostat, dielectric and enclosure dimensions. Clearly an optimization process suggests itself. The most direct method will use an iteration process. In some cases it may be possible to combine the controlling relations into a closed-form algorithm, but the effort is usually not trivial and often not justified.

The methods of calculation will be presented by groups, somewhat in the order that they impact the general analysis of the cable system. Superconductor performance and the

ohmic losses in the system are dependent on the magnetic fields throughout the system. It is, therefore, appropriate to begin with a review of the relevant magnetic field calculations.

Magnetic field calculations

The behavior of superconducting material is dependent on the magnetic field that exists at its surface. In addition, normal metal components of the cables, cryostat and/or enclosures that are exposed to time-varying fields will suffer eddy current losses that must be acknowledged in the thermal design of the system. Clearly, an accurate knowledge of the magnetic fields produced by the cables is mandatory.

Engineering materials are classified into one of three groups based on their internal reaction to a magnetic field. Diamagnetic materials set up atomic dipoles that oppose the externally applied magnetic field. Paramagnetic materials enhance the field and ferromagnetic materials enhance it dramatically. The contribution to an applied field H by the magnetization M of the material is called its susceptibility χ_m which is defined by the ratio of M to H.

$$\chi_m = \frac{M}{H} \tag{3-2}$$

The magnetic flux density B in the material is the sum of the applied magnetization H and the internal magnetization M times the permeability of free space, or,

$$B = \mu_0 (H + M) = \mu_0 (H + \chi_m H) = \mu H \quad \frac{Webers}{m^2} \tag{3-3}$$

where $\mu = \mu_0(1 + \chi_m)$. The susceptibility of diamagnetic materials is slightly less than zero while that of paramagnetic materials is slightly greater than zero. The χ_m of ferromagnetic materials is much greater than zero, is a function of magnetization and magnetic history, and is specific not only to a particular material but also to its geometry.

Superconductors are close to perfectly diamagnetic ($\chi = -1$, $\mu = 0$) in the classical sense, for magnetic intensities below H_c in Type I or H_{c1} in Type II materials. Type II materials exhibit a finite negative susceptibility above H_{c1} and a marked hysteresis that is responsible for their AC loss characteristic. Fortunately, it is not necessary to combine the internal workings of the superconductor with the calculation of the fields external to the superconductor to obtain an approximation of the fields that exist elsewhere in the system. When dealing with a specific assembly of different materials where one or more of the materials is a superconductor (or a magnetic material), the magnetic field outside of those materials can be calculated by adding a surface current distribution to the magnetic material that reflects the impact of their magnetization. In a superconductor, this surface current is known as the shielding current and is equal to the induction H acting parallel to the surface. It has units of Amps per unit width in the direction orthogonal to the vector H. However, if one desires to define the local fields in the vicinity of superconducting elements precisely or determine the impact of the magnetic shielding and field distortion created by the superconductor and its tendency to exclude fields, the field calculations must recognize the diamagnetic nature of the material.

The susceptibilities of the non-magnetic materials found in the cable system are so small that they can be neglected for all practical calculations. Thus, in a superconducting cable system, the magnetic flux B can be related to the magnetic intensity H by the magnetic permeability of free space μ_0 everywhere in the system except within the superconductor or in ferromagnetic components, which may include steel formers, steel pipes, nickel, and nickel alloys (e.g. Hastalloy).

The SI unit of the magnetic flux density vector B is the Tesla or Weber/m^2. The cgs unit is the gauss. One gauss is equal to 10^{-4} Tesla. When calculating power or energy it is helpful to remember that the Weber is equivalent to a Volt-second. The magnetic

intensity vector H has SI units of Amps/m but is more frequently stated in Amps/cm. The permeability of free space in SI units is:

$$\mu_0 = 4\,\pi \times 10^{-7} \quad \frac{Webers}{Amp\text{-}m} \quad or \quad \frac{Tesla\text{-}m}{Amp} \quad or \quad \frac{Henry}{m} \tag{3-4}$$

The cgs emu system of units does not recognize a free space permeability. In cgs emu units, H is expressed in Oersteds (Oe) and is numerically equal to the flux density B in Gauss (G). The conversion of H from cgs emu to SI units is best visualized by comparison of the relation between flux density B and magnetic induction H. In cgs emu units, Equation 3-3 becomes:

$$B = H + 4\pi M \quad Gauss \tag{3-5}$$

The 4π factor stems from the basic formulations of Maxwell's equations which use 4π rather than μ_0 and ε_0. Unfortunately, much of the scientific literature uses the cgs emu set of units. The 4π factor enters into both approaches frequently since it is fundamental to area and volume calculations. Needless to say, the potential for confusion cannot be over-stressed. When working with equations in emu units, the conversion to SI units is best done by a complete term-by-term substitution, the rules of which are not immediately obvious. These rules are summarized in Appendix A.

The major use of superconductors is for the windings of magnets. The performance achieved by superconducting materials and the requirements of potential applications are often related on a plot of critical current density against the magnetic field B acting parallel to the material surface. Figure 3-1 reproduces a popular plot which relates the performance level required by various applications to the results achieved so far. The performance range of interest to the magnet designer is from less than one Tesla to perhaps fifty Tesla, the largest field produced in the laboratory to date being about 35 Tesla. Future applications sometimes envision fields up to a few hundred Tesla, so graphs with this range are occasionally seen in the literature reporting long-range targets and advances in material performance. Cable applications require fields on the order

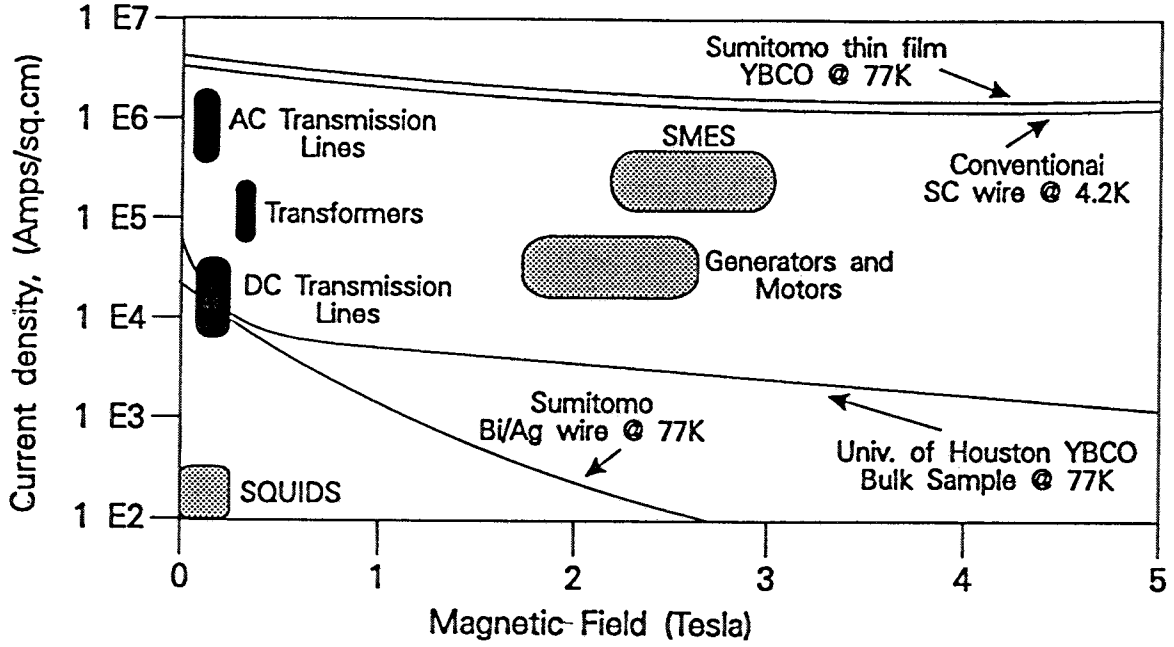

Figure 3-1 Critical current density and Magnetic Field for typical applications.

of 100 to 1000 gauss, or 0.01 to 0.1 Tesla, one of the lowest field requirements in power applications. To convert a magnetic field in Tesla to Gauss, simply divide it by 10,000.

In a cable system the magnetic field is created by currents (flow of charges). The calculation of the field at any point P begins with the Biot law which relates the differential contribution to the local field, dB, to the current i in a differential element of the system, dl, as illustrated in Figure 3-2.

The Biot law is expressed mathematically in Equation 3-6 where the direction of the field element is determined using the right hand rule (when thumb points in direction of current element, rolled fingers point in direction of field).

$$dB = \frac{\mu_0}{4\pi} \frac{i\ dl\ \sin(\theta)}{r^2} \quad \frac{Webers}{m^2} \tag{3-6}$$

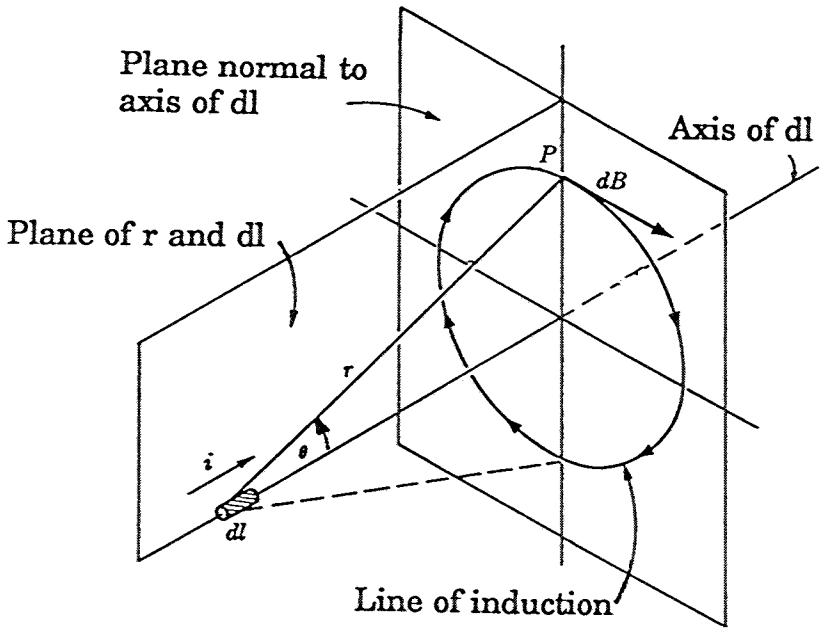

Figure 3-2 Magnetic Field due to current element.

If we assume that a superconductor is in the form of a long straight thin wire, the magnetic field at radius r anywhere outside of this wire is calculated using the Biot-Savart law which results from the integration of Equation 3-6 along the axis of the wire from minus to plus infinity. This integration yields Equation 3-7.

$$B = \frac{\mu_0 I}{2\pi r} \quad \frac{Webers}{m^2} \tag{3-7}$$

The magnetic field resulting from the current I is in the circumferential direction, tangent to the conductor surface and parallel to the local material surface. The field at the surface of a wire is known as the self-field, a term that is often used in conjunction with tests of a wire's capacity. In SI units, with I in Amps and r in meters, Equation 3-7 reduces to the simple relation,

$$B = 2\times10^{-7} \frac{I}{r} \quad Tesla \tag{3-8}$$

If r is in centimeters, B can be computed directly in Gauss as

$$B = 0.2 \frac{I}{r} \quad Gauss \qquad (r \ in \ cm) \tag{3-9}$$

Figure 3-3 illustrates the magnetic field of a coaxial tubular cable with the outer conductor carrying a return current that is equal and opposite to the central conductor's current.

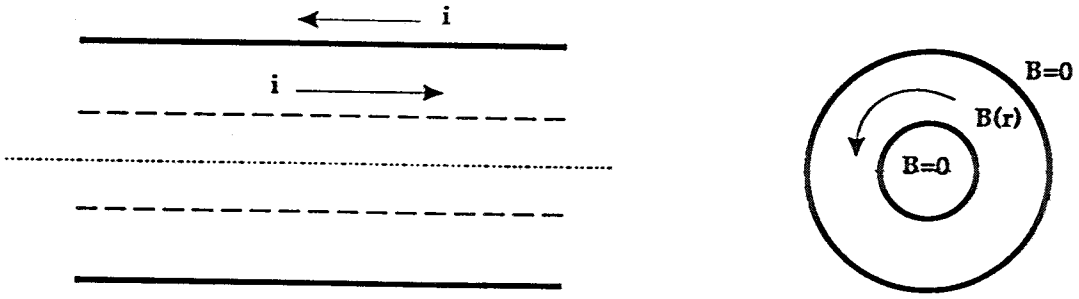

Figure 3-3 Magnetic Field in coaxial Cable

Equations 3-7, 3-8 and 3-9 define the magnitude of the field in the space between the inner and outer conductors where r is the radius to an arbitrary point in this space. For this case there is no field inside the inner conductor or outside the outer conductor.

The magnetic intensity H is a measure of the effective surface current density per unit width of the current path. For a tubular conductor the total "width" of the axial path is the circumference. For this ideal configuration H is related to the current as follows:

$$H_1 = \frac{I}{2\pi r_1} \quad \frac{Amps}{m} \tag{3-10}$$

The unit of H is amps per unit length (of circumference). This result can also be obtained using Equations 3-7 and 3-3. H_1 is the magnetic intensity at r_1, the outer surface of the inner conductor. The magnetic field parallel to the inner surface of the

outer conductor at radius r_2 causes the superconductor to react with a shielding current that produces a magnetic intensity in opposition to the inner conductor's field. This H_2 value is computed from the flux density at r_2 using Equations 3-7 and 3-3 which shows that the magnetic intensity acting on the outer conductor is reduced by the ratio of the inner and outer radii as given by Equation 3-11.

$$H_2 = H_1 \frac{r_1}{r_2} \quad \frac{Amps}{m} \tag{3-11}$$

The reduction in surface current density is exactly compensated by the increase in circumference such that the total shielding current is equal to the current flowing in the inner conductor. This return current will flow provided a complete path is available, even in a three phase assembly where the three cable outer conductors (shields) are connected together and/or grounded at each end to eliminate the need for these currents by phase cancellation. If the return conductors are, however, open circuited, the supercurrents required to prevent the field from entering the superconductor will take the form of internally circulating currents, following whatever path they can find. The local return path of these currents may be on the outer surface of the superconducting tube, effectively recreating the field they canceled inside the return conductor. In this case there will be no shielding effect. When shielding currents must flow from the inner surface to the outer surface of a superconducting layer they may have to traverse normal resistive material which will create an I^2R loss. When helical tapes are used, the nature of the tape edge can have a major effect on the losses in the assembly, an effect that may be difficult to recognize.

Figure 3-4 shows a family of curves which plot the peak values of magnetic intensity H and flux density B at the surface of a round conductor as a function of current, for several radii. Note that B in Gauss is equal to 1.26 times H in amps per centimeter.

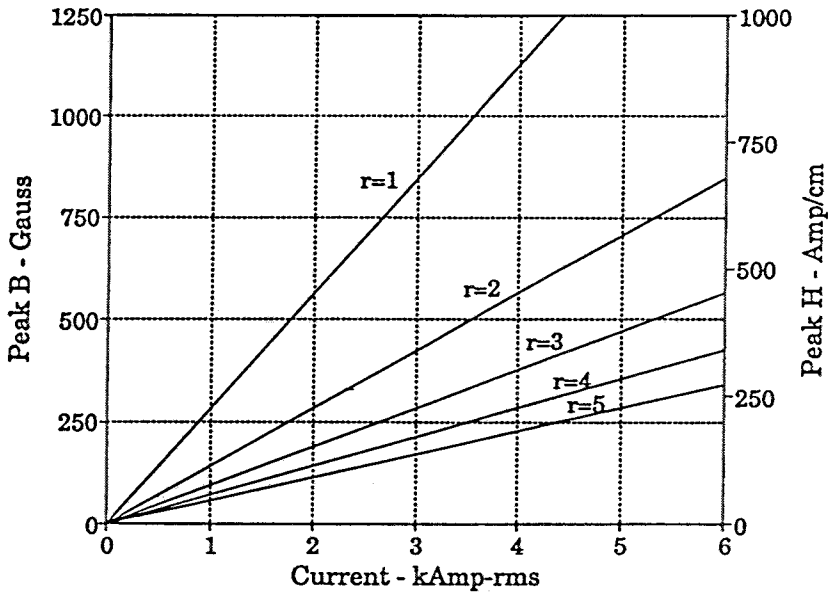

Figure 3-4 Magnetic Field and Intensity at Conductor Surface.

The above discussion has concerned coaxial cable where a return current flows on the outer conductor which exactly cancels the field from the central conductor's current. This arrangement makes a cable autonomous. The number of phases in the system, or other circuits near-by have no influence on the electrical behavior of this cable type because the outside surface of the outer superconductor shields the cable from external fields.

If the cable does not have a superconducting return, the field due to the current flowing in the conductor will not be canceled but will extend to act on other nearby conducting materials. In DC systems, the steady component of the magnetic field stores inductive energy, but has little further effect except on another superconductor that may be close by, such as the return conductor in a bipole system. Steady fields induce no voltage gradient or current flow in normal materials, but cause an opposing shielding current to flow in superconducting material. This current flow may "use up" some of the available cross-section of the other superconductor and reduce its effective capacity. Of course, this effect is mutual.

AC cables experience more magnetic activity because the fields are time varying. Any conducting material exposed to the field will experience eddy currents caused by the voltage gradients induced by the changing fields, and any eddy current flow will create additional fields in opposition to the driving field. Each superconductor is exposed to fields from its neighbors that tend to degrade its capacity, and penetration of these fields will increase hysteretic loss where the local peak field exceeds H_{c1}.

A first approximation of the total field at a point on the outside surface of one of the superconductors in a three phase cable system without coaxial superconducting returns can be made by superposition of the fields caused by each phase current using Equation 3-9 and the assumption that each phase is made up of parallel current elements uniformly spaced around the circumference of the conductor. This configuration leads to the ability to represent these elements as a line source located at the conductor's axis. Figure 3-5 illustrates the three fields at a point on the surface of one conductor for three cables in a triangular configuration. Each field's direction is tangential to the radius from its source, as defined by the right hand rule.

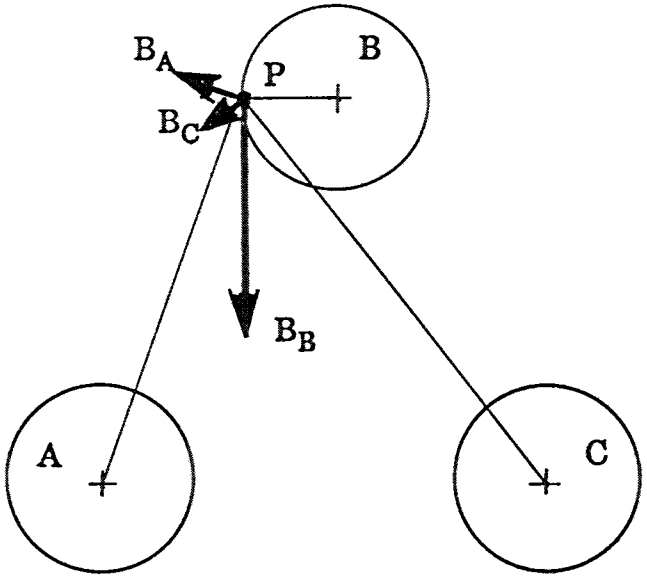

Figure 3-5 Magnetic field of each conductor in triangular configuration.

Figure 3-6 shows a variation when the cables lie in a cradled configuration. The magnitudes of the field from each conductor are 120 or 240 electrical degrees out of phase with each other.

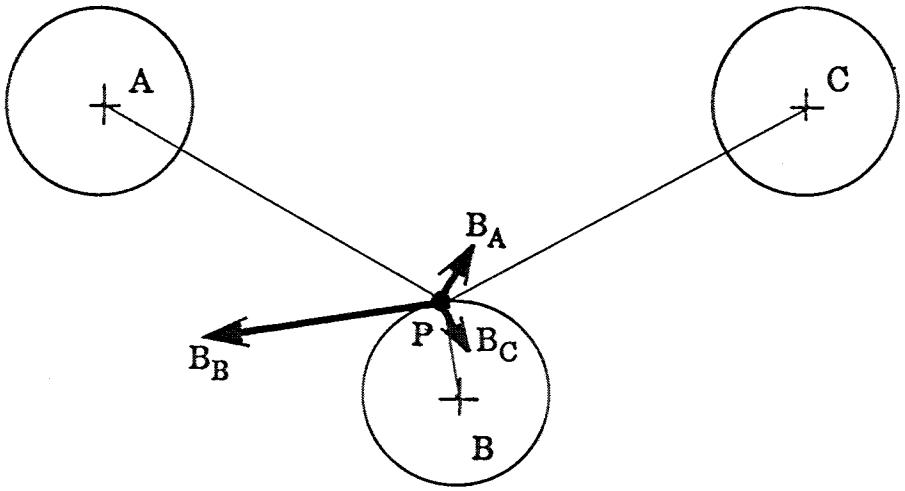

Figure 3-6 Magnetic field of each conductor in cradled configuration.

The total field at any point on the conductor surface is best described by a normal and parallel component. (The "parallel" rather than the "tangential" designation is often used to clarify its relation to the local superconductor surface, even though the term "tangential" is more precise.) These are easily obtained by applying the appropriate trigonometry to each field contribution to determine its normal and parallel components and adding the components due to each phase current. A unique field pattern results for each point on each conductor.

A magnetic field acting normal to the surface of a superconductor is perceived to degrade its performance more than a field that is parallel to its surface. A major concern for any superconducting cable system that does not have a superconducting outer conductor is the magnitude of the unwanted normal field that results from the phase

interaction. Calculations were performed for the triangular three phase configuration shown in Figure 3-5 and the cradled configuration shown in Figure 3-6. These calculations do not include a magnetic pipe, and the assumption is made that shielding and eddy currents do not significantly change the fundamental field configuration. The results of interest are a first approximation of the magnitudes of the field components parallel to and normal to the surface of each tubular superconductor. Appendix B gives a summary of the calculation procedure and results and includes a BASIC program listing that was used to generate the data. Appendix C is an independent report prepared by Magsoft Corp. confirming the validity of this procedure and presenting additional results.

The behavior of the fields acting on the surface of each superconductor in an unshielded three phase cable system is difficult to visualize because both the normal and the tangential components vary in electrical phase and magnitude with azimuthal position around each conductor. Figure 3-7 graphs the normalized maximum magnitude of the tangential field that occurs in one electrical cycle verse azimuthal position for the triangular configuration of Figure 3-5, and compares it to the field in a coaxial cable.

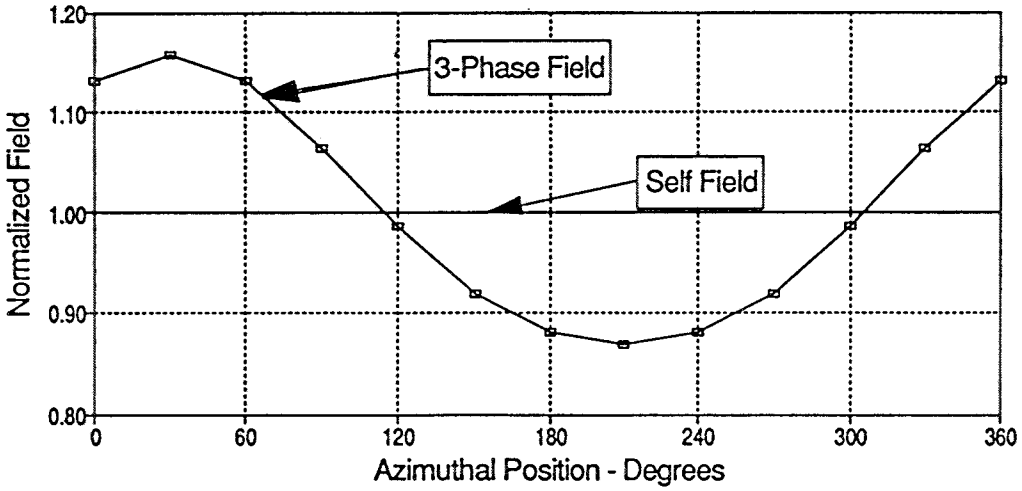

Figure 3-7 Maximum tangential field in triangular configuration.

Figure 3-8 shows the maximum peak normal component over one cycle verse position for the same cable arrangement with a 2.54 cm conductor diameter and an O.D. of 7.62 cm carrying 3000 amperes RMS.

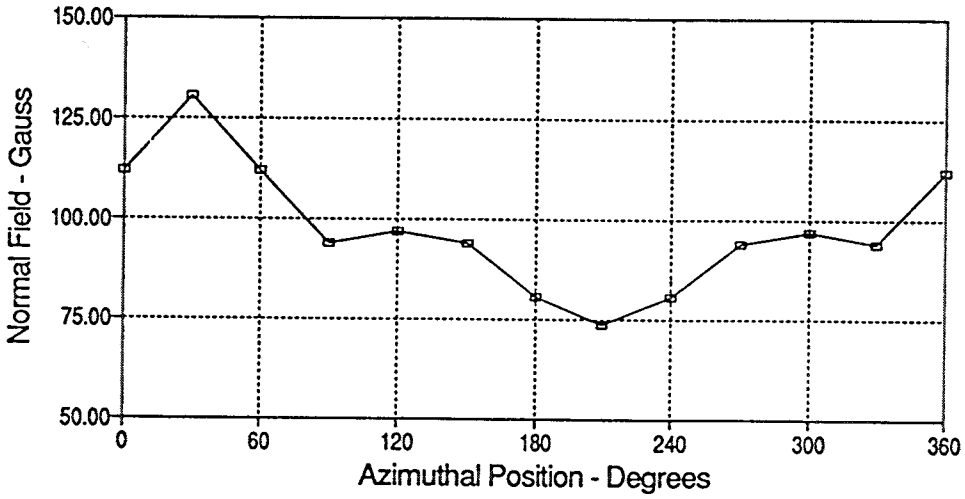

Figure 3-8 Maximum normal field in triangular configuration.

Figures 3-9 and 3-10 illustrate the field behavior for the cradled configuration in the same order. Two curves are shown for each case because the center and outer phases differ. Figures 3-11 and 3-12 are three-dimensional surface plots of typical data for a triangular geometry for cables carrying 1000 amperes. Figure 3-13 and 3-14 are three-dimensional surface plots of similar typical data for a cradled geometry. These plots illustrate the complexity of the tangential and normal field as a function of azimuthal position and electrical phase.

If a steel pipe surrounds the cables as in a room temperature dielectric cable installed in a pipe-type configuration, the fields inside the pipe are distorted, and fields at the surface of the steel cause hysteretic loss and eddy current loss in the steel. The field distortion inside the pipe can be envisioned by noting that the high permeability of the steel lowers the reluctance of the magnetic circuit for the flux lines generated by each

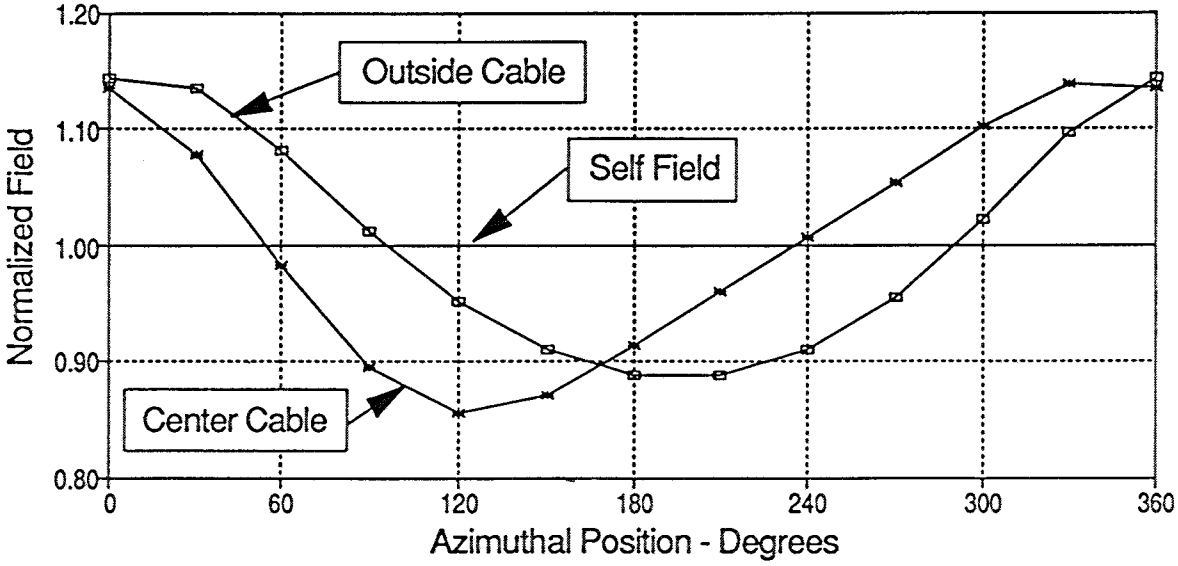

Figure 3-9 Maximum tangential fields in cradled configuration

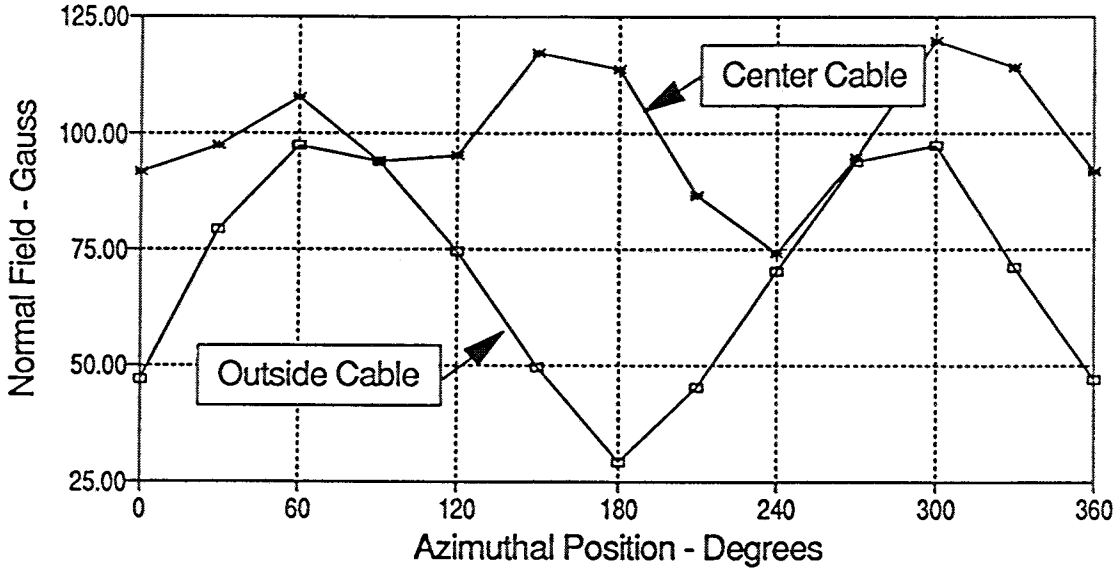

Figure 3-10 Maximum normal fields in cradled configuration

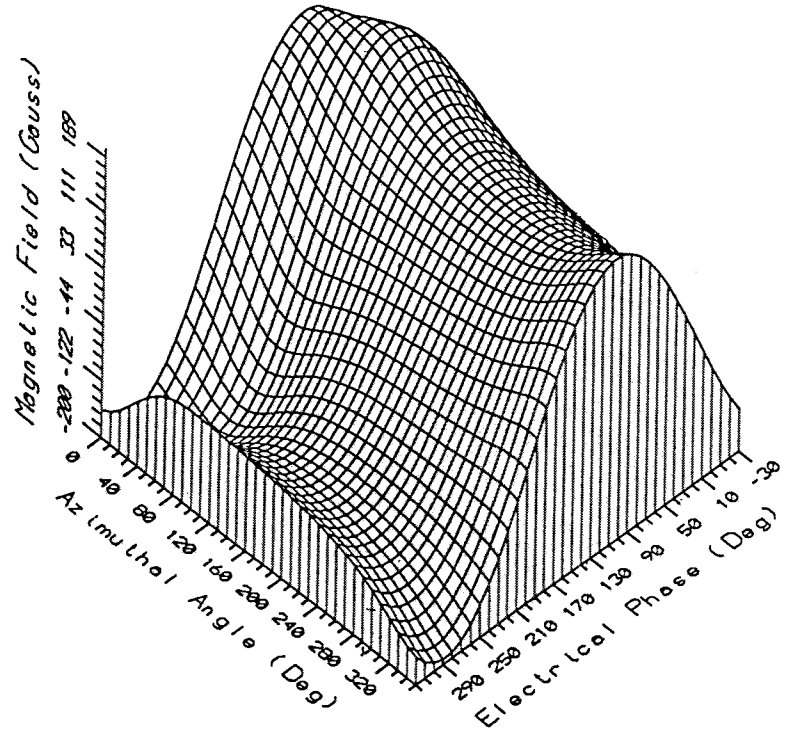

Figure 3-11 Surface plot of tangential field in triangular configuration

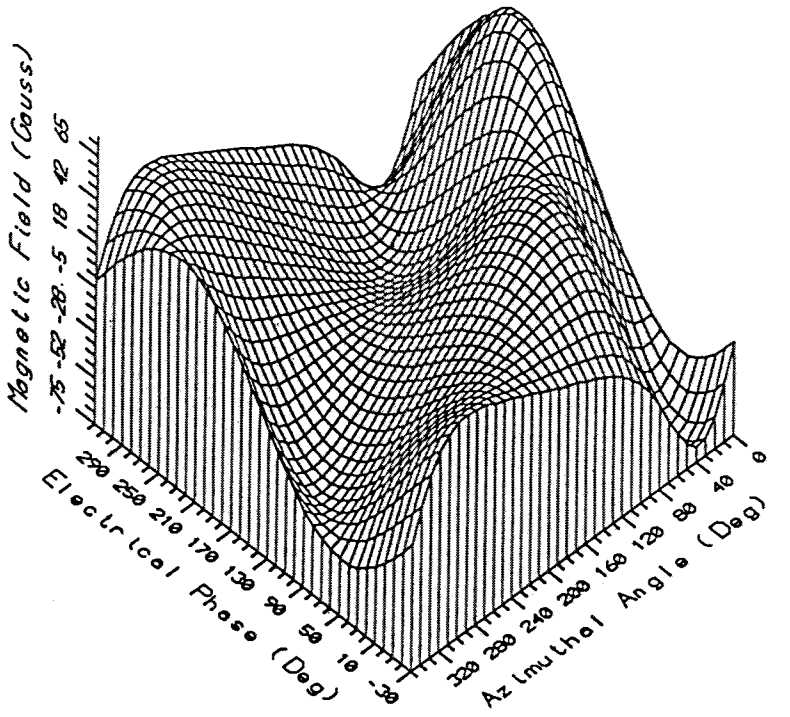

Figure 3-12 Surface plot of normal field in triangular configuration

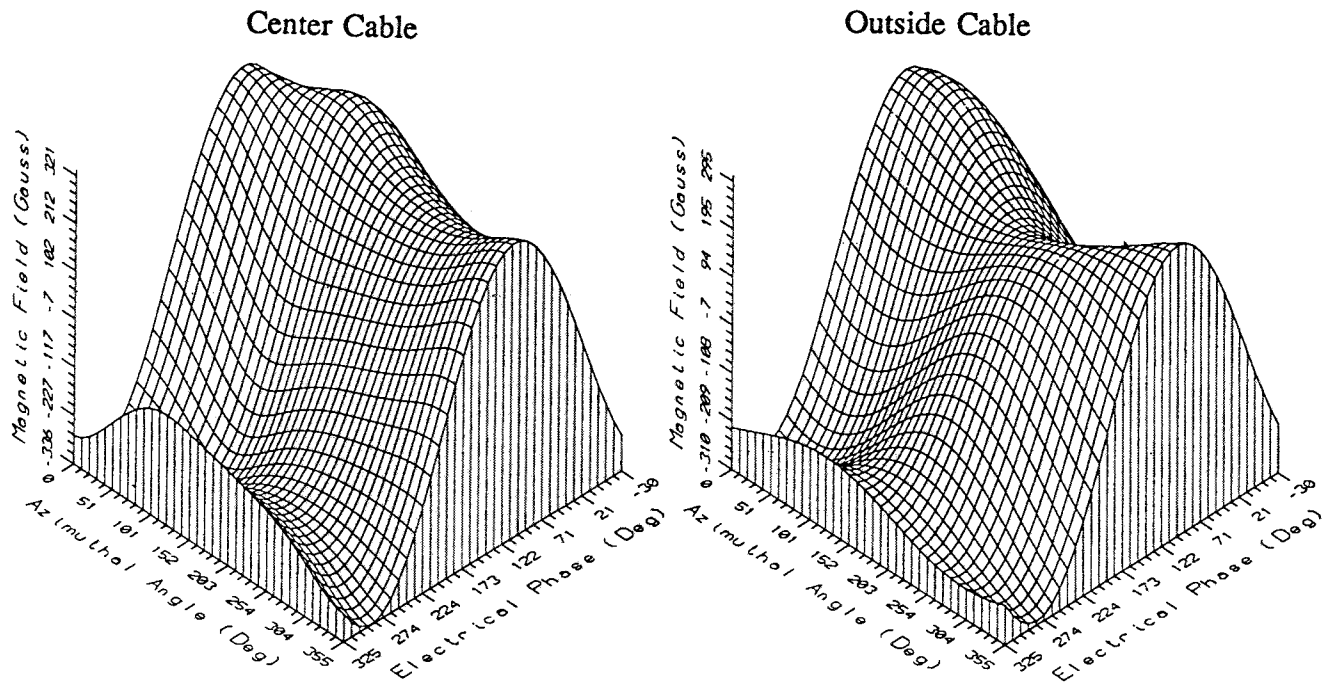

Figure 3-13 Surface plot of tangential field in cradled configuration

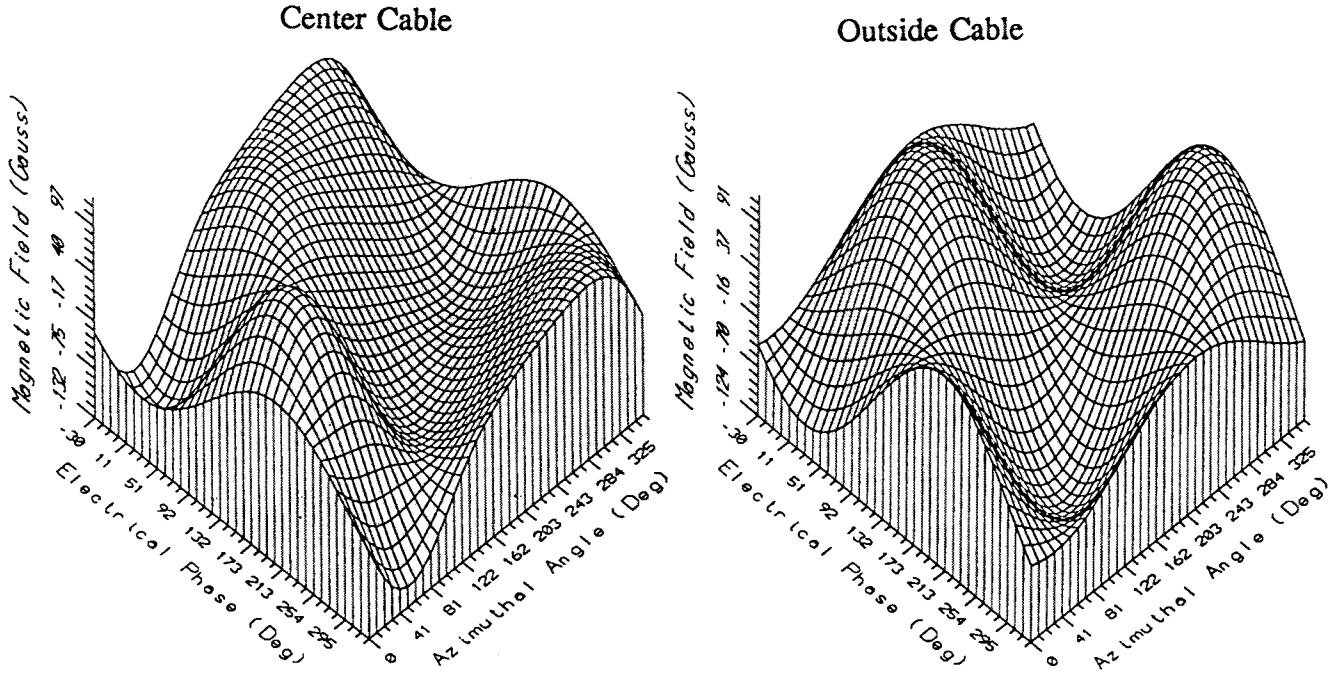

Figure 3-14 Surface plot of normal field in cradled configuration

conductor. This has the effect of expanding the flux lines inside the pipe which increases the magnitude of the field at any specific point. The result is equivalent to an increase in the effective separation of the cables which increases their inductance. The losses associated with a steel pipe will be discussed later.

The generalized technique for the complete analysis of fields is to iterate on the calculation of the field at a specific point by superposition of the field contribution from all current sources. Shielding currents and eddy currents are calculated from the local conditions and their effect added to the analysis for the next step of the iteration. The presence of steel complicates matters, not only because of the discontinuity of permeability but also due to the nonlinearity of the steel's permeability. In the final analysis, a measurement program may yield more accurate results with less effort.

The above discussion has centered on a cable system that is composed of uniform tubular members each with a single conducting layer or filaments all parallel to the axis. A more likely scenario involves superconductors in tape form applied in a helical fashion. The analysis of the fields in helical cables is far more interesting and involves the specific characteristics of the tape. As shown in the Appendices, Equation 3-7 can be used to compute the field due to any number of parallel current filaments. If, however, the filaments are helically applied, the field calculation becomes more difficult, but not impossible. It is then necessary to revert to the integral version of Equation 3-7 that is the foundation of the Biot-Savart equation, stated in Equation 3-12.

$$B = \frac{\mu_0}{4\pi} \int \frac{i\ dl\ \sin(\theta)}{r^2} \quad \frac{Webers}{m^2} \tag{3-12}$$

This relation in the integral form gives the field at a point in space due to a filament of arbitrary shape carrying a current I. The field can be computed numerically by summing the vector field component from individual elements of the length of the filament moving from far away on one side of the plane of interest to far away on the other side. For each element, the "radius" r is the distance from the element to the point,

and the angle θ is the angle between r and the axis of the element. The incremental field at the point will be normal to the plane formed by the radius and the element's axis. The total field at P is the vector sum of the field increments from each filament in the system. Figure 3-15 illustrates the geometrical arrangement of these parameters for an element of a single helical filament.

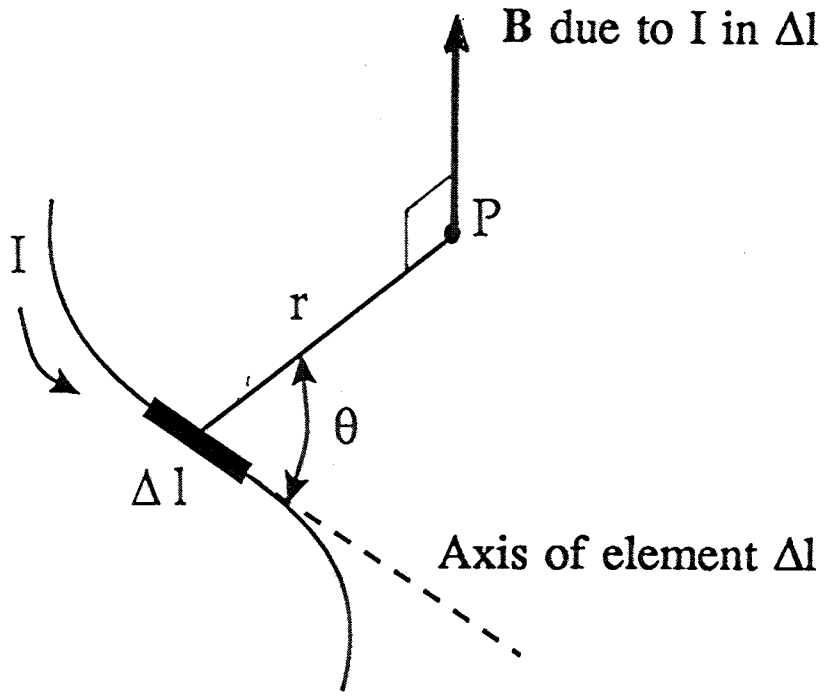

Figure 3-15 Field from element of helical filament

One critical aspect of a helical taped conductor involves the number of layers that will be applied. The magnetic aspect of this question can be addressed with the following intuitive analysis. If the conductor is formed of only one layer, the helical current path will create an axial field inside the conductor as in a solenoid. The current in each tape is equal to the total (delivered) current divided by the number of tapes n. If α is the lay angle of the helix relative to the cable axis, the axial surface current density I_a is the total current times cos(α) divided by the circumference, and the circumferential surface

current density I_c is the total current times sin(α) divided by the lay length. The axial field B_a will be given by the circumferential current density I_c and the equation for the field in a solenoid:

$$B_a = \mu_0 \frac{I_c}{2} \quad Tesla \tag{3-13}$$

The direction of B_a is given by the right hand rule applied to the circumferential current. The axial field increases the self inductance of the conductor assembly (and the cable's surge impedance) and will cause eddy current loss in any normal metal that lies inside of the superconducting layer.

The current flowing in a helical outer conductor also sets up an axial field. If the lay direction is the same as the tapes on the inner conductor, the axial field due to the outer conductor will be in the opposite direction and tend to cancel the field inside the inner conductor. This field will exist in the dielectric space between the two conductors. By judicious choice of the lay angle, it is possible to control the interaction of the two solenoidal fields. However, there are other restrictions on the lay angle, the most important being the control of thermal contraction. If a net axial field exists inside of the outer superconducting layer, a voltage will be induced in any closed conducting path that surrounds the cable, and this voltage will cause a circumferential current to flow which will generate an ohmic loss. If externally closed layers are inevitable it may be necessary to optimize the external loss with that in the core when selecting lay angles.

The interaction of superconducting layers can result in surprising behavior. For example, if a tubular conductor is made of two superconducting layers separated by a thin insulating layer, and the two layers are solidly connected together at each end or a joint, the question arises as to the division of current between the two layers. If the layers were resistive then DC current would divide in the inverse ratio of each layer's resistance. For the AC case, the inductance of each layer (without resistance) should perform the same function on the basis of equalizing the axial voltage drop between the

two layers. However, if a current were to flow on the inner layer, it would set up a field on the inside surface of the outer layer that would require an opposite surface current to prevent field penetration. These two currents would effectively cancel each other and the imposed transport current would have to flow on the outer surface of the outer layer. In fact, a preliminary analysis indicates that the two inner currents cannot flow because their respective inductive voltages are of opposite sign, end-to-end. Thus, the second (inside) layer provides no useful current transport. This situation is exactly analogous to the skin effect with infinite conductivity.

The current paths in cables made of multiple layers of helical tapes are difficult to establish by calculation. An approximate analysis can be done by noting that current can and will flow on both surfaces of any superconducting layer and since the tapes are at an angle to the axis of the cable, both circumferential and axial field components can cause currents to circulate around a tape. If a tape current is vectorially divided into a circumferential component and an axial component, the former will create a solenoidal field internal to its diameter and the latter will create a circumferential field external to its diameter. A tape lying inside will see the axial field and set up an opposing current. A tape lying outside will see the circumferential field and also set up an opposing current. How the driving currents and reaction currents combine to satisfy conflicting effects will depend on the relative lay direction of alternate layers. A more detailed analysis remains to be done when materials become available that will enable some experimental input to justify that effort.

Loss Calculations

This section will deal with the existing knowledge and computational methods for predicting the energy dissipation in an HTSC power cable.

The losses can be grouped into three categories; those due to current, those due to the voltage, and the heat in-leak through the cryostat. The elements for which losses must

be predicted include the conductor and its supporting components, the dielectric, the cable shield structure, the cryostat or cryogenic enclosure and/or the cable pipe or sheath. The heat in-leak is treated as a loss because this energy must also be removed by the cryogen.

We begin with a discussion of the loss calculations for the superconducting conductor assembly. The superconductor properties will be a function of magnetic field and actual temperature. The parameters to be used in the performance calculations should be determined experimentally for a specific material in its final form. At this point in time, performance levels for the HTSC materials have not been firmly established making it difficult to predict what will be achieved. What follows is a description of the nature of the loss characteristics that are expected with some guidelines as to the magnitudes that should be obtainable. The easiest form to analyze is the tubular conductor which represents the ideal (most efficient) arrangement of superconducting material. Calculations will be developed for this geometry which is characterized by a uniform current density and a well-defined magnetic field with no axial component. Assemblies of tapes or wires or the use of corrugated tubes complicate the analytical situation and most likely will result in a higher loss for the same amount of superconductor.

Conductor losses: AC cables

The conductor loss calculations are dependent on the configuration of the conductor, the application, and the magnitude of the current. AC cables at low current levels may have detectable resistive loss due to low level surface phenomena which generate a loss proportional to the square of the transport current, but it's apparent resistance may not pass through the zero current/zero loss intercept.

The dominant AC loss mechanism in the operating current range should be the hysteretic loss that is proportional to frequency and the magnetic intensity H (current) cubed, and inversely proportional to J_c. Eddy current loss will be present in this range

which will vary with the square of the frequency as well as the current. Finally, if the current density is forced to exceed J_c the superconductor will become normal and the loss will jump discontinuously into a resistive mode. In this state, the resistivity of the metal in the conductor structure will combine in parallel with the normal resistivity of the superconductor material to determine the loss behavior.

The combination of these mechanisms will establish three operating zones that define the loss per meter of conductor as a function of the phase current and the temperature of operation. They will be unique to a material in its service configuration. The lowest zone will be resistive and might contain an offset. The second zone can be thought of as the operational zone and should extend beyond the normal operating range of the cable to include light fault and overload conditions. The third or normal zone will only be active as a result of an extreme fault or the loss of temperature control.

AC cables will have a broad operational zone representing the combination of hysteretic loss and eddy current loss. The superconductor's J_c may show a tendency to decrease as the field increases. This was a dramatic effect for materials that were weak-linked. However, HTSC materials that have J_c's in the required range will not be weak-linked and will show a very mild fall-off of J_c with increasing field in the range of operation. This will result in an apparent increase of the exponent of the field dependence above three.

The total loss in the conductor assembly Q_c under normal design operating conditions is modeled as the sum of the three losses, namely, a small resistive loss (Q_r), hysteretic loss (Q_h), and the eddy current loss (Q_e):

$$Q_c = Q_r + Q_h + Q_e \quad \frac{W}{m} \tag{3-14}$$

Resistive loss. At low currents, the loss can be approximated by a resistivity ρ, that depends on the nature of the material including its surface treatment and structure. This component will be a function of temperature. This behavior should extend to a field level of about H_{c1}. A resistivity value equal to 0.001 times that of copper at the same temperature can be used for design purposes. At 77 K, the resistivity of oxygen-free copper (resistivity ratio of 100) is 0.20×10^{-8} Ω-m. The corresponding suggested limiting design value of resistivity, ρ_{77}, for the superconductor is 0.20×10^{-11} Ω-m at 77 K. The temperature coefficient of copper can be used. At 77 K, α will be approximately 0.005 K^{-1}. The equation for loss in one phase conductor for this range is,

$$Q_r = \rho_{77}\left(1+\alpha(T_{sc}-77)\right)\frac{I^2}{A_{sc}}\quad\frac{W}{m} \tag{3-15}$$

where T_{sc} is the Superconductor temperature in K, A_{sc} is the cross sectional area of superconducting material in the conductor assembly in square meters, and I is the rms phase current in amperes.

Hysteretic loss. The hysteretic loss of an idealized tubular superconductor can be estimated using the classic Bean-London "critical state" model[21] applied to a flat superconducting surface with an alternating field parallel to the surface, modified to recognize that the field exists only on the outer surface in the cylindrical form. Equation 3-16 describes the loss due to flux moving into and out of one side of the material.

$$Q_{surface} = \frac{2f\mu_0}{3}\frac{H^3}{J_c}\quad\frac{W}{m^2} \tag{3-16}$$

This is a surface loss and must be multiplied by the conductor surface area $2\pi R$ m^2/m when R is in meters to arrive at the loss per unit length shown in Equation 3-17.

$$Q_h = 2\pi R\,\frac{2f\mu_0}{3}\frac{H^3}{J_c}\quad\frac{W}{m} \tag{3-17}$$

In Equations 3-16 and 3-17, f is 60 Hz, H is the peak field at the surface in Amps/m as defined by Equation 3-10 and J_c is the effective critical current density in Amps/m^2. These equations apply to a tubular surface which is approximated by a flat surface when the thickness of the active superconductor is small relative to the tube radius.

The situation for a cylindrical conductor has been expressed by an equation derived first by London and again by Carr for the case of a solid wire[22]. The London-Carr equation is,

$$Q_h = 4f\,(\pi R^2)^2\,J_c^2\,f(\Gamma) \times 10^{-7} \quad \frac{W}{m} \tag{3-18}$$

where $\Gamma = (I/I_c)$, $I_c = \pi R^2 J_c$ amps, and the function $f(\Gamma)$ is defined by Equation 3-19.

$$f(\Gamma) = \Gamma - \frac{\Gamma^2}{2} + (1-\Gamma)\ln(1-\Gamma) \tag{3-19}$$

I and I_c are the peak currents, not the rms values. Even though Equation 3-18 applies to a solid wire, it can be valid for a hollow tube if the current flow and field penetration are limited to the outer portion of the material which is less than t, the thickness of the superconducting layer. When this is true the superconducting material in the central portion of the wire sees no electrical activity and can be "removed" with no effect. For this condition to be satisfied, the peak value of the current I must be less than the actual critical current of the assembly I_c', where I_c' is given by Equation 3-20.

$$I_c' = 2\pi\,(R-t)\,t\,J_c \quad Amps \tag{3-20}$$

Equations 3-17 and 3-18 give essentially identical results for a tubular conductor in the size range of interest.

Another effect that should be added to the above analysis is that of a surface barrier to the entrance of flux, which could be on the order of H_{c1}. This barrier effect on the field

penetration into flat surfaces has been studied by Fournet, et al.[23], who suggested the following modification to Equation 3- 17 which can be used when the operating range is above ΔH.

$$Q_h = 2\pi R \frac{2f\mu_0}{3} \left(\frac{(H-\Delta H)^3 + 3(H-\Delta H)^2}{J_c} \right) \frac{W}{m} \qquad (3\text{-}21)$$

where ΔH is the surface barrier field in Amps/m. The value of ΔH can be determined by fitting Equation 3-21 to experimental data. H_{c1} is a reasonable choice for the starting point for a numerical iteration procedure.

An additional consideration for the topic of hysteretic loss is the effect of field interaction with other conductors for the non-shielded case applicable to a room temperature dielectric cable, or a cryogenic dielectric cable without a superconducting outer conductor. An approximation to the field conditions shown earlier appears in Carr's analysis where he presents the loss of a wire carrying an AC transport current in an AC transverse field that is in phase with the current and its self field. If we define a loss Q' that results from an in-phase transverse field H_t superimposed on the self-field H_s, the loss Q_h given above should be corrected as follows:

$$Q_h' = Q_h \left(1 + \frac{8}{3} \left(\frac{H_t}{H_s}\right)^2 \frac{\Gamma^3}{2\, f(\Gamma)} \right) \frac{W}{m} \qquad (3\text{-}22)$$

Recognizing that Γ is very small because of the solid wire to hollow tube transformation implicit in Equation 3-18, Equation 3-22 for transverse fields less than the self field can be simplified to that shown as Equation 3-23.

$$Q_h' = Q_h \left(1 + 8 \left(\frac{H_t}{H_s}\right)^2 \right) \frac{W}{m} \qquad (3\text{-}23)$$

Typically H_t might be 20% of H_s in the unshielded configuration. This will cause a loss correction of 32% using Equation 3-23. However, as discussed above and in appendices B and C, the transverse field has a complex phase relation to the self field. It can be seen in Figures 3-7 and 3-11 that, in the triangular configuration, the resultant maximum tangential fields around the conductor are increased over only about one third of the circumference and actually decreased over the remaining two thirds when compared to the self field that would apply in a coaxial configuration. One means to estimate this effect is to compute the tangential and normal components of field as a function of angular position around the conductor, and to integrate Equation 3-23 around the conductor using the tangential field for H_s and the normal field for H_t. This procedure is amenable to numerical approximation which treats the conductor as a group of segments, each with unique field components.

Figure 3-16 plots loss characteristics (loss vs current) computed for a 4 cm diameter superconductor assembly with a J_c of 50,000 amps/cm^2, using Equation 3-17 for a coaxial

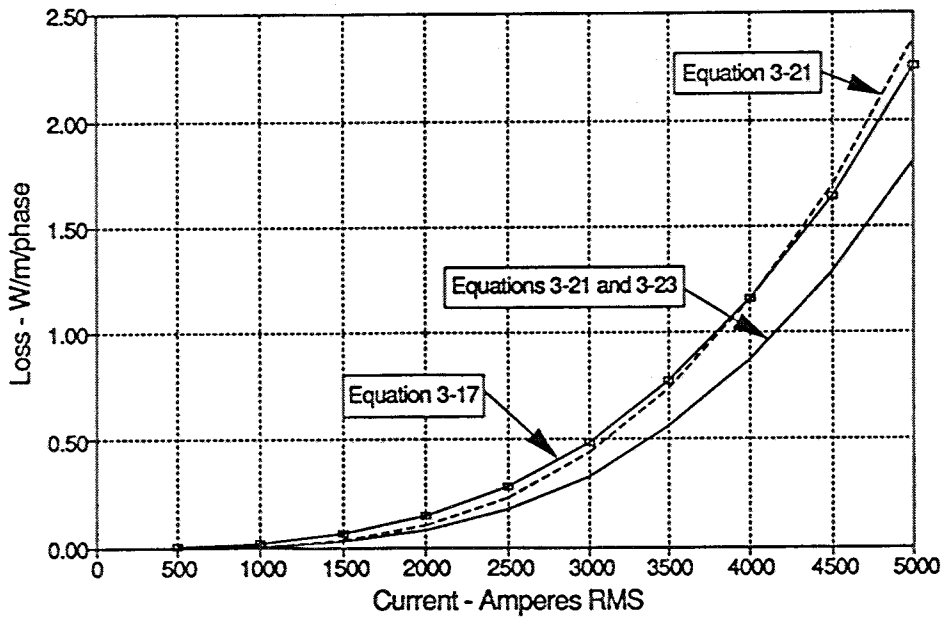

Figure 3-16 Hysteretic loss as estimated by Equations 3-17, 3-21 and 3-23.

configuration with ΔH=0, Equation 3-21 with ΔH =4000 amps/m, and Equation 3-23 in combination with Equation 3-21 for a Room-Temperature Dielectric configuration with a peak transverse field equal to 10% of the self field and ΔH =4000 amps/m.

The above analysis can be applied directly to an idealized tubular outer conductor of a coaxial cryogenic dielectric cable with the use of Equation 3-11 to define the magnetic intensity at the inner surface of the outer conductor.

The temperature dependence of the superconductor properties has a strong influence on the loss behavior because the operating temperature will be relatively close to it's critical temperature. Temperature effects are important in the design of the temperature control system and impact the overload capability of the system. The variation of J_c will have the biggest effect on the losses calculated with the above equations. Theoretical considerations indicate that J_c will fall off parabolically as the temperature rises toward T_c as described by the following relation.

$$J_c(T) = J_c(0)\left(1-(\frac{T}{T_c})^n\right) \quad \frac{Amps}{m^2} \qquad (3\text{-}24)$$

The value of 'n' in Equation 3-24 can vary between 1 and 4, the most common reported value being 2. However, experimental results have shown that the exponent n is not always 2. The determination of $J_c(0)$ and n can be done if T_c is known and J_c has been measured at two or more temperatures by fitting Equation 3-24 to the data. If only one temperature measurement of J_c is available, n should be set equal to 2 to calculate $J_c(0)$.

Equation 3-24 can be used to compute the behavior of J_c in the operating temperature range expected for HTSC cables, and for comparison of the attributes of materials with different T_c's. Such calculations are plotted in Figure 3-17 for the three popular superconductor materials with critical temperatures of 91 K (Y system), 104 K (Bi system) and 107 K (Tl system), against a J_c normalized at 77 K.

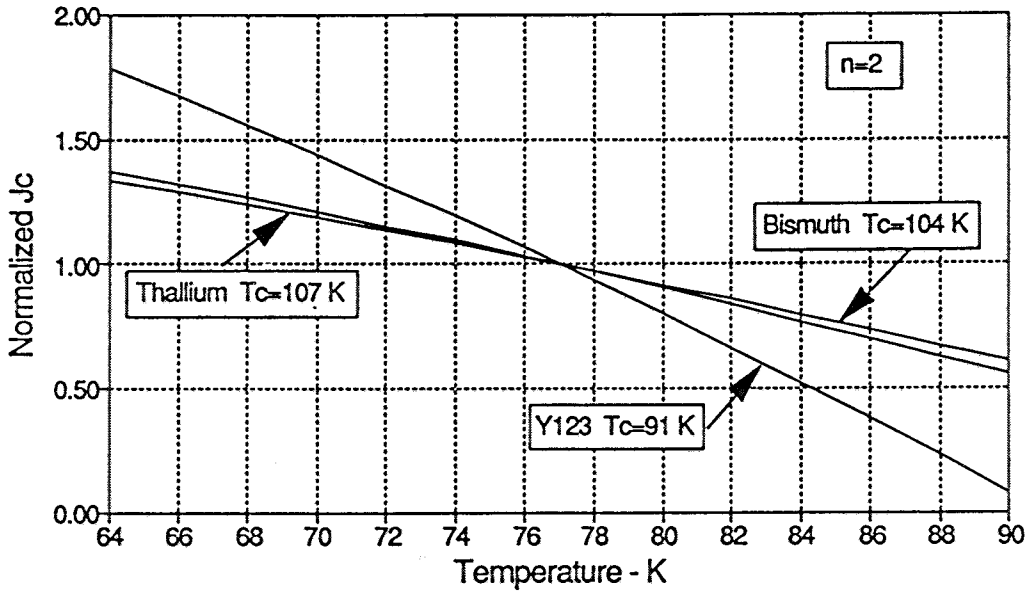

Figure 3-17 Variation of J_c with temperature.

Figure 3-17 illustrates the importance of both J_c and T_c in the prediction of conductor performance.

The critical fields H_{c1} and H_{c2} show a temperature dependence defined by the same relation as J_c where the exponent is expected to be 2. The impact of the field-temperature dependence will be minimal because the normal operating range for cables should be well into the mixed state, but far below H_{c2}. However, if the surface barrier field ΔH used in Equation 3-21 is found to exist, it should also be adjusted for the temperature as follows:

$$\Delta H(T) = \Delta H(0)\left(1 - \left(\frac{T}{T_c}\right)^2\right) \quad \frac{Amp}{m} \tag{3-25}$$

Finally, one comes to the crucial question of whether these fundamental theoretical formulae, which are derived from Maxwell's equations and assumptions concerning the nature of magnetic fields in superconductors, accurately represent reality for HTSC materials. As discussed in Section 2, the conductor assembly in the Brookhaven LTSC

cable design exhibited losses significantly higher than predicted by these theoretical expressions[24]. The excess losses have been attributed to current flow in normal metal between the two layers of the counter-spiraled superconductor tapes and to currents flowing around the tape across its non-superconducting edges.

In the summer of 1991, USi made AC loss measurements on HTSC samples from different manufacturers. One sample of melt-textured YBCO displayed a self field loss proportional to I^2 at very low currents and proportional to I^3 over two orders of magnitude of loss, in accordance with the expectations described above[25]. These experimental data are shown in Figure 3-18. These losses, however, are seen to be an order of magnitude greater than predicted by the above theories. Other samples, including different materials from different manufacturers were also measured, and they showed similar behavior. Generally losses were an order of magnitude greater than predicted by the theory. In essence, this implies that the J_c relevant to the computation of AC losses was an order of magnitude smaller than the measured DC J_c employing the 1 microvolt/cm criterion to define J_c.

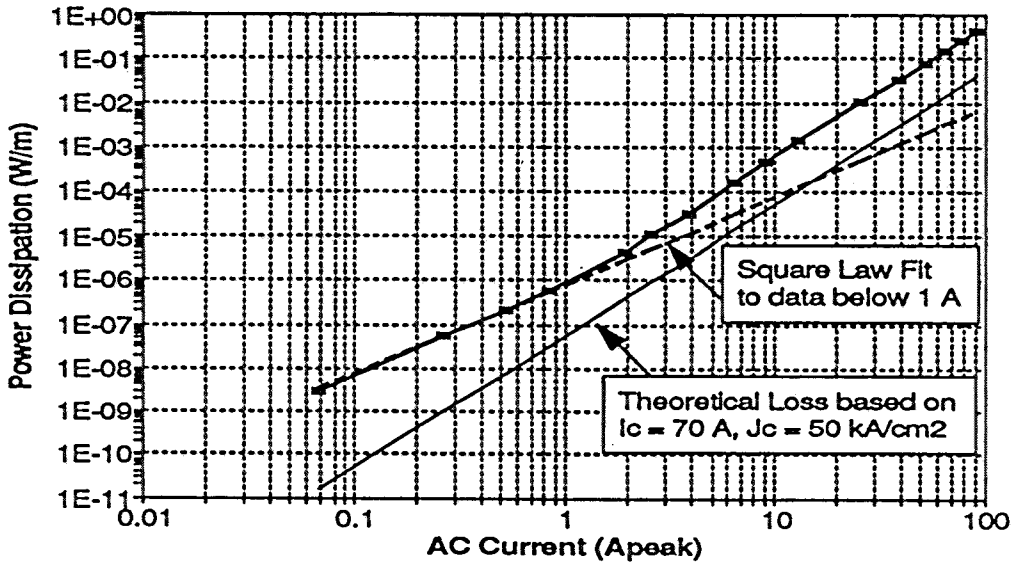

Figure 3-18 Loss data on early bundled fiber one meter long.

The source of the discrepancy between theoretical predictions and experimental observations is not yet known. Certainly, both samples were far from ideal in the sense that the magnetic J_c measured by AC susceptibility was substantially greater than the conduction J_c measured by a DC transport current. The difference could be the result of something as simple as the manner in which a measured J_c is defined. The DC conduction J_c is generally defined as the current which causes a 1 μV/cm voltage drop. However, the resistive sample characteristic does not sharply disappear below this voltage, but, simply approaches zero almost asymptotically. Perhaps a smaller voltage drop, say 10 nV/cm, would better suit the experimental data. This would imply that normal conduction that begins at substantially lower current may be relevant to the AC loss mechanism.

There are two other factors that might explain the higher losses observed experimentally. While their discussion goes beyond the intent of this section, it may be helpful to mention them briefly. First, the AC loss may affect whole grains and grain boundaries in a different manner due to the same phenomena that cause the observed differences in transport current and susceptibility measurements of J_c. This behavior is attributed to the tendency for weak links at grain boundaries to be enhanced by the field while the intra-grain field dependency is much smaller. A second possibility is that the magnetization characteristics that drive the loss may differ substantially from the behavior assumed in the Bean-London critical state model. Careful measurements of the magnetization should be carried out on HTSC materials in the proper tubular configurations at realistic levels of field and current to provide the basis for a more accurate analysis of the transmission line application.

Eddy current loss. The third conductor loss component is that due to eddy currents. Eddy currents will exist where there is a time-varying magnetic field within a conducting media because of the voltage gradient resulting from the changing flux through closed loops in the material. The nature of the closed loops relative to the field

will determine how much and where current can flow and the resulting loss. When changing flux lines pass through a body of conducting material, eddy currents will flow around the surface of the body. The loss is minimized by maximizing the ratio of the length of the surface path to the area it encloses. It is common practice in high flux magnetic devices to break up iron core components into thin sheets to minimize the eddy current loop area and subsequent losses.

Eddy current analysis can be a complex three dimensional problem, but there are some applications where the analysis can be greatly simplified. Eddy current behavior is dependent on the skin depth δ and relative permeability μ_r of the material which is exposed to the field. The skin depth δ is a measure of the depth of field penetration and is defined in Equation 3-26.

$$\delta = \sqrt{\frac{2\rho}{\omega \mu_r \mu_0}} \quad m \tag{3-26}$$

In Equation 3-26 ρ is the electrical resistivity in Ohm-m, $\omega=2\pi f=377$ at 60 Hz and μ_r is the relative permeability of the material. For all practical non-magnetic metals Equation 3-26 can be simplified to,

$$\delta = 6.497 \sqrt{\rho} \quad mm \tag{3-27}$$

where ρ is expressed in $\mu\Omega$-cm and the frequency of interest is 60 Hz.

Table 3-10 gives the resistivity and 60 Hertz skin depth at 293 K (room temperature) and 77 K for several materials that are used frequently in cable constructions. It is clear that the skin depth will be large relative to the thickness of the materials that might be exist within flexible cables.

Table 3-10

Resistivity and skin depth of normal metals at 293 K and 77 K

Metal	Room Temperature - 293 K		LN_2 Temperature - 77 K	
	Resistivity Ω-m x 10^8	Skin depth mm (ins)	Resistivity Ω-m x 10^8	Skin depth mm (ins)
Silver	1.59	8.19 (.323)	0.18	2.76 (.109)
Copper	1.67	8.4 (.331)	0.19	2.83 (.111)
SS - 304	72	55 (2.17)	55	48.2 (1.9)
Aluminum	2.65	10.6 (.417)	0.23	3.12 (.123)
Brass	7.2	17.4 (.686)	4.7	14.1 (.555)
Bronze	3.92	12.9 (.51)	2.5	10.3 (.404)
Zinc	5.92	15.8 (.62)	1.12	6.87 (.270)
Lead	20.6	29.5 (1.16)	4.73	14.1 (.556)
Tin	11.8	22.3 (.88)	2.1	9.4 (.37)
Steel	12-20	1-2 (.04-.08)*	-	-

* Range of μ_r: 100 to 1000

An idealized cable which has a uniform tubular superconductor with a thin metal covering will experience eddy current losses in the metal layer due to the circumferential magnetic field. This arrangement approximates a thin flat plate in a field parallel to the surface. Eddy currents will form small circumferential vortices that will result in opposite axial surface currents on the inner and outer surfaces of the normal metal; there will be no net axial current and there will be no significant reaction field caused by the eddy currents. Eddy currents of this type are said to be resistance-limited as opposed to plates where the thickness is much greater then δ which are said to be inductance-limited. An expression for the power loss of such a plate has been derived by Stoll[26] and is presented as Equation 3-28 which can be used to calculate the power dissipation

in any layer of normal metal of thickness t meters that is not carrying significant transport current.

$$P_{layer} = \frac{\omega^2 \mu_0^2}{3 \rho} H_s^2 \frac{t^3}{8} \frac{W}{m^2} \quad (3\text{-}28)$$

H_s is the peak magnetic intensity in the material caused by the conductor current. To determine the loss per conductor meter, Equation 3-28 must be multiplied by the area of the layer per meter of conductor length, $2\pi R$. Gathering constants and simplifying Equation 3-28 with the help of Equation 3-10 results in Equation 3-29 which defines the loss per layer at 60 Hz as a function of conductor current.

$$P_{layer} = 29.748 \frac{I^2 t^3}{\rho R} \frac{mW}{m} \quad (3\text{-}29)$$

In Equation 3-29 I is the rms current in kiloamps inside the layer, t is the layer thickness in mm, ρ is the resistivity in $\mu\Omega$-cm, and R is the layer radius in cm.

Equation 3-30 illustrates the eddy current loss dependence on the variables specific to a cable design. This relation can be helpful to the experimentalist trying to separate hysteretic loss from eddy current loss because of the different powers associated with the parameters that can be experimentally varied, notably frequency and current or field.

$$P_{layer} \propto \frac{f^2 I^2 t^3}{\rho R} \quad (3\text{-}30)$$

For an example of an eddy current loss calculation, consider a tube with a superconducting layer which has an outside diameter of 4 cm covered by 0.1 mm of silver that is exposed to the field of the superconductor. At an rms current of 2500 amps the loss in the silver using Equation 3-29 and a mean radius of 2.01 cm computes to 0.514 mW/m. If the covering layer were increased in thickness to 1.0 mm, the loss would jump to 0.514 W/m.

The eddy current loss in the inner wall of a stainless steel cryostat for a room temperature dielectric cable design can be estimated using Equation 3-29. If the mean radius is 2.3 cm and the metal thickness is 0.635 mm (25 mils) the loss is 0.376 mW/m at an rms current of 2500 amps. The loss in the outer wall which is at or above room temperature will be 0.189 mW/m. The cubic dependence on metal thickness clearly indicates the importance of careful design to minimize the thickness of all normal metals that must lie in the field of the cable's current. However, these loss values will have little effect on the system design and operational costs, even after applying a factor of 10 to 15 to the inner (cryogenic) loss. Note that doubling the wall thickness of the cryostat members would increase the above values eight times, still insignificant.

The total eddy current loss to be assigned to the conductor assembly is the sum of the losses in each layer:

$$Q_e = \sum P_{layer} \quad \frac{W}{m} \tag{3-31}$$

Equation 3-29 can be used to calculate these losses for all layers that approximate the tubular geometry and lie in the field of the conductor current. More complex geometries such as the edges of superconducting tapes in a taped assembly require a more thoughtful analysis based on the specific magnetic field that will exist within the material and the surface paths for the eddy current vortex.

Conductor losses: DC cable

DC cable using a superconductor should exhibit no ohmic loss carrying a steady DC current. Truly loss-free conduction is difficult to achieve, and practical conductors will suffer small losses from several effects, two which are significant being AC harmonics and time variations in load, including start-up. If the superconductor is operated above its H_{c1} level, it will be in the mixed state, and flux will exist in the material. A changing magnetic field will cause fluxoids to move into or out of the superconductor, and their motion will result in a hysteretic loss as in the AC case. The rate of change of load

current during start-up and system disturbances may be large enough to yield losses that have an effect on the cryogen temperature profile. Loss generation, including its temperature dependence, must be carefully determined for harmonics and under the worst transient conditions possible as defined by the DC rectifier and inverter characteristics.

In magnet applications where the superconductor carries a DC current but is exposed to a transverse applied AC field due to the device function, as in a motor, for example, a loss mechanism is caused by the Lorentz force due to the DC transport current acting on the fluxoids. If the force exceeds the pinning force, energy is dissipated by movement of the fluxoid. This type of loss extracts its energy from the transport current and appears to be a resistive loss to the outside world. The phenomena is characterized as a dynamic resistivity and is well-known[27]. Equations for cylindrical wires carrying DC transport current in a transverse AC field are presented in the analysis performed by Carr[22]. The dynamic resistivity is zero at H_{c1} and rises to a constant value as the transverse field approaches the full penetration field.

Fortunately, this configuration does not apply to the DC power cable system. In a coaxial DC transmission cable, the conductor current will have AC harmonics that will superimpose an AC self-field onto the DC self-field. Harmonic currents and fields will be much smaller than the DC current and field, a situation opposite that of most magnet applications where the DC contribution of a single element accounts for only a small portion of the total field. The loss characteristic will resemble an AC loss and can be approximated using Equation 3-17, where H is the magnitude of the AC component of the field. Relatively slow time variation of the current can also be approximated by adjusting the frequency 'f' to correspond to one full cycle of the field change, recognizing that the loss will be in effect only for the time that the change is occurring. The reader is cautioned that the use of Equation 3-17 might be misleading. Hysteretic loss involves the magnetization curve for the material and the presence of the DC field will bias the

operating point on this curve. Critical state theory assumes a rectangular curve, the worst case, with results that have been reasonably accurate for self field due to AC transport currents. The DC bias combined with small field variations may establish operating points that differ greatly with DC bias level and conductor history. Such affects may be misinterpreted. The magnetization characteristic for a conductor assembly should be experimentally determined so that the loss analysis can be performed accurately. Eddy currents will be present in normal metals associated with the superconductor assembly due to harmonics and this loss, proportional to the square of frequency, may behave in a fashion similar to hysteretic loss, confusing the analysis of loss data.

Other loss mechanisms may result in the appearance of a finite resistivity. Examples include surface effects, small field interactions between the DC field which penetrates the surface layer and the transport current, and fluxoid instabilities which cause irregular or random flux motion, sometimes referred to as flux creep. These losses will be specific to the physical condition of the material and can vary with field, transport current and temperature. It should be possible to reduce these mechanisms by modification of the surface and/or the microstructure, but the optimization process will be one of trial and error as the quantitative correlation of the loss characteristics with the ceramic surface and microstructure is yet unavailable.

A major loss affecting DC transport current might arise due to defects in the superconductor that cause the current to move into adjacent normal metal paths. Large defects will be like cracks and effectively separate superconducting regions, forcing the current to follow a normal metallic path for a short distance. This type of defect can only be characterized after it has been established, suggesting that performance specifications should be based on measured loss after installation, or at least a clear demonstration that handling and service conditions will not aggravate the defect structure. Of course, the tendency for a material to have random defects, or to suffer

damage during installation should be quantified as part of the conductor application development process.

Dielectric Loss

AC HTSC cable designs that are based on the use of "solid" materials will experience dielectric losses that can be computed in the conventional way. They will depend on the characteristics of the dielectric selected, the dimensions, and possibly the nature of the dielectric shielding materials. The loss is easily derived by multiplying the phase-to ground voltage by the real component of the capacitive current flowing radially through the dielectric.

The capacitance of a coaxial cable with a uniform dielectric constant, ε, is given by Equation 3-32.

$$C = \frac{2\pi\,\varepsilon}{\ln(D_o/D_i)} \quad \frac{F}{m} \tag{3-32}$$

The dielectric constant is the product of the permittivity of free space, $\varepsilon_0 = 8.85 \times 10^{-12}$ Farads/meter, and the SIC (Specific Inductive Capacitance) of the material. For any practical dielectric material the capacitive current that flows radially because of the phase-to-ground voltage V is accurately approximated by Equation 3-33 which ignores the resistive component.

$$I_c = \omega C\, V \quad \frac{amps}{m} \tag{3-33}$$

The power dissipated in the dielectric is simply the product of the voltage, current and the cosine of the angle between them. The compliment of this angle is denoted the loss angle δ and the tangent of δ is numerically equal to the cosine of its compliment for small values of δ. The tan δ is called the dissipation factor which is a well-defined characteristic of any dielectric material. Equation 3-34 defines the dielectric loss of a single coaxial cable.

$$Q_d = V\ I\ \tan(\delta) \quad \frac{W}{m} \tag{3-34}$$

The above equations can be simplified to Equations 3-35 and 3-36 which give the capacitance and dielectric loss in more convenient units.

$$C = \frac{55.606\ SIC}{\ln(D_o/D_i)} \quad \frac{pF}{m} \tag{3-35}$$

$$Q_d = \frac{0.02096\ SIC\ \tan(\delta)\ V^2}{\ln(D_o/D_i)} \quad \frac{W}{m} \tag{3-36}$$

In these equations V is the phase-to-ground voltage in kV and D_o and D_i are the outside and inside diameters of the dielectric. The relevant diameters are those that represent the interface between the inner and outer shields and the dielectric. Representative values of SIC and tan δ for liquid and solid dielectric materials are given in Table 3-11.

Table 3-11

SIC and tan δ of cable dielectrics

Material	SIC		tan δ - %	
	293 K	77 K	293 K	77 K
Paper	3.4-3.6	1.9-2.4	0.15-0.28	0.13-0.20
PPP	2.6-2.8	2.25	0.06-0.10	0.04-0.09
XLP	2.3	2.2-2.3	<0.01	<0.01
EPR	2.8	2.5-3.0	0.35	0.03-0.06
Tyvek	-	1.7	-	<0.01
Dielectric Fluid	2.0-2.2	-	0.01-0.50	-
Liquid Nitrogen	-	1.454	-	0.01-0.04

* Bi-axially Oriented Polymer (Polyethylene or Polypropylene) Tape

In some constructions, the resistance of the shield layers may contribute a significant loss. This loss is computed as the product of the capacitive radial current (charging current) and the radial resistance of the shield layer. The resistance of the shield layer is given by Equation 3-37.

$$R_{radial} = \rho_s \frac{t}{A} \quad \frac{\Omega}{m} \tag{3-37}$$

In Equation 3-37, ρ_s is the resistivity of the shield material at its operating temperature, t is the shield thickness in meters and A is the area per meter of conductor, equal to πD_m where D_m is the mean shield diameter in meters. This resistance should be calculated for both the inner and outer shield layers. Table 3-12 provides representative resistivity values for shield materials that might be found in HTSC cables.

Table 3-12

Resistivity of shield materials

Shield material	Resistivity (ρ) ohm-m at 293 K	Resistivity (ρ) ohm-m at 77 K
Carbon Black Paper	500-5000	1.0-10
Carbon Black PE	50-100	5.4[28]

The loss in each layer is an I^2R loss given by Equation 3-38.

$$Q_{ds} = R_{radial} I_c^2 \quad \frac{W}{m} \; per\ layer \tag{3-38}$$

Shield Losses

Most high voltage cable designs are based on electrostatically shielded single conductor cable with the shielding structure held at or near ground potential. Currents that flow in this shield assembly create ohmic loss, unless the shield is superconducting. In that

case, the losses will follow the behavior outlined above for the superconducting conductor assembly, except the field due to the conductor current is lower at the shield radius than at the conductor radius. This discussion will concentrate on the calculation of losses in the so-called "non-coaxial" case where the shield structure is comprised of normal metals.

In the context of discussions on superconducting cables, a coaxial cable is one that carries the full conductor current in its shield structure. This situation can be forced to occur in any shielded cable by not grounding the shield at one end and floating the load or system between the conductor and its shield. In an ideal coaxial superconducting cable with a tubular outer shield conductor, the inner (phase) conductor current flows in the shield as a shielding current created by the superconductor to prevent field penetration. The outer conductor must have connections at its ends that allow this current to flow, otherwise the axial shielding current generated on the inside surface of the superconductor will return on its outside surface. Fortunately, the end connections can be as simple as connecting the three shields together, since the three phase shield currents vectorially add to zero.

Normal cables try to carry a return current on their shield due to the axial voltage gradient induced in that conducting path by the field of the conductor current. The amount of current that flows, assuming the appropriate connections at the cable ends, is determined by the voltage gradient and the impedance of the shield path. If there are multiple end-to-end paths, such as an external ground, or isolated armor layers, the current will divide in inverse proportion to the impedance of each path. The calculation of shield currents in self-contained cable systems is a formidable task, too complex to include in this discussion. Most self-contained systems have heavy shield assemblies to handle fault currents and their shield systems require special design consideration or cross-bonded connection schemes to control both the induced voltage and the current losses.

The pipe-type cable system is the most likely system for HTSC consideration in the U.S., at least in the early days of HTSC technology. We will therefore limit detailed discussion of the loss calculations to this configuration, applicable to both a room temperature dielectric cable or a cryogenic cable without a superconducting shield assembly.

Losses that are proportional to the square of the phase current occur in the shield structure and the pipe. They are calculated in accordance with the classic Neher-McGrath paper which derives these formulations for the calculation of cable ampacity[29]. The Neher-McGrath procedure for pipe-type cables defines the ohmic losses in each cable component as a portion of a total AC/DC resistance ratio using y-factors, y_c, y_s, and y_p, and an "in-pipe" factor PF which is in the range of 1.5 to 1.7. The total ohmic loss Q_t is the sum of the conductor loss Q_c, the shield loss Q_s, and the pipe loss Q_p. It can be written as I^2 times an overall AC resistance, R_{ac}, or as a function of the conductor's DC resistance R_{dc} using the y-factors and the in-pipe factor PF as shown in Equation 3-39.

$$Q_t = I^2 R_{ac} = I^2 R_{dc} (1 + PF (y_c + y_s) + y_p) \quad watts/m \tag{3-39}$$

The individual component losses are related to the y-factors and PF by Equations 3-40, 41 and 42 defined below.

$$Q_c = I^2 R_{dc} (1 + PF y_c) \quad watts/m \quad Conductor\ loss \tag{3-40}$$

$$Q_s = I^2 R_{dc} PF\, y_s \quad watts/m \quad Shield\ loss \tag{3-41}$$

$$Q_p = I^2 R_{dc}\, y_p \quad watts/m \quad Pipe\ loss \tag{3-42}$$

The HTSC application does not contain a meaningful R_{dc} so it is necessary to eliminate R_{dc} from the equations. Fortunately, the Neher-MacGrath equations that define the y-factors all contain R_{dc} in the denominator. If R_{dc} is simply removed from the defining y-factor equations, then Equations 3-40, 41 and 42 must also remove R_{dc} to properly define the component losses. The modified y-factor equations then define an effective resistance for the loss in each component.

There are three mechanisms that create losses in the metallic shield structure of a pipe-type cable assembly. These are circulating currents, eddy currents due to the fields of the three conductors, and charging currents that are collected by the shield structure but must flow some axial distance. Charging current loss is dependent on the type of contact that exists between the three shield assemblies because these currents are radial and the three phases will cancel each other locally if possible. The nature of the contact can only be speculated if a positive system is not applied.

Circulating current is an axial current that flows when the shield is not an open circuit. The loss it creates is proportional to the phase current squared, and is calculated with an equivalent resistance, R_{circ}, using Neher-McGrath Equations 26 and 27 with R_{dc} removed which results in Equation 3-43.

$$R_{circ} = \frac{R_s}{1 + (R_s/X_m)^2} \quad \frac{\Omega}{m} \tag{3-43}$$

The shield resistance, R_s, is the result of the parallel combination of all metal tapes and skid wires for one cable. Each is calculated using Neher-McGrath Equation 13 which, after adjustment of units results in Equation 3-44,

$$R(per\ path) = \frac{\rho_s}{A_s} \sqrt{1 + \left(\frac{\pi D_{sm}}{pitch}\right)^2} \quad \frac{\Omega}{m} \tag{3-44}$$

where ρ_s is the resistivity of the metal at the specific temperature as given in Table 3-10, A_s is the cross-sectional area of the tape or skid wire, D_{sm} is the mean skid wire diameter, and the pitch is defined as the distance between successive turns of the tape or skid wire. A typical value for shielding tape is 1.06 times the tape width. Skid wires are normally applied with a pitch (lay) of 7.62 cm (3"). Two skid wires, equally spaced, are used in conventional pipe cable unless the cable is small, less then about 5 cm (2") in diameter. HTSC cables may be able to use only one skid wire because they will be much lighter then conventional cables, and the elimination of a skid wire will reduce the shield loss considerably. The total R_s is given by Equation 3-45.

$$R_s = \frac{1}{\sum \frac{1}{R_{per\ path}}} \quad \frac{\Omega}{m} \tag{3-45}$$

X_m is the mutual reactance between the conductor and the shield. X_m is a function of D_{sm}, the mean shield diameter and S, the axial spacing between the centerlines of the phases. S is nominally equal to the shield diameter plus 1.5 times the thickness of the skid wire. X_m is defined by Equation 3-46 for a triangular cable arrangement (Neher-McGrath Equation 28A) and Equation 3-47 for a cradled configuration (Neher-McGrath Equation 29), the latter applicable if the ratio of the pipe inside diameter to the cable outside diameter is greater than 2.5.

$$X_m = 75.36 \times 10^{-6} \ln\left(\frac{2S}{D_{sm}}\right) \quad \frac{\Omega}{m} \quad triangular \tag{3-46}$$

$$X_m = 75.36 \times 10^{-6} \ln\left(\frac{2.52\,S}{D_{sm}} \sqrt[6]{1 - \left(\frac{S}{D_p - S}\right)^2}\right) \quad \frac{\Omega}{m} \quad cradled \tag{3-47}$$

Eddy currents flow locally due to the oscillating magnetic field in the metallic shield components. The loss these currents create is proportional to the phase current squared, and is calculated as an equivalent resistance using Neher-McGrath Equation 30A modified for the shorted shield configuration, which produces Equation 3-48.

$$R_{eddy} = 0.0013 \frac{R_s}{R_s^2+X_m^2} \left(\frac{D_{sm}}{2S}\right)^2 \left(1 + \frac{5}{12}\left(\frac{D_{sm}}{2S}\right)^2\right) \quad \frac{\Omega}{m} \tag{3-48}$$

The total loss in the shield proportional to the square of the phase current is the sum of the circulating current and eddy current loss and is given by the following equation:

$$Q_s = (R_{circ} + R_{eddy})\, I^2 \quad \frac{W}{m} \tag{3-49}$$

The loss given by Equation 3-49 should be multiplied by 1.5 if the cables are installed directly in a steel pipe to account for the magnetic effects of the steel. This factor should not be applied to cryogenic dielectric cables where only the outer wall of the cryostat is steel.

Since R_s is normally much greater then X_m, both of these losses are seen to be inversely proportional to R_s. For this reason, it is desirable to make R_s as large as possible.

Typical shield loss calculations were performed to illustrate the magnitude of these losses for a cable construction that uses one 304 SS tape and one 1/16" X 3/16" 304 SS skid wire. The results are shown in Table 3-13. The calculations cover a range of shield diameters from 2" (5.1 cm) to 4" (10.2 cm). The skid wire dominates the shield resistance, and results in marginally high loss for the cryogenic dielectric design. An alternative that uses a hollow skid wire of the same dimensions, but half the cross-section cuts the loss almost in half, as shown.

Table 3-13

Shield losses due to phase current

D_{sm} (cm)	Solid skid wire			Hollow skid wire		
	R_s Ω/m	R_{eff} μΩ/m	Total Loss W/m	R_s μΩ/m	R_{eff} μΩ/m	Total Loss W/m
5.1	0.0937	0.0443	1.189	0.1705	0.0246	0.654
6.35	0.0956	0.0430	1.150	0.1767	0.0233	0.622
7.62	0.0969	0.0420	1.125	0.1812	0.0226	0.602
8.9	0.0979	0.0413	1.107	0.1846	0.0220	0.587
10.2	0.0986	0.4091	1.094	0.1873	0.0217	0.576

R_{eff} is the effective loss resistance for one phase that yields one third of the total loss when multiplied by the square of the phase current in kAmps. R_{eff} is the sum of R_{circ} and R_{eddy} and is inversely proportional to R_s.

The Total Loss is in Watts per meter for all three shield assemblies with a phase current of 3000 Amps. Losses due to axial flow of charging currents and those in the surrounding pipe or pipes are not included in this example.

Charging currents flowing radially through the cable capacitance will create a loss if they are forced to flow axially in the shield structure for any appreciable distance. When the three shields are in continuous contact, the three phase charging currents add to zero everywhere so there is no ohmic loss in the shields other then that due to radial current flow. However, when the points of contact between phases are not continuous, currents will flow axially. When skid wires are present, the shortest possible distance between contacts is half of the pitch, but the cables could be floating for distances of several meters. If insulating skid wires are used to reduce losses, the shields would be connected only at splices. The distance between splices is on the order of a kilometer.

The insulating skid wire concept would generally be counter-productive; however, a semi-conducting polymer skid wire might provide adequate shield-to-shield contact and also satisfy the high resistivity goal mentioned above.

The charging current is calculated using Equation 3-33. If the distance between phase contacts is L meters, then the average loss due to the charging current flowing into that distance equally from each end can be found by integrating the square of the local current flow times R_s over the length L, and dividing by L to get an equivalent loss per unit length. The result is given in Equation 3-50.

$$Q = \frac{R_s L^2 I_c^2}{3} \quad \frac{W}{m\text{-}phase} \tag{3-50}$$

Unlike the circulating and eddy current losses, this component is directly proportional to R_s. Fortunately, L can be kept small by using a conducting or semi-conducting material for the skid wire and ensuring radial continuity through the shield structure. This means that all tapes applied over the dielectric must have a radial current transfer mechanism. Polyester moisture seal tapes are commonly used in pipe cable constructions. It is imperative that insulating tapes such as these have a metalized surface and that are applied in pairs, half-lapped with the pairs on opposite faces, or half-lapped with a metal tape. Tying the three cables together is also suggested, to maintain an equilateral formation and positive phase-to-phase contact, even though this practice admittedly slows down the cable pulling operation. Tying the cables into a positive triangular configuration also tends toward minimizing the magnetic interaction of the cables with each other and with the pipe enclosure, and yields the lowest shield loss configuration.

Table 3-14 summarizes calculations of the loss that might occur due to the axial flow of charging current in a 138 kV cable with a cryogenic paper dielectric. This table is based on a cable with a 5.08 cm diameter core with 12.83 mm (0.505") of paper insulation

Table 3-14

Losses caused by charging current

Contact Distance (m)	Solid Skidwire Total Loss (W/m)	Hollow Skidwire Total Loss (W/m)
1	1.6×10^{-6}	3.1×10^{-6}
10	1.6×10^{-4}	3.1×10^{-4}
100	1.6×10^{-2}	3.1×10^{-2}
1000	1.6	3.1
10000	160	310

which has an SIC of 2.0 at 77 K. The outside diameter of the insulation is 7.65 cm. This cable has a capacitance of 274.2 pF/m and a charging current of 8.23 Amps/km. The Total Loss listed is for the three phases. It is clear that cable-to-cable contacts must be assured more frequently then at splice locations, which could be a kilometer apart, in order to keep this loss insignificant.

Enclosure Losses

Pipe losses represent a potential upper limit to the current capacity of an AC HTSC power cable without a superconducting ground shield. Pipe losses are the result of eddy currents which are created by the magnetic fields from the phase currents in the three conductors. Since these currents add vectorially to zero, there are no continuous flux lines within the pipe material encircling the three cables. Magnetic flux penetration into the pipe material occurs locally near each phase conductor resulting in an eddy current and small hysteretic loss that varies with azimuthal position around the pipe. The loss in the pipe or enclosure is minimized by positioning the three conductors as close together as possible. Some utilities have recognized the importance of cable position on losses as mentioned above and have tied the cables into an equilateral configuration as

they enter the pipe, a tedious process that slows down the pulling operation. Tying cables during the pull is no longer a common installation practice.

The Neher-McGrath procedures contain equations for the losses in both magnetic and non-magnetic enclosures. The non-magnetic case involves only eddy current loss which can be roughly approximated using Neher-McGrath Equation 31, presented as Equation 3-51 with R_{dc} removed, adjusted for SI units and multiplied by three to represent an effective resistance that yields the total three phase loss when multiplied by the square of the phase current. It is applicable to non-magnetic pipes (e.g. stainless steel) in the room temperature dielectric pipe type configuration, and both walls of the cryostat in a non-coaxial cryogenic configuration if a steel pipe is not used for the outer wall.

$$R_{eff} \approx 9\, R_p \left(\frac{A^2}{B+1} + \frac{A^4}{4B+1} + \frac{A^8}{16B+1} \cdots \right) \quad \frac{\Omega}{m} \tag{3-51}$$

Rp and the A and B parameters are defined below,

$$R_p = \frac{\rho_p}{\pi\, D_{pm}\, t} \quad \frac{\Omega}{m} \tag{3-52}$$

$$A = \frac{2\,s}{D_{pm}} \quad and \quad B = \left(\frac{1.585 \times 10^6\, R_p}{f} \right)^2 \tag{3-53}$$

where D_{pm} is the mean pipe diameter and t is the thickness of the pipe, both in meters, and ρ_p = resistivity of the pipe in Ohm-m. The resistivity can be taken from Table 3-10. A temperature coefficient of 0.001 can be used to adjust the resistivity of stainless steel.

When calculating the pipe loss for a room temperature dielectric system in triangular configuration ($D_p/D_s < 2.5$) in a non-magnetic pipe, the spacing factor s is equal to 0.578 times the cable diameter over the skid wire, D_s. This accounts for the relatively small conductor diameter. If the cables can lie cradled ($D_p/D_s > 2.5$), the Neher-McGrath

procedure suggests that the loss be obtained by averaging the two losses calculated using $s = 0.578\ D_s$ and $s = (D_{pm}-D_s)/2$. When calculating the loss for the inner cryostat pipe in the non-coaxial cryogenic dielectric case, the latter definition of s should be used. The loss in the outer cryostat pipe wall is reduced because the cables are more closely centered with respect to that pipe. Its effective resistance can be calculated using $s = 0.578\ D_s$.

The effective pipe resistance is more conveniently stated in units of μΩ/m which gives Watts/m when multiplied by the square of the phase current in kAmps. The effective resistance is seen to be roughly proportional to the inverse of the pipe resistance which means that the loss increases with thickness and decreases with increasing temperature. At cryogenic temperatures, the thinnest possible wall thickness should be used to counteract the decrease in resistance at those temperatures.

To illustrate the magnitude of this loss, the effective resistance was calculated for a range of applicable Type 304 stainless steel pipe sizes using a thickness of 3.175 mm (1/8 inch) and a resistivity adjusted to 55 C, the practical limiting pipe temperature for the room temperature dielectric design. These results are plotted in Figure 3-19 against the ratio of pipe ID to D_s for both possible cable configurations.

The effect of pipe wall thickness is illustrated in Figure 3-20 for a 20.64 cm (8 1/8") ID pipe, a pipe to cable diameter ratio of 2.4 for the triangular arrangement and a pipe to cable diameter ratio of 2.8 for the cradled configuration.

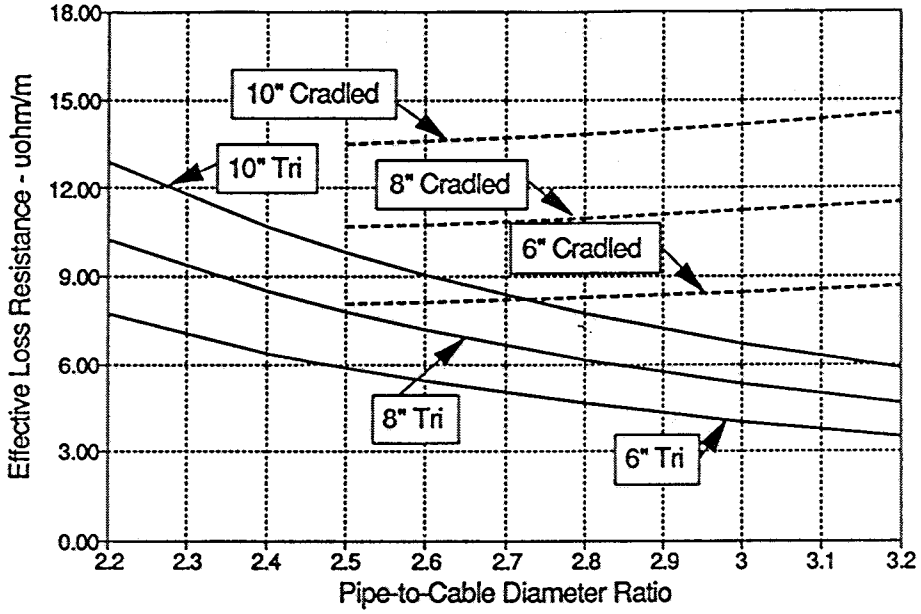

Figure 3-19 Effective resistance of 304 Stainless steel pipe.

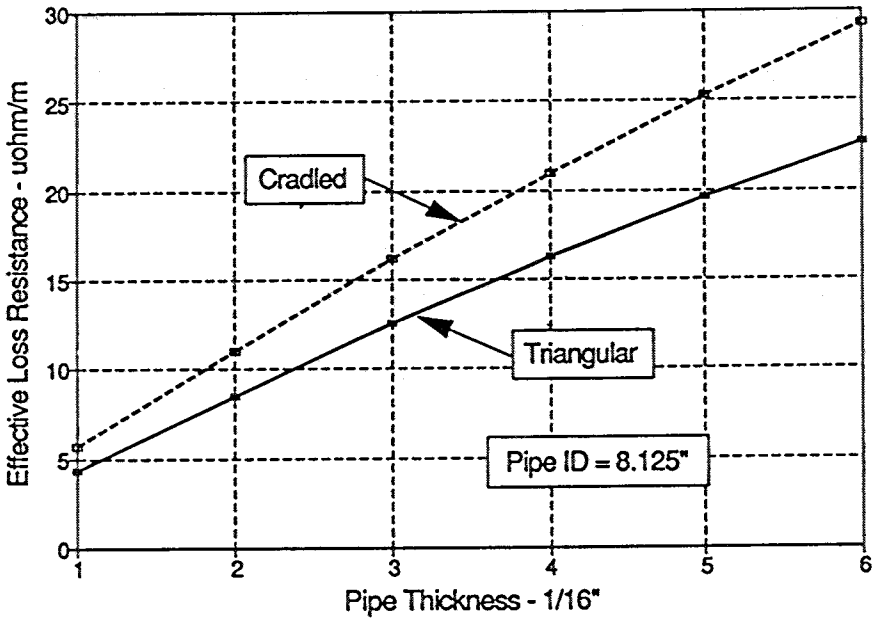

Figure 3-20 Effect of wall thickness on 304 stainless steel pipe loss.

Systems that use a steel pipe suffer higher losses. The Neher-McGrath procedure uses two empirical formulas to calculate y_p, Neher-McGrath Equations 34 and 35 for triangular and cradled cable configurations, respectively. These are repeated below with R_{dc} removed to define an effective pipe resistance. This resistance yields the total loss in the pipe directly when multiplied by the square of the phase current.

$$R_{eff} = 9.843 \times 10^{-6} \left(35.04\, D_{skid} - 4.53\, D_p \right) \frac{\Omega}{m} \qquad (3\text{-}54)$$

$$R_{eff} = 9.843 \times 10^{-6} \left(13.39\, D_{skid} + 6.89\, D_p \right) \frac{\Omega}{m} \qquad (3\text{-}55)$$

The analysis of losses in steel pipes is more complex than these empirical equations imply because of the interaction between the magnetic flux entering the pipe material and the magnitude of the phase current creating the flux. In fact, the effective pipe resistance decreases as the field strength caused by the phase currents increases. Also, the pipe loss being an eddy current loss decreases with increasing resistivity. Thus, an elevated pipe temperature reduces it's loss. While the Neher-McGrath equations are adequate for the current range of typical pipe cables, on the order of 1000 Amps, the equations must be recognized as simplified empirical relations that ignore magnetization and pipe temperature effects.

The use of HTSC Room Temperature Dielectric cables in steel pipes will demand higher current levels then those possible with conventional cables. The losses in the pipe will cause the pipe temperature to rise so that this loss is removed by conduction to the surrounding earth. This cable style will continue to have temperature limitations dictated by the soil's thermal stability, as do conventional HPFF cables. It is therefore desirable to be able to estimate the pipe loss with some degree of confidence because it will define the upper capacity limit possible with this simple design.

There has been much work published on losses in pipe-type cables as evidenced in the literature. EPRI funded an extensive study in project RP7832[30]. This program acquired a large amount of data and also provided a comprehensive theoretical analysis. Several observations which are listed below emerged from a review of the literature and the EPRI reports generated in RP7832.

1. The pipe loss mechanism is predominantly an eddy current loss rather than a hysteretic loss. The flux creating the eddy currents is, however, increased by the magnetization of the steel.

2. The loss decreases with increasing permeability. This makes the loss a decreasing function of current since current translates to magnetization, and the permeability increases with magnetization up to the saturation level of steel. Increasing permeability decreases the skin depth.

3. The loss, being an eddy current loss, decreases with increasing temperature.

4. The position of the three conductors relative to each other and with respect to the pipe exert a major influence on the magnitude of the loss. The configuration in which the cables are close to the pipe and far from each other (open triangular) results in the highest losses. The configuration in which the cables are close to each other and far away from the pipe (close triangular) and centered in the pipe offers the lowest loss scenario. The losses for the cradled formation are intermediate between these two cases. The loss increases with cable diameter for the close triangular configuration which rests on the pipe.

5. The loss is proportional to the inside surface area of the pipe per unit of length. That is, for the same conductor arrangement and current level the loss per unit length increases with pipe diameter.

While all studies that reported loss data as a function of current show the decrease of loss with increasing current, no one has produced a calculation method that predicts such behavior. The closest is the work reported in EL-3977[31] which develops a generalized calculation procedure for pipe loss as a function of permeability. The permeability increases with magnetization up to saturation. Unfortunately, there is no method to quantify the effective magnetization as a function of the phase current. It is

necessary to correlate the calculation with measured data as a means to estimate the permeability in effect.

The prediction of pipe loss is also complicated by the interaction of the pipe and the current distribution in the conductors inside the pipe. The presence of the steel pipe causes the loss in the conductors and shields to increase in a somewhat uncertain manner. When the total loss is measured it is difficult to accurately separate the losses in the pipe from those in the conductors and shields.

The evaluation of experimental data has usually been done by measuring the total loss and using it to establish the overall AC/DC ratio, since the direct measurement of the individual losses is very difficult. The data reported in EPRI EL-1125[30] is presented this way. The total loss is measured first in air and then in the pipe. The increase over the loss in air is attributed to the combination of an in-pipe factor and the actual pipe loss.

Equation 3-39 can be re-arranged to define the AC/DC ratio as in Equation 3-56.

$$R_{ac/dc} = 1 + PF(y_c + y_s) + y_p \qquad (3\text{-}56)$$

If the in-pipe factor can be separated from the pipe loss it is possible to estimate the pipe loss from total loss measurements. Data from EL-1125 is amenable to such treatment. Total loss data was obtained for several constructions using copper and aluminum in three pipe sizes as a function of load and temperature.

A unique aspect of this data collection is the use of the same geometries for several conductor types. When the geometry, load and temperature are the same, the pipe loss should be the same independent of the conductor style if the field distortions caused by changes in the current distribution for each member of the conductor are small. Because the conductors tested were all segmental the current density distortion in the individual segments which increases the conductor loss will not change the overall field interaction

with the pipe. Local changes will average out because the pipe length is several segment lay lengths. If this is true, variations in the total loss with conductor style must be accommodated by variation of the in-pipe factor, not the actual pipe loss.

The copper segments, whether bare, tinned, or lead alloy-coated have good contact between strands that tends to negate the benefit of multi-strand assemblies verse solid rods. These conductor segments have relatively high skin and proximity effects because the current distribution is easily distorted. Their in-pipe factor can also be expected to be high and somewhat uncertain. This was confirmed by the erratic behavior of the loss for the copper conductors due to load (temperature) cycling that was attributed to changes in the inter-strand contact resistance with physical motion. Both the enameled copper and the aluminum conductor are expected to exhibit higher inter-strand resistance which reduces skin and proximity effects and should stabilize their in-pipe factors.

Data for the aluminum conductors, which did not exhibit variation of AC/DC ratios with temperature cycling, was selected from EL-1125 for analysis of load and temperature effects to determine if an adjustment to the Neher-McGrath equations could be justified. Table 3-15 summarizes the basic geometric parameters of this study for the aluminum conductor data.

Table 3-15

Dimensions of cables and pipes in pipe loss study

	2000 kcmil Segmental		4700 kcmil Segmental	
Pipe ID	D_s	D_p/D_s	D_p	D_p/D_s
8.125"	2.60"	3.125	3.48"	2.34
10.25"	3.87"	2.649	4.75"	2.16
12.25"	4.86"	2.521	5.70"	2.15

Only the close triangular configuration was studied because HTSC applications are expected to be near the maximum diameters that will fit in a given pipe. Using the recommended in-pipe factor of 1.5, the aluminum conductors yielded the lowest pipe loss. Data was obtained for the 2000 kcmil aluminum conductor with currents of 200, 400, 600 and 800 amperes at 23C in all pipe sizes, and at a conductor temperature of 63C and a pipe temperature of 50C in the 8" pipe. Data was obtained for the 4700 kcmil conductor in each pipe size at 23C and 800 amperes. This data is summarized in Table 3-16 and 3-17. Included in these tables is an estimated value of the AC/DC ratio projected to a current of 2500 amperes, the range of interest of room temperature dielectric HTSC cables.

Table 3-16

AC/DC Ratio Measurements - 2000 kcmil Aluminum Conductor

Current amps	8" pipe @ 23C $R_{AC/DC}$	10" pipe @ 23C $R_{AC/DC}$	12" pipe @ 23C $R_{AC/DC}$	8" pipe @ 50C $R_{AC/DC}$
200	1.25	1.32	1.42	1.21
400	1.22	1.29	1.39	1.19
600	1.21	1.27	1.37	1.165
800	1.205	1.26	1.36	1.155
2500*	1.19	1.24	1.34	1.145

* Estimated value by projection of data

Table 3-17

AC/DC Ratio Measurements - 4700 kcmil Aluminum Conductor

Current amps	8" pipe @ 23C $R_{AC/DC}$	10" pipe @23C $R_{AC/DC}$	12" pipe @ 23C $R_{AC/DC}$
800	1.67	1.83	2.02
2500*	1.60	1.70	1.85

* Estimated value by projection of data

Table 3-18 gives the R_{dc} of each conductor and the factor $1 + y_c + y_s$ for each pipe size as measured in air in the close triangular configuration.

The Neher-McGrath Equations 3-54 and 3-55 define the effective pipe loss resistance as a function only of geometry. The data presented in Tables 3-16 and 3-17 illustrate behavior as a function of load for two distinct temperatures. The combination of these effects can yield a means for estimating the effective pipe loss resistance needed for the

Table 3-18

R_{dc} and $(1 + y_c + y_s)$ at 23C for each Case

Conductor Size	R_{dc}	$1 + y_c + y_s$ (measured in air)		
kcmil	uΩ/ft	8" pipe	10" pipe	12" pipe
2000	8.57	1.04	1.03	1.02
2000 @ 63C	9.935	1.04*	1.03*	1.02*
4700	3.29	1.12	1.08	1.09

* Values at 63C assumed identical to those at 23C

design of HTSC cable systems. This is done by converting the AC/DC ratio data to an effective resistance using the DC resistance and an assumed value of 1.5 for the in-pipe factor as suggested by RP7812. The relation is shown in Equation 3-57.

$$R_{eff} = 3R_{dc}\left(R_{ac/dc} - 1 - PF(y_c + y_s)\right) \quad \frac{\mu\Omega}{m} \tag{3-57}$$

The results of this exercise are shown in Figure 3-21 which plots the effective pipe loss resistance against load, and Figure 3-22 which plots the Neher-McGrath relations for the triangular configuration as a function of D_p/D_s to illustrate the relation between Equation 3-54 and this experimental data.

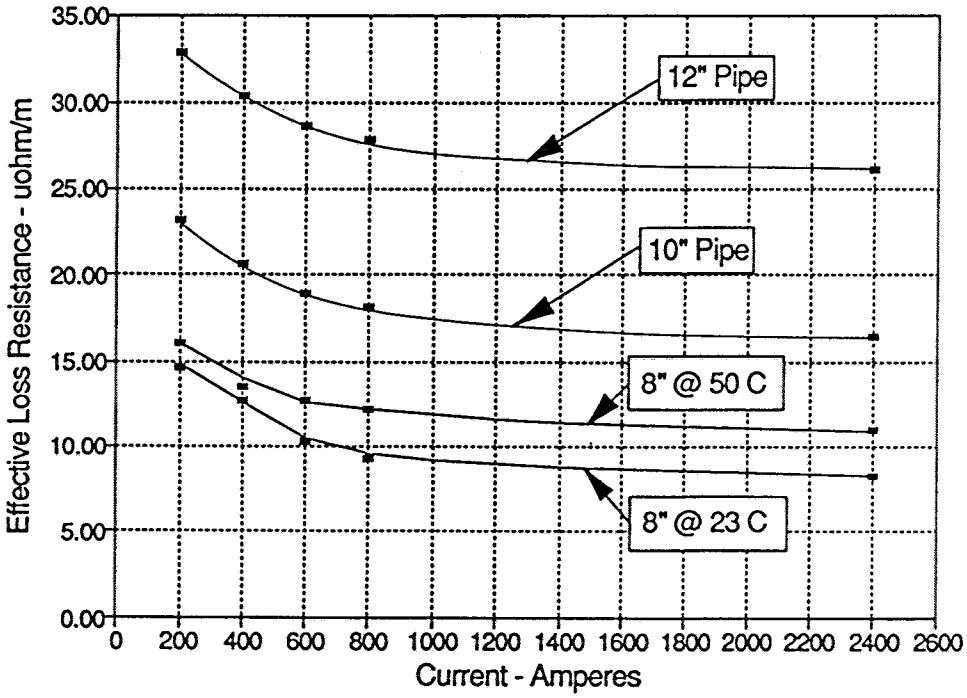

Figure 3-21 Variation of measured pipe loss resistance with load.

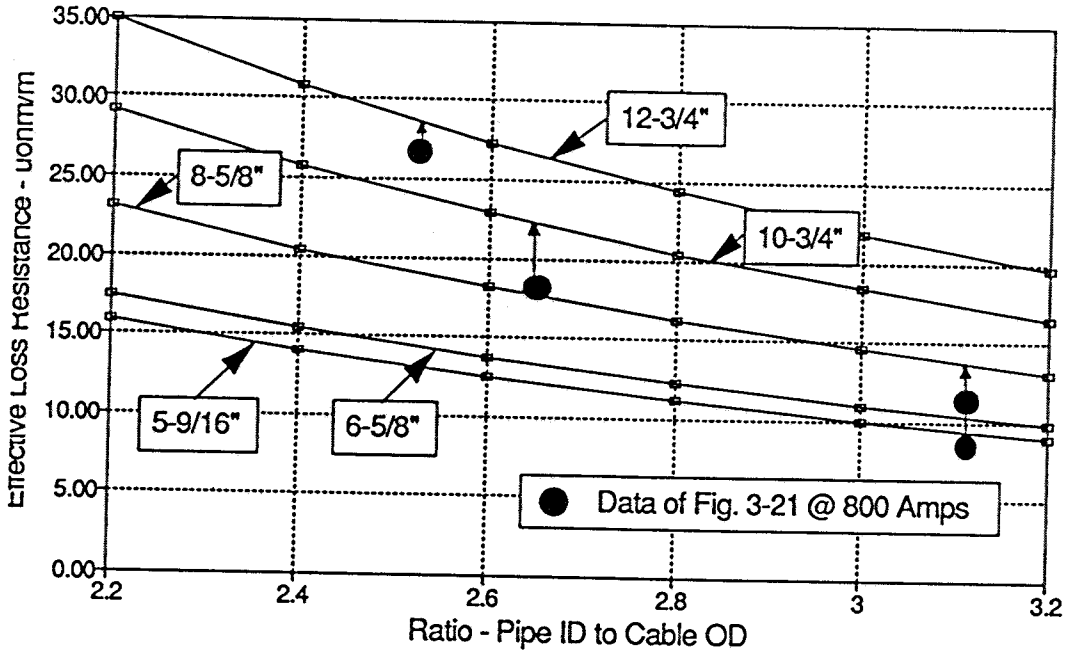

Figure 3-22 Neher-McGrath predicted pipe loss and data from Figure 3-21.

Consideration of this data leads to a modification of the constants in Equation 3-54 for the purpose of predicting the pipe loss of Room Temperature Dielectric HTSC cables in steel pipes. The modified equation is:

$$R_{eff} = 9.843\ (38.544\ D_s\ -7.258\ D_p)\quad \frac{\mu\Omega}{m} \tag{3-58}$$

Figure 3-23 plots the effective resistance relations computed with Equation 3-58 as a function of the pipe to cable diameter ratio R, defined as D_p/D_s.

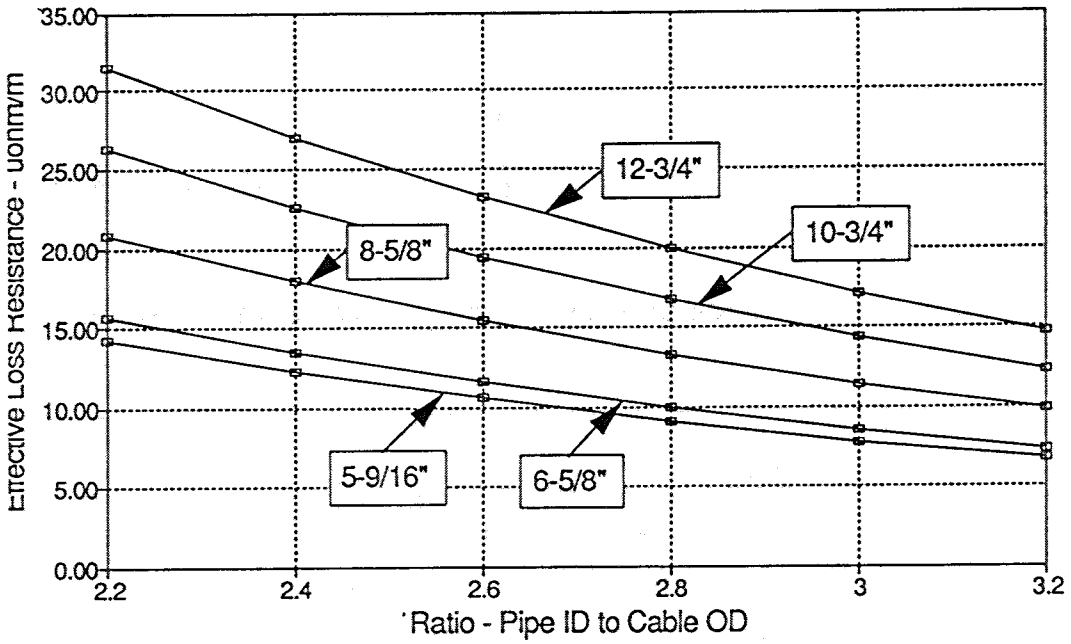

Figure 3-23 Effective pipe loss resistance for HTSC cables in Steel Pipe.

The total pipe loss for magnetic or non-magnetic pipes is calculated as R_{eff} times the square of the current as shown in Equation 3-59.

$$Q_p = R_{eff}\, I^2\quad \frac{W}{m} \tag{3-59}$$

The correct loss is obtained when R_{eff} is in $\mu\Omega/m$ and I is in kA or R_{eff} is in Ω/m and I is in Amperes. R_{eff} is defined by Equation 3-51 for non-magnetic pipe or Equation 3-58

for magnetic steel pipe. This loss, when combined with the total dielectric loss and the thermal resistance and temperature of the surrounding earth, defines the magnitude of current that results in the limiting pipe interface temperature for the room temperature dielectric configuration. If higher currents are required, supplemental cooling will be necessary to control the temperature of the pipe and earth. The cooling can be in the form of conventional forced cooling by circulating dielectric fluid, or other innovative means might be explored.

New installations have the option of using stainless steel pipe in place of steel pipe. The increase in capacity afforded by the stainless steel pipe can be estimated on the basis that the allowed temperature rise will be the same for both cases. Therefore, the square root of the ratio of effective pipe loss resistances will relate the currents of the two cases. Considering pipes with an ID of 0.2604 m (8 1/8") and a pipe-to-cable diameter ratio of 2.4, the steel pipe effective resistance of 17.908 μΩ/m is obtained from Equation 3-58. Equation 3-51 defines the stainless steel effective pipe loss resistance as 8.512 μΩ/m using a stainless steel resistivity corrected to 55 C (74.52×10^{-8} Ω-m) and a thickness of 3.175 mm (1/8"). The root of the ratio of these resistances is 1.45 in favor of the stainless steel, indicating that for these circumstances the stainless steel pipe will yield a 45% higher current capacity if both are limited by the 55 C pipe temperature.

Heat In-leak

The subject of heat in-leak is discussed in depth in Section 4. The type of cryostat that should be used for either a room temperature or cryogenic dielectric system will employ multi-layer evacuated superinsulation because of its superior thermal insulation capabilities. Heat transfer in this medium takes place by two mechanisms, radiation and conduction. Radiative heat transfer between two surfaces varies as the difference of fourth power of the surface temperatures. The purpose of the multi-layer insulation is to provide a series of low emissivity surfaces which grade the temperature from one surface to the next and take advantage of the fourth power dependence of heat transfer

on surface temperatures. It can be shown that the radiative transfer across a series of "n" layers is approximately 1/[2(n+1)] times the transfer without intermediate layers.

Heat is also transferred by conduction between layers due to layer-to-layer contact and the solid paths afforded by the support structure. Conductive heat transfer is directly proportional to temperature difference and thermal conductivity of the materials involved. The thermal conductivity of many materials varies substantially with temperature over the range of interest for cryogenic applications.

In Section 4 the combined heat transfer of superinsulation is shown to behave like a conduction phenomena in the range of room temperature (293 K) to liquid nitrogen temperature (77 K) if the high temperature is fixed, regardless of small variations in the liquid nitrogen temperature because of the T^4 dependence. An effective overall thermal resistivity ρ_{eff} of 12000 K-m/W has been found to correlate well with measured data for this temperature range. The thermal resistance between two coaxial cylinders with an inner diameter D_i and an outer diameter D_o is given by Equation 3-60.

$$R_{thermal} = \frac{\rho_{eff}}{2\,\pi} \ln\left(\frac{D_o}{D_i}\right) \quad \frac{C-m}{watt} \tag{3-60}$$

If the cryostat is corrugated, the diameters that define its thermal performance are the maximum outer surface diameter of the inner tube and the minimum inside diameter of the outer tube.

The high temperature side of the cryostat may operate well above room temperature, which will have a substantial impact on the radiation heat transfer because of the T^4 dependence on T_h. In this case, the value of resistivity mentioned above should be adjusted downward. Such an adjustment can be approximated if the assumption is made that at 293 K the radiative and conductive heat transfers are equal. Then the

conductive heat transfer effective resistivity is twice that noted above, or 24000 K-m/watt, and the radiation half of the heat transfer should use 24000 K-m/watt adjusted by the ratio of 293 to the actual temperature (in Kelvin) of the cryostat shell, raised to the fourth power. If the high temperature is 55C (328K), the effective resistivity of the radiative portion is reduced to 15,282 K-m/watt which when combined with the conduction component reduces the net effective resistivity by 21.2% to 9337 K-m/watt.

The variable of interest to the system designer is the heat in-leak as a function of cryostat dimensions. This heat can be found using the thermal equivalent of Ohm's Law, shown in Equation 3-61, where T_h will be determined only by factors external to the cryogenic system, and the thermal resistance is adjusted as discussed above.

$$Q_{in-leak} = \frac{T_h - T_c}{R_{Thermal}} \quad \frac{W}{m} \tag{3-61}$$

If the diameter ratio is 1.4 and the temperature difference is 258 K (328-70), the target heat in-leak of 0.5 w/m requires an effective resistivity of about 10,000 K-m/watt.

Hydraulic Calculations

The hydraulic design of HTSC cable systems is discussed in Section 4 in conjunction with refrigeration system options. Pertinent points are repeated here to provide the calculation procedures necessary to continue the design process. All HTSC systems under consideration will use liquid nitrogen as the coolant in configurations that are similar to forced cooled pipe cable or self-contained cable systems. The liquid nitrogen will be kept at a pressure sufficiently high to insure that boiling cannot take place anywhere in the cooling section, whether or not the liquid nitrogen is in contact with the dielectric. This will be accomplished by a "pumping plant" whose function is the control of pressure by the addition or release of liquid nitrogen in the same manner that a dielectric fluid pumping plant controls the pressure in a conventional cable system.

Flow parameters

The analysis of liquid nitrogen flow uses equations common to most low viscosity liquids. Liquid nitrogen has physical properties similar to water except it exists in a different temperature range. There are five liquid properties that must be known for the hydraulic calculation procedures. All are functions of temperature, and to a lesser degree, pressure. These properties are presented in Table 3-19 for a temperature of 70 K and a pressure of 1.379 MPa (200 psi), both typical of the expected operating range.

Table 3-19

Properties of Liquid Nitrogen at 70 K, 200 psi

Density	Viscosity	Specific heat	Thermal conductivity	Coeff. of expansion
840 kg/m^3	220 μPa-s	2.024 kJ/(kg-K)	149.9 mW/(m-K)	4.91 x 10^{-3} /K

Density and viscosity are involved in pressure drop calculations while specific heat, thermal conductivity, and the thermal expansion coefficient are required for thermal calculations. Variations of these properties with pressure in our range of interest are small enough to be ignored. The behavior of these properties with temperature are shown graphically in Figure 3-24 normalized to the values given in Table 3-19.

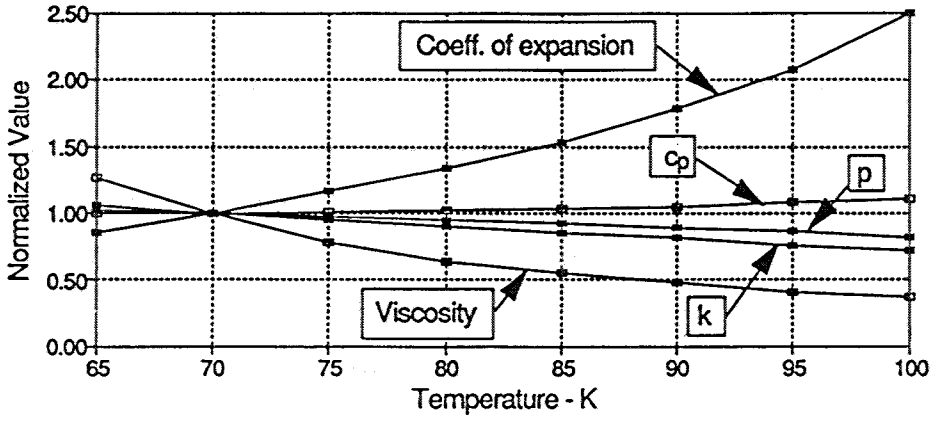

Figure 3-24 Variation of Liquid Nitrogen Properties with temperature.

Pressure drop

Hydraulic calculations involve the coordination of three variables that characterize the system. These are the flow rate, the pressure drop and the temperature rise. For a given geometry, the pressure drop per unit length will increase with the square of the flow rate and the temperature rise per unit length will be directly proportional to flow rate and heat load. Pressure drop and flow rate are related by the duct or channel dimensions. Temperature rise is a function of heat load and flow rate only, but heat transfer coefficients must be considered in the calculation of the temperature of cable components such as the actual superconducting materials. The cooling section length is an important independent variable that ties the flow rate, temperature rise and pressure drop together.

The calculation procedure begins with the definition of the flow geometry. Ducts are characterized by a hydraulic diameter D_h and a flow area A_f. The hydraulic diameter of a circular duct is simply its diameter, and its flow area is its cross-section.

If the duct is not circular the hydraulic diameter is defined on the basis of the flow area divided by the wetted perimeter:

$$D_h = 4 \frac{A_f}{wetted\ perimeter} \quad m \tag{3-62}$$

The space surrounding the three cables inside the cryostat of a cryogenic dielectric design can be described analytically as given in Equations 3-63 and 3-64,

$$A_f = \frac{\pi}{4} (D_p^2 - 3D_s^2) \quad m^2 \tag{3-63}$$

$$Wetted\ Perimeter = \pi (D_p + 3D_s) \quad m \tag{3-64}$$

where D_p is the inside diameter of the pipe (m) and D_s is the cable diameter over the skid wire (m).

If the flow space is not analytically defined, both the flow area and the wetted perimeter can be found by graphical means.

The average velocity V is computed by dividing the flow rate in m^3/s by the flow area.

$$V = \frac{Flow\ Rate}{A_f} \quad \frac{m}{s} \tag{3-65}$$

The hydraulic flow is characterized by its Reynolds Number defined in Equation 3-66,

$$N_R = \frac{\rho\ V\ D_h}{\mu} \quad (dimensionless) \tag{3-66}$$

where ρ is the density in kg/m^3 and μ is the viscosity in (kg/m-s). The Reynolds Number establishes the nature of the flow, laminar or turbulent. A Reynolds Number of 2000 is considered to be the typical point where the flow changes from laminar to turbulent, at least for flow in pipes or channels that are roughly circular. Flow in a cable pipe containing three cables in random, variable configuration with skid wires makes the laminar-to-turbulent transition at a lower Reynolds Number, on the order of 800.

The pressure drop is calculated with the aid of a friction factor that is empirically defined by the magnitude of the Reynolds Number. Because the behavior of the friction factor is strongly dependent on the type of flow, it is common to define separate factors for the two flow types. The friction factor in laminar flow is a simple function of the Reynolds Number, given by Equation 3-67.

$$f_l = \frac{K}{N_R} \quad (dimensionless) \tag{3-67}$$

The constant K is 64 for flow in conductor ducts or circular pipes. A value of 45 should be used when calculating pressure drop in a cable pipe containing three cables, to be consistent with the above definition of hydraulic diameter and empirical data.

The friction factor in turbulent flow is obtained from an experimentally determined "Moody Diagram" which plots f_t as a function of Reynolds Number for smooth pipe walls and as a function of a surface roughness parameter. The Moody Diagram for water can be found in Figure 4-57. The friction factor is seen to become essentially constant for rough pipes at high Reynolds Numbers.

The friction factor for conductor ducts is complicated by the presence of either a helical former or a corrugated surface. Data for such configurations is sparse. Therefore, it is necessary to estimate what friction factor might be expected, or what the equivalent surface roughness might be. Supplier data for corrugated pipes suggests increasing the smooth pipe friction factor by four times. In Section 4, Los Alamos suggests this multiplication factor might be as high as seven for helical formers or a corrugated duct. Until further data become available, we suggest the following philosophy for the definition of friction factor: Use $f=64/N_{Re}$ for Reynolds Numbers below 2000, otherwise use f=0.1.

Experimental data for the turbulent flow friction factor in pipes with cables and skid wires obtained in EPRI RP7801-5[32] yielded the following relation between the friction factor and Reynolds number. Until experimental data becomes available this relation for flow in a cabled pipe is recommended.

$$f_t = \frac{0.2}{N_R^{0.1}} \qquad (3\text{-}68)$$

Finally, the pressure drop is defined by the Darcy-Weisbach equation.

$$\frac{\Delta P}{\Delta L} = f \frac{\rho V^2}{2 D_h} \quad \frac{N}{m^2} \ per\ meter \qquad (3\text{-}69)$$

The flow configuration for the Room Temperature Dielectric system requires one duct to carry twice the flow of the other two ducts. In laminar flow the pressure drop is proportional to the flow rate so two thirds of the loop pressure drop occurs in the double flow duct, but the temperature rise in that duct will be roughly half that in the other two (if heat inputs are the same). In turbulent flow, if the friction factor is independent of Reynolds Number, the pressure drop is proportional to the square of the flow rate, making the pressure drop in the double flow duct 80% of the total.

The relatively high pressure drop in the single duct could be reduced by making that duct (and the rest of that phase) larger. For a given flow rate in laminar flow the pressure drop varies inversely with the fourth power of the diameter. A 19% increase in duct diameter of the single duct would equalize the pressure drops between the go and return paths and reduce the pressure drop and pumping energy by 33%.

If the flow is in the turbulent regime the pressure drop dependence on diameter approaches an inverse fifth power. In this case a 32% increase in duct diameter is required to equalize the go and return pressure drops. The total pressure drop and pumping energy would then be reduced by 58%.

The unequal cable diameters would complicate the manufacture of the cables and result in unbalanced capacitive and inductive reactances. The unbalanced capacitance could be corrected by transposing the larger cable twice if at least three cooling sections are required in the circuit. If a circuit is short enough to be designed with one or two cooling sections, a small unbalance in the cable reactances probably will not impact the system. An alternate approach would use a larger wall thickness to reduce the capacitance to match the smaller cables. If the system has multiple loops and multiple cooling plants, the differing pressure drops are more easily accommodated.

Noting that the pressure drop varies with the inverse fourth or fifth power emphasizes the desirability for making the cryogen duct diameter as large as practical. For a given mass flow, if the duct diameter is increased by 10% the pressure drop in laminar flow is reduced by 46% and by 61% in turbulent flow.

Temperature rise

The temperature rise of the fluid per unit length is a function of the mass flow rate and heat capacity of the liquid nitrogen, and the heat load that is being absorbed by the liquid nitrogen stream. The general equation for the rate of temperature rise is,

$$\frac{dT}{dx} = \frac{Q}{M\,C_p} \quad \frac{K}{m} \tag{3-70}$$

where,

$$M = \rho \times flow\,rate \quad \frac{kg}{s} \tag{3-71}$$

In Equations 3-70 and 3-71, Q is the heat being absorbed in W/m, the liquid nitrogen flow rate is in m^3/s, and C_p is the liquid nitrogen heat capacity in (W-s/kg-K), given in Table 3-19 and Figure 3-24.

Equation 3-70 can be integrated over the cooling section length to determine the total temperature rise, recognizing that both Q and C_p vary with temperature and position. The approximate temperature rise will be dT/dx evaluated at the mid-point of the cooling section multiplied by the section length. More exact calculations should integrate along the length using an approximation to the temperature dependence of the heat capacity shown in Figure 3-24. This type of analysis would also incorporate the temperature dependence of the superconducting conductor assembly losses discussed above.

The application of the above equations in a complete system design will depend on the configuration of the flow channels and their interaction. Such problems are identical to those of forced cooled conventional cable systems. The analysis of these situations is covered thoroughly in EPRI's Forced Cooling Handbook[32] and are not repeated here. Following are some general comments that should help the potential user, should he wish to pursue a more detailed analysis.

The room temperature dielectric system is easier to analyze because the three flow paths are thermally isolated by the individual cryostats. The heat load on the cryogen flow is just the heat in-leak, the ohmic losses in the superconductor assembly and the pumping loss.

If cooling is done at one end only, there is a preferred arrangement which will minimize the superconductor losses based on the variation of loss with temperature. If the loss did not vary with temperature then it wouldn't matter whether the cold cryogen is pumped into one or two phases since the total loss going around the loop would be the same for either flow arrangement. However, since the losses increase with temperature, the total loss will be lower if the cold cryogen is pumped into the single phase because the temperature at the turn-around point and the average system temperature will be lower with this arrangement.

Cryogenic dielectric systems that use the three conductor ducts as the "go" path and the space within the pipe as the "return" will be more difficult to design because of the thermal coupling between the two sides of the cooling loop. If the go and return streams are at different temperatures there will be heat flow between the two streams, in addition to the heat load of the system. When such an arrangement has only one cooling plant, the temperature far from the cooling plant is difficult to control, and tends to rise above the return temperature at the cooling end. It is suggested that loop designs with single point cooling be avoided with this type of system. This tendency can be

reduced if a thermal insulation barrier can be applied between the two flow paths. One way to accomplish this would be to apply the thickest possible layer of thermal insulation over each cable, under the skid wire, but electrically connecting the cable shield to the skid wire.

Thermal Calculations

The HTSC cable system operating temperature profile will be established by heat flow into the cryogen and to the earth's surface, and the thermal impedances between the heat sources and these two heat sinks. Thermal calculations at the design stage are generally made on the basis of steady state operation. This eliminates the necessity to use a dynamic technique to study temperature-time variations which inevitably impact the actual operation of transmission systems.

Thermal models. The steady state temperature profile of a cross-section of the cable system can be established by using the resistive analog models shown in Figures 3-25 and 3-26 for the room temperature dielectric and the cryogenic dielectric pipe type systems, respectively.

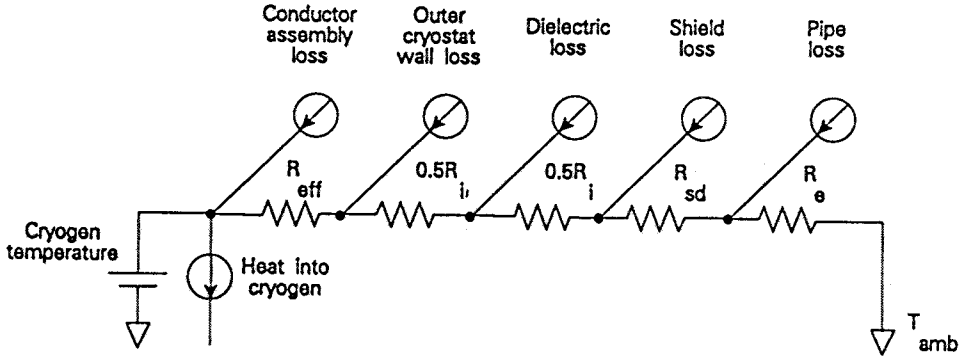

Figure 3-25 Thermal model of Room Temperature Dielectric Cable System.

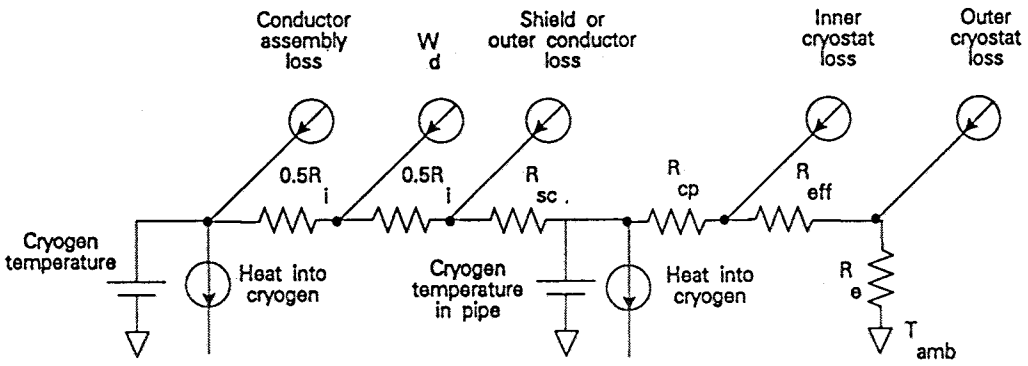

R_i = Thermal resistance of the cable dielectric

R_{sc} = Thermal resistance between the surface of the three cables and the cryogen

R_{cp} = Thermal resistance between the cryogen and the outer pipe

R_e = Thermal resistance between the cable enclosure and the surface of the earth

Figure 3-26 Thermal model of Cryogenic Dielectric Cable System.

A preliminary analysis of the heat flow and operating temperature profile over the length of the cooling loop can be made using these simple resistive models applied at many equally spaced locations along the cooling section, adjusting the cryogen temperature for its axial temperature profile based on the average heat input and local rate of rise at each model section. The various methods for dealing with this type of three dimensional problem can be found in the Forced Cooling Handbook.

Thermal resistances. Several thermal resistances must be computed in addition to R_{eff}, the effective resistance of the cryostat defined above. R_i is the thermal resistance of the cable dielectric. It is a simple annulus which has a thermal resistance defined by Equation 3-72 where D_i is the diameter of the inner metallic surface at high voltage and D_o is the inside diameter of the outer ground surface, in like units. For thermal considerations the dielectric material includes all semi-conducting non-metallic shielding material.

$$R_i = \frac{\rho_i}{2\pi} \ln\left(\frac{D_o}{D_i}\right) \quad \frac{C-m}{Watt} \tag{3-72}$$

A similar conduction resistance is R_e, the resistance between the cable pipe or enclosure and the earth surface. It is given by the Kennelly formula[29],

$$R_e = \left(\frac{\rho_{eff}}{2\pi}\right) \ln\left(\frac{4L}{D_p}\right) \quad \frac{K\text{-}m}{W} \tag{3-73}$$

where L is the depth from the surface of the earth to the centerline of the pipe and D_p is the diameter over the pipe coating. The thermal resistivity of dielectrics and earth materials needed to define R_i and R_e are summarized in Table 3-20.

Table 3-20

Thermal resistivity of materials in K-m/W

Room Temperature Dielectrics	
Fluid-impregnated paper	5.5 K-m/W
Fluid-impregnated PPP	6.0 K-m/W
Polyethylene	3.5 K-m/W
EPR/EPDM	5.0 K-m/W
Earth materials - Effective overall resistivity	
Thermal sands	0.6 K-m/W
Native soils - typical	1.0 K-m/W
Poor soils, fine sand	2.0 K-m/W

The resistance R_{sd} between the surface of the three cables and the pipe in the room temperature dielectric configuration is calculated using Neher-McGrath Equation 41 repeated below:

$$R_{sd} = \frac{A}{1 + \{84.6 \times (B + CT_m)D_s\}} \quad \frac{K\text{-}m}{W} \tag{3-66}$$

The constants for this equation are given in Table 3-21 for the two common pipe filling media, dielectric fluid or nitrogen gas, both at 1.38 MPa (200 psi). T_m is the mean media temperature (C, not K) between the cable surfaces and the pipe. D_s is the cable diameter over the skid wire in meters.

Table 3-21

Numerical values of constants employed for computation of R_{sd}

Pipe filling medium	A	B	C
Dielectric fluid	0.256	0	0.0065
Nitrogen gas	0.945	1.16	0.0053

Cryogen heat transfer. The other resistances in these models involve the heat transfer between duct or pipe walls or the cable surfaces and the flowing cryogen. Heat transfer of this type is characterized by the dimensionless Nusselt number which contains a heat transfer film coefficient. The standard analytical approach is to define the Nusselt Number in terms of the Prandtl Number and the Grasof Number for laminar flow or the Reynolds Number in turbulent flow with empirically determined exponents. The Prandtl and Grashof Numbers are defined as follows:

$$N_{Pr} = \frac{C_p\ \mu}{k} \quad \textit{Prandtl Number} \tag{3-75}$$

$$N_{Gr} = \frac{g\ \beta\ \rho^2 \Delta T\ D_h^3}{\mu^2} \quad \textit{Grashof Number} \tag{3-76}$$

where g is the acceleration due to gravity (9.807 m/s^2).

The Nusselt relations can be arranged to provide a direct calculation of a thermal resistance between the surface and fluid. This procedure has been developed for pipe cable surface-to-fluid thermal resistances in the Forced Cooling Handbook leading to the following definitions of the resistances used in the above models between the surface of each of the three cables and the cryogen (R_{sc}), and between the cryogen and the outer pipe (R_{cp}). For Laminar flow,

$$R_{sc} = \frac{D_h A_c}{k} (N_{Gr} N_{Pr})^{0.2} \quad \frac{K\text{-}m}{W} \tag{3-77}$$

and,

$$R_{cp} = \frac{D_h A_p}{k} (N_{Gr} N_{Pr})^{0.25} \quad \frac{K\text{-}m}{W} \tag{3-78}$$

In turbulent flow,

$$R_{sc} = \frac{28}{k} (N_R^{0.8} N_{Pr}^{0.33}) \quad \frac{K\text{-}m}{W} \tag{3-79}$$

and,

$$R_{cp} = \frac{R_{sc}}{2} \tag{3-80}$$

In these equations $A_c = \pi D_s$ m^2/m, $A_p = \pi D_p$ m^2/m and D_p = ID of the pipe. The Reynolds number that marks the change from laminar flow to turbulent flow in the above equations is 800.

Heat transfer from the conductor duct into the cryogen flow is similar to that of water flowing in a circular tube being heated and will be improved by the presence of corrugations or a spiral former. Rough calculations of the expected heat transfer ignoring these enhancements indicate that the temperature differences between the duct wall and the flowing liquid nitrogen will not exceed 0.3 K in laminar flow and will be less than 0.1 K in turbulent flow. Such a small resistance can be neglected.

The above equations provide all of the information necessary to calculate the heat balance for the thermal models shown in Figures 3-25 and 3-26. The manipulation of this type of model is routine for the electrical or mechanical engineer and will not be discussed further. The reader in need of more guidance is directed to the literature.

Electrical Characteristics

The analysis of superconducting cables forming part of a utility transmission system requires knowledge of the electrical parameters of the cable system. The generalized transmission line is characterized by its R, L, C and G parameters that are sufficient to describe its behavior completely in any electrical circumstance. Most of the problems facing transmission engineers (with the exception of dielectric loss) will be such that the shunt conductance G will have no significance and can be ignored. For balanced three phase power flow analysis the series resistance is of minor significance. However, a superconducting cable can exhibit a non-linear behavior during extreme overload or fault conditions if the current and/or field is high enough to drive the conductor into the normal state. The following discussion will concentrate first on the definition of the reactive components, the shunt capacitance C and the effective series inductance L, and then AC resistance. Calculation of the sequence impedances will also be discussed. Some discussion of the impact of the unique characteristics of superconducting lines on long distance transmission will be included, addressing the pros and cons of surge impedance loading as it affects the need for some form of reactive compensation.

Capacitive reactance

The capacitance of a coaxial cable system was defined earlier by Equations 3-33 and 3-36 in conjunction with the dielectric constants tabulated in Table 3-11. This definition applies to essentially all HTSC cable designs under consideration because all are electrostatically coaxial.

The shunt capacitive reactance of one phase is defined as,

$$X_C = \frac{1}{\omega C} \quad \frac{\Omega}{m} \tag{3-81}$$

where C is the cable's capacitance in F/m.

The charging current has been expressed by Equation 3-34 which is equivalent to Equation 3-82 below when multiplied by the circuit length L in meters.

$$I_C = \frac{L\,V}{X_c} \quad amperes \tag{3-82}$$

The voltage V is the phase-to-ground voltage. The capacitive reactance of a cable system is sometimes stated as the total MVAR for the three phases combined. This is approximated by three times the charging current times the phase-to-ground voltage.

Inductive Reactance

The inductance of HTSC cable systems will depend on the nature of the cable design. Inductance is a measure of the energy stored in the magnetic field set up by current flow, and is influenced by the geometry of the return current path or paths and other conductors near-by. The generalized formulations for three phase single conductor cable systems include a self inductance term and mutual inductance terms with the other phase conductors, the shields of every cable, and any parallel ground conductors. A general routine to determine the inductive reactance of one conductor in a system of conductors involves the calculation of the induced voltage over the length of the conductor in question from all related sources. Reference 33 contains a clear summary of this procedure applicable to the generalized three phase cable system which would also be appropriate for Room Temperature Dielectric HTSC non-coaxial cables installed as single conductor cables with metallic sheaths.

The two most probable forms of HTSC cables are special cases which have relatively simple relations that describe their inductance and inductive reactance. The cryogenic dielectric coaxial arrangement where both the inner and outer conductors are superconducting effectively shields itself from the other phases and ground conductors. This configuration has the lowest possible inductance. The Room temperature dielectric pipe-type system has mutual relations only with its two neighboring phases, the three cable shields, and the pipe.

Conventional conductors that approximate a solid shape create magnetic fields that can be separated into an internal component and an external component. The internal component of magnetic flux does not link the entire conductor, only that portion within the flux circle. Outside of the conductor all flux links all of the conductor. The inductance for conventional conductors is calculated as the sum of the two parts which describe the internal and external flux fields. These two parts can be combined into a single expression by the use of the Geometric Mean Radius (GMR). The resulting general formula for the inductance of a conductor is given in Equation 3-83,

$$L = 2\times10^{-7} \ln(\frac{S}{r}) \quad \frac{Henry}{m} \tag{3-83}$$

where S is the spacing between the conductor's center and an effective return and r is the GMR of the conductor. Solid conductors of radius r_c have a GMR=0.779r_c. If the conductor has the form of a thin tube, the internal flux becomes very small and the GMR approaches r_c. An ideal HTSC conductor made of an HTSC layer on the surface of a tube would represent the limit where the internal flux would vanish. HTSC conductors made of several layers of tapes or wires will approximate a thin tube and should use the radius of the outermost layer as the GMR unless contrary data is available.

A fully coaxial cable that carries a return current equal to the conductor current has the minimum inductance of any cable type because the external field is limited to the space

between the inner and outer conductors. The inductance of a coaxial cable is given by Equation 3-83 with S set equal to the radius of the inner layer of the outer conductor.

HTSC Room Temperature Dielectric Cables installed in stainless steel pipe exhibit a net inductance also defined by Equation 3-83 where S is equal to the diameter over the skid wire for cables in a triangular configuration or S is the cube root of the product of the three center-to-center spacings defining the cradled arrangement. When a steel pipe is used Equation 3-83 should be increased by 15% to account for the high permeability of the steel and S for cables in a cradled configuration is given by Equation 3-84,

$$S = 1.26\, D_s \sqrt[6]{1 - \left(\frac{D_s}{D_p - D_s}\right)^2} \quad meters \tag{3-84}$$

where D_p is the inside diameter of the pipe.

The inductive reactance of each phase of the cable system at 60 Hz is given by Equation 3-85.

$$X_L = \omega L \quad \frac{\Omega}{m} \tag{3-85}$$

AC Resistance

The AC resistance of a superconducting cable is not determined as a ratio of the AC to DC resistance because the DC resistance is presumably zero. To the system, however, all losses created by the flow of current appear as a resistance. The calculation of this resistance parameter requires the summation of all relevant current-dependent loss terms. Each of the loss mechanisms has been described in the above sections. The effective AC resistance can be expressed as the summation of losses divided by the square of the phase current as shown in Equation 3-86 where Q(I) represents each of the current-dependent losses.

$$R_{AC} = \frac{\sum Q(I)}{I^2} \qquad (3\text{-}86)$$

The Cryogenic Dielectric coaxial system will experience hysteretic loss in both the inner and outer superconductor and eddy current loss in normal metal claddings that lie in the magnetic field. The Room Temperature Dielectric assembly has superconductor losses only in the superconductor assembly but must add shield and enclosure losses to the summation.

Phase Sequence Impedances

The method of symmetrical components is used by utility planners to study the behavior of the power system when phase conditions are unbalanced or when faults occur from one phase to ground or between two phases. This method breaks the three phase system voltage and current phasors into the sum of three balanced phasor systems, the positive sequence with phase sequence defined in one direction, the negative sequence which has its phase sequence in the opposite direction, and the zero sequence which is made up of three equal phasor sets that are in phase with each other. Analysis of this type requires knowledge of impedances of the system to each sequence. For transmission lines and cable systems, the positive and negative sequence impedances are assumed equal but the zero phase sequence impedance will generally differ because of changes in mutual reactive effects. Also, in the case of pipe-type cables single phase current flow within the pipe is highly non-linear because of the permeability of the steel pipe.

The Cryogenic Dielectric coaxial cable zero sequence impedance will be identical to the positive/negative sequence impedance as long as both the inner and outer superconductor assemblies are not driven into the normal state by the higher fault current. At some current level the inner conductor may switch to the normal state due to excess field. This change will dramatically increase the AC resistance but not the reactance, as long as the outer conductor remains superconducting. At a higher current

level the outer conductor will also go normal and the cable will take on the behavior of conventional cable in pipe where the return current will divide among the three outer conductors and the pipe. If the inner and outer conductor cross-sections were equalized by design the transition out of the superconducting state may occur simultaneously if current density rather than magnetic field is limiting the superconducting state.

The zero sequence impedance defines the system impedance parameters when all three cables carry single phase current. If only one cable is carrying fault current the other two may remain in the shielded superconducting state. This would upset analysis by symmetrical components because the zero sequence impedance of individual phases would differ. However, the field from the normal cable may be high enough to drive near-by cables normal and the fault current may try to return on the outer conductor of the other cables as well. It is therefore likely that all three cables will go normal under extreme fault conditions. When all cables are in the normal state the sequence impedances can be calculated as for conventional cables using the methods suggested by Neher[34], or empirical data. The AC resistance will be increased substantially because superconductivity has been lost leaving only the normal metal components of the conductor assembly to carry current. The AC resistance of a tubular assembly of tapes or wires will be approximately equal to the DC resistance of the assembly if the thickness of the assembly is less than 10% of the mean radius.

The series resistance and reactance defined above by Equations 3-83 through 3-86 describe the positive, negative and zero sequence resistance and reactance of Cryogenic Dielectric coaxial cables for normal loading conditions as shown in Equation 3-87.

$$Z_{(+,-,0)} = R_{AC} + j\,X_L \qquad (3\text{-}87)$$

The positive and negative sequence impedances for Room Temperature Dielectric cables at normal power levels installed in stainless steel or steel pipes can also be computed using Equations 3-83 through 3-86. If fault currents will drive the superconductor into

its normal state then R_{AC} will be increased dramatically and should be estimated to be the DC resistance of the conductor and cryostat assembly.

The zero sequence impedance of non-superconducting cables in pipes is based on the flow of the single phase return current, equal to three times the phase current, in the pipe and the cable shield structures. Following Neher's analysis[34], the zero sequence resistance and reactance for cables in non-magnetic pipe are developed as follows:

$$R_0 = R_c + 3R_r \quad \frac{\Omega}{m} \ per\ phase \tag{3-88}$$

$$X_0 = 3(X_c + X_r) \quad \frac{\Omega}{m} \ per\ phase \tag{3-89}$$

R_c is the DC resistance of the conductor assembly in the normal state, which includes the cryostat in the Room Temperature Dielectric cable structure. X_c is the conductor reactance defined by Equation 3-90.

$$X_c = 132.92\times10^{-6} \ln\left(\frac{(D_p + t)^3}{3.115 D_c S^2}\right) \quad \frac{\Omega}{m} \ per\ phase \tag{3-90}$$

In Equation 3-90 the geometrical variables expressed in meters are:

D_p = inside diameter of pipe.
t = pipe thickness.
D_c = diameter over conductor assembly.
S = spacing, either the diameter over the skid wire or as defined in Equation 3-84.

The return resistance R_r and reactance X_r are somewhat complicated. These terms are defined by Equations 3-91 and 3-92 for cables in non-magnetic pipes.

$$R_r = R_p - real\ part\ of \frac{(R_p + jX_m)^2}{R_s/3 + R_p + jX_m} \quad \frac{\Omega}{m} \ per\ phase \tag{3-91}$$

$$X_r = imag\ part\ of\ -\frac{(R_p + jX_m)^2}{R_s/3 + R_p + jX_m}\ \frac{\Omega}{m}\ per\ phase \qquad (3\text{-}92)$$

where X_m is given by Equation 3-90 with D_c replaced by D_s, and the constant 3.115 replaced by 4. R_p and R_s are the DC resistance of the pipe and one cable shield (including skid wires) respectively.

The zero sequence impedance parameters of cables in steel pipes are not well behaved because of magnetic effects in the steel. It is customary to use empirical data to estimate the zero sequence parameters which are functions of the zero sequence current. Review of data published by Thomas and Kershaw[35] and by Neher[34] shows that the zero sequence reactance X_0 does not vary much with cable and pipe size but is moderately dependent on the ratio of pipe to cable diameter which defines how the cables fit in the pipe. It is possible to estimate X_0 as a function of only the current and this ratio with suitable accuracy for preliminary studies. Figure 3-27 presents a graph which plots X_0 for the three cables in parallel against the total zero sequence current.

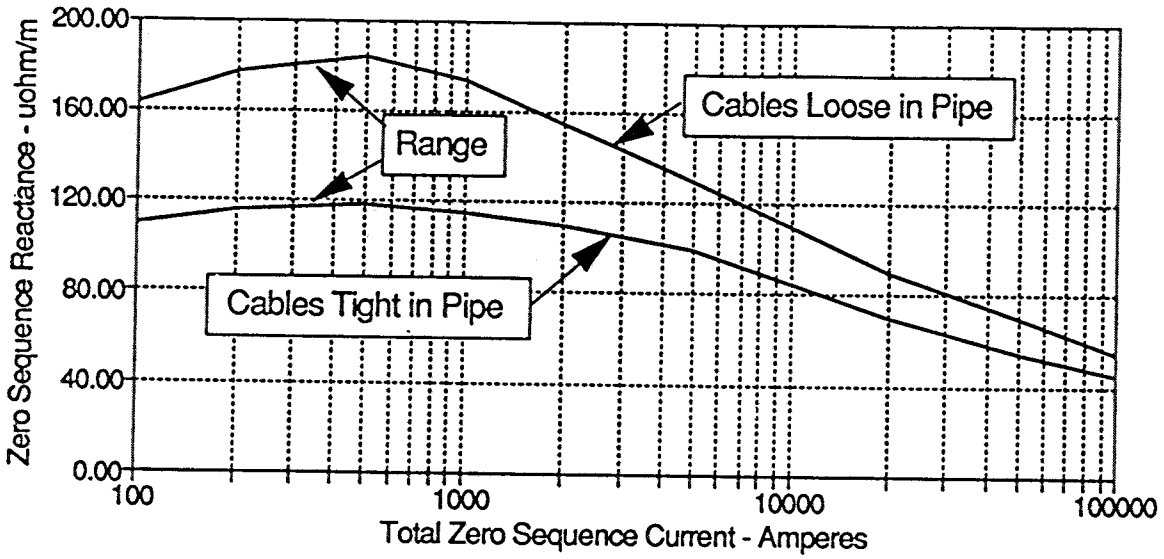

Figure 3-27 Estimated zero sequence reactance of cables in steel pipe.

The zero sequence resistance for the three cables in parallel in a steel pipe can be estimated by Equation 3-88 with R_c divided by three and the return resistance R_r, which varies only with zero sequence current and pipe diameter, obtained from Figure 3-28.

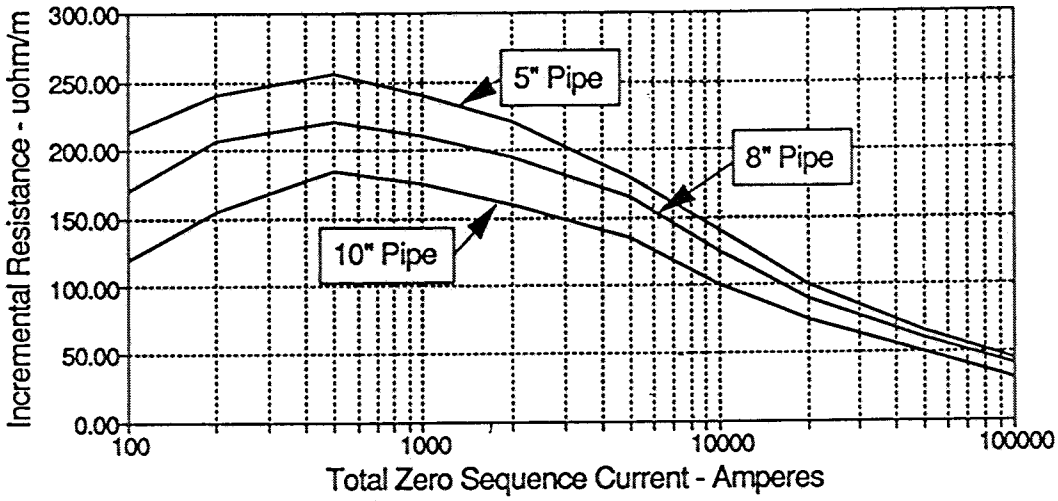

Figure 3-28 Incremental zero sequence resistance for cables in steel pipe.

Long Line Considerations

The R, L and C and G parameters discussed above can be used to analyze an HTSC cable system as an electrical transmission line using traveling wave techniques. The shunt conductance G can usually be ignored but it will be included in the following presentation of the transmission line equations for thoroughness.

A transmission line is described by several traveling wave parameters that are functions of the line's electrical characteristics[36]. These are summarized below:

Characteristic Impedance: Z_0 is the impedance of the infinite line seen by the source. It represents the load which will have no wave reflections. When a line is terminated with Z_0, there will be no reactive energy exchange with the system.

$$Z_0 = \sqrt{\frac{R + j\omega L}{G + j\omega C}} \quad \Omega \tag{3-93}$$

It is customary to express Z_0 in its approximate form by neglecting both R and G.

$$Z_0 = \sqrt{\frac{L}{C}} \quad \Omega \tag{3-94}$$

Propagation Constant: This parameter defines the attenuation and phase shift that occur along the line.

$$\gamma = \sqrt{(R + j\omega L)(G + j\omega C)} = \alpha + j\beta \tag{3-95}$$

where α is the attenuation constant and β is the phase constant.

Velocity of Propagation:

$$v_p = \frac{\omega}{\beta} \quad \frac{m}{s} \tag{3-96}$$

Wavelength:

$$\lambda = \frac{2\pi}{\beta} \quad m \tag{3-97}$$

For the lossless line,

$$v_p \approx \frac{1}{\sqrt{LC}} \quad \frac{m}{s} \quad and \quad \lambda \approx \frac{1}{f\sqrt{LC}} \quad m \tag{3-98}$$

Reflection Coefficient: This parameter defines the magnitude of reflected voltage and current waves for an arbitrary load impedance in terms of the characteristic impedance of the line. The Reflection Coefficient can be a complex number if the load impedance is complex.

$$\Gamma_r = \frac{Z_L - Z_0}{Z_L + Z_0} \tag{3-99}$$

The voltage and current at any point on the line are given by Equations 3-100 and 3-101.

$$V_x = V_L \frac{e^{\gamma x} + \Gamma_r e^{-\gamma x}}{1 + \Gamma_r} \quad (3\text{-}100)$$

$$I_x = I_L \frac{e^{\gamma x} - \Gamma_r e^{-\gamma x}}{1 - \Gamma_r} \quad (3\text{-}101)$$

These two equations can be used to study the behavior of transmission cables of any length. The parameters of interest are the voltage and current at the sending and receiving ends of system, and the power angle, defined as the phase shift between the sending and receiving voltages.

One problem with long cable systems in sharp contrast with overhead lines is their low surge impedance which generally makes their SIL much larger than their thermal capability. Table 3-22 summarizes the relations between surge impedance and load limits for overhead and conventional underground systems. It tabulates typical surge impedances, SIL's and thermal limits, and the ratios of thermal rating to SIL.

Table 3-22

Surge Impedance and Load Limits

Voltage (kV)	Zo - ohms		SIL - MW		Thermal Limits - MW			
	OH	UG	OH	UG	OH	%SIL	UG	%SIL
69	250	24	19	200	200	1050	150	75
115-161	260	27	73	705	350	480	320	45
230	270	33	196	1603	600	306	460	29
345	280	41	425	2900	1400	330	650	22
500	290	50	862	5000	2800	325	930	19
765	300	61	1950	9600	7000	360	1300	13

Overhead lines have a characteristic impedance of 200 to 400 ohms which depends on conductor size more than voltage level but tends to increase with voltage. Z_0 for conventional pipe-type cables is in the range of 20 to 70 ohms, increasing significantly with voltage. Room Temperature Dielectric HTSC cables in steel pipes will have a Z_0 in the same range as conventional HPFF cables. Cryogenic Dielectric coaxial cables will have a Z_0 in the range of 10 to 40 ohms.

The thermal limits of EHV overhead lines tend to be about three times SIL. Conventional underground cables are thermally limited to a fraction of their SIL. This fraction also varies inversely with the voltage due to increasing dielectric loss and thermal resistance at higher voltages. As voltages increase, the thermal limit of a single overhead line becomes much larger than its underground counterpart. Room Temperature Dielectric HTSC cables will have a load limit rough half of SIL. Cryogenic Dielectric coaxial cables should be able to achieve capacities in excess of SIL if the performance of the superconducting material can be improved to the level of LTSC materials.

Cable systems tend to be designed to achieve a particular capacity which is well below SIL, and operated at even lower loadings. As a result the cable system is capacitive and contributes leading VARS to the system. One consequence of operation well below SIL is the fact that the sending voltage is lower than the receiving voltage. Utility systems tend to operate in the constant voltage mode wherein bus voltages are controlled within limits that are typically +/- 10%. This operating range may limit the length of a cable system for a fixed load, or, conversely it may dictate the minimum load that a line of fixed length can support. Another problem that must be acknowledged is the degree of voltage rise at the receiving end of an open circuited line, as might occur when a breaker opens to shed load or when an unenergized line is first energized from one end. The variation of sending voltage with line parameters and load is easily studied using Equation 3-100.

The more common application problem for long cable circuits is the accommodation of the capacitive charging current which can use up much of the thermal capacity of the cable system. The "critical length" of an uncompensated cable is that length at which the charging current, which is proportional to length, equals the thermal capacity of the cable so that the cable cannot deliver useable power. Fortunately the charging current is in quadrature with load current so that the useable load increases rapidly as length is reduced below the critical. Also, by insuring that the charging current is supplied equally from each end, often by the use of fixed shunt reactors at the cable ends, the critical length is doubled. The variation of sending end current with line parameters and load is easily studied using Equation 3-101.

Examination of Equation 3-94 for the surge impedance reveals that Z_0 is proportional to inductance and inversely proportional to capacitance. Since most applications will be at loads that are below SIL for the two types of HTSC cables, it would be desirable to make the surge impedance as large as possible within the design constraints of a particular situation. This is done by increasing the wall thickness of the dielectric. This increases inductance and lowers capacitance, with the added benefit of operating the dielectric at lower stress. Moderate increases in wall thickness should not have a significant effect on the cable cost.

References

1. *Specification for Impregnated Paper and Laminated Polypropylene Insulated Cable, High-Pressure Pipe-Type,* 5th Edition, Association of Edison Illuminating Companies, Birmingham, Alabama, May 1990.

2. *Specification for Impregnated-Paper-Insulated Low and Medium Pressure Self Contained Liquid Filled Cable,* 8th Edition, Association of Edison Illuminating Companies, Birmingham, Alabama, January 1993.

3. *Specifications for Crosslinked Polyethylene Insulated Shielded Power Cables Rated 46 Through 138 kV,* 2nd Edition, Association of Edison Illuminating Companies, Birmingham, Alabama, October 1987.

4. *Specifications for Ethylene Propylene Rubber Insulated Shielded Power Cables Rated 5 Through 69 kV,* 5th Edition, Association of Edison Illuminating Companies, Birmingham, Alabama, October 1987.

5. E.B. Forsyth, et al, "The Performance of Power Cables with Fully Synthetic Taped Insulation", (90WM 253-5), *IEEE Transactions on Power Delivery,* July 1990.

6. "Status of 138 kV Solid Dielectric Cables being Evaluated at Waltz Mill", EPRI High-Voltage Solid Dielectric Operating Committee, *IEEE Transactions on Power Apparatus and Systems,* July/August 1975.

7. W.G. Lawson, P.K.Padgham, P. Metra, "The Effect of Polarity Reversals on the Dielectric Strength of Oil-Impregnated Paper Insulation for HVDC Cables", Paper F 77 546-5, IEEE PES Summer Meeting, Mexico City, Mexico, July 17-22, 1977.

8. *Design Limits of Oil/Paper High-Voltage Direct-Current Cable,* EPRI EL-3973 Final Report, Project 7859, July 1985.

9. E.B. Forsyth, "The Dielectric Insulation of Superconducting Power Cables", *Proceedings of the IEEE,* Vol 79, No. 1, January 1991.

10. R.J. Densley, A.T. Bulinski, T.S. Sudarshan, "Short-Term Electrical Insulating Characteristics of some Polymeric Materials immersed in Liquid Nitrogen", *IEEE Transactions on Electrical Insulation,* Vol EI-14, No. 4, August 1979.

11. J.S. Engelhardt, *Final Report on Preliminary Dielectric Studies - Spir-O-Line Cable for Application at Power Frequencies,* US DOE HCP/T5054-01, April 1979.

12. *Resistive Cryogenic Cable, Phase II Final Report*, GE Contract 14-01-0001-1483 with EEI/DOE/TVA, Work performed between April 1972 and April 1974.

13. *Development of Cross-Linked Polyethylene Insulated Cable for Cryogenic Operation*, EPRI EL-3907 Final Report, Project 7892-1, February 1985.

14. M. Kosaki, M. Nagao, Y. Mizano, N. Shimizui, K. Horii, "Development of Extruded Polyethylene-Insulated Superconducting Cable", *Electrical Engineering in Japan*, Vol 109, No. 1, 1989.

15. *Development of Low-Loss 765 kV Pipe-Type Cable*, EPRI EL-2196 Final Report, Project 7812-1, January 1982.

16. M.J. Jeffries, K.N. Mathes, "Insulation Systems for Cryogenic Cable", Paper 70 TP 44-PWR, IEEE Winter Power Meeting, New York, N.Y., January 25-30, 1969.

17. *Resistive Cryogenic Cable - Phase III*, EPRI EL-503 Final Report, Project 7806, October 1977.

18. "Experimental Research on 1100 kV Self-Contained High-Pressure Oil-Filled Cable", *Cable Review* by Pirelli, Milan, Italy, 1983.

19. *Waltz Mill Cable Test Facility - Part 1: Introduction to Facility and review of HPOF Pipe-Type Cable Tests*, EPRI Report No. 5-A, Project 7801, April 1979.

20. J.B. Prime, "Progress Report - Stainless Steel Line Pipe for Pipe Cable Applications", Appendix F-1, *IEEE PES ICC Minutes*, 54th Meeting, Niagara Falls, Ontario, Canada, May 20-22, 1974.

21. C.P. Bean, "Magnetization of Hard Superconductors", *Physics Review Letters*, Vol 8, No. 250, March 15, 1962.

22. W.J. Carr Jr., AC Loss and Macroscopic Theory of Superconductors, Gordon and Breach Science Publishers, New York, 1983.

23. G. Fournet, A. Mailfert, "Penetration de L'induction Champ Electrique et Pertes Dans Les Supraconducteurs de Seconde Espece Impurs Presentant un Courant de Surface", *Journel de Physique*, Vol 31, April 1970.

24. E.B. Forsyth, "Energy Loss Mechanisms of Superconductors Used in Alternating Current Power Transmission Systems", (to be published in) Science Magazine, 1988.

25. S.A. Boggs, E.W. Collings, M.V. Parish, "AC Losses in HTSC Conductor Elements", Fifth Annual Conference on Superconductivity and Applications, Buffalo, N.Y., September 24 1991.

26. R.L. Stoll, The Analysis of eddy Currents, Clarendon Press - Oxford, London, England, 1974.

27. S.A. Boggs, J.R. Clem, E.W. Collings, K.R. Marken, M.V. Parish, M.D. Sumption, "AC Loss and Dynamic Resistance of a High-Tc Strand Carrying a Direct Current in a Transverse AC Magnetic Field", CEC/ICMC Conference, Huntsville, Alabama, June 10-14, 1991.

28. G. Bahder, M. Rabinowitz, M. Sosnowski, "Bulk Solid Dielectric for Cryogenic Cables", *Cryogenics*, February 1983.

29. J.H. Neher, M.H. McGrath, "The Calculation of Temperature Rise and Load Capability of Cable systems", *AIEE Transactions*, Vol 76, No. 3, 1957.

30. *Determination of AC Conductor and Pipe Loss in Pipe-Type Cable Systems*, EPRI EL-1125 Final Report, Project RP7832-1, July 1979.

31. *Calculating AC/DC Resistance Ratios for High-Pressure Oil-Filled Cable Designs, Volume 1: Designer's Guide*, EPRI EL-3977 Final Report, Project 7832-3, April 1985.

32. *Designer's Handbook for Forced-Cooled High-Pressure Oil-Filled Pipe-Type Cable Systems*. EPRI EL-3624 Final Report, Project 7801-5, July 1984.

33. Underground Transmission Systems Reference Book, 1992 Edition, EPRI Project 7909-01, Palo Alto, CA.

34. J.H. Neher, "The Phase Sequence of Pipe-Type Cables", *IEEE Transactions on Power Apparatus and Systems*, Vol PAS 83, August 1964.

35. E.R. Thomas, R.H. Kershaw, "Impedance of Pipe-Type Cable", *IEEE Transactions on Power Apparatus and Systems*, Vol PAS 84, October 1965.

36. R.K. Moore, Traveling-Wave Engineering, McGraw-Hill Book Company, New York, 1960.

Appendix 3-A

Units for magnetic parameters

The bulk of the scientific literature that discuss magnetic phenomena tend to use the CGS electro magnetic unit (emu) system of units. The conversion to SI units, now the standard in the US, can present some problems because of the difference in the fundemental definition of the magnetic properties of space and matter between these two systems of units.

In SI units, the flux density **B** is related to the magnetic strength vector **H** by the permeability of the medium μ. $\mathbf{B} = \mu\mathbf{H}$, where $\mu = \mu_0 \times \mu_r$. μ_0 is the permeability of free space which is equal to $4\pi \times 10^{-7}$ Henries/meter. The unit of **B** is the Tesla which is equivalent to a Weber/m^2. **H** has units of amperes/meter. The relative permeability μ_r is dimensionless and defined as:

$$\mu_r = 1 + \mathbf{M}/\mathbf{H} = 1 + \chi \quad \text{where } \chi \text{ is the susceptability of the medium.}$$

In CGS units the magnetic flux density **B** in free space is equal to the magnetic strength vector **H**. **H** is expressed in Oersteds which are numerically equal to the Gauss, the unit of flux density. The Gauss is a much smaller unit of flux than the Tesla being equal to a Tesla $\times 10^{-4}$. The Oersted is a large unit of field strength when compared to the ampere/meter in SI units. One Oersted = $10^3/4\pi$ ampere/meter. A permeability of free space is not defined. In materials that exhibit a non-zero susceptibility χ,

$$\mathbf{B} = \mathbf{H} + 4\pi\mathbf{M} = \mu\mathbf{H} \quad \text{so that } \mu = 1 + 4\pi\mathbf{M}/\mathbf{H} = 1 + 4\pi\chi$$

In CGS the permeability is dimensionless and appears to be the same as the relative permeability μ_r in SI units except for the 4π factor in front of the ratio of M to H. So far this does not present a problem because the conversion from one system to the other is

taken care of by the $4\pi \times 10^{-7}$ factor which results from the combination of the conversions for **B** and **H**. However, some scientists working in CGS emu include the 4π in their definition of susceptibility. The reader is cautioned to be aware of this discrepancy when reviewing data, particularly data involving magnetic measurements of the properties of superconductors. Also, since **B** and **H** have equivalent units in CGS it is possible to confuse one for the other. Measurements of the effect of a magnetic field on a superconducting material, or the field produced by a superconductor can be ambiguous when reported in CGS. The interpretation of units and conversions is discussed in References 1 and 2 and any good modern text which addresses the magnetic properties of matter.

Conversion of the primary magnetic parameters from the CGS system to the SI system is summarized in the following table:

Factors for conversion of CGS emu units to SI units

Quantity	Symbol	Multiply CGS emu unit	By the factor	To obtain SI unit
Permeability	μ	Dimensionless	$4\pi \times 10^{-7}$	H/m
Relative permeability	μ_r	Not defined		Dimensionless
Magnetic flux density	B	Gauss(G)	10^{-4}	Tesla (T), Wb/m^2
Magnetic flux	ϕ	Maxwell (Mx)	10^{-8}	Weber (Wb)
Magnetomotive force	F	Gilbert (Gb)	$10/4\pi$	Ampere (A)
Magnetic field strength	H	Oersted (Oe), Gb/cm	$10^3/4\pi$	A/m
Intensity of magnetization	J, I	emu/cm^3	$4\pi \times 10^{-4}$	T, Wb/m^2

References

1. Alternating-Field Susceptometry and Magnetic Susceptibility of Superconductors, R.B. Goldfarb, M. Lelental, C.A. Thompson, U.S. Deptartment of Commerce Publication NISTIR 3977, October 1991.

2. Engineering Guide to High-Temperature Superconductivity, J.D. Doss, John Wiley and Sons, New York, 1989.

Appendix 3-B

NOTES ON COMPUTATION OF THE MAGNETIC FIELD IN A THREE PHASE CONFIGURATION

INTRODUCTION

This note documents the calculation of the magnetic field at the surface of a conductor (conductor 3 in the accompanying figure) caused by the self current in that conductor along with the current in the other two conductors of a three phase circuit. In the following, eddy currents are neglected and S, r, and θ given.

BASIC IDENTITIES

$C = [(S-r\cdot\cos\theta)^2 + (r\cdot\sin\theta)^2]^{0.5} = [S^2+r^2-2rS\cos\theta]^{0.5}$

$\alpha = \tan^{-1}[(r\cdot\sin\theta)/(S - r\cdot\cos\theta)] = \cos^{-1}[(S - r\cdot\cos\theta)/C] = \sin^{-1}[r\cdot\sin\theta/C]$

COMPUTATION OF THE NORMAL FIELD FROM 1 AT THE SURFACE OF 3

$NF1 = (\mu_0 I/2\pi C)\sin\omega t\cdot\sin(\alpha+\theta)$, expanding $\sin(\alpha+\theta)$,

$NF1 = (\mu_0 I/2\pi C)\sin\omega t\cdot(\sin\alpha\cos\theta+\sin\theta\cos\alpha)$, substituting for α from the identities,

$NF1 = (\mu_0 I/2\pi C)\sin\omega t\cdot(r\sin\theta\cos\theta/C + (S-r\cos t\theta)\sin\theta/C)$, rearranging

$NF1 = (\mu_0 I/2\pi C)\sin\omega t\cdot[(r/C)(\sin\theta\cos\theta-\text{sein}\theta\cos\theta)+S\sin\theta/C]$

$NF1 = (\mu_0 I/2\pi C)\sin\omega t\cdot(S/C)\sin\theta$

$NF1 = (S\mu_0 I\sin\theta\sin\omega t/[2\pi(S^2+r^2-2rS\cos\theta)]$

The field from conductor two can be computed by substituting as follows:

ωt goes to $\omega t+2\pi/3$ and θ goes to $\theta-\pi/2$. The total Normal field is NF1 + NF2, since the self field has no Normal component. Thus

$NF2 = (S\mu_0 I\sin(\theta-\pi/3)\sin(\omega t+2\pi/3)/[2\pi(S^2+r^2-2rS\cos(\theta-\pi/3))]$

COMPUTATION OF THE PARALLEL FIELD FROM 1 AT THE SURFACE OF 3

$PF1 = (\mu_0 I/2\pi C)\sin\omega t\cdot\sin(\pi/2-\alpha-\theta)$, but since $\sin(\pi/2-x)=\cos(x)$,

$PF1 = (\mu_0 I/2\pi C)\sin\omega t\cdot\cos(\alpha+\theta)$, expanding,

$PF1 = (\mu_0 I/2\pi C)\sin\omega t\cdot(\cos\theta\cos\alpha-\text{sein}\theta\sin\alpha)$, substituting for α,

$PF1 = (\mu_0 I/2\pi C)\sin\omega t\cdot[(S-r\cos\theta)\cos\theta/C - r\sin^2\theta/C]$, expanding and rearranging,

$PF1 = (\mu_0 I/2\pi C)\sin\omega t\cdot[S\cos\theta/C - (r/C)(\cos^2\theta-\sin^2\theta)]$, using the identity for $\cos 2\theta$,

$PF1 = (\mu_0 I/2\pi C)\sin\omega t\cdot[S\cos\theta/C - r\cos 2\theta/C]$

$PF1 = [\mu_0 I(S\cos\theta-r\cos 2\theta)\sin\omega t/2\pi(r^2+S^2-2rS\cos\theta)]$

For PF2, ωt goes to $\omega t+2\pi/3$ and θ goes to $\theta-\pi/3$.

PF3 is the self field from conductor 3 and is given by

$PF3 = \mu_0 I\sin(\omega t-2\pi/3)/2\pi r$

The total parallel field is PF1 + PF2 + PF3.

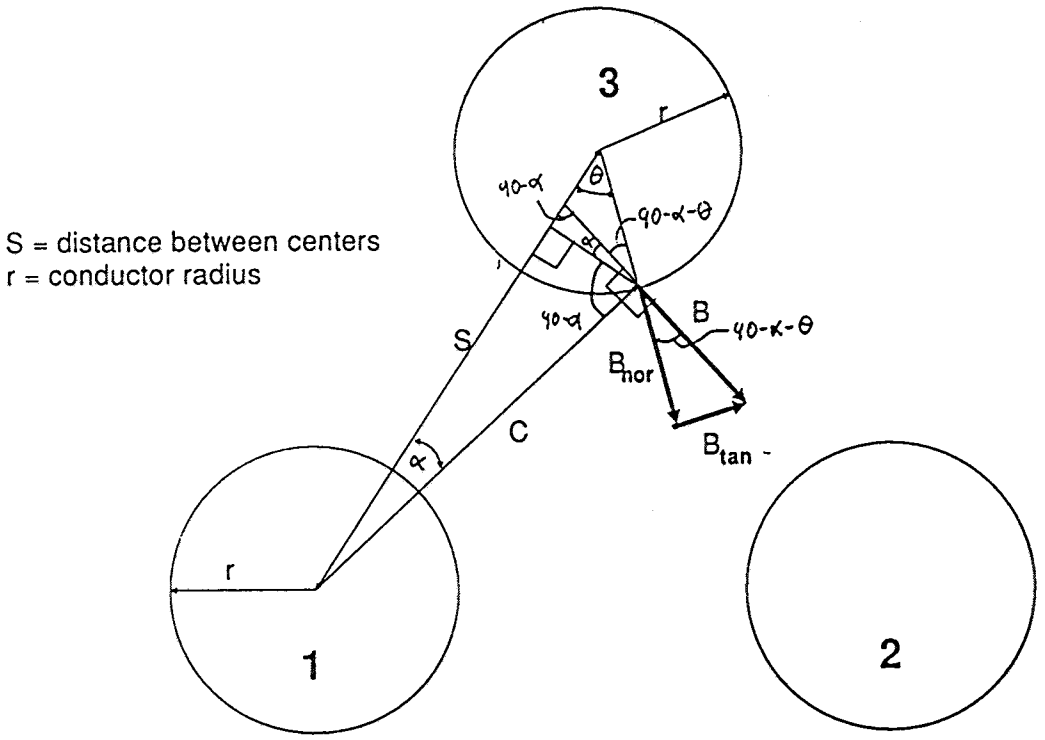

Geometry for computation of the magnetic field at the surface of conductor 3 caused by current in conductor 1.

PROGRAM FOR COMPUTATION OF NORMAL AND PARALLEL MAGNETIC FIELDS

```
5 DIM PTM(200),PFM(200),NTM(200),NFM(200),PFMIN(200),NFMIN(200),
    PTMIN(200),NTMIN(200)
10 INPUT "PEAK CURRENT (AMPS)=",I
20 INPUT "CONDUCTOR RADIUS (cm)",R:R=.01*R
30 INPUT "CENTER-TO-CENTER CONDUCTOR SEPARATION (cm)",S:S=.01*S
40 PI=3.14159265359#:MU=1.26E-06
50 FOR TH = 0 TO 2*PI STEP PI/36
60 TC=INT((TH+.01)/(PI/36))
65 PRINT TC
70 CSQTH1 = 2*PI*(S^2+R^2-2*R*S*COS(TH))
80 CSQTH2 = 2*PI*(S^2+R^2-2*R*S*COS(TH-PI/3))
90 COSTH = COS(TH)
100 SINTH = SIN(TH)
110 COSTHP = COS(TH-PI/3)
120 SINTHP = SIN(TH-PI/3)
130 COS2TH = COS(2*TH)
140 COS2THP = COS(2*(TH-PI/3))
150 FOR T = 0 TO 2*PI STEP PI/36
160 NF1 = (S*MU*I*SINTH*SIN(T))/CSQTH1
170 NF2 = (S*MU*I*SINTHP*SIN(T+2*PI/3))/CSQTH2
180 PF1 = MU*I*(S*COSTH-R*COS2TH)*SIN(T)/CSQTH1
190 PF2 = MU*I*(S*COSTHP-R*COS2THP)*SIN(T+2*PI/3)/CSQTH2
200 PF3 =MU*I*SIN(T-2*PI/3)/(2*PI*R)
202 PFT = (PF1+PF2+PF3)*10000:NFT=(NF1+NF2)*10000
204 IF PFT>PFM(TC) THEN PFM(TC)=PFT:PTM(TC)=T
206 IF NFT>NFM(TC) THEN NFM(TC)=NFT:NTM(TC)=T
208 IF PFT < PFMIN(TC) THEN PFMIN(TC)=PFT:PTMIN(TC)=T
209 IF NFT < NFMIN(TC) THEN NFMIN(TC)=NFT:NTMIN(TC)=T
210 ':PRINT INT((TC/(2*PI))*360+.01),INT((T/(2*PI))*360+.01),PFT,NFT
220 NEXT T,TH
232 FOR TH = 0 TO 2*PI/(PI/36)
234 LPRINT TH*5,INT((PTM(TH)/(2*PI))*360+.01),PFM(TH),
    INT((NTM(TH)/(2*PI))*360+.01),NFM(TH)
236 NEXT TH
240 FOR TH = 0 TO 2*PI/(PI/36)
250 LPRINT INT((PTMIN(TH)/(2*PI))*360+.01),PFMIN(TH),
    INT((NTMIN(TH)/(2*PI))*360+.01),NFMIN(TH)
260 NEXT TH
270 END
```

Appendix 3-C

Magnetic field calculations done by Magsoft Corporation

Confirmation of the methods used to calculate the magnetic fields in cable systems was obtained from Magsoft Corporation, an analytical consulting firm headed by Professor Shep Salon of RPI, Troy, N.Y.

Attached are the following documents:

1. Letter from USI to Magsoft explaining the problem with background information on pipe cable systems.
2. Drawings illustrating the cable geometries to be studied.
3. Report from Magsoft detailing their results.

The study was performed by Philip Wendling of Magsoft. The dimensions used in the study were:

	Concept #1	Concept #3
Conductor diameter:	1"	2"
Outer Cryostat Diameter:	2"	-
Dielectric Diameter:	3"	3.5"
Inner Cryostat OD:	-	8-5/8"x1/8" SS
Outer Pipe OD:	8-5/8"x1/4" steel	12-3/4"x1/4" steel

UNDERGROUND SYSTEMS, INC. • 84 BUSINESS PARK DRIVE, SUITE 109 • P.O. BOX 27 • ARMONK, NEW YORK 10504
TEL: (914) 273-8727 • FAX: (914) 273-6909

April 17, 1990

Professor Shep Salon
Magsoft Corporation
1223 Peoples Avenue
Troy, NY 12180

Dear Professor Salon,

Our project involves the development of superconducting cables using the new High Temperature SuperConducting materials which can operate at temperatures obtainable in liquid Nitrogen. While we are developing both AC and DC cable systems, the calculation of magnetic fields and the losses they create is of particular concern with our AC systems. This is due partly to the sensitivity of these new HTSC materials to magnetic fields, and partly to the effect of losses on critical system parameters such as cryogen channel diameter, the distance between refrigeration plants, and the energy cost of removing those losses.

Attached are two isometric drawings which illustrate our AC design concepts. These are referred to as our "room Temperature" dielectric, Cable Concept #1, and our "cryogenic" dielectric, Cable Concept #3. These designs are "radical" in that they do not rely on a superconducting outer shield over each phase conductor to minimize the shield loss, as do all of the AC flexible cable designs that emerged in the seventies, based on Low Temperature SuperConducting materials. When the outer cable conductor is a superconductor, it carries a current equal to and opposite to the inner conductor current. As a result, there is no magnetic field outside of the cable to interact with the other two phases. The magnetic field associated with these currents exists only in the dielectric that separates them, and there is no component of field normal to the surface of either conductor. This is the way coaxial cables work when they are far away from other phases and the shield system is heavy enough to carry the "return" phase current, as in widely-spaced submarine cable systems. An immediate reaction we get from someone who is familiar with the LTSC systems of the seventies is that our designs are not viable because of the large magnetic fields and losses that must exist if the outer shield conductor is not superconducting. This has created a third concern about the validity of our analysis of magnetic fields and losses.

Following, for your information, is a brief overview of pipe-type cable systems, which are the most common type of underground transmission system in the US, and the

superconducting transmission line's chief competitor. Both of our AC design concepts closely parallel standard pipe cable design. The room temperature concept is a pipe cable system except for the substitution of the HTSC conductor systems for the copper or aluminum conductors.

PIPE CABLE OVERVIEW

Pipe cable was first introduced by the Okonite Company in the 30's. They called it "Oil-O-Static" because the pipe is filled with oil which is maintained at 200 psi static pressure by mechanical pumps.

A pipe cable consists of three copper or aluminum conductors, each insulated with many layers of paper tape and shielded with thin metal tapes and "D" shaped skid wires, which are pulled into a steel pipe. The standard pipe sizes are 5 9/16", 6 5/8", 8 5/8" and 10 3/4" O.D. with a 1/4" wall thickness, the larger sizes being used with higher voltage cables. The usual operating voltages range from 69 KV to 345 KV. 500 KV and even 765 KV are feasible, but have not been needed so far in the US.

Power levels range from 20 MVA to a maximum of about 750 MVA, per pipe. Their limitation is determined by their maximum operating temperature. 85 C is the common normal limit for the conductor temperature. Short time emergencies allow this temperature to go to 105 C, and longer excursions are limited to 100 C. Like transformers, these temperature limits have come about to limit the thermal aging which takes place in the paper dielectric. Aging becomes detectable above the 100 C level, but is dependent on paper properties and oil cleanliness.

Cables are manufactured in lengths up to 8000 feet, and all three phases are pulled into the pipe together. The sections of cables are joined in manholes using pressed or welded connectors and hand-built insulation. They are sealed in welded steel casings. The splicing process is tedious and requires skilled "splicers". A 345 KV splice can take up to 8 days working around the clock.

The three cables are brought out of the pipe at each end through a trifurcating end-plate and carried to individual terminations, called "potheads" in stainless steel riser pipes. After installation, the entire system is evacuated, which may take a few weeks, and filled with high-quality dielectric oil, fondly referred to as "dielectric fluid" since oil became an environmental no-no. A 345 KV cable in 10 3/4" pipe requires about three gallons of oil per foot. A typical 18 mile circuit in the New York area holds 500,000 gallons of "dielectric fluid".

The cable dielectric requires pressure to operate properly. The electric stress in the dielectric is the highest of any utility equipment in use. The pressure is maintained by pumps in one or more pumping plants, which also have storage tanks to contain the oil expelled when the cables heat up, and supply oil when they cool down. Tank sizes may range from 1,000 to 50,000 gallons, depending on the amount of oil in the circuit. Thermal expansion can cause a volume change of up to 4%.

3

Some pipe cable systems are set up for oil circulation which can help smooth hot spots in the line, and some are force-cooled, by passing the oil through oil-air heat exchangers or refrigeration systems to remove the heat generated by the electrical losses, both ohmic and dielectric, in the cables. Obviously, such systems need at least two pipes in parallel to form a loop. Sometimes the second pipe is installed the same size as the cabled pipe to allow for future installation of a second cable circuit. Sometimes a smaller pipe is used just to provide for oil circulation.

The pipe is usually buried and coated to protect the steel from corrosion. Cathodic protection is almost always used to make the pipe or pipes the most negative metal in the vicinity. This is done by impressing a negative DC voltage of about 0.8 volts on the pipe relative to driven grounds or ground beds at the substations. The voltage is supplied by rectifiers or sacrificial anode beds, the former being more popular. The pipes are not directly grounded, but provision for the passage of fault currents to ground is always made. This is done by using polarization cells, or a high current rectifier driving a DC current into a heavy stainless steel resistor that can pass 50,000 to 100,000 amps without burning up. Polarization cells are like storage batteries. They are very high impedance up to about 2 volts, but switch to a very low impedance quickly if the voltage between the pipe and ground tries to go higher because of a fault.

The three cables lay randomly in the pipe. If the cables are small, they will most likely lie in a cradled configuration. If their diameter is greater then (pipe I.D)/2.5, they must lie in a triangular configuration. The pipe-to-cable diameter ratio is typically in the 2.3 to 2.8 range. A ratio of 2.15 represents the largest cable that can fit into a pipe, and if the ratio is too close to three, the cables might damage themselves during the pull, or in service, by trying to cross and jamming themselves in the pipe. Ratios greater then three can be used but are not usually justified.

The skid wires and shielding tapes make casual electrical contact with each other. The pipe I.D. is coated with epoxy to prevent rust from forming before the system is sealed. The skid wires may scratch through this coating during the pull, and in service due to repetitive thermal motion, but contact is not required. The cable shields are heavily bonded to the pipe at each joint by connecting the skid wires to the pipe and adding heavy jumpers between the joint shielding and the pipe. However, there have been cases where it is thought that induced voltages on the cable shields due to the currents in the conductors have caused sparking between the shield/skid wire assembly and the pipe. This has been detected by noting an increase in acetylene dissolved in the pipe oil.

A typical cable drawing is attached. Conductors larger then one million circular mils are usually segmental as shown. Four segments, each stranded with 37, 61 or 91 bare strands, are cabled together with a 4 to 10 foot lay. Each segment starts as a concentric round conductor of 4,5 or 6 layers of strands with each layer applied with a lay opposite to the previous layer. It is then rolled into the quarter circle segment shape and compacted at the same time. Two of the four segments are wrapped with a few layers of paper to insulate the four from each other. This improves the AC/DC resistance ratio by reducing skin and proximity effects. The four segments are

wrapped with a copper, bronze or stainless steel binder tape intercalated with a carbon black paper tape. A well-compacted conductor will have a volume efficiency of about 90%. i.e., its cross-section will be 90% metal and 10% oil.

The paper insulation thickness ranges from 1/4" for 69 KV cables to almost 1" for 345 KV cables. The outer assembly includes one or two pairs of intercalated metalized mylar tapes which act as a moisture barrier/oil seal, a copper or stainless steel tape intercalated with a metalized mylar tape which is the primary electrostatic conductor, and one or two "D" shaped skid wires of stainless steel, bronze, brass or zinc. The skid wires do just that; they facilitate the pulling operation. The three cables required for a three-phase system are connected to a common pulling yoke and pulled into the pipe with a steel rope and heavy winch. Pulling lengths are usually in the 2,000 to 3,000 foot range, but pulls up to 8,000 feet have been made. Pulling tensions generally run about 30,000 pounds. On long pulls of heavy cables, pulling tensions of up to 150,000 pounds have been experienced.

ELECTRICAL CALCULATIONS

The current-carrying capacity, or ampacity, of cables is limited by their maximum allowable operating temperature. The heat generated by their ohmic and dielectric losses is dissipated to the surrounding environment by conduction. The parameters that govern the temperature rise above ambient are the losses and the thermal resistances. The calculation of ohmic losses of pipe cables is complicated by the magnetic properties of the steel pipe and the uncertain configuration of the cables in the pipe. The classic work in this area is the well-known Neher-McGrath paper of 1957 (Reference 16 of the attached list). This work culminated a lot of published methods and approximations, and has withstood the test of time. Much of the work we do deals with the dynamic modeling of cable systems and the real-time measurement and calculation of operating temperatures. Models based on the Neher-McGrath equation set, with thermal capacitances added, can closely match the behavior of all of the systems we have monitored, once we zero in on the local characteristics of the earth.

Another important set of calculations involve the electrical modeling of the cable system so it can be represented as a part of the electrical transmission system in a system study. The shunt admittance of cables is well defined, since they are just capacitors with well-known, easily measured dielectric constants and loss angles. The series impedance, however, is again complicated by the steel pipe. Both the AC resistance and the self and mutual inductances are difficult to pin down. Empirical relations have developed over the years, but a good deal of uncertainty is to be expected.

In general, power cables that operate above 4 KV are coaxial in nature with an outer shield enclosing each phase to control the dielectric stress. (Some older paper-lead cables did not have individual shields, but only a shield over all three phases. These were known as belted cables because the three insulated conductors were covered by an additional layer of insulation called a belt.) A coaxial cable carrying AC current

tries to induce an equal and opposite return current in its outer conductor if the other two phases are not close by and in a triangular configuration. If the connections of the outer conducting shield allow this current to flow, and the impedance of the outer shield is low, this current will flow and generate ohmic loss in the shield. If, however, the shield is interrupted, the current path is broken and axial current does not flow; instead, an axial voltage is induced which must be controlled. Most distribution cables and high power transmission cables outside the US are self-contained coaxial cables and must contend with the electrical activity in the shield/sheath. A solidly grounded cable tolerates the shield current and provides enough metal to carry it without too much heat generation. That can get expensive, so some more sophisticated systems choose to interrupt the shield and deal with the induced voltages instead. Safety is the primary concern, followed by the integrity of the shield jacket which provides corrosion protection. One method is to install shield interrupts frequently, using single point grounding for each independent section. Other schemes involve the use of transformers to cross-bond the three cable shields periodically. This arrangement takes advantage of the three-phase nature of the system and periodically interrupts each cable shield and cross-connects them so that the induced voltages cancel over the length of the circuit. This still provides a solid path to ground in the event of a fault, but eliminates the normal flow of current under balanced three-phase operation.

Pipe cables are considered to be solidly grounded, but the high resistance of the light shield and skid wires limits the axial current component to a very small level. Losses also occur in the shield due to eddy currents. Since the magnetic fields of the current in each phase conductor are not counteracted by circulating current in the shields, they penetrate to the pipe and cause eddy current and hysteretic loss in the pipe. Some have tried to minimize this effect by tying the cables into a tight triangular configuration as they are being pulled into the pipe. As you can imagine, tying these cables on the fly as they come off of their reels is not easy, and the benefit is usually not justified by the time and trouble of the tying operation.

The details of the conductor construction also affect the magnetic fields. Normal metal conductors generally do not carry high enough currents to cause concern for such things as the axial fields caused by helical current paths. However, superconductor assemblies will probably be more delicate and susceptible to Lorentz forces caused by non-ideal geometrical arrangements, and current densities perhaps one hundred times the normal level. If the superconductor can be deposited on the surface of a smooth tube such that the current flows axially in a continuous sheet around the circumference of the tube, then there should be no axial magnetic field component. If, however, the conductor is made up of many strands of wire or helically applied flat ribbons, the current will follow the helix and will generate an axial magnetic field component. The magnetic fields and forces that are created, and the additional losses that occur are difficult to visualize. The standard approach to control axial fields is to apply an even number of layers with opposite lay so that the net axial field is zero, or close to it.

SCOPE OF WORK

The area where we need your help is in the calculation of the magnetic fields that characterize our two Cable Concepts. This may involve several combinations of conductor assembly, cable shielding, and surrounding metallic components. We will need to calculate losses in all of the conducting components that result from the induced circulating currents and eddy currents, and hysteretic losses when magnetic components are involved. I would like to set up generalized programs in a PC environment that will allow us to quickly evaluate the cause and effect of various design iterations.

The first level of calculation should be done with idealized conducting assemblies. Full-scale cross-section drawings for our two Cable Concepts are enclosed. For these cases, all conducting surfaces can be modeled as continuous tubular components. The variables will be the type of metal for each layer, and its effective thickness. In both cases, the HTSC superconductor is taken as a layer deposited on the outer surface of the innermost tube. We have made calculations of the tangential and normal fields acting on the surface of the HTSC tube to ballpark the magnitudes of the fields interacting with the HTSC material. These calculations are enclosed. However, the current distribution will be distorted by the fields of the two other phases, and the resulting fields will be (slightly?) different. An iterative approach suggests itself to establish the true current distribution in the HTSC tube. The next question is: what goes on in the surrounding metal components, and does their presence alter the field distribution both globally and at the HTSC surface? We expect dramatically different results dependent on whether the outermost pipe is magnetic steel or a non-magnetic alternative.

For Cable Concept #1, the cable shields can be considered to be in continuous contact with each other and with the pipe, but no external ground connection exists that might form an external return path for stray currents. The outer tube of the cryostat could be connected to the HTSC conductor continuously, periodically at splices, or only once per cable section which would break its parallel connection with the HTSC conductor.

The cross-section for Cable Concept #1 shows cable B in three different positions. Our simple field calculations considered phase A to be the reference phase, and the three positions of B represent triangular, cradled with A in the center, and cradled with A on the outside, respectively. This representation assumes that there is no field distortion due to eddy currents or circulating currents in any of the conducting members. When this is not the case, the triangular case will yield different field effects for the top phase and the bottom two.

Cable Concept #3 is shown in one triangular position only. Since this system will always be a new installation, and the losses that occur at cryogenic temperatures are leveraged by the refrigeration penalty, we expect that the enclosure diameter will always be less then 2.5 times the cable diameter, and the cables will always be tied to enforce a tight triangular arrangement.

For both Concepts, the outermost pipe would be cold-rolled resistance-welded steel line pipe with a 1/4" wall, designated as grade A, API Standard 5L, in accordance with ASTM A-523 which restricts the interior surface quality.

The cross-section for Cable Concept #3 shows a thin tubular conductor rather then the double layer of wires depicted in the isometric drawing. The second level of calculation complexity introduces this type of conductor assembly, where the HTSC elements may be wires or tapes in one or more layers, applied helically. Multiple layers might be applied with alternating lay for mechanical reasons, but this is not mandatory if electrical behavior is significantly degraded.

When the helical current paths are used, the magnetic fields will have an axial component that might really mess things up. Induced current flows in the outer components may result in disproportionate increases in losses, and the fields in the immediate vicinity of the HTSC elements must be examined in detail to evaluate their interaction with the HTSC material.

The third level of calculation detail involves the specific cable shield and skid wire assemblies that will be used. The typical cable assembly will have one metal tape intercalated with a semi-conducting (carbon black paper) tape, and two metal skid wires applied with the opposite lay at an axial spacing of about 1-1/2", as shown on the isometric views. This assembly is necessary because it is the outer electrode of the cable capacitance and must be able to carry the capacitive currents to an effective ground. However, these currents are low, on the order of a few amps per thousand feet, so these shields can be interrupted at splices if losses can be lowered by so doing. We have a lot of flexibility with the choice of metals. The skid wires could be non-metallic, if that would improve the situation. Note that losses occurring in the cable shields and enclosures are not leveraged by the refrigeration system for Cable Concept #1, but are for Cable Concept #3. I've enclosed a brief note on the calculation of shield losses for our cases using the Neher-McGrath equations, which are a combination of rigorous mathematics and empirical data. These calculations indicate that our design yields rather high losses, so we must take steps to maximize the shield resistance for our Cable Concept #3. On the other hand, shield loss is not so important for Cable Concept #1, so there may be reason to reduce shield resistance if the current flows improve the magnetics in the conductor system. A design power level of 3000 amps at 138 KV is a reasonable level to use for all calculations. However, we will ultimately have to know how the losses vary with current below the maximum rating, to assess operating costs and refrigeration loading.

Our first concern is for some level one calculations that (hopefully) back up our own to define the order of magnitude of fields interacting with the HTSC material, and establish the appropriate calculating procedure for shield and enclosure loss. A list of references that might be helpful with this general problem is attached. If you choose to review any of this material, we can provide copies from our files and save you some library time. We would like your numerical work to be made available to us in a PC environment which we can manipulate so we could use it throughout our project, as

this aspect of these systems has to be presented to many different audiences, each with a different concern.

The second and third levels of complexity would be built on the first, depending on your projected costs to the project and a successful completion of the first stage.

Please review this material and send us a proposal that we can use to prepare a purchase order. Our timing is not urgent, but we would like some preliminary results by the end of June, if possible. If you have any questions, please call me. We would be happy to sit down with you either in Troy or Armonk at your convenience to go over what I've tried to explain above, if you'd like.

I think you'll agree that ours is an interesting, but solvable problem, and one which will be both challenging and rewarding. I look forward to hearing from you.

Sincerely,

John S. Engelhardt
President

JSE:jlm

cc: S. A. Boggs
D. K. Sharma

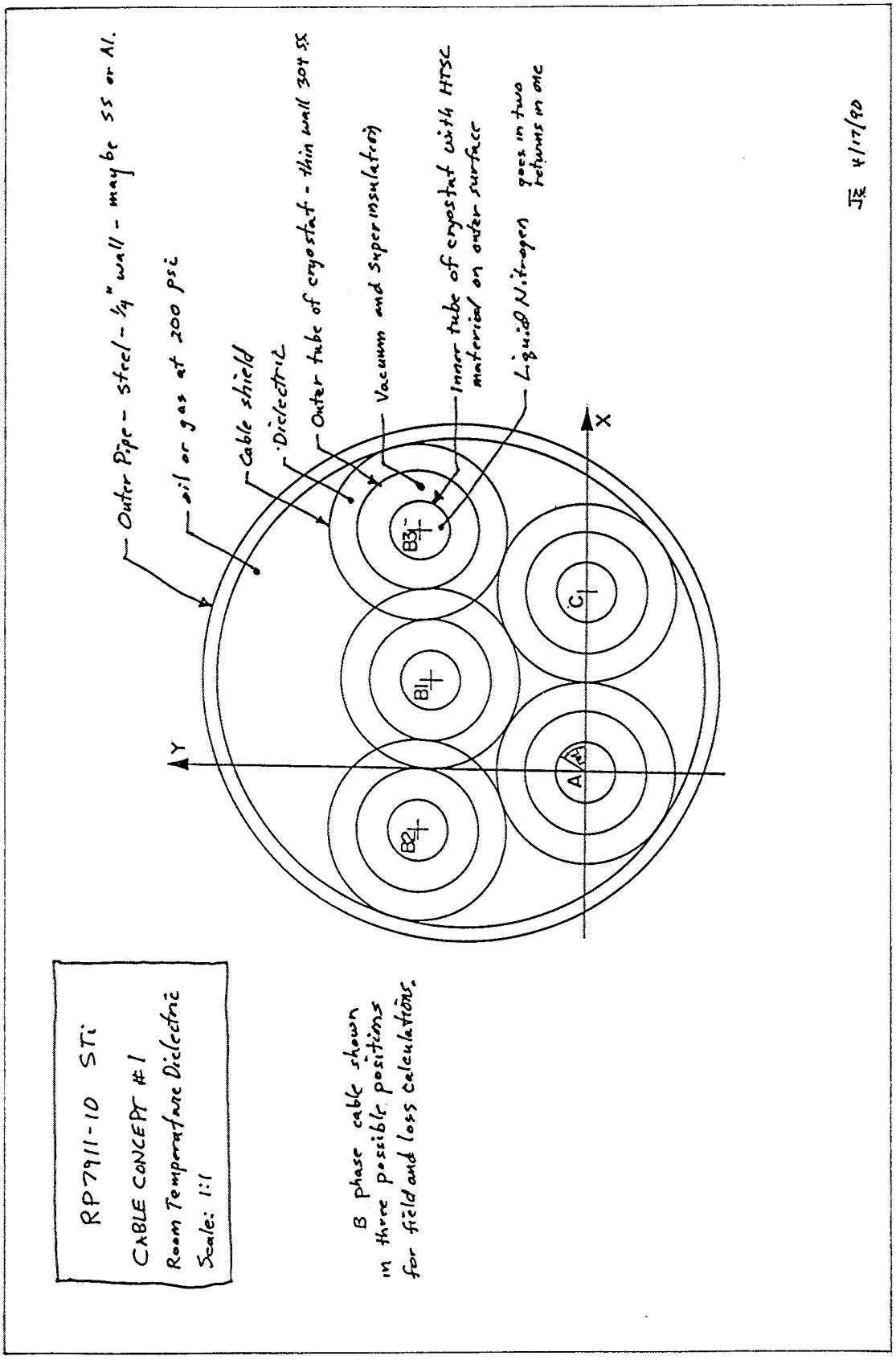

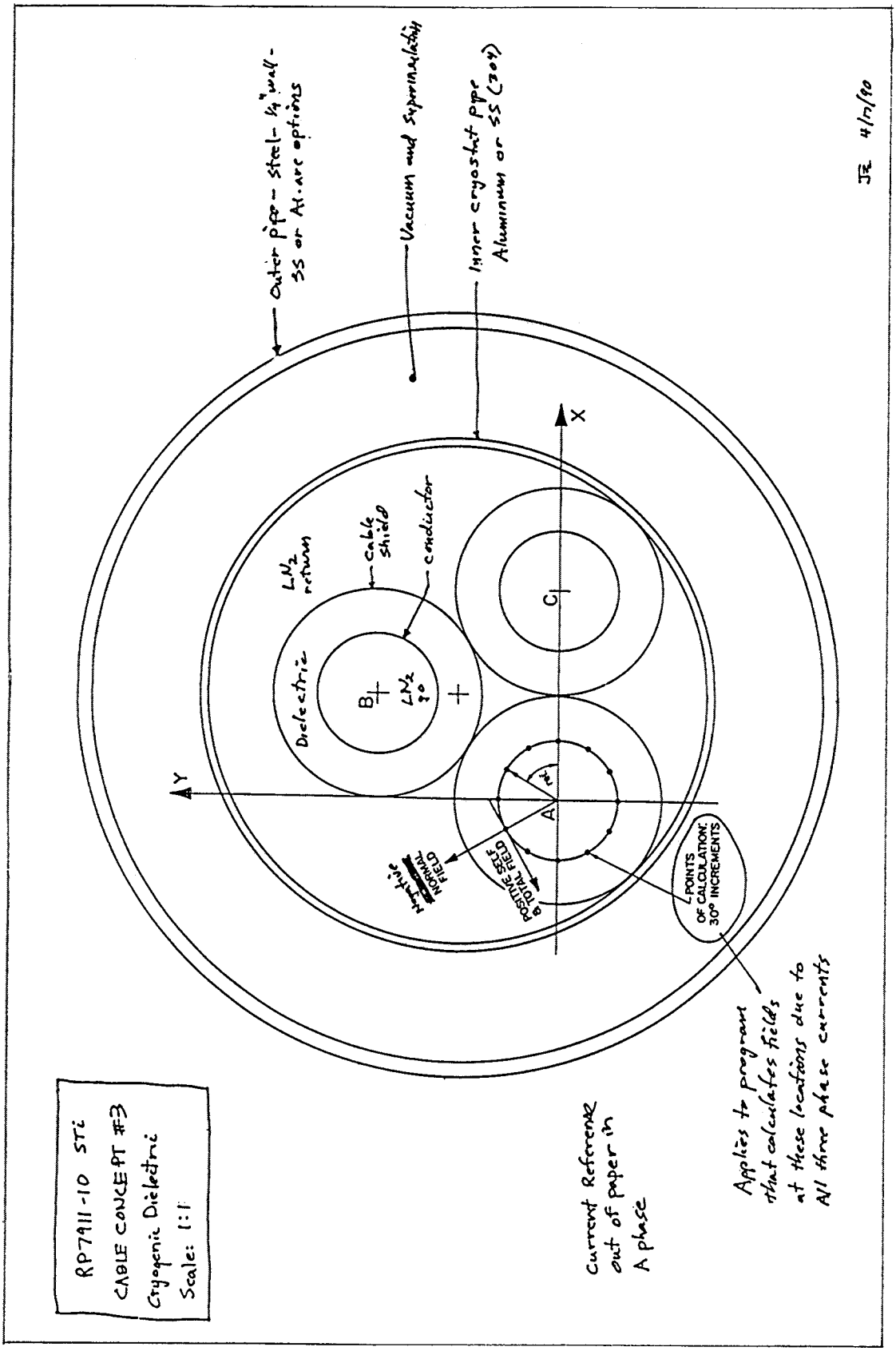

Notes On Magnetic Field Calculations

1. Closed Form Computations

We checked the computation presented in the Basic program.

Let us do the computation for the following case; The three conductors A, B and C are positioned as in concept #1 with conductor B in a triangular configuration between conductor A and C (see figure #1).

We want the field along the surface of conductor A.

We have:

$$\int H.dl = I$$

Along the conductor surface:

$$2*\pi*R_a * H = I_a$$

$$H = \frac{I_a}{2*\pi*R}$$

$$B = \mu H$$

R is the distance between the conductor center and the point considered. I_a is the value of the current going through conductor A.

We perform the computation at the surface of the conductor.

$$\mu = 4*\pi*10^{-7} \text{ (henries/meter)}$$

If R is in centimeters and B in Gauss, we find:

$$B = .2 * I_a / R_a$$

This gives a flux density parallel to the surface of the conductor.

We will decompose the field into two components: a tangential and a normal component.

Conductor A only contributes to the tangential component.

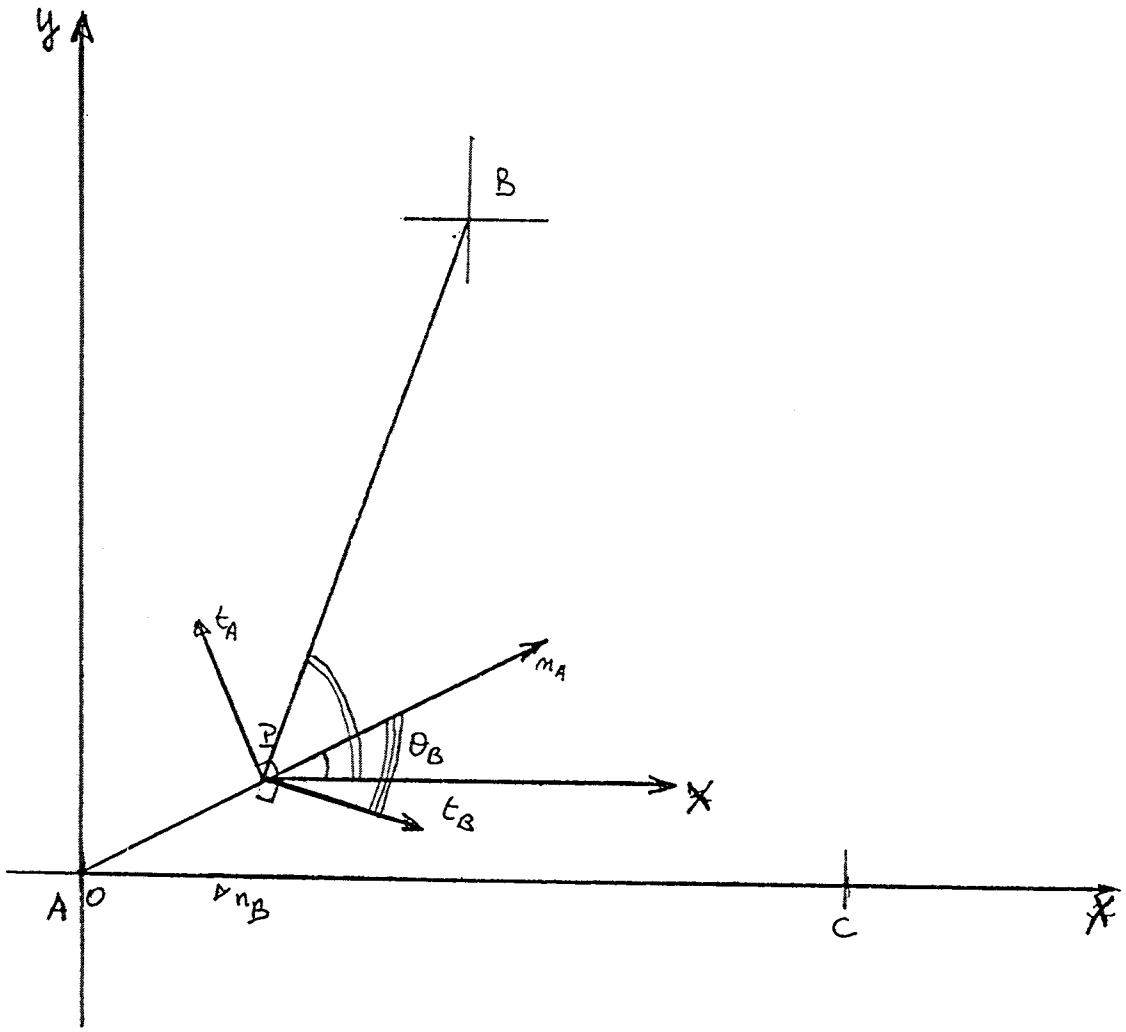

FIGURE 1: DECOMPOSITION OF THE ANGLES

Let us evaluate the tangential and normal component at point P on the surface of conductor A due to conductor B. As simplification, we will assume that conductor A is centered on the origin of the coordinate system. We will use the common convention for the orientation of vector: positive rotation is counter clockwise, normal vector oriented from the center of the circle towards the outside, tangential vector oriented counter clockwise.

We know the angle (Ox,OP) and the angle (Px,PB). The angle between the vector field generated by conductor B in point P and the vector normal to conductor A at point P is:

$$\theta_b = (Px,PB) - (Ox,OP) - 90°$$

$$(Ox,OB) = \text{atan}[(y_b - y_p)/(x_b - x_p)]$$

$$(Ox,OP) = \text{atan}(y_p/x_p)$$

The normal component of the flux density due to conductor B at point P along conductor A is:

$$H_{bn} = H_b * \cos(\theta)$$

The tangential component of the flux density due to conductor B at point P along conductor A is:

$$H_{bt} = H_b * \sin(\theta)$$

We ran a test to make sure this closed form solution and Flux2D were giving the same results in the case where there is no magnetic material involved in the problem. The following table gives a comparison of the results obtained by these two methods of computation.

The value of current was at peak negative value in conductor A.

$$I_a = -4243.0 \text{ A}$$
$$I_b = -2121.5 \text{ A}$$
$$I_c = -2121.5 \text{ A}$$

The results are presented in the following tables. The first column of the table is the angular position of point P on the surface of the conductor. Position 0° is for P on the X axis.

There are then one or two sets of three columns. The first column gives the value of the flux density computed using the closed form solution, the second column gives the value computed using Flux2D and the third the difference in percent between these two values.

Tangential component of flux density at point P along the surface of conductor A due to conductor A only.

Angular Position	Tangential C. Form	Tangential Flux	δ %
0	-668.19	-666.29	0.29
30	-668.19	-654.23	2.13
60	-668.19	-659.59	1.30
90	-668.19	-664.40	0.57
120	-668.19	-672.69	-0.67
150	-668.19	-688.46	-2.94
180	-668.19	-662.10	0.92
210	-668.19	-657.17	1.68
240	-668.19	-660.56	1.15
270	-668.19	-665.82	0.36
300	-668.19	-652.78	2.36
330	-668.19	-649.54	2.87

Flux density at point P along the surface of conductor A due to conductor B only.

Angular Position	Normal Component C. Form	Normal Component Flux	δ %	Tangential Component C. Form	Tangential Component Flux	δ %
0	56.00	55.71	0.52	-21.55	-21.57	-0.07
30	37.67	37.26	1.10	-52.69	-52.52	0.32
60	0.00	0.00	0.00	-66.82	-66.34	0.72
90	-37.67	-37.59	0.21	-52.69	-52.43	0.49
120	-56.00	-55.79	0.38	-21.55	-21.23	1.53
150	-54.18	-53.88	0.55	9.03	9.03	-0.01
180	-40.37	-40.09	0.70	31.08	31.09	-0.04
210	-21.15	-20.86	1.38	43.68	43.51	0.39
240	-0.00	0.00	0.00	47.73	47.48	0.52
270	21.15	21.11	0.18	43.68	43.35	0.76
300	40.37	40.25	0.30	31.08	30.82	0.84
330	54.18	53.92	0.48	9.03	8.85	2.03

Flux density at point P along the surface of conductor A due to conductor C only.

Angular Position	Normal Component C. Form	Flux	δ %	Tangential Component C. Form	Flux	δ %
0	0.00	0.00	0.00	-66.82	-66.57	0.37
30	-37.67	-37.42	0.67	-52.69	-52.51	0.34
60	-56.00	-55.77	0.41	-21.55	-21.64	-0.40
90	-54.18	-54.09	0.16	9.03	8.998	0.35
120	-40.37	-40.13	0.60	31.08	31.07	0.03
150	-21.15	-21.09	0.28	43.68	43.51	0.39
180	-0.00	0.00	0.00	47.73	47.63	0.21
210	21.15	21.06	0.42	43.68	43.53	0.34
240	40.37	40.03	0.85	31.08	31.13	-0.17
270	54.18	54.00	0.33	9.03	9.07	-0.45
300	56.00	55.73	0.48	-21.55	-21.64	-0.40
330	37.67	37.47	0.53	-52.69	-52.49	0.38

Flux density at point P along the surface of conductor A. his is the total flux density to conductor A, B and C.

Angular Position	Normal Component C. Form	Flux	δ %	Tangential Component C. Form	Flux	δ %
0	-756.56	-754.43	0.28	56.00	60.30	-7.13
30	-773.56	-759.26	1.88	-0.00	2.36	-99.99
60	-756.56	-747.57	1.20	-56.00	-55.55	0.81
90	-711.85	-707.84	0.57	-91.85	-86.18	6.57
120	-658.67	-662.85	-0.63	-96.37	-100.62	-4.22
150	-615.48	-635.91	-3.21	-75.33	-72.22	4.30
180	-589.38	-583.37	1.03	-40.37	-42.38	-4.74
210	-580.83	-570.13	1.88	-0.00	-0.03	-99.84
240	-589.38	-581.94	1.28	40.37	41.40	-2.48
270	-615.48	-613.40	0.34	75.33	76.08	-0.99
300	-658.66	-643.59	2.34	96.37	98.59	-2.25
330	-711.85	-693.18	2.69	91.85	86.97	5.61

This comparison shows that, for a device in free space (no permeable material), the closed form computation and the Finite Elements computation from Flux2d give us the same results within a margin of less than 10%. The large differences between both methods were obtained for value of flux density close to zero.

2. Results provided by the computation performed by USI

We found a mistake going through the basic program provided with the computation. Let us assume that point P is the point of interest on the surface of conductor A. The angle between the field due to conductor B or C at point P and the normal vector (or tangent vector) to the circle at point P is wrong.

The component computed as "Parallel field"/"Other field" is in fact the normal component of the field at point P. The component computed as "normal field" is the tangential component of the field at point P on the surface of conductor A due to conductors B and C. This component is the one to add to the main tangential field due to conductor A itself.

Note: the convention of orientation used in the calculation presented before differs from the one presented in the Basic program: the vector normal to the circle is oriented towards the inside in the Basic program.

Results Of The FEM Computation

We performed computations for three geometries: cable concept #1 with conductor B in a triangular configuration between cable A and C, cable concept #1 with cable B cradled between cable A and the outside pipe and cable concept #3.

Each set of results is for a time instant. The reference is Phase A. Current is described as a sinusoidal function so that phase A current is 0 at T = 0.

The computations were made in magnetostatics (no eddy current) with non linear material for the steel pipes.

The orientation of the tangential component of the field is counter clockwise. The orientation of the normal of the field is from the circumference of the circle towards the center of the circle.

Cable concept #1 with conductor B in a triangular configuration between cable A and C

```
*******************************************
*     CEDRAT                    MAGSOFT     *
* Grenoble, France             Troy, N.Y.   *
*                                           *
*              FLUX2D  6.36                 *
*                                           *
*                      Serial # MAGSOFT     *
*                                           *
*     copyright (all rights reserved)       *
* ENSIEG - LABORATOIRE D'ELECTROTECHNIQUE   *
* BP46 38402 Saint Martin d'Heres France    *
*******************************************

       expgen    6/25/90  7:51:02

Problem : CACOM1

Time : 0°


********
Integrals
********


Integrals on region  A

Surface of the region          308.8672     (square mm)
Flux through one turn       = -0.9095555E-04 (Weber)
```

Integrals on region B

Surface of the region		308.8672	(square mm)
Integ. (A.J) dv	=	5.352037	
Total ampere turn(s)	=	3674.563	(Ampere)
Inductance (1 turn)	=	0.3963764E-06	(Henry)

Integrals on region C

Surface of the region		308.8672	(square mm)
Integ. (A.J) dv	=	6.782731	
Total ampere turn(s)	=	-3674.563	(Ampere)
Inductance (1 turn)	=	0.5023346E-06	(Henry)

CURVES
******

Flux density
arc : center X = 0; Y = 0; R = 12.7 (0 -> 360 deg.)

ABSCISSA Deg	MAGNITUDE Tesla	NORMAL C. Tesla	TANGENTIAL C. Tesla
0.00000	0.1738970E-01	-0.1283555E-01	0.1173244E-01
30.00000	0.1771938E-01	-0.1762906E-01	0.1786820E-02
60.00000	0.1672037E-01	-0.1436319E-01	-0.8559752E-02
90.00000	0.1504144E-01	-0.6489208E-02	-0.1356964E-01
120.0000	0.1335049E-01	0.9357831E-03	-0.1331765E-01
150.0000	0.1219276E-01	0.6177209E-02	-0.1051215E-01
180.0000	0.1164118E-01	0.9551216E-02	-0.6655179E-02
210.0000	0.1167431E-01	0.1147648E-01	-0.2140059E-02
240.0000	0.1219667E-01	0.1180294E-01	0.3073975E-02
270.0000	0.1318749E-01	0.9904055E-02	0.8707437E-02
300.0000	0.1459645E-01	0.4907536E-02	0.1374673E-01
330.0000	0.1618675E-01	-0.3442451E-02	0.1581646E-01
360.0000	0.1738970E-01	-0.1283555E-01	0.1173244E-01

Time : 30°

****
Integrals
****

Integrals on region A

Surface of the region		308.8672	(square mm)
Integ. (A.J) dv	=	2.026393	
Total ampere turn(s)	=	2121.485	(Ampere)
Inductance (1 turn)	=	0.4502395E-06	(Henry)

Integrals on region B

Surface of the region		308.8672	(square mm)
Integ. (A.J) dv	=	8.844061	
Total ampere turn(s)	=	-4243.001	(Ampere)
Inductance (1 turn)	=	0.4912532E-06	(Henry)

Integrals on region C

Surface of the region		308.8672	(square mm)
Integ. (A.J) dv	=	1.772314	
Total ampere turn(s)	=	2121.485	(Ampere)
Inductance (1 turn)	=	0.3937864E-06	(Henry)

CURVES
******

Flux density
arc : center X = 0; Y = 0; R = 12.7 (0 -> 360 deg.)

ABSCISSA Deg	MAGNITUDE Tesla	NORMAL C. Tesla	TANGENTIAL C. Tesla
0.00000	0.5269206E-01	-0.5825947E-02	0.5236900E-01
30.00000	0.4723244E-01	-0.1508313E-01	0.4475939E-01
60.00000	0.3743369E-01	-0.1640915E-01	0.3364552E-01
90.00000	0.2921290E-01	-0.1324218E-01	0.2603917E-01
120.0000	0.2389426E-01	-0.7947152E-02	0.2253394E-01
150.0000	0.2058182E-01	-0.2505751E-02	0.2042872E-01
180.0000	0.2020076E-01	0.2429067E-02	0.2005418E-01
210.0000	0.2358834E-01	0.8280257E-02	0.2208726E-01
240.0000	0.3018203E-01	0.1386137E-01	0.2681077E-01
270.0000	0.3843045E-01	0.1663393E-01	0.3464407E-01
300.0000	0.4624612E-01	0.1375757E-01	0.4415239E-01
330.0000	0.5185165E-01	0.5907666E-02	0.5151400E-01
360.0000	0.5269205E-01	-0.5825952E-02	0.5236898E-01

Time : 60°

****
Integrals
****

Integrals on region A

Surface of the region		308.8672	(square mm)
Integ. (A.J) dv	=	6.783132	
Total ampere turn(s)	=	3674.564	(Ampere)
Inductance (1 turn)	=	0.5023642E-06	(Henry)

Magsoft Corporation/112_01 USI Page 9

Integrals on region B

Surface of the region 308.8672 (square mm)
Integ. (A.J) dv = 5.351643
Total ampere turn(s) = -3674.563 (Ampere)
Inductance (1 turn) = 0.3963472E-06 (Henry)

Integrals on region C

Surface of the region 308.8672 (square mm)
Flux through one turn = 0.9106284E-04 (Weber)

CURVES
******

Flux density
arc : center X=0 Y=0R = 12.7 (0 -> 360 deg.)

ABSCISSA Deg	MAGNITUDE Tesla	NORMAL C. Tesla	TANGENTIAL C. Tesla
0.00000	0.6902311E-01	0.1558017E-01	0.6724171E-01
30.00000	0.7451448E-01	0.9133197E-02	0.7395263E-01
60.00000	0.7539649E-01	0.3047772E-03	0.7539587E-01
90.00000	0.7292409E-01	-0.9957788E-02	0.7224102E-01
120.0000	0.6750183E-01	-0.1563646E-01	0.6566580E-01
150.0000	0.5882704E-01	-0.1669448E-01	0.5640846E-01
180.0000	0.5030172E-01	-0.1489511E-01	0.4804580E-01
210.0000	0.4339984E-01	-0.8611047E-02	0.4253700E-01
240.0000	0.4029234E-01	0.4028324E-03	0.4029033E-01
270.0000	0.4353225E-01	0.9002824E-02	0.4259114E-01
300.0000	0.5094679E-01	0.1401382E-01	0.4898151E-01
330.0000	0.6008272E-01	0.1711729E-01	0.5759280E-01
360.0000	0.6902309E-01	0.1558017E-01	0.6724168E-01

Time : 90°

****
Integrals
****

Integrals on region A

Surface of the region 308.8672 (square mm)
Integ. (A.J) dv = 8.844812
Total ampere turn(s) = 4243.002 (Ampere)
Inductance (1 turn) = 0.4912948E-06 (Henry)

Integrals on region B

Surface of the region		308.8672	(square mm)
Integ. (A.J) dv	=	1.771942	
Total ampere turn(s)	=	-2121.485	(Ampere)
Inductance (1 turn)	=	0.3937039E-06	(Henry)

Integrals on region C

Surface of the region		308.8672	(square mm)
Integ. (A.J) dv	=	2.026019	
Total ampere turn(s)	=	-2121.485	(Ampere)
Inductance (1 turn)	=	0.4501565E-06	(Henry)

CURVES
******

Flux density
arc : center X = 0; Y = 0; R = 12.7 (0 -> 360 deg.)

ABSCISSA Deg	MAGNITUDE Tesla	NORMAL C. Tesla	TANGENTIAL C. Tesla
0.00000	0.8507769E-01	0.1057974E-01	0.8441731E-01
30.00000	0.8642507E-01	0.3679805E-03	0.8642429E-01
60.00000	0.8250027E-01	-0.7940572E-02	0.8211724E-01
90.00000	0.7710401E-01	-0.1524466E-01	0.7558193E-01
120.0000	0.7035032E-01	-0.1751499E-01	0.6813511E-01
150.0000	0.6111918E-01	-0.1571058E-01	0.5906548E-01
180.0000	0.5294160E-01	-0.1168492E-01	0.5163599E-01
210.0000	0.4799657E-01	-0.3317233E-02	0.4788180E-01
240.0000	0.4884338E-01	0.7279493E-02	0.4829787E-01
270.0000	0.5655130E-01	0.1611352E-01	0.5420704E-01
300.0000	0.6724001E-01	0.1901496E-01	0.6449535E-01
330.0000	0.7769492E-01	0.1777769E-01	0.7563369E-01
360.0000	0.8507767E-01	0.1057974E-01	0.8441728E-01

Time : 120

****
Integrals
****

Integrals on region A

Surface of the region		308.8672	(square mm)
Integ. (A.J) dv	=	6.783132	
Total ampere turn(s)	=	3674.564	(Ampere)
Inductance (1 turn)	=	0.5023642E-06	(Henry)

Integrals on region B

Surface of the region		308.8672	(square mm)
Integ. (A.J) dv	=	5.351643	
Total ampere turn(s)	=	-3674.563	(Ampere)
Inductance (1 turn)	=	0.3963472E-06	(Henry)

Integrals on region C

Surface of the region		308.8672	(square mm)
Flux through one turn	=	0.9106284E-04	(Weber)

CURVES
******

Flux density
arc : center X = 0; Y = 0; R = 12.7 (0 -> 360 deg.)

ABSCISSA Deg	MAGNITUDE Tesla	NORMAL C. Tesla	TANGENTIAL C. Tesla
0.00000	0.6902311E-01	0.1558017E-01	0.6724171E-01
30.00000	0.7451448E-01	0.9133197E-02	0.7395263E-01
60.00000	0.7539649E-01	0.3047772E-03	0.7539587E-01
90.00000	0.7292409E-01	-0.9957788E-02	0.7224102E-01
120.0000	0.6750183E-01	-0.1563646E-01	0.6566580E-01
150.0000	0.5882704E-01	-0.1669448E-01	0.5640846E-01
180.0000	0.5030172E-01	-0.1489511E-01	0.4804580E-01
210.0000	0.4339984E-01	-0.8611047E-02	0.4253700E-01
240.0000	0.4029234E-01	0.4028324E-03	0.4029033E-01
270.0000	0.4353225E-01	0.9002824E-02	0.4259114E-01
300.0000	0.5094679E-01	0.1401382E-01	0.4898151E-01
330.0000	0.6008272E-01	0.1711729E-01	0.5759280E-01
360.0000	0.6902309E-01	0.1558017E-01	0.6724168E-01

Time : 150°

****
Integrals
****

Integrals on region A

Surface of the region		308.8672	(square mm)
Integ. (A.J) dv	=	2.360661	
Total ampere turn(s)	=	2121.485	(Ampere)
Inductance (1 turn)	=	0.5245097E-06	(Henry)

Integrals on region B

Surface of the region		308.8672	(square mm)
Integ. (A.J) dv	=	7.159194	
Total ampere turn(s)	=	-4243.000	(Ampere)
Inductance (1 turn)	=	0.3976655E-06	(Henry)

Integrals on region C

Surface of the region		308.8672	(square mm)
Integ. (A.J) dv	=	2.360659	
Total ampere turn(s)	=	2121.485	(Ampere)
Inductance (1 turn)	=	0.5245093E-06	(Henry)

CURVES
******

Flux density
arc : center X = 0; Y = 0; R = 12.7 (0 -> 360 deg.)

ABSCISSA Deg	MAGNITUDE Tesla	NORMAL C. Tesla	TANGENTIAL C. Tesla
0.00000	0.3600303E-01	0.1640572E-01	0.3204795E-01
30.00000	0.4443726E-01	0.1545108E-01	0.4166454E-01
60.00000	0.4920554E-01	0.8468463E-02	0.4847134E-01
90.00000	0.4958278E-01	-0.2002618E-02	0.4954231E-01
120.0000	0.4659360E-01	-0.9567965E-02	0.4560063E-01
150.0000	0.4083043E-01	-0.1320491E-01	0.3863617E-01
180.0000	0.3459159E-01	-0.1411400E-01	0.3158120E-01
210.0000	0.2828122E-01	-0.1159744E-01	0.2579393E-01
240.0000	0.2247200E-01	-0.6581779E-02	0.2148653E-01
270.0000	0.1956938E-01	-0.5202816E-03	0.1956246E-01
300.0000	0.2101094E-01	0.5257519E-02	0.2034252E-01
330.0000	0.2688196E-01	0.1187012E-01	0.2411929E-01
360.0000	0.3600303E-01	0.1640572E-01	0.3204793E-01

Time : 180°

****
Integrals
****

Integrals on region A

Surface of the region		308.8672	(square mm)
Flux through one turn	=	0.9095555E-04	(Weber)

Integrals on region B

Surface of the region		308.8672	(square mm)
Integ. (A.J) dv	=	5.352037	
Total ampere turn(s)	=	-3674.563	(Ampere)
Inductance (1 turn)	=	0.3963764E-06	(Henry)

Integrals on region C

Surface of the region		308.8672	(square mm)
Integ. (A.J) dv	=	6.782731	
Total ampere turn(s)	=	3674.563	(Ampere)
Inductance (1 turn)	=	0.5023346E-06	(Henry)

CURVES
******

Flux density
arc : center X = 0; Y = 0; R = 12.7 (0 -> 360 deg.)

ABSCISSA Deg	MAGNITUDE Tesla	NORMAL C. Tesla	TANGENTIAL C. Tesla
0.00000	0.1738970E-01	0.1283555E-01	-0.1173244E-01
30.00000	0.1771938E-01	0.1762906E-01	-0.1786820E-02
60.00000	0.1672037E-01	0.1436319E-01	0.8559752E-02
90.00000	0.1504144E-01	0.6489208E-02	0.1356964E-01
120.0000	0.1335049E-01	-0.9357831E-03	0.1331765E-01
150.0000	0.1219276E-01	-0.6177209E-02	0.1051215E-01
180.0000	0.1164118E-01	-0.9551216E-02	0.6655179E-02
210.0000	0.1167431E-01	-0.1147648E-01	0.2140059E-02
240.0000	0.1219667E-01	-0.1180294E-01	-0.3073975E-02
270.0000	0.1318749E-01	-0.9904055E-02	-0.8707437E-02
300.0000	0.1459645E-01	-0.4907536E-02	-0.1374673E-01
330.0000	0.1618675E-01	0.3442451E-02	-0.1581646E-01
360.0000	0.1738970E-01	0.1283555E-01	-0.1173244E-01

Time = 210°

****
Integrals
****

Integrals on region A

Surface of the region		308.8672	(square mm)
Integ. (A.J) dv	=	2.026393	
Total ampere turn(s)	=	-2121.485	(Ampere)
Inductance (1 turn)	=	0.4502395E-06	(Henry)

Integrals on region B

Surface of the region		308.8672	(square mm)
Integ. (A.J) dv	=	1.772314	
Total ampere turn(s)	=	-2121.485	(Ampere)
Inductance (1 turn)	=	0.3937864E-06	(Henry)

Integrals on region C

Surface of the region		308.8672	(square mm)
Integ. (A.J) dv	=	8.844061	
Total ampere turn(s)	=	4243.001	(Ampere)
Inductance (1 turn)	=	0.4912532E-06	(Henry)

CURVES
******

Flux density
arc : center X = 0; Y = 0; R = 12.7 (0 -> 360 deg.)

ABSCISSA Deg	MAGNITUDE Tesla	NORMAL C. Tesla	TANGENTIAL C. Tesla
0.00000	0.5269206E-01	0.5825947E-02	-0.5236900E-01
30.00000	0.4723244E-01	0.1508313E-01	-0.4475939E-01
60.00000	0.3743369E-01	0.1640915E-01	-0.3364552E-01
90.00000	0.2921290E-01	0.1324218E-01	-0.2603917E-01
120.0000	0.2389426E-01	0.7947152E-02	-0.2253394E-01
150.0000	0.2058182E-01	0.2505751E-02	-0.2042872E-01
180.0000	0.2020076E-01	-0.2429067E-02	-0.2005418E-01
210.0000	0.2358834E-01	-0.8280257E-02	-0.2208726E-01
240.0000	0.3018203E-01	-0.1386137E-01	-0.2681077E-01
270.0000	0.3843045E-01	-0.1663393E-01	-0.3464407E-01
300.0000	0.4624612E-01	-0.1375757E-01	-0.4415239E-01
330.0000	0.5185165E-01	-0.5907666E-02	-0.5151400E-01
360.0000	0.5269205E-01	0.5825952E-02	-0.5236898E-01

Time: 240°

****
Integrals
****

Integrals on region A

Surface of the region		308.8672	(square mm)
Integ. (A.J) dv	=	6.448885	
Total ampere turn(s)	=	-3674.564	(Ampere)
Inductance (1 turn)	=	0.4776097E-06	(Henry)

Integrals on region B

Surface of the region		308.8672	(square mm)
Integ. (A.J) dv	=	6.448140	
Total ampere turn(s)	=	3674.563	(Ampere)
Inductance (1 turn)	=	0.4775545E-06	(Henry)

Integrals on region C

Surface of the region		308.8672	(square mm)
Flux through one turn	=	-0.1004824E-06	(Weber)

CURVES
******

Flux density
arc : center X = 0; Y = 0; R = 12.7 (0 -> 360 deg.)

ABSCISSA Deg	MAGNITUDE Tesla	NORMAL C. Tesla	TANGENTIAL C. Tesla
0.0000000	0.7902183E-01	-0.2744628E-02	-0.7897416E-01
30.00000	0.7621447E-01	0.8495854E-02	-0.7573946E-01
60.00000	0.6829866E-01	0.1405841E-01	-0.6683612E-01
90.00000	0.6093303E-01	0.1644699E-01	-0.5867138E-01
120.0000	0.5437316E-01	0.1470067E-01	-0.5234816E-01
150.0000	0.4708594E-01	0.1051728E-01	-0.4589632E-01
180.0000	0.4173418E-01	0.5343908E-02	-0.4139063E-01
210.0000	0.4049843E-01	-0.2865419E-02	-0.4039694E-01
240.0000	0.4504933E-01	-0.1220576E-01	-0.4336429E-01
270.0000	0.5467187E-01	-0.1890688E-01	-0.5129856E-01
300.0000	0.6551984E-01	-0.1892137E-01	-0.6272823E-01
330.0000	0.7467209E-01	-0.1367484E-01	-0.7340925E-01
360.0000	0.7902181E-01	-0.2744621E-02	-0.7897413E-01

Time = 270°

****
Integrals
****

Integrals on region A

Surface of the region		308.8672	(square mm)
Integ. (A.J) dv	=	8.844812	
Total ampere turn(s)	=	-4243.002	(Ampere)
Inductance (1 turn)	=	0.4912948E-06	(Henry)

Integrals on region B

Surface of the region		308.8672	(square mm)
Integ. (A.J) dv	=	2.026019	
Total ampere turn(s)	=	2121.485	(Ampere)
Inductance (1 turn)	=	0.4501565E-06	(Henry)

Integrals on region C

Surface of the region		308.8672	(square mm)
Integ. (A.J) dv	=	1.771942	
Total ampere turn(s)	=	2121.485	(Ampere)
Inductance (1 turn)	=	0.3937039E-06	(Henry)

CURVES
******

Flux density
arc : center X = 0; Y = 0; R = 12.7 (0 -> 360 deg.)

ABSCISSA Deg	MAGNITUDE Tesla	NORMAL C. Tesla	TANGENTIAL C. Tesla
0.00000	0.8507769E-01	-0.1057974E-01	-0.8441731E-01
30.00000	0.8642507E-01	-0.3679805E-03	-0.8642429E-01
60.00000	0.8250027E-01	0.7940572E-02	-0.8211724E-01
90.00000	0.7710401E-01	0.1524466E-01	-0.7558193E-01
120.0000	0.7035032E-01	0.1751499E-01	-0.6813511E-01
150.0000	0.6111918E-01	0.1571058E-01	-0.5906548E-01
180.0000	0.5294160E-01	0.1168492E-01	-0.5163599E-01
210.0000	0.4799657E-01	0.3317233E-02	-0.4788180E-01
240.0000	0.4884338E-01	-0.7279493E-02	-0.4829787E-01
270.0000	0.5655130E-01	-0.1611352E-01	-0.5420704E-01
300.0000	0.6724001E-01	-0.1901496E-01	-0.6449535E-01
330.0000	0.7769492E-01	-0.1777769E-01	-0.7563369E-01
360.0000	0.8507767E-01	-0.1057974E-01	-0.8441728E-01

Time : 300°

****
Integrals
****

Integrals on region A

Surface of the region		308.8672	(square mm)
Integ. (A.J) dv	=	6.783132	
Total ampere turn(s)	=	-3674.564	(Ampere)
Inductance (1 turn)	=	0.5023642E-06	(Henry)

Magsoft Corporation/112_01 USI Page 17

Integrals on region B

Surface of the region = 308.8672 (square mm)
Integ. (A.J) dv = 5.351643
Total ampere turn(s) = 3674.563 (Ampere)
Inductance (1 turn) = 0.3963472E-06 (Henry)

Integrals on region C

Surface of the region = 308.8672 (square mm)
Flux through one turn = -0.9106284E-04 (Weber)

CURVES
******

Flux density
arc : center X = 0; Y = 0; R = 12.7 (0 -> 360 deg.)

ABSCISSA Deg	MAGNITUDE Tesla	NORMAL C. Tesla	TANGENTIAL C. Tesla
0.00000	0.6902311E-01	-0.1558017E-01	-0.6724171E-01
30.00000	0.7451448E-01	-0.9133197E-02	-0.7395263E-01
60.00000	0.7539649E-01	-0.3047772E-03	-0.7539587E-01
90.00000	0.7292409E-01	0.9957788E-02	-0.7224102E-01
120.0000	0.6750183E-01	0.1563646E-01	-0.6566580E-01
150.0000	0.5882704E-01	0.1669448E-01	-0.5640846E-01
180.0000	0.5030172E-01	0.1489511E-01	-0.4804580E-01
210.0000	0.4339984E-01	0.8611047E-02	-0.4253700E-01
240.0000	0.4029234E-01	-0.4028324E-03	-0.4029033E-01
270.0000	0.4353225E-01	-0.9002824E-02	-0.4259114E-01
300.0000	0.5094679E-01	-0.1401382E-01	-0.4898151E-01
330.0000	0.6008272E-01	-0.1711729E-01	-0.5759280E-01
360.0000	0.6902309E-01	-0.1558017E-01	-0.6724168E-01

Time : 330°

****
Integrals
****

Integrals on region A

Surface of the region = 308.8672 (square mm)
Integ. (A.J) dv = 2.360661
Total ampere turn(s) = -2121.485 (Ampere)
Inductance (1 turn) = 0.5245097E-06 (Henry)

Integrals on region B

Surface of the region		308.8672	(square mm)
Integ. (A.J) dv	=	7.159194	
Total ampere turn(s)	=	4243.000	(Ampere)
Inductance (1 turn)	=	0.3976655E-06	(Henry)

Integrals on region C

Surface of the region		308.8672	(square mm)
Integ. (A.J) dv	=	2.360659	
Total ampere turn(s)	=	-2121.485	(Ampere)
Inductance (1 turn)	=	0.5245093E-06	(Henry)

CURVES
******

Flux density
arc : center X = 0; Y = 0; R = 12.7 (0 -> 360 deg.)

ABSCISSA Deg	MAGNITUDE Tesla	NORMAL C. Tesla	TANGENTIAL C. Tesla
0.00000	0.3600303E-01	-0.1640572E-01	-0.3204795E-01
30.00000	0.4443726E-01	-0.1545108E-01	-0.4166454E-01
60.00000	0.4920554E-01	-0.8468463E-02	-0.4847134E-01
90.00000	0.4958278E-01	0.2002618E-02	-0.4954231E-01
120.0000	0.4659360E-01	0.9567965E-02	-0.4560063E-01
150.0000	0.4083043E-01	0.1320491E-01	-0.3863617E-01
180.0000	0.3459159E-01	0.1411400E-01	-0.3158120E-01
210.0000	0.2828122E-01	0.1159744E-01	-0.2579393E-01
240.0000	0.2247200E-01	0.6581779E-02	-0.2148653E-01
270.0000	0.1956938E-01	0.5202816E-03	-0.1956246E-01
300.0000	0.2101094E-01	-0.5257519E-02	-0.2034252E-01
330.0000	0.2688196E-01	-0.1187012E-01	-0.2411929E-01
360.0000	0.3600303E-01	-0.1640572E-01	-0.3204793E-01

Cable concept #1 with cable B cradled between cable A

```
*****************************************
*     CEDRAT                    MAGSOFT   *
* Grenoble, France             Troy, N.Y. *
*                                         *
*             FLUX2D  6.36                *
*                                         *
*                     Serial # MAGSOFT    *
*                                         *
*     copyright (all rights reserved)     *
* ENSIEG - LABORATOIRE D'ELECTROTECHNIQUE *
* BP46 38402 Saint Martin d'Heres France  *
*****************************************

        expgen    6/25/90  7:51:02

Problem : CACOL1

time : 0°


********
Integrals
********


Integrals on region  A

Surface of the region          309.0320      (square mm)
Flux through one turn      = -0.1818753E-06 (Weber)

Integrals on region  B

Surface of the region          309.0320      (square mm)
Integ. (A.J) dv            =   8.818553
Total ampere turn(s)       =   3676.524      (Ampere)
Inductance (1 turn)        =  0.6524129E-06 (Henry)

Integrals on region  C

Surface of the region          309.0319      (square mm)
Integ. (A.J) dv            =   8.819891
Total ampere turn(s)       =  -3676.523      (Ampere)
Inductance (1 turn)        =  0.6525122E-06 (Henry)
```

CURVES
******

Flux density
arc : center X = 0; Y = 0; R = 12.7 (0 -> 360 deg.)

ABSCISSA Deg	MAGNITUDE Tesla	NORMAL C. Tesla	TANGENTIAL C. Tesla
0.00000	0.2692444E-01	-0.1270786E-01	0.2373680E-01
30.00000	0.2779189E-01	-0.2426335E-01	0.1355282E-01
60.00000	0.2800591E-01	-0.2794715E-01	-0.1813209E-02
90.00000	0.2765482E-01	-0.2220395E-01	-0.1648556E-01
120.0000	0.2664622E-01	-0.9533279E-02	-0.2488248E-01
150.0000	0.2514216E-01	0.4385129E-02	-0.2475680E-01
180.0000	0.2366945E-01	0.1492675E-01	-0.1836940E-01
210.0000	0.2268290E-01	0.2079516E-01	-0.9059527E-02
240.0000	0.2240524E-01	0.2237477E-01	0.1167913E-02
270.0000	0.2284446E-01	0.1985477E-01	0.1129855E-01
300.0000	0.2396594E-01	0.1293586E-01	0.2017497E-01
330.0000	0.2551271E-01	0.1445377E-02	0.2547173E-01
360.0000	0.2692444E-01	0.1270786E-01	0.2373680E-01

Time : 30°

****
Integrals
****

Integrals on region A

Surface of the region 309.0320 (square mm)
Integ. (A.J) dv = 2.140718
Total ampere turn(s) = 2122.617 (Ampere)
Inductance (1 turn) = 0.4751338E-06 (Henry)

Integrals on region B

Surface of the region 309.0320 (square mm)
Integ. (A.J) dv = 3.716959
Total ampere turn(s) = 2122.617 (Ampere)
Inductance (1 turn) = 0.8249821E-06 (Henry)

Integrals on region C

Surface of the region 309.0319 (square mm)
Integ. (A.J) dv = 10.20428
Total ampere turn(s) = -4245.264 (Ampere)
Inductance (1 turn) = 0.5662041E-06 (Henry)

CURVES
******

Flux density
arc : center X = 0; Y = 0; R = 12.7 (0 -> 360 deg.)

ABSCISSA Deg	MAGNITUDE Tesla	NORMAL C. Tesla	TANGENTIAL C. Tesla
0.00000	0.6002053E-01	-0.5721146E-02	0.5974723E-01
30.00000	0.5375725E-01	-0.1823458E-01	0.5057017E-01
60.00000	0.4464291E-01	-0.2469374E-01	0.3719151E-01
90.00000	0.3284260E-01	-0.2231414E-01	0.2409803E-01
120.0000	0.2149975E-01	-0.1430706E-01	0.1604828E-01
150.0000	0.1271486E-01	-0.3879684E-02	0.1210850E-01
180.0000	0.1448905E-01	0.6309312E-02	0.1304320E-01
210.0000	0.2274900E-01	0.1403076E-01	0.1790683E-01
240.0000	0.3307642E-01	0.2028110E-01	0.2612904E-01
270.0000	0.4228443E-01	0.2237314E-01	0.3588057E-01
300.0000	0.5103873E-01	0.1886914E-01	0.4742264E-01
330.0000	0.5709950E-01	0.8028647E-02	0.5653223E-01
360.0000	0.6002052E-01	-0.5721150E-02	0.5974723E-01

Time : 60°

****
Integrals
****

Integrals on region A

Surface of the region = 309.0320 (square mm)
Integ. (A.J) dv = 6.455760
Total ampere turn(s) = 3676.524 (Ampere)
Inductance (1 turn) = 0.4776090E-06 (Henry)

Integrals on region B

Surface of the region = 309.0320 (square mm)
Flux through one turn = 0.6433631E-03 (Weber)

Integrals on region C

Surface of the region = 309.0319 (square mm)
Integ. (A.J) dv = 6.453900
Total ampere turn(s) = -3676.523 (Ampere)
Inductance (1 turn) = 0.4774718E-06 (Henry)

CURVES
******

Flux density
arc : center X = 0; Y = 0; R = 12.7 (0 -> 360 deg.)

ABSCISSA Deg	MAGNITUDE Tesla	NORMAL C. Tesla	TANGENTIAL C. Tesla
0.00000	0.7979853E-01	0.2798473E-02	0.7974944E-01
30.00000	0.7439914E-01	-0.7320071E-02	0.7403816E-01
60.00000	0.6787018E-01	-0.1482396E-01	0.6623150E-01
90.00000	0.6050307E-01	-0.1644554E-01	0.5822513E-01
120.0000	0.5484161E-01	-0.1524744E-01	0.5267938E-01
150.0000	0.4705880E-01	-0.1110497E-01	0.4572975E-01
180.0000	0.4115604E-01	-0.3998604E-02	0.4096133E-01
210.0000	0.4022874E-01	0.3507007E-02	0.4007558E-01
240.0000	0.4589701E-01	0.1275336E-01	0.4408953E-01
270.0000	0.5424692E-01	0.1889690E-01	0.5084914E-01
300.0000	0.6503465E-01	0.1974666E-01	0.6196430E-01
330.0000	0.7350972E-01	0.1246072E-01	0.7244591E-01
360.0000	0.7979851E-01	0.2798468E-02	0.7974942E-01

Time : 90°

****
Integrals
****

Integrals on region A

Surface of the region = 309.0320 (square mm)
Integ. (A.J) dv = 8.630217
Total ampere turn(s) = 4245.266 (Ampere)
Inductance (1 turn) = 0.4788637E-06 (Henry)

Integrals on region B

Surface of the region = 309.0320 (square mm)
Integ. (A.J) dv = 1.351516
Total ampere turn(s) = -2122.617 (Ampere)
Inductance (1 turn) = 0.2999699E-06 (Henry)

Integrals on region C

Surface of the region = 309.0319 (square mm)
Integ. (A.J) dv = 1.351516
Total ampere turn(s) = -2122.616 (Ampere)
Inductance (1 turn) = 0.2999701E-06 (Henry)

CURVES
******

Flux density
arc : center X = 0; Y = 0; R = 12.7 (0 -> 360 deg.)

ABSCISSA Deg	MAGNITUDE Tesla	NORMAL C. Tesla	TANGENTIAL C. Tesla
0.00000	0.7909111E-01	0.1056823E-01	0.7838186E-01
30.00000	0.7786525E-01	0.5555958E-02	0.7766678E-01
60.00000	0.7753026E-01	-0.9818971E-03	0.7752404E-01
90.00000	0.7699779E-01	-0.6170149E-02	0.7675017E-01
120.0000	0.7616214E-01	-0.1210209E-01	0.7519448E-01
150.0000	0.6883170E-01	-0.1535456E-01	0.6709723E-01
180.0000	0.5939676E-01	-0.1323507E-01	0.5790343E-01
210.0000	0.5211657E-01	-0.7956512E-02	0.5150563E-01
240.0000	0.5026827E-01	0.1808191E-02	0.5023574E-01
270.0000	0.5320981E-01	0.1035700E-01	0.5219211E-01
300.0000	0.6183312E-01	0.1533282E-01	0.5990191E-01
330.0000	0.7026646E-01	0.1355380E-01	0.6894686E-01
360.0000	0.7909110E-01	0.1056822E-01	0.7838184E-01

Time : 120°

****
Integrals
****

Integrals on region A

Surface of the region = 309.0320 (square mm)
Integ. (A.J) dv = 6.456371
Total ampere turn(s) = 3676.524 (Ampere)
Inductance (1 turn) = 0.4776542E-06 (Henry)

Integrals on region B

Surface of the region = 309.0320 (square mm)
Integ. (A.J) dv = 6.453290
Total ampere turn(s) = -3676.524 (Ampere)
Inductance (1 turn) = 0.4774263E-06 (Henry)

Integrals on region C

Surface of the region = 309.0319 (square mm)
Flux through one turn = 0.6435295E-03 (Weber)

CURVES
******

Flux density
arc : center X = 0; Y = 0; R = 12.7 (0 -> 360 deg.)

ABSCISSA Deg	MAGNITUDE Tesla	NORMAL C. Tesla	TANGENTIAL C. Tesla
0.00000	0.5811933E-01	0.1550636E-01	0.5601259E-01
30.00000	0.6281361E-01	0.1694334E-01	0.6048531E-01
60.00000	0.6929865E-01	0.1312325E-01	0.6804471E-01
90.00000	0.7493232E-01	0.5758459E-02	0.7471072E-01
120.0000	0.7777213E-01	-0.5714141E-02	0.7756191E-01
150.0000	0.7216859E-01	-0.1549011E-01	0.7048661E-01
180.0000	0.6227609E-01	-0.1892539E-01	0.5933077E-01
210.0000	0.5208783E-01	-0.1728820E-01	0.4913512E-01
240.0000	0.4398680E-01	-0.9621458E-02	0.4292162E-01
270.0000	0.3956218E-01	-0.9579197E-03	0.3955057E-01
300.0000	0.4234065E-01	0.6810766E-02	0.4178929E-01
330.0000	0.4824837E-01	0.1101534E-01	0.4697412E-01
360.0000	0.5811933E-01	0.1550636E-01	0.5601257E-01

Time : 150

****
Integrals
****

Integrals on region A

Surface of the region = 309.0320 (square mm)
Integ. (A.J) dv = 2.141344
Total ampere turn(s) = 2122.617 (Ampere)
Inductance (1 turn) = 0.4752729E-06 (Henry)

Integrals on region B

Surface of the region = 309.0320 (square mm)
Integ. (A.J) dv = 10.20303
Total ampere turn(s) = -4245.265 (Ampere)
Inductance (1 turn) = 0.5661342E-06 (Henry)

Integrals on region C

Surface of the region = 309.0319 (square mm)
Integ. (A.J) dv = 3.717587
Total ampere turn(s) = 2122.616 (Ampere)
Inductance (1 turn) = 0.8251217E-06 (Henry)

CURVES
******

Flux density
arc : center X = 0; Y = 0; R = 12.7 (0 -> 360 deg.)

ABSCISSA Deg	MAGNITUDE Tesla	NORMAL C. Tesla	TANGENTIAL C. Tesla
0.00000	0.2475026E-01	0.1628938E-01	0.1863414E-01
30.00000	0.3605815E-01	0.2379052E-01	0.2709614E-01
60.00000	0.4678597E-01	0.2371185E-01	0.4033206E-01
90.00000	0.5507112E-01	0.1614399E-01	0.5265168E-01
120.0000	0.5918682E-01	0.2204962E-02	0.5914573E-01
150.0000	0.5617280E-01	-0.1147491E-01	0.5498827E-01
180.0000	0.4893241E-01	-0.1954442E-01	0.4485974E-01
210.0000	0.4015329E-01	-0.2198730E-01	0.3359829E-01
240.0000	0.3037031E-01	-0.1847291E-01	0.2410617E-01
270.0000	0.2025925E-01	-0.1201612E-01	0.1631103E-01
300.0000	0.1297017E-01	-0.3536290E-02	0.1247878E-01
330.0000	0.1358820E-01	0.5525190E-02	0.1241417E-01
360.0000	0.2475026E-01	0.1628938E-01	0.1863414E-01

Time : 180°

****
Integrals
****

Integrals on region A

Surface of the region 309.0320 (square mm)
Flux through one turn = 0.1818753E-06 (Weber)

Integrals on region B

Surface of the region 309.0320 (square mm)
Integ. (A.J) dv = 8.818553
Total ampere turn(s) = -3676.524 (Ampere)
Inductance (1 turn) = 0.6524129E-06 (Henry)

Integrals on region C

Surface of the region 309.0319 (square mm)
Integ. (A.J) dv = 8.819891
Total ampere turn(s) = 3676.523 (Ampere)
Inductance (1 turn) = 0.6525122E-06 (Henry)

CURVES
******

Flux density
arc : center X = 0; Y = 0; R = 12.7 (0 -> 360 deg.)

ABSCISSA Deg	MAGNITUDE Tesla	NORMAL C. Tesla	TANGENTIAL C. Tesla
0.00000	0.2692444E-01	0.1270786E-01	-0.2373680E-01
30.00000	0.2779189E-01	0.2426335E-01	-0.1355282E-01
60.00000	0.2800591E-01	0.2794715E-01	0.1813209E-02
90.00000	0.2765482E-01	0.2220395E-01	0.1648556E-01
120.0000	0.2664622E-01	0.9533279E-02	0.2488248E-01
150.0000	0.2514216E-01	-0.4385129E-02	0.2475680E-01
180.0000	0.2366945E-01	-0.1492675E-01	0.1836940E-01
210.0000	0.2268290E-01	-0.2079516E-01	0.9059527E-02
240.0000	0.2240524E-01	-0.2237477E-01	-0.1167913E-02
270.0000	0.2284446E-01	-0.1985477E-01	-0.1129855E-01
300.0000	0.2396594E-01	-0.1293586E-01	-0.2017497E-01
330.0000	0.2551271E-01	-0.1445377E-02	-0.2547173E-01
360.0000	0.2692444E-01	0.1270786E-01	-0.2373680E-01

Time : 210°

****
Integrals
****

Integrals on region A

Surface of the region = 309.0320 (square mm)
Integ. (A.J) dv = 2.140718
Total ampere turn(s) = -2122.617 (Ampere)
Inductance (1 turn) = 0.4751338E-06 (Henry)

Integrals on region B

Surface of the region = 309.0320 (square mm)
Integ. (A.J) dv = 3.716959
Total ampere turn(s) = -2122.617 (Ampere)
Inductance (1 turn) = 0.8249821E-06 (Henry)

Integrals on region C

Surface of the region = 309.0319 (square mm)
Integ. (A.J) dv = 10.20428
Total ampere turn(s) = 4245.264 (Ampere)
Inductance (1 turn) = 0.5662041E-06 (Henry)

CURVES
******

Flux density
arc : center X = 0; Y = 0; R = 12.7 (0 -> 360 deg.)

ABSCISSA Deg	MAGNITUDE Tesla	NORMAL C. Tesla	TANGENTIAL C. Tesla
0.00000	0.6002053E-01	0.5721146E-02	-0.5974723E-01
30.00000	0.5375725E-01	0.1823458E-01	-0.5057017E-01
60.00000	0.4464291E-01	0.2469374E-01	-0.3719151E-01
90.00000	0.3284260E-01	0.2231414E-01	-0.2409803E-01
120.0000	0.2149975E-01	0.1430706E-01	-0.1604828E-01
150.0000	0.1271486E-01	0.3879684E-02	-0.1210850E-01
180.0000	0.1448905E-01	-0.6309312E-02	-0.1304320E-01
210.0000	0.2274900E-01	-0.1403076E-01	-0.1790683E-01
240.0000	0.3307642E-01	-0.2028110E-01	-0.2612904E-01
270.0000	0.4228443E-01	-0.2237314E-01	-0.3588057E-01
300.0000	0.5103873E-01	-0.1886914E-01	-0.4742264E-01
330.0000	0.5709950E-01	-0.8028647E-02	-0.5653223E-01
360.0000	0.6002052E-01	0.5721150E-02	-0.5974723E-01

Time : 240°

****
Integrals
****

Integrals on region A

Surface of the region 309.0320 (square mm)
Integ. (A.J) dv = 6.455760
Total ampere turn(s) = -3676.524 (Ampere)
Inductance (1 turn) = 0.4776090E-06 (Henry)

Integrals on region B

Surface of the region 309.0320 (square mm)
Flux through one turn = -0.6433631E-03 (Weber)

Integrals on region C

Surface of the region 309.0319 (square mm)
Integ. (A.J) dv = 6.453900
Total ampere turn(s) = 3676.523 (Ampere)
Inductance (1 turn) = 0.4774718E-06 (Henry)

CURVES
******

Flux density
arc : center X = 0; Y = 0; R = 12.7 (0 -> 360 deg.)

ABSCISSA Deg	MAGNITUDE Tesla	NORMAL C. Tesla	TANGENTIAL C. Tesla
0.00000	0.7979853E-01	-0.2798473E-02	-0.7974944E-01
30.00000	0.7439914E-01	0.7320071E-02	-0.7403816E-01
60.00000	0.6787018E-01	0.1482396E-01	-0.6623150E-01
90.00000	0.6050307E-01	0.1644554E-01	-0.5822513E-01
120.0000	0.5484161E-01	0.1524744E-01	-0.5267938E-01
150.0000	0.4705880E-01	0.1110497E-01	-0.4572975E-01
180.0000	0.4115604E-01	0.3998604E-02	-0.4096133E-01
210.0000	0.4022874E-01	-0.3507007E-02	-0.4007558E-01
240.0000	0.4589701E-01	-0.1275336E-01	-0.4408953E-01
270.0000	0.5424692E-01	-0.1889690E-01	-0.5084914E-01
300.0000	0.6503465E-01	-0.1974666E-01	-0.6196430E-01
330.0000	0.7350972E-01	-0.1246072E-01	-0.7244591E-01
360.0000	0.7979851E-01	-0.2798468E-02	-0.7974942E-01

Time : 270°

****
Integrals
****

Integrals on region A

Surface of the region 309.0320 (square mm)
Integ. (A.J) dv = 91.09959
Total ampere turn(s) = 4245.266 (Ampere)
Inductance (1 turn) = 0.5054831E-05 (Henry)

Integrals on region B

Surface of the region 309.0320 (square mm)
Integ. (A.J) dv = 43.42131
Total ampere turn(s) = 2122.617 (Ampere)
Inductance (1 turn) = 0.9637393E-05 (Henry)

Integrals on region C

Surface of the region 309.0319 (square mm)
Integ. (A.J) dv = 43.43432
Total ampere turn(s) = 2122.616 (Ampere)
Inductance (1 turn) = 0.9640286E-05 (Henry)

CURVES
******

Flux density
arc : center X = 0; Y = 0; R = 12.7 (0 -> 360 deg.)

ABSCISSA Deg	MAGNITUDE Tesla	NORMAL C. Tesla	TANGENTIAL C. Tesla
0.00000	0.6505242E-01	-0.4685245E-02	0.6488348E-01
30.00000	0.6017641E-01	-0.1189679E-02	0.6016465E-01
60.00000	0.5939512E-01	-0.1194365E-03	0.5939500E-01
90.00000	0.5985418E-01	0.2564195E-02	0.5979923E-01
120.0000	0.6360879E-01	0.5030883E-02	0.6340952E-01
150.0000	0.6609199E-01	0.6868094E-02	0.6573416E-01
180.0000	0.6940607E-01	0.7131923E-02	0.6903867E-01
210.0000	0.7240531E-01	0.3526220E-02	0.7231939E-01
240.0000	0.7412264E-01	0.2480298E-03	0.7412222E-01
270.0000	0.7136797E-01	-0.3711129E-02	0.7127141E-01
300.0000	0.6850316E-01	-0.6196396E-02	0.6822233E-01
330.0000	0.6527621E-01	-0.8038426E-02	0.6477936E-01
360.0000	0.6505241E-01	-0.4685245E-02	0.6488346E-01

Time : 300°

****
Integrals
****

Integrals on region A

Surface of the region = 309.0320 (square mm)
Integ. (A.J) dv = 6.456371
Total ampere turn(s) = -3676.524 (Ampere)
Inductance (1 turn) = 0.4776542E-06 (Henry)

Integrals on region B

Surface of the region = 309.0320 (square mm)
Integ. (A.J) dv = 6.453290
Total ampere turn(s) = 3676.524 (Ampere)
Inductance (1 turn) = 0.4774263E-06 (Henry)

Integrals on region C

Surface of the region = 309.0319 (square mm)
Flux through one turn = -0.6435295E-03 (Weber)

CURVES
******

Flux density
arc : center X = 0; Y = 0; R = 12.7 (0 -> 360 deg.)

ABSCISSA Deg	MAGNITUDE Tesla	NORMAL C. Tesla	TANGENTIAL C. Tesla
0.00000	0.5811933E-01	-0.1550636E-01	-0.5601259E-01
30.00000	0.6281361E-01	-0.1694334E-01	-0.6048531E-01
60.00000	0.6929865E-01	-0.1312325E-01	-0.6804471E-01
90.00000	0.7493232E-01	-0.5758459E-02	-0.7471072E-01
120.0000	0.7777213E-01	0.5714141E-02	-0.7756191E-01
150.0000	0.7216859E-01	0.1549011E-01	-0.7048661E-01
180.0000	0.6227609E-01	0.1892539E-01	-0.5933077E-01
210.0000	0.5208783E-01	0.1728820E-01	-0.4913512E-01
240.0000	0.4398680E-01	0.9621458E-02	-0.4292162E-01
270.0000	0.3956218E-01	0.9579197E-03	-0.3955057E-01
300.0000	0.4234065E-01	-0.6810766E-02	-0.4178929E-01
330.0000	0.4824837E-01	-0.1101534E-01	-0.4697412E-01
360.0000	0.5811933E-01	-0.1550636E-01	-0.5601257E-01

Time : 330

****
Integrals
****

Integrals on region A

Surface of the region = 309.0320 (square mm)
Integ. (A.J) dv = -37.98927
Total ampere turn(s) = -2122.617 (Ampere)
Inductance (1 turn) = -0.8431746E-05 (Henry)

Integrals on region B

Surface of the region = 309.0320 (square mm)
Integ. (A.J) dv = 85.74953
Total ampere turn(s) = 4245.265 (Ampere)
Inductance (1 turn) = 0.4757974E-05 (Henry)

Integrals on region C

Surface of the region = 309.0319 (square mm)
Integ. (A.J) dv = 40.73574
Total ampere turn(s) = 2122.616 (Ampere)
Inductance (1 turn) = 0.9041334E-05 (Henry)

CURVES
******

Flux density
arc : center X = 0; Y = 0; R = 12.7 (0 -> 360 deg.)

ABSCISSA Deg	MAGNITUDE Tesla	NORMAL C. Tesla	TANGENTIAL C. Tesla
0.00000	0.3821819E-01	-0.9685840E-02	-0.3697045E-01
30.00000	0.3963788E-01	-0.8015196E-02	-0.3881904E-01
60.00000	0.4188276E-01	-0.4627419E-02	-0.4162635E-01
90.00000	0.4414390E-01	0.1755222E-03	-0.4414354E-01
120.0000	0.4473730E-01	0.7208157E-02	-0.4415279E-01
150.0000	0.3986486E-01	0.1222467E-01	-0.3794423E-01
180.0000	0.3246623E-01	0.1224267E-01	-0.3006946E-01
210.0000	0.2575983E-01	0.8948278E-02	-0.2415569E-01
240.0000	0.2179680E-01	0.2607380E-02	-0.2164029E-01
270.0000	0.2179505E-01	-0.3632100E-02	-0.2149028E-01
300.0000	0.2651959E-01	-0.8427052E-02	-0.2514505E-01
330.0000	0.3207140E-01	-0.9688448E-02	-0.3057301E-01
360.0000	0.3821818E-01	-0.9685839E-02	-0.3697044E-01

Cable Concept #3: triangular configuration

```
*****************************************
*     CEDRAT                    MAGSOFT   *
* Grenoble, France             Troy, N.Y. *
*                                         *
*              FLUX2D  6.36               *
*                                         *
*                     Serial # MAGSOFT    *
*                                         *
*     copyright (all rights reserved)     *
* ENSIEG - LABORATOIRE D'ELECTROTECHNIQUE *
* BP46 38402 Saint Martin d'Heres France  *
*****************************************

        expgen    6/27/90 13:26:22

Problem : CACOM3

Time: 0°


********
Integrals
********


Integrals on region  A

Surface of the region          887.2899     (square mm)
Flux through one turn      = -0.3452014E-04 (Weber)

Integrals on region  B

Surface of the region          887.2899     (square mm)
Integ. (A.J) dv            =   1.883959
Total ampere turn(s)       =   2451.227     (Ampere)
Inductance (1 turn)        =  0.3135482E-06 (Henry)

Integrals on region  C

Surface of the region          887.2905     (square mm)
Integ. (A.J) dv            =   2.279996
Total ampere turn(s)       =  -2451.229     (Ampere)
Inductance (1 turn)        =  0.3794603E-06 (Henry)
```

CURVES
******

Flux density
arc : center X=0 Y=OR = 25.4 (0 -> 360 deg.)

ABSCISSA Deg	MAGNITUDE Tesla	NORMAL C. Tesla	TANGENTIAL C. Tesla
0.0000000	0.1192485E-01	-0.8491942E-02	0.8371920E-02
30.00000	0.1256801E-01	-0.1255791E-01	0.5039391E-03
60.00000	0.1143367E-01	-0.8852823E-02	-0.7235770E-02
90.00000	0.9471628E-02	-0.2261126E-02	-0.9197773E-02
120.0000	0.7832722E-02	0.2094033E-02	-0.7547619E-02
150.0000	0.6742144E-02	0.4315466E-02	-0.5180082E-02
180.0000	0.6249743E-02	0.5491274E-02	-0.2984156E-02
210.0000	0.6171927E-02	0.6125384E-02	-0.7565485E-03
240.0000	0.6499480E-02	0.6274795E-02	0.1694164E-02
270.0000	0.7261434E-02	0.5650300E-02	0.4560979E-02
300.0000	0.8485103E-02	0.3500310E-02	0.7729476E-02
330.0000	0.1018272E-01	-0.1241212E-02	0.1010678E-01
360.0000	0.1188857E-01	-0.8440922E-02	0.8371917E-02

Test: 30°

****
Integrals
****

Integrals on region A

Surface of the region 887.2899 (square mm)
Integ. (A.J) dv = 0.7048281
Total ampere turn(s) = 1415.227 (Ampere)
Inductance (1 turn) = 0.3519093E-06 (Henry)

Integrals on region B

Surface of the region 887.2899 (square mm)
Integ. (A.J) dv = 0.6292171
Total ampere turn(s) = 1415.227 (Ampere)
Inductance (1 turn) = 0.3141580E-06 (Henry)

Integrals on region C

Surface of the region 887.2905 (square mm)
Integ. (A.J) dv = 2.981182
Total ampere turn(s) = -2830.457 (Ampere)
Inductance (1 turn) = 0.3721136E-06 (Henry)

CURVES
******

Flux density
arc : center X = 0; Y = 0; R = 25.4 (0 -> 360 deg.)

ABSCISSA Deg	MAGNITUDE Tesla	NORMAL C. Tesla	TANGENTIAL C. Tesla
0.0000000	0.2399303E-01	-0.4509361E-02	0.2356546E-01
30.00000	0.1998516E-01	-0.1079136E-01	0.1682121E-01
60.00000	0.1414477E-01	-0.1054942E-01	0.9422528E-02
90.00000	0.8691693E-02	-0.6509297E-02	0.5759737E-02
120.0000	0.5785968E-02	-0.3368680E-02	0.4704191E-02
150.0000	0.4363650E-02	-0.8456894E-03	0.4280917E-02
180.0000	0.4129861E-02	0.1721753E-02	0.3753840E-02
210.0000	0.6706257E-02	0.4523931E-02	0.4950548E-02
240.0000	0.1071279E-01	0.7927670E-02	0.7205275E-02
270.0000	0.1526690E-01	0.9717399E-02	0.1177499E-01
300.0000	0.1958581E-01	0.9008205E-02	0.1739127E-01
330.0000	0.2270287E-01	0.3943225E-02	0.2235780E-01
360.0000	0.2397962E-01	-0.4437476E-02	0.2356546E-01

Time: 60°

****
Integrals
****

Integrals on region A

Surface of the region 887.2899 (square mm)
Integ. (A.J) dv = 2.194385
Total ampere turn(s) = 2451.227 (Ampere)
Inductance (1 turn) = 0.3652126E-06 (Henry)

Integrals on region B

Surface of the region 887.2899 (square mm)
Flux through one turn = -0.4140336E-06 (Weber)

Integrals on region C

Surface of the region 887.2905 (square mm)
Integ. (A.J) dv = 2.196395
Total ampere turn(s) = -2451.229 (Ampere)
Inductance (1 turn) = 0.3655465E-06 (Henry)

CURVES
******

Flux density
arc : center X = 0; Y = 0; R = 25.4 (0 -> 360 deg.)

ABSCISSA Deg	MAGNITUDE Tesla	NORMAL C. Tesla	TANGENTIAL C. Tesla
0.0000000	0.3245150E-01	0.6815398E-03	0.3244435E-01
30.00000	0.2928055E-01	-0.6133155E-02	0.2863101E-01
60.00000	0.2536932E-01	-0.9419190E-02	0.2355592E-01
90.00000	0.2118664E-01	-0.9013218E-02	0.1917382E-01
120.0000	0.1758438E-01	-0.7928691E-02	0.1569542E-01
150.0000	0.1385781E-01	-0.5780186E-02	0.1259478E-01
180.0000	0.9812193E-02	-0.2509080E-02	0.9485970E-02
210.0000	0.9486578E-02	0.1710261E-02	0.9331141E-02
240.0000	0.1311207E-01	0.7456207E-02	0.1078570E-01
270.0000	0.1938333E-01	0.1118056E-01	0.1583377E-01
300.0000	0.2545395E-01	0.1210221E-01	0.2239285E-01
330.0000	0.2973412E-01	0.8071010E-02	0.2861777E-01
360.0000	0.3245313E-01	0.7550271E-03	0.3244434E-01

Time : 90°

****
Integrals
****

Integrals on region A

Surface of the region 887.2899 (square mm)
Integ. (A.J) dv = 2.978941
Total ampere turn(s) = 2830.455 (Ampere)
Inductance (1 turn) = 0.3718343E-06 (Henry)

Integrals on region B

Surface of the region 887.2899 (square mm)
Integ. (A.J) dv = 0.6303512
Total ampere turn(s) = -1415.227 (Ampere)
Inductance (1 turn) = 0.3147242E-06 (Henry)

Integrals on region C

Surface of the region 887.2905 (square mm)
Integ. (A.J) dv = 0.7059554
Total ampere turn(s) = -1415.228 (Ampere)
Inductance (1 turn) = 0.3524717E-06 (Henry)

CURVES
******

Flux density
arc : center X = 0; Y = 0; R = 25.4 (0 -> 360 deg.)

ABSCISSA Deg	MAGNITUDE Tesla	NORMAL C. Tesla	TANGENTIAL C. Tesla
0.0000000	0.3312257E-01	0.5689826E-02	0.3263021E-01
30.00000	0.3276996E-01	0.1683412E-03	0.3276953E-01
60.00000	0.3190306E-01	-0.5765214E-02	0.3137782E-01
90.00000	0.2892027E-01	-0.9102177E-02	0.2745054E-01
120.0000	0.2475534E-01	-0.1036432E-01	0.2248127E-01
150.0000	0.1978526E-01	-0.9165958E-02	0.1753402E-01
180.0000	0.1405377E-01	-0.6067621E-02	0.1267645E-01
210.0000	0.1131982E-01	-0.1561622E-02	0.1121159E-01
240.0000	0.1251298E-01	0.4986972E-02	0.1147627E-01
270.0000	0.1838508E-01	0.9648039E-02	0.1565013E-01
300.0000	0.2450748E-01	0.1195358E-01	0.2139459E-01
330.0000	0.2900190E-01	0.1003626E-01	0.2720999E-01
360.0000	0.3313212E-01	0.5745226E-02	0.3263020E-01

Time: 120°

****
Integrals
****

Integrals on region A

Surface of the region 887.2899 (square mm)
Integ. (A.J) dv = 2.278949
Total ampere turn(s) = 2451.227 (Ampere)
Inductance (1 turn) = 0.3792865E-06 (Henry)

Integrals on region B

Surface of the region 887.2899 (square mm)
Integ. (A.J) dv = 1.885027
Total ampere turn(s) = -2451.227 (Ampere)
Inductance (1 turn) = 0.3137258E-06 (Henry)

Integrals on region C

Surface of the region 887.2905 (square mm)
Flux through one turn = 0.3408459E-04 (Weber)

CURVES
******

Flux density
arc : center X = 0; Y = 0; R = 25.4 (0 -> 360 deg.)

ABSCISSA Deg	MAGNITUDE Tesla	NORMAL C. Tesla	TANGENTIAL C. Tesla
0.0000000	0.2576109E-01	0.9173471E-02	0.2407242E-01
30.00000	0.2885151E-01	0.6424743E-02	0.2812707E-01
60.00000	0.3079689E-01	-0.5663745E-03	0.3079168E-01
90.00000	0.2916399E-01	-0.6752104E-02	0.2837159E-01
120.0000	0.2531192E-01	-0.1002274E-01	0.2324302E-01
150.0000	0.2044179E-01	-0.1009565E-01	0.1777482E-01
180.0000	0.1481582E-01	-0.8000324E-02	0.1247009E-01
210.0000	0.1101155E-01	-0.4415071E-02	0.1008769E-01
240.0000	0.9168015E-02	0.1181445E-02	0.9091572E-02
270.0000	0.1255629E-01	0.5530253E-02	0.1127284E-01
300.0000	0.1700022E-01	0.8601874E-02	0.1466340E-01
330.0000	0.2072133E-01	0.9312198E-02	0.1851098E-01
360.0000	0.2576910E-01	0.9195937E-02	0.2407241E-01

Time: 150°

****
Integrals
****

Integrals on region A

Surface of the region = 887.2899 (square mm)
Integ. (A.J) dv = 0.7893629
Total ampere turn(s) = 1415.227 (Ampere)
Inductance (1 turn) = 0.3941162E-06 (Henry)

Integrals on region B

Surface of the region = 887.2899 (square mm)
Integ. (A.J) dv = 2.509706
Total ampere turn(s) = -2830.455 (Ampere)
Inductance (1 turn) = 0.3132640E-06 (Henry)

Integrals on region C

Surface of the region = 887.2905 (square mm)
Integ. (A.J) dv = 0.7893562
Total ampere turn(s) = 1415.228 (Ampere)
Inductance (1 turn) = 0.3941123E-06 (Henry)

Magsoft Corporation/112_01 USI

CURVES
******

Flux density
arc : center X = 0; Y =0; R = 25.4 (0 -> 360 deg.)

ABSCISSA Deg	MAGNITUDE Tesla	NORMAL C. Tesla	TANGENTIAL C. Tesla
0.0000000	0.1364529E-01	0.1019922E-01	0.9064761E-02
30.00000	0.1935111E-01	0.1095973E-01	0.1594835E-01
60.00000	0.2247055E-01	0.4784224E-02	0.2195534E-01
90.00000	0.2184529E-01	-0.2592890E-02	0.2169086E-01
120.0000	0.1910409E-01	-0.6995687E-02	0.1777714E-01
150.0000	0.1564844E-01	-0.8320352E-02	0.1325313E-01
180.0000	0.1184432E-01	-0.7789467E-02	0.8922568E-02
210.0000	0.8731195E-02	-0.6085591E-02	0.6260937E-02
240.0000	0.5185366E-02	-0.2940654E-02	0.4270898E-02
270.0000	0.3875732E-02	-0.6928587E-04	0.3875113E-02
300.0000	0.4970135E-02	0.2945428E-02	0.4003335E-02
330.0000	0.7789056E-02	0.6093069E-02	0.4852206E-02
360.0000	0.1363297E-01	0.1018273E-01	0.9064759E-02

Time: 180°

****
Integrals
****

Integrals on region A

Surface of the region 887.2899 (square mm)
Flux through one turn = 0.3452014E-04 (Weber)

Integrals on region B

Surface of the region 887.2899 (square mm)
Integ. (A.J) dv = 1.883959
Total ampere turn(s) = -2451.227 (Ampere)
Inductance (1 turn) = 0.3135482E-06 (Henry)

Integrals on region C

Surface of the region 887.2905 (square mm)
Integ. (A.J) dv = 2.279996
Total ampere turn(s) = 2451.229 (Ampere)
Inductance (1 turn) = 0.3794603E-06 (Henry)

CURVES
******

Flux density
arc : center X = 0; Y = 0; R = 24.5 (0 -> 360 deg.)

ABSCISSA Deg	MAGNITUDE Tesla	NORMAL C. Tesla	TANGENTIAL C. Tesla
0.0000000	0.1177551E-01	0.8452904E-02	-0.8198231E-02
30.00000	0.1237667E-01	0.1236676E-01	-0.4950990E-03
60.00000	0.1133925E-01	0.8800203E-02	0.7150867E-02
90.00000	0.9513879E-02	0.2368708E-02	0.9214288E-02
120.0000	0.7824738E-02	-0.2008906E-02	0.7562461E-02
150.0000	0.6800383E-02	-0.4307486E-02	0.5262202E-02
180.0000	0.6307960E-02	-0.5530372E-02	0.3034030E-02
210.0000	0.6227249E-02	-0.6183227E-02	0.7391439E-03
240.0000	0.6548780E-02	-0.6316306E-02	-0.1729392E-02
270.0000	0.7272988E-02	-0.5635940E-02	-0.4597012E-02
300.0000	0.8438771E-02	-0.3369040E-02	-0.7737081E-02
330.0000	0.1009430E-01	0.1356179E-02	-0.1000279E-01
360.0000	0.1172889E-01	0.8387840E-02	-0.8198228E-02

Time: 210°

****
Integrals
****

Integrals on region A

Surface of the region = 887.2899 (square mm)
Integ. (A.J) dv = 0.7048281
Total ampere turn(s) = -1415.227 (Ampere)
Inductance (1 turn) = 0.3519093E-06 (Henry)

Integrals on region B

Surface of the region = 887.2899 (square mm)
Integ. (A.J) dv = 0.6292171
Total ampere turn(s) = -1415.227 (Ampere)
Inductance (1 turn) = 0.3141580E-06 (Henry)

Integrals on region C

Surface of the region = 887.2905 (square mm)
Integ. (A.J) dv = 2.981182
Total ampere turn(s) = 2830.457 (Ampere)
Inductance (1 turn) = 0.3721136E-06 (Henry)

CURVES
******

Flux density
arc : center X = 0; Y = 0; R = 25.4 (0 -> 360 deg.)

ABSCISSA Deg	MAGNITUDE Tesla	NORMAL C. Tesla	TANGENTIAL C. Tesla
0.0000000	0.2399303E-01	0.4509361E-02	-0.2356546E-01
30.00000	0.1998516E-01	0.1079136E-01	-0.1682121E-01
60.00000	0.1414477E-01	0.1054942E-01	-0.9422528E-02
90.00000	0.8691693E-02	0.6509297E-02	-0.5759737E-02
120.0000	0.5785968E-02	0.3368680E-02	-0.4704191E-02
150.0000	0.4363650E-02	0.8456894E-03	-0.4280917E-02
180.0000	0.4129861E-02	-0.1721753E-02	-0.3753840E-02
210.0000	0.6706257E-02	-0.4523931E-02	-0.4950548E-02
240.0000	0.1071279E-01	-0.7927670E-02	-0.7205275E-02
270.0000	0.1526690E-01	-0.9717399E-02	-0.1177499E-01
300.0000	0.1958581E-01	-0.9008205E-02	-0.1739127E-01
330.0000	0.2270287E-01	-0.3943225E-02	-0.2235780E-01
360.0000	0.2397962E-01	0.4437476E-02	-0.2356546E-01

Time: 240°

****
Integrals
****

Integrals on region A

Surface of the region 887.2899 (square mm)
Integ. (A.J) dv = 2.194385
Total ampere turn(s) = -2451.227 (Ampere)
Inductance (1 turn) = 0.3652126E-06 (Henry)

Integrals on region B

Surface of the region 887.2899 (square mm)
Flux through one turn = 0.4140336E-06 (Weber)

Integrals on region C

Surface of the region 887.2905 (square mm)
Integ. (A.J) dv = 2.196395
Total ampere turn(s) = 2451.229 (Ampere)
Inductance (1 turn) = 0.3655465E-06 (Henry)

CURVES
******

Flux density
arc : center X = 0; Y = 0; R = 25.4 (0 -> 360 deg.)

ABSCISSA Deg	MAGNITUDE Tesla	NORMAL C. Tesla	TANGENTIAL C. Tesla
0.0000000	0.3245150E-01	-0.6815398E-03	-0.3244435E-01
30.00000	0.2928055E-01	0.6133155E-02	-0.2863101E-01
60.00000	0.2536932E-01	0.9419190E-02	-0.2355592E-01
90.00000	0.2118664E-01	0.9013218E-02	-0.1917382E-01
120.0000	0.1758438E-01	0.7928691E-02	-0.1569542E-01
150.0000	0.1385781E-01	0.5780186E-02	-0.1259478E-01
180.0000	0.9812193E-02	0.2509080E-02	-0.9485970E-02
210.0000	0.9486578E-02	-0.1710261E-02	-0.9331141E-02
240.0000	0.1311207E-01	-0.7456207E-02	-0.1078570E-01
270.0000	0.1938333E-01	-0.1118056E-01	-0.1583377E-01
300.0000	0.2545395E-01	-0.1210221E-01	-0.2239285E-01
330.0000	0.2973412E-01	-0.8071010E-02	-0.2861777E-01
360.0000	0.3245313E-01	-0.7550271E-03	-0.3244434E-01

Time: 270°

****
Integrals
****

Integrals on region A

Surface of the region 887.2899 (square mm)
Integ. (A.J) dv = 2.978941
Total ampere turn(s) = -2830.455 (Ampere)
Inductance (1 turn) = 0.3718343E-06 (Henry)

Integrals on region B

Surface of the region 887.2899 (square mm)
Integ. (A.J) dv = 0.6303512
Total ampere turn(s) = 1415.227 (Ampere)
Inductance (1 turn) = 0.3147242E-06 (Henry)

Integrals on region C

Surface of the region 887.2905 (square mm)
Integ. (A.J) dv = 0.7059554
Total ampere turn(s) = 1415.228 (Ampere)
Inductance (1 turn) = 0.3524717E-06 (Henry)

CURVES
******

Flux density
arc : center X = 0; Y = 0; R = 25.4 (0 -> 360 deg.)

ABSCISSA Deg	MAGNITUDE Tesla	NORMAL C. Tesla	TANGENTIAL C. Tesla
0.0000000	0.3312257E-01	-0.5689826E-02	-0.3263021E-01
30.00000	0.3276996E-01	-0.1683412E-03	-0.3276953E-01
60.00000	0.3190306E-01	0.5765214E-02	-0.3137782E-01
90.00000	0.2892027E-01	0.9102177E-02	-0.2745054E-01
120.0000	0.2475534E-01	0.1036432E-01	-0.2248127E-01
150.0000	0.1978526E-01	0.9165958E-02	-0.1753402E-01
180.0000	0.1405377E-01	0.6067621E-02	-0.1267645E-01
210.0000	0.1131982E-01	0.1561622E-02	-0.1121159E-01
240.0000	0.1251298E-01	-0.4986972E-02	-0.1147627E-01
270.0000	0.1838508E-01	-0.9648039E-02	-0.1565013E-01
300.0000	0.2450748E-01	-0.1195358E-01	-0.2139459E-01
330.0000	0.2900190E-01	-0.1003626E-01	-0.2720999E-01
360.0000	0.3313212E-01	-0.5745226E-02	-0.3263020E-01

Time: 300°

****
Integrals
****

Integrals on region A

Surface of the region 887.2899 (square mm)
Integ. (A.J) dv = 2.278949
Total ampere turn(s) = -2451.227 (Ampere)
Inductance (1 turn) = 0.3792865E-06 (Henry)

Integrals on region B

Surface of the region 887.2899 (square mm)
Integ. (A.J) dv = 1.885027
Total ampere turn(s) = 2451.227 (Ampere)
Inductance (1 turn) = 0.3137258E-06 (Henry)

Integrals on region C

Surface of the region 887.2905 (square mm)
Flux through one turn = -0.3408459E-04 (Weber)

CURVES
******

Flux density
arc : center X = 0; Y = 0; R = 25.4 (0 -> 360 deg.)

ABSCISSA Deg	MAGNITUDE Tesla	NORMAL C. Tesla	TANGENTIAL C. Tesla
0.0000000	0.2576109E-01	-0.9173471E-02	-0.2407242E-01
30.00000	0.2885151E-01	-0.6424743E-02	-0.2812707E-01
60.00000	0.3079689E-01	0.5663745E-03	-0.3079168E-01
90.00000	0.2916399E-01	0.6752104E-02	-0.2837159E-01
120.0000	0.2531192E-01	0.1002274E-01	-0.2324302E-01
150.0000	0.2044179E-01	0.1009565E-01	-0.1777482E-01
180.0000	0.1481582E-01	0.8000324E-02	-0.1247009E-01
210.0000	0.1101155E-01	0.4415071E-02	-0.1008769E-01
240.0000	0.9168015E-02	-0.1181445E-02	-0.9091572E-02
270.0000	0.1255629E-01	-0.5530253E-02	-0.1127284E-01
300.0000	0.1700022E-01	-0.8601874E-02	-0.1466340E-01
330.0000	0.2072133E-01	-0.9312198E-02	-0.1851098E-01
360.0000	0.2576910E-01	-0.9195937E-02	-0.2407241E-01

Time: 330°

****
Integrals
****

Integrals on region A

Surface of the region 887.2899 (square mm)
Integ. (A.J) dv = 0.7893629
Total ampere turn(s) = -1415.227 (Ampere)
Inductance (1 turn) = 0.3941162E-06 (Henry)

Integrals on region B

Surface of the region 887.2899 (square mm)
Integ. (A.J) dv = 2.509706
Total ampere turn(s) = 2830.455 (Ampere)
Inductance (1 turn) = 0.3132640E-06 (Henry)

Integrals on region C

Surface of the region 887.2905 (square mm)
Integ. (A.J) dv = 0.7893562
Total ampere turn(s) = -1415.228 (Ampere)
Inductance (1 turn) = 0.3941123E-06 (Henry)

CURVES
******

Flux density
arc : center X = 0; Y = 0; R = 25.4 (0 -> 360 deg.)

ABSCISSA Deg	MAGNITUDE Tesla	NORMAL C. Tesla	TANGENTIAL C. Tesla
0.0000000	0.1364529E-01	-0.1019922E-01	-0.9064761E-02
30.00000	0.1935111E-01	-0.1095973E-01	-0.1594835E-01
60.00000	0.2247055E-01	-0.4784224E-02	-0.2195534E-01
90.00000	0.2184529E-01	0.2592890E-02	-0.2169086E-01
120.0000	0.1910409E-01	0.6995687E-02	-0.1777714E-01
150.0000	0.1564844E-01	0.8320352E-02	-0.1325313E-01
180.0000	0.1184432E-01	0.7789467E-02	-0.8922568E-02
210.0000	0.8731195E-02	0.6085591E-02	-0.6260937E-02
240.0000	0.5185366E-02	0.2940654E-02	-0.4270898E-02
270.0000	0.3875732E-02	0.6928587E-04	-0.3875113E-02
300.0000	0.4970135E-02	-0.2945428E-02	-0.4003335E-02
330.0000	0.7789056E-02	-0.6093069E-02	-0.4852206E-02
360.0000	0.1363297E-01	-0.1018273E-01	-0.9064759E-02

Magsoft Corporation 113_01/USI Plot Page 1

Magnetic Field Calculations: Plot

1. Cable Concept #1: Position B1.

This plot shows the flux lines at t = 90°.

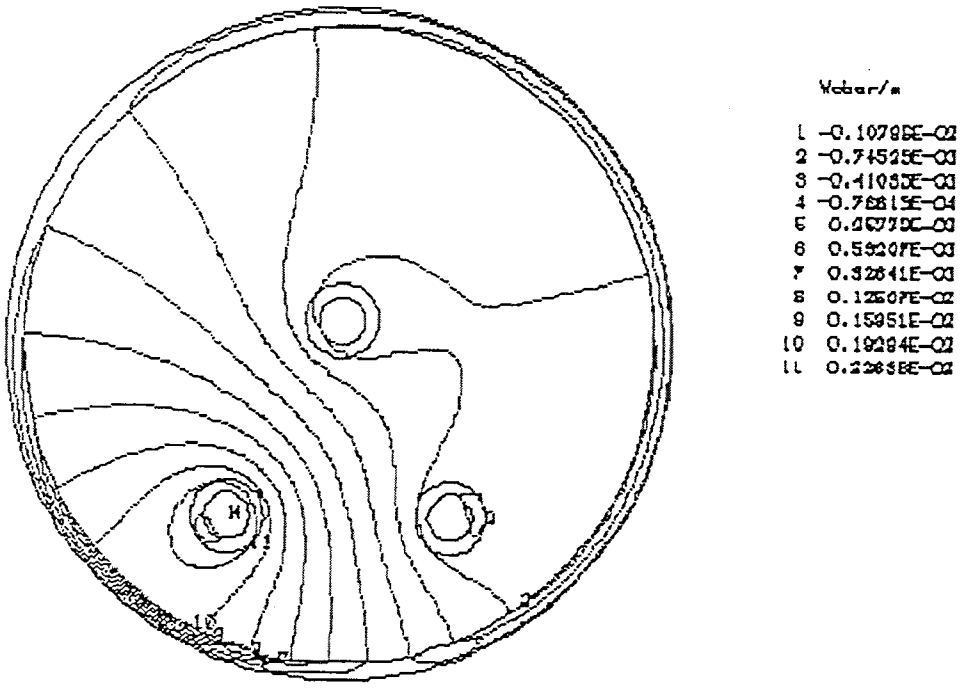

The domain modelled is actually larger than the one shown on this plot. However, there is almost no field outside the pipe. This is in fact the case for any of the studied geometry.

Magsoft Corporation 113_01/USI Plot Page 2

This plot shows the variation of the flux density along the surface of the conductor. Both the variation of the normal component and of the tangential component are shown on this plot.

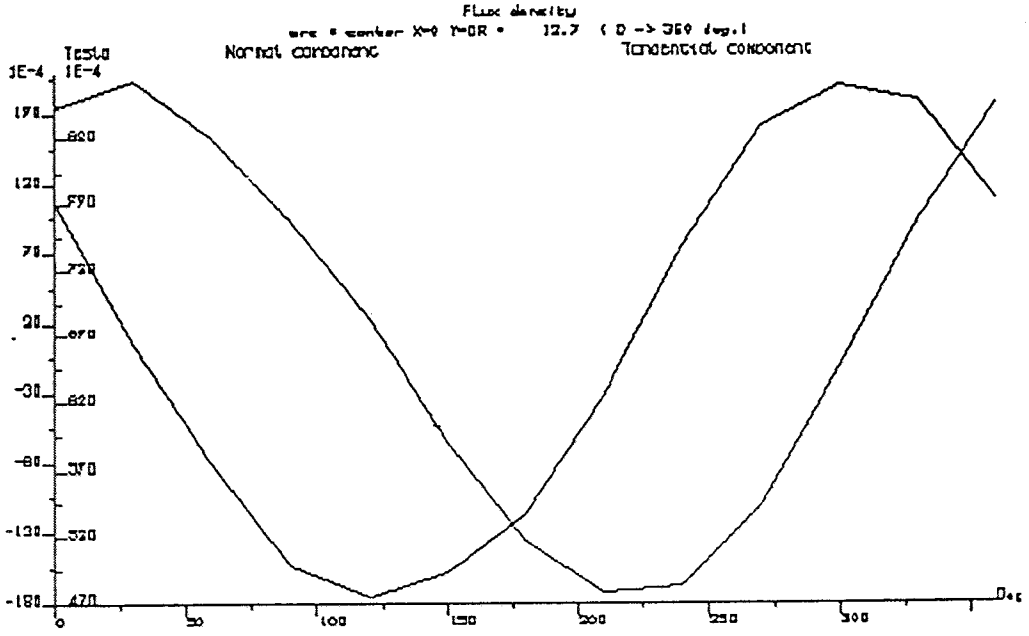

Magsoft Corporation 113_01/USI Plot Page 3

This plot shows the flux lines at t = 0°.

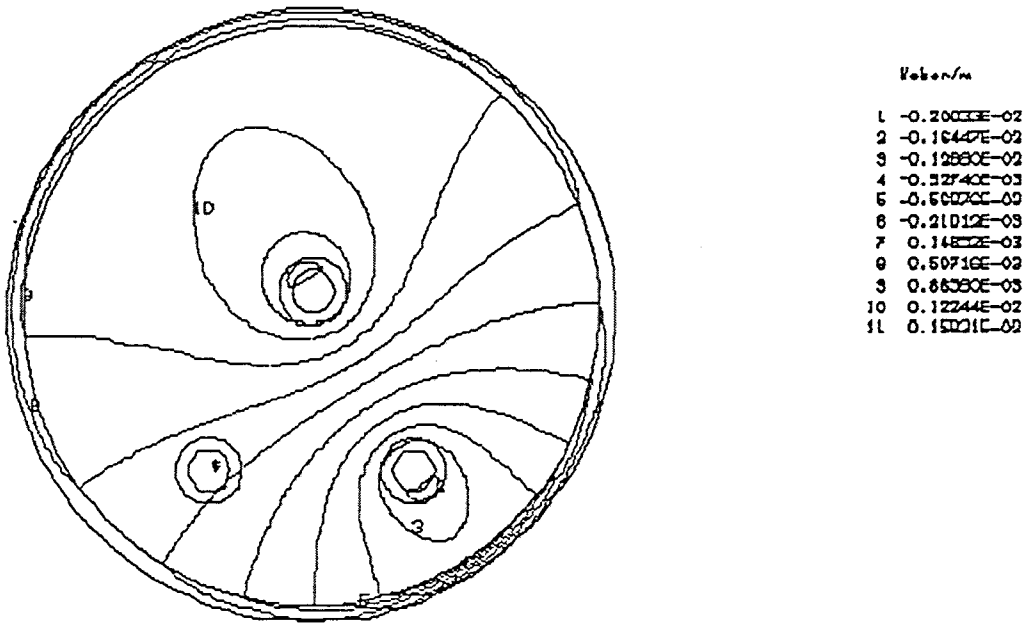

Magsoft Corporation 113_01/USI Plot Page 4

2. Cable Concept #1: Position B2.

This plot shows the flux lines at t = 90°.

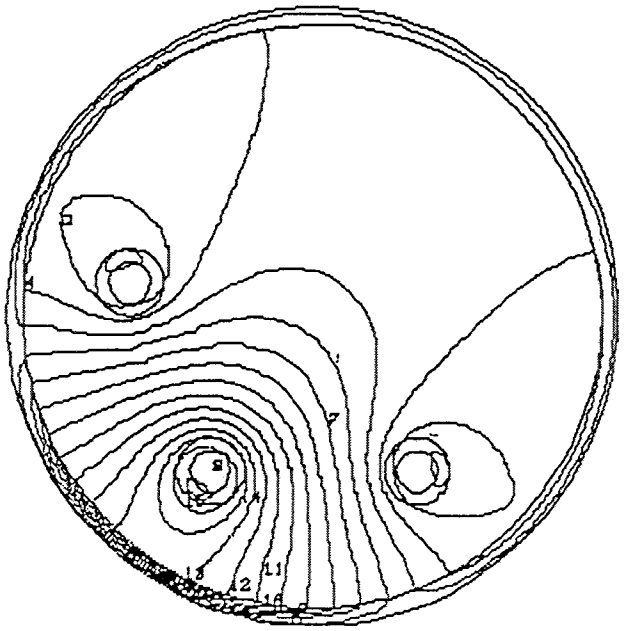

Magsoft Corporation 113_01/USI Plot Page 5

3. Cable Concept #3

This plot shows the flux lines at t = 90°.

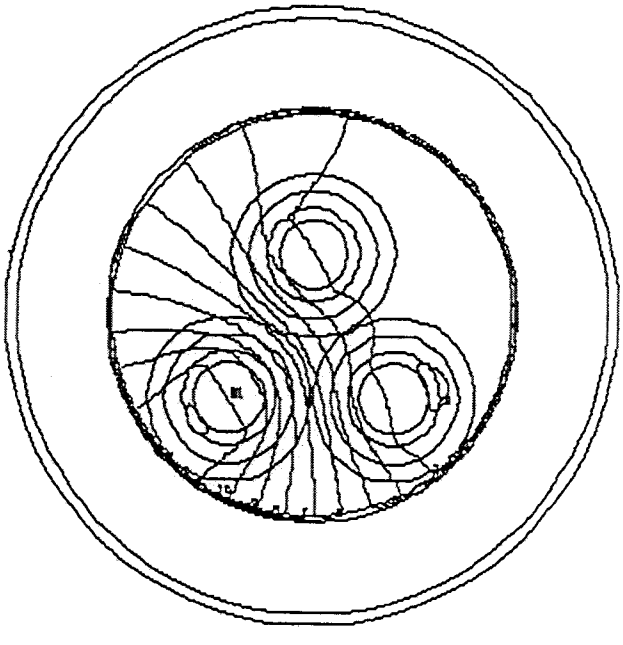

Magsoft Corporation 113_01/USI Plot Page 6

4. Cable Concept #3: Diamagnetic conductor

This plot shows the flux lines at t = 90°.

FLUX2D 6.36 CACOM3 6/28/90 15:41 EXPLOITATION Display Equi flux

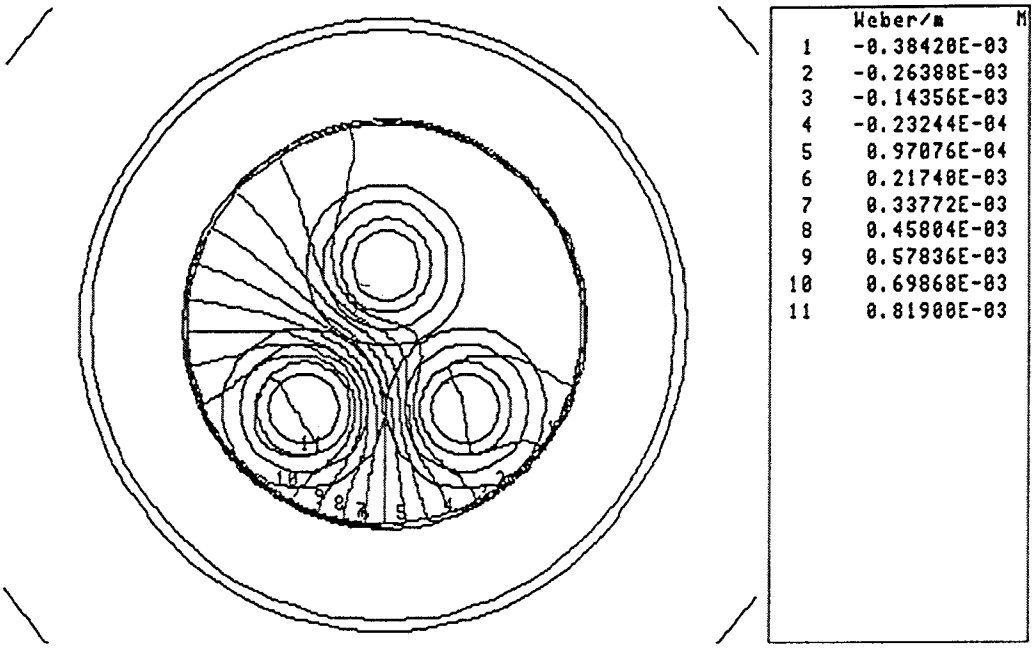

The magnetic permeability of these conductors was set to μ = .75. Less flux lines are actually crossing the conductor than when we use a μ = 1 magnetic permeability.

Magsoft Corporation 113_01/USI Plot Page 7

5. Cable Concept #3: Mesh

The next plot shows the mesh of the complete domain.

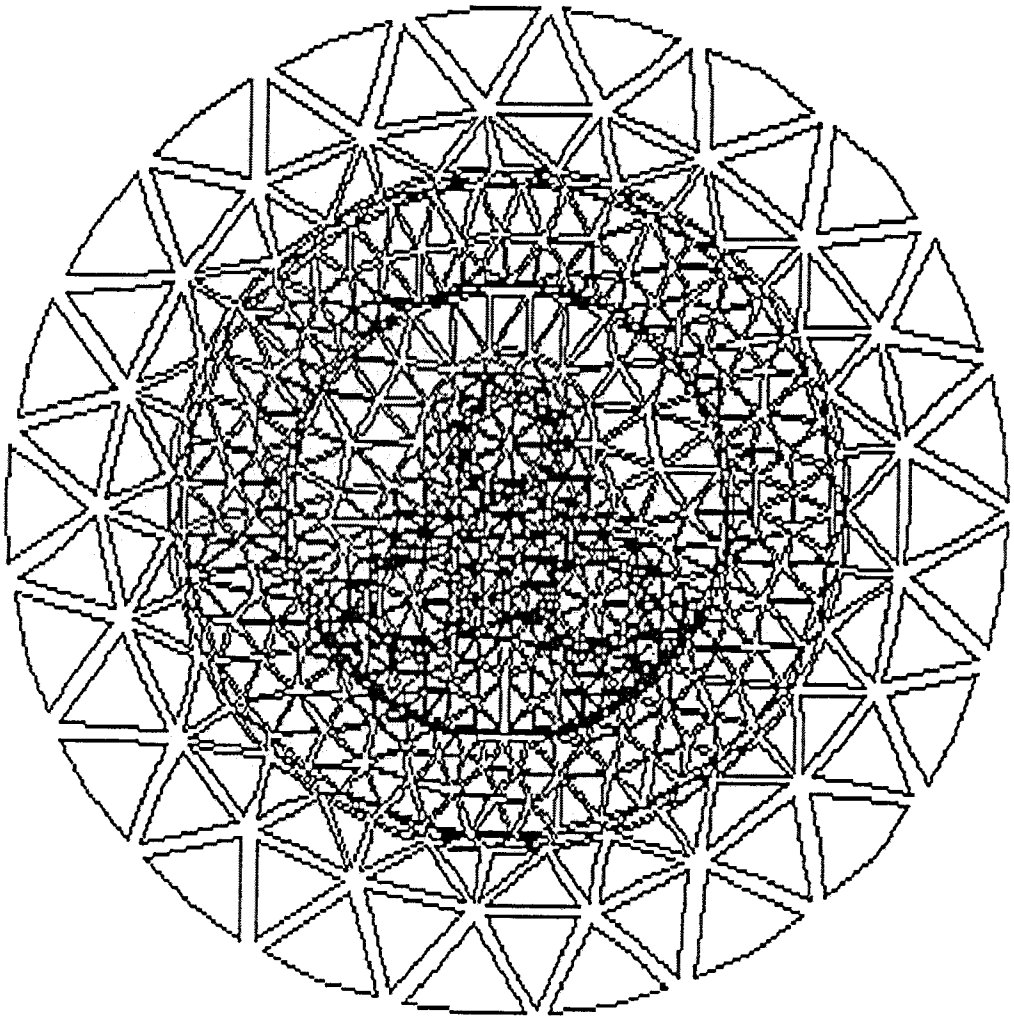

The number of nodes for each of the geometry is around 2000.

Magsoft Corporation 113_01/USI Plot Page 8

The next plot shows a detail of the mesh.

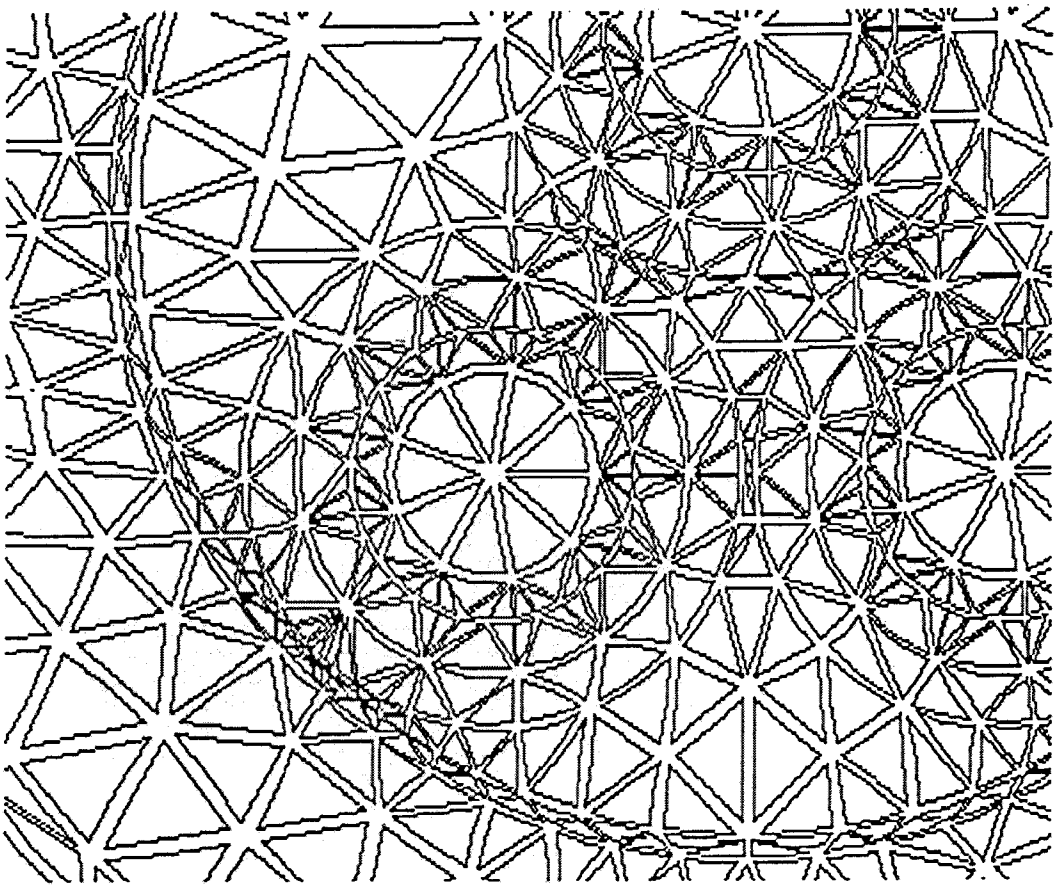

4

CRYOGENIC SYSTEMS

Introduction

This section details the concepts and design parameters for cryogenic systems employed in HTSC based cable systems. The design of the cryogenic system can be subdivided into; (a) design of thermal insulation and (b) design of refrigeration systems. A project team was assembled at the Los Alamos National Laboratory as part of the STI effort to review these two aspects of the cryogenic systems and make suitable recommendations. This effort produced two reports which have been combined to form this section.

Thermal Insulation Options

Four Superconducting Power Transmission Line (SPTL) concepts as shown in Figure 4-1 through Figure 4-4 are being considered in the STI Project; two ac systems (Figures 4-1 and 4-3) and two dc systems (Figures 4-2 and 4-4). The cable concepts shown in Figures 4-1 and 4-2 involve a room-temperature dielectric; thus, the dielectric is on the outside of the thermal insulation. Consequently, existing, widely-used, dielectric technology is applicable because in these two concepts the dielectric operates in the normal condition for conventional electrical insulation. The cable concepts shown in Figures 4-3 and 4-4 have the dielectric on the inside of the thermal insulation; therefore, the dielectric must provide electrical insulation at the cryogenic conditions of the coolant, for which conventional dielectric technology may not be suitable.

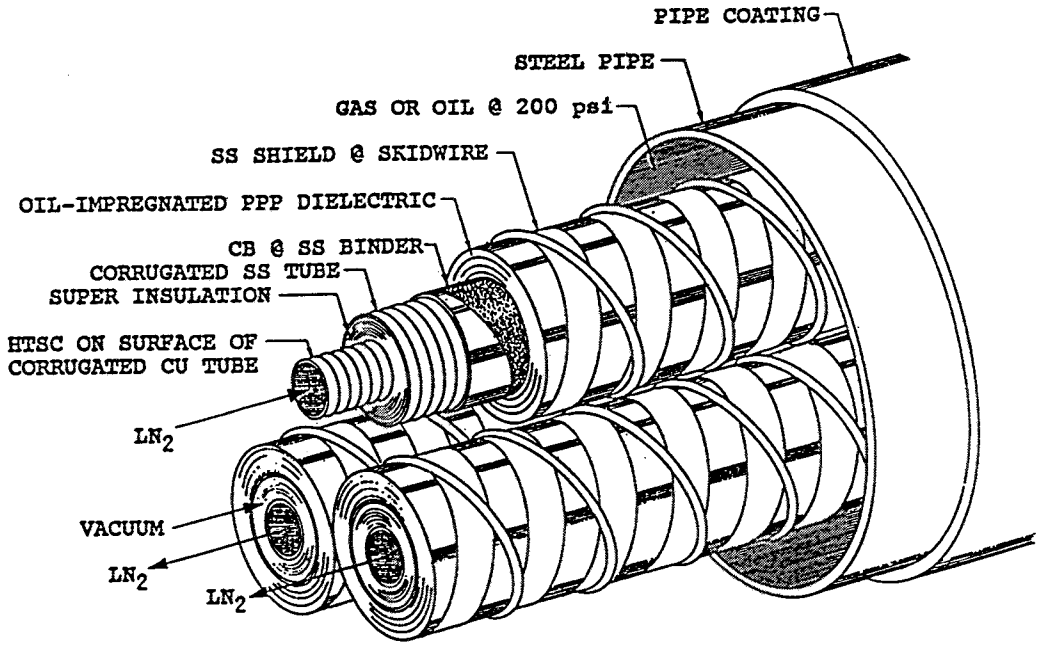

Figure 4-1 High temperature superconducting cable concept for 3-phase ac system with room temperature dielectric.

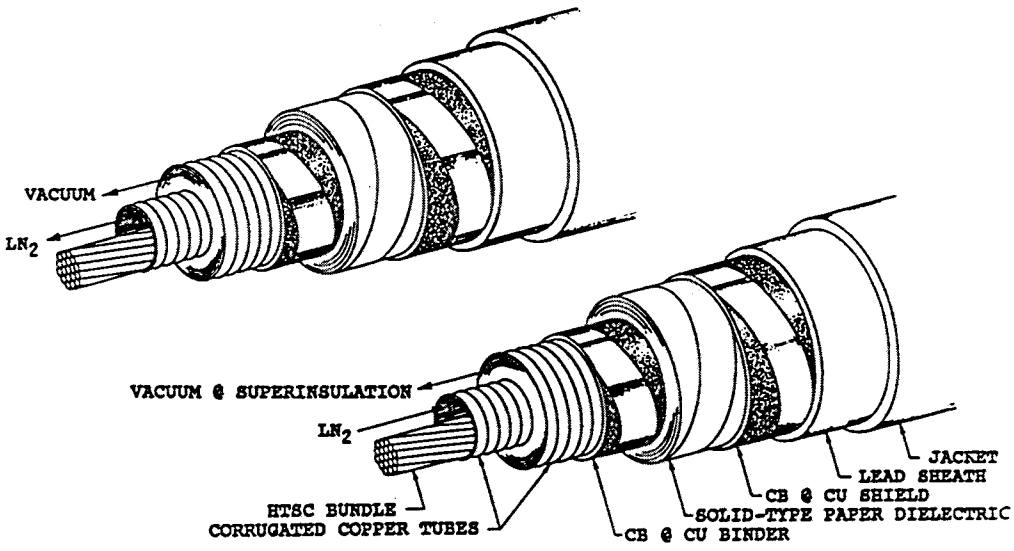

Figure 4-2 High temperature superconducting bipole dc cable concept with room temperature dielectric.

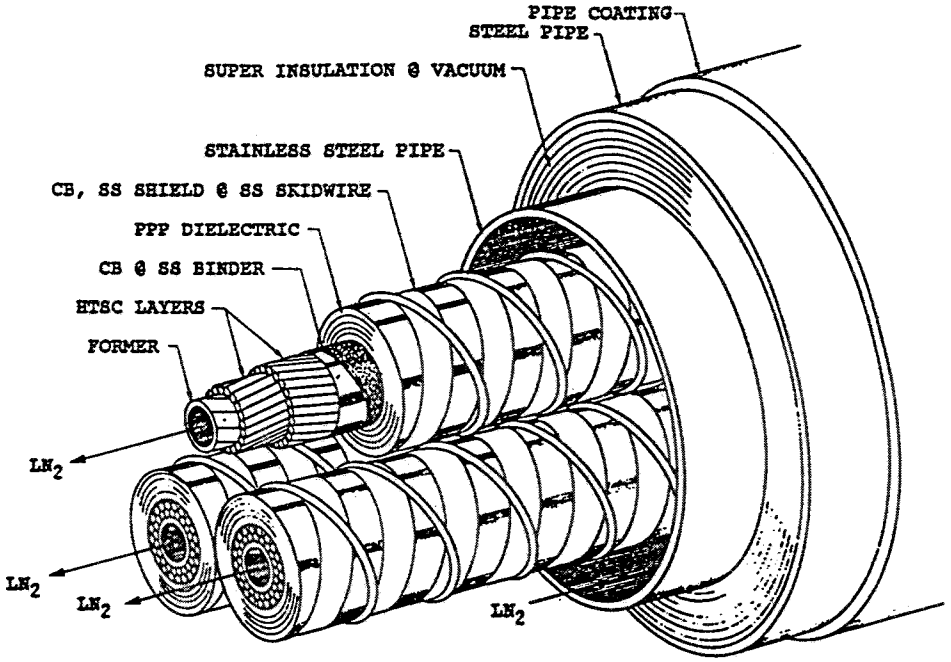

Figure 4-3 High temperature superconducting cable concept for 3-phase ac system with dielectric at cryogenic temperatures.

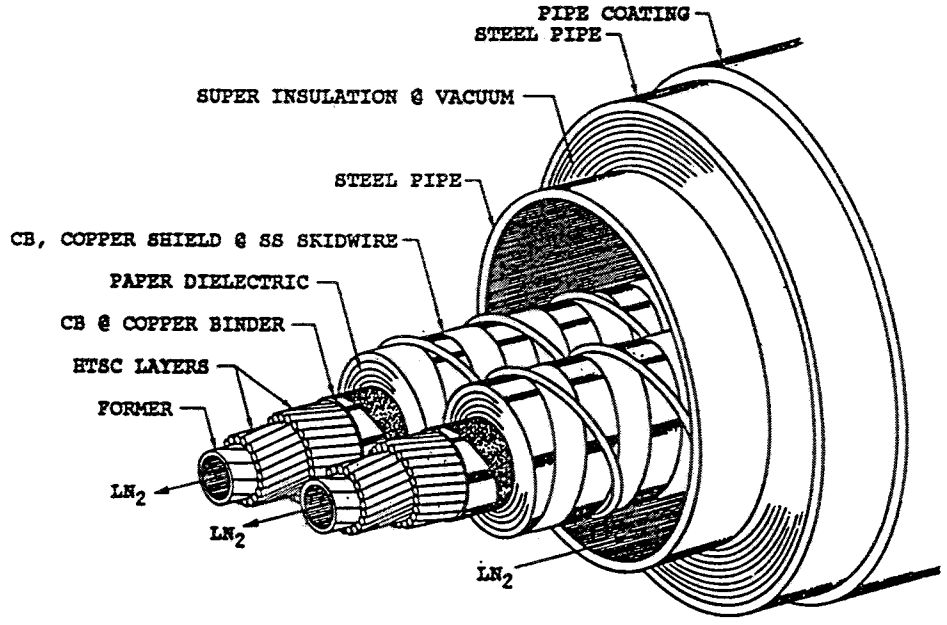

Figure 4-4 High temperature superconducting bipole dc cable concept with dielectric at cryogenic temperature.

The thermal insulation design aspects addressed herein include the following:

* heat transfer mechanisms applicable to an SPTL;
* various thermal insulation types used in cryogenic applications;
* a comparison of the various insulation types;
* outgassing;
* getters;
* an application of the above information for the STI Project;
* issues recommended for further investigation.

Some useful conversion factors are given in the Appendix.

For reasonable values of heat leak and insulation thickness, the most practical insulation for the SPTL application appears to be a multilayer insulation. However, there is some uncertainty in the effective thermal conductivity of multilayer insulation when it is used in an SPTL configuration. This uncertainty should be investigated further. As much as possible, the information presented in the following sections is oriented to an SPTL configuration with upper and lower temperatures of about 300 and 77 K. Because multilayer insulation appears to be the most appropriate insulation type for the SPTL application, more data are presented herein for multilayer insulation than for the other insulation types.

Heat Transfer Mechanisms

The thermal load for an SPTL refrigeration system comes from several sources that include, for example, resistive heating, ac losses in the superconductor, dielectric losses, and heat leak through the cryogenic enclosure. Only the latter source is addressed in this report. An SPTL must have thermal insulation to reduce heat transfer from the ambient environment to the coolant fluid in the transmission line. Four heat transfer mechanisms associated with the thermal insulation that must be considered in an SPTL design are:

* conduction through solid supports, wires, etc.;

* conduction through gas;
* convection; and
* radiation.

Each of these heat transfer mechanisms will be described briefly, and special cases applicable to an SPTL configuration will be discussed.

Conduction

The transfer of heat by conduction occurs when two regions of a medium are maintained at different temperatures and the heat flow rate (transfer) by conduction is given by the Fourier heat conduction equation

$$Q = k(T)A\frac{dT}{dx}, \text{ or } Q = k(T)A\frac{1}{r}\frac{dT}{dr} \quad (1)$$

for rectangular and cylindrical coordinates, where Q is the heat transfer rate (W), k(T) is the temperature-dependent thermal conductivity of the solid (W/m·K), A is the cross-sectional heat conduction area (m^2), T is temperature (K), x is conduction distance (m), and r is conduction radius (m) for cylindrical systems. Eq. 1 is commonly given as

$$Q = k_{eff}\, A\, \frac{T_h - T_c}{S}, \text{ or } \quad Q = 2\pi L k_{eff}\, \frac{T_h - T_c}{\ln\left(\frac{R_h}{R_c}\right)} \quad (2)$$

where k_{eff} is the effective thermal conductivity (W/m·K) over the temperature range of T_h to T_c, T_h and T_c are the temperatures (K) at the hot and cold boundaries of the insulation, S is the length (m) of the conduction path from the hot to the cold boundaries of the insulation, R_h and R_c are the radii (m) at the hot and cold boundaries of the insulation, and L is the length (m) of the cylindrical insulation. Values of k_{eff} for many materials for various temperature ranges, such as 300 to 77 K, are given in Tables 4-5 through 4-11 and compared herein later. Eq. 1 is also often expressed as follows:

$$Q = \frac{A}{S}\left(\int_0^{T_h} k(T)dT - \int_0^{T_c} k(T)dT\right), \text{ or } \quad Q = \frac{2\pi L}{\ln\left(\frac{R_h}{R_c}\right)}\left(\int_0^{T_h} k(T)dT - \int_0^{T_c} k(T)dT\right) \qquad (3)$$

where values of the integrals (in W/m) are tabulated for many materials and at various temperatures as shown in Table 4-1.

Table 4-1 Thermal conductivity integral for several materials commonly used in cryogenic systems.

Material	$\int_{77}^{300} k dT$ (W/m)
Copper	
Electrolytic Tough Pitch (ETP)	93,400
Oxygen Free, High Conductivity (OFHC)	93,400
Phosphorus Deoxidized	40,700
Aluminum	
Commercial pure (99%)	50,800
6063-T5	45,300
Stainless Steel (average types: 303, 304,316,347)	2,740
Glass (average, Pyrex, Quartz, Borosilicate)	182
Nylon	76
PTFE (Teflon)	57
Perspex (organic glass thermoplastic:Lucite, Plexiglas)	53

Heat may be transferred through a gas by conduction without convection. For helium gas at pressures in the range of a few microns (< 10 μ), heat conduction is given by Eq. 4[1] where Q_i is the heat transfer rate to the inner surface as a result of free molecule gas conduction between concentric cylinders (W/m^2), P is the pressure (Pa), C is a constant

$$Q = C\alpha P(T_h - T_c) \tag{4}$$

(with units of m/s·K) defined by Eq. 5, and α is the overall accommodation coefficient (dimensionless) as given by Eq. 6.

$$C = \frac{\gamma+1}{\gamma-1}\sqrt{\frac{R}{8\pi MT}} \tag{5}$$

where γ is the specific heat ratio of the gas ($\gamma = c_p/c_v$) and is assumed constant, R is the universal gas constant (8,314.3 J/kg-mole·K), M is the molecular weight of the gas (kg/kg-mole), and T is the absolute temperature (K) where the pressure P is measured. The temperature at the pressure gage is assumed to be 300 K. Values for the constant C are given in Table 4-2[1].

$$\alpha = \frac{\alpha_i\alpha_0}{\alpha_0 + \alpha_i(1 - \alpha_0)\left(\frac{A_i}{A_0}\right)} \tag{6}$$

where A_i and A_o are the inner and outer surface areas and α_i and α_o are the accommodation coefficients for the inner and outer surfaces. Some suggested values for the individual accommodation coefficients are given in Table 4-3[1].

Table 4-2
Constant C for the Gas Conduction Equation

Gas	Th and Tc (K)	Constant C
Nitrogen	<400	0.0159
Oxygen	<300	0.0149
Hydrogen	(300 and 77)/(300 and 90) 77 and 20	0.0528 0.0398
Helium	any	0.0280

Table 4-3
Approximate Accommodation Coefficients

Temperature (K)	Helium	Hydrogen	Air
300	0.3	0.3	0.3-0.9
77	0.6	0.5	1
20	0.6	1	1

Convection

Heat transfer by convection is a combination of conduction and mass transfer in the fluid and results in the transfer of heat between a solid surface and a fluid (either a gas or a liquid). The heat transfer rate for convective heat transfer is given by

$$Q = hA_c(T_s - T_g) \tag{7}$$

where T_s is the temperature of the surface (K), T_g is the temperature of the fluid (K), h is the convective heat transfer coefficient (W/m^2K), and A_c is the area of the surface in contact with the fluid (m^2).

Radiation

Heat transfer by radiation is different from both convection and conduction heat transfer in that energy transfer occurs by electromagnetic radiation; therefore, physical contact between two objects is not necessary for heat transfer to take place. The single similarity between radiant heat transfer and convection or conduction heat transfer is that there must be a temperature difference between the radiating source and the receiving body. Radiant heat transfer from the hot to the cold surface, $Q_{h,c}$, is given by

$$Q = \sigma \mathcal{F}_{h,c}\, t\, (T_h^4 - T_c^4) \tag{8}$$

where σ is the Stefan-Boltzmann constant equal to 5.67×10^{-12} W/cm^2K^4, $\mathcal{F}_{h,c}$ is a factor involving the emissivities of the two surfaces, A_h is the area of the hot surface (cm^2).

For a cylindrical geometry (which is typical for the SPTL application), A_h is the area of the enclosing (outer) cylindrical surface. The value of $\mathcal{F}_{h,c}$ for a cylindrical geometry depends on whether the reflections at the enclosing surface are specular (mirror-like) or diffuse (i.e., with intensity proportional to the cosine of the angle between the direction of emission and the surface). The mode of reflection at the enclosed surface is immaterial. For long coaxial cylinders $\mathcal{F}_{h,c}$ is given for specular reflection by

$$\mathcal{F}_{h,c} = \frac{e_i e_0}{e_0 + (e_i)(1 - e_0)} \tag{9}$$

and for diffuse reflection by

$$\mathcal{F}_{h,c} = \frac{e_i e_0}{e_0 + (e_i)\left(\frac{A_i}{A_0}\right)(1-e_0)} \tag{10}$$

where A_i and A_o are the areas of the inner and outer surfaces respectively, and e_i and e_o are the emissivities of the inner and outer surfaces respectively (for grey surfaces -- that is, surfaces for which the emissivity is independent of wave length). (The assumption of greyness is not strictly correct but can be shown to introduce negligible error in practical applications)[2]. Typical values for total normal emissivity (rate of radiant energy emission normal to the surface divided by the corresponding rate from a black body) for several materials are given in Table 4-4. If a number, n, of parallel sheets of highly reflective material are positioned between the surfaces at T_h and T_c in such a way that the sheets are thermally isolated from each other, then the radiative exchange between the surfaces will approach a steady-state distribution such that the net heat flow by radiation, Q_n, is[3]

$$Q_n = \sigma \mathcal{F}_{h,c} A_h \frac{(T_h^4 - T_c^4)}{2(n+1)} \tag{11}$$

Table 4-4
Emissivity of various materials

Material	Material treatment	Temperature (K)	Emissivity[e]
Aluminum	annealed (electropolished)	300	0.03
			0.018 (76 K) [a]
Aluminum with oxide layer	0.25 micron thick	311	0.06
	1 micron thick	311	0.30
	7 micron thick	311	0.75
Vaporized Aluminum	onto 0.5 mil Mylar plastic [d]	300	0.04 (76 K) [a]
Copper	black oxidized	300	0.78
	scraped	300	0.07
	commercial polish	300	0.03
	electrolytic, careful polish	295	0.015 (76 K) [a]
	chromic acid dip	295	0.017 (76 K) [a]
	polished	295	0.019 (76 K) [a]
	liquid honed [b]	295	0.088 (76 K) [a]
	carefully prepared surface of pure Cu	295	0.0082 (90 K) [a]
Gold	15 mil foil (on glass or Lucite plastic)	295	0.01 (76 K) [a]
	5 mil foil (on glass or Lucite plastic)	295	0.016 (76 K) [a]
	vaporized onto 0.5 mil Mylar plastic[d]	295	0.02 (76 K) [a]
	0.2 mil plate[c] on stainless steel	295	0.025 (76 K) [a]
	0.05 mil plate[c] on stainless steel	295	0.027 (76 K) [a]
Lacquer	white	373	0.925
	black matte	373	0.97
Nickel	electroplated on copper	300	0.03 (76 K) [a]
	electrolytic	295	0.04
	4 mil foil	295	0.022 (76 K) [a]
Paper		373	0.92
Silver		295	0.022
		295	0.01 (76 K) [a]
Stainless steel	polished	373	0.08
	type 302	300	0.048 (76 K) [a]

[a] Total hemispherical absorptivity,
[b] A commercial liquid "sandblast",
[c] 1% Ag in Au,
[d] Both sides,
[e] An emissivity value followed by a temperature denotes absorptivity at that temperature for black body radiation of the temperature listed in the "Temperature" column.

The mean effective thermal conductivity of MLI, assuming that there is only radiative heat flux through the MLI, can then be defined by[3]

$$k_{eff} = \sigma \mathcal{F}_{h,c} t \frac{(T_h^4 - T_c^4)}{(n+1)(T_h - T_c)} \quad (12)$$

where t is the thickness of the total space occupied by the MLI; this is not necessarily the distance between the inner and outer walls because the MLI may not fill this space completely.

Special Cases Applicable to a Superconducting Power Transmission Line

SPTL With Convection to Air. An SPTL installed above ground will involve heat transfer by both conduction through the thermal insulation and convection to the surroundings (air). For this situation, a combination of Eqs. (2) and (7) applies, giving[4]

$$Q = \frac{2 \pi L k_{eff} (T_h - T_c)}{\ln\left(\frac{R_h}{R_c}\right) + \frac{k_{eff}}{hR_h}} \quad (13)$$

for cylindrical coordinates and those thermal insulations described later except for the vacuum only case. For this case Eqs. (7) and (8) can be used to determine the impedance to heat transfer of the vacuum and the convection film resistance to the external atmosphere.

SPTL Buried in Ground. An SPTL buried in the ground will involve heat transfer by conduction through the thermal insulation and the soil. For this situation, the heat transfer is given by the following relationship[5]

$$Q = \frac{2\,\pi\,L\,k_i\,k_s\,(T_a - T_c)}{k_s \ln\left(\frac{R_{oi}}{R_{ii}}\right) + k_i \ln\left(\frac{2Z}{R_{oi}}\right)} \qquad (14)$$

where k_i and k_s are the effective thermal conductivity (W/m·K) of the thermal insulation and the soil, respectively; T_a is the ambient temperature (K) at the top of the soil; R_{oi} and R_{ii} are the radius (m) of the outside and inside of the thermal insulation, respectively; and Z is the distance (m) from the top of the soil to the center line of the SPTL. Eq. 14 applies for cylindrical coordinates and those thermal insulations described later except for the vacuum only case.

SPTL with Dielectric Outside the Thermal Insulation. One of the designs being considered for the STI project involves the location of the electrical dielectric outside the thermal insulation so that the dielectric is near room temperature, not at cryogenic temperature. For this situation the heat transfer is given by

$$Q = \frac{2\,\pi\,L\,k_i\,k_d\,(T_a - T_c)}{k_d \ln\left(\frac{R_{oi}}{R_{ii}}\right) + k_i \ln\left(\frac{R_{od}}{R_{oi}}\right)} \qquad (15)$$

where k_d is the effective thermal conductivity (W/m·K) of the electrical dielectric, R_{od} is the outer radius (m) of the electrical dielectric, and T_a is the ambient temperature on the outside of the electrical dielectric. Eq. 15 applies for cylindrical coordinates and those thermal insulations described later except for the vacuum only case.

Multilayer Insulation. Heat transfer through multiple shields [multilayer insulation (MLI) -- also called superinsulation in high vacuum ($< 10^{-3}$ torr) is by radiation, residual gas conduction, and solid conduction. A semiempirical relationship that has been used to predict the performance of MLI systems is[6]

$$k = C_s N^{1.56} (T_h + T_c) + \frac{C_r \varepsilon_{tr} \left(T_h^{4.67} - T_c^{4.67}\right)}{N (T_h - T_c)} \quad (16)$$

where k is the effective thermal conductivity (W/cm·K) of the MLI, $C_s = 4.48 \times 10^{-12}$, $C_r = 5.40 \times 10^{-14}$, N = layers/cm, and ε_{tr} is the room-temperature total hemispherical emittance (commonly 0.03 is used). The first term on the right side of this expression is the conductive component and the second term is the radiative component of heat transfer. This semiempirical relationship is based on flat-plate measurements for a system using double aluminized Mylar shields separated by two silk net layers, with layer densities ranging from 18 to 50 layers/cm.[6]

The heat transfer through MLI in high (< 10^{-3} torr) vacuum considering radiation, residual gas conduction, and solid conduction is given by[7]

$$Q = \frac{\sigma A \varepsilon_0 \varepsilon_s (T_h^4 - T_c^4)}{\varepsilon_0 (N_t - 1) + 2\varepsilon_s} + \alpha C A P (T_h^{0.5} - T_c^{0.5}) + \frac{k A_c (T_h - T_c)}{N\delta} \quad (17)$$

where Q is the total heat transfer rate, A is the total area of the inner plate, A_c is the average layer to layer contact area, C is a residual gas conductivity factor, ε_o is the emissivity of the boundary, ε_s is the emissivity of the layers, k is the average solid thermal conductivity, N_t is the total number of MLI layers, P is the absolute pressure in the MLI system, α is the accommodation coefficient for residual gas conduction, d is the thickness of the Mylar on the MLI, and s is the Stefan-Boltzmann constant.[7]

A product specification brochure by R. G. Hansen & Associates gives the following expression for the heat transfer between two parallel surfaces of equal area in a vacuum better than 10^{-4} torr for MLI consisting of thin layers of crinkled aluminized mylar that is 0.00025 in. thick:

$$Q = \left\{\frac{A_{1s}}{N}\right\} \{(1 \times 10^{-12})(T_h^4 - T_c^4) + (4.2 \times 10^{-8})(S_d^{1.5})(T_h - T_c)\} \quad (18)$$

where A_{1S} is the area of one of the surfaces (in.^{2}), N_m is the number of Mylar layers, and S_d is the layer density in sheets per inch. A summary of various analytical and empirical equations for predicting the performance of multilayer insulation is given in Ref. 8.

Thermal Insulation

Although no material in any presently conceived arrangement can completely obstruct the flow of heat, the flow can be reduced.[9] The starting point for the improvements in the effectiveness of thermal insulations was the development of the double-wall, vacuum-insulated Dewar flask.[9] Since that time, the field has been characterized by steady progress rather than brilliant new discoveries; new materials, improved methods of heat transfer analysis, and experimental measurements of thermal properties have been developed.[9] However, because economic considerations very often govern the choice of materials, insulations are usually selected on the basis of application requirements and cost as well as insulation effectiveness.[9]

Thermal insulations are designed to reduce heat flow between their boundary surfaces over a specified temperature range. They can consist of either a single material, a mixture of materials, or a composite structure.[9] The effectiveness of a thermal insulation, determined by its effective thermal conductivity, is a function of the physical structure of the material.[9] In general, its effectiveness depends on the temperature and emittance of the boundary surfaces, the density of the material, the type and pressure of gas contained within the insulation, the arrangement of the insulation components, and the compressive loads, vibration, and mechanical and thermal shocks to which the insulation is subjected.[9]

A single homogeneous material cannot withstand all of the extreme temperature conditions encountered by thermal insulations at cryogenic temperatures without introducing serious design penalties.[9] Therefore, combinations of materials with desired properties have been found to be more effective.[9] These combinations may take the form of a matrix characterized by a discontinuous phase, such as particles, flakes, or fibers dispersed in various proportions, a laminate of two or more layers either bonded together or held loosely in a multilayer fabric, or a low-density core of a honeycomb or foamed material having acceptable structural and mechanical properties when encased by sheaths of higher-density material.[9] Such composite materials can be assembled into a thermal insulation system to combine maximum insulating effectiveness with desired structural integrity.[9] The system approach to thermal insulation permits the choice of different materials according to physical, chemical, or mechanical properties which make them suitable for particular functions.[9] The most effective load-carrying elements can be used to bear such outside forces as compressive loads, vibration, and shock, and to support an outer environment-excluding structure.[9] The integration of the insulating material and load-bearing elements requires careful selection of the component materials and care in the design and application of the system.[9]

Types of thermal insulation commonly used in cryogenic applications are listed below in order of increasing cost and increasing effectiveness; however, the selection of a thermal insulation material will also involve other factors such as ease of application, weight, and ruggedness.[10] Some of the common materials for each of these types are also given below, but not in any particular order of effectiveness, cost, etc.

* expanded foams;
  - polyurethane
  - polystyrene
  - epoxy
  - rubber
  - silica

- glass

* gas-filled powders;
  - -perlite (a crushed and expanded volcanic rock, made primarily of silica and alumina)
  - Cab-O-Sil (silica powder)
  - Microcel (calcium silicate)
  - Santocel (silica aerogel)
  - diatomaceous earth
  - powdered cork
  - Vermiculite
* gas-filled fibers (loosely compacted fibrous insulation);
  - Fiberglas
* vacuum alone (both static and dynamic vacuum systems);
* vacuum with powder or fibrous materials;
* vacuum with opacified powders; and
  - copper flakes
  - aluminum flakes
  - silver flakes
  - nickel flakes
* vacuum with multilayer insulation.

The performance of any insulation in an actual installation will be greatly affected by the applied compressive loads, the design of supports, the manner in which the insulation is attached, and the means devised to prevent thermal short-circuiting as a result of penetrations.[9]

The technique of using a refrigerated shield at a temperature between ambient temperature and the temperature of the cryogen to reduce heat input to the cryogen has

not been considered for use in the design of a high-temperature superconducting power transmission line because of the added complexity and expense, decreased reliability, and minimal benefit for operation at liquid nitrogen temperature.

Expanded-Foam Insulations (Nonevacuated and Evacuated)

Expanded-foam insulations have a cellular structure formed by the evolution of a large volume of gas during the manufacture of the foam.[2,10] The materials formed in this manner are useful for insulation for low-temperature applications if the cells in the material are small and do not communicate with each other.[2] However, the insulating capability of such foams seldom approaches that of ordinary permeable materials such as powder because the solid conducting paths in the foam are continuous even though they may be tortuous.[2] Carbon dioxide, which has a low vapor pressure at liquid nitrogen temperature, is the foaming gas used with many of the expanded foams.[2,10]

The foams of most interest in cryogenic applications are the "more or less closed-cell" foams of polystyrene, epoxy, polyurethane, rubber, silica, and glass.[1] Polyurethane and polystyrene foams are the two most commonly used foams for cryogenic applications.[11]

Organic foams are made in a low density range, exhibit good fabrication properties, and are relatively low in cost.[12] The two basic types of organic foams are thermoplastic (heat softening) and thermosetting (heat hardening).[12] The typical thermoplastic foams which soften at temperatures of 258 to 394 K are made from polystyrene, polyvinyl chloride, polyethylene, and polypropylene.[12] Thermosetting foams are usually made with phenolic, ureaformaldehyde, epoxy, and polyurethane resins.[12]

In general, the thermal conductivity of a foam is determined by the interstitial gas contained in the cells plus internal radiation and a contribution from solid conduction.[1] The thermal conductivity of foams is usually dominated by the conduction of the interstitial gas.[11] The thermal conductivity of some selected foam types is given in Table 4-5.

Table 4-5
Apparent mean thermal conductivity of selected foam and other solid insulations for boundary temperatures of approximately 300 K and 77 K.

Foam	Density (kg/m^3)	Gas pressure (torr)	Thermal Conductivity (mW/m-K)	Reference
Balsa Wood (across grain)	117	760	47[a]	34
	141	760	55[a]	34
	320	760	83[a]	34
Corkboard -- no added binder	86	760	36[a]	34
no added binder	112	760	39[a]	34
no added binder	170	760	43[a]	34
no added binder	224	760	48[a]	34
with asphalt binder	232	760	47[a]	34
Epoxy resin	80	760	33	1,34
	80	10^{-2}	16.8	1
	80	4×10^{-3}	13	1
Glass	140	760	35	1,10
Polystyrene	32		33	2
	38	760	33	34
	39	760	33	1,10
	46	760	26	1,10,34
	80	760	33	34
Polyurethane	11	--	33	10
	32	--	12	35
	32	760	28	36
	80-140	760	33	1,34
	---	10^{-3}	12	1
Rubber	80	760	36	1,10,34
Silica	160	760	55	1,10,34
Silica Aerogel	136	760[b]	16.8	36

[a] Boundary temperatures not specified
[b] Air environment

Evacuation of most foams reduces the thermal conductivity as shown in Figure 4-5 and Table 4-5, thus showing the partial open-cell nature of most of these materials.[1]

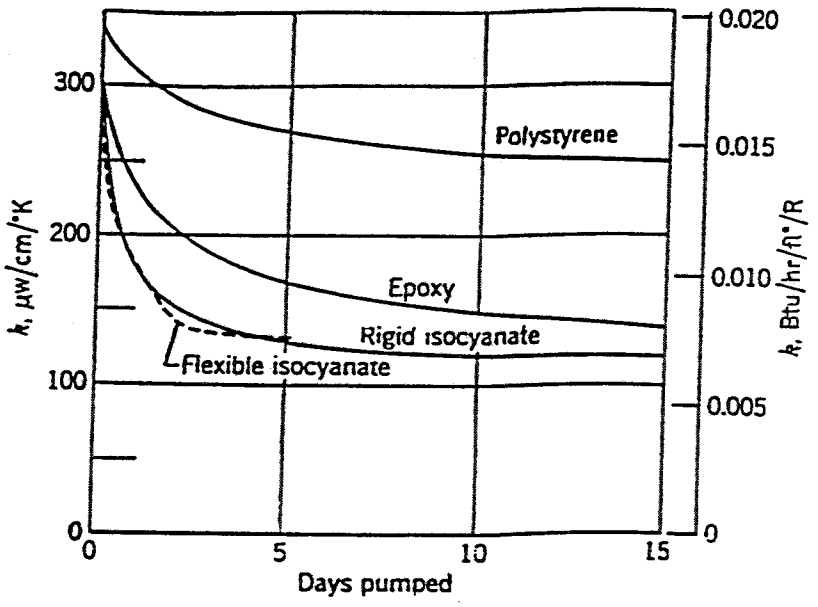

Figure 4-5. Apparent mean thermal conductivity between 300 K and 76 K of some selected foams as a function of time under evacuation (SOURCE: Reference 1)

However, even under evacuation, foam insulations have much higher conductivities than the other types of insulation described herein.[1]

The thermal conductivity of fresh (newly manufactured) foam is decreased when one side is initially cooled to liquid-nitrogen temperature because much of the CO_2 (or other foaming agent) condenses within the insulation. However, after the foam has been exposed to ambient air for a few months air diffuses into the cells and replaces some of the CO_2 and the thermal conductivity may increase as much as 40%. If the foam is exposed to an atmosphere of hydrogen or helium for an extended period of time, the thermal conductivity may be increased by as much as a factor of 3 or 4 because of the higher thermal conductivity of H_2 or He gas, compared with CO_2.[1,10] In this aspect Freon-blown foams are similar to the CO_2-blown foams.[1]

Cost and ease of application are major advantages for the use of foam insulations. Some of the foams can be foamed in place by mixing the appropriate monomer, foaming agent, and catalyst and pouring this mixture into the space that is to be filled with foam.

A major disadvantage of foams is their large thermal contraction, and not necessarily their high thermal conductivity[10]. When applied to a metal surface that experiences thermal cycling from room temperature to low temperatures, the foams tend to crack and lose their insulation capability[10,11]. The foams shrink more (eg., by a factor of 5) than the metal during cooldown and, consequently, the foam cracks, which allows air and water vapor to enter the cracks and seriously degrade the insulating performance. This problem is often addressed by using contraction joints in the foam and enclosing the foam in a plastic liner (such as Mylar) to prevent diffusion of air and water vapor into the joints[10].

Powder and Fibrous Insulations (Gas-Filled, Evacuated, and Opacified)

Gas-Filled. Permeable materials of low density, such as powders and fibers with gas at atmospheric pressure in the interstices, can be used for insulation in cryogenic applications where the low temperature does not go below liquid nitrogen temperature[2]. In this type of insulation, the volume of the gas in the voids may be 10 to 100 times the volume of the solid material[2].

The primary mechanism for insulation in gas-filled powders and fibrous materials is the reduction or elimination of convection as a result of the small size of the voids within the material[10]. Thermal radiation is also reduced by this type of insulation. In addition, with very fine powders, the distance between the powder particles may become smaller than the mean free path of the gas within the insulation, and the gaseous conduction mechanism shifts from continuum to free molecular conduction[1,10]. In this case, the effective thermal conductivity of the gas is decreased, and the thermal conductivity of the material is correspondingly smaller than that for powders with larger particles[10].

Powder (finely divided particulate materials) and fibrous insulations include fiber glass, powdered cork, perlite (a naturally occurring siliceous volcanic rock that when heated to a suitable point expands four to twenty times its original volume), Santocel (silica

aerogel), rock wool, expanded SiO_2, calcium silicate, diatomaceous earth, and Vermiculite[1,10,11]. Some representative thermal conductivity values for these insulations are given in Table 4-6, and some thermal conductivity values as a function of temperature are shown in Fig. 4-6. The thermal conductivity of the better insulators shown in Fig. 4-6 approaches the thermal conductivity of air (26.4 mW/m·K at 300 K and 7.5 mW/m·K at 80 K),[2] indicating that air, which occupies the voids, is responsible for most of the heat conduction.[2] This suggests the principle of gas-filled insulation.[2] The solid portion of the insulation stops radiation and gas convection.[2] In the ideal case the conduction through the solid would be negligible and the gas in the voids would be responsible for the heat flow.[2] In actual insulations the solid particles of powder or the fibers short-circuit the heat flow through the gas to some extent and the resultant thermal conductivity is usually somewhat greater than that of the gas alone.[2] There is one exception; very fine powders sometimes have such small distances between the solid particles that the mean free path of the gas is greater than the interstitial distance; hence its thermal conductivity is reduced as it would be by decreasing the pressure.[2] Thus it is possible for a powder insulation to have a thermal conductivity less than that of the gas that fills the voids even when the gas is at atmospheric pressure.[2]

One disadvantage of gas-filled fibrous materials is that moisture and air can diffuse through the material to the cold surface unless a vapor barrier, or a continual purge of dry nitrogen, is used.[10] If the warm surface of an insulation of this type is exposed to the atmosphere, water vapor will diffuse through and deposit as ice in the cold inner layers of the insulation, greatly increasing the thermal conductivity.[2]

Because the gas in the insulation is at atmospheric pressure, the temperature of the cold surface must not go below the condensing point of the gas (about 81.5 K for air, or 77 K for nitrogen).[2] If the gas in the insulation condenses, it will constitute a large heat leak as a result of reflux -- condensation on the cold surface, dripping of liquid into the warmer insulation and evaporation from the warm surface.[2] Also, if the insulation is

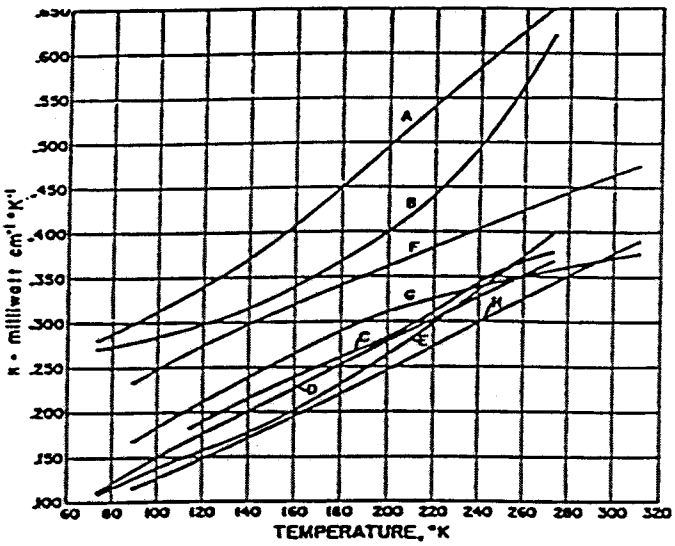

A- Vermiculite 10-14 mesh
B- Sawdust
C- Granulated cork, 50% 10-20 mesh, 50% less than 20 mesh
D- Seaweed product (powder)
E- Crude cotton wadding
F- Vegetable fiber board
G- Cork board
H- Glass fiber board

Figure 4-6 Thermal conductivity of several permeable materials at low temperatures.

combustible, the condensation of air constitutes a fire hazard.[2] Helium can be used in a gas-permeated insulation below 77 K, but the high thermal conductivity of He (7.5 times that of N_2 at 100 K) is a serious disadvantage.[2] By using helium the thermal conductivities of the better materials shown in Fig. 4-6 would be increased by a factor of 5 or more.[2] However, for a very fine powder such as silica aerogel or some grades of perlite, the ordinary thermal conductivity of He may not apply.[2] Because He has a mean free path about 3 times that of air its thermal conductivity would be reduced more by the small interstitial distances.[2] Values of thermal conductivity of several materials filled with N_2, H_2, and He are shown in Table 4-6.

Perlite is a very common powder used for cryogenic applications down to liquid hydrogen temperature; its thermal conductivity as a function of density is given in Fig. 4-7. These data represent perlite (1) of various particle sizes, (2) fired in several types of furnaces, and (3) manufactured from various ore deposits.[1,11] The dashed curves in Fig 4-7 indicate maximum deviation for 95% of the samples.

Table 4-6
Apparent mean thermal conductivity of several gas-filled powders and fibrous insulations for boundary temperatures of approximately 300 K and 77 K

Insulation	Density (kg/m^3)	Gas pressure (torr)	Thermal conductivity (mW/m-K)	Reference
Calcium silicate (synthetic)[l]	360	628[e]	45.5[n]	1
Fiber glass	110	---	25[a]	10
Fiber glass [p]	64	760	29.4	36
Mica, expanded	150[k]	628[e]	50.3[n]	1
	150	628[b]	150[n]	1
Perlite	50	---	26[a]	10
	210	---	44[a]	10
	80.3-96.3	---	126[b,c]	2
	80.3-96.3	---	32[c,e]	2
	96	760	28[o]	36
	100[h]	628[e]	33.2[n]	1
	100[h]	628[b]	127[n]	1
	100[h]	628[f]	146[n]	1
	130[i]	628[e]	32.5[n]	1
	130[i]	628[b]	126[n]	1
	130	628[f]	145[n]	1
	140 [j]	628[e]	35[n]	1
	140 [j]	628[b]	135[n]	1
	140 [j]	628[f]	145.3[n]	1
Rock wool	160	---	35[a]	10
Silica [g]	60	630[e]	18.5[n]	1
Silica aerogel [m]	80	---	19[a]	10
	100 [d]	628[e]	19.6[n]	1
	100	628[b]	62[n]	1
	100	628[f]	80[n]	1
Vermiculite	120	---	52[a]	10

[a] Lower boundary temperature = 90K,
[b] Helium filled,
[c] 15 cm-layer,
[d] 250A,
[e] Nitrogen filled,
[f] Hydrogen filled,
[g] Flame prepared, 150-200A,
[h] +30 mesh,
[i] 0.02 to 0.07 micron
[j] 80 mesh
[k] -30 to 15 mesh 70%,
[l] 0.02 to 0.07 micron,
[m] Santocel = Silica Aerogel. Aerogel = SiO_2
[n] 2.54 cm thick sample. Wall emissivities greater than 0.8,
[o] Boundary temperatures and fill gas not specified,
[p] AAAA 0.56 micron dia. fiber-heat felt.

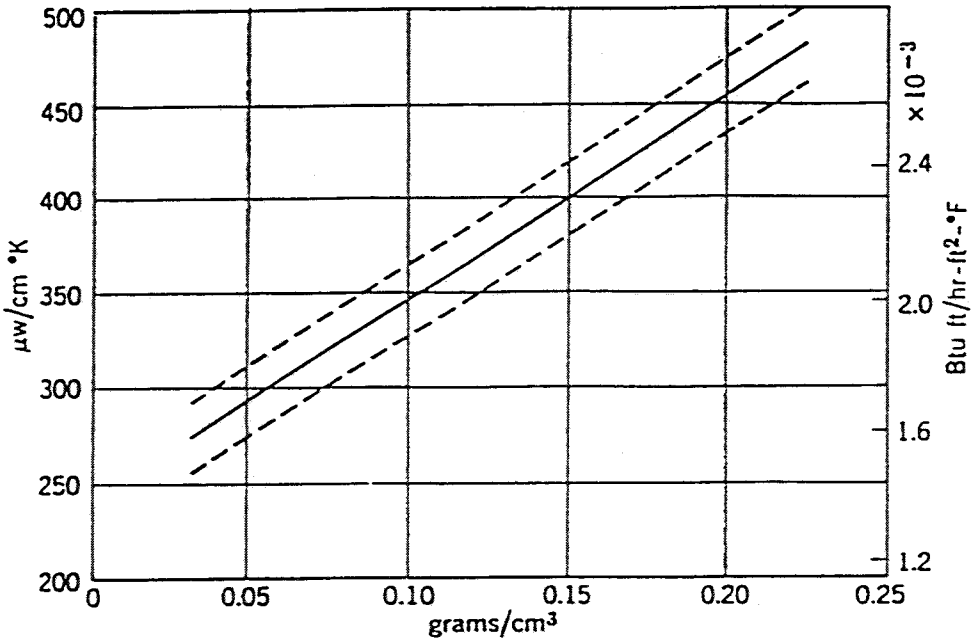

Figure 4-7 Thermal conductivity vs. density for unevacuated perlite in air for boundary temperatures of 300 K and 77 K.

Evacuated. Because gaseous conduction is one of the primary modes of heat transfer within powder and fibrous insulations, one obvious method of reducing the heat-transfer rate through these insulations is to evacuate the gas from the insulation.10 When powder is used at low pressure (10m Hg or less), gas conduction is negligible and heat transport is primarily by radiation and solid conduction. For some powders, radiation absorption reduces heat transfer more than solid conduction increases it, and these powders thus reduce the overall heat transport.[1]

The desirable properties of evacuated powder or fiber insulations are[9]

- low overall thermal conductivity;
- low density;
- particle size small enough so that the pressure-dependent region of gas conduction can be obtained with a moderate vacuum;
- satisfactory load-bearing ability;

- low vapor pressure;
- particle size distribution to minimize effects of vibration and low vapor pressure at operating temperature;
- low cost; and
- ease of installation.

Consideration also has to be given to the cost of the materials, the quantity in which they are available, the ease with which they can be used, and their compatibility (in terms of potential hazards) with the cryogens which have to be thermally insulated.[9]

When an insulating space is filled with a powder having a low gross density (a large ratio of volume of gas-filled voids to that of the solid material) the apparent thermal conductivity is approximately that of the gas and the amount of heat transferred by solid conduction through the powder appears to be relatively small.[2] Also the presence of the powder inhibits, to some extent, heat transfer by convection and radiation.[2] If the gas pressure in the interstices is reduced by pumping the enclosure, the rate of heat transfer is little affected at first because the thermal conductivity of the gas is almost independent of pressure in this higher-pressure region.[2] However, when the gas pressure approaches the value at which the mean free paths of the molecules are comparable with interstitial distances, there is a marked reduction in the apparent thermal conductivity, as shown in Figure 4-8.[2] For most powders used with nitrogen as the interstitial gas it appears that the condition of free molecule conduction sets in at pressures of the order 1.0 to 0.1 torr.[2] If the only mechanism for heat transfer were that of gaseous conduction, the rate of heat transfer at all lower pressures would be proportional to the pressure of the gas.[2] However this is not the case; at quite low pressures the rate of heat transfer becomes almost independent of pressure, showing that heat is being transmitted by other means. This residual heat transfer can be by solid conduction through the powder or by radiation or by both.[2] Figure 4-8 is somewhat idealized to represent the behavior of a powder with voids of uniform size and therefore having a rather sharp transition into

the range of free molecule conduction.[2] For most actual powders this transition is more diffuse,[2] as shown in Figure 4-9, which gives the thermal conductivity of perlite as a function of residual gas pressure.[10] The thermal conductivity of several evacuated insulating fibers and powders is given in Table 4-7, and thermal conductivity as a function of residual gas pressure is shown in Figure. 4-10. The thermal conductivity of evacuated perlite as a function of density is shown in Figure 4-11 and as a function of particle size in Figure 4-12. It may be noted that further investigation has shown that the thermal conductivity does not become constant with small particle size as shown in Figure 4-12, but continues to decrease.[1]

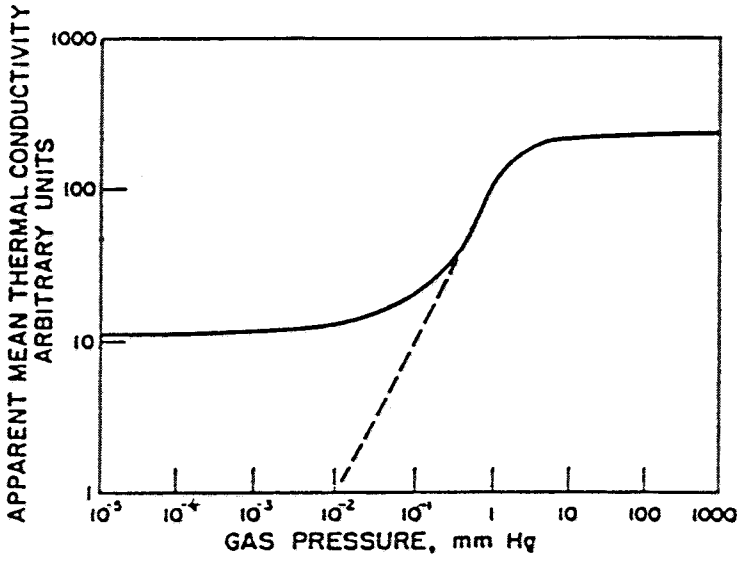

Figure 4-8 Variation of the apparent thermal conductivity of an insulating powder as the pressure of the interstitial gas is changed.

The data shown in Fig. 4-10 indicate that when the cold surface is at liquid nitrogen temperature the apparent thermal conductivity is reduced only slightly by lowering the pressure below 10^{-2} mm Hg.[2] An investigation of this result revealed that solid conduction was unimportant for this temperature span; however, solid conduction through the powder is a major factor for heat transfer from a surface at 76 K to one at 20 K.[2]

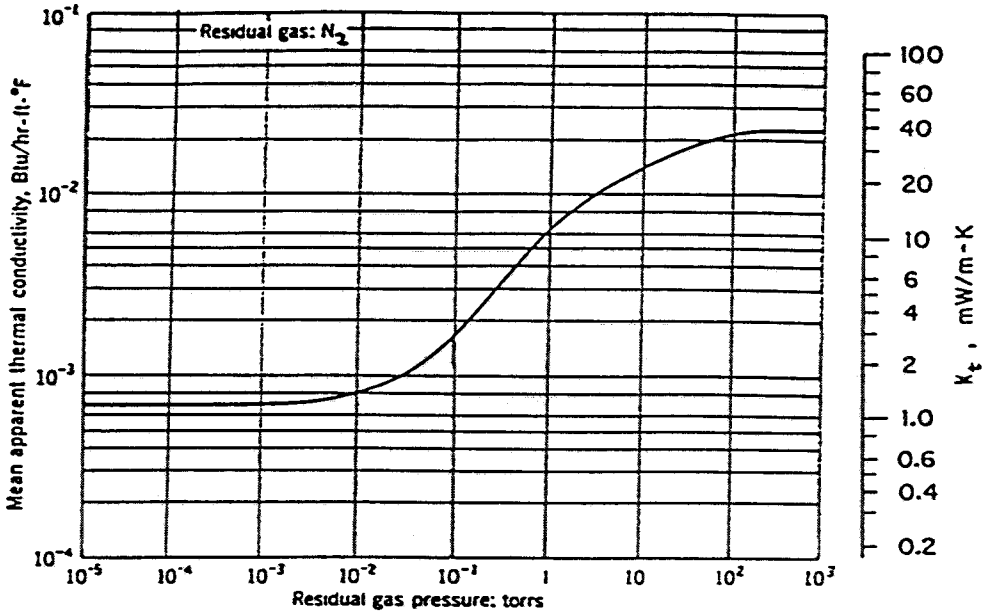

Figure 4-9 Variation of mean thermal conductivity with residual gas (N_2) pressure for 30 to 80 mesh perlite. Boundary temperatures are 300 K and 78 K.

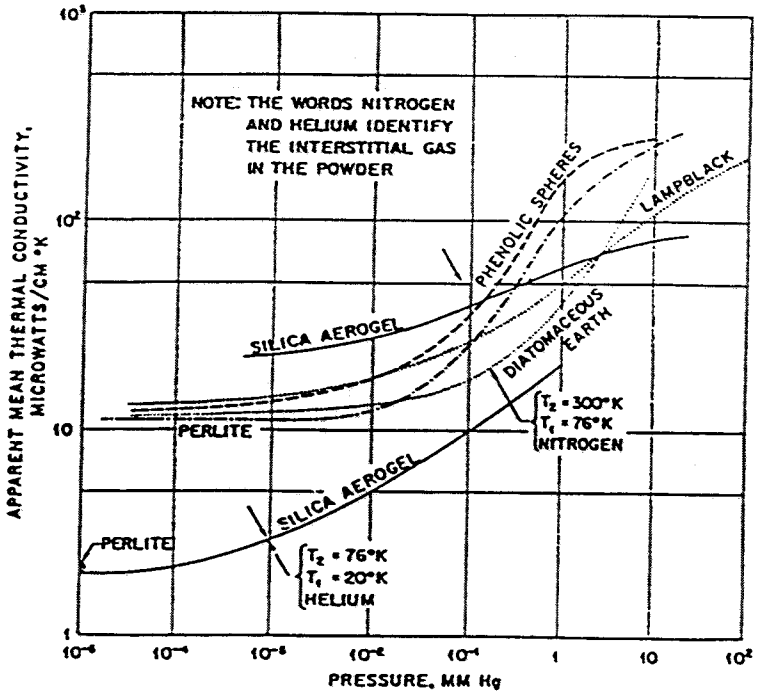

Figure 4-10 Thermal conductivity of several insulating powders and the variation with interstitial gas pressure. (SOURCE: Reference 2)

Table 4-7
Apparent mean thermal conductivity of several evacuated powders and fibrous insulations for boundary temperatures of approximately 300 K and 77 K and gas pressure $\leq 10^{-3}$ torr

Insulation	Density (kg/m^3)	Thermal conductivity (mW/m-K)	Reference
Alumina -- fused (-50 +100 mesh)	2,000	1.8[b]	1
Alumina -- laminar (0.1 to 10 micron)	70	2.3[b]	1
Calcium silicate (synthetic) -- 0.02 micron	170	0.75[b]	1
Calcium silicate (synthetic) --0.02 to 0.07 micron	360	0.55[b]	1
	210	0.59	10
Carbon plus 7% ash[a] (30% <44 micron)	200	0.6[b]	1
Charcoal peach pits (20-30 mesh)	490	1.8[b]	1
Diatomaceous earth (1-100 micron)	240	1.6[b]	1
	250	1.4[b]	1
	290	1.0[b]	1
	--	1.1	2
Fiber glass	50	1.7	10
Fiber glass *	64	1.4[c]	36
Fiber glass *	16	4.2	36
Iron oxide (Fe_2O_3), 200A	190	1.4[b]	1
Lampblack	200	1.25[b]	1
	193	1.1	2
	200	1.2	10
Mica, expanded (-20 +30 mesh 30%)	150	1.8[b]	1
Perlite -- +30 mesh	60	2.1[b]	1
Perlite -- coarse	64	1.9	10
Perlite -- 15-cm layer	80.3-96.3	1.1	2
Perlite -- +30 mesh	100	1.8[b]	1
Perlite -- 30 mesh	106	1.7	2
Perlite -- -30 to 80 mesh	130	1.2[b]	1
Perlite -- 30 to 80 mesh	135	1.2	2
Perlite -- -80 mesh	140	1.0[b]	1
Perlite -- -30 mesh	140	1.0[b]	1
Perlite -- 80 mesh	140	1.0	2
Perlite --	160	1.47[c]	36
Perlite -- fine	180	0.95	10
Phenolic spheres (25 to 100 micron)	200	1.3[b]	1
Silica (flame prepared, 150-200A)	60	2.1[b]	1
Silica aerogel [d] -- Chemically prepared	100	2.1[b]	1
Silica aerogel [d] -- +10% free silicon dust, by weight	110	1.8[b]	1
Silica aerogel [d] ---	80	1.6	10
Silica aerogel [d] ---	80	2.2	2
Silica aerogel [d] ---	96	1.96[c]	36
Talc	1,200	1.6[b]	1
Titanium dioxide (1,100A)	350	1.6[b]	1

[a] Ash= mostly SiO_2 and Al_2O_3
[b] 2.54 cm thick sample, wall emissivities >0.8.
[c] Boundary temperatures not specified * AAAA 0.56 micron dia. fiber-heat felt
[d] Santocel = Silica aerogel. Aerogel = SiO_2

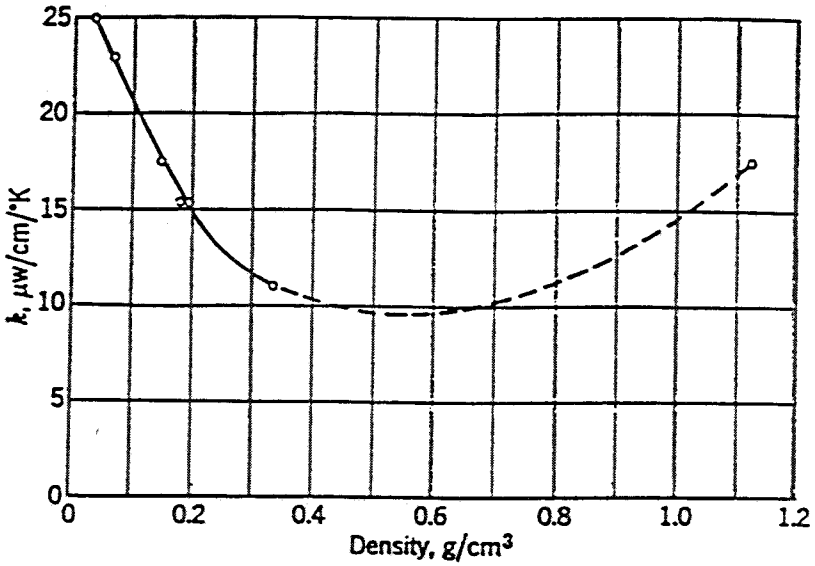

Figure 4-11 Thermal conductivity vs. density for evacuated perlite (80% of particles 450+150 micron. Boundary temperatures 300 K and 76 K.

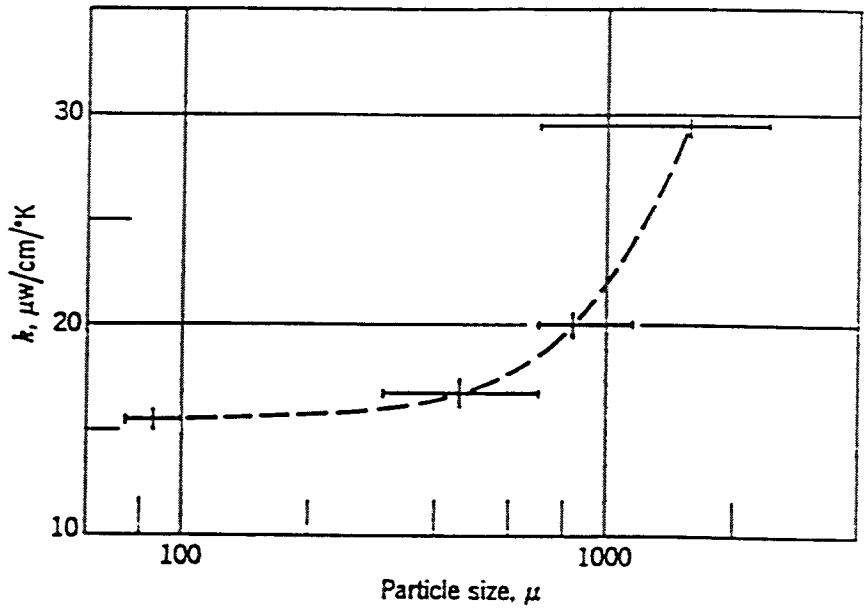

Figure 4-12 Thermal conductivity vs. particle size for evacuated perlite, ρ=190kg/m^3. Boundary temperatures 300 K and 77 K.

The radiant heat transmission through a partially transparent powder is not simple: some of the heat is radiated directly from the warm to the cold surface; some is absorbed by the powder and re-radiated; and some is reflected by the powder.[2] For layers of silica aerogel (less than 25.4 mm thick) the apparent thermal conductivity depends upon the thickness and upon the emissivity of the boundaries. Thus the concept of thermal conductivity cannot be properly applied to thin layers. However for layers 25.4 mm or more in thickness the apparent thermal conductivities given in Fig. 10 may be employed in the conventional way with errors not exceeding 10%.[2]

The difficulty of evacuation is a major consideration in the use of evacuated powders as an insulation although the vacuum required with powder insulations is much less extreme than with high-vacuum or multilayer insulation.[1,2] The gas being removed from the powder usually has to filter through the powder for rather long distances, and the resistance to flow is considerable.[2] Evacuation time can be reduced by providing a number of pumping taps, or better still, a number of pumping channels with many openings distributed so that the paths of the gas through the powder are short.[2] Since the powders are light and fine, they tend to be carried along with the gas; so the openings must be protected by filters.[2] Also, some of the powders, notably silica aerogel, adsorb large amounts of water from a humid atmosphere.[2] Thus, they should be dried by heating before being installed into the insulation space to save evacuation time.[2] Evacuation time can also be reduced by heating during evacuation to drive off adsorbed gases. Fine mesh filters must be used to protect vacuum pumps from these highly abrasive particles.[1]

Opacified. The amount of heat transport as a result of radiation through the dielectric powders Cab-O-Sil (diatomaceous earth), Santocel, and perlite can be reduced by adding metallic powders (such as flakes of copper or aluminum) to the dielectric powders.[1] (The dielectric properties of these powders may provide an opportunity for innovation in combining the electrical and thermal insulation requirements for an SPTL.) Radiant

heat transfer accounts for a large portion of the total heat transferred through evacuated powders having one surface at room temperature and the other at cryogenic temperatures. The thermal conductivity of an evacuated powder can be reduced by a factor of 5 by using the optimum quantity of opacifier (between 40 and 50% by weight). The conductivity is dependent upon the amount of metal added, and the effect is much more pronounced for Cab-O-Sil than for perlite[1]. Values of thermal conductivity for some evacuated opacified-powder insulations are given in Table 3-8.

Table 4-8
Apparent mean thermal conductivity of several opacified powder insulations for boundary temperatures of approximately 300 K and 77 K and gas pressure $\leq 10^{-3}$ Torr.

Insulation	Density (kg/m^3)	Thermal conductivity ($\mu W/m\text{-}K$)	Reference
Aluminum - Santocel [a] (40/60 wt%)	160	350	10
Bronze - Santocel [a] (50/50 wt%)	179	580	10
Copper - Santocel [a] (50/50 wt%)	180	330	10
Silica - carbon	80	480	10
Santocel "A"	96	154[b]	36
Perlite	128	121[b]	36
Cab-O-Sil [c]	72	296[b]	36
Micro-cell	---	588[b]	36
Cabotherm A	55	1400[b]	36
Silver - Cab-O-Sil (66/34 wt%)	---	240	26
Nickel - Cab-O-Sil (53/47 wt%)	---	349	26
Copper - Cab-O-Sil (55/45 wt%)	---	370	26
Aluminum - Cab-O-Sil (20/80 wt%)	---	569	26
Aluminized flakes[d] - perlite	---	1450[e]	37
Aluminized flakes [f] - perlite	---	1540[g]	37
Aluminized flakes [h] - perlite	---	1530	37

[a] Santocel = silica aerogel. Aerogel = SiO_2
[b] Boundary temperatures unspecified
[c] Cab-O-Sil = silica powder
[d] Square mylar flakes aluminized on one side
[e] Average of four data points
[f] Square Mylar flakes aluminized both sides
[g] average of two data points
[h] Square paper flakes aluminized one side

A disadvantage of opacified powders is that vibration can cause packing of the metal flakes. If many flakes get packed together, a "thermal short" develops, and the thermal conductivity of the insulation is increased[10]. Copper flakes are preferable to aluminum from a safety standpoint because of the large heat of combustion of aluminum in combination with oxygen[10]. Copper opacified powders have been successfully used.

Vacuum Insulation

Vacuum insulation consists of an evacuated space between two surfaces; preferably two highly reflecting surfaces. Vacuum insulation essentially eliminates two components of heat transfer -- solid conduction and gaseous convection; consequently, heat transport is predominately by radiation and gas conduction. Heat is transferred across the space between two surfaces by radiation from the hot outer surface to the cold inner surface, and by gaseous conduction through the residual gas within the evacuated space. The net radiant heat transfer from a surface at 300 K to one at 77 K is shown for various surface emissivity values in Figure 4-13[1,10,11].

A technique that can be used for obtaining a vacuum insulation consists of attaching a layer of fiber glass to the inner surface of a cryostat (such as a transfer line) and holding the fiber glass in place with a perforated aluminum foil[13]. The vacuum space is then charged with pure carbon dioxide to a pressure of about 152 kPa and sealed off from the atmosphere[13]. When the inner surface is cold (such as transfer of a cryogen through a transfer line) the CO_2 condenses onto the inner line and is held there by the glass wool resulting in a pressure of less than 10^{-5} torr. When the inner surface warms to ambient temperature the CO_2 pressure returns to 152 kPa, thus allowing the cryostat to be stored for extended periods with less danger of developing small leaks[13].

Multilayer Insulation

Multilayer insulation consists of alternating layers of a highly reflecting material (such as aluminum foil, copper foil, or aluminized Mylar) referred to as radiation-reflecting

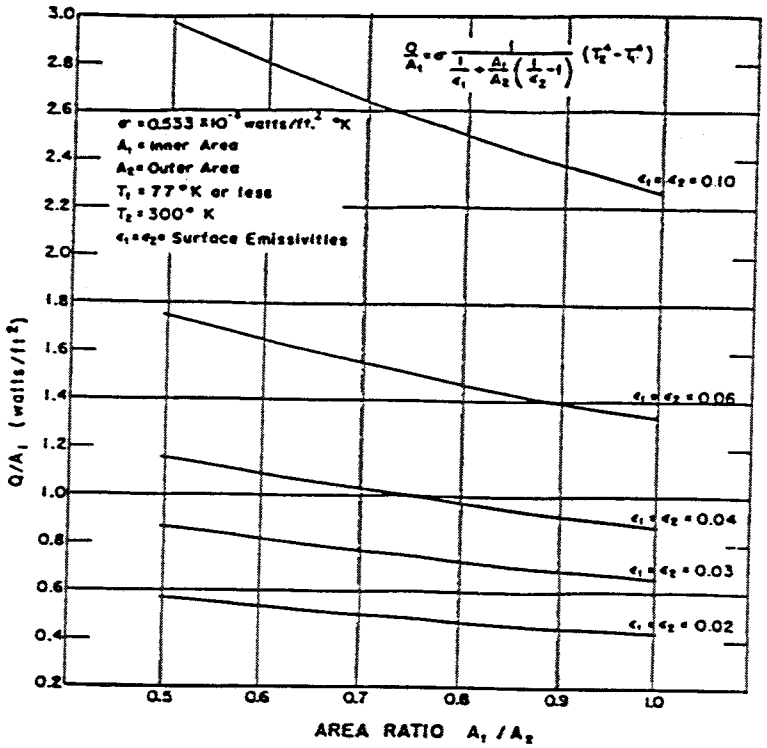

Figure 4-13 Net radiant heat transfer from a surface at 300 K to 77 K or lower (SOURCE: Reference 2)

shields (or just shields herein) and a low-conductivity spacer (such as fiber glass mat or paper, glass fabric, or nylon net) to reduce heat transfer by solid conduction from shield to shield[1,9-11]. The spaces thus formed between the shields are evacuated to decrease heat transfer by gas conduction[9]. The reflecting layers may also be separated by crinkling or embossing the sheets so that they touch only at a few discrete points, and a spacer is not required[10]. Some forms of multilayer insulation have yielded the lowest thermal conductivity of any bulk cryogenic insulation[1]. The effective thermal conductivity of multilayer insulation is a function of various parameters, such as the emissivity of the shields, the type of spacer material, the number of shields, the density of the layers, the contact pressure, and the annulus and interstitial pressure[8].

All modes of heat transfer (radiation, solid conduction, and gaseous conduction) are reduced considerably by multilayer insulation[10]. Radiation is minimized by using many

layers of a highly reflecting metal foil (shields)[10]. Solid conduction through a spacer material between the shields is minimized by using a low-conductivity fiberous material for the spacer or by crinkling the shield material to allow contact at only a few points[10]. Gaseous conduction is minimized by reducing the residual gas pressure to values on the order of 1.3 mPa (105 torr). The contribution of solid conduction and radiant heat transfer to the thermal conductivity of MLI is shown in Figure 4-14.

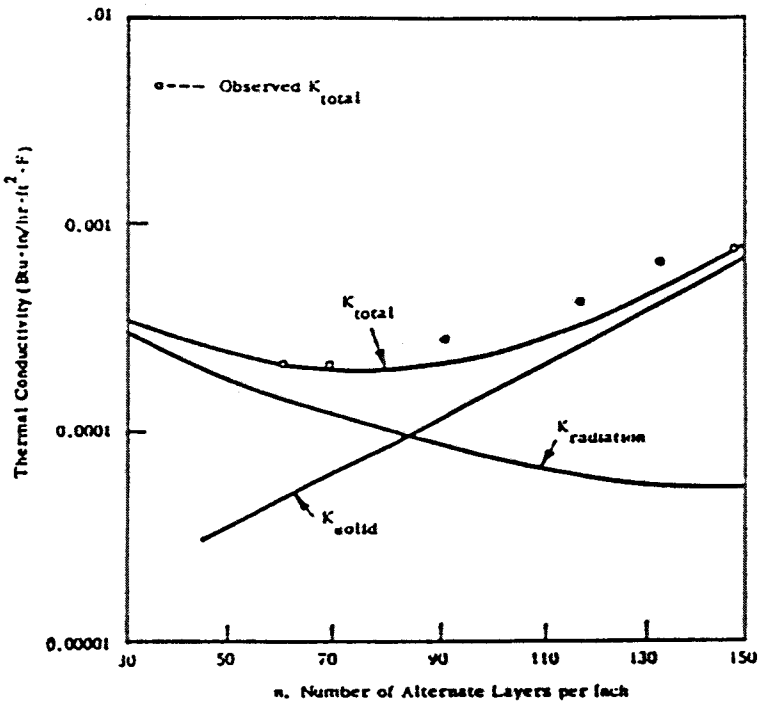

Figure 4-14 The contribution of solid conduction and radiant heat transfer to the thermal conductivity of mutilayer insulations (SOURCE: Reference 21)

Each component of an MLI system is designed specifically to perform one function[9]. For example, radiation shields attenuate radiation; spacers decrease solid conduction; and the evacuated enclosure surrounding the insulation decreases gas conduction[9].

Multilayer insulations can be classified according to the type of spacer used[9]. Multiple resistance spacers are fibrous mats with the fibers arranged parallel. Point-contact spacers are approximated by a netting, the crossover points (knots) of which are spheres twice as thick as the connecting threads[9]. To produce random small-area contacts, radiation shields can be embossed or crinkled and thus spaced without spacers[9]. Composite spacers are combinations of two or more materials, in which a material of acceptable thermal properties (such as thin foam) is attached to a carrier material of good tensile properties[9].

Radiation shields can be either thin metal foils or vacuum-deposited metal coating on thin polyester films[9]. They require a low emittance metal, such as silver, aluminum, or gold; aluminum is used most frequently because it is readily available in various foil thicknesses and as a coating on a variety of metallic and nonmetal surfaces[9]. Metal coatings about 1000 thick and vacuum-deposited on film are nontransparent to radiation and are clean, uniform, and highly reflective[9].

Representative thermal conductivity values for several MLI configurations are summarized in Tables 4-9, 4-10, and 4-11. The data in these tables show a large difference in published thermal conductivity values. These differences are partially the result of a large number of different MLI systems, and partially the result of differences in experimental techniques and results. Although the apparent thermal conductivity is a common parameter for comparing MLI systems, it contains the independent variables Q, T, and H that are measured with different degrees of accuracy. The measurement of MLI height, H, (or thickness build) has an inherently large reading error as a result of the difficulty of maintaining a constant layer thickness and layer density during the fabrication of the MLI and its later installation into a cryostat. Heat flux per unit area (Q) and temperature (both T_h and T_c) are measured with much better accuracy[14].

Table 4-9
Summary of apparent mean thermal conductivity of multilayer insulation with aluminum foil radiation shield, boundary temperatures of approximately 300 K and 77 K and residual gas pressure of $\leq 10^{-4}$ Torr.

Insulation	Number of layers	Density (layers/cm)	Insulation thickness (cm)	Thermal conductivity (μW/m-K)	Ref
Aluminum foil [a] &Fiber glass paper [a]	—	20	—	37	10
Aluminum foil & Glass-fiber paper [b]	—	22	3.3	55	1
Aluminum foil & Glass-fiber paper [b]	—	20	3.8	50	1
Aluminum foil & Glass-fiber paper [b]	—	20	2.5	70	1
Aluminum foil & Glass-fiber paper [b]	—	20	3.0	130	1
Aluminum foil & Glass-fiber paper [c]	—	30	3.8	100	1
Aluminum foil & Glass - fiber paper [c]	—	14	4.3	70	1
Aluminum foil & Glass -fiber paper [b]	—	24	1.9	140	1
Aluminum foil & Glass -fiber paper [c]	—	21	1.9	90	1
Aluminum foil [d]&Fiber glass paper [e]	—	31	—	33.6	3.4
Aluminum foil [d] &Fiber glass paper [f]	—	39	—	55.5	3.4
Aluminum foil [g] & DexterFiber glass paper [h]	—	22	—	56	3
Aluminum foil [g] & DexterFiber glass paper [d]	—	20	—	52	3
Aluminum foil [i] & Glass -fiber paper [j]	—	4-8	—	180	3
Aluminum foil [k] & Glass -fiber paper [l]	—	16-32	—	42	3
Aluminum foil [m] & Glass -fiber paper [n,o],PP[q]	10	—	0.285	28.1	3
Aluminum foil [m] & Glass -fiber paper [n,o],AP[q]	10	—	0.285	22.8	3
Aluminum foil [m] & Glass -fiber paper [n,r],PP	10	—	0.209	23.9	3
Aluminum foil [m] & Glass -fiber paper [n,r],AP	10	—	0.209	17.9	3
Aluminum foil [m] & Glass -fiber paper [n,r,s],PP	10	—	0.209	11	3
Aluminum foil [m] & Glass -fiber paper [n,r,s],AP	10	—	0.209	10.8	3
Aluminum foil & Glass -fiber paper (unbonded)	—	6	4.5	390	1
Aluminum foil & Glass -fiber paper (unbonded)	—	6	2.2	300	1
Aluminum foil & Glass fabric	60	28.1	—	82.7[t]	15
Aluminum foil & Glass fabric	40	28.45	—	73.5[t]	15
Aluminum foil & Glass fabric	20	32.35	—	48.5[t]	15
Aluminum foil & Silk fabric	60	32.34	—	94.9[t]	15
Aluminum foil & Silk fabric	40	33.64	—	61.6[t]	15
Aluminum foil & Silk fabric	20	33.8	—	38[t]	15
Aluminum foil & glass texture	—	—	—	56.9[u]	
Aluminum foil & glass texture	10	—	—	207[v]	39
Aluminum foil & Glass fiber mat	—	26	3.7	70	1
Aluminum foil & Fiber glass mat[w]	—	26	—	70	3
Aluminum foil[x] & Rayon net[y]	—	10	—	78	10
Aluminum foil & Nylon net[y]	—	11	—	34	10
Aluminum foil & Nylon net	—	24	2.5	230	1
Aluminum foil & Nylon net[z]	—	24	—	230	3
Aluminum foil & Nylon net[o],PP	10	—	0.311	65.5	3
Aluminum foil & Nylon net[o], AP	10	—	0.311	13.1	17
Aluminum foil & Nylon net[o], Tightly wound ,PP	10	—	0.184	61.2[aa]	3
Aluminum foil & Nylon net[o], tightly wound,AP	10	—	0.184	17	3

Table 4-9 (Continued...)

[a] 15 mm thick

[b] Paper thickness = 0.2mm

[c] Paper thickness = 0.12 mm

[d] 12 micron thick

[e] 0.2-0.5 micron thick

[f] 0.5 to 0.7 micron thick

[g] 6.4 micron thick

[h] 20 micron thick

[i] Linde SI 12

[j] 3 micron thick

[k] Linde SI 4

[l] Sub micron thickness

[m] 8.7 micron thick

[n] Paper spacer was Whatman GFG3 glass-fiber paper containing no binder, a nominal weight of 18g/m^2 and a nominal thickness of 100 microns

[o] As received from manufacturer

[p] PP = passive pumping (i.e. vacuum pump not running)

[q] AP = active pumping (i.e. vacuum pump was running)

[r] Paper baked at 180C with either a vacuum pump-out or a dry nitrogen purge

[s] Plus getter on cold surface

[t] Thermal conductivity may have been affected by the interstitial pressure

[u] Low temperature~90K

[v] Low temperature~125K

[w] 20 micron thick polystyrene binder

[x] 6 micron thick

[y] 2 mm mesh

[z] 15 micron

[aa] Pressure was 10^{-3} torr

Table 4-10
Summary of apparent mean thermal conductivity of multilayer insulation with aluminized plastic film, boundary temperatures of approximately 300 K and 77 K and residual gas pressure of $\leq 10^{-4}$ Torr

Insulation	No. of layers	Density (layers per cm)	Insulation thickness (cm)	Thermal conductivity (μW/m-K)	Ref.
NRC	---	---	---	36[a]	36
NRC-2 Crinkled aluminized Mylar film [b]	---	35	---	42	10
NRC-2 Crinkled aluminized Mylar film [b]	---	20	---	28	3
Dimplar dimple & Smooth Mylar film	---	8	---	42	10
Dimplar dimpled & Smooth Mylar film [c]	---	3-12	---	42	3
Double Aluminized PET[d] &PET[d]	32	---	---	30	40
Aluminized Mylar [e]	---	24	3.5	85	1
Aluminized Mylar [e]	---	47	1.3	180	1
Aluminized Mylar [e,f] & no spacer	---	24	---	85	3
Aluminized Mylar & Silk Fabric	60	31.9	---	71.5[g]	15
Aluminized Mylar & Silk Fabric	40	32.4	---	58.6[g]	15
Aluminized Mylar & Silk Fabric	20	33.2	---	19[g]	15
Aluminized Mylar [h] &Glass fabric [i]	60	30.28	---	62.1	15
Aluminized Mylar [h] &Glass fabric [i]	40	28.3	---	57	15
Aluminized Mylar [h] &Glass fabric [i]	20	28.75	---	51.5	15
Aluminized Mylar[j] & Dexter Fiber glass paper [h]	---	9	---	200	3
Aluminized Mylar[h] & Dexter Fiber glass paper [j,k], PP[l]	10	---	0.267	41.7[m]	3
Aluminized Mylar[h] & Dexter Fiber glass paper [j,k], AP[n]	10	---	0.267	30.5	3
Aluminized Mylar[o] & Fiber glass mat [p]	10	---	---	71.9	41
Aluminized Mylar [o] & Spun Nylon	24	---	---	55.5	41
Aluminized Mylar[o] & no spacer	20	---	---	15.9	41
Aluminum coated polyester [r] & Polyurethane foam [s]	---	59	---	14.4	26

[a] Boundary temperature unspecified
[b] 6 micron thick
[c] Alternate layers of dimpled and smooth Mylar film
[d] PET = Polyethylene terephthalate
[e] Aluminized on one side
[f] 12.7 micron thick
[g] κ may have been affected by high interstitial pressure
[h] 12 micron thick
[i] 76.2 micron thick
[j] Paper spacer was Whatman GFG3 glass-fiber paper containing no binder, a nominal weight of 18g/m^2, and a nominal thickness of 100 microns
[k] As received from the manufacturer
[l] PP = passive pumping
[m] Pressure=10^{-3} Torr
[n] AP=active pumping
[o] Aluminized on both sides
[p] Polyester bonded fiberglass mat
[q] Double aluminized dimpled perforated polyester film
[r] 6.4 micron thick
[s] Density=32 kg/m^3

Table 4-11
Summary of apparent mean thermal conductivity of multilayer insulation with adsorbent-loaded spacer, boundary temperatures of approximately 300 K and 77 K and residual gas pressure of $\leq 10^{-4}$ Torr

Insulation	No. of layers	Density (layers/cm)	Insulation thickness (cm)	Thermal conductivity (μW/m-K)	Ref
Aluminum foil & carbon-loaded glass-fiber paper [a]	--	--	--	7.6	18
Aluminum foil & paper with 0% carbon loading	--	--	--	63.4[b]	19
Aluminum foil & paper with 2% carbon loading	--	--	--	83.5[b]	19
Aluminum foil & paper with 10% carbon loading	--	--	--	79.7[b]	19
Aluminum foil & paper with 20% carbon loading	--	--	--	82.5[b]	19
Aluminum foil & carbon with 30% loading	--	--	--	76[b]	19
Aluminum foil[c] & Carbon loaded paper [d], PP[e]	10	--	0.324	15.2	3
Aluminum foil[c] & Carbon loaded paper [d], AP[f]	10	--	0.324	15.2	3
Aluminum foil[c] & Carbon loaded paper [g], PP	10	--	0.298	9.2	3
Aluminum foil[c] & Carbon loaded paper [g], AP	10	--	0.298	10.7	3
Aluminum foil[c] & Carbon loaded paper [a,d], PP	10	--	0.305	15.2	3
Aluminum foil[c] & Carbon loaded paper [a,d], AP	10	--	0.305	12.8	3
Aluminum foil[c] & Carbon loaded paper [a,g], PP	10	--	0.324	7.9	3
Aluminum foil[c] & Carbon loaded paper [a,g] AP[e]	10	--	0.324	7.7	3
Aluminum foil[c] & Carbon loaded paper [a,g], PP	10	--	0.324	9.9[h]	3
Aluminum foil[c] & Carbon loaded paper [a,g], AP	10	--	0.324	7.6[h]	3
Aluminized Mylar[i] & Carbon loaded paper [d], PP	10	--	0.184	35.7	3
Aluminized Mylar[i] & Carbon loaded paper [d], PP	10	--	0.216	25.6	3
Aluminized Mylar[i] & Carbon loaded paper [d], AP	10	--	0.184	31.2	3
Aluminized Mylar[i] & Carbon loaded paper [d], AP	10	--	0.216	21.5	3
Aluminized Mylar[i] & Carbon loaded paper [g], PP	10	--	0.324	26.3	3
Aluminized Mylar[i] & Carbon loaded paper [g], AP	10	--	0.324	26.5	3
Aluminized Mylar[i] & Carbon loaded paper [j,k], AP	9	--	0.28	15	3
Aluminized Mylar[i] & Carbon loaded paper [j,k], AP	5	--	0.18	12	3
Aluminized Mylar[i] & Carbon loaded paper [j,k], AP	3	--	0.15	16	3
Aluminized Mylar[i] & Alumina loaded paper [d], PP	10	--	~0.3	43	3
Aluminized Mylar[i] & Alumina loaded paper [g], AP	10	--	~0.3	35	3
Aluminized Mylar[i] & Molecular-sieve loaded paper [g,k], PP	10	--	~0.3	59	3
Aluminized Mylar[i] & Molecular-sieve loaded paper [g,k], AP	10	--	~0.3	41	3
Aluminum foil & paper with 30% zeolite loading	--	--	--	89.4[b]	19
Aluminum foil & Molecular sieve loaded glass paper	10	--	--	128[l]	39

[a] Plus getter on cold surface
[b] Low temperature~90K
[c] 8.7 micron thick
[d] As received from the manufacturer
[e] PP = passive pumping (vacuum pump not running)
[f] AP = active pumping (vacuum pump was running)
[g] Paper baked at 180C with either a vacuum pump-out or a dry nitrogen purge
[h] Rotary pumpdown only
[i] 12 micron thick
[j] Paper spacer was Whatman GFG3 glass-fiber paper containing no binder, a nominal weight of 18g/m^2, and a nominal thickness of 100 microns.
[k] Handmade
[l] Low temperature~125K

Effect of Residual Gas Pressure. Multilayer insulation must be evacuated to a pressure below 10 mPa (7.5 X 10-5 torr) to be effective[10]. The dependence of the apparent thermal conductivity on residual gas pressure for a typical multilayer insulation is shown in Figure 4-15[10]. One of the problems associated with multilayer insulation is the effective evacuation of the residual gas from the space within the insulation layer[10]. Small vent holes may be used in the foil layers to allow more effective removal of the trapped gas[10]. Outgassing of the shields can also introduce significant quantities of gas within the insulation[10]. A carbon-filled glass-fiber paper can be used for the spacer material and the carbon will adsorb the outgassing load and maintain a low pressure within the insulation[10]. The effective thermal conductivity of MLI increases with increase in the number of layers for a given layer density; this may be attributed to gas conduction[8,15]. The interstitial pressure may be orders of magnitude higher than the vacuum chamber pressure[15]. Thus, gas conduction through MLI should not be neglected in calculating its performance[15]. The interstitial pressure can be predicted within an accuracy of 16 - 47%, and the performance of MLI can be predicted within an accuracy range of 4.9 - 30.6% using the techniques described in Refs. 8 and 15, which shows that this is a difficult parameter to control.

Effect of Layer Density. The variation of apparent thermal conductivity with layer density is shown in Figure 4-16 for a typical multilayer insulation [10]. Figure 4-16 shows that the apparent thermal conductivity of MLI is reduced by increasing the layer density up to about 30 layers/cm, but if the insulation is compressed too tightly by going to higher layer density, the solid conductance increases causing the insulation conductivity to increase [10,11]. However, data presented in Ref. 15 did not show an increase in effective thermal conductivity as layer density decreased below about 30 layers/cm as shown in Figure 4-16. This is probably a result of insufficient or no test data for layer densities < 30 layers/cm. However, data presented in Ref. 16 and plotted in Fig. 17 show a minimum k_{eff} at about 100 layers/cm for 20 layers of Mylar (12 m thick) with an aluminum coating on both sides and boundary temperatures of 300 and 77 K. Other

data presented in Ref. 16 showed a minimum k_{eff} as high as 500 layers/cm for other MLI systems.

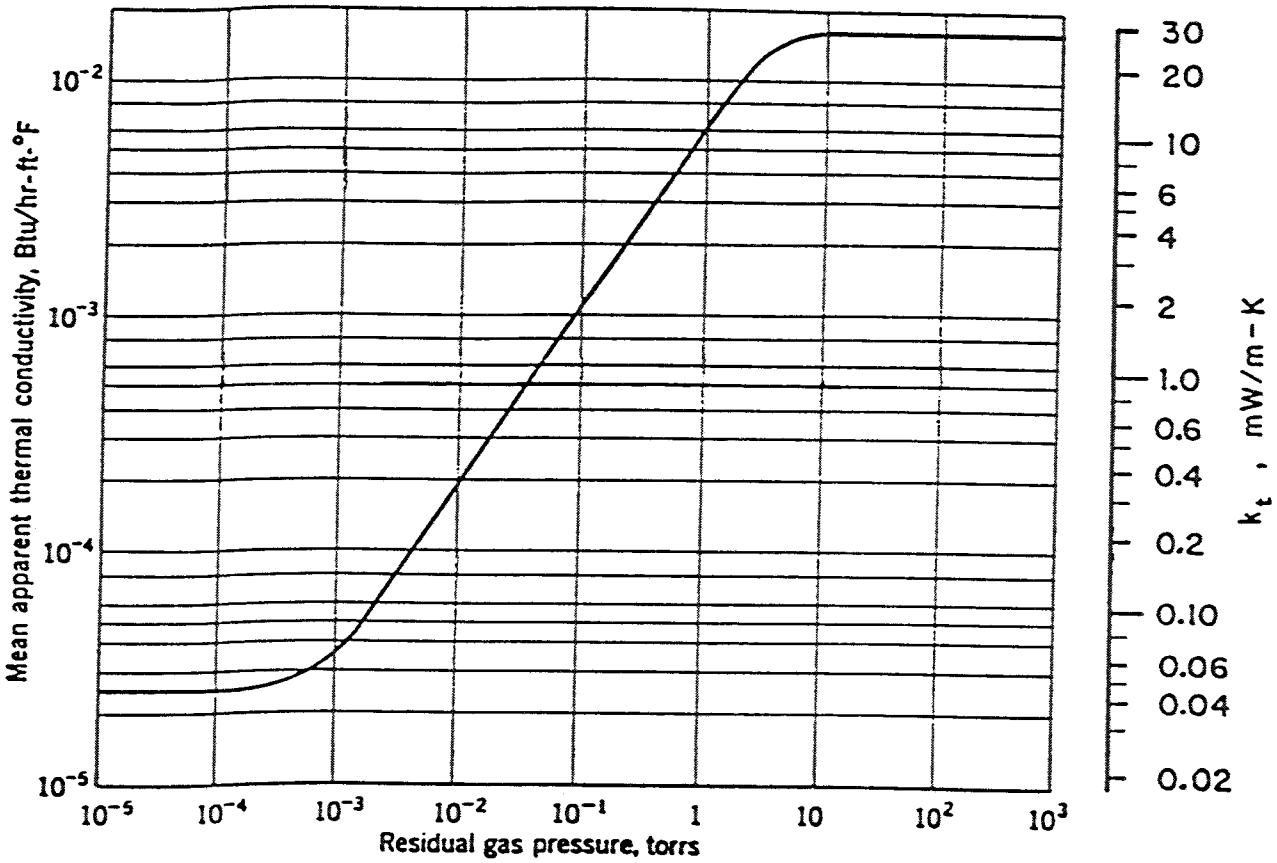

Figure 4-15 Thermal conductivity vs. residual gas pressure for a typical MLI. Layer density = 24 layers/cm, Boundary temperatures are 300 K and 90.5 K.

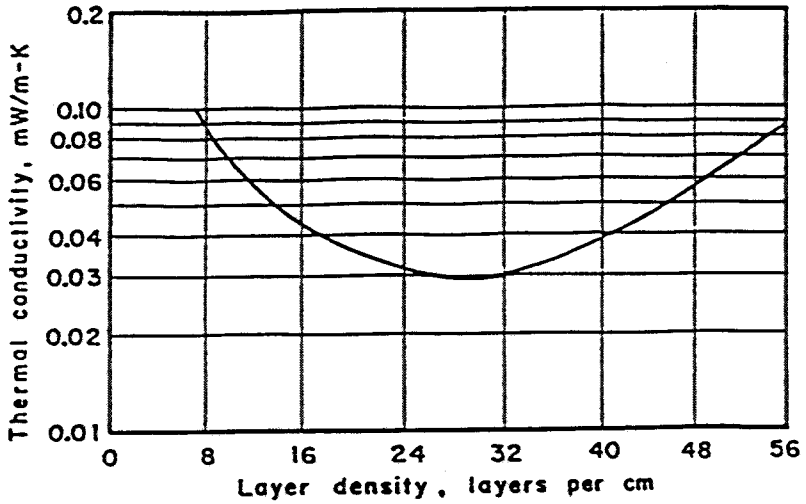

(a) Typical multilayer insulation with boundary temperatures of 294 K and 78 K (SOURCE: Ref. 10)

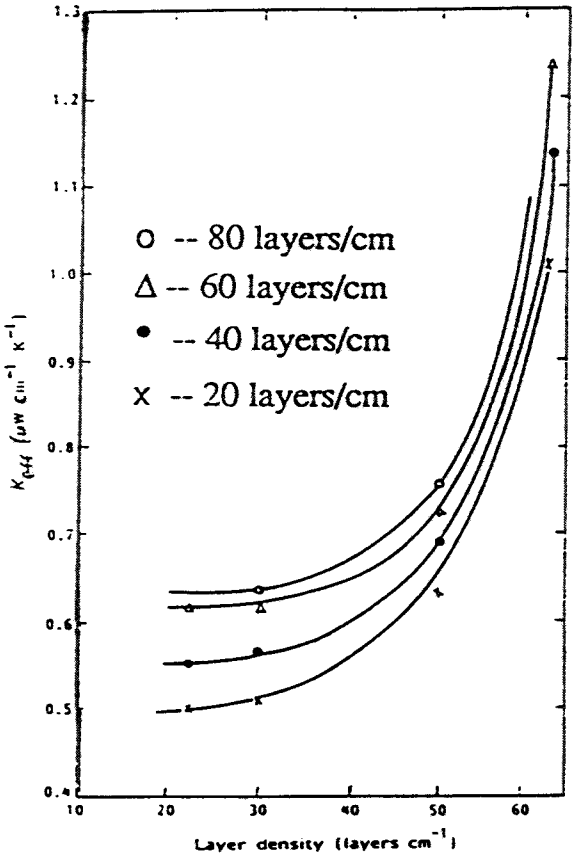

(b) aluminized Mylar and glass fabric multilayer system with boundary temperatures of 300 K and 80 K (SOURCE: Ref. 15)

Figure 4-16 Variation of thermal conductivity with layer density for two types of insulation

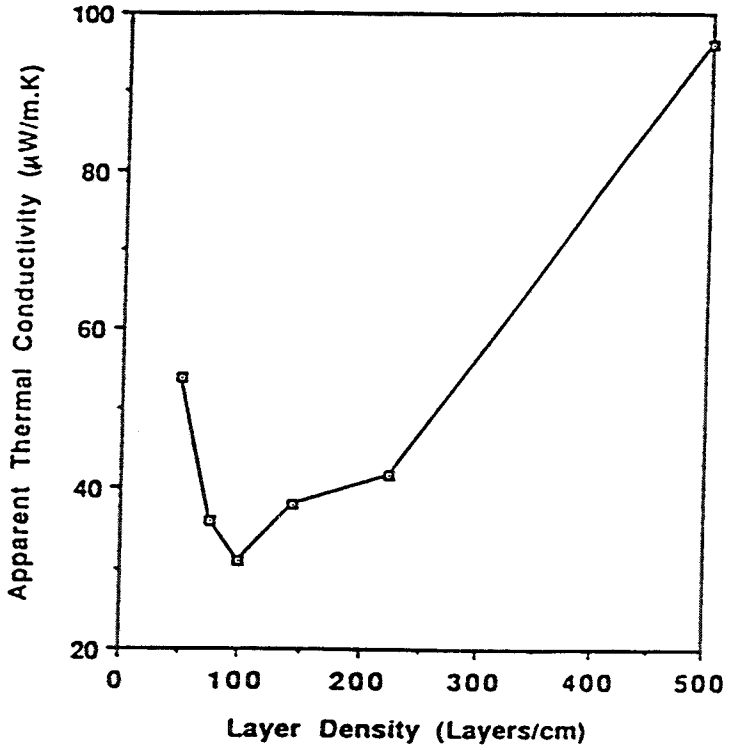

Figure 4-17 Apparent thermal conductivity for 20 layers of 12 micron thick Mylar with aluminum coating on both sides. Boundary temperatures ~300 Kand 78 K.

Effect of Number of Layers. Experimental data indicate a marginal benefit of using more than about 30 layers of MLI[7]. These data were obtained in tests in which the layer density was 11±2 layers/cm[7]. Although increasing the number of layers plays an important role in decreasing the heat flux when the number of layers is < 30 or 40, the improvement from additional layers is small[17].

Data from Ref. 15 on thermal conductivity as a function of number of layers for four MLI configurations with a layer density of approximately 30 layers/cm are shown in Figure 4-18. Experimental and calculated heat flow rates and effective thermal conductivity as a function of number of layers are shown in Figure 4-19 (from Ref. 15) for an aluminumized Mylar and glass fabric MLI at four layer densities (63.28, 50.0, 30.0, and 24.2 layers/cm)[15]. As shown in this figure, the heat flow rate decreases with increase in number of layers but increases with increase in layer density, because an

increase in the layer density increases both the contact pressure between the layers and the interstitial pressure[15]. Disagreement between experimental and calculated heat flow rates varies from 4.9 to 30.6%[15]. The minimum disagreement is at a layer density of 30 layers/cm and with the number of layers at 20[15]. The maximum disagreement is observed for a layer density of 30 layers/cm and with the number of layers at 80[15]. Also shown in Figure 4-19 is that the measured effective thermal conductivity increases with number of layers for the same layer density; however, the variation of effective thermal conductivity with number of layers as calculated using the numerical technique presented in Ref. 8 is shown to be negligible[15].

A product information brochure by King-Seeley Thermos Co. presented the data given in Figure 4-20 for NRC-2 multilayer insulation to show the relationship between the number of layers and heat flux for various packing densities.

Covering a heavily oxidized surface with an aluminum tape appears to be an effective way to reduce the emissivity of the surface, although this could complicate the evacuation of the vacuum space. An aluminum-taped surface should be better than a bare, heavily oxidized surface regardless of the number of layers of MLI applied[17]. A few layers of MLI play an important role in reducing the heat flux[17]. For example, the heat flux can be reduced by a factor of 17 with the application of aluminum tape and 5 MLI layers to a heavily oxidized surface[17]. The use of aluminum tape on the cold surface permits the number of layers of MLI to be reduced by approximately one-half for the same heat flux[7]. This could reduce the time required for evacuation of the MLI[7]. However, the use of only a few layers of MLI, while speeding pump down, does not provide much protection in the event of a poor vacuum[17].

For an experiment in which the first layer of MLI was wrapped directly on the cold surface and the last layer was separated from the warm surface, the temperature of the last layer was closer to the temperature of the warm surface than the temperature of the

first layer was to the cold surface temperature. A temperature difference of only a few degrees Kelvin existed between the last layer and the warm surface when > 10 or 20 layers were used. This implies that if the outermost layer touches the warm surface the heat flux will not increase significantly; however, touching should be avoided when using only a few MLI layers[17].

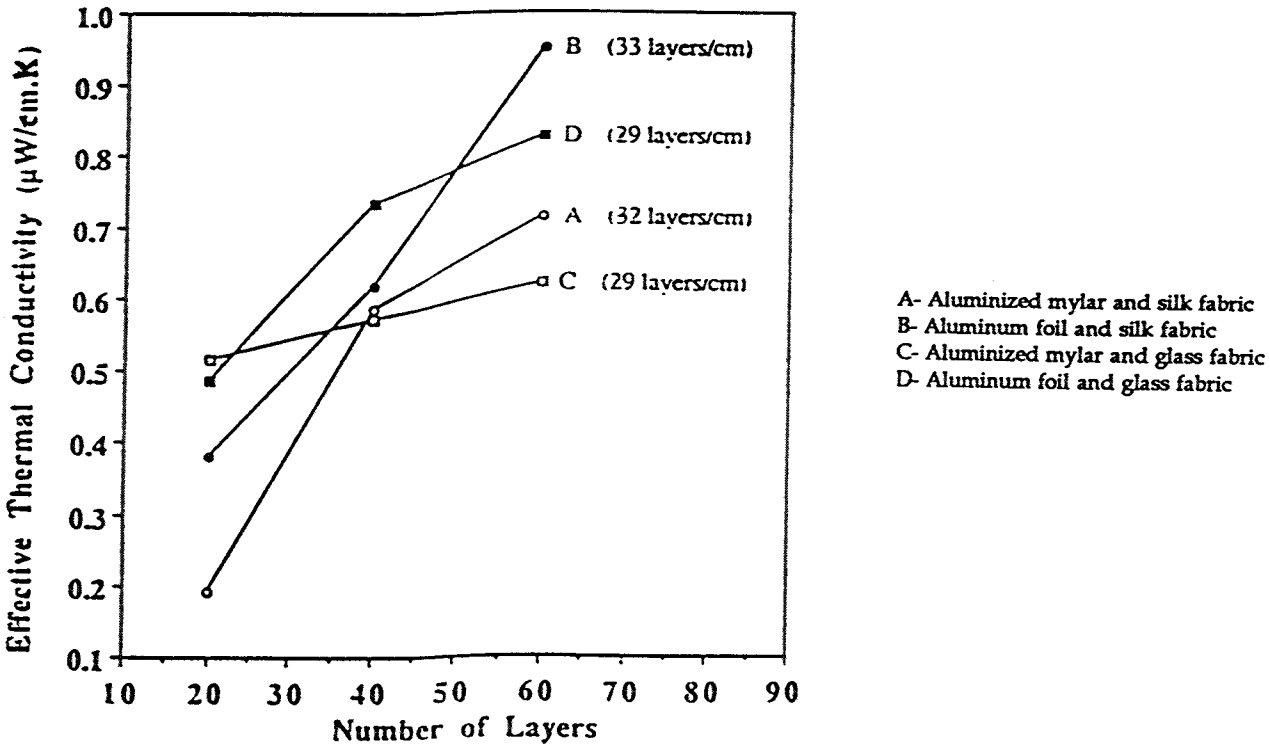

Figure 4-18 Effective thermal conductivity of four multilayer insulation systems as a function of number of layers

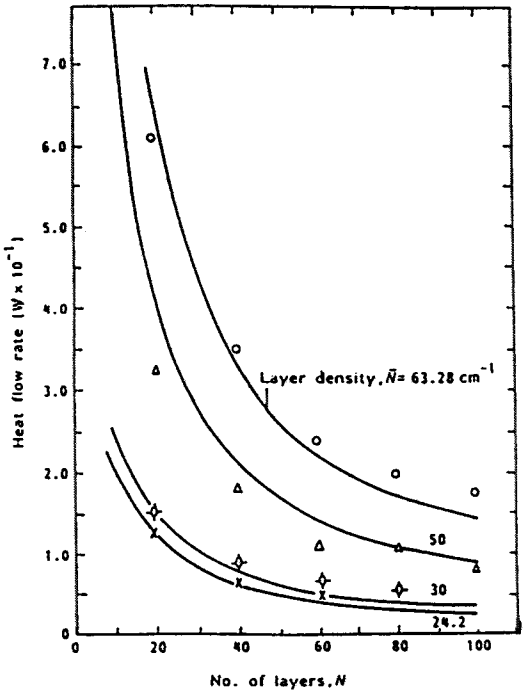

(a) Variation of heat flow with number of layers and layer density

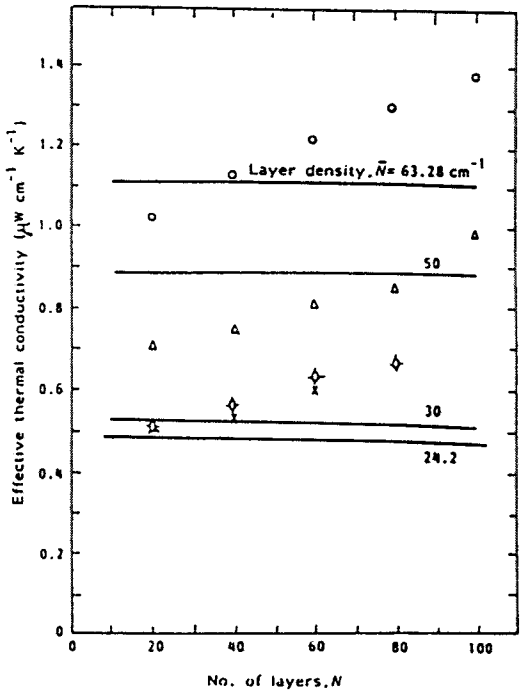

(b) Variation of effective thermal conductivity with number of layers and layer density

Figure 4-19 Heat flow and thermal conductivity data for aluminized Mylar and glass fabric multilayer insulation with boundary temperatures of 300 K and 80 K and pressure of 2 X 10^{-5} Torr. SOURCE: Reference 15

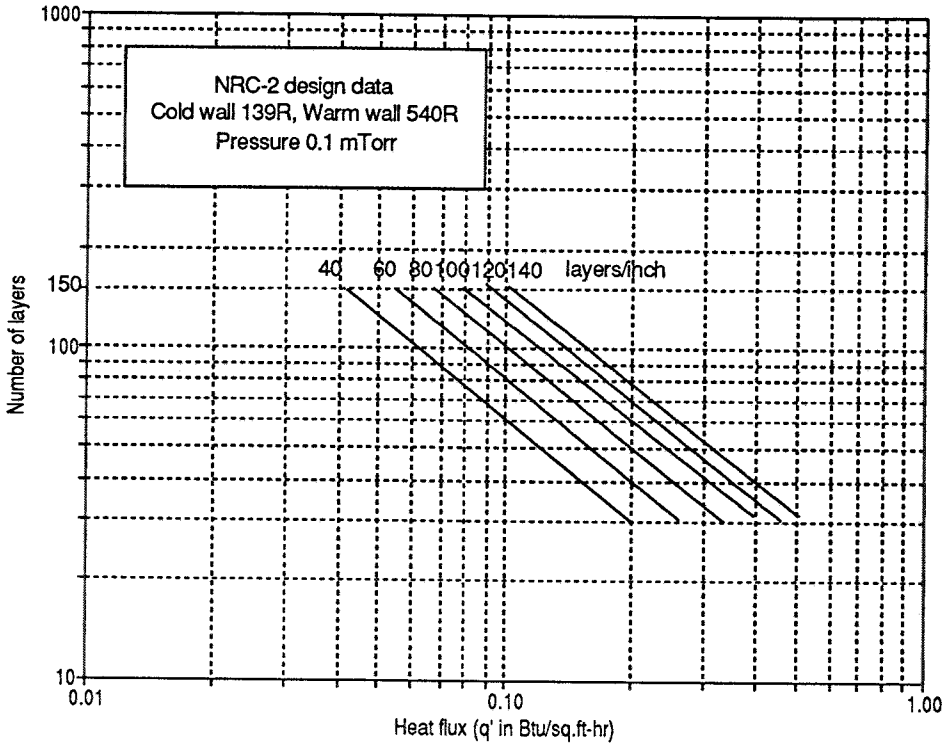

Figure 4-20 Relationship between the number of layers and heat flux for various packing densities for NRC-2 MLI. Boundary temperatures of 300 K and 77 K.

Effect of Adsorbent-Loaded Spacer Material. The theoretical minimum value of k_{eff} for MLI is about 6.5 W/m.K (for given assumptions), but experimentally obtained values exceed this by a factor of 5 or more[18]. Thus, the major heat flow is not by radiation[18]. This observation led to the conclusion that residual gas pressure within the layers of insulation (probably from outgassing) was the probable cause[18]. To overcome this, an adsorbent-loaded paper spacer material was developed using carbon, alumina, zeolite, and molecular-sieve adsorbents. The use of carbon as the adsorbent gave a thermal conductivity at least 20% lower than unloaded paper (compare data in Tables 4-9, 4-10, and 4-11)[3,18]. Also, it was found that the carbon-loaded paper spacer permitted an almost complete recovery of the insulation capability after small quantities of air were admitted into the vacuum space[3,18]. A different experimental investigation[19] found that the carbon-loaded paper had a slightly higher, not a significantly lower, k_{eff} (see data in

Table 4-11). This was attributed to heat conduction inside the paper[20]. An explanation for the differences between the results of these two experimental groups is not known.

Effect of Mechanical Load. The effect of mechanical load on the density and thereby on the heat flux through MLI is of considerable interest. An increase in mechanical load will cause the radiation shields and spacers to be compressed into a thinner sandwich of higher density[21]. Then the radiation shield and spacers will return to their original density upon a decrease in the mechanical load, provided that no permanent deformation has occurred[21]. Forces that can compress MLI and reduce its effectiveness include[9]

* tension applied during wrapping of the MLI;
* thermal expansion or contraction of the MLI and the cryostat inner and outer surfaces;
* localized loads in the vicinity of supports;
* compressive loading by atmospheric pressure if the cryostat outer surface is flexible; and
* bending of flexible sections of the cryostat.

As shown in Figure 4-21, the compression of multilayer insulation by the application of an external load results in a significant increase in the thermal conductivity of the insulation[11]. For example, the initial conductivity of a sample increased from 36 mW/m.K to 880 mW/m.K when the sample was subjected to a load of 101 kPa[11,22] and in addition, the thickness of the sample decreased to approximately 25% of its original thickness[11,22]. Thus the overall heat flux increased approximately one hundred times[11,22]. Upon releasing the load, the sample returned to within 90% of its original thickness and to approximately its original thermal conductivity[11]. Maintaining the compression load for periods up to 48 hours has been shown to have no deleterious effect on the recovery characteristics of the insulation system[22]. Others also have reported that compressed MLI will return to nearly its original condition when the

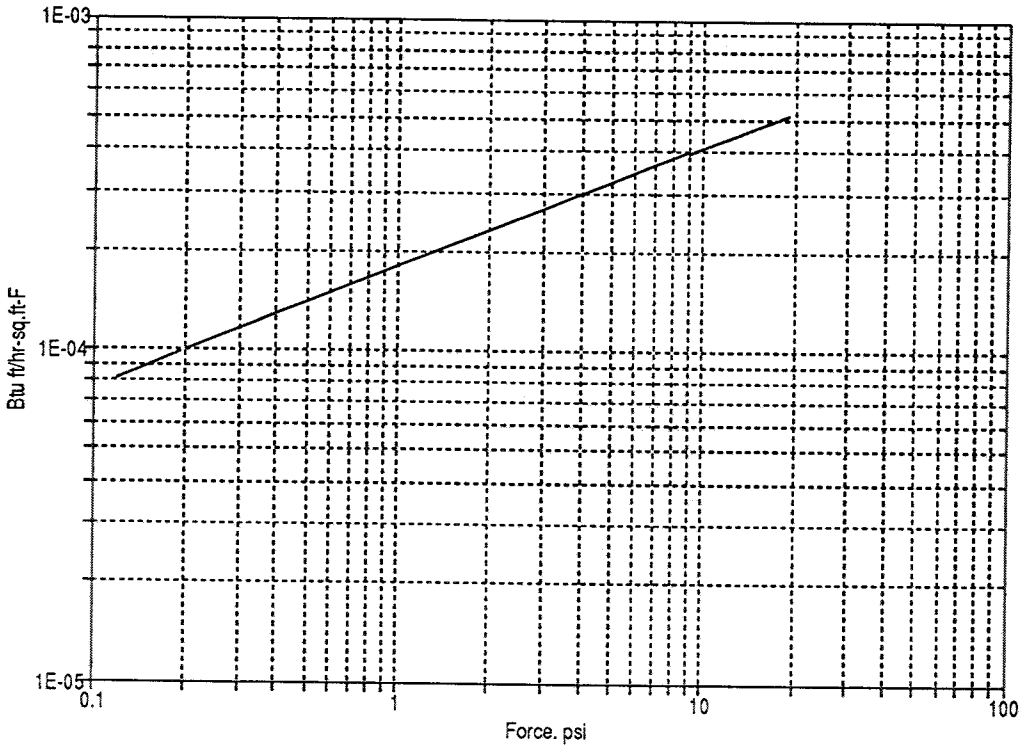

Figure 4-21 Thermal conductivity vs. applied force for multilayer insulation with boundary temperatures of 300 K and 77 K. Under zero load, the conductivity is 346μW/m-K (2x10-4 Btu.ft/hr.ft^2-F). SOURCE: Reference 11

compressive load is removed[23]. Compaction has been reported, as a result of other experiments, to increase conductivity by as much as ten to forty times[1]. The Linde Company reported results for external bearing pressure tests on its superinsulation in which the apparent thermal conductivity varied from about 35 W/m.K at no external bearing pressure, to about 138 W/m.K at an external bearing pressure of 0.7 kPa, and to about 865 W/m.K at an external bearing pressure of 101 kPa[24]. For the increase of pressure from zero to 101 kPa, a physical compression of the insulation by a factor of 4 took place[24]. Compressive loads as low as a few Pa have been reported to result in a significant increase in heat flux[25]. One experiment found that when MLI was compressed up to 13.8 kPa the heat flux was about 200 times greater than at the no-load

condition as shown in Figure 4-22 for various MLI systems[25]. Still others report that a compressive load of 13.8 kPa increased the heat flux by a factor of as much as 100[26].

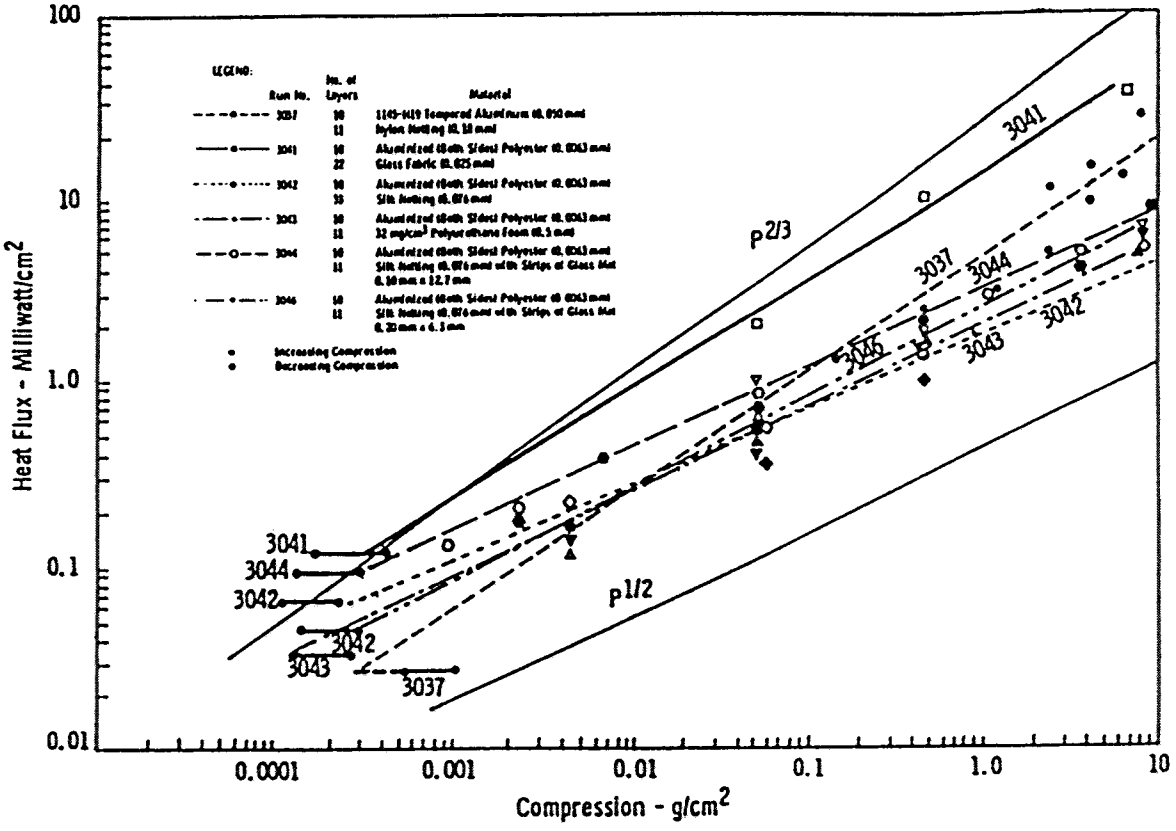

Figure 4-22 Effect of external compression on heat flux through several multilayer insulation systems. SOURCE: References 9 and 25

For most MLIs the increase in heat flux is proportional to P^n, where P is the compressive load and n is between one-half and two-thirds as shown in Figure 4-22[9,26]. Assuming elastic deformation[26], the contact area between two cylinders pressed together with the axes at right angles is proportional to the force raised to the 2/3 power, and for two cylinders with their axes parallel, the contact area is proportional to the force raised to the 1/2 power. For the random orientation of the fibers in multilayer insulation spacers, the heat flux (which is proportional to the contact area, if solid conduction dominates) would be expected to be proportional to the compressive pressure raised to a power between 1/2 and 2/3[26].

The effect of mechanical loading on thermal conductivity of several MLI systems is shown in Figure 4-23. The data shown in Figure 4-23 illustrate the following[21]:

(1) With an increase in mechanical load, the solid conduction contribution to heat transfer becomes dominant.

(2) The differences in thermal conductivity at optimum layer density are the result of differences in the spacer materials. Spacers consisting of fibers have a high contact resistance which impedes solid conduction. With no external load on the insulation, the closeness of the packing of these fibers (and hence the contact resistance) depends upon previous history such as number of load applications, method of manufacture, and storage conditions. The crinkled polyester film is subject to a greater increase in thermal conductivity under compressive loading compared to other multilayer insulation. The lack of mechanical strength of the thin film leads to a greater increase in solid conduction by flattening out crinkles. Multilayer insulations using fiber spacers have comparable thermal conductivities for loads exceeding 20.7 kPa.

(3) After an initial sharp rise the thermal conductivity is a function of the two-thirds power of the mechanical load. This relationship corresponds to the deformation of a sphere resting on a plane and appears to approximate the deformation of the contact areas between the spacers and the radiation shields. The trend of the effects of mechanical load on thermal conductivity indicates that the insulating effectiveness of most multilayer insulations is greatly reduced under compressive loads.

The effect of mechanical loads on density for different MLI systems is shown in Figure 4-24. Because a considerable choice exists in the thickness of radiation shields and spacers, the insulation density can be adjusted to meet a particular set of conditions. The selection of a combination of materials may be more influenced by specific design requirements including the effects of lateral heat conduction through the radiation shield, structural integrity, high-temperature stability, and production considerations[21].

The density of the crinkled polyester film is strongly dependent on repeated mechanical load application. The results of compression on a sample consisting of 20 shields are given in Table 4-12, and indicate the hysteresis effect obtained by repeated compression causing a flattening out of the crinkles. The density of the sample was calculated from the thickness, which was measured during the test in a fixture constructed for this purpose[21].

Spacer materials consisting of two or more substances have been suggested for use in an MLI system to mitigate the effects of compressive loads[25]. The spacer may be a separate material consisting of very light webs of stable thin materials with tensile properties that will permit easy application of the insulation, or the spacer may be physically attached to the radiation shield (for example, by "flocking" a pattern of short, fine fibers onto the radiation shield)[25]. The effect of mechanical loading on heat flux through MLI systems with a variety of shield and spacer materials is shown in Fig. 4-25[25], and the results of other experiments[11,27] are provided in Table 4-13.

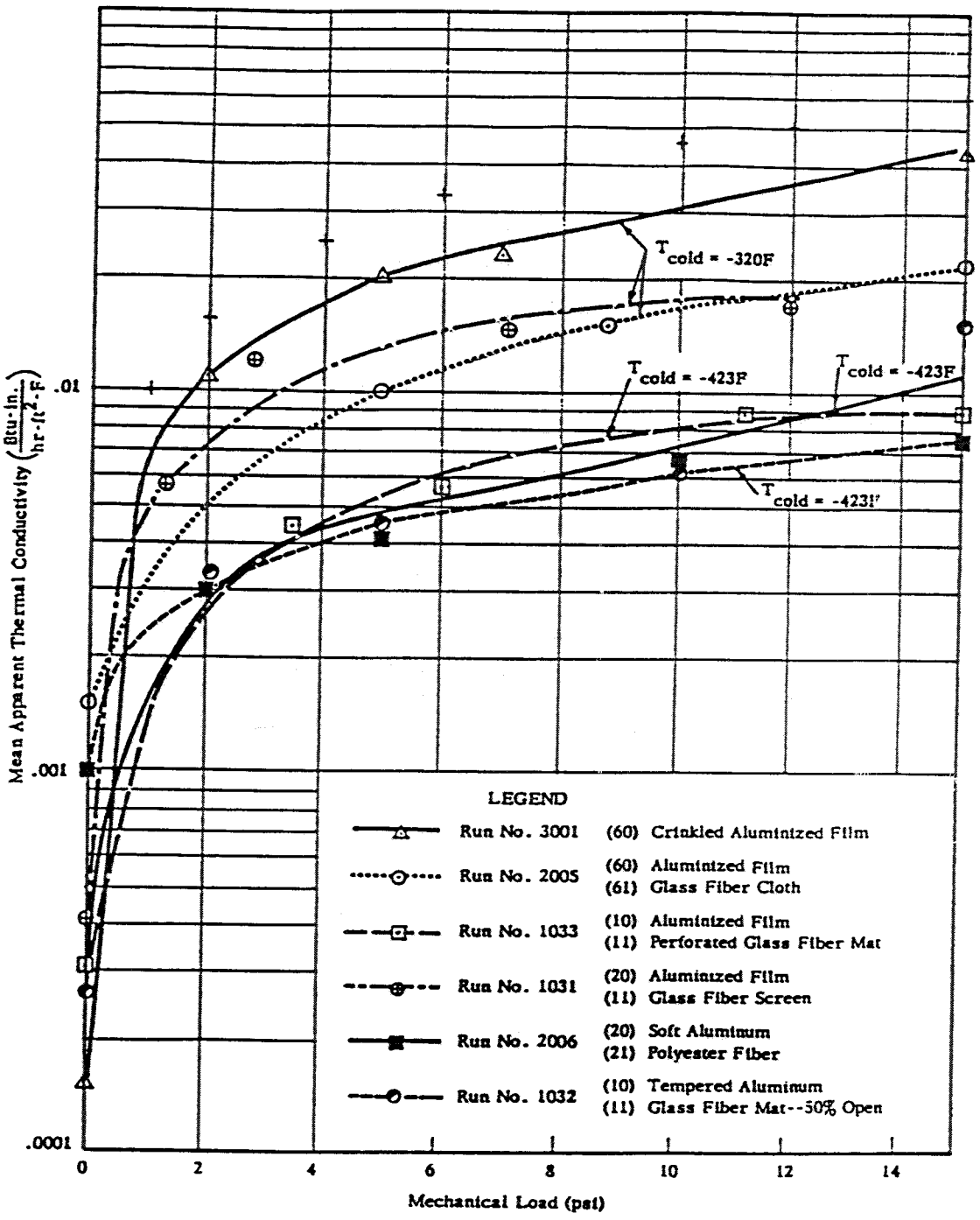

Figure 4-23 Effect of mechanical loading on thermal conductivity for various multilayer insulation systems. SOURCE: Reference 21.

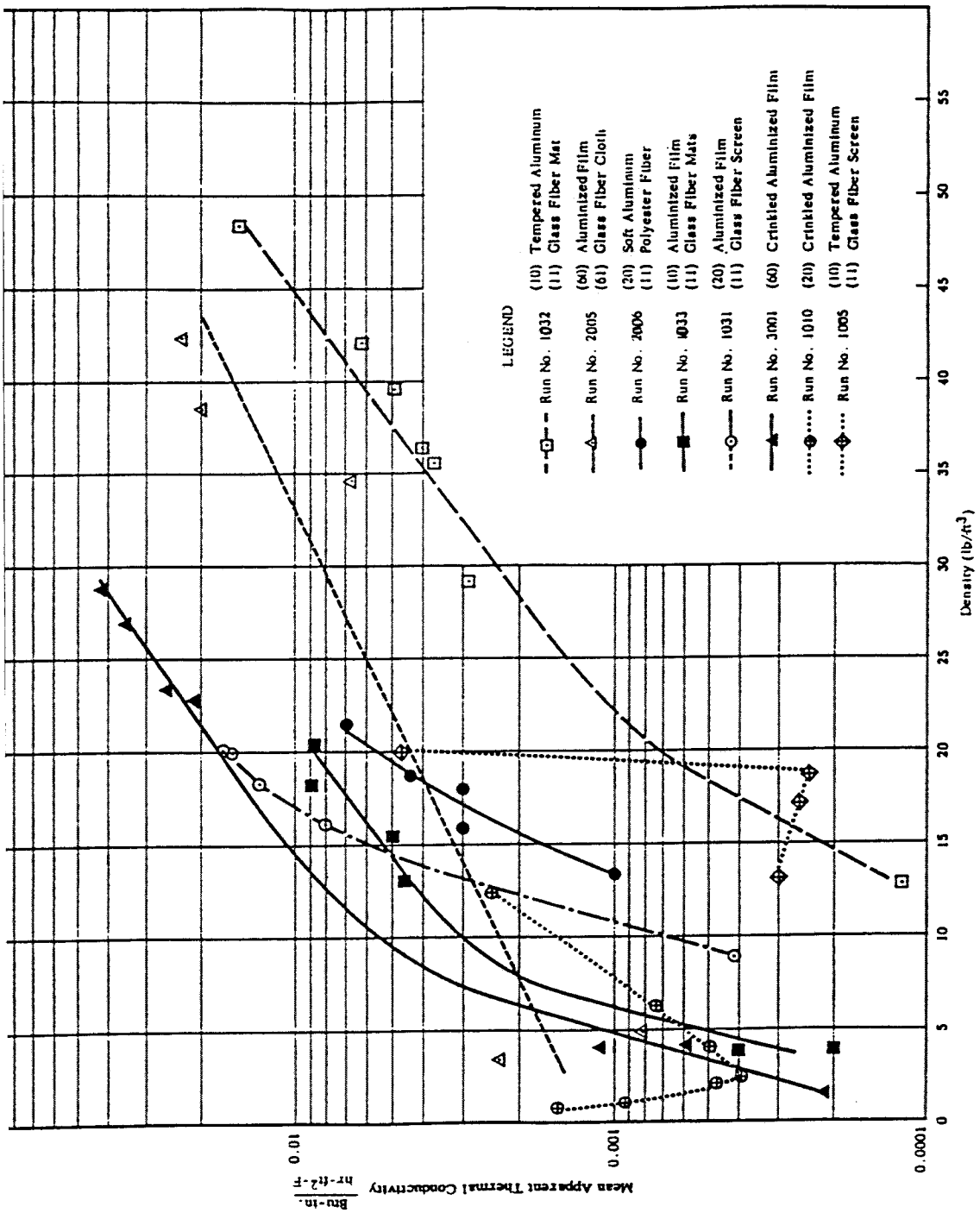

Figure 4-24 Effect of density on mean apparent thermal conductivity for several multilayer insulation systems. SOURCE: Reference 21

Table 4-12
Results of compression tests on crinkled polyester film, 6.35μm thick uncompressed
(SOURCE: Reference 21)

	Compressive load (Pa)	Sample thickness (mm)	Density (kg/m^2)
A. First test	0	25.4	2.15
	41	12.7	4.25
	124	7.87	6.79
	372	4.57	11.28
	807	3.18	16.89
B. Repeat test	117	3.61	14.89
	372	2.03	26.46
	1,131	1.4	38.57
	1,276	1.12	48.19
C. Repeat test	124	1.5	35.93
	372	1.3	41.5
	1,131	1.19	45.01
D. Repeat test	1,276	1.07	50.33

Table 4-13
Summary of effect of compression on thermal conductivity of multilayer insulation for boundary temperatures of approximately 300 K and 77 K.

Insulation	Shields per cm	Compression pressure (kPa)	Thermal conductivity (μW/m-K)	Ref
Shield: Polyethyleneterephtalate (PEPT) film, double aluminized, crinkled, **Spacer:** Basalt (75%) and Cellulose (25%) (δ=400 micron)	15	20	1,100	27
Shield: Polyethyleneterephtalate (PEPT) film, double aluminized, crinkled, **Spacer:** Basalt (75%) and Cellulose (25%) (δ=400 micron)	20	100	1,600	27
Shield: Aluminum,1145-H19, 50 micron **Spacer:** Nylon mesh, 18 micron thick	--	100	2,300[b]	9
Shield: Polyester film, double -coated aluminized, 6.3 micron thick **Spacer:** Nylon mesh, 18 micron thick	--	100	2,600[b]	9
Shield: Soft aluminum, 12 micron thick **Spacer:** Fiber glass cloth (3 layers), 25 micron thick	--	100	4,800[b]	9
Shield: Soft aluminum, 12 micron thick **Spacer:** Fiber glass mat	--	100	640[b]	9
Shield: Soft aluminum, 25 micron thick **Spacer:** Fiber glass mat, 76 micron thick	--	100	1,100[b]	9
Polyester film, one side aluminized, crinkled	--	100	5,900[b]	9
Shield: Aluminum foil **Spacer:** Glass fiber	--	101	880	11
Linde Super Insulation (SI-62)	--	101	865	24
Linde Super Insulation (SI-62)	--	103	1010[a]	36

[a] Boundary temperatures not specified
[b] Boundary temperatures 293 and 20K

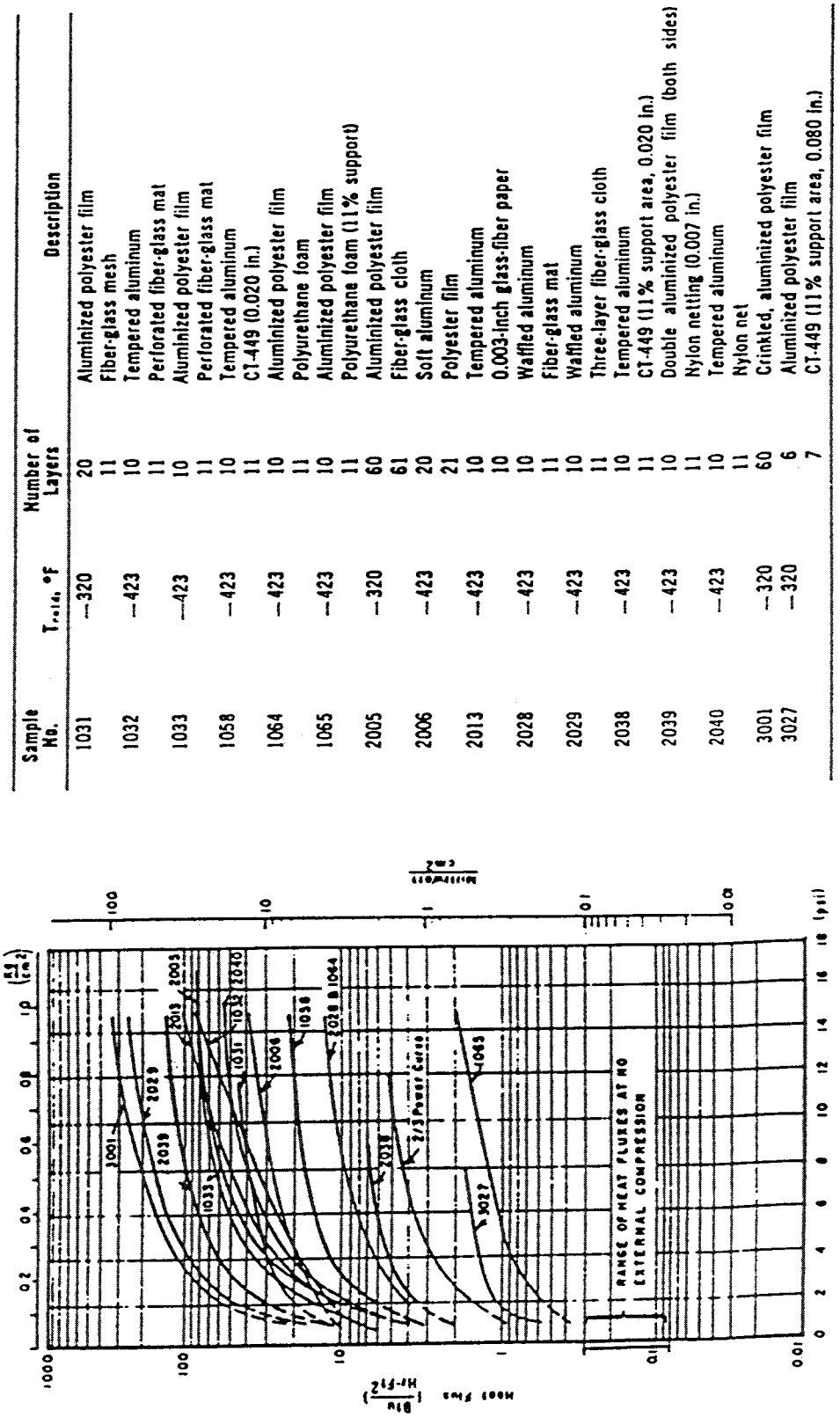

Sample No.	T_{cold}, °F	Number of Layers	Description
1031	−320	20	Aluminized polyester film
		11	Fiber-glass mesh
1032	−423	10	Tempered aluminum
		11	Perforated fiber-glass mat
1033	−423	10	Aluminized polyester film
		11	Perforated fiber-glass mat
1058	−423	10	Tempered aluminum
		11	C1-449 (0.020 in.)
1064	−423	10	Aluminized polyester film
		11	Polyurethane foam
1065	−423	10	Aluminized polyester film
		11	Polyurethane foam (11% support)
2005	−320	60	Aluminized polyester film
		61	Fiber-glass cloth
2006	−423	20	Soft aluminum
		21	Polyester film
2013	−423	10	Tempered aluminum
		10	0.003-inch glass-fiber paper
2028	−423	10	Waffled aluminum
		11	Fiber-glass mat
2029	−423	10	Waffled aluminum
		11	Three-layer fiber-glass cloth
2038	−423	10	Tempered aluminum
		11	C1-449 (11% support area, 0.020 in.)
2039	−423	10	Double aluminized polyester film (both sides)
		11	Nylon netting (0.007 in.)
2040	−423	10	Tempered aluminum
		11	Nylon net
3001	−320	60	Crinkled, aluminized polyester film
3027	−320	6	Aluminized polyester film
		7	C1-449 (11% support area, 0.080 in.)

Figure 4-25 Effect of mechanical loading on the heat flux through various multilayer insulation systems. SOURCE: Reference 25.

Effect of Gaps, Penetrations, and Joints. Gaps between the edges of adjacent shields at corners or joints can add significantly to the total heat transport[1]. Thus, design considerations and techniques of application are very important[1]. In addition, the insulation must be installed clean and dry because an interstitial gas pressure lower than 10^{-4} torr is required to attain low conductivities[1].

The thermal conductivity of multilayer insulation in the direction parallel to the shields is about three orders of magnitude greater than the thermal conductivity in the direction normal to the shields[10]. Consequently, insulation around penetrations through the insulation must be installed carefully to avoid seriously degrading the performance of the insulation by contact between edges of the insulation with the penetrations[10]. The aluminum foil/glass fiber combination has a low thermal conductivity perpendicular to the foil, but the lateral conduction has been estimated to be thousands of times greater[11]. The advantage of aluminized Mylar is its reduced lateral conduction (although it is significantly greater than the transverse conductivity) and its relatively low density[11]. Under optimum conditions, its density is two to three times less than other multilayer insulations[11].

The overall thermal performance of MLI systems used in large scale cryogenic applications is often not as good as expected based on experimental measurements. This performance degradation is often qualitatively attributed to penetrations through the MLI and to joints between prefabricated MLI blankets. The effect of joints in MLI was investigated by cutting slots in an MLI blanket installed over a black painted copper surface. The heat load increased by a factor of 3.5 over the calculated increase. Furthermore, the degradation was even greater when the vacuum got poorer by an order of magnitude[7]. A theoretical model was developed to predict the effect of joints in MLI[28]. One observation from this model is that interleaving patches between layers of aluminized Mylar MLI is more effective than putting the same number of patches on top of a crack[28]. Experimental results indicate that the use of a patch every few layers is

almost as effective as using a patch every layer[29]. Placing the patches in the upper (higher temperature) half of the blanket is observed to be much better than in the lower (lower temperature) half and can reduce the heat load essentially to that without joints[29].

As a rough guide, no more than 30% of the total heat leak into the cryogenic system should be caused by discontinuities such as joints, supports, and piping attachments[21]. Heat leaks that are higher would tend to nullify the effectiveness of the insulation and might make the use of a simpler system more desirable. Heat leaks can be classified as[21]:

(1) Weak thermal shorts where a linearized radiation boundary condition can be applied with an acceptable accuracy, e.g., where the surface temperature is within 10% of the adiabatic wall temperature.

(2) Strong thermal shorts when the depression of the temperature at the outer surface of a foil exceeds 10% of the adiabatic wall temperature and when the analytical solution of the problem requires a nonlinear boundary condition.

(3) Absolute thermal shorts where the penetration is so highly conductive that the cold wall of the cryogenic system and the outside surface of the short are nearly at the same temperature.

Multilayer insulations can be used with spacers made with materials such as Teflon to meet the structural requirements and to satisfy the weak thermal short condition. Steel or other separators would not fall into the category of weak thermal shorts unless an insulator was installed between the multilayers and the penetration. In the case of aluminized film, weak thermal shorts could be obtained for a structural material of reasonable thickness and low thermal conductivity when the thickness of the film assembly is greater than 2.54 cm (1 in.). The maximum widths of various materials penetrating multilayer insulations when the weak thermal short approximation is applicable are shown in Figure 4-26. The design of a thermal insulation system, even with weak thermal shorts, may have to be modified so that the overall heat leak is within permissible limits[21].

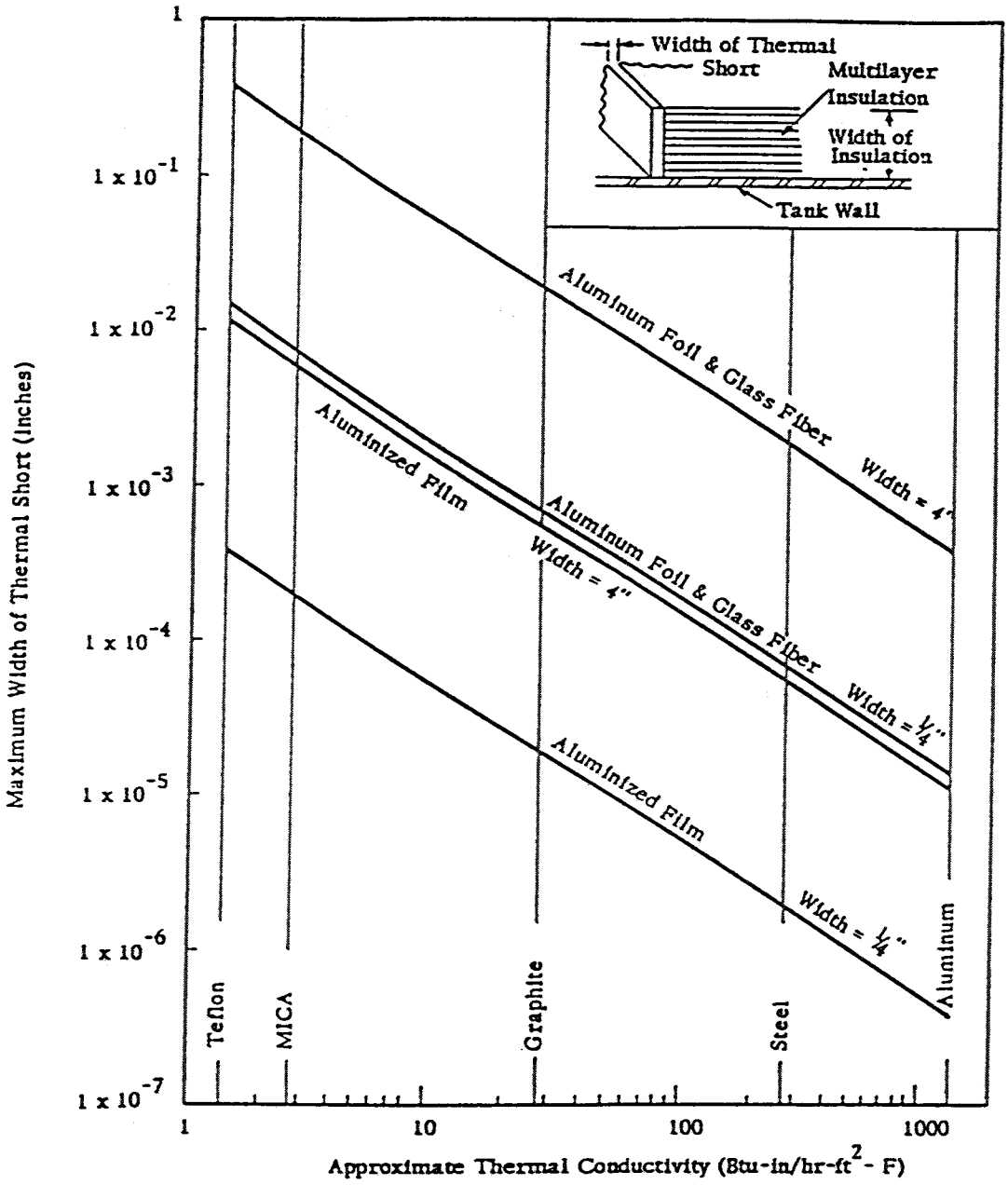

Figure 4-26 Maximum width of various thermal short materials penetrating multilayer insulations. SOURCE: Reference 21.

Effect of Perforations. Interstitial gas within MLI must be evacuated through the edges of the insulation unless other provisions are made[26]. Generally, edge pumping alone is not adequate to remove the absorbed gases from within an MLI in a reasonable length of time. Also, a pressure gradient may build up within the insulation during the initial pump down causing mechanical damage to the insulation[26]. Finally, the edges must be exposed for edge pumping to be effective, and radiant energy may strike the exposed edges and be "tunneled" between the layers of insulation[26]. Because of this lateral heat transport, the performance of the insulation would be degraded[26].

More effective pump down of the insulation is made possible by perforating the radiation shields[26]. If the perforations comprise 10% of the surface area of the shields, the pumping rate of gas from the insulation is increased by a factor of approximately 1000 compared with edge pumping; however, for the same percentage perforation area, the radiant heat flux is increased by a factor of 5. A compromise must be reached in a specific application between attaining a sufficiently high pumping speed from the insulation and preventing degradation of the insulation thermal performance[26]. A 1% open area with holes of 3.175-mm diameter spaced on 25.4-mm centers is often used as a satisfactory compromise[26].

For the same perforation area, the pumping is more effective when many small holes are used instead of a few large holes[26]. However, the radiant heat flux is higher for the situation of many small holes as shown in Figure 4-27[26]. Generally, perforations have a smaller effect on the insulations using crinkled aluminized Mylar shields than on the insulations with aluminum foil shields and glass fiber spacers[26].

Effect of Diameter. Calculated and experimental data indicate that the heat flux through a fixed insulation system (constant number of layers and layer density) increases as the diameter of a cylindrical cold surface decreases[30]. Heat flux is inversely proportional to the radius of the insulation [as shown in Eq. (1)]; this applies to MLI

when the apparent thermal conductivity is used to estimate the heat flux. Heat flux for a 10-mm o.d. tube with 30 layers was about twice as large as that for a 65-mm o.d. tube with the same number of insulators[30]. However, this increase in heat flux is reduced as the number of layers is reduced[30].

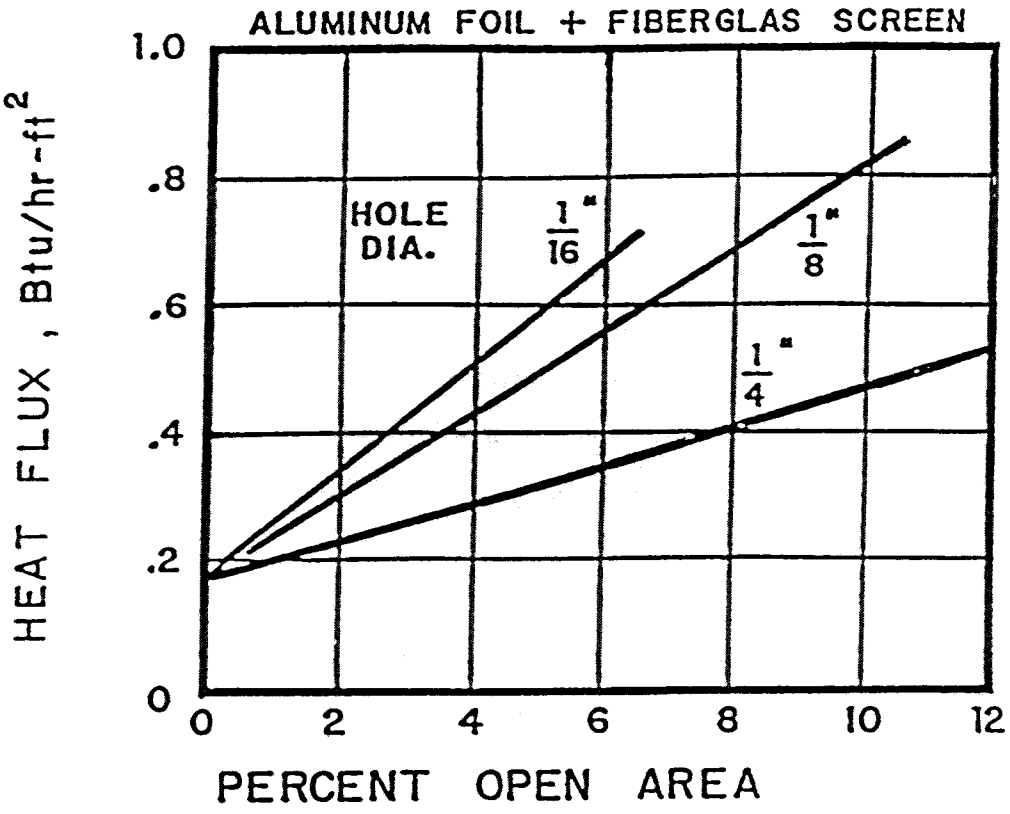

Figure 4-27 Effect of perforation of the radiation shields on the heat flux through a multilayer insulation

Fabrication. A technique for fabricating MLI blankets in lengths up to 17 m has been developed at Fermilab and is available for licensing to industry[31,32].

Comparison Of Cryogenic Insulations

An overall comparison of the mean effective thermal conductivity of various insulation types with boundary temperatures of approximately 300 and 77 K is given in Figure 4-28. A comparison of the dependence of thermal conductivity on residual gas pressure for various insulation types is given in Figure 4-29[21]. A comparison of the advantages and disadvantages of various insulations that are commonly used in cryogenic systems is given in Table 4-14[10].

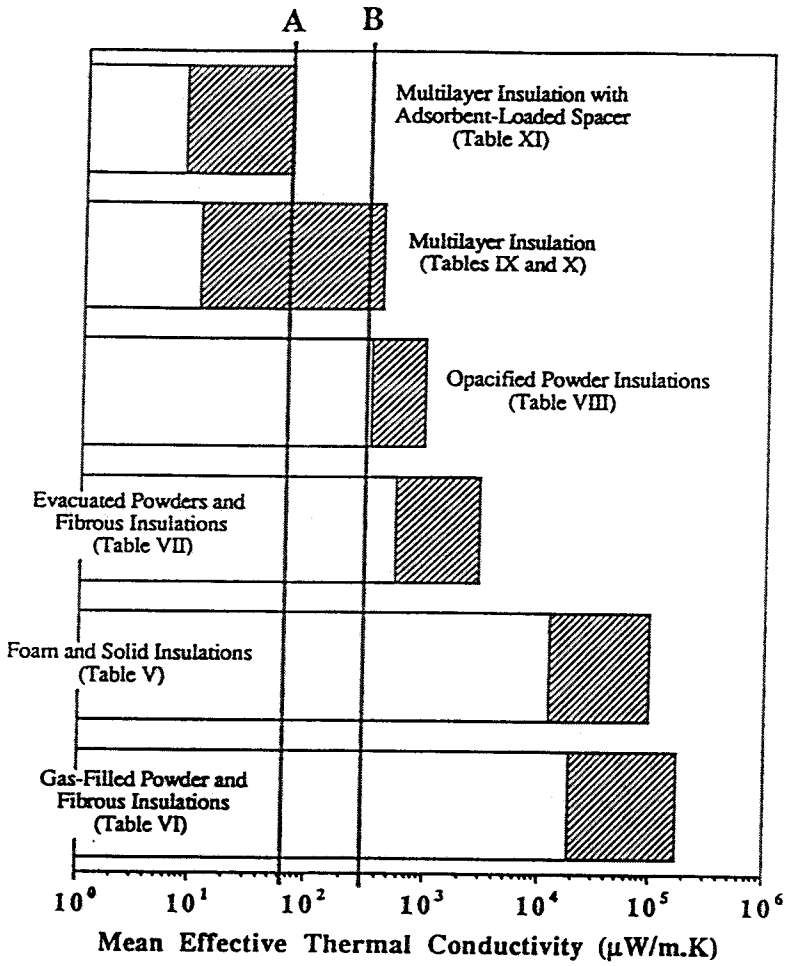

Figure 4-28 Comparison of mean effective thermal conductivity for various insulations with boundary temperatures of approximately 300 K and 77 K. Lines A and B are for k_{eff}=69 and 293μW/m-K; the values required for thermal heat leak of 1W/m for a cryogenic enclosure with an i.d. of 25 cm and 5 cm, respectively.

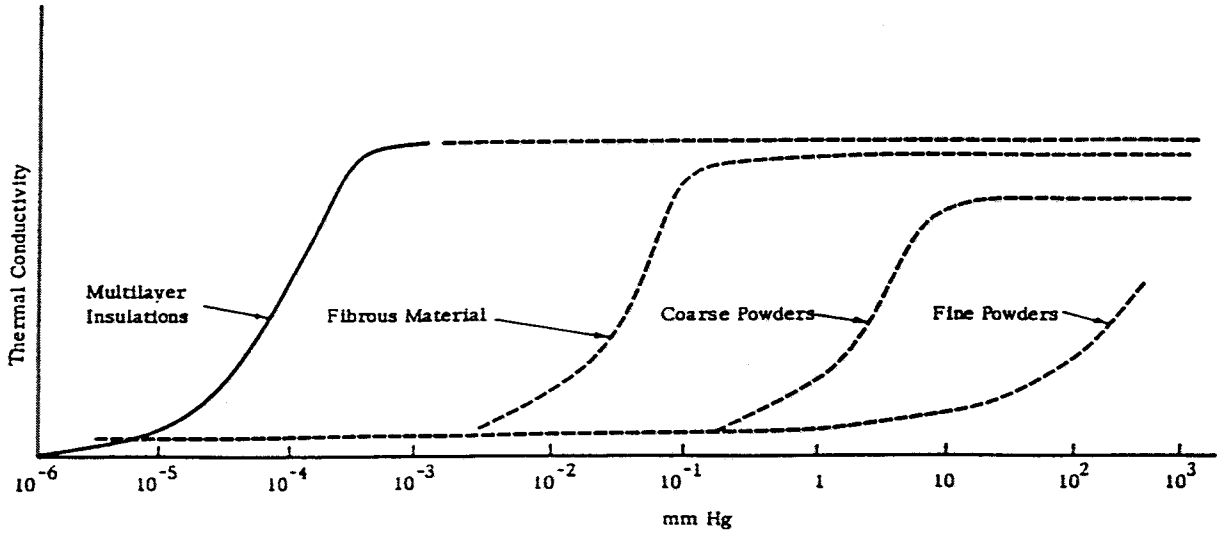

Figure 4-29 Dependence of thermal conductivity on pressure for various particle spacings for several cryogenic insulation types. SOURCE: Reference 21.

The boundary temperatures that are of most interest for a high-temperature superconducting power transmission line are room temperature (about 300 K) and the boiling point of nitrogen (about 77 K). When high-vacuum insulation is used, heat is transferred from a surface at 300 K to one at 77 K almost entirely by radiation, and the radiant heat transfer is practically unaffected by reducing the temperature of the cold surface below 77 K because of the T^4 temperature difference[2]. However, with the cold boundary at 77 K, even a small amount of residual gas (hydrogen or helium) will account for a large part of the total heat flow[2]. If the surfaces that are at 300 K and 77 K are separated by a few inches, evacuated powder will usually improve the insulation by reducing the radiant heat transfer[2]. This applies to surfaces having emissivities of ~0.01.[2] If the emissivities can be made low enough, the powder will not help[2]. However, the additional heat capacity of the powder will result in a greater cooldown load[2].

Table 4-14
Summary of the advantages and disadvantages of various insulation systems
SOURCE: Reference 10.

Advantages	Disadvantages
Expanded Foams *Low cost * No need for rigid vacuum jacket * Good mechanical strength	* High thermal contraction * Conductivity may change with time
Gas-Filled Powders and Fibrous materials * Low cost * Easily applied to irregular shapes * Not flammable	* Vapor barrier is required * Powder can pack and conductivity is increased
Vacuum alone * Complicated shapes may easily insulated * Small cooldown loss * Low heat flux for small gap between inner and outer vessel	* Permanent high vacuum required * Low-emissivity boundary surfaces needed
Evacuated powders and fibrous materials * Vacuum levels less stringent than for MLI * Complicated shapes may be easily insulated * Relatively easy to evacuate	* May pack under vibratory loads and thermal cycling * Vacuum filters are required * Must be protected when exposed to moist air (retains moisture)
Opacified powders * Better performance than straight evacuated powders * Complicated shapes may be easily insulated * Vacuum requirement not as stringent as for MLI and vacuum alone	* Higher cost than evacuated powders * Explosion hazards with Al in O_2 atmosphere * Problems of settling of metallic flakes
Multilayer insulation * Best performance of all insulations * Low weight * Lower cooldown loss compared with powders * Better stability than powders	* High cost per unit volume * Difficult to apply to complicated shapes * Problems with lateral conduction * More stringent vacuum requirements than powders

Permeable insulations, such as gas-filled powders, are at least an order of magnitude poorer than vacuum insulation for the 300 to 77 K boundary temperatures because the gases available for filling the voids have high thermal conductivities[2]. The principle virtue of this type of insulation is that it does not require vacuum tight boundaries and therefore can be lighter and less expensive than most evacuated insulations[2].

Solid insulation materials are inferior to gas-filled permeable insulation in the upper temperature region, but they usually improve greatly as the temperature is lowered to 20 K because the gas in the cells is condensed and the thermal conductivity of the solid constituting the cell walls is greatly reduced[2]. One notable exception is a glass foam which contains hydrogen gas in the cells[2]. Solid foams also can be used without vacuum-tight boundaries[2].

A large number of variables is involved in determining the thermal conductivity of an insulation; consequently, the values given herein should be considered accordingly. The total heat leak through any insulation system, especially for circular geometries of small diameter, is usually greater than that predicted by analysis. Therefore, a design margin should be included in the absence of measured performance data for the proposed system.

Thermal insulations for a superconducting power transmission line should not be compared strictly on the basis of thermal conductivity only. Consideration should also be given to durability, ease of manufacturing, and ease of maintenance.

Outgassing

Attaining a good vacuum can be considerably limited by the release of gases (often in large quantities) from the materials and surfaces within the enclosure during, or following, evacuation. This gas release can often be a very gradual process. Several sources exist for the gases that are released during evacuation including gases bound to

the surfaces by physical adsorption, gases dissolved in the solid materials, and gases existing in chemical combination (for example, in oxides on the surfaces). By heating during the evacuation process these gases can be removed effectively and, thus, minimize evacuation time and achieve a better vacuum. If heating during evacuation is not feasible, heating the components in a vacuum before assembly into the vacuum system is also effective[2].

Organic materials, such as rubber and phenolic plastics, should not be used in a vacuum system because they often contain appreciable quantities of air in solution and may also contain entrapped or dissolved plasticizer. (Large quantities of outgassing plasticizer and solvents can present a contamination problem for a vacuum pumping system, especially the vacuum pump oil.) Teflon, Kel-F, polyethylene, polystyrene, and epoxy resins are often used in vacuum systems without causing too much difficulty with outgassing[2]. The inside surfaces of a vacuum enclosure and the components within the enclosure should be very clean, especially of oil films, water, cleaning fluids and solvents, and soldering flux. Detergents with hot water and/or solvents are commonly used for the cleaning process[2].

Outgassing is a major consideration in deciding whether to provide continuous pumping of a vacuum system or whether to use adsorbents to trap such gases. Typical values for the specific outgassing rate for several materials are given in Table 4-15[10]. The specific outgassing rate is defined as the outgassing rate per unit surface area after a certain time has elapsed[10]. The outgassing rate depends strongly upon the condition of the surface exposed to vacuum[10].

Getters

Getters are often used in vacuum systems to improve or maintain vacuum, especially when outgassing occurs in passive vacuum systems. The getter is a material that takes up gas at very low pressures through various processes which include physical

adsorption of the gas upon an extended surface adsorbent, chemical combination with suitable active materials, and solution of gases in certain metals[2].

Table 4-15
Outgassing rates for several materials. SOURCE: Reference 10

Material	Condition	Specific outgassing Rate (μPa-m/s)	
		1 hour	10 hours
Mild steel	Shotblasted	---	80
	---	670	67
	As received (450°C)	560	---
	Degreased (450°C)	480	---
	As received (200°C)	---	11.5
	As received (400°C)	---	11.2
	Baked 15 h (400°C)	---	0.016
Stainless Steel	---	270	27
	Polished,degreased	---	1.9
	As received (450°C)	850	---
	Degreased (450°C)	530	---
	Annealed (450°C)	71	---
	Baked 12 h (400°C)	---	0.0012
Aluminum	Anodized	---	130
	As received (450°C)	1,730	---
	As received	---	3.3
	As received (200°C)	---	6.0
	Baked 13.5 h (200°C)	---	0.49
	Baked 15 h (300°C)	---	0.21
Copper	---	3,100	---
	As received (450°C)	2,100	---
	Degreased	1,900	---
Neoprene	---	40,000	20,000
	As received	267,000	---
Teflon	As received	6,700	---
	---	610	280
Butyl Rubber	---	2,000	---
Kel-F	---	53	---
Mylar	As received	4,000	---
Polyethylene	---	350	---
Nylon	---	16,000	---
Plexiglas	Outgassed	1,330	---

The use of chemical getters (such as barium and alkali and alkaline earth metals) requires that the pressure achieved be greater than the dissociation pressure of the compound formed by the metal and the gas and that the reaction take place with reasonable speed[2].

Titanium, zirconium, palladium, and thorium are transition metals commonly used as solution getters. These take common gases such as N_2, O_2, and H_2 into solid solution either as dissociated atoms or possibly by dissolving compounds formed by the gas and the metal. The more active of these metals may absorb very large quantities of gas. Gas/metal systems of this type show decreasing gas solubility, but increasing rate of solution, with increasing temperature. The optimum operating temperature is obtained by a balance of these factors[2].

Adsorbents such as activated coconut charcoal are used to adsorb gases in a vacuum enclosure. The adsorbents' effectiveness is increased at low temperatures; consequently, the adsorbent is usually thermally connected to the lowest temperature in the system. The vacuum in an enclosure may not be very good at room temperature, but as soon as a cryogen is introduced into the system the adsorber will take up gas and greatly improve the vacuum[2].

Using an adsorbent to improve a high vacuum requires that the adsorbent be able to adsorb gas at a very low pressure. The adsorption of nitrogen and hydrogen by carbon is shown in Figure 4-30. The differences shown in Figure 4-30 reflect a wide variation in the adsorptive capacity between the various types of carbon used[2].

Thermal Insulation for a Superconducting Power Transmission Line

The equations and data presented above were used to estimate the heat leak through various insulation systems as a function of insulation thickness for two SPTL sizes (cryogenic enclosure i.d. = 5 and 25 cm). These estimates were made for SPTLs with

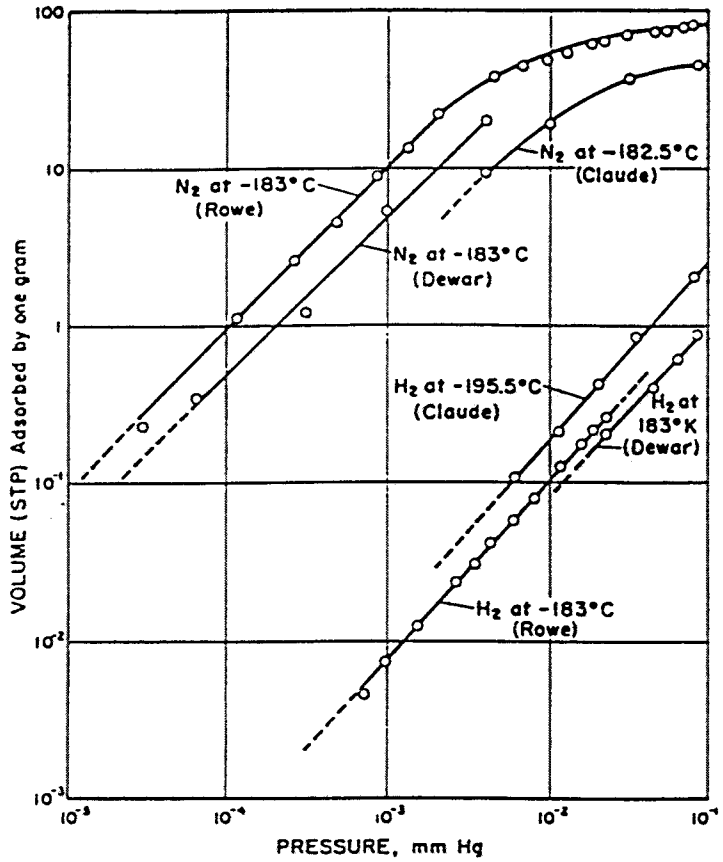

Figure 4-30 Volume (cm^3 at STP) of nitrogen and hydrogen adsorbed by activated charcoal at low temperatures and pressures. SOURCE: Reference 2

heat transfer from the environment as a result of (1) overhead installation with convection to air; (2) burial in soil with conduction through the surrounding soil; and (3) dielectric layer installation on the outside of the cryogenic enclosure with convection to air on the outer surface of the dielectric. Assumptions that were used in making these estimates are summarized in Table 4-16. The results of these heat leak estimates are presented in Figures 4-31 through 4-35. The results from these estimates indicate that MLI is the only insulation that will provide a heat leak of 1 W/m with reasonable insulation thickness (a few centimeters). A similar conclusion has been reached by others[33]. that have considered a high-temperature superconducting power transmission line. The heat leak through the low-temperature superconducting power transmission

lines at the Brookhaven National Laboratory and at the Los Alamos National Laboratory was about 0.25 W/m[33]. There is a tradeoff between heat leak and the complexity of an SPTL (in its size, coolant pressure drop, refrigeration load, etc.).

Table 4-16
Assumptions used in thermal insulation comparison

Insulation Boundary temperature (K)	
Outer	300
Inner	77
Insulation Mean Effective Thermal Conductivity (mW/m-K)	
Foam	12
Gas Filled Powder and Fiber	32
Evacuated Powder and Fiber	1.1
Multilayer	0.08
Emissivity for Vacuum alone Insulation	
Inner surface	0.04
Outer surface	0.05
Convective Heat Transfer Coefficient to Air (W/m^2-K)	8.51 [a]
Soil Mean Effective Thermal Conductivity (mW/m-K)	1,039 [a]
Depth of Soil Above Thermal Insulation (m)	1
Dielectric Thickness (cm)	5
Dielectric [b] Mean Effective Thermal Conductivity (mW/m-K)	104

[a] Source = Reference 4
[b] Mylar

The effect of heat transfer boundary conditions (such as convection to air, conduction through soil, or conduction through a dielectric layer with convection to air) may be neglected in making first order estimates of heat leak through an insulation that is of practical thickness with reasonably low values of heat leak such as would be necessary for an SPTL. This effect is shown in Figure 4-36 for a foam insulation. The results for a foam insulation are presented in Figure 4-36 to show the divergence of the curves for a thin insulation with large heat transfer values. The same cases with MLI, instead of foam, have essentially no divergence of the curves.

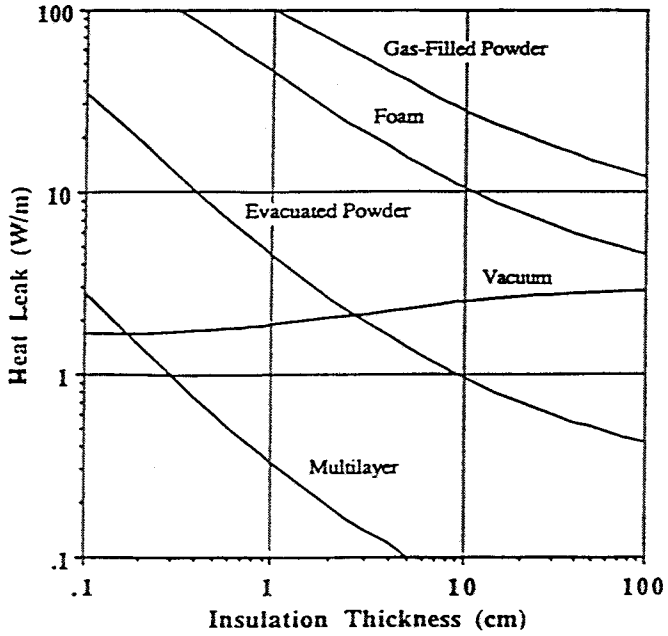

Figure 4-31 Heat leak comparison for several thermal insulations with convection to air and cryogenic enclosure i.d. = 5 cm

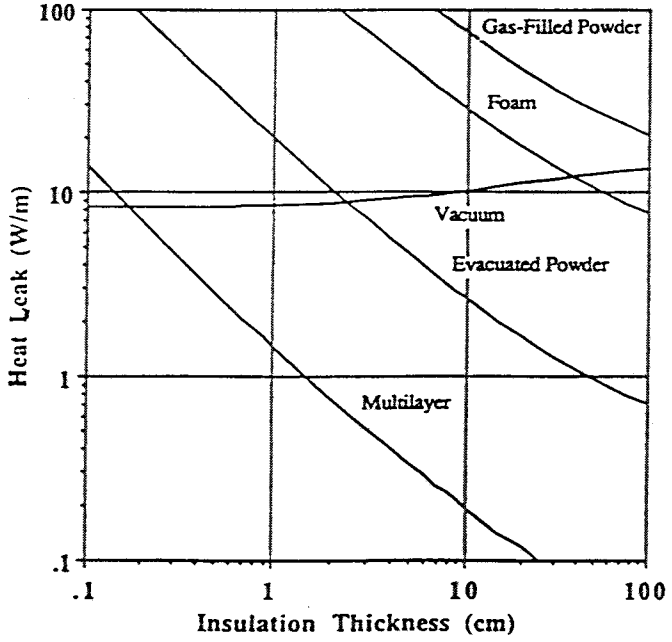

Figure 4-32 Heat leak comparison for several thermal insulations with convection to air and cryogenic enclosure i.d. = 25 cm.

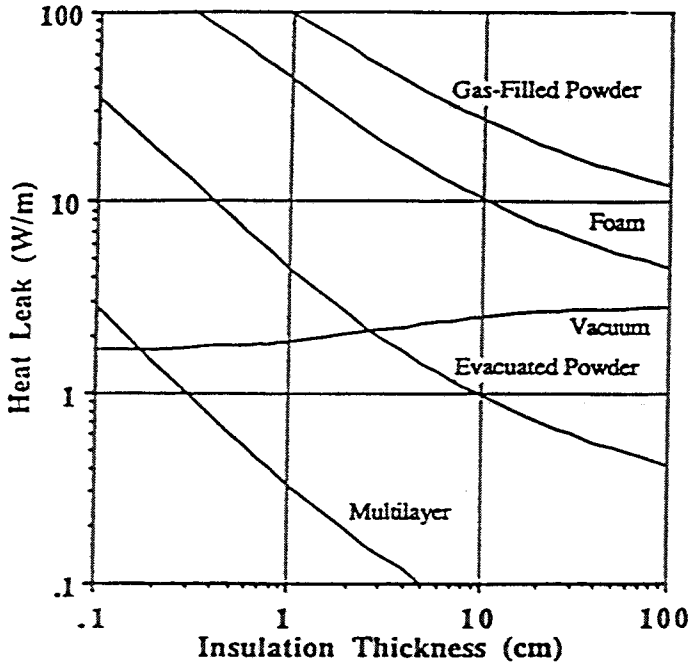

Figure 4-33 Heat leak comparison for several thermal insulations with cable buried in soil and cryogenic enclosure i.d. = 5 cm.

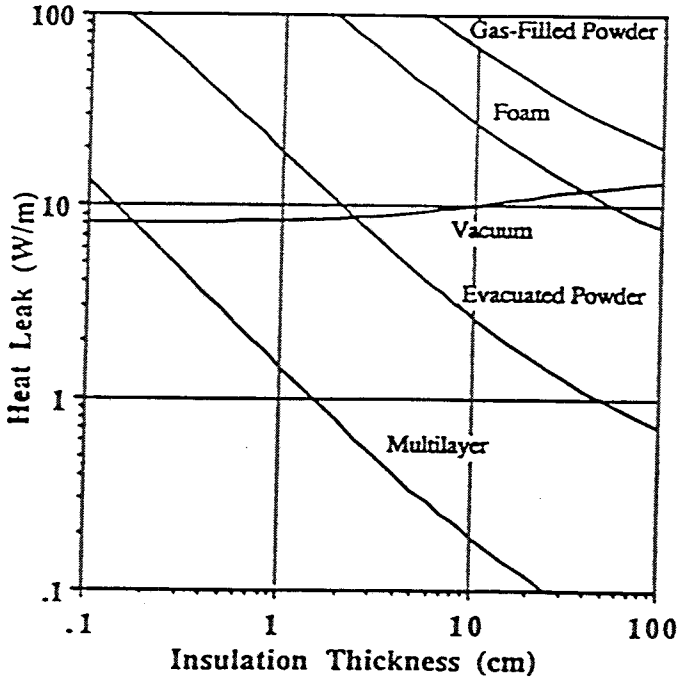

Figure 4-34 Heat leak comparison for several thermal insulations with cable buried in soil and cryogenic enclosure i.d. = 25 cm.

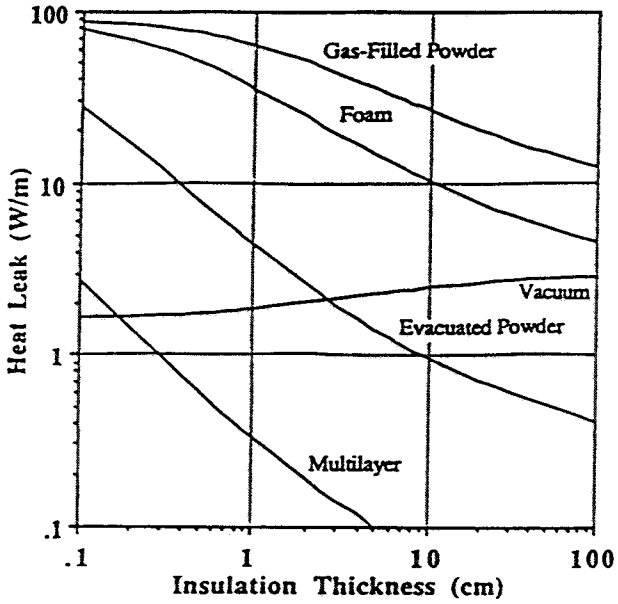

Figure 4-35 Heat leak comparison for several thermal insulations with dielectric layer on outside of cryogenic enclosure (i.d. = 5 cm) and convection to air.

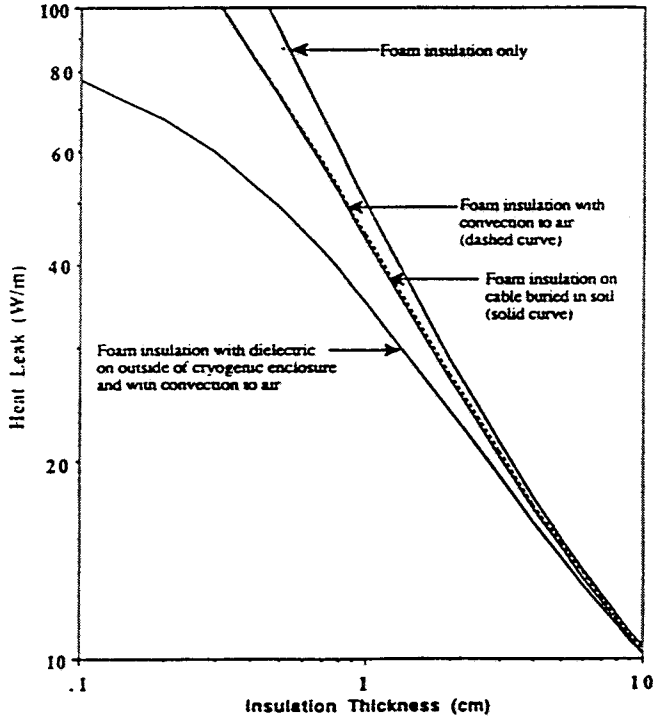

Figure 4-36 Effect of convection to air, burial in soil, and dielectric on outside of cryogenic enclosure (i.d. = 5 cm) for foam insulation.

Heat leak through MLI as a function of the cryogenic enclosure i.d. for MLI thicknesses from 0.1 to 10 cm is shown in Figure 4-37. This figure may be used to estimate the insulation thickness for a given cryogenic enclosure i.d. for a desired heat leak.

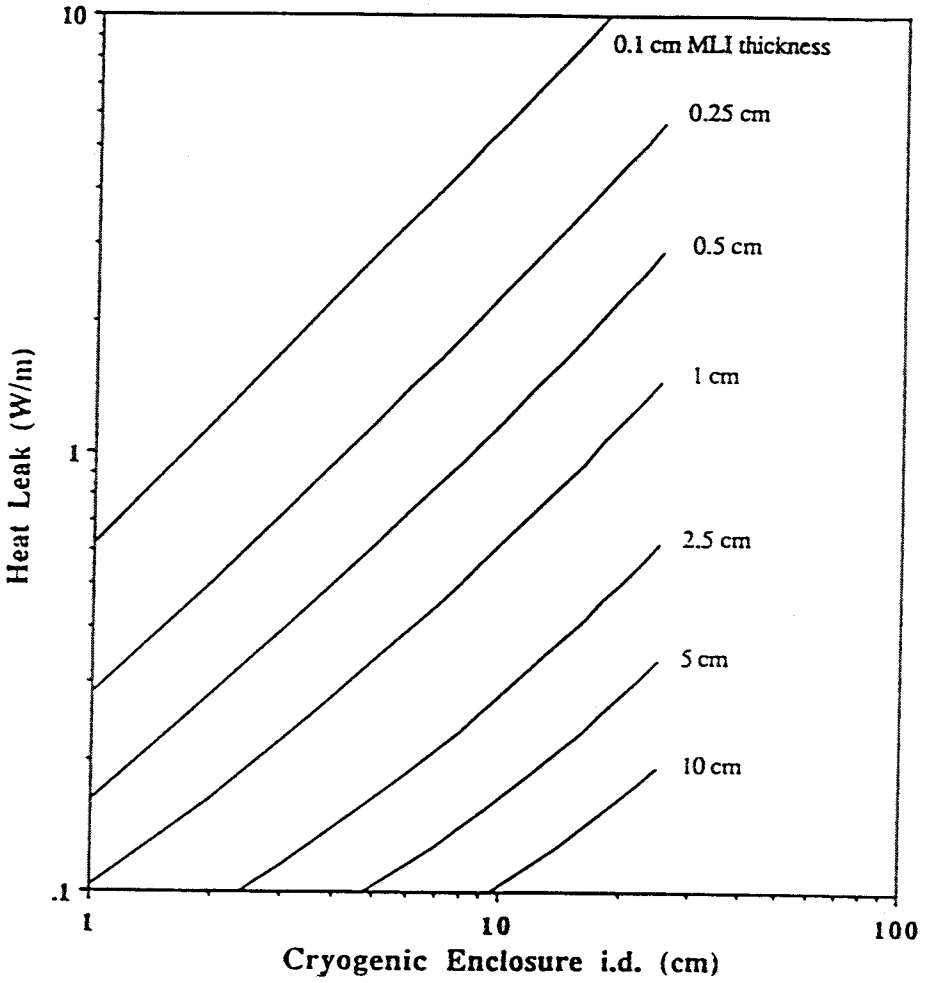

Figure 4-37 Heat leak as a function of cryogenic enclosure inside diameter for several multilayer insulation thicknesses.

The results presented in Figures 4-29 and Figures 4-31 through 4-35 indicate that MLI is the only insulation system that should be considered for an SPTL operating in the 65

to 80 K temperature range. Thus, the disadvantages and special considerations of MLI must be addressed;

* the installation of MLI on a long length (say about 600 m) of a corrugated, flexible tube;

* the need for a support mechanism to permit an MLI wrapped flexible tube to be rolled onto a spool without compressing the MLI;

* the effects (such as forces) on the MLI and the support for rolling the tube onto a spool; and

* the evacuation of a long length of an annular space between two corrugated tubes with evacuation only at the ends of the tubing.

It seems reasonable that a fabrication process is possible (such as described in Refs. 31 and 32) in which MLI is wrapped onto a corrugated tube after the tube has been formed and then has been cleaned and prepared properly. One type of support that could be used to hold the insulated inner tube inside an outer tube without compressing the MLI is a ribbon (say of Teflon) that is spirally wrapped onto the inner tube along with the MLI. An alternative is to replace the ribbon with a wire that has Teflon balls at fixed intervals along the wire. The additional heat leak from the support mechanism must be considered. Only materials that have a low outgassing property should be used in the annular space that must be evacuated.

The annular space between the MLI and the outer corrugated tube can be made large enough to facilitate evacuation of a long length of the assembly. The use of a getter attached to the outer surface of the inner corrugated tube and carbon-loaded paper spacers in the MLI could reduce the need for a high vacuum throughout the length of the assembly. One disadvantage of a long length of hose with a continuous vacuum space is that a leak into the vacuum space would have a greater effect on the SPTL; i.e., a longer length of damaged line would have a much greater heat leak than would a shorter length.

Insulation Related Issues for Further Investigation

There is a large uncertainty in the effective thermal conductivity of MLI in the configuration applicable for an SPTL; consequently, a test program is recommended to address this uncertainty. This test program could also address the issue of evacuation of a long length of corrugated tubing with multilayer insulation. Additionally, the test program could address the heat leak and effectiveness of the support concept. The vacuum pumpout connection between the vacuum space and the exterior of the cable must be electrically insulated and isolated from the high voltage in the cable. In some design concepts under consideration this connection must penetrate the dielectric layer. This connection may represent a discontinuity in the external shape of the assembly and may present a problem in rolling the assembly onto a spool or in pulling the assembly into a conduit. Hence, the vacuum connection must be addressed to consider these conditions and requirements.

Refrigeration Options

The function of the refrigeration system in an SPTL is to maintain the operating temperature of the superconductor sufficiently below its critical temperature that it can provide a useful and desirable current density, typically 10^5 to 10^6 amperes/cm^2. Several options for providing the necessary refrigeration to the SPTL are discussed herein. The application of this refrigeration to the extremely long length-to-diameter ratio of an SPTL complicates the design of the cooling process. Methods by which the refrigeration can be applied to the SPTL are also discussed in this section.

The higher critical temperatures of the new HTSC materials can greatly reduce the input energy requirement needed to produce the refrigeration of the SPTL. For this report a base operating temperature in the range available with liquid nitrogen will be considered. Thus, for the use of liquid nitrogen as the coolant, an operating temperature range of 64 K to 77 K would be practical for the SPTL conductors. If the HTSC can operate with sufficient current density at a higher temperature, the liquid nitrogen

coolant can undergo a larger temperature rise with only a modest increase in pressure and corresponding decrease in coolant flow. For example, an increase of system pressure sufficient to permit the return of the coolant to the refrigerator at a pressure no less than 0.69 MPa (100 psia) would allow the extending of the upper end of the temperature range to 98 K, with corresponding decrease of a factor of approximately 2.5 in liquid nitrogen flow rate. In addition to nitrogen, other refrigerating working media could be employed for this same temperature range.

Refrigeration Techniques

The cooling of an SPTL to its operating temperature requires the occurrence of two simultaneous processes; first, a heat sink (refrigeration) must be produced, and second, this heat sink must be applied (thermal coupling) to the entire length of the SPTL in such a way as to ensure a relatively uniform, and acceptably low temperature at all points along the length of the SPTL. The desire for uniform temperature results from a need to keep the maximum temperature sufficiently below the critical temperature that the current-carrying capacity of the superconductor is adequately high. On the other hand the cost of the refrigeration is almost inversely proportional to the minimum temperature required by the system. Thus, there is a benefit in operating at as high a temperature as possible.

The cooling of an SPTL using an HTSC involves a number of variables, including the refrigeration cycle, the cooling fluid, and the method of circulating the cooling fluid through the length of the SPTL. In turn, each of these variables involves numerous options and operating conditions.

In general, the cooling concepts for the SPTL configurations being considered for the STI Project involve using a refrigerator to cool a fluid that is circulated through the SPTL, or through a section of the SPTL. The fluid is heated by the heat leak from the environment into the cooled SPTL and by any heat generated within the SPTL. Thus,

upon its return to the refrigerator, the cooling fluid is at a higher temperature than when it left the refrigerator. The following requirements are typical of what might be expected for the refrigerator; (a) Fluid Outlet Temperature = 64 K, (b) Fluid Return Temperature = 77 K, and Cooling Load = 20 to 500 kW (depending upon several factors, such as the length of the SPTL being cooled).

Summary Description of Several Refrigeration Cycles

The efficiency of an ideal refrigerator can not exceed that of a machine operating on a Carnot Cycle. For an ideal system removing heat from a low temperature, T_c, and rejecting heat to a warm temperature, T_h, the ratio of input energy to heat energy removed is equal to

$$\frac{(T_h - T_c)}{T_c} \qquad (19)$$

In practice this limit is never attained, and only a fraction of the Carnot efficiency can be achieved. With the present status of development of cryogenic refrigerators, the type of refrigerator that will be required for SPTL application will depend upon many components, such as compressors, heat exchangers, and expansion engines. Voth[42] has considered the effects of the inefficiencies that each of these items might be expected to contribute and concludes that practical refrigeration systems can reach within about 42% of the Carnot limit. Strobridge[43] has shown that, in general, the closest approach to the theoretical Carnot efficiency is achieved in the largest machines, where the Carnot limit is within about 40% of being reached.

Although several processes have been used to produce cooling effects in the cryogenic range of temperatures, the only machines that have been developed with the cooling capacity required for an SPTL rely on closed-cycle compression and expansion of a gas working fluid. Cooling processes, such as the Joule-Thomson expansion (isenthalpic expansion through a restriction), or nearly isentropic expansion through an expansion

engine, are frequently employed. A number of different cryogenic refrigeration cycles have been developed, and could be successfully used in an SPTL application. A brief discussion of several of these cycles follows.

The Linde-Hampson Refrigerator. The Linde-Hampson refrigerator[44] in its simplest form (Figure 4-38) makes use of a compressor, a high-temperature heat exchanger, a Joule-Thomson expansion valve, and a low-temperature vessel (refrigerated space). The gas working fluid, after leaving the compressor after-cooler, passes through the heat exchanger where it is cooled by the cold gas returning from the cold end of the system. The gas exits the heat exchanger at a lower temperature and then is cooled further by free expansion through the Joule-Thomson valve. The cold gas then passes through the cold (possibly liquid) vessel where it picks up heat in performing the desired cooling. Before returning to the compressor inlet, the still cold, low-pressure gas then returns to the heat exchanger where the gas is heated by cooling the high-pressure gas exiting the compressor aftercooler. This simple arrangement is suitable for obtaining refrigeration at temperatures in the liquid nitrogen range. For cooling to be obtained by this process the working gas must be below its inversion temperature so that cooling will occur during the Joule-Thomson expansion. Even lower temperatures can be obtained by adding liquid nitrogen precooling (Figure 4-39).

The Reverse Brayton Cycle. The reverse Brayton cycle[45] is similar to the above-mentioned Linde-Hampson cycle, except that the Joule-Thomson expansion is replaced with expansion of the gas through an expander (Figure 4-40). The expander can be either a reciprocating expander (piston in a cylinder) or a turbine-type expander. In either case the gas does work in expanding so that cooling of the gas always occurs, regardless of the inlet temperature.

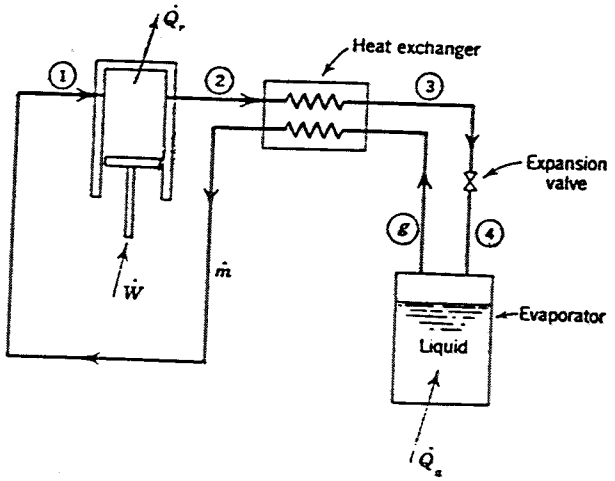

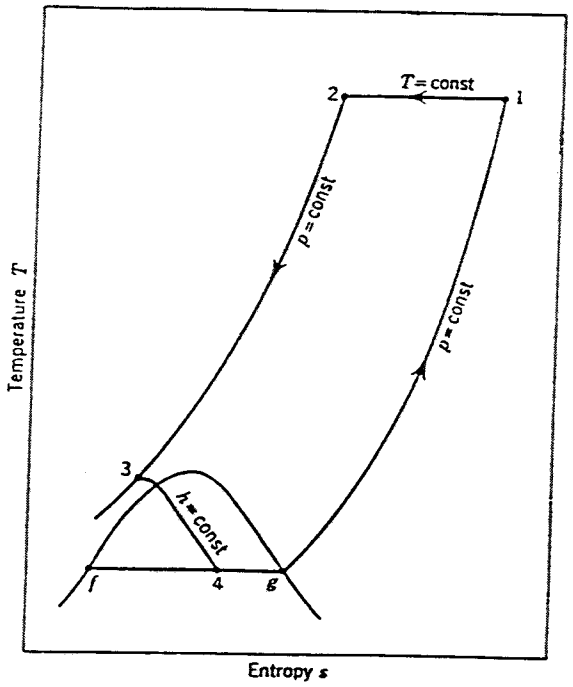

Figure 4-38 The Linde-Hampson refrigerator schematic diagram and its thermodynamic cycle T-S diagram. The numbers on the schematic diagram correspond to the state points on the T-S diagram. SOURCE: Reference 44

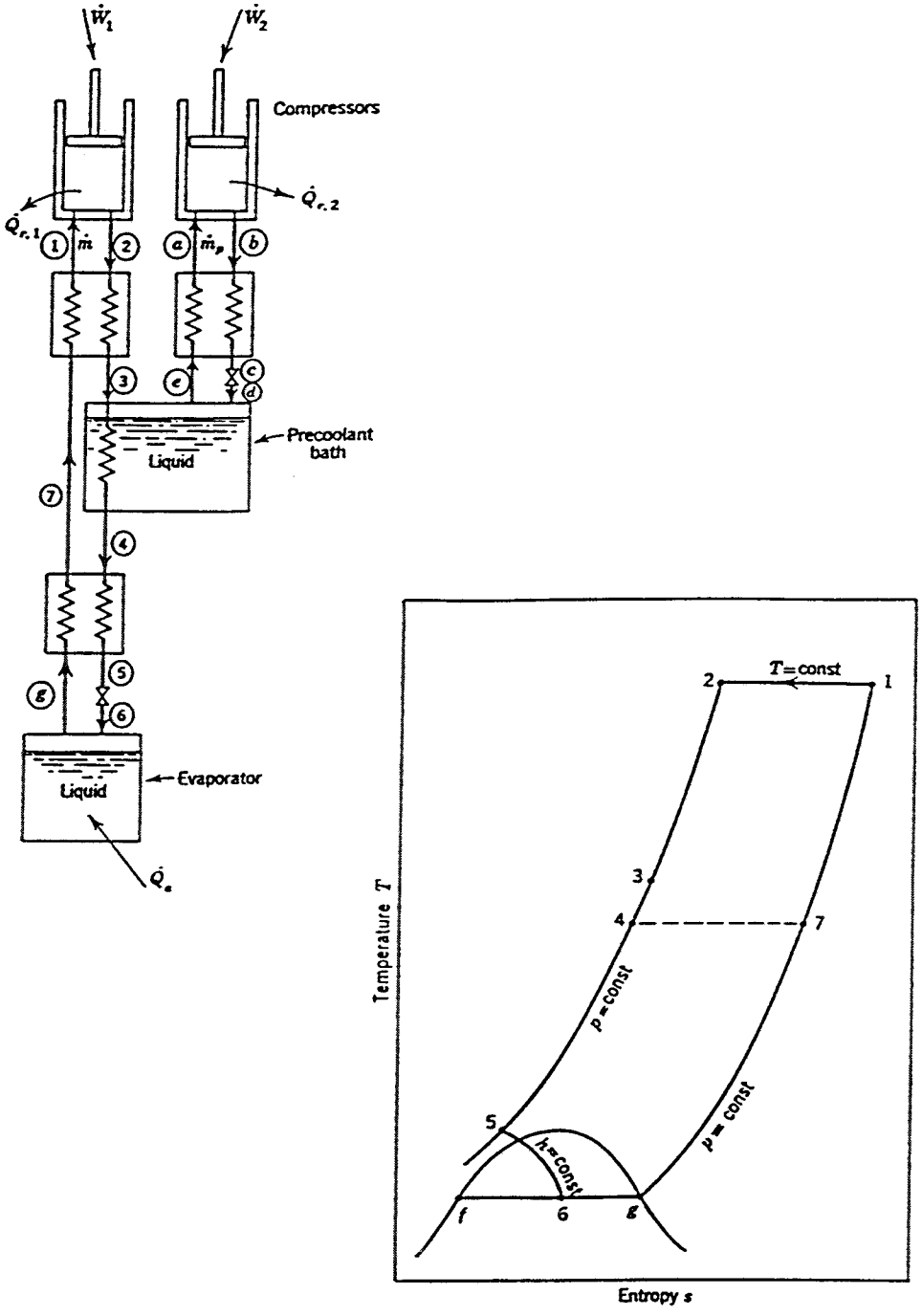

Figure 4-39 The pre-cooled Linde-Hampson refrigerator schematic diagram and its thermodynamic cycle T-S diagram. The numbers on the schematic diagram correspond to the state points on the T-S diagram. SOURCE: Reference 44

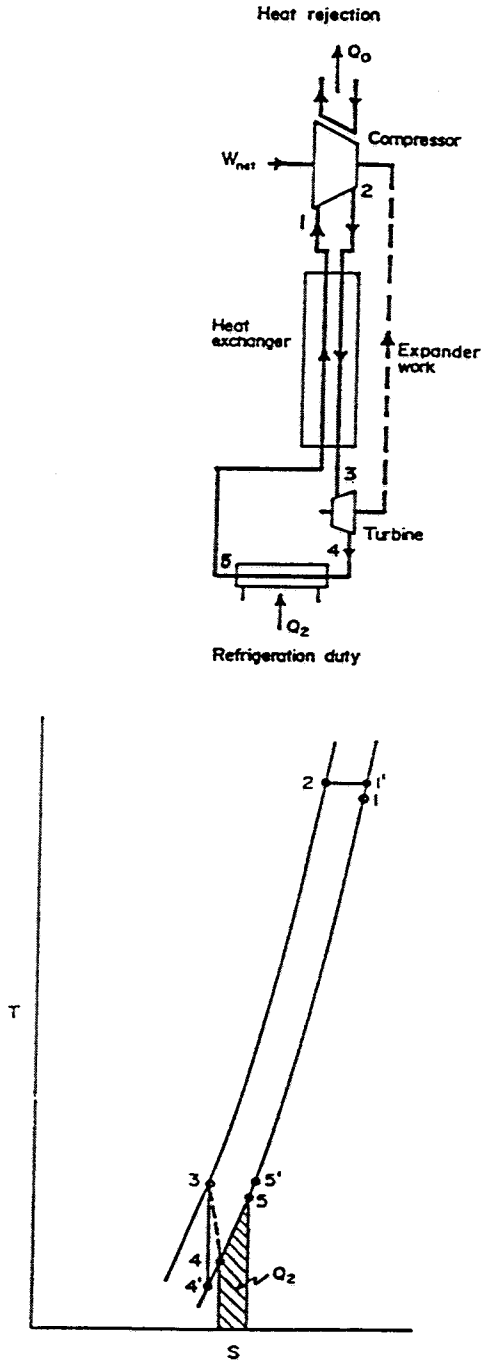

Figure 4-40 The reverse Brayton cycle refrigerator schematic diagram and its thermodynamic cycle T-S diagram. The numbers on the schematic diagram correspond to the state points on the T-S diagram. SOURCE: Reference 45.

Other Expansion Refrigerators. The above-mentioned refrigerators are commonly used to obtain temperatures down to the liquid nitrogen range, as well as to liquefy air for the subsequent production of liquid nitrogen by distillation. These types of cryogenic refrigerators have also been used in conjunction with liquid nitrogen precooling, multiple expanders, and different heat exchanger arrangements to effect a number of different refrigeration cycles. These cycles are usually used to reach temperatures well below that of liquid nitrogen. For the production of liquid nitrogen at a temperature below its normal boiling point (77 K), the use of some such cycle with a different working fluid might be more advantageous than its alternative of vacuum pumping the surface of a liquid nitrogen bath (down to a minimum of just below 64 K at an absolute pressure of 12.5 kPa {94 Torr}). One example of another refrigerator arrangement is the Claude refrigerator[44] shown in Figure 4-41.

The Stirling (or Phillips) Refrigerator. The Stirling refrigerator[44] is based on a cycle in which the working fluid (gas) is compressed isothermally while rejecting heat to a warm reservoir. Next, the motion of a displacer forces the gas to flow through a regenerator where it is cooled, while passing into a low-temperature chamber where it is expanded isothermally while extracting heat from the cold reservoir. Refrigerators of this type (Figure 4-42), using helium gas as a working fluid, have been built in large sizes, are very reliable, and might be a good choice to provide refrigeration for a liquid nitrogen-cooled SPTL operating in the vicinity of 64 K.

Other Regenerator Refrigerators. There are several ways similar to those used in the Stirling cycle to arrange the cooling functions. In the Gifford-McMahon cycle[44] (Figure 4-43) a compressor is used to provide a constant supply of high-pressure gas that can be fed to the displacer for passage through the regenerator as controlled by cycling valves. Several other regenerator-type arrangements are possible, and the Gifford-McMahon refrigerators, as well as other similar types, have been built and operate very successfully with excellent maintenance records. However, as currently developed, the

limited cooling capacity of this type of machine (say 250 Watts) will restrict its use for an SPTL application.

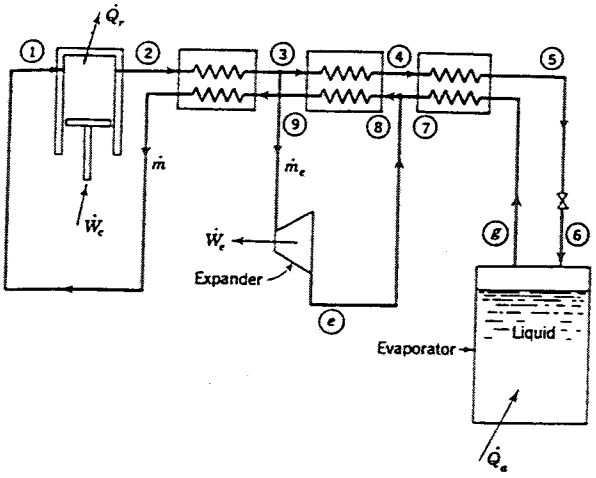

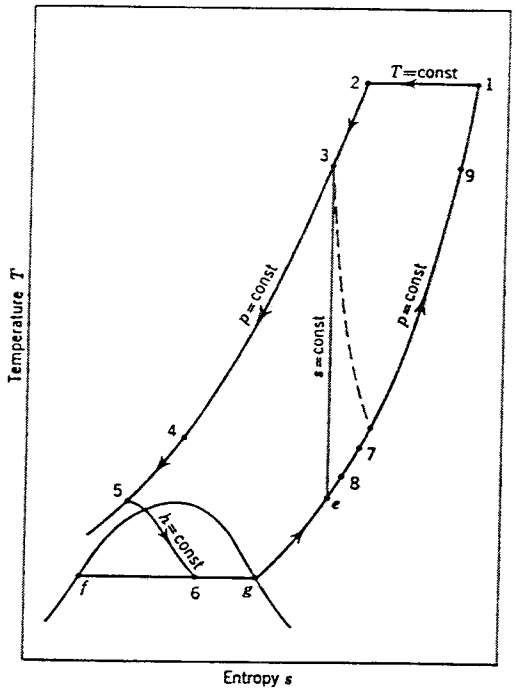

Figure 4-41 The Claude refrigerator schematic diagram and its thermodynamic cycle T-S diagram. The numbers on the schematic diagram correspond to the state points on the T-S diagram. SOURCE: Reference 44

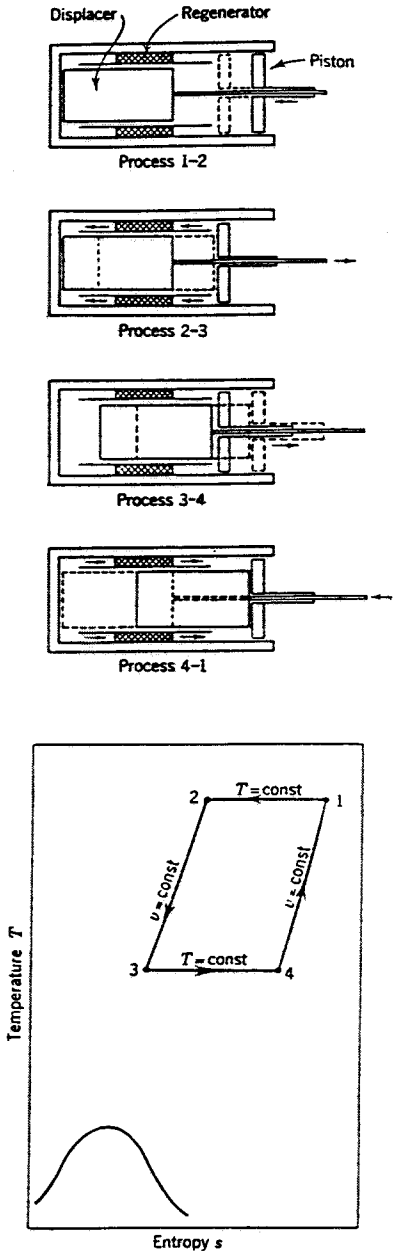

Figure 4-42 The Stirling refrigerator schematic diagram and its thermodynamic cycle T-S diagram. The numbers on the schematic diagram correspond to the state points on the T-S diagram. SOURCE: Reference 44

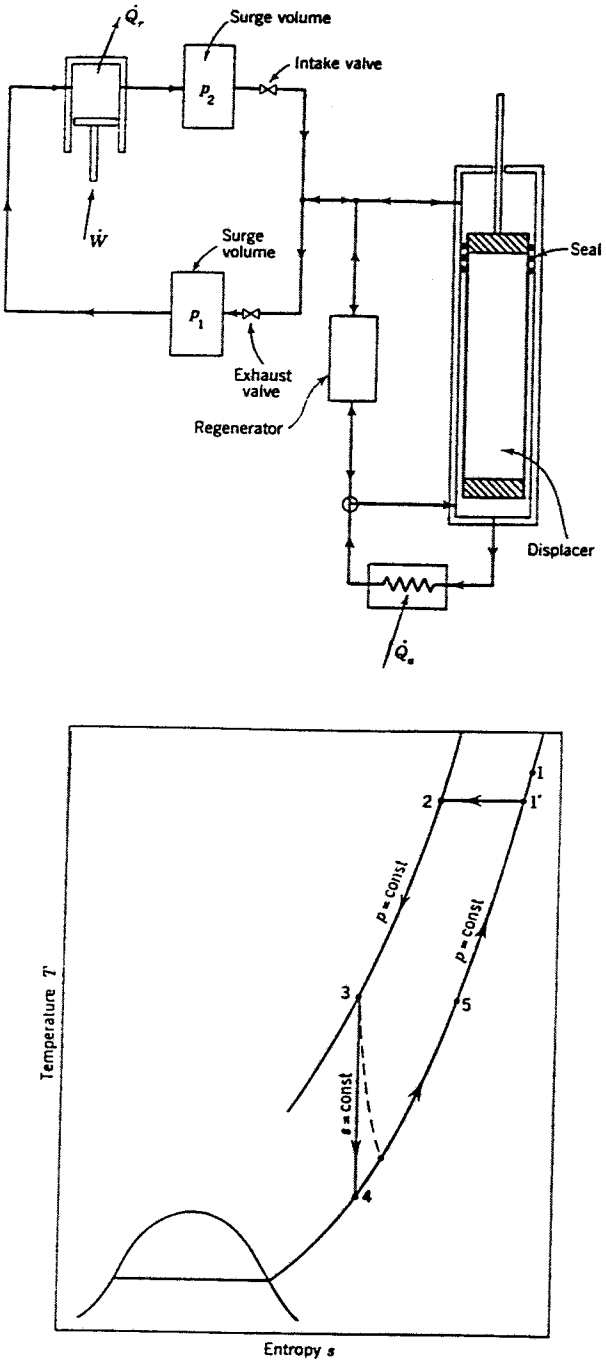

Figure 4-43 The Gifford-McMahon refrigerator schematic diagram and its thermodynamic cycle T-S diagram. The numbers on the schematic diagram correspond to the state points on the T-S diagram. SOURCE: Reference 44

Application of the Refrigeration

The application of cryogenic refrigeration to an SPTL presents a problem in intercepting the heat leaking into the system through the thermal insulation and the lead conductors that make the electrical connections to the external (ambient temperature) system, as well as removing any heat generated by the transmission of the electricity. In the case of dc power transmission, the latter heat source is minimal. In the case of ac transmission, the electrical heating depends upon several factors but can be about equal to the heat leaking into the system through the thermal insulation. In contrast to most other applications of cryogenic refrigeration, the SPTL requires that the refrigeration be applied over very long lengths that can approach distances of tens of kilometers. Furthermore, the conductors must be kept at or below the temperature at which they can conduct electricity with a sufficiently high current density without going normal. At the same time, for economic reasons, it is desirable to perform the refrigeration at as high a temperature as possible. These limitations require that the temperature be as uniform as possible along the length of the SPTL.

There are several possibilities for the design of the system that is to perform the cooling of the SPTL. First, the decision must be made as to whether the cooling in the SPTL will take place at essentially a constant temperature with boiling of the coolant or whether the coolant, will remain in a single-phase and increase in temperature as it passes through the system. In the latter case the liquid coolant should enter the line subcooled and at a sufficiently elevated pressure to suppress boiling at the maximum temperature to be reached before returning to the refrigeration system for recooling. Although it was recently suggested that the coolant be allowed to boil, and the resulting vapor removed from the line through a porous inner wall, the technology for doing this would represent a further development. The problems of handling a coolant in two-phase flow, with the accompanying increased pressure drop and tendency toward increased vibration, have made this option unattractive to most previous investigators. Thus, most investigations have only considered the use of a subcooled coolant, pressurized sufficiently to ensure

single-phase flow throughout the entire system, and only this type of cooling is considered here.

Because the cooling of the SPTL must be accomplished in a closed system it is necessary to return the coolant to the refrigeration system for recooling after it has exited the SPTL. Several methods have been proposed to accomplish this closed-loop concept. Graneau[46] proposed a dual-line system in which one transmission line circuit served as the "go" conduit with the coolant flowing in parallel through the interior of three hollow conductors, while another similar circuit provided the "return" path (Figure 4-44).

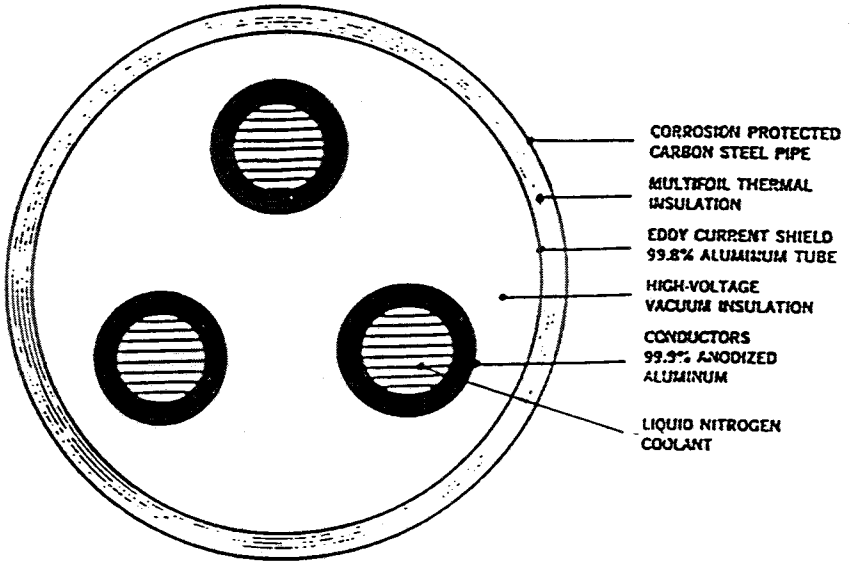

Figure 4-44 Schematic diagram of an SPTL design in which separate circuits are provided for "go" and "return" coolant streams. SOURCE: Reference 46

An alternate scheme was proposed by Longsworth and Schoch[47], who have considered an SPTL with the current conductors immersed in the "go" stream with a separate cryogenic line for the return of the coolant (Figure 4-45). If the conducting cables are made with a hollow core and contained within a cryogenic enclosure, then both the "go" and the "return" stream of coolant can be accommodated within a single cryogenic

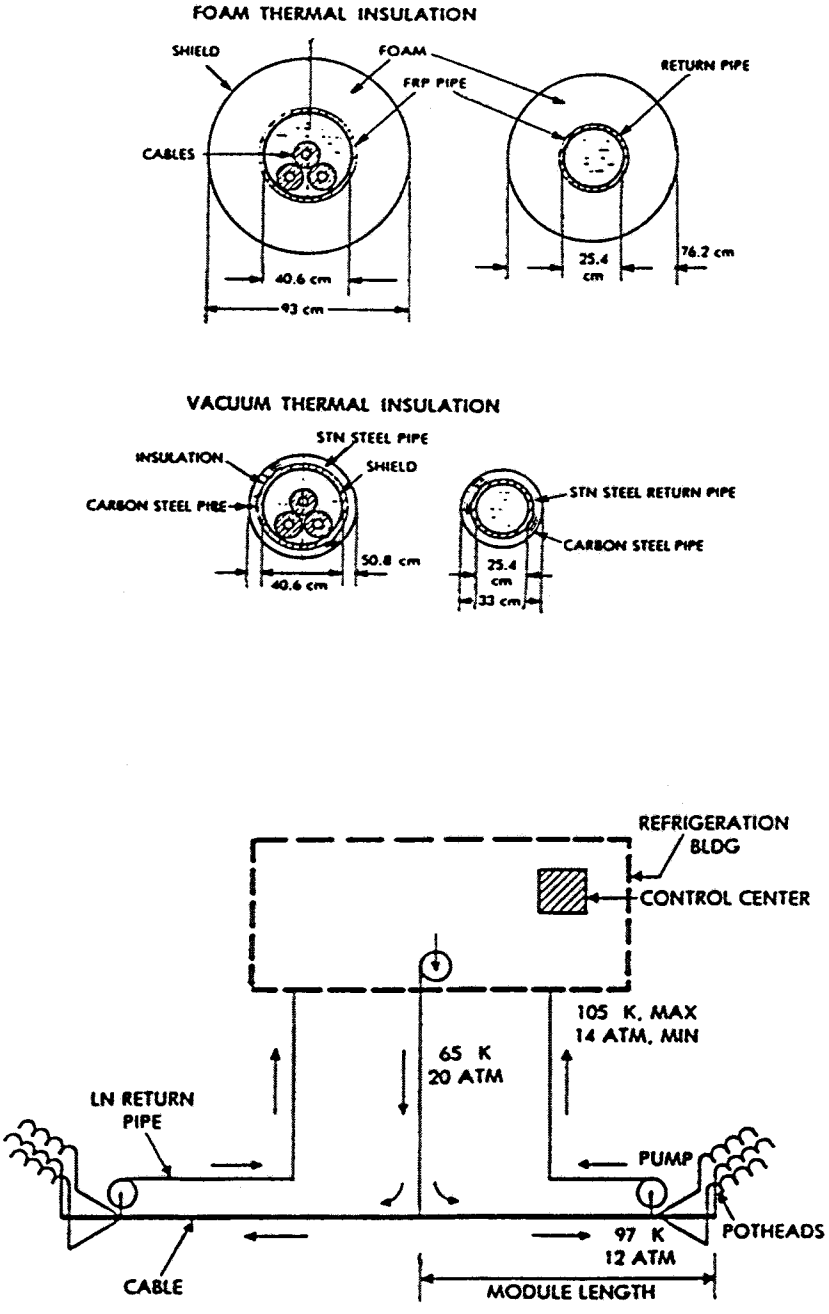

Figure 4-45 Schematic diagram of an SPTL design in which the "go" coolant stream flows through three hollow cables. The "return" coolant stream is in a separate return line (not an SPTL). SOURCE: Reference 47.

enclosure by having the "go" stream of coolant flow through the hollow core of the cables and the return stream flow in the annular space around the outside of the cable but within the cryogenic enclosure[48] (Figure 4-46).

Another decision that must be made in developing an SPTL concept is with respect to the working fluid within the refrigerator and the fluid that will be used to perform the SPTL cooling. It is possible to use the same fluid for the SPTL coolant as the working fluid used in the refrigeration system. In this case the pressure needed to circulate the coolant through the SPTL can be supplied by the compressor of the refrigerator (Figure 4-47). Alternatively, the cooling can be provided by a so-called referee fluid, which, in turn, is cooled in a heat exchanger by the working fluid of the refrigerator (Figure 4-48).

Refrigerant-Coolant as a Single Fluid. Although using the same fluid as both the refrigerant and the coolant offers the simplification of having only a single refrigeration/cooling system, other complications arise. If nitrogen is chosen as the working fluid it, will be necessary to split the product stream of liquid nitrogen to provide a subcooled pool of liquid nitrogen at below atmospheric pressure to allow subcooling of the separate coolant stream before it passes into the SPTL. The vacuum pump must be of sufficient capacity to remove all of the nitrogen vapor resulting from the evaporation of the fluid in the subcooling pool. The output from the pump can be returned to the input of the compressor of the refrigeration system. The heat exchanger of the refrigeration system must be large enough to accommodate the entire flow of the coolant system, which will be warmed to ambient temperature, be compressed by the compressor, and be recooled back to the operating input conditions.

Use of a Referee Fluid. The use of a referee fluid permits the separation of the refrigeration and coolant functions. This choice offers several advantages. First, a refrigeration system can be utilized that can easily attain as cold an operating temperature as desired without the need for large-scale vacuum pumping and a separate

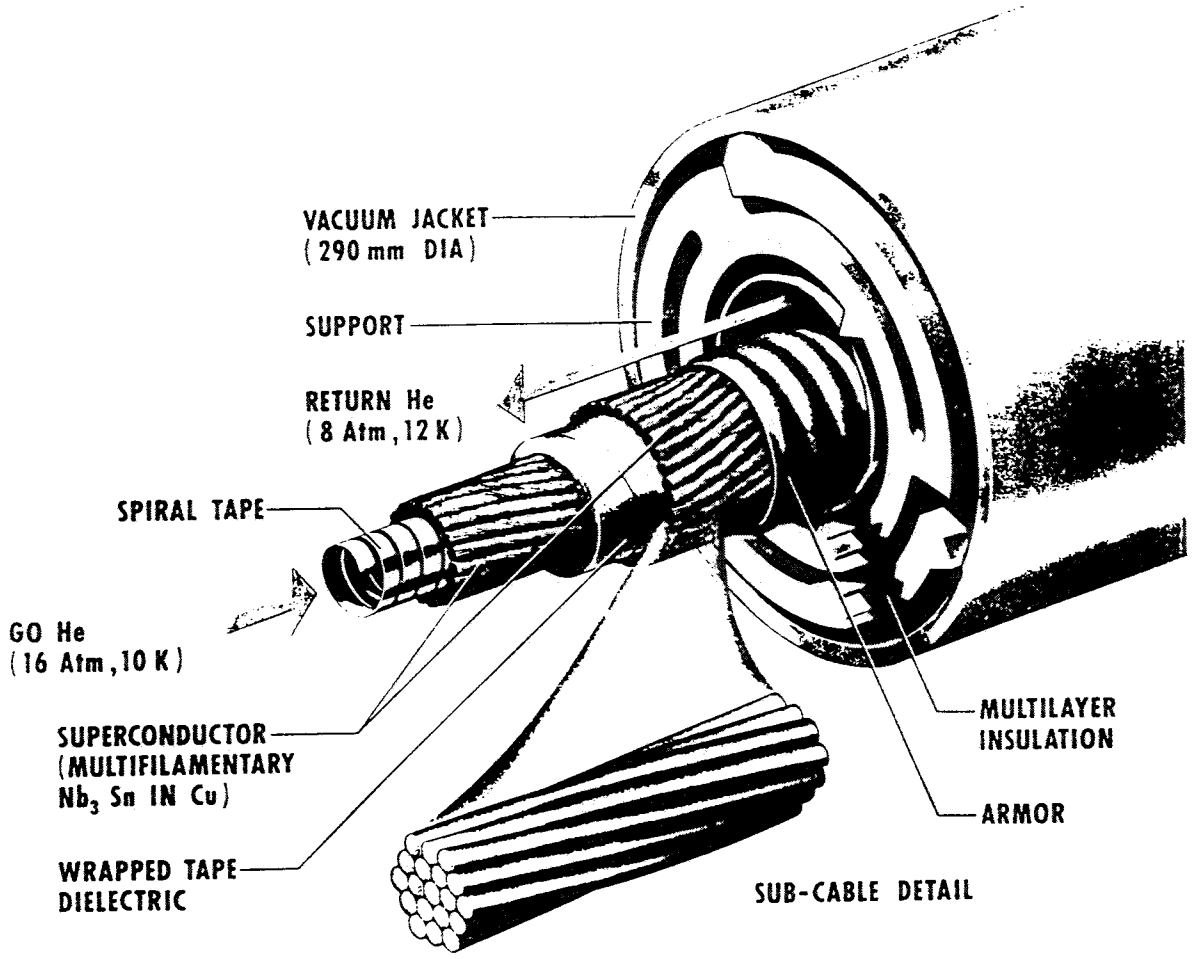

Figure 4-46 Schematic diagram of an SPTL design in which the "go" coolant stream flows through the interior of a hollow cable and the "return" coolant stream flows in the annulus around the cable but within the cryogenic enclosure. SOURCE: Reference 48.

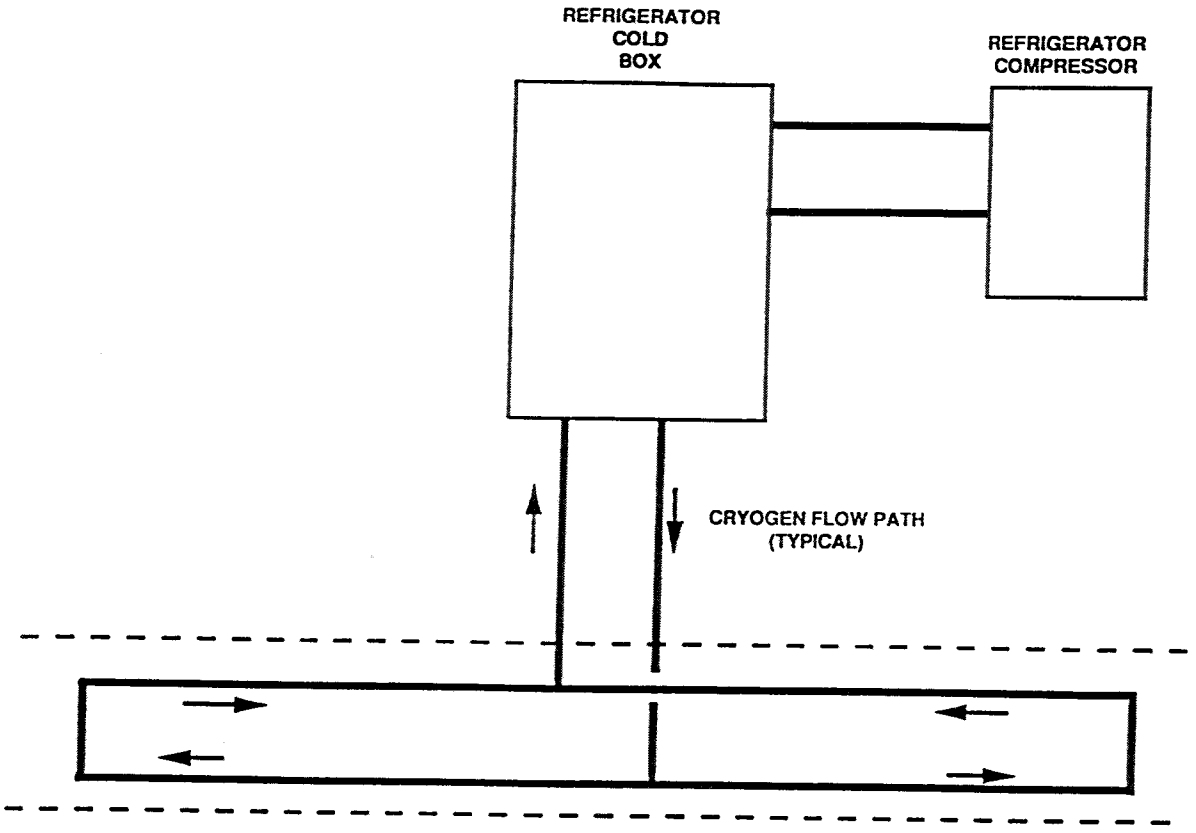

Figure 4-47 SPTL cooling scheme with a single fluid for refrigerator working fluid and SPTL coolant.

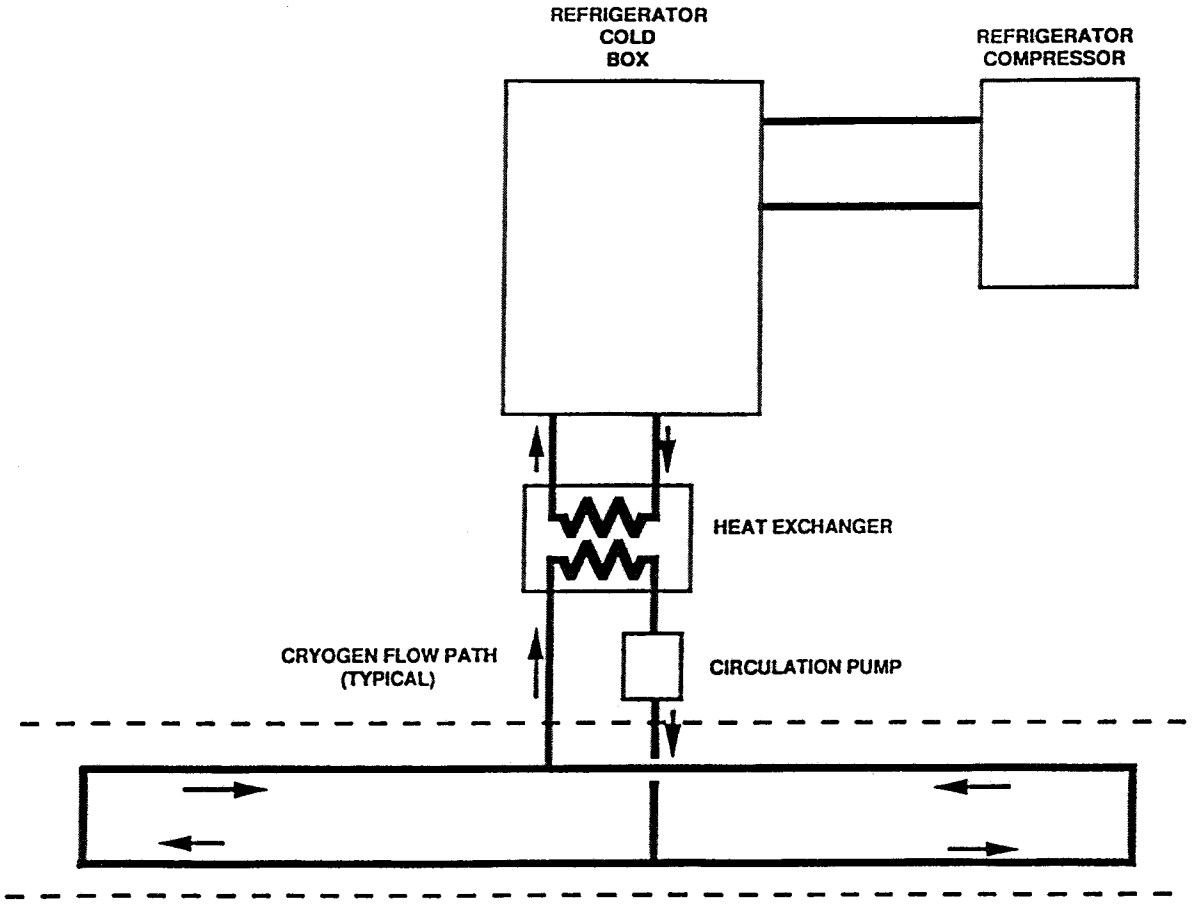

Figure 4-48 SPTL cooling scheme with separate fluids for refrigerator working fluid and SPTL coolant

pool of subatmospheric liquid for subcooling the coolant. In addition, for standby operation, the same refrigerator can be used to provide a reservoir of subcooled coolant to be used for short-term operation during down-time of the refrigerator without the complication of using a vacuum pump to cool the referee fluid. However, the necessary, although small,delta T of the heat exchanger (1 to 2 K) will require that the refrigeration be supplied at a slightly lower temperature. Such a system requires the use of a cold, circulating pump that would have to overcome the small pressure drop within the SPTL. Such pumps are already commercially available. Figure 4-48 shows a possible arrangement for this type of system. The circulation pump can be located either upstream or downstream of the heat exchanger. The upstream location has the advantage that the heat of compression can be removed in the heat exchanger, but the disadvantage that the circulation pump would operate at a higher, and possibly variable, temperature. The downstream location has the advantage of operating the pump at a constant lower temperature, but has the disadvantage that the heat of compression (and small temperature increase) is carried through the entire length of the SPTL flow circuit.

Line Cooling Options. There are several ways to utilize cryogenic refrigerators for the cooling of an SPTL. In general the SPTL will be sufficiently long that it will not be practical to perform the entire line cooling with a single refrigerator. Furthermore, there is a requirement that lead cooling must be provided by means of a bleed stream exiting the cryogenic system along the path of the current leads to intercept the heat leaking along the leads and to sweep out the heat generated by resistive heating in the non-superconductive part of the leads. Because the coolant gas in this bleed stream will exit the system at close to ambient temperature, it represents a greater load than the same quantity of coolant gas returning to the refrigeration system at the upper temperature of the SPTL operation. This is more like a liquefier load than a refrigerator load, and the refrigerator heat exchangers will have unequal mass flows. Thus, the question arises as to whether to perform the two types of refrigerator loads in separate refrigerators or to combine them in a single refrigerator.

Figure 4-49 shows an SPTL being cooled by one refrigerator at each end, with each refrigerator performing both the line cooling and lead cooling functions. Figure 4-50 shows an arrangement with separate refrigerators for line and lead cooling. In this concept the terminal refrigerators and the line refrigerators can be optimized separately for their differing refrigeration requirements, whereas a refrigerator arrangement such as shown in Figure 4-49 may not be optimized for either a line load or a terminal load. In the system shown in Figure 4-50, the line-cooling refrigerators are located at intermediate points along the SPTL to allow each refrigerator to provide cooling in each direction and, thus, shorten the coolant paths. Figure 4-51 shows another possibility utilizing refrigerators combining both cooling functions at each end of the line and line cooling refrigerators along the length of the line.

For any of the above arrangements, the coolant is circulated in a closed cycle. Therefore, it is necessary to provide a return path for the coolant. This can be done either in a separate cryogenic enclosure, or within the same cryogenic enclosure, with the proper design of the flow system. It is necessary to discuss further the use of liquid nitrogen as the coolant for the SPTL under the conditions assumed herein, namely a temperature of 64 K and a pressure sufficiently high to suppress boiling after the fluid has been heated to 77 K, and with the pressure decrease due to system pressure drop. Consequently, the fluid will have to enter the line at a pressure in excess of 0.10 MPa (15 psia), with the excess pressure being equal to the line pressure drop plus an additional amount for a safety factor. The line pressure drop cannot be determined without knowing the length of the SPTL to be cooled, along with channel dimensions and the required mass flow rate. A safety factor of perhaps 3 to 4 atmospheres might be acceptable. It is not necessary to know the absolute value here, but at 64 K, the vapor pressure of nitrogen is only about 0.014 MPa (2 psia). Because of this constraint on total system pressure, the total system pressure must be, everywhere, considerably above the vapor pressure of nitrogen.

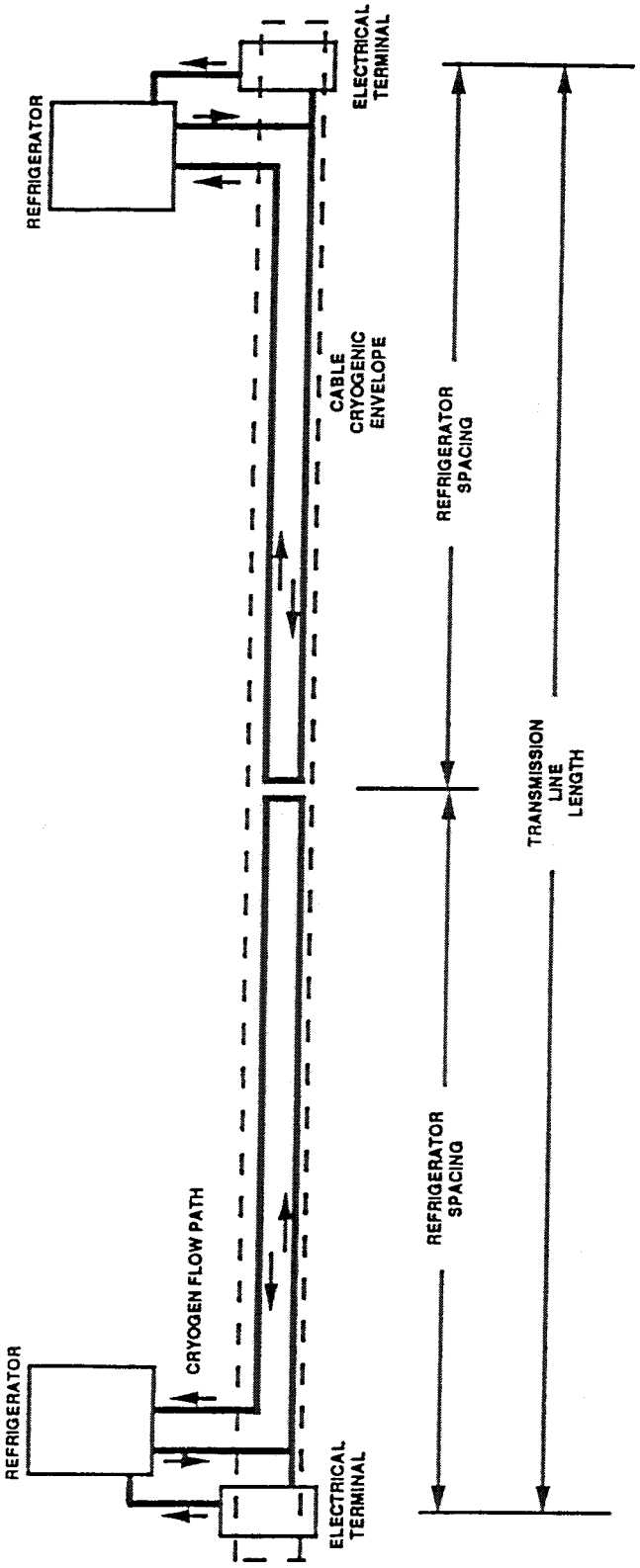

Figure 4-49 SPTL single fluid cooling scheme with a single refrigerator providing both line cooling and lead cooling.

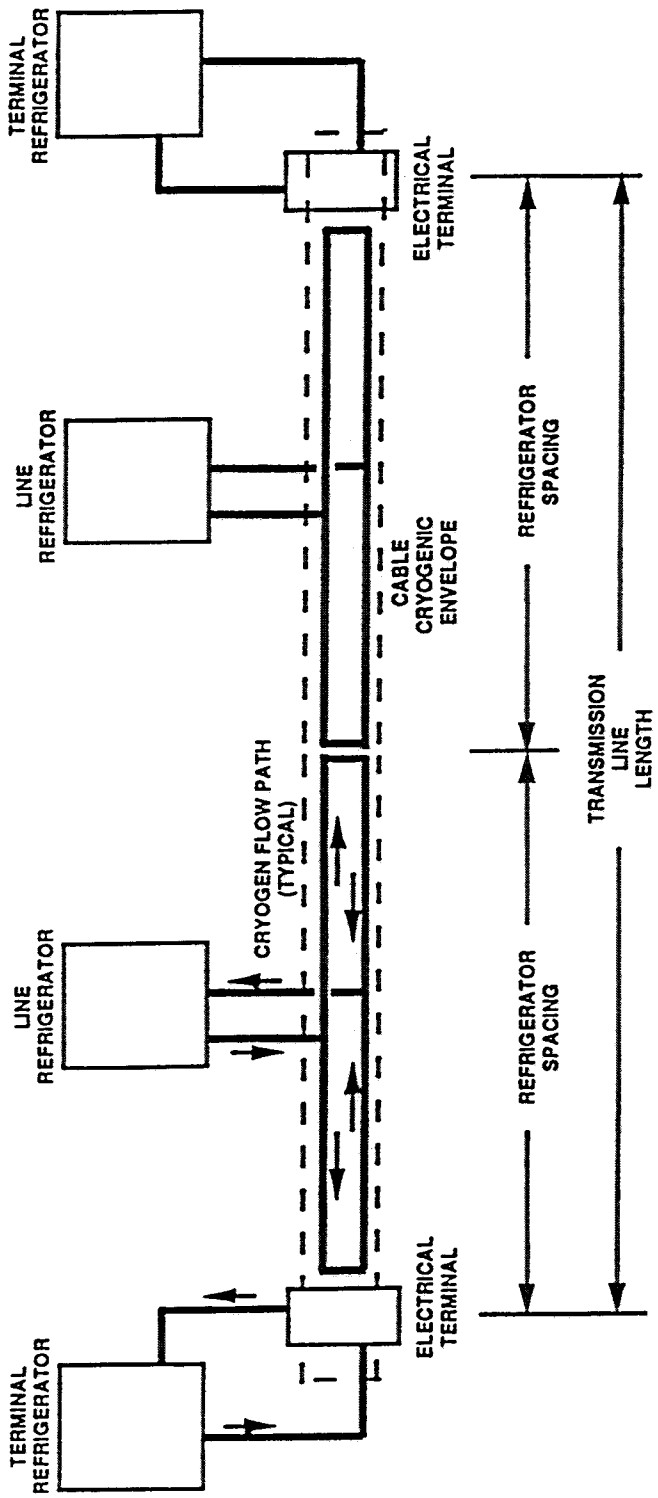

Figure 4-50 SPTL cooling scheme with separate refrigerators for line cooling and lead cooling.

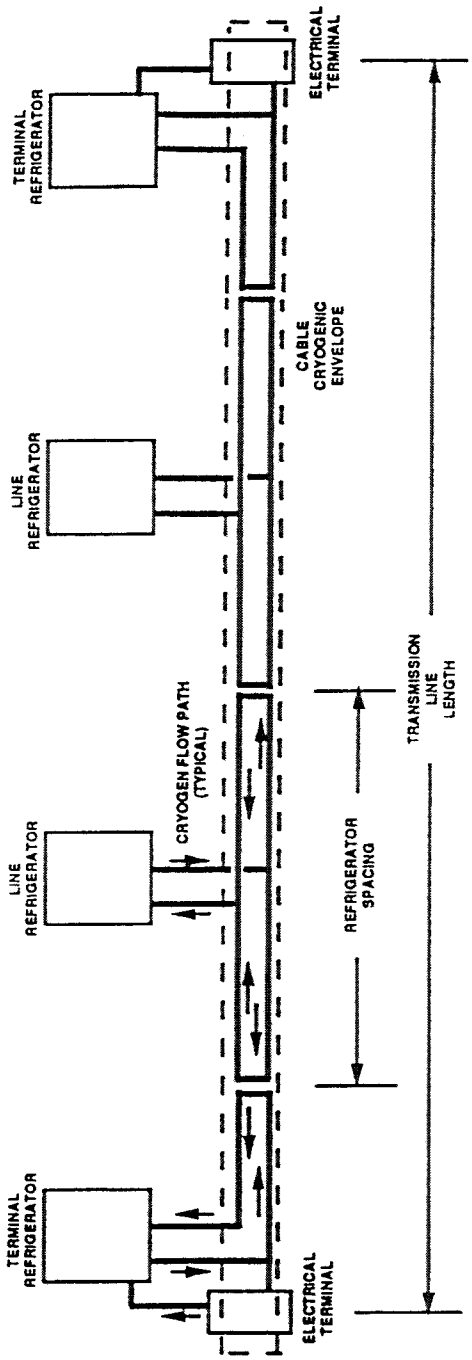

Figure 4-51 SPTL cooling scheme showing both line cooling refrigerators and refrigerators performing both line cooling and lead cooling functions.

Consequently, there are two ways to maintain the desired system pressure. One way would be to pressurize the nitrogen circulation system with a noncondensible gas, such as helium. However, with this method, gas bubbles could occur somewhere in the system if dissolved gas were to come out of solution. The other way to maintain pressure would be to have only one phase (liquid nitrogen) present in the SPTL coolant system. Because of the change of density with temperature, in such a system, it will be necessary to make provisions for relieving the system pressure by discharging some of the coolant, if the temperature rises above the specified value, or to add some coolant, if the temperature drops within the system. The discharge of fluid can be handled by spring-loaded pressure relief valves, and whether the discharged fluid should be recovered and reused or merely discharged to the atmosphere is a matter for economic analysis. The schematic diagram in Figure 4-52 shows a method of pressure control that provides for the recovery of discharged coolant, and for the insertion of additional coolant, if either of these processes becomes necessary. Because the system will be operating at an elevated pressure, adding fluid would require a liquid nitrogen pump. Relief valves and liquid nitrogen pumps are readily available, but the required specifications for these units will have to be determined.

Refrigerants

In principle a number of refrigerants can be used either for the refrigerator working fluid or to perform the cooling function for the SPTL. These fluids include helium, hydrogen, neon, nitrogen, and oxygen.

Neon is obtained by separation from the earth's atmosphere, where it is present in the amount of 18 parts per million by volume.[49] Because of its low concentration, neon is very expensive. Its expense, coupled with the facts that cryogenic refrigerators that utilize neon as the working fluid are not currently available and that its physical properties are not as well known in the range of cryogenic temperatures, make it

unlikely that neon will be a practical candidate for use in cryogenic refrigerators. Furthermore, the availability of neon in sufficiently large quantities is questionable.

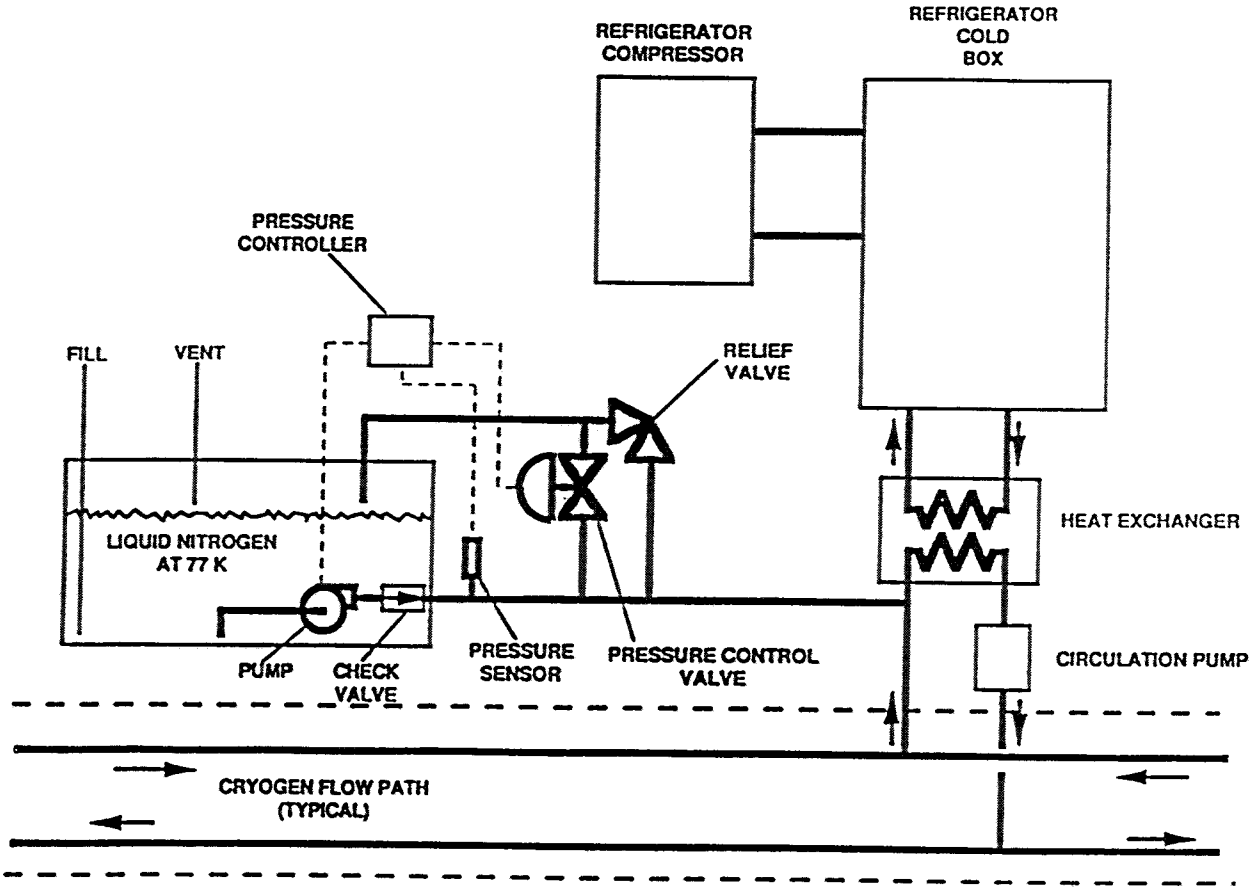

Figure 4-52 Schematic diagram of a pressure control system.

All of the other gases mentioned above are easily available in large quantities and in a sufficiently pure state to be useful as a refrigerator working fluid and as a coolant. However, hydrogen and oxygen can be eliminated as SPTL coolants on the basis of safety. Although these gases can be handled safely, doing so requires additional safety precautions to preclude unwanted combustion reactions. Hydrogen is flammable over a very wide range of composition in air mixtures (mixtures of 4% to 75% hydrogen in air are combustible). Although oxygen is not a fuel itself, it is extremely reactive and makes the combustion process much more vigorous and dangerous[50].

In addition to the above considerations, for HTSC SPTL applications, there are no disadvantages to the use of helium or nitrogen rather than neon, hydrogen, or oxygen. We will also be dealing with closed systems, with no expected large losses of the refrigerating and cooling system fluids, so the cost of these relatively inexpensive fluids will not be of primary importance. Thus, we are left with helium and nitrogen as useful options for the refrigerant and coolant roles. Table 4-17 gives pertinent thermophysical properties of nitrogen, over the temperature range of interest, for its use as a refrigerant or coolant in an SPTL.

The costs of the above-mentioned gases vary considerably with quantity and purity requirements. Nevertheless, costs that can be estimated show the economic disadvantage of neon as an SPTL coolant. Table 4-18 shows some estimated costs for helium, neon, and nitrogen.

Helium. The use of helium gas as the working fluid for the refrigeration process offers a number of advantages. First, it is already used as the working fluid in most of the available cryogenic refrigerators intended for cooling below the nominal temperature of liquid nitrogen (77 K). As shown in Table 4-18, the expense of helium gas, although greater than that of nitrogen, is not too great, and its properties are well known and understood over the entire temperature range of interest. Although perhaps not a shelf

item, the refrigerators needed for SPTL operation will be available. Helium can also be used as the coolant in the SPTL. However, its low density will probably require operation at a higher pressure than would nitrogen to achieve adequate cooling capacity with an acceptable pressure drop. However, helium is an attractive candidate for the refrigeration process. The desired temperature (about 64 K) can be easily attained with no vacuum pumping, and existing refrigerators are close to what would be needed. Figure 4-53 is a temperature-entropy diagram for helium over the range of temperature of interest to this study.

Table 4-17
Pertinent thermophysical properties of nitrogen (SOURCE: Reference 20)

Temperature (K)	Pressure (MPa)	Density (kg/m^3)	Enthalpy (kJ/kg)	Viscosity (centipoise)
64	0.689	866	-147	0.298
	1.379	866	-147	0.302
	2.068	868	-147	0.307
	2.758	868	-146	0.310
	3.447	---	---	---
77	0.689	812	-122	0.153
	1.379	813	-121	0.156
	2.068	815	-121	0.158
	2.758	816	-120	0.159
	3.447	818	-120	0.161
98	0.689	703	-77.6	0.088
	1.379	706	-77.4	0.090
	2.068	709	-77.4	0.092
	2.758	712	-77.2	0.094
	3.447	716	-81.6	0.097

Nitrogen. Nitrogen can also be used as the refrigerant, although attaining the lower end of the desired temperature range (64 K) will require additional equipment to provide a subcooling process to be carried out. It will not be as easy to use developed and readily

available equipment over the entire temperature range of interest in an SPTL when specifying nitrogen as the working fluid in the refrigerator. However, nitrogen is a very promising candidate for a referee coolant fluid for an SPTL.

Table 4-18
Cost of some coolants

Coolant	Cost ($/m^3) at STP
Helium	1.76
Neon	150
Nitrogen	0.11

Another possibility for cooling an SPTL to the nitrogen temperature range might be the use of nitrogen slush, which is a mixture of solid and liquid nitrogen. If the nitrogen is cooled to just below 64 K, further cooling will result in some of the nitrogen freezing. Experiments, mostly performed with liquid hydrogen (but also some with liquid nitrogen), have shown that, if flow rates are not too slow, slush mixtures with up to 50% solid can flow like a liquid without separation or settling out of the solid phase. Although there would be some complications in operating with a system in which the vapor pressure of the nitrogen would be subatmospheric, the additional cooling capability provided by the heat of melting can be as much as an additional 15% for a coolant mixture of 50% solid nitrogen by weight. Figure 4-54 is a temperature-entropy diagram for nitrogen.

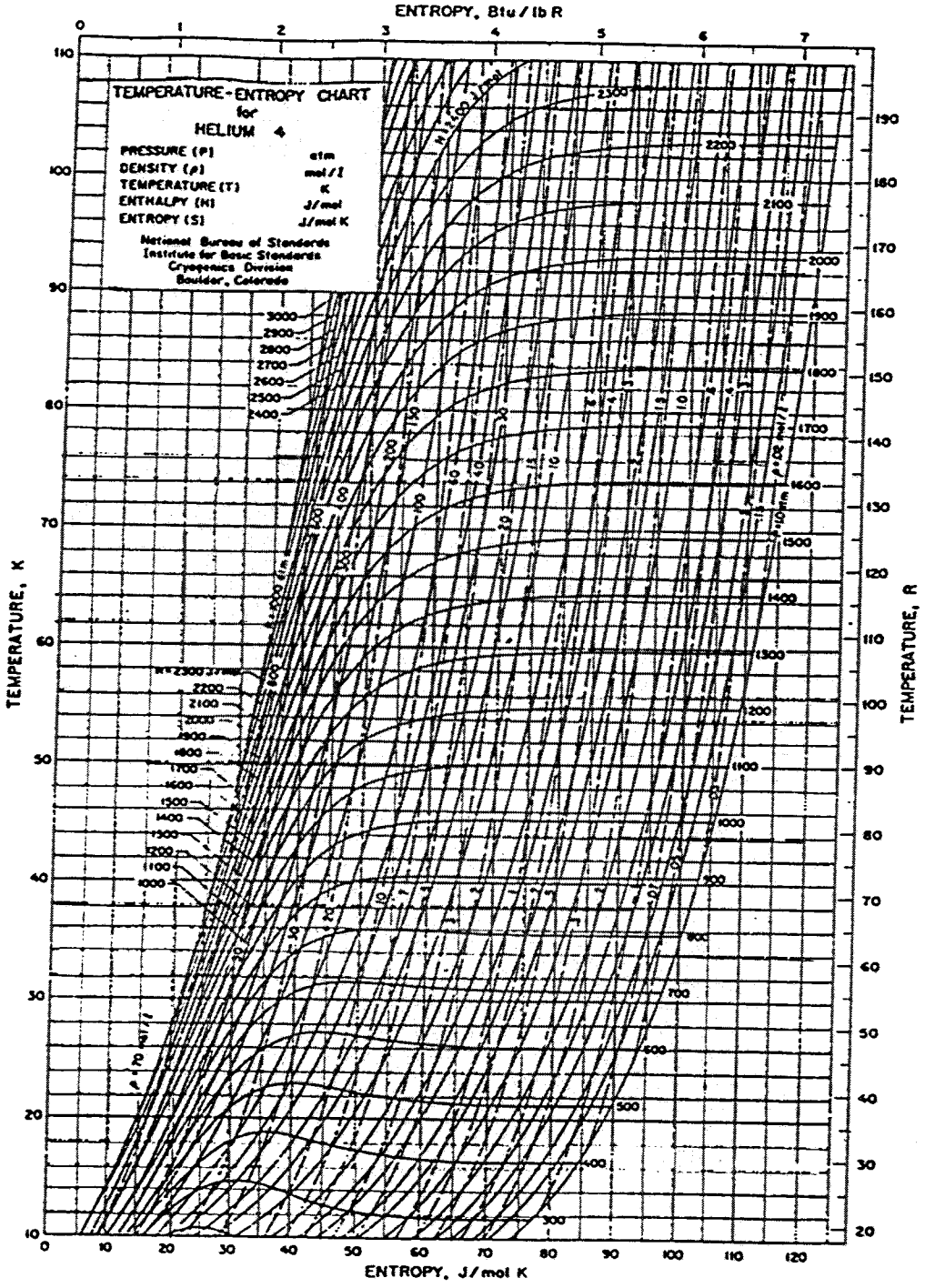

Figure 4-53 Temperature-entropy diagram for helium. SOURCE: Reference 44

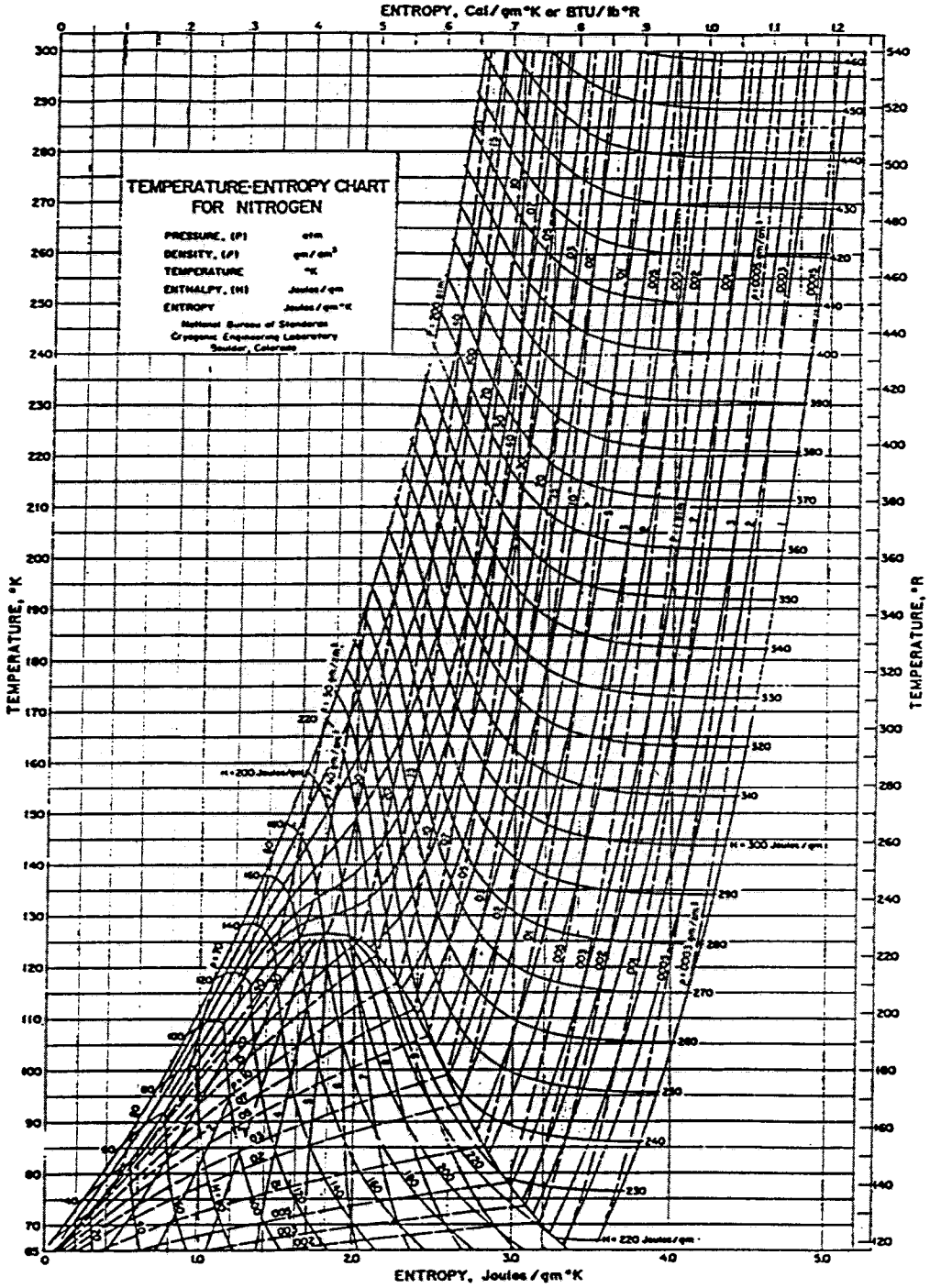

Figure 4-54 Temperature-entropy diagram for nitrogen. SOURCE: Reference 44

Components

Equipment

The major components in a large-scale cryogenic refrigerator are the compressor, the expansion devices, and the heat exchangers. The importance of each of these components was examined by Voth,[42] who found that the most important contribution to refrigerator inefficiency was in the inefficiency of the compressor. Typically, the maximum efficiency that can be expected in a compressor is about 60%. This limit has not been improved to any extent in the past decade. The screw compressor was relatively new a decade ago, but it has now been accepted and is the most commonly employed type of compressor in the cryogenic refrigerator industry. Although it offers no significant improvement in efficiency, it does offer very reliable performance,[51] and for larger capacity systems, it occupies less space than a reciprocating compressor, resulting in an overall smaller plant size.

More recently, progress has been made in the development of the cold compressor. This type of compressor can operate with the cold vapors in the low temperature end of the refrigeration system without having to warm the gas up to ambient temperature in heat exchangers. To date this type of compressor is being used to produce subcooled cryogenic liquids with a more practical sized compressor than would be the case if the initial stage of compression were to take place at ambient temperature and subambient pressure.

Heat exchangers can contribute to the overall inefficiency of the cryogenic refrigerator both in the pressure drop they contribute and in their thermal inefficiency. The latter effect is limited only by the economic effect of the cost of the heat exchanger. However, the heat exchangers are already quite efficient, and contribute little to the overall inefficiency of the system.

Expansion engines in recent large cryogenic refrigerators are almost always of the turbine type, utilizing either gas bearings or oil bearings. The development of gas bearings allows very high rotational speeds and very reliable operation, especially in continuous service.

For the type of cooling system that utilizes a referee fluid, a cold, circulating pump is also required. Units of this type have been developed for service in cold helium and hydrogen. The successful operation of these units is encouraging[52,53].

Reliability

For a previous study of SPTLs utilizing low-temperature superconductors, the reliability of cryogenic refrigerators was addressed by Kadi and Longsworth[54] and Manatt et al[55]. The refrigerator reliability requirements for these studies are appropriate for the present study. Kadi and Longsworth[54] showed that the thermal capacity of the system was sufficient that a loss of refrigeration for up to 8 hours would not result in the inability of the SPTL to transmit power at full load. At the higher operating temperature of the HTSC SPTL (64 K to 77 K vs 9 K to 12 K for low temperature SPTLs), all of the system's components will have a higher heat capacity as well as a smaller temperature difference from ambient, which reduces heat leak into the system. For these reasons it is felt that routine maintenance or system repairs requiring less than 8 hours to complete are acceptable. A condition exceeding this limit, that would shut down the entire SPTL system, was deemed acceptable[54] no more frequently than once in ten years.

Kadi and Longsworth[54] conclude that an even stricter reliability condition of one failure every 20 years can be achieved with existing equipment (as of 1976) by providing a duplicate compressor and cold box, as well as a backup cryogen storage Dewar. Manatt et al[55]. considered the refrigeration system in greater detail and estimated the maintenance and repair times (usually less than 8 hours) that were required for diagnosis, part replacement, and startup. They recommended that more reliability data

be gathered before a decision could be made on the mean time before failure of individual equipment items. In contrast, Kadi and Longsworth made use of complete duplicate systems. Since that time, Longsworth and Schoch[47] have presented some reliability data on a number of refrigerator components taken from the actual operation of an air separation and liquefaction plant over a period of more than 8 years. Some of their data (which is reproduced in Table 4-19) shows that, with the exception of the main nitrogen compressor, the reliability of the other components had reached a satisfactory state more than a decade ago.

Table 4-19
Reliability data from APCI Wharton plant. SOURCE: Reference 47

Item	Number of outages	MTBF (hr)	MTTR (hr)	Outages exceeding	
				6 hr	24 hr
Power Failures	13	5,800	2.6	0	0
Main Air Compressor (5,000 hp)	2	37,700	5.8	1	0
N_2 Make-up compressor (1,700 hp)	4	18,800	4.1	1	0
Main N_2 compressor(17,000 hp)	17	4,700	24.7	15	7
Companders (2 sets)	16	9,400 each	16.1	10	3
Nitrogen cold boxes (2)	1	150,000	5.8	0	0
Electrical equipment	4	18,800	12.5	4	0
Major scheduled maintenance	5	15,100	185.7	5	5
Minor scheduled maintenance	14	5,400	46.5	14	10
Storage tanks (two, 2000 tons)	0	--	---	0	0

Notes:
1. MTBF = Mean time between failures
2. MTTR = Mean time to repair
3. Total on stream time was 75,350 hours
4. Maintenance done while plant was shut down because of power interruption or full storage is not included; however, maintenance extending beyond normal restart time is included.
5. Compressor failures include controls, instrumentation, and coolers. Main nitrogen compressor includes 1 cooling tower and 11 cooler failures.
6. Outage time includes time to cooldown, typically 2 hr. from a warm condition.
7. Previous studies have shown that rotating machinery, expanders and compressors, typically have MTBF's in the range of 20,000 to 30,000 hr. when controls are included.

Storage Requirements

An important adjunct in providing reliability to the refrigeration system is local storage of the cryogen coolant. This storage, along with a circulation pump, can hold the system at operating temperature for any length of time desired, provided the storage volume is large enough. The coolant stored in this manner would be circulated through the system and discarded at the system exit because no refrigerator would be available to recool it. Because of the low cost of the nitrogen gas, its recovery is not felt to be economical.

Let us consider the storage volume required for a holding period of 8 hours for a refrigeration system with a capacity of 5 kW. For such a system liquid nitrogen would be maintained at 64 K and at a sufficiently high pressure so that it could be exhausted from the SPTL as a liquid at 77 K. For these conditions, a storage volume of 6450 liters (1700 gallons) would be required. The total backup system would consist of the storage volume, with its submerged heat exchanger for subcooling, and gas storage (probably helium) for system pressurization. The volume of storage required for an 8-hour outage of the cryogenic refrigerator operating at a capacity of 5 kW is small compared with the volume of existing trailer-transports that are 15,000 liters (4000 gallons) or more. With no subcooling, the system would have to be operated at an elevated pressure, for example 0.69 MPa (100 psia) and a liquid nitrogen discharge temperature of 98 K. For these conditions, the 8-hour liquid nitrogen requirement for standby operation would amount to 3800 liters (1000 gallons). Thus, there are at least two ways to assure the desired reliability of providing the needed refrigeration to an SPTL on a standby basis.

Algorithms and Calculation Aids

Refrigerator Capacity and Cost

The cost of cryogenic refrigerators is most easily estimated on the basis of their input power requirements. The theoretical power requirement for an ideal cryogenic refrigerator can be obtained by multiplying the desired refrigeration capacity by the

Carnot efficiency, as given by Eq. 19. Strobridge has correlated the degree to which actual refrigerators approach this limit as a function of refrigerator capacity[43] A copy of Strobridge's graph of this correlation is given in Figure 4-55. The actual input power requirement can then be estimated by dividing the theoretical input power by the fraction of the Carnot efficiency, as obtained from Figure 4-55.

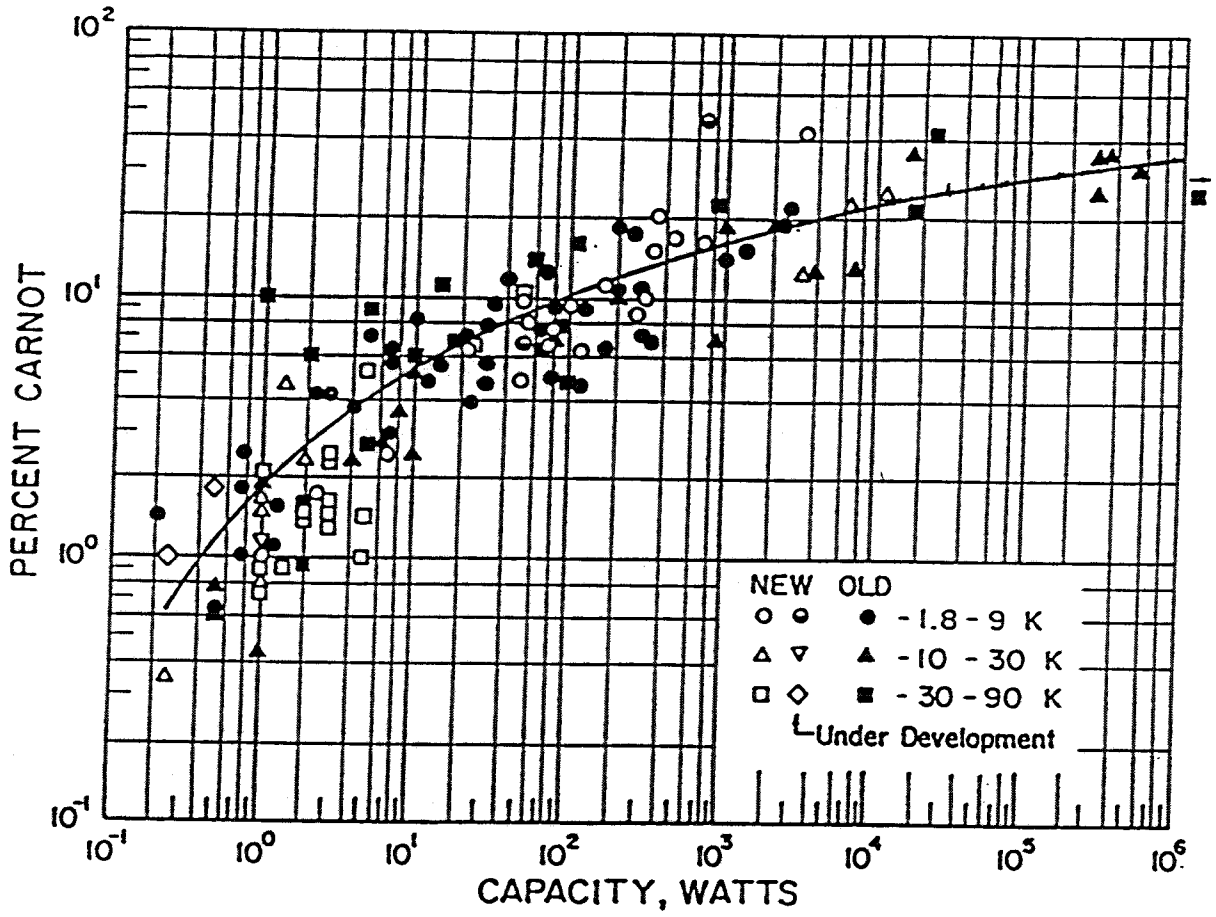

Figure 4-55 The percent of Carnot efficiency realized in practical cryogenic refrigerators as a function of refrigerator capacity. SOURCE: Reference 43

Strobridge has also given the following equation for predicting the cost of cryogenic refrigerators:

$$C = 6000 \times (P)^{0.7} \quad \$ \tag{20}$$

where C = cost in $ and P = input power in kW. The selection of 0.7 as the exponent in the above equation is not universally accepted, and values of 0.6 have also been used. For this study, we have obtained a budgetary cost estimate from a refrigerator manufacturer over a range of refrigerator capacities (see Table 4-20). These data are plotted in Figure 4-56, which shows a better fit to the data if we use an exponent of 0.626. The corresponding equation then becomes:

$$C = 23700 \times (P)^{0.626} \quad \$ \tag{21}$$

Table 4-20
Helium refrigeration cost, power and efficiency data

Refrigeration capacity at 64K (kW)	Input Power (kW)	Cost ($)	Efficiency (% of Carnot)
10	175	600,000	21
20	350	900,000	21
50	850	1,600,000	22
100	1,600	2,400,000	23
200	3,100	3,600,000	24
300	4,500	4,600,000	25

Because of the change in the exponent, the constant, 23,700 can not be compared with Strobridge's value of 6000 to imply a corresponding value of inflation over the period from 1974 (the date of Strobridge's paper) to 1992 (the date of the current cost estimates). An alternative way to estimate refrigerator costs would be to use Strobridge's equation, as shown above, and then multiply the 6000 by the amount of inflation that has occurred

since 1974. Values for the inflation of capital equipment costs were obtained from the *Statistical Abstract of the US - 1990*[56] and the *Monthly Labor Review*,[57] and from these data a cumulative inflation factor of 2.48 was calculated. The fitting of a curve through the center of the recently obtained cost data with an exponent of 0.7 (also shown on Figure 4-55) predicts a constant for Strobridge's equation of 13,900, which corresponds to an inflationary increase of 2.32. This is in relatively good agreement with the 2.48 obtained from U.S. Government figures on inflation for the same period.

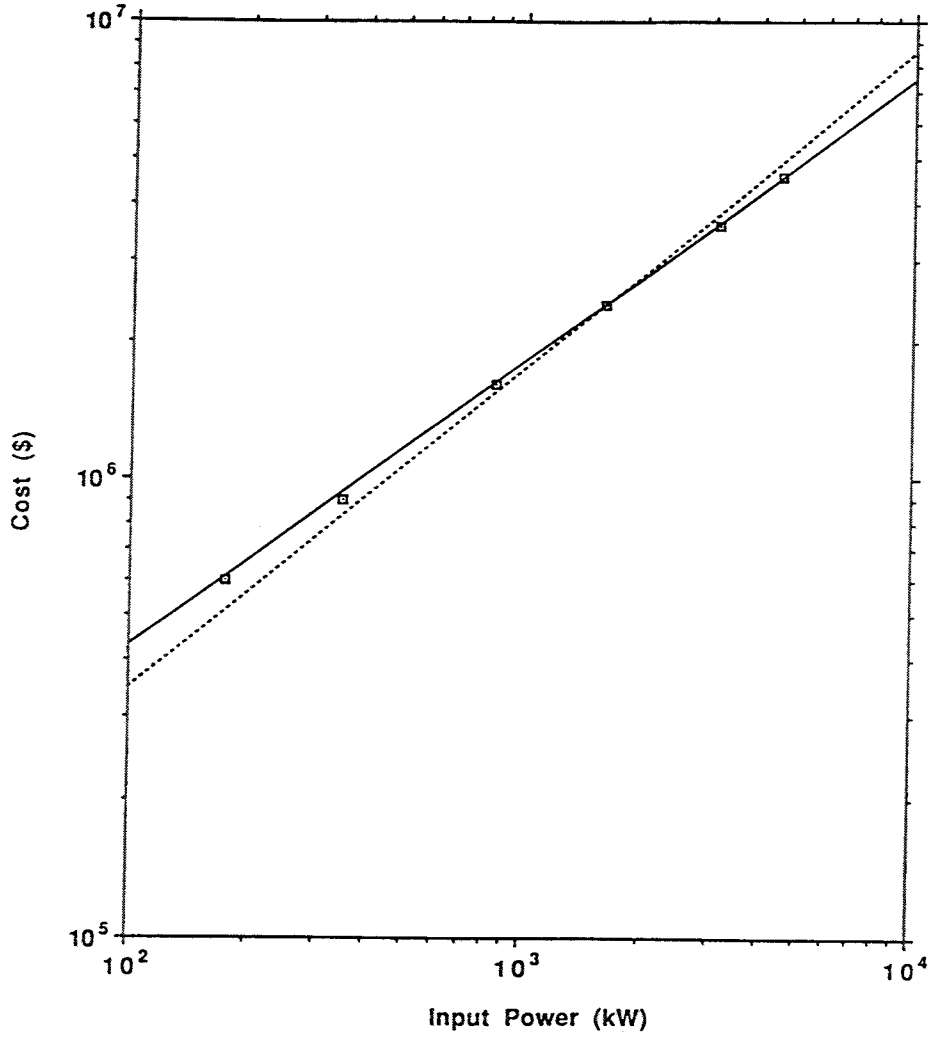

Figure 4-56 Cost of cryogenic refrigerators vs. input power. The solid line is the best fit to the data. The broken line is a fit forcing the exponent of 0.7 to the input power.

Mass Flow

The necessary mass flow of coolant within the SPTL will depend upon the heat leak and internal heat generation, if any, and on the enthalpy of the coolant at the entrance and exit to the SPTL. The mass flow can be calculated from:

$$M = \frac{Q}{(H_{exit} - H_{input})} \tag{22}$$

where M = mass flow of coolant (in kg/s), Q = total heat (in Watts) to be extracted from the SPTL section being cooled, H_{exit} = the enthalpy of the exit coolant stream (in J/kg), and H_{input} = the enthalpy of the entering coolant stream (in J/kg). Some pertinent values of the enthalpy of nitrogen are listed in Table 4-17.

Pressure Drop

The pressure drop within the SPTL system will depend upon the mass flow rate, the fluid density, the dimensions and shape of the channel through which the coolant must flow, and the length of the cooling passage. A method for determining the mass flow is described above. The other factors are the result of the design of the total system including the method of application of the refrigeration, also described earlier.

The pressure drop can be calculated from the following relationship;

$$\Delta P = f\,(\frac{L}{D})\times(\frac{v^2}{2})\rho \tag{23}$$

where ΔP = the pressure drop (Pa), f = friction factor (dimensionless), L and D are the length and diameter of the cooling passage (both in m), v = the fluid velocity (m/s), and ρ = the coolant density (kg/m^3). The literature contains two different expressions for the friction factor: the Fanning friction factor and the Moody (also called Darcy) friction factor. These differ by a factor of 4; consequently, care must be taken to use the proper one. The Moody friction factor and its appropriate equation are used both here and in Figure 4-57. The density is only a weak function of the pressure, but a stronger function

of the temperature (see Table 4-17). Therefore, for maximum accuracy, the pressure drop must be calculated for small increments of path length, thus indicating the desirability of a computer solution. The velocity should be kept reasonably low to avoid too large a pressure drop and can be directly calculated from the mass flow rate, M (in kg/s), channel dimensions (in m), and appropriate coolant density (in kg/m) for that section of the cooling passage. Because of the relationship that

$$M = \rho v A \tag{24}$$

where A = the area of the flow channel (in m^2), we can rewrite the above equation for pressure drop as follows;

$$\Delta P = f \left(\frac{L}{D}\right) \left(\frac{M^2}{2\rho A^2}\right) \tag{25}$$

and if the channel is circular in cross section

$$A = \frac{\pi}{4} D^2 \tag{26}$$

so that

$$\Delta P = \frac{8 f L m^2}{\pi^2 \rho D^5} \tag{27}$$

The value of f may be obtained from a graph, such that in as Figure 4-57, or from the Colebrook equation for turbulent flow (3000 < Reynolds Number < 10^8);

$$\frac{1}{f^{0.5}} = 2 \log_{10} \left(\frac{(e/D)}{3.7} + \frac{2.51}{Re\, f^{0.5}} \right) \tag{28}$$

where e is the relative roughness (same units as the diameter), and Re = the dimensionless Reynolds number given by the following relationship:

$$Re = Dv \frac{\rho}{\mu} \tag{29}$$

where μ = the viscosity (kg/(m s).

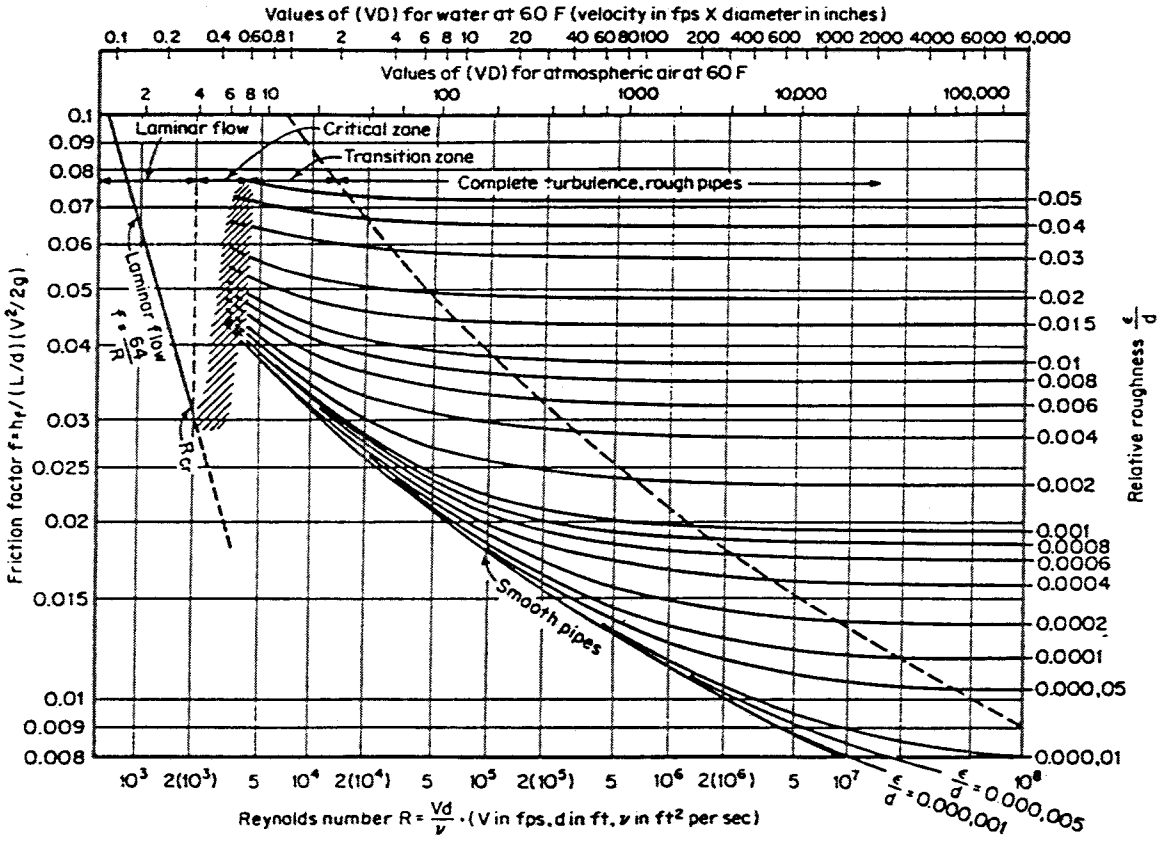

Figure 4-57 Friction factor as a function of Reynolds number. SOURCE: Reference 61.

The Reynolds number must be evaluated for either of the above methods for determining f. The effect of including the roughness, e, allows this method to be used

for determining pressure drop in rough pipes up to the point where the roughness dimension is 5% of the pipe diameter[58].

For noncircular flow passages, an equivalent diameter can be used in which D is replaced by D_{eq}, which is four times the hydraulic radius, or,

$$D_{eq} = 4 \times \frac{(flow\ area)}{(wetted\ perimeter)} \tag{30}$$

Flow within a bellows-type construction has been investigated by Weisend and Van Sciver,[59] who give alternative methods for determining f. The friction factor for flow within corrugated channels can be increased by a factor of 7 or more over the value for smooth channels. For greater roughnesses than 5%, or for the influence of other geometries, such as the presence of a spiral tape that could induce a swirl to the flow pattern, an experimental determination of the friction factor is recommended.

Refrigeration at Lower Temperatures

It is possible to cool an SPTL to lower temperatures than those considered so far. The cryogenic refrigerator, as currently available, is capable of cooling at temperatures down to 4.2 K. However, the use of nitrogen is no longer possible below 63.2 K, the triple point temperature below which nitrogen exists only as either a gas (at very low vapor pressure) or a solid. The use of liquid oxygen as a coolant would be possible down to 54.3 K, but the inconvenience of handling the oxygen safely does not make this small decrease in operating temperature attractive. Neon could extend the operating range down to 24.6 K and hydrogen to 13.8 K, but neither of these fluids is practical, for the reasons mentioned earlier. However, helium gas could be used over this entire temperature range, with little disadvantage other than the possibly higher operating pressure and the lower efficiency inherent with lower temperatures.

The lower operating temperature also carries with it an additional cost for performing the refrigeration at that lower temperature. Because the degree of approach to the

Carnot limit depends only upon capacity[43], a comparison of the Carnot limits for ideal refrigerators will also give us the ratio of power inputs for practical refrigerators. We can use the results from above in which the refrigerator cost was shown to be proportional to the 0.626 power of the input power. Taking operation at 64 K as a basis, Table 4-21 shows the increase in input power, and, consequently, the increase in cost of operating an SPTL at 50, 40, and 20 K.

Table 4-21
Relative costs of SPTL refrigeration at various temperatures

Temperature (K)	Input power ratio	Cost ratio
64	1	1
50	1.36	1.21
40	1.76	1.42
20	3.80	2.31

Summary

In the design of an SPTL there are numerous interrelated parameters that must be considered. A variety of refrigeration methods are available, and several cryogens are available to serve as the working fluid for the refrigerator and as the coolant for the SPTL. Other parameters include the flow path of the coolant, the dimensions of the cable and cooling channels, the type of thermal insulation, the size of the cryogenic enclosure, and the distance between the refrigeration stations. These items are of direct importance to the cryogenic system. The importance of the optimization of the total system becomes obvious from the results of a previous study[60], which showed that the cost of the cryogenic system (refrigerator and cryogenic enclosure) can amount to 35% to 50% of the total system cost.

The selection of a refrigerator type, the method of application of the refrigeration to the SPTL, and the SPTL design are so interrelated that not one of these items can be treated independently. Consequently, no specific recommendations can be made for these items

for the STI Project without doing a more extensive study that would integrate the design of the cable, the cryogenic enclosure, and reliability and redundancy requirements. It might also be advisable to tie this study to a specific application, including such details as location, capacity, and other use conditions. This might be done by picking a niche, or specific application in which an SPTL could offer a definite advantage or capability over a conventional power transmission system.

Thus, we recommend that an electric utility become involved in selecting the site and the appropriate SPTL capacity and use conditions. Then the study could proceed with the design of the cable, the cryogenic enclosure, and refrigeration system for that use.

References

1. R. H. Kropschot, "Low-Temperature Insulation," in Applied Cryogenic Engineering, R. W. Vance and W. M. Duke, Eds. (John Wiley & Sons, New York, 1963), Chapter 6, pp. 152-169.

2. R. B. Scott, Cryogenic Engineering, (Met-Chem Research, Inc., Boulder Colorado, 1988).

3. R. G. Scurlock and B. Saull, "Development of Multilayer Insulations with Thermal Conductivities below 0.1 W/cm.K," *Cryogenics* 16, 303-311 (1976).

4. Frank Kreith, Principles of Heat Transfer, 2nd Ed., (International Textbook Co., Scranton, Pennsylvania, 1965), p. 39.

5. P. J. Schneider, "Conduction," in Handbook of Heat Transfer, W. M. Rohsenow and J. P. Hartnett, Eds. (McGraw-Hill, New York, 1973), pp. 3-121.

6. I. E. Spradley, T. C. Nast, and D. J. Frank, "Experimental Studies of MLI Systems at Very Low Boundary Temperatures," in Advances in Cryogenic Engineering, Vol. 35, R. W. Fast, Ed. (Plenum Press, New York, 1990), pp 477-486.

7. Q. S. Shu, R. W. Fast, and H. L. Hart, "An Experimental Study of Heat Transfer in Multilayer Insulation Systems from Room Temperature to 77 K," in Advances in Cryogenic Engineering, Vol. 31, R. W. Fast, Ed. (Plenum Press, New York, 1986), pp.455-463.

8. S. L. Bapat, K. G. Narayankhedkar, and T. P. Lukose, "Performance Prediction of Multilayer Insulation," *Cryogenics* 30, 700-710 (1990).

9. P. E. Glasser, "The Development of Thermal Insulations and Techniques for Use at Very Low Temperature," Progress in Refrigeration Science and Technology, *Proc. XIII International Congress of Refrigeration*, Vol. 2 (Inst. Int. Froid, Paris, 1967), pp. 3-27.

10. R. F. Barron, Cryogenic Systems, 2nd Ed. (Oxford University Press, New York, 1985), pp. 383-400.

11. R. H. Kropschot, "Insulation Technology," in Cryogenic Technology, (John Wiley & Sons, New York, 1963), Chapter 7, pp. 239-250.

12. "Low Temperature Insulations - Foams and Composites," *Cryogenic Engineering News* 4, No. 5, 20-25 (1969).

13. R. H. Kropschot, "Cryogenic Insulation," *ASHRAE Journal* 1, 48-54 (1959).

14. W. N. Boroski, J. D. Gonczy, and R. C. Niemann, "Thermal Performance Measurements of a 100 Percent Polyester MLI System for the Superconducting Super Collider; Part II: Laboratory Results (300 K - 80 K)," in Advances in Cryogenic Engineering, Vol. 35, R. W. Fast, Ed. (Plenum Press, New York, 1990), pp. 497-506.

15. S. L. Bapat, K. G. Narayankhedkar, and T. P. Lukose, "Experimental Investigation of Multilayer Insulation," *Cryogenics* 30, 711-719 (1990).

16. K. Kutzner, F. Schmidt, and I. Wietzke, "Radiative and Conductive Heat Transmission Through Superinsulations -- Experimental Results for Aluminum Coated Plastic Foils," *Cryogenics* 13, 396-404 (1973).

17. Q. S. Shu, R. W. Fast, and H. L. Hart, "Heat Flux From 277 to 77 K Through a Few Layers of Multilayer Insulation," *Cryogenics* 26, 671-677 (1986).

18 .R. G. Scurlock and B. Saull, "Development of Multi-layer Insulations with Thermal Conductivities below 0.1 W/cm.K," Proceedings 6th International Cryogenic Engineering Conference, Grenoble, May 11-14, 1976 (IPC Science and Technology Press, Guildford, Surrey, England, 1976), pp. 169-172.

19. T. L. Halaczek and J. Rafalowicz, "Heat Transport in Self-Pumping Multilayer Insulation," *Cryogenics* 26, 373-376 (1986).

20. T. L. Halaczek and J. Rafalowicz, "Temperature Variation of Thermal Conductivity of Self-Pumping Multilayer Insulation," *Cryogenics* 26, 544-546 (1986).

21. *"Design of Thermal Protection Systems for Liquid Hydrogen Tanks,"* Arthur D. Little, Inc. Report no. 65008-03-01, April 1963.

22. C. R. Lindquist, *"Linde Company Super Insulation Applied to Space Vehicles,"* Linde Company report, December 1, 1962.

23. P. J. Perkins, L. S. Smith, and M. A. Colaluca, "Preliminary Test Results on a Compressed Multilayer Insulation System for a Liquid-Hydrogen Fueled Rocket," in Advances in Cryogenic Engineering, Vol. 9, K. D. Timmerhaus, Ed. (Plenum Press, New York, 1964), pp. 38-45.

24. C. R. Lindquist, "Advances in Cryogenic Technology," Linde Company report, March 1, 1963.

25. P. E. Glasser, "Effective Thermal Insulation: Multi-layer Systems," *Cryogenic Engineering News* 4, No. 4, 16-24 (1969).

26. R. F. Barron, "Principles of Evacuated Cryogenic Insulations," AIChE Symposium Series, Vol. 68, No. 125, pp. 40-49.

27. R. S. Mikhalchenko, V. F. Getmanets, N. P. Pershin, and Yu. V. Batozshii, "Study of Heat Transfer in Multilayer Insulations Based on Composite Spacer Materials," *Cryogenics* 23, 309-311 (1983).

28. Q. S. Shu, "Systematic Study to Reduce the Effects of Cracks in Multilayer Insulation, Part I: Theoretical Model," *Cryogenics* 27, 249-256 (1987).

29. Q. S. Shu, "Systematic Study to Reduce the Effects of Cracks in Multilayer Insulation, Part II: Experimental Results," *Cryogenics* 27, 298-311 (1987).

30. N. Saho and T. Takada, "Influence of Tube Diameter on Heat Transfer in Multilayer Insulation," presented at Cryogenic Engineering Conference, Colorado Springs, Colorado, August 15-19, 1983, paper IC-11.

31. "Fermilab Licensing Insulation System," *Superconductor Industry* 2, No. 3, 32-33 (1989).

32. J. D. Gonczy, W. N. Boroski, R. C. Niemann, J. G. Otavka, M. K. Ruschman, and C. J. Schoo, "A Blanket Design, Apparatus, and Fabrication Techniques for the Mass Production of Multilayer Insulation Blankets for the Superconducting Super Collider," in Advances in Cryogenic Engineering, Vol. 35 (Part A), R. W. Fast, Ed.(Plenum Press, New York, 1990), pp. 507-516.

33. G. B. Andeen and R. L. Provost, "Preliminary Design of a High-Temperature Superconducting Transmission Line," in Advances in Cryogenic Engineering (Materials), Vol. 36 (Part A), A. F. Clark and R. P. Reed, Eds. (Plenum Press, New York, 1988), pp. 557-564.

34. K. D. Williamson, Jr., F. J. Edeskuty, and F. G. Brickwedde, "Cryogenics," in Marks' Standard Handbook for Mechanical Engineers, Ninth Edition, E. A. Avallone and T. Baumeister III, Eds. (McGraw-Hill Book Co., New York, 1987), Chap. 19.2, pp. 19-21 - 19-37.

35. *"Resistive Cryogenic Cable, Phase III - Final Report,"* Cryogenics Branch, Power Generation and Propulsion Laboratory, General Electric Co., prepared for the Electric Power Research Institute, EPRI EL-503, Project 7806, October 1977.

36. "Low Temperature Insulations," *Cryogenic Engineering News* 4, No. 1, 123-125 (1969).

37. G. X. Yu, Y. X. Zhou, and Z. Y. Zhang, "Research on Heat Transfer Process in Evacuated Powder Insulation with Square Flakes," *Cryogenics* 30 (September Supplement), 335-339 (1990).

38. M. P. Hnilicka, "Engineering Aspects of Heat Transfer in Multilayer Reflective Insulation and Performance of NRC Insulation," in Advances in Cryogenic Engineering, Vol. 5, (Plenum Press, New York, 1960), pp. 199-208.

39. T. L. Halaczek and J. Rafalowicz, "Unguarded Cryostat for Thermal Conductivity Measurements of Multilayer Insulation," *Cryogenics* 25, 529-530 (1985).

40. W. N. Boroski, J. D. Gonczy, and R. C. Niemann, "Thermal Performance Measurements of a 100 Percent Polyester MLI System for the Superconducting Super Collider; Part I: Instrumentation and Experimental Preparation (300 K - 80 K)," in Advances in Cryogenic Engineering, Vol. 35, R. W. Fast, Ed. (Plenum Press, New York, 1990), pp. 487-496.

41. T. Ohmori, W. N. Boroski, J. D. Gonczy, R. C. Niemann, M. K. Ruschman, T. Taira, K. Takahashi, A. Yamamoto, and H. Hirabayashi, "Thermal Performance of Candidate SSC Magnet Thermal Insulation Systems," in Advances in Cryogenic Engineering, Vol. 33, R. W. Fast, Ed. (Plenum Press, New York, 1988), pp. 323-331.

42. R. O. Voth, "Maximum Practical Efficiency of Helium Temperature Refrigerators," *Cryogenics* **21**, 635-640 (1981).

43. T. R. Strobridge, "Cryogenic Refrigerators - an Updated Survey," National Bureau of Standards Report NBS Technical Note 655, June, 1974.

44. R. F. Barron, *Cryogenic Systems* (Oxford University Press, New York, 1985).

45. G. G. Haselden, "Refrigeration and Liquefaction Cycles," Chapter 2 in *Cryogenic Fundamentals*, G, G, Haselden, Ed. (Academic Press, London, 1971) p 50.

46. P. Graneau, H. C. Parish, and J. L. Smith, Jr., "Refrigeration Requirements of the LN2 Cryo-Cable," Transactions of the ASME *Journal of Engineering for Industry* (November 1971), pp 1161-1165.

47. R. C. Longsworth and K. F. Schoch, "A Study of Refrigeration for Liquid-Nitrogen-Cooled Power Transmission Cables," *Advances in Cryogenic Engineering*, **Vol. 25**, K. D. Timmerhaus, Ed. (Plenum Press, New York, 1980), pp 585-596.

48. P. Chowdhuri and H. L. Laquer, "Some Electrical Characteristics of a DC Superconducting Cable," *IEEE Transactions on Power Apparatus and Systems*, **Vol. PAS-97, no. 2**, March/April, 1978, pp 399-408.

49. G. A. Cook, *Argon, Helium, and the Rare Gases*, **Vol. 1** (Interscience Publishers, New York, 1961), p 42.

50. C. F. Key, "Compatibility of Materials with Liquid Oxygen," NASA Technical Memorandum NASA TM X-64711 (October 1972).

51. K. Tsuchiya, N. Ohuchi, and A. Torashimi, "Cryogenic System of the Superconducting Insertion Quadrupole Magnet for Tristan Main Ring," *Advances in Cryogenic Engineering*, **Vol. 35B**, R. Fast, Ed. (Plenum Press, New York, 1990), pp 941-948.

52. J. D. Fuerst, "Trial Operation of Cold Compressors in Fermilab Satellite Refrigerator," *Advances in Cryogenic Engineering*, **Vol 35B**, R. Fast, Ed. (Plenum Press, New York, 1990), pp 1023-1030.

53. T. Jasinski, W. D. Stacy, S. C. Honkonen, and H. Sixsmith, "Generic Pump/Compressor Design for Circulation of Cryogenic Fluids," *Advances in Cryogenic Engineering*, **Vol. 31**, R. Fast, Ed. (Plenum Press, New York, 1986) pp 991-997.

54. F. J. Kadi and R. C. Longsworth, "An Assessment and Study of Existing Concepts and Methods of Cryogenic Refrigeration for Superconducting Transmission Cables," Air Products and Chemicals, Inc. report to the US Energy Research and Development Administration no. C00-02552-6 (February 1976).

55. S. A. Manatt, P. G. Wapato, J. Stanke, and J. P. Baumgartner, "Concepts and Methods of Refrigeration of Superconducting Power Transmission Cables,"AiResearch Mfg. Co. report to the US Energy Research and Development Administration no. CONS/1061-1 (June 1976).

56. *Statistical Abstract of the US - 1990, The National Data Book*, US Department of Commerce, The Bureau of the Census, p 468.

57. Monthly Labor Review, D. P. Klein, Ed., US Department of Labor (October 1991) pp 90-91.

58. Marks' Standard Handbook for Mechanical Engineers, Ninth Edition, E. A. Avallone and T. Baumeister III, Eds. (McGraw-Hill Book Co., New York, 1987), pp 56-57.

59. J. G. Weisend II and S. W. Van Sciver, "Pressure Drop from Flow of Cryogens in Corrugated Bellows," *Cryogenics*, **30**, 935-941 (1990).

60. F. J. Edeskuty, E. M. Honig, W. F. Stewart, L. K. Trocki, J. L. Smith, Jr., J. L. Kirtley, and S. D. Umans, "The Impact of High Temperature Superconductors on the Transmission and Generation of Electricity," Los Alamos National Laboratory internal report no. A-4/88-1 submitted to the Electric Power Research Institute (Palo Alto, CA, June 1988).

61. R. T. Jacobsen, R. B. Stewart, R. D. McCarty, and H. M. J. Hanley, "Thermophysical Properties of Nitrogen from the Fusion Line to 3500 R (1944 K) for Pressures to 150,000 PSIA (10342 x 10^5 N/m^2)," NBS Technical Note 648, National Bureau of Standards, Boulder, CO (December 1973).

Bibliography

1. W. P. Dube, L. L. Sparks, A. J. Slifka, R. M. Bitsy, "Apparatus for Measurement of Thermal Conductivity of Insulation Systems Subjected to Extreme Temperature Differences," in *Advances in Cryogenic Engineering (Materials)*, Vol. 36, R. P. Reed and F. R. Fickett, Eds. (Plenum Press, New York, 1990), pp. 853-859.

2. L. L. Sparks, W. P. Dube, and A. J. Slifka, *"Thermal Conductivity of Selected Foams and Systems from 100 to 300 K,"* National Bureau of Standards report NBSIR 88-3086, January 1988.

3. W. P. Dube, L. L. Sparks, and A. J. Slifka, "Thermal Conductivity of Evacuated Perlite at Low Temperatures as a Function of Load and Load History," presented at 7th Intersociety Cryogenics Symposium, Houston, Texas, January 22-25, 1989.

4. J. K. Novak, "Compressive Behavior of Perlite Insulating Powder," Los Alamos Scientific Laboratory report LA-DC-7158, 1965.

5. *"Cryogenic Insulation Systems for the RIFT Vehicle,"* Aerojet-General Corporation Report No. 2339, July 1962.

6. J. D. Gonczy, M. Kuchnir, T. H. Nicol, R. C. Niemann, and R. J. Powers, "HeatLeak Measurements Facility," in *Advances in Cryogenic Engineering*, Vol. 31, (Plenum Press, New York, 1986), pp. 1291-1298.

7. T. L. Halaczek and J. Rafalowicz, "Flat-Plate Cryostat for Measurements of Multilayer Insulation Thermal Conductivity," *Cryogenics* 25, 593-595 (1985).

8. A. S. Adorjan, D. B. Crawford, and S. E. Handman, "Double-Walled Cryogenic Storage Tanks -- Effect of Perlite/Fiberglass Insulation on Dynamic Loads in Case of Inner Tank Failure," in *Cryogenic Processes and Equipment* 1982, Vol. 79, No. 224, AIChE Symposium Series, pp. 46-50.

9. C. R. Maiti, "Some Aspects of the Thermal Performance of Indigenous Powder Insulators," *Cryogenics* 22, 518-522 (1982).

10. C. R. Maiti, "The Insulation Effectiveness of a Porous Material as Measured by the Screening Technique," *Cryogenics* 23, 207-208 (1983).

11. M. M. Yovanovich, "Apparent Conductivity of Glass Microspheres from Atmospheric Pressure to Vacuum," presented at ASME-AIChE Heat Transfer Conference, Atlanta, Georgia, August 5-8, 1973, ASME paper # 73-HT-43.

12. J. B. Loser, C. E. Moeller, and M. B. Thompson, "Thermophysical Properties of Thermal Insulating Materials," Wright Patterson Air Force Base Technical Documentary Report No. ML-TDR-64-5, April 1964.

13. C. F. Sindt, "Insulation of Liquid Oxygen Dewars," National Bureau of Standards report NBSIR 73-308, April 1973.

14. R. T. Parmley, "Evacuated Load-Bearing High Performance Insulation Study," NASA Lewis Research Center Contract NAS 3-17817, May 1974 - August 1977.

15. R. T. Parmley, "Microsphere Insulation Systems," in Applications of Cryogenic Technology, Vol. 8, S. H. Booth and R. W. Vance, Eds. (Scholium International Inc., Flushing, New York, 1976), pp. 161-167.

16. W. P. Dube, L. L. Sparks, and A. J. Slifka, "NBC Boil-Off Calorimeter for Measuring Thermal Conductivity of Insulating Materials," in *Advances in Cryogenic Engineering (Materials)*, Vol. 34, A. F. Clark and R. P. Reed, Eds. (Plenum Press, New York, 1988), pp. 67-73.

17. L. L. Scull and J. M. Arvidson, "Low Temperature Mechanical Property Measurements of Silica Aerogel Foam," *in Advances in Cryogenic Engineering (Materials)*, Vol. 34, A. F. Clark and R. P. Reed, Eds. (Plenum Press, New York, 1988), pp. 413-418.

18. N. Saho and T. Takada, "Thermal Characteristics of Multilayer Insulation," in Proceedings of the Ninth International Cryogenic Engineering Conference, K. Yasukochi and H. Nagano, Eds., Kobe, Japan, May 11-14, 1982, pp. 572-575.

19. I. Ishaghoff and J. M. Canty, "Quilted Superinsulation," in Advances in Cryogenic Engineering (Materials), Vol. 9, K. D. Timmerhaus, Ed. (Plenum Press, New York, 1964), pp. 46-51.

20. L. L. Sparks, "Cryogenic Foam Insulations: Polyurethane and Polystyrene," in Nonmetallic Materials and Composites at Low Temperatures, A. F. Clark, R. P. Reed, and G. Hartwig, Eds., (Plenum Press, New York, 1979), pp. 165-205.

21. W. P. Dube, L. L. Sparks, and A. J. Slifka, "Thermal Conductivity of Evacuated Perlite at Low Temperatures as a Function of Load and Load History," Cryogenics 31, 3-6 (1991).

22. "Low Temperature Insulations: Powders and Fibers," Cryogenic Engineering News 4, No. 2, 18-21 (1969).23. A. H. Taylor, P. S. McAuliffe, L. L. Sparks, "An Advanced Reusable Cryogenic Foam Insulation System," NASA Langley Research Center report LAR-14014, 1987.

ABOUT EPRI

The mission of the Electric Power Research Institute is to discover, develop, and deliver high value technological advances through networking and partnership with the electricity industry.

Funded through annual membership dues from some 700 member utilities, EPRI's work covers a wide range of technologies related to the generation, delivery, and use of electricity, with special attention paid to cost-effectiveness and environmental concerns.

At EPRI's headquarters in Palo Alto, California, more than 350 scientists and engineers manage some 1600 ongoing projects throughout the world. Benefits accrue in the form of products, services, and information for direct application by the electric utility industry and its customers.

EPRI—*Leadership in Electrification through Global Collaboration*

(continued from front cover)

4. TERM AND TERMINATION

This license and this agreement are effective until terminated. You may terminate them at any time by destroying this report. EPRI has the right to terminate the license and this agreement immediately if you fail to comply with any term or condition of this agreement. Upon any termination you may destroy this report, but all obligations of nondisclosure will remain in effect.

5. DISCLAIMER OF WARRANTIES AND LIMITATION OF LIABILITIES

NEITHER EPRI, ANY MEMBER OF EPRI, ANY COSPONSOR, NOR ANY PERSON OR ORGANIZATION ACTING ON BEHALF OF ANY OF THEM:

(A) MAKES ANY WARRANTY OR REPRESENTATION WHATSOEVER, EXPRESS OR IMPLIED, (I) WITH RESPECT TO THE USE OF ANY INFORMATION, APPARATUS, METHOD, PROCESS OR SIMILAR ITEM DISCLOSED IN THIS REPORT, INCLUDING MERCHANTABILITY AND FITNESS FOR A PARTICULAR PURPOSE, OR (II) THAT SUCH USE DOES NOT INFRINGE ON OR INTERFERE WITH PRIVATELY OWNED RIGHTS, INCLUDING ANY PARTY'S INTELLECTUAL PROPERTY, OR (III) THAT THIS REPORT IS SUITABLE TO ANY PARTICULAR USER'S CIRCUMSTANCE; OR

(B) ASSUMES RESPONSIBILITY FOR ANY DAMAGES OR OTHER LIABILITY WHATSOEVER (INCLUDING ANY CONSEQUENTIAL DAMAGES, EVEN IF EPRI OR ANY EPRI REPRESENTATIVE HAS BEEN ADVISED OF THE POSSIBILITY OF SUCH DAMAGES) RESULTING FROM YOUR SELECTION OR USE OF THIS REPORT OR ANY INFORMATION, APPARATUS, METHOD, PROCESS OR SIMILAR ITEM DISCLOSED IN THIS REPORT.

6. EXPORT

The laws and regulations of the United States restrict the export and re-export of any portion of this report, and you agree not to export or re-export this report or any related technical data in any form without the appropriate United States and foreign government approvals.

7. CHOICE OF LAW

This agreement will be governed by the laws of the State of California as applied to transactions taking place entirely in California between California residents.

8. INTEGRATION

You have read and understand this agreement, and acknowledge that it is the final, complete and exclusive agreement between you and EPRI concerning its subject matter, superseding any prior related understanding or agreement. No waiver, variation or different terms of this agreement will be enforceable against EPRI unless EPRI gives its prior written consent, signed by an officer of EPRI.

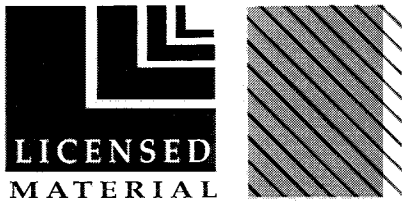

Printed with soya inks on recycled paper (50% recycled fiber, including 10% postconsumer waste) in the United States of America.